

**NANOTECHNOLOGY FOR DRUG AND VACCINE DELIVERY:  
FORMULATION AND BIOPHARMACEUTICAL  
CHARACTERIZATION OF MUCOSAL TUBERCULOSIS DRUG AND  
VACCINE DELIVERY SYSTEMS**

A thesis submitted to  
THE MAHARAJA SAYAJIRAO UNIVERSITY OF BARODA  
for the award of Degree of

**DOCTOR OF PHILOSOPHY  
IN  
PHARMACY**

By  
**Kailash C. Petkar**

Supervised by  
**Dr. (Mrs.) Krutika Sawant**  
Professor of Pharmaceutics



**Pharmacy Department**  
Faculty of Technology and Engineering  
The Maharaja Sayajirao University of Baroda  
Vadodara

**September 2013**

## DECLARATION

In accordance with the University Ordinance no. ACED/510 Ph. D., I, undersigned, hereby declare that the work presented in this thesis entitled “Nanotechnology for Drug and Vaccine Delivery: Formulation and Biopharmaceutical Characterization of Mucosal Tuberculosis Drug & Vaccine Delivery Systems”, comprises of independent investigations carried out by me in the Pharmacy Department, The M. S. University of Baroda, India and University College London, School of Pharmacy, UK. Whenever references have been made to the work of others, it has been clearly indicated with the source of information under the chapters of references. I further declare that the results of this work have not been previously submitted for the award of any degree or fellowship.

Candidate  
(Kailash C. Petkar)

Certified by and forwarded through Research Supervisor,

Krutika K. Sawant, M. Pharm., PhD  
Professor,  
Pharmacy Department,  
Faculty of Technology & Engineering,  
The M.S. University of Baroda,  
Vadodara - 390 001



Pharmacy Department,  
Faculty of Technology & Engineering  
The Maharaja Sayajirao University of Baroda

Post Box No.: 51, Kalabhavan, Vadodara - 390 001, INDIA.

Phone: (+91-0265) 2434187

Fax: (0265) 2423898/2418927

Email: head-pharm@msubaroda.ac.in

September 18, 2013

### CERTIFICATE

This is to certify that the thesis entitled "Nanotechnology for Drug and Vaccine Delivery: Formulation and Biopharmaceutical Characterization of Mucosal Tuberculosis Drug and Vaccine Delivery Systems" submitted for the award of Ph.D. degree in Pharmacy by Mr. Kailash C. Petkar, incorporating original research work carried out by him under my supervision and no part of the thesis has been submitted for the award of any other degree.

  
Dr. Krutika K. Sawant  
Research Supervisor  
Pharmacy Department

  
Head  
Pharmacy Department,  
Faculty of Tech. & Engg.  
M.S. Univ. of Baroda,  
Kalabhavan, BARODA

  
Dean  
Faculty of Technology & Engineering  
The M. S. University of Baroda  
Faculty of Tech. & Engg.  
M. S. University of Baroda,  
Baroda.

Department of Special Assistance (Phase-I) of University Grants Commission  
Centre of Relevance & Excellence in New Drug Delivery Systems of TIFAC  
Department of Science & Technology, Government of India



## STATEMENT OF STUDENT STATUS

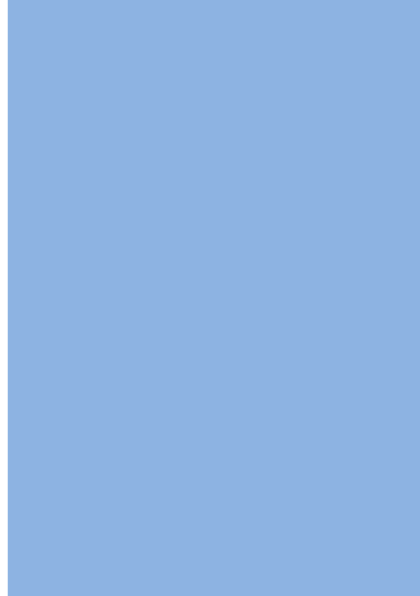
This is to confirm that the student named below was registered at UCL as follows:

<b>Student Number:</b>	011119346
<b>Full Name as registered:</b>	Kailash Petkar
<b>Programme of Study:</b>	Affiliate Pharmacy
<b>Department:</b>	School Of Pharmacy
<b>Current Student Status:</b>	Permanent Leaver- Previously Enrolled
<b>Current Mode of Attendance:</b>	Full-time
<b>Date of Registration:</b>	07/Nov/2011
<b>End of Registration:</b>	20/Nov/2012

Students registered on a full-time basis were expected to devote approximately 35 hours per week to their studies and to attend the course for periods of at least 24 weeks in the year. Students registered on a part-time basis were permitted to be in attendance for a maximum of 15 hours per week.

---

Printed on 25 March 2013



**Dedicated To  
My Family**



### Acknowledgements

During the course of my PhD, large number of people have given me assistance. I want to thank everyone for their unconditional help and support throughout my studies in The M.S. University of Baroda and UCL School of Pharmacy.

First and foremost, I would like to express my deep sense of gratitude and thank to my mentor Prof. Krutika K. Sawant (Pharmacy Department, The M. S. University of Baroda) for her unending and untiring support, timely advice and constructive suggestions. Her constant encouragement and meticulous attention throughout the course of this research work has made me competent enough to carry out this work with the patience.

I would also like to thank Dr. Satyanarayana Somavarapu and Prof. Kavin Taylor (University College London, School of Pharmacy) in a capacity of my mentors in UK under Commonwealth Fellowship Plan, UK for introducing me to the world of chitosan and their never-ending enthusiasm while carrying out this research work. In particular, Dr. Soma has always been by my side during my happy and despair moments. He has been great support during my stay at UCL SOP, UK.

I am thankful to Dr. Jayashree Pohnerkar (Department of Biochemistry, The M. S. University of Baroda) for exposing me to the globe of protein biochemistry and providing hands on training on various molecular biology techniques.

I extend my thanks to Prof. A. N. Misra, Dean, Faculty of Technology and Engineering, The M. S. University of Baroda for his friendly and encouraging suggestions while carrying out this work and providing timely, invaluable suggestions on scientific and personal life.

I would like to thank Prof. M. R. Yadav, Head, Department of Pharmacy, Prof. S. J. Rajput and R. Girdhar (the then Co-ordinator of Shri. G. H. Patel Pharmacy Building) of The M. S. University of Baroda for providing necessary facility to carry out this research work.

I would like to extend my sincere thanks to Prof. Ijeoma Uchegbu and Dr. Sudax (UCL, SOP, UK) for providing timely access to her lab to carry out required studies. Moreover, I also thank Dr. Khalid Sheikh for his encouraging words during my stay at UCL, SOP, UK and Sunny (Dr. Hardyal Gill) for providing timely help while carrying out HPLC. In addition, their enthusiasm on discussing wide variety of topics from social to scientific has always energized me.

I also want to thank David McCarthy for his assistance with the Scanning & Transmission electron microscopy and wonderful discussions with him. I must thank Dr. Gary Parkinson for his timely help in carrying out XRD studies.

I wish to extend my thanks to Dr. Imran and Nitesh from School of Pharmacy and Biomolecular Science Liverpool John Moores University for providing assistance in carrying out cytotoxicity studies.

## Acknowledgements

---

I am thankful to Helen Mokhtar from Veterinary Laboratories Agency, Department of Environmental, Food and Rural Affairs (DEFRA), Government of UK for providing assistance throughout in-vitro cell line studies.

I would also like to thank Dr. M. N. Satish Kumar, (Prof. J.S.S. College of Pharmacy, Ooty) and Mr. Raju for their valuable support during the course of animal studies.

Financial support from All India Council of technical Education (AICTE), India for granting National Doctoral Fellowship and Commonwealth Scholarship Commission, UK for awarding Commonwealth Fellowship are gratefully acknowledged without which it would have been difficult to carry out the entire work.

I would like to mention special thanks to Mycobacteria Research Laboratories, Department of Microbiology, Colorado State University for providing necessary materials for research as part of NIH, NIAID Contract, entitled "Tuberculosis Vaccine Testing and Research Materials", (contract no. HHSN266200400091C).

I also thank former and present members of our research group and friends from Pharmacy Department, M.S.U. Baroda, India; Sandip, Anand, Garima, Heena, Kaustubh, Mukesh, Niraj, Ashish, Nirav, Mohan and all other friends for always taking time to help me in any way they can.

I would also like to thank members of our research group and friends from School of Pharmacy, UK; Naba, Zeeneh, Garima, Hamid, Zip, Alberto, Abeer, Nicola, Asma for providing constant help throughout my stay wonderful and comfortable at UCL SOP.

I would like to sincerely thank all the teaching and non-teaching staff members of Department of Pharmacy, The M. S. University of Baroda and UCL, School of Pharmacy, London for supporting me throughout the research work.

I want to thank my first angel who entered into my life during the course of PhD and emerged as a constant source of encouragement throughout this research work. Secondly, I must thank “cherry” our baby angel who came while being in London and arrived few months ago in our life with lots of happiness, I must thank for her innocent support.

I owe deep gratitude to my parents, who have been seeing me since I am 0 year old. They have always kept me at comfort to continue my education and tasks at level best. All other family members particularly my sister’s family, late brother and parents in laws are equally responsible for completion of my PhD thesis patiently.

Last but not least, I thank to almighty for empowering me with courage, keeping me at peace to take up and accomplish the tasks during the course of my PhD.

**Table of Contents**

LIST OF TABLES .....	I
LIST OF FIGURES .....	V
LIST OF ABBREVIATIONS .....	IX
ABSTRACT .....	XI
<b>CHAPTER 1: INTRODUCTION .....</b>	<b>1</b>
1.1 General Overview on vaccine and drug development for Tuberculosis .....	1
1.2 Objective of the Research .....	5
1.2 Innovation of the thesis .....	5
1.3 Plan of work.....	5
References.....	7
<b>CHAPTER 2: LITERATURE REVIEW.....</b>	<b>11</b>
2.1 History and Epidemiology of TB.....	11
2.2 Pathogen, Pathogenesis and Progression of TB.....	13
2.3 Macrophage activation and immune response.....	15
2.4 Current status of TB vaccine development .....	17
2.4.1 BCG vaccine.....	17
2.4.2 Live and attenuated mycobacterial vaccines .....	19
2.4.3 DNA vaccines .....	20
2.4.4 Subunit vaccines.....	22
2.5 Evolution and current status of TB chemotherapy.....	32
2.6 Pulmonary mucosal delivery of vaccines and drugs - an alternative route .....	39
2.6.1 Anatomy of Lung.....	39
2.6.2 Rational behind delivery of drug and vaccines to lungs.....	40
2.6.3 Advances in pulmonary drug and vaccine delivery .....	43
2.6.4 Polymeric carrier based delivery systems.....	47
2.6.5 PLGA and Chitosan for pulmonary vaccine and drug delivery systems .....	49
2.6.5.1 PLGA.....	49
2.6.5.2 Chitosan.....	50
2.7 Formulation and characterization of Nanoparticle .....	54
2.8 Techniques for the preparation of Dry powders .....	58
2.9 Characterization of Nanoparticulate formulations.....	59
References.....	65
<b>CHAPTER 3: ANALYTICAL METHODS.....</b>	<b>75</b>
3.1 Materials .....	75
3.2 TNBS Assay for determination of degree of acylation in HCD (octanoyl chitosan) .....	75
3.3 Estimation of FITC using Fluorometric method of analysis.....	76
3.4 Estimation of BSA using QuantiPro™ BCA protein assay kit by UV Spectroscopy.....	76

## Table of Contents

3.4.1 Calibration curve of BSA in water using QuantiPro™ BCA assay kit .....	76
3.4.2. Calibration curve of BSA in SDS/NaOH solution using QuantiPro™ BCA assay kit .....	77
3.4.3 Calibration curve of BSA in Simulated Lung Fluid (SLF) using QuantiPro™ BCA assay kit.....	78
3.5 Results and Discussion .....	79
3.6 Estimation of Rifampicin by Ultraviolet Spectroscopy.....	84
3.6.1 Calibration curve in water .....	84
3.6.2 Calibration curve in SLF (pH 7.4) .....	85
3.7 Results and Discussion .....	86
3.8 Estimation of rifampicin in double distilled water and SLF by HPLC .....	89
3.9 Results and Discussions .....	90
References .....	94
<b>CHAPTER 4: VACCINE PREPARATION, EXTRACTION AND PURIFICATION .....</b>	<b>95</b>
4.1 Materials .....	95
4.2 Transformation of pDNA into <i>E. Coli</i> DH5 $\alpha$ and BL21 DE3 pLysS .....	95
4.3 Plasmid preparation using Alkaline Lysis method for isolation of pDNA .....	96
4.4 Restriction analysis of small-scale preparations of plasmid DNA (PMRL B41/Rv3804c /Ag85A in pET15b) in <i>E. coli</i> DH-5 $\alpha$ by Xho I Digestion .....	98
4.5 Agarose Gel Electrophoresis.....	99
4.6 Protein expression and purification (Ag85A) .....	101
4.7 ELISA (criss cross) assay to optimize reagent concentration and Ag85A activity .....	110
4.8 Fluorometric analysis of native, urea-denatured and refolded Ag85A .....	113
4.9 Results and Discussion .....	113
References .....	120
<b>CHAPTER 5: SYNTHESIS AND CHARACTERIZATION OF HYDROPHOBIC CHITOSAN DERIVATIVE.....</b>	<b>121</b>
5.1 Materials .....	121
5.2 Equipments .....	121
5.3 Methods .....	121
5.3.1 <i>Synthesis of hydrophobic chitosan derivative (HCD)</i> .....	121
5.4 Solubility study .....	122
5.5 Degree of Substitution.....	122
5.6 Structural analysis of HCD .....	122
5.6.1 <i>Fourier Transform Infrared Spectroscopy (FTIR)</i> .....	122
5.6.2 <i>Nuclear magnetic resonance (<sup>1</sup>H-NMR) spectroscopy</i> .....	122
5.6.3 <i>Differential Scanning Calorimetry (DSC)</i> .....	122
5.6.4 <i>X-Ray diffractometry (XRD)</i> .....	123
5.7 Result and Discussion.....	123
References .....	129

<b>CHAPTER 6: SYNTHESIS AND CHARACTERIZATION OF MODIFIED CHITOSAN DERIVATIVE.....</b>		<b>131</b>
6.1 Materials .....		131
6.2 Equipments.....		131
6.3 Methods.....		131
6.3.1 <i>Synthesis of modified chitosan derivative (MCD)</i> .....		131
6.4 Solubility study .....		132
6.5 Degree of Acylation.....		132
6.6 Structural analysis of MCD .....		132
6.6.1 <i>Fourier Transform Infrared Spectroscopy (FTIR)</i> .....		132
6.6.2 <i>Nuclear magnetic resonance (<sup>1</sup>H-NMR) spectroscopy</i> .....		132
6.6.3 <i>Differential Scanning Calorimetry (DSC)</i> .....		132
6.6.4 <i>X-Ray diffractometry (XRD)</i> .....		133
6.7 Result and Discussion .....		133
References.....		139
<b>CHAPTER 7: PREPARATION AND CHARACTERIZATION OF Ag85A LOADED PLGA NANOPARTICLES (NPs).....</b>		<b>141</b>
7.1 Materials .....		141
7.2 Equipments.....		141
7.3 Preparation of PLGA nanoparticles .....		141
7.3.1 <i>Optimization of preliminary parameters</i> .....		142
7.3.2 <i>Optimization by Factorial design</i> .....		142
7.3.3 <i>Optimization Data Analysis</i> .....		143
7.3.4 <i>Lyophilization of PLGA-Ag85A NPs</i> .....		143
7.4 Characterization of Nanoparticle formulation.....		144
7.4.1 <i>Particles size and zeta potential characterization</i> .....		144
7.4.2 <i>Encapsulation efficiency (EE) and Protein loading (PL)</i> .....		145
7.4.3 <i>Morphology</i> .....		145
7.4.4 <i>DSC and XRD</i> .....		145
7.5 Antigen Integrity by SDS-PAGE Analysis .....		145
7.6 In-vitro aerosolization & lung deposition using Twin Stage Impinger (TSI).....		146
7.7 In-vitro release studies .....		147
7.8 Stability study.....		147
7.9 Statistical analysis .....		147
7.10 Result and Discussion .....		147
References.....		167
<b>CHAPTER 8: PREPARATION AND CHARACTERIZATION OF RIFAMPICIN LOADED HCD NPs .....</b>		<b>171</b>
8.1 Materials .....		171
8.2 Equipments.....		171
8.3 Preparation of HCD-Rif nanoparticles (HCD-Rif NPs).....		171

## Table of Contents

8.3.1 Optimization of preliminary parameters.....	172
8.3.2 Optimization of MPS and EE by Factorial design .....	173
8.3.3 Optimization Data Analysis .....	174
8.3.4 Lyophilization of NPs .....	175
8.4 Characterization of HCD-Rif Nanoparticles .....	175
8.4.1 Mean particles size (MPS) and zeta potential (ZP) characterization.....	175
8.4.2 Rifampicin encapsulation efficiency (EE) and loading .....	175
8.4.3 Morphology .....	176
8.4.4 DSC and XRD.....	176
8.5 In-vitro aerosolization & lung deposition using Twin Stage Impinger (TSI).....	176
8.6 In-vitro release studies.....	177
8.6.1 HPLC Analysis.....	178
8.7 Stability study .....	178
8.8 Statistical analysis.....	178
8.9 Result and Discussion.....	178
References .....	198
<b>CHAPTER 9: PREPARATION AND CHARACTERIZATION OF Ag85A LOADED HCD NPs.....</b>	<b>201</b>
9.1 Materials.....	201
9.2 Equipments .....	201
9.3 Preparation of HCD-Ag85A nanoparticles (HCD-Ag85A NPs).....	201
9.3.1 Optimization of parameters .....	202
9.4 Preparation of FITC labeled HCD.....	202
9.5 Protein (Ag85A) adsorption onto HCD nanoparticles .....	203
9.6 Characterization of HCD-Ag85A Nanoparticles .....	203
9.6.1 Particles size and zeta potential characterization .....	203
9.6.2 Loading efficiency (LE) and protein loading (PL) .....	203
9.6.3 Morphological evaluation .....	204
9.6.4 DSC and XRD studies.....	204
9.7 Antigen Integrity by SDS-PAGE Analysis.....	204
9.8 In-vitro aerosolization & lung deposition using Twin Stage Impinger (TSI).....	204
9.9 In-vitro release studies.....	205
9.10 Stability study .....	205
9.11 Statistical analysis.....	205
9.12 Result and Discussion.....	206
References .....	217
<b>CHAPTER 10: PREPARATION AND CHARACTERIZATION OF HCD-RIFAMPICIN NANO SPRAY DRIED (NSD) POWDER FOR INHALATION .....</b>	<b>291</b>
10.1 Materials.....	219
10.2 Equipments .....	220
10.3 Preparation of nano-spray dried powder formulation for inhalation (NSDPI).....	221

## Table of Contents

10.3.1 Principle of Nano Spray Dryer B-90.....	220
10.3.2 Drug loading (DL) and encapsulation efficiency (EE) .....	221
10.3.3 Particle size and Zeta potential.....	221
10.3.4 Shape, surface morphology and solid state characterization .....	221
10.3.5 Powder characterization using Sympatech .....	221
10.4 In-vitro aerosolization & lung deposition studies .....	222
10.5 In-vitro release studies .....	222
10.5.1 HPLC Analysis .....	223
10.6 Stability study.....	223
10.7 Statistical analysis .....	223
10.8 Result and Discussion .....	223
References.....	236
<b>CHAPTER 11: PREPARATION AND CHARACTERIZATION OF MCD-RIFAMPICIN NANO SPRAY DRIED (NSD) POWDER FOR INHALATION.....</b>	<b>239</b>
11.1 Materials .....	239
11.2 Equipments.....	239
11.3 Preparation of nano-spray dried powder formulation for inhalation (NSDPI) .....	239
11.3.1 Drug loading (DL) and encapsulation efficiency (EE) .....	240
11.3.2 Particle size and Zeta potential.....	240
11.3.3 Shape, surface morphology and solid state characterization .....	240
11.3.4 Powder characterization using Sympatech .....	240
11.4 In-vitro aerosolization & lung deposition studies .....	241
11.5 In-vitro release studies .....	241
11.5.1 HPLC Analysis .....	242
11.6 Stability study.....	242
11.7 Statistical analysis .....	242
11.8 Result and Discussion .....	242
References.....	256
<b>CHAPTER 12: IN-VITRO CELL LINE STUDIES .....</b>	<b>259</b>
12.1 Materials .....	259
12.2 Equipments.....	259
12.3 Cytotoxicity studies.....	259
12.4 MTT assays HCD and MCD .....	260
12.5 Cell viability and cellular uptake studies.....	261
12.6 Immune-stimulatory study .....	261
12.6.1 Isolation and culture of Peripheral blood mononuclear cells (PBMCs).....	262
12.6.2 Cytokine ELISA assay.....	263
12.6.3 Analysis of T cell activation (Maturation Marker Staining) .....	264
12.7 Result and Discussion .....	265
References.....	275

## Table of Contents

---

<b>CHAPTER 13: IN-VIVO IMMUNIZATION STUDIES</b> .....	<b>277</b>
13.1 Materials .....	277
13.2 Equipments .....	277
13.3 In-vivo immunization studies.....	277
13.3.1 <i>Animals</i> .....	277
13.3.2 <i>Immunization procedure</i> .....	277
13.3.3 <i>Collection of samples</i> .....	278
13.4 Cytokine Assay.....	280
13.5 ELISA assay for detection of Ag85A specific IgG2a antibody .....	282
13.6 Histopathology studies of lung tissue .....	282
13.7 Statistical analysis.....	283
13.8 Result and Discussion.....	283
References .....	292
<b>CHAPTER 14: SUMMARY AND CONCLUSIONS</b> .....	<b>293</b>

List of Tables

Chapter & Table No.	Title of Table	Page No.
<b>Chapter 2</b>		
Table 2.1	Various vaccine candidates and their current research status	27
Table 2.2	Progress in Tuberculosis (TB) chemotherapy	35
Table 2.3	New Anti-TB molecules in Preclinical and clinical trials	37
Table 2.4	Comparison of Systemic and Mucosal Immunity	42
Table 2.5	Advantages and Disadvantages and Advancements in different inhalers	44
Table 2.6	Nanoparticles prepared using modified chitosan derivatives	55
Table 2.7	Methods of NP preparation and their advantages and disadvantages	60
Table 2.8	Methods for the preparation of dry powder formulations	62
Table 2.9	Major Techniques used for the Characterization of Nanoparticulate Drug/Vaccine Delivery System	64
<b>Chapter 3</b>		
Table 3.1	Protocol for TNBS assay	75
Table 3.2	Working reagent preparation for BSA estimation	76
Table 3.3	Sample preparation for standard protein (BSA) estimation in water	77
Table 3.4	Sample preparation for protein estimation in NaOH/SDS solution	78
Table 3.5	Sample preparation for protein estimation in SLF	79
Table 3.6	Calibration data for chitosan using TNBS assay	79
Table 3.7	Parameters for TNBS assay of chitosan	80
Table 3.8	Calibration data for FITC at emission wavelength (520 nm)	80
Table 3.9	Parameters for FITC at emission wavelength 520 nm	81
Table 3.10	Calibration data of FITC at excitation wavelength (490 nm)	81
Table 3.11	Parameters for FITC at excitation wavelength of 490 nm	81
Table 3.12	Calibration data for BSA in water by visible spectroscopy	82
Table 3.13	Parameters for BSA estimation using QuantiPro™ BCA assay kit in water	82
Table 3.14	Calibration data for BSA in NaOH/SDS solution	83
Table 3.15	Parameters for BSA protein estimation using QuantiPro™ BCA assay kit in NaOH/SDS solution	83
Table 3.16	Calibration data for standard protein (BSA) in SLF	84
Table 3.17	Parameters for standard protein (BSA) estimation using QuantiPro™ BCA assay kit in	84
Table 3.18	Calibration data for Rifampicin in water	86
Table 3.19	Parameters for UV spectrometric method of analysis for Rifampicin in water	87
Table 3.20	Intraday precision and accuracy for rifampicin assay in water by UV spectroscopy.	87
Table 3.21	Interday precision and accuracy for rifampicin assay in water by UV spectroscopy.	87
Table 3.22	Calibration data for Rifampicin in SLF	88
Table 3.23	Parameters for UV spectrometric method of analysis for	88

## List of Tables

	Rifampicin in SLF	
Table 3.24	Intraday precision and accuracy for rifampicin assay in SLF by UV spectroscopy.	89
Table 3.25	Interday precision and accuracy for rifampicin assay in SLF by UV spectroscopy	89
Table 3.26	Concentration of THF in mobile phase reached at a given time during one run	90
Table 3.27	Calibration data for rifampicin in water	91
Table 3.28	Parameters for method of analysis of Rifampicin by HPLC	91
Table 3.29	Intraday precision and accuracy for rifampicin assay in water by HPLC	91
Table 3.30	Interday precision and accuracy for rifampicin assay in water by HPLC	92
Table 3.31	Calibration data for rifampicin in water	92
Table 3.32	Parameters for method of analysis of Rifampicin by HPLC	93
Table 3.33	Intraday precision and accuracy for rifampicin assay in SLF by HPLC	93
Table 3.34	Interday precision and accuracy for rifampicin assay in SLF by HPLC	93
<b>Chapter 4</b>		
Table 4.1	Composition of Different Alkaline Lysis solutions	96
Table 4.2	Fragment size and Res for Rv3804c	98
Table 4.3	Composition of Restriction enzyme digestion studies	99
Table 4.4	Percentage of agarose in gel for effective separation of linear pDNA	100
Table 4.5	Reagents for SDS-PAGE	100
Table 4.6	Composition of Separating (Resolving) Gel and stacking Gel	103
Table 4.7	Compositions of buffers and reagents for expression & purification Studies	103
Table 4.8	Protocol for refolding of the denatured protein	107
Table 4.9	Reagents for ELISA assay	110
Table 4.10	Criss Cross analysis to determine optimal reagent concentration	112
Table 4.11	Criss Cross analysis to determine optimal reagent concentration	118
Table 4.12	Optimized parameters for ELISA	118
<b>Chapter 5</b>		
Table 5.1	Solubility of Chitosan and HCD	124
<b>Chapter 6</b>		
Table 6.1	Solubility of Chitosan and MCD	133
<b>Chapter 7</b>		
Table 7.1	Composition of nanoparticles	142
Table 7.2	Factorial design parameters for optimization of nanoparticle formulation	143
Table 7.3	Formulation of the nanoparticles utilizing 3 <sup>2</sup> factorial design	143
Table 7.4	Selection of solvent for the preparation of PLGA NPs	148
Table 7.5	Optimization of sonication time during primary and secondary emulsion	148
Table 7.6	Optimization of Sonication pulse and Surfactant (PVA) concentration	150
Table 7.7	Response parameters for NPs prepared as per 3 <sup>2</sup> factorial design.	151
Table 7.8	Other production evaluation parameters for NPs prepared as per 3 <sup>2</sup>	151

## List of Tables

	factorial design	
Table 7.9	Observed and Predicted values of response parameter – MPS (Y1)	152
Table 7.10	Observed and Predicted values of response parameter - EE (Y2)	153
Table 7.11	Response of full model of PLGA- O-alb NPs	154
Table 7.12	Analysis of variance (ANOVA) of MPS for full models of PLGA-O-alb NPs	156
Table 7.13	Analysis of variance (ANOVA) of EE for full models of PLGA-O-alb NPs	158
Table 7.14	Optimized formula for PLGA- O-alb NPs	160
Table 7.15	The predicted and observed response variables of the optimized PLGA-O-alb NPs	160
Table 7.16	Parameters for optimized formulation of PLGA-Ag85A NPs	160
Table 7.17	Pulmonary deposition Parameter of the PLGA-Ag85A NPs Measured by TSI	164
Table 7.18	Release kinetics of PLGA-Ag85A NPs	165
Table 7.19	Stability of PLGA-Ag85A NPs at RT	166
<b>Chapter 8</b>		
Table 8.1	Composition of blank nanoparticles	172
Table 8.2	Preliminary parameters for optimization of blank nanoparticle formulation	173
Table 8.3	Formulation of the blank nanoparticles using 2 <sup>3</sup> factorial design (Coded values)	173
Table 8.4	Factorial design parameters for optimization of HCD-Rif nanoparticle formulation	174
Table 8.5	Formulation of the nanoparticles utilizing 3 <sup>2</sup> factorial design	174
Table 8.6	Optimization of sonication time during primary and secondary emulsion	179
Table 8.7	Results of optimization parameters (solvent, surfactant & surfactant concentration)	181
Table 8.8	Response parameters for NPs prepared as per 3 <sup>2</sup> factorial design	183
Table 8.9	Other evaluation parameters for NPs prepared as per 3 <sup>2</sup> factorial Design	184
Table 8.10	Observed and Predicted values of response parameter – MPS (Y1)	184
Table 8.11	Observed and Predicted values of response parameter - EE (Y2)	184
Table 8.12	Response of full model of HCD-Rif NPs	186
Table 8.13	Analysis of variance (ANOVA) of MPS for full models of HCD-Rif NPs	188
Table 8.14	Analysis of variance (ANOVA) of EE for full models of HCD-Rif NPs	188
Table 8.15	Optimized formula for HCD-Rif NPs	191
Table 8.16	The predicted and observed response variables of the optimized HCD-Rif NPs	191
Table 8.17	Parameter for Pulmonary Deposition of HCD-Rif NPs measured by TSI	195
Table 8.18	Release kinetics Rifampicin from HCD-Rif NPs	197

## List of Tables

Table 8.19	Stability of HCD-Rif NPs at RT	197
<b>Chapter 9</b>		
Table 9.1	Optimization of sonication time during primary and secondary emulsification	207
Table 9.2	Formulation of HCD-Ag NPs	207
Table 9.3	MPS, PDI and ZP of HCD-Ag85A NPs before freeze drying	208
Table 9.4	MPS, PDI and ZP with LC and LE of HCD-Ag85A NPs after freeze drying	208
Table 9.5	LC and LE of Ag85A adsorbed on blank HCD NPs (A-HC-Ag 0)	209
Table 9.6	Parameter for Pulmonary Deposition of FITC-HCD NPs as Measured by TSI	215
Table 9.7	Kinetics model fitting of in vitro release data of HCD-Rif NPs	216
Table 9.8	Stability of HCD-Ag85A NPs at RT (10-15 °C)	216
<b>Chapter 10</b>		
Table 10.1	Percent yield, Drug loading and Entrapment efficiency	224
Table 10.2	Particle Size Distribution Data of Dry Powders Analyzed by Sympatec	226
Table 10.3	Deposition Parameter of the Different Formulations Measured by NGI	232
Table 10.4	Stability of HCD-Rif NSD formulation at RT	235
<b>Chapter 11</b>		
Table 11.1	Percent yield, Drug loading (%DL) and Entrapment efficiency (%EE)	243
Table 11.2	Particle Size Distribution Data of Dry Powders Analyzed by Sympatec	244
Table 11.3	Deposition Parameter of the Different Formulations Measured by NGI	252
Table 11.4	Kinetics model fitting of in vitro release data of MCD-Rif NSD powder formulation	254
Table 11.5	Stability of MCD-Rif NSD formulation at RT	255
<b>Chapter 12</b>		
Table 12.1	In vitro cytotoxicity of controls and polymers HCD & MCD in A549 cells	265
<b>Chapter 13</b>		
Table 13.1	Group of animals under immunization study	278
Table 13.2	Composition of Cytokine (Mouse INF- $\gamma$ ) ELISA assay kit	280
Table 13.3	Preparation of Standard Solutions	281
Table 13.4	Cytokine (INF- $\gamma$ ) levels in BALF, Lymph node (LN) and spleen after 42 days immunization	289
Table 13.5	Specific antibody (IgG2a) levels in Blood at different time point	289
Table 13.6	Specific antibody (IgG2a) levels in BALF, lymph node and spleen after 42 days immunization	290

List of Figures

Chapter & Figure No.	Title of Figure	Page No.
<b>Chapter 2</b>		
Figure 2.1	History Timeline of TB	12
Figure 2.2	Estimated TB incidence rate in the year 2011	13
Figure 2.3	Pathogenesis of LTBI and TB disease	16
Figure 2.4	Progression of LTBI and active TB	16
Figure 2.5	Macrophage-Lymphocyte Interaction in TB	16
Figure 2.6	Various strategies for post exposure TB vaccination	25
Figure 2.7	Vaccines in preclinical and clinical trials	26
Figure 2.8	Anatomy Human Lung	40
Figure 2.9	Depiction of Common Mucosal Immune System	42
Figure 2.10	Structure of chitosan	51
<b>Chapter 3</b>		
Fig. 3.1	Calibration curve for chitosan using TNBS assay	79
Fig. 3.2	Calibration Curve of FITC at emission wavelength (520 nm)	80
Fig. 3.3	Calibration Curve of FITC at excitation wavelength of 490 nm	81
Fig. 3.4	Calibration Curve of BSA in water by visible spectroscopy	82
Fig. 3.5	Calibration Curve of BSA in NaOH/SDS solution by visible spectroscopy	83
Fig. 3.6	Calibration Curve of standard protein (BSA) in SLF by visible spectroscopy	84
Fig. 3.7	Standard Curve of Rifampicin in water	86
Fig. 3.8	Standard Curve of Rifampicin in SLF	88
Fig. 3.9	Calibration Curve of rifampicin in water by HPLC	91
Fig. 3.10	Calibration Curve of rifampicin in SLF by HPLC	93
<b>Chapter 4</b>		
Figure 4.1	pMRLB.41 - Rv 3804c - Ag85A in pET15b	99
Figure 4.2	Schematic representation of protein synthesis	102
Figure 4.3	Ag85A by Xho I digestion	113
Figure 4.4	Protein expression in cell lysate	114
Figure 4.5	Protein expression in cell suspension and pellet	115
Figure 4.6	Standardization of inclusion bodies solubilization using different molar urea	116
Figure 4.7	Protein expression in inclusion bodies after urea solubilisation	116
Figure 4.8	Refolded protein on SDS PAGE	116
Figure 4.9	Purified protein 1 (Ag85A)	117
Figure 4.10	Purified protein R1 (Refolded Ag85A)	117
Figure 4.11	Fluorimetric Emission Spectra of Tryptophan, BSA, native Ag85A, refolded Ag85A and denatured Ag85A	119
<b>Chapter 5</b>		
Figure 5.1	Scheme for synthesis of HCD	121
Figure 5.2	FTIR Spectra of – a) Chitosan; and b) HCD	125
Figure 5.3	NMR spectra of – Chitosan (a) and HCD (b)	126
Figure 5.4	X-Ray Diffratograms of – a) Chitosan and b) HCD	126
Figure 5.5	DSC Thermograms of Chitosan (a) and HCD (b)	127

## List of Figures

<b>Chapter 6</b>		
Figure 6.1	Scheme for synthesis of MCD	131
Figure 6.2	FTIR Spectra of – (a) Chitosan ; and (b) MCD	135
Figure 6.3	NMR spectra of – (a) Chitosan ; and (b) MCD	135
Figure 6.4	X-Ray Diffratograms of – a) Chitosan ; and b) MCD	137
Figure 6.5	DSC Thermograms of (a) Chitosan ; and (b) MCD (Octanoyl Chitosan)	138
<b>Chapter 7</b>		
Figure 7.1	X-Y scatter plot showing the predicted vs actual values of MPS	153
Figure 7.2:	X-Y scatter plot showing the predicted vs actual values of EE	153
Figure 7.3(a)	Contour plot showing the effect of independent factors on MPS	155
Figure 7.3(b)	Response surface plot showing the effect of independent factors on MPS	156
Figure 7.3(c)	Interaction plot showing the interaction between PLGA and ova on MPS	156
Figure 7.4(a)	Contour plot showing the effect of independent factors on EE	157
Figure 7.4(b)	Contour plot showing the effect of independent factors on EE	157
Figure 7.4(c)	Interaction plot showing the interaction between PLGA and O-alb on EE	157
Figure 7.5a	Particle size distribution of PLGA-Ag85A NPs before freeze drying	161
Figure 7.5b	Particle size distribution of PLGA-Ag85A NPs after freeze drying	161
Figure 7.6a	Scanning Electron micrograph of PLGA-Ag85A NPs	161
Figure 7.6b	Transmission Electron micrograph (TEM) of PLGA-Ag85A NPs	161
Figure 7.7	DSC Thermograms of – a) Ovalbumin (O-alb); b) Pure PLGA; c) PLGA-O-alb physical mixture; d) Blank PLGA NPs ; e) PLGA-Ag85A NPs	162
Figure 7.8	X-Ray Diffratograms of – a) PLGA ; b) Blank PLGA NPs; c) PLGA-Ag85A NPs	163
Figure 7.9	SDS-PAGE analysis of PLGA-Ag85A NPs, 1) Protein Marker; 2) Native Ag85A; 3) Blank PLGA-NPs; 4) PLGA-Ag85A NPs; 5) PLGA-Ag85A NPs after 2 months	163
Figure 7.10	Percent cumulative release (PCR) of Ag85A from Ag85A loaded PLGA NPs	165
<b>Chapter 8</b>		
Figure 8.1	Assembly of Twin stage Impinger	177
Figure 8.2(a)	Contour plot showing the effect of independent factors on MPS	187
Figure 8.2(b)	Response surface plot showing the effect of independent factors on MPS	187
Figure 8.3(a)	Contour plot showing the effect of independent factors on EE	188
Figure 8.3(b)	Contour plot showing the effect of independent factors on EE	188
Figure 8.4a	Particle size distribution of HCD-Rif NPs before freeze drying	192
Figure 8.4b	Particle size distribution of HCD-Rif NPs after freeze drying	192
Figure 8.5a	Scanning Electron micrographs of HCD-Rif NPs	193
Figure 8.5b	Transmission Electron micrographs of HCD-Rif NPs	193
Figure 8.6	DSC Thermograms of – a) Rif; b) chitosan; c) HCD; d) HCD-Rif physical mixture; e) HCD-Rif NPs	194
Figure 8.7	X-Ray Diffratograms of – a) Rif ; b) Chitosan ; c) HCD; d) HCD-Rif NPs.	194

## List of Figures

Figure 8.8	Percent cumulative release (PCR) of HCD-Rif nanoparticles	196
<b>Chapter 9</b>		
Figure 9.1	Schematic of FITC-HCD preparation	203
Figure 9.1a	Particle size distribution of HCD-Ag85A NPs before Freeze Drying	210
Figure 9.1b	Particle size distribution of HCD-Ag85A NPs after Freeze Drying	210
Figure 9.1c	Zeta potential of HCD-Ag85A NPs after Freeze Drying	210
Figure 9.2a	Particle size distribution of FITC-HCD NPs after Freeze Drying	211
Figure 9.2b	Zeta potential of FITC-HCD NPs after Freeze Drying	211
Figure 9.3	a) Scanning Electron micrographs of HCD-Ag85A NPs ; b) Transmission Electron micrographs of HCD-Ag85A NPs	211
Figure 9.4	DSC Thermograms of – a) O-alb; b) Chitosan; c) HCD; d) HCD-O-alb physical mixture; e) HCD-O-alb NPs; f) HCD-Ag85A NPs	212
Figure 9.5	X-Ray Diffratograms of – a) HCD-Ag85A NPs; b) Blank HCD NPs; c) HCD; d) Chitosan	213
Figure 9.6	SDS-PAGE analysis of HCD-Ag85A NPs, 1) HCD-Ag85A NPs after 2 months of storage ; 2) HCD-Ag85A NPs; 3) Blank HCD-NPs; 4) Native Ag85A; 5) Protein Marker	213
Figure 9.7	Cumulative % release of Ag85A from HCD-Ag 02 NPs.	216
<b>Chapter 10</b>		
Figure 10.1	Buchi B-90, Nano Spray Dryer; a) Nano spray dryer; b) spray pattern produced by nozzle; c) representative SEM image	220
Figure 10.2	Particle size distributions of nano spray dried particles - A) HCD-Rif NSD; B) HCD-Rif-NaSt NSD	226
Figure 10.3	Scanning Electron micrographs of ; a) Rif as supplied; NSD powder of - b) Rif ; c) HCD-Rif ; d) HCD-Rif-NaSt	226
Figure 10.4	FTIR Spectra of - a) Rif; b) HCD; c) HCD-Rif NSD formulation	227
Figure 10.5	DSC Thermograms of – a) Rif; b) Chitosan; c) HCD; d) HCD+Rif physical mixture; e) HCD-Rif NSD formulation; f) HCD-Rif-NaSt NSD formulation	229
Figure 10.6	X-Ray Diffratograms of – a) Rif ; b) Sodium Stearate; c) Chitosan d) HCD; e) HCD-Rif NSD formulation	230
Figure 10.7	Next Generation Impactor stage deposition of pure rifampicin, HCD-Rif NSD, HCD-Rif-NaSt NSD	232
Figure 10.8	Percent cumulative drug release (CDR) of rifampicin, HCD-Rif NSD and HCD-Rif-NaSt NSD powder formulation	234
<b>Chapter 11</b>		
Figure 11.1	Particle size distributions of nano spray dried particles – MCD-Rif NSD & MCD-Rif-L NSD	244
Figure 11.2	Scanning Electron micrographs of nano spray dried particles of ; a) Rifampicin; b) MCD-Rif; c) MCD-Rif-Leu	245
Figure 11.3	FTIR Spectra of - a) Chitosan; b) MCD; c) Rifampicin; d) MCD-Rif NSD & e) MCD-Rif-Leucin NSD formulation	247
Figure 11.4	DSC Thermograms of – a) Rif; b) Chitosan; c) MCD; d) MCD+Rif physical mixture; e) MCD-Rif NSD formulation	248
Figure 11.5	X-Ray Diffratograms of – a) Rif; b) Chitosan c) MCD; d) MCD-Rif NSD & e) MCD-Rif-Leu NSD formulation	249
Figure 11.6	Next Generation Impactor stage deposition of Rifampicin, MCD-Rif NSD, MCD-Rif-Leucine NSD	252

## List of Figures

Figure 11.7	Percent cumulative drug release (% CDR) of Rifampicin, MCD-Rif NSD and MCD-Rif-L NSD powder formulation	254
<b>Chapter 12</b>		
Figure 12.1a	In vitro cytotoxicity of RPMI control and HCD in A 549 cells	266
Figure 12.1b	In vitro cytotoxicity of RPMI control and MCD in A 549 cells	266
Figure 12.1c	In vitro cytotoxicity of DMSO control in A 549 cells	266
Figure 12.2	In vitro cytotoxicity of HCD polymers and HCD NPs in porcine monocytes	267
Figure 12.3a	Cell uptake of formulation and polymers at 37 and 4 °C	268
Figure 12.3b	Cell uptake of formulation and polymers at 37 and 4 °C	268
Figure 12.4a	Cytokine, IL-10 induction in monocyte, B Cells and Enriched DCs upon immunostimulation by Nanoparticles	271
Figure 12.4b	Cytokine, IL-12 induction in monocyte, B Cells and Enriched DCs upon immunostimulation by Nanoparticles	271
Figure 12.4c	Cytokine, TNF- $\alpha$ induction in monocyte, B Cells and Enriched DCs upon immunostimulation by Nanoparticles	272
Figure 12.5a	Expression of CD 16 upon immunostimulation with formulation and polymers	273
Figure 12.5b	Expression of MHC-II upon immunostimulation with formulation and polymers	274
<b>Chapter 13</b>		
Figure 13.1	Process for collection of BALF	279
Figure 13.2	Cytokine (INF- $\gamma$ ) levels in BALF, lymph node and spleen after 42 days immunization in mice with different formulations	284
Figure 13.3	Levels of IgG2a in BALF, blood, LN and spleen after 42 days immunization in mice. BALF - Bronchoalveolar fluid, LN - Lymph node	288
Figure 13.4	Levels of IgG2a in blood at different time points after immunization of mice with different formulations	288
Figure 13.5	Histopathological changes in mice lung samples after 42 days immunization	291

List of Abbreviations

ABB	- Ammonium bicarbonate buffer pH 7.0
AFB	- Acid fast bacilli
AGE	- Agarose Gel Electrophoresis
ALP	- Alkaline phosphatase
AMs	- Alveolar macrophages
APC	- Antigen presenting cells
APS	- Ammonium persulphate
ATDs	- Antitubercular drugs
BALF	- Bronchoalveolar fluid
BCA	- Biscinchoninic acid
BCG	- Bacillus Calmette Guerin
BMRC	- British Medical Research Council
BSA	- Bovine Serum Albumin
CDCl <sub>3</sub>	- Deuterated chloroform
CDR	- cumulative drug release
CMI	- Cell Mediated Immunity
CPR	- Cumulative percent release
CTL	- Cytotoxic T-lymphocytes
D <sub>2</sub> O	- Deuterium oxide
DC	- Dendritic Cells
DCM	- Dichloromethane
DDA	- Degree of deacetylation
DESE	- Double emulsion solvent evaporation method
DL	- Drug Loading
DLS	- Dynamic light scattering
DMSO	- Dimethyl sulfoxide
DNA	- Deoxy ribose nucleic acid,
DOTS	- Directly observed therapy
DPI	- Dry Powder Inhaler
DS	- Degree of Substitution
DSC	- Differential Scanning Calorimetry
ED	- Emitted dose
EE	- Entrapment efficiency
ELISA	- Enzyme linked immunosorbent assay
EMA	- European Medicine Agency
EMB	- Ethambutol
EtOAc	- Ethyl Acetate
FTIC	- Fluorescein isothiocyanate
FPD	- Fine particle dose
FPF	- Fine particle fraction;
FTIR	- Fourier Transform Infrared Spectroscopy
GMP	- Good Manufacturing Practice
GSD	- Geometric standard deviation
GTE	- Glucose Tris EDTA
HCD	- Hydrophobic chitosan derivative
IDRI	- Infectious Disease Research Institute
IFN- $\gamma$	- Interferon gamma
IGRA	- Interferon-gamma release assay
IL	- Inter leukin
IN	- Intra nasal
IPTG	- Isopropyl $\beta$ -D-1-thiogalactopyranoside
Isoniazid	- INH
LB	- Luria broth

## List of Abbreviations

---

LDH	- Lactate dehydrogenase
LDV	- Laser doppler velocimetry
Leu or L	- Leucine
LTBI	- Latent TB Infection
MACs	- Magnetic-activated cell sorting
MCD	- Codified chitosan derivative
MDR-TB	- Multi drug resistant Tuberculosis
MHC	- Major Histocompatibility complex
MLRA	- Multiple regression analysis
MMAD	- Mass median aerodynamic diameter
MMR	- Macrophage mannose receptor
MPS	- Mean particle size
MTB	- <i>Mycobacterium tuberculosis</i>
MTT	- (3-[4,5-dimethyl-thiazole-2-yl]-2,5-diphenyl tetrazolium bromide)
NaSt	- Sodium Stearate
NE	- Nebulization efficiency
NGI	- Next Generation Impactor
NIH	- National Institute of Health
NOS	- Nitric oxide synthase
NSDPI	- Nano-spray dried powder for inhalation
O-alb	- Ovalbumin
OC	- Octanoyl chloride
OETC	- Oxford Emergent Tuberculosis Consortium
PAS	- Para amino salicylic acid
PBS	- Phosphate buffer saline
PDI	- Poly dispersity Index
PDMI	- Phthiocerol dimycocerosate
PLGA	- Poly(lactic-co-glycolic acid)
pMDI	- Pressurized Metered Dose Compact Inhalers
pNPP	- p-nitrophenyl phosphate
PPD	- Purified protein derivative
PRESS	- Predicted residual sum of squares
PVA	- Poly vinyl alcohol
PZA	- Pyrazinamide
RF	- Respirable fraction;
Rif	- Rifampicin
RNA	- Ribose nucleic acid
RSM	- Response Surface Methodology
SC	- Subcutaneous
SDS PAGE	- Sodium Dodecyl Sulphate Poly acrylamide gel electrophoresis
SEM	- Scanning Electron Microscopy
SLF	- Simulated Lung Fluid
SM	- Streptomycin
TEM	- Transmission Electron Microscopy
TEMED	- N,N,N,N'-tetramethylethylenediamine
T <sub>g</sub>	- Glass transition temperature
THF	- Tetrahydrofuran
TNBS	- Trinitrobenzene sulfonic acid
TNF- $\alpha$	- Tumor Necrosing Factor alpha
TPP	- Tri-polyphosphate
TSI	- Twin Stage Impinger
TST	- Tuberculin skin test
WHO	- World health organization
XDR	- Extensive drug resistance
XRD	- X-Ray diffractometry
ZP	- Zeta Potential

---

---

**ABSTRACT**

Tuberculosis (TB) is a major global health problem and a leading cause of morbidity with globally prevalent cases of 16-20 million, despite the use of currently available BCG vaccine and chemotherapy due to drawbacks associated with them. Worldwide, scientists in the biomedical research are exploring chitosan for its possible application as drug and vaccine carrier owing to its varied benefits. However, inherent insolubility in water and organic solvents limits its application in drug delivery. Therefore, two chitosan derivatives, hydrophobic chitosan derivative (HCD) and modified chitosan derivative (MCD) were synthesized to overcome current limitations of chitosan. Thereafter, nanoparticulate delivery systems were prepared by double emulsion solvent evaporation using PLGA and HCD for pulmonary delivery of Ag85A and rifampicin to improve immunostimulatory effect of Ag85A and therapeutic efficacy of rifampicin. In addition, nano spray drying (NSD) of rifampicin with HCD and MCD was carried out to prepare particles for dry powder inhalation. Results of physicochemical characterization showed successful entrapment of Ag85A and rifampicin in HCD, whereas in-vitro lung deposition and release studies revealed more than 30-40 % deposition of nanoparticles in lungs and sustained with biphasic release pattern respectively. Results of the physicochemical properties of MCD NSD particles indicated successful formation of rifampicin entrapped MCD particles, whereas in-vitro lung deposition studies showed more deposition of MCD-rif NSD particles as compared to HCD-Rif particles. Non-toxic nature of HCD and MCD based on MTT assay and almost 100 % uptake of FITC-HCD NPs in porcine monocyte indicated their suitability for application in delivery of vaccines and drugs. In-vitro cytokine assay showed production of IL-10, IL-12 and TNF- $\alpha$  in porcine monocyte, B cells and enriched dendritic cells in response to the stimuli conferred by HCD-Ag85A NPs, whereas up-regulation of MHC II and down regulation of CD 16 was also observed. Thus, activation of Th1 and Th2 cells indicated induction of cell mediated and humoral immunity conferred by HCD-Ag85A NPs. In-vivo studies confirmed generation of INF- $\alpha$  in bronchoalveolar fluid (BALF), spleen and lymph nodes, whereas Ag85A specific IgG2a antibody was detected in BALF, serum, lymph node and spleen indicating mucosal and systemic immunological response. In sum, based on the results of in vivo immunization study, HCD-Ag85A NPs may be considered as a new and promising adjuvant candidate for enhancing and prolonging the immune response of Ag85A after SC and IN administration. PLGA-Ag85A NPs demonstrated best immunological responses among all formulations after both SC and IN administration, whose immunostimulatory properties for various protein antigens are already reported. However, interesting feature of our experiment was achievement of higher immunological responses from HCD-Ag85A NPs and PLGA-Ag85A NPs as compared to marketed BCG vaccine, which is known to be standard and alum adsorbed Ag85A, which is traditional and only approved adjuvant to date. In sum, the new hydrophobic chitosan derivative synthesized by us, which exhibited interesting in vitro and in vivo features hold promise as a better alternative for vaccine delivery of subunit antigens over conventional or routine adjuvants such as alum.

## 1.0 Introduction

### *End of Dream*

*“He wanted to be an IITian like his father, got a JEE rank of 224 and admission in IIT-B. But Shreeram Radhakrishnan couldn’t attend a single lecture; he was diagnosed with **MDR-TB** in 2011, shortly after he topped the CBSE class XII exams in Maharashtra. Unconscious for 10 months, Shreeram died last December.”*

## 1.1 General Overview on vaccine and Drug development for tuberculosis

Tuberculosis (TB) is a major global health problem caused by *Mycobacterium tuberculosis* (MTB) and *Mycobacterium bovis*. It is a leading cause of morbidity, which infects one-third of the world’s population of which 8-10 million develop active disease and 2 million die every year. (Shegokar et al., 2011) Despite the impressive results and remarkable accomplishments, there is a still need to further improve on vaccine and drug delivery research and development to combat deadly tuberculosis to provide complete protection, especially in developing nations (Schroder et al., 2001). It is essentially an uncontrolled problem despite the use of BCG vaccine ‘the world’s widely used and only currently licensed TB vaccine for use in humans for more than 75 years’. Because currently available TB vaccine (BCG) presents various drawbacks like - 1) Varied efficacy and ineffectiveness against pulmonary TB; 2) Systemic vaccine administration affects the rate of adverse reactions and efficacy; 3) The available BCG vaccine formulation requires skilled personnel for administration and preparation of the vaccine from freeze dried product and decent facilities in order to avoid contamination; 4) BCG is not recommended for children and adults who are infected with HIV; 5) BCG lacks important antigens; 6) BCG is not including T cell subsets; 7) BCG efficacy wanes over time (Yeboah et al., 2008 ; Agger et al., 2002). Moreover, treatment of TB with the antitubercular drugs (ATD’s) is tedious and lengthy process requiring combination antibiotics therapy to be administered orally in high systemic doses over a period of 4-10 month. The prolong duration of anti-tubercular chemotherapy may lead to various systemic side effects and poor patient compliance (Manca et.al, 2012). Co-infection with HIV and mutation of MTB (due to generation of drug resistant mutants of MTB) make the disease even worse. (Pawlowski et al., 2012) Therefore, effective vaccination for TB with the subunit vaccines and treatment of TB with less frequent dosing, reduced dose of drugs and duration of therapy are at the priority in order to save many lives.

Large numbers of protein vaccine candidates have been selected from *MTB* antigens in animal models. *MTB* proteins such as ESAT-6, Ag85 complex, Hsp60 and fusion proteins of ESAT-6 and Ag85B, a 72kDa fusion protein based upon the *MTB32* and *MTB39* antigens of *MTB* have shown protective capacity. Among which Ag85 complex protein (including Ag85A, B and C) has presented promising characteristics due to its ability to bind fibronectin and promote their adherence to mucosal surfaces thereby facilitating their entry into host cells. Moreover, Ag85 complex interacts with the immune system at an early stage of the infectious process and induces both humoral and cell-mediated immune responses in *MTB*-infected patients and animal models (Lu D, 2007). The early-stage antigens would be most useful in a preventive vaccine. A mycolyl-transferase member, Ag85A is well characterized antigen 85 complex of *MTB* and is a promising vaccine candidate which has shown to

induces strong protective responses in experimental animal models (Tanghe et.al., 2001). It is also used (as Modified Vaccinia Ankara 85A) in phase 2b clinical trials as a boosting vaccine of BCG vaccines and PPD positive persons (Todoroff et.al., 2013 ; in press). Recently, Yu et. al., developed and highlighted the potential utility of Fe<sub>3</sub>O<sub>4</sub>-Glu-polyethyleneimine nanoparticles encapsulated with the DNA (Ag85A-ESAT-6-IL-21) as a prophylactic vaccine in the MTB infected mouse model (Yu et. al., 2012). Todoroff et.al., investigated the potential of Poloxamer 407 (P407) combined with a CpG oligonucleotide (CpG) to enhance immune responses to MTB antigen 85A (Ag85A) following pulmonary delivery in BALB/c mice and reported generation of strong immune responses, with a polyfunctional T cells phenotype (Todoroff et. al., 2013). Similarly, few other studies also confirms the efficacy of nanoparticulate DNA vaccine delivery system to enhance T cell responses through pulmonary delivery in a DNA prime/protein boost vaccine regimen (Merdan Bivas-Benita et.al., 2004 ; Bivas-Benita et.al., 2009). Thus, Ag85A is the most investigated protein and examined at preclinical and clinical level. However, a major drawback of protein vaccine is low immunogenicity especially by mucosal routes, therefore adjuvant co-administration is advised and currently research is still under progress to increase the immunogenicity of subunit protein vaccines by adjuvant effects of nanoparticulate delivery systems with due concerns to its safety. Considering this fact, research was envisaged to formulate Ag85A (proteins) entrapped nanoparticulate delivery systems for the localized delivery to lung.

Amongst various antitubercular drugs, rifampicin is a first-line drug for the treatment of tuberculosis and is included in the list of recommended drug regimens for treatment of MTB infection (Esmaeili et.al., 2007). Despite the availability of an effective therapeutic regimen for TB, high dose, patient non-compliance (due to frequent dosing regimens of antitubercular drugs (ATDs) including rifampicin, daily or several times a week) led to emergence of multi drug resistance (MDR) and extensive drug resistance (XDR) and thus unsuccessful treatment of tuberculosis. Moreover, less macrophage uptake of rifampicin, causing less concentration to reach at macrophages (where TB bacilli resides), non-localized delivery of drugs and associated adverse effects are another concerns with the current rifampicin therapy (Kumar et al., 2006). As rifampicin is a first line drug for the treatment of TB, many research groups have addressed these challenges by reporting different strategies such as encapsulation of rifampicin in polymeric microparticles, nanoparticles and liposomes etc. where sustained release, improved intracellular delivery and high drug loading can be achieved (Booyesen et.al., 2013; Doan et.al., 2011 ; Esmaeili et.al., 2007 ; Pandey et.al., 2003 ; Vyas et.al., 2004). These systems are also known to minimize first pass metabolism by protecting drug inside the polymeric shell (Couvreur and Vauthier, 2006) and contribute toward protein binding, biodistribution, cellular uptake and immune response due to their various physicochemical properties. Ultimately, it may reduce dose and dosing frequency and improve patient compliance, macrophage uptake, antitubercular activity, thereby overall management of therapy. However, research is still underway to accomplish bountiful delivery system for ATDs, using alternative route of administration. Thereof, we have chosen rifampicin to address the challenges associated with the current therapy by formulating it into a newly developed polymeric system via alternative route.

During the last few years, it has been shown that the body has a very effective immunological system that resides in the mucosa. It has also been shown that vaccines and drugs can be administered by nasal, oral, pulmonary, rectal and vaginal routes. Majority of pathogens invade into the body via one or more of the mucosal routes. Oral, nasal, pulmonary, and urino-genital routes are the most common pathways for entry of infectious pathogens into the human host. Therefore, generating a “first-line of defense” at the site of entry is gaining importance. (Shahiwala et. al., (2007); Schroder et. al., (2001)) The mucosal routes and the ducts of all endocrine glands are endowed with powerful mechanical and chemical cleansing mechanism (e.g. antigen presenting cells (APC) like dendritic cells, macrophages) that degrade and repel the foreign matter. Thus, success of a vaccine depends on an efficient presentation of vaccine antigens to APC and most importantly long lasting immunological memory which helps to clear infectious agent through recall immunity. Among various APCs, dendritic cells are the most effective due to their flexible morphology and variant phenotypes. (Garcia et.al., (2012))

TB bacilli usually multiply first in the macrophages, in the lung alveoli and alveolar ducts and in draining lymph nodes. Infected macrophages eventually get killed, progressively creating a primary tubercle. (Girard et al., (2005)) Hence, alveolar macrophages (AMs) are the most vital regulators in the first line defense and lung homeostasis upon infection with MTB. As discussed earlier, the current problems with the vaccination and drug therapy for TB resides in low and varied efficacy of existing vaccine and frequent administration of large daily doses of antibiotics (usually in grams quantity) respectively, which distributes systematically throughout the body without targeting specific cell (may lead to systemic toxicity). Consequently, delivering antigens and drugs to the lungs (which is primary site of infection of TB) allows its increased local concentration to combat TB. It also supplies antigens and drug for non-pulmonary TB by inducing systemic immunity and providing drug concentration in the systemic circulation thereby provides many advantages over conventional delivery. Thus, there is a therapeutic rationale for the delivery of subunit protein Ag85A and rifampicin to the lungs (where large number of tubercle bacilli harbor) using novel delivery systems for the prevention and improved chemotherapy of TB respectively.

Recently, novel vaccine and drug delivery systems have opened up new vistas in the management of TB by providing sustained release of antigens and drug to the respiratory tract. This helps extending duration of action, minimizing dosing frequency, reducing the therapeutic dose, thereby improving patient compliance and overall management of therapy. Moreover, it also helps delivering antigens and drugs at the specific site of action (Manca et.al, 2012).

Sustained delivery of antigens and drugs to the pulmonary site is usually achieved by formulating them in microparticle or nanoparticle formulations as they provide uniform dose distribution among the alveoli, delay drug residence time in the tissue and control its release. Over the past decade, large numbers of biodegradable materials of natural and synthetic origin have been utilized in controlled drug delivery for the formulation of micro and nanoparticles. They are either hydrophobic polymers synthesized chemically or amphiphilic

macromolecules obtained from natural sources. The most widely investigated synthetic polymers include poly(lactic-co-glycolic acid), (PLGA), poly(alkylcyanoacrylate) (PACA), poly(butylcyanoacrylate) (PBCA), poly(ethylcyanoacrylate) (PECA), poly(caprolactone) (PCL), poly(lactic acid) (PLA), and poly(methacrylic acid-coethacrylate) block co-polymer, whereas, albumin, chitosan, hyaluronan, gelatin, alginates and inorganic material like hydroxyapatite are categorized as natural polymers (Makadia et.al., 2011). Both types of polymers present their own advantages and drawbacks. A detailed review on this is recently discussed (Hans et.al., 2002; Nair et al., 2007; Petkar et al., 2011). Amidst, chitosan and PLGA are most abundantly employed polymers in the vaccine and drug delivery systems, as both polymers are biodegradable, biocompatible and non-toxic in nature and present unique characteristics for the formulation of vaccine and drug delivery systems.

Firstly, PLGA is a copolymer of poly lactic acid (PLA) and poly glycolic acid (PGA) and it is the best copolymeric elastomer available to date for vaccine and drug delivery with respect to design and performance of delivery systems (Makadia et.al., 2011). It is approved by the US FDA and European Medicine Agency (EMA) in various drug delivery systems in humans owing to its biodegradability, biocompatibility and safety. In addition, ease of preparation of micro/nanoparticles, drug-polymer compatibility, predictable drug release behavior, targeting ability make it widely acceptable material in vaccine and drug delivery (Petkar et al., 2011).

Nevertheless, major limitation in the application of synthetic polymers like PLGA (in the context of DNA/RNA and protein delivery), lies primarily in their negative charge, which confines the interaction with the negatively charged DNA, RNA and proteins (Merdan et.al., 2002; Luten et.al., 2008). Therefore, surface modification of PLGA using various poly-cations (including chitosan) has been used to overcome this disadvantage, owing to the unique properties of chitosan. Hence, considering the advantages of PLGA, the present research was undertaken using PLGA as a carrier system to encapsulate a model antigen pMRLB.41/Ag85A for pulmonary vaccine delivery in the TB.

Secondly, chitosan, one of the most handsome natural polymer (polysaccharide) after cellulose, having similar structure to that of cellulose, as both are made up of linear  $\beta$ - (1 to 4)-linked monosaccharides. However, chitosan is different to that of cellulose due to presence of 2-amino-2-deoxy- $\beta$ -d-glucan combined with glycosidic linkages. The primary amine groups in chitosan furnish very special properties making it extensively used polymer in biomedical and pharmaceutical (including drug delivery) applications among all natural polymers. Unusual combination of biological activities plus mechanical and physical properties including presence of primary amine groups, positive charge, mucoadhesive nature and its ability to efficiently permeate across absorptive epithelia makes it more suitable in sustained and targeted drug delivery (Maurya et.al., 2008 ; Nafee et.al., 2007; Praveen et.al., 2011; Cho et.al., 2012; Agnihotri et. al., 2004). It has been also reported that chitosan particles interact with the mannose receptors of macrophages, which results in the phagocytosis of the particles in macrophages followed by the degradation of lysozymes and N-acetyl- $\beta$ -d-glucosaminidase in phagosomes, thus presenting inherent immunoadjuvant activity (Bianco et.al., 2000; Suh et al., 2000 ; Peluso et.al., 1994). Notwithstanding, one of the serious disadvantages of the chitosan is its poor water and organic solubility due to its crystalline structure leading to limited use in pharmaceutical and biomedical industry.

Furthermore, solubility of chitosan in acetic acid containing water demonstrates another limitation while using for the delivery of bioactive materials like protein/peptides, DNA/RNA and anticancer drugs, as it may harm them (Jang et. al., 2001). In addition, cumbersome methods of nanoparticle preparation (e.g. complexation-coacervation methods) usually involving crosslinking agent (e.g. tri-polyphosphate (TPP) poses another problem in the preparation of delivery systems (Salamanca et. al., 2006; Agnihotri et. al., 2004 ; Bivas-Benita et.al., 2004).

In order to solve these problems and avail the important features of chitosan, many studies have been undertaken either to enhance the solubility of chitosan in water and organic solvents by chemical modification of chitosan (as it would bring new and improved properties to chitosan without changing its basic skeleton and physicochemical and biochemical properties) (Maurya et.al., 2008 ; Jang et. al., 2001; Huang Y., et.al., 2010) or surface modification of synthetic polymers using chitosan and thus presenting characteristics of chitosan onto synthetic polymers for their improved application in vaccine and drug delivery (Danhier et.al., 2012). Recently, Maurya et.al., have most beautifully elaborated modifications and applications of chitosan in their review (Maurya et.al., 2008).

Looking at the benefits and limitations associated with the chitosan, the present investigation was perused to synthesize chitosan derivatives and determine their applicability in the preparation of nanoparticles incorporating Ag85A and rifampicin.

Thus, the present research was proposed - 1) to formulate and evaluate PLGA and cationic chitosan nanoparticles encapsulating Ag85A protein for pulmonary delivery in TB; 2) to formulate and evaluate rifampicin entrapped cationic chitosan nanoparticles for pulmonary delivery for the treatment of TB, in order to, 1) improve the immunogenicity of subunit vaccine and provide its sustained localized delivery to the lungs owing to its incorporation into nanoparticulate delivery system; 2) ameliorate antitubercular activity of rifampicin and overall management of TB by increasing the macrophage uptake, improving patient compliance and reducing adverse effects due to localized pulmonary delivery of rifampicin from nanoparticulate delivery system.

### **1.2 Objectives**

The present investigation was aimed at the development of nanoparticulate vaccine and drug delivery systems loaded with Ag85A and rifampicin for pulmonary mucosal delivery.

### **1.3 Innovation of the thesis**

Literature review revealed that, we are the first to prepare and utilize octanoyl chitosan nanoparticles for the delivery of vaccine and drug in the treatment of TB.

### **1.4 Hypothesis of the Study**

Hypothesis of the present study is based on the fact that the antigens can be better recognized by body when they interact directly with APCs. In connection to this, it is reported that mucosal immunity renders better disease protection as compared to systemic

immunity. Moreover, study is based on the reports that nano-particles (in the range of 200-500 nm) fabricated from biodegradable polymers are more suitable than micro-particles for surface presentation of antigens and subsequent interaction with APCs. In addition, application of chitosan for the formation of nanoparticles gives additional benefits while interacting with the cells due to its cationic charge and mucoadhesive property. The nanoparticles given through mucosal route localize in lymphoidal tissues and stimulate M cell for the production of the specific antibody. Due to the size of the particles, the uptake by lymphoid cells will be immediate and surface presentation of antigens will facilitate interaction with APCs. Thus, the nanoparticulate vaccine delivery system is expected to provide efficient and effective immunization.

### 1.5 Plan of Work

Following tasks will be undertaken as a part of the proposed research -

- 1) Literature review and procurement of APIs and excipients.
- 2) To synthesize and characterize derivatives of chitosan to overcome limitation of chitosan.
- 3) To prove the feasibility of synthesized polymer in the preparation of nanoparticles.
- 4) To find out analytical methods for estimation of protein and rifampicin.
- 5) To formulate and evaluate Ag85A loaded nanoparticles using PLGA and chitosan derivative.
- 6) To formulate and evaluate rifampicin loaded nanoparticles using chitosan derivatives.
- 7) To assess the performance of vaccine formulations by *in-vitro* and *in-vivo* studies.
- 8) To evaluate nanoparticles of PLGA and chitosan derivative for adjuvant activity.

### References

Agger E.M., Andersen, P. (2002) A novel TB vaccine; towards a strategy based on our understanding of BCG failure, *Vaccine*, 21, 7–14.

Agnihotri S.A., Mallikarjuna N.N., Aminabhavi T.M. (2004) Recent advances on chitosan-based micro- and nanoparticles in drug delivery, *Journal of Controlled Release*, 100, 5–28.

Bianco I.D., Balsinde J.S., Beltramo D.M., Castagna L.F., Landa C.A., Dennis E.A. (2000) Chitosan-induced phospholipase A2 activation and arachidonic acid mobilization in P388D1 macrophages, *FEBS Letters*, 466, 292-294.

Bivas-Benita M., Van Meijgaarden K.E., Franken K.EMC., Junginger H.E., Borchard G., Ottenhoff T.H.H., Geluk A. (2004) Pulmonary delivery of chitosan-DNA nanoparticles enhances the immunogenicity of a DNA vaccine encoding HLA-A 0201-restricted T-cell epitopes of *Mycobacterium tuberculosis*, *Vaccine*, 22, 1609–1615.

Bivas-Benita M., Lin M.Y., Bal S.M., Meijgaarden K.E.V., Franken K.EMC., Friggen A.H., Junginger H.E., Borchard G., Klein M.R., Ottenhoff T.H.H. (2009) Pulmonary delivery of DNA encoding *Mycobacterium tuberculosis* latency antigen Rv1733c associated to PLGA–PEI nanoparticles enhances T cell responses in a DNA prime/protein boost vaccination regimen in mice, *Vaccine*, 27 (30), 4010–4017.

Booyesen L.L.I.J., Kalombo L., Brooks E., Hansen R., Gilliland J., Gruppo V., Lungenhofer P., Semete-Makokotela B., Swai H.S., Kotze A.F., Lenaerts A., Plessis L.H. (2013) In vivo/in vitro pharmacokinetic and pharmacodynamic study of spray-dried poly-(dl-lactic-co-glycolic) acid nanoparticles encapsulating rifampicin and isoniazid, *International Journal of Pharmaceutics*, In Press.

Couvreur P., Vauthier C. (2006). Nanotechnology: intelligent design to treat complex 615 disease. *Pharm. Res.* 23, 1417–1450.

Danhier F., Ansorena E., Silva J.M., Coco R., Breton A.L., Pr at V. (2012) PLGA-based nanoparticles: An overview of biomedical applications, *Journal of Controlled Release*, 161, 505–522.

Doan T.V.P., Couet W., Olivier J.C. (2011) Formulation and in vitro characterization of inhalable rifampicin-loaded PLGA microspheres for sustained lung delivery, *International Journal of Pharmaceutics* 414, 112– 117

Eyles, J.E., Williamson, E.D., Alpar, H.O. (1999). Immunological response to nasal delivery of free and encapsulated tetanus toxoid: studies on the effect of vehicle volume. *Int. Jour. Pharmaceutics*, 189, 75-79.

Garcia C., Awasthi S., Hanif SNM., Hickey A.J. J. (2012) Inhaled Vaccines for the prevention of Tuberculosis. *J Mycobac Dis.*, S1:002, 1-13.

Girard M.P., Fruth U., Kieny M.P. (2005) A review of vaccine research and development: tuberculosis, , 23(50), 5725-31.

Hans M.L., Lowman A.M. (2002) Biodegradable nanoparticles for drug delivery and targeting, *Current Opinion in Solid State and Materials Science*, 6, 319–327.

Huang Y., Yu H., Guo L., Huang Q. (2010) Structure and Self-Assembly Properties of a New Chitosan-Based Amphiphile, *J. Phys. Chem. B*, 114, 7719-7726.

Jang M., and Nah J. (2001) The synthesis of LMWSC for pharmaceutical application, *Applied Chemistry*, 6(2), 611-614.

Kumar P.V., Asthana A., Dutta T., Jain N.K. (2006) Intracellular macrophage uptake of rifampicin loaded mannosylated Dendrimers, *J Drug Targeting*, 14 (8) 546-556.

Lu D. (2007) Aerosol Delivery of Recombinant Antigen 85B in Microparticle Vaccine Systems for Protection against Tuberculosis, Chapel Hill, NC. PhD Dissertation.

Luten J., Van Nostrum C.F., De Smedt S.C., Hennink W.E. (2008) Biodegradable polymers as non-viral carriers for plasmid DNA delivery *Journal of Controlled Release*, 126, 97–110.

Makadia H., and Siegel S. (2011) Poly Lactic-co-Glycolic Acid (PLGA) as Biodegradable Controlled Drug Delivery Carrier, *Polymers*, 3, 1377-1397.

Manca M.L., Sinico C., Maccioni A.M., Diez O., Fadda A.M., and Manconi M. (2012) Composition Influence on Pulmonary Delivery of Rifampicin Liposomes, *Pharmaceutics*, 4, 590-606.

Marques M.R.C, Loebenberg R., Almukainzi M. (2011) Simulated Biological Fluids with Possible Application in Dissolution Testing, *Dissolution Technology*, August 2011.

Maurya V.K. and Inamdar N.N. (2008) Chitosan modifications and applications: Opportunities galore, *Reactive and Funtional Polymers*, 68, 1013-1051.

Merdan T., Kopecek J., Kissel T. (2002) Prospects for cationic polymers in gene and oligonucleotide therapy against cancer, *Adv. Drug Del. Rev.* 54, 715–758.

Nafee N., Taetz S., Schneider M., Schaefer, U.F., Lehr C.M. (2007) Chitosan-coated PLGA nanoparticles for DNA/RNA delivery: effect of the formulation parameters on complexation and transfection of antisense oligonucleotides, *Nanomedicine: Nanotechnology, Biology and Medicine*, 3(3), 173–183.

Nair L.S. and Laurencin C.T. (2007) Biodegradable polymers as biomaterials, *Prog. Polym. Sci.* 32, 762–798.

Pawlowski A., Jansson M., Skoř M., Rottenberg M.E., Kař llenius G. (2012) Tuberculosis and HIV Co-Infection, *PLOS Pathogens*, Vol 8, 2, 1-7.

Pandey R., Zahoor A., Sharma S., Khuller G.K. (2003) Nanoparticle encapsulated antitubercular drugs as a potential oral drug delivery system against murine tuberculosis, *Tuberculosis*, 83, 373–378.

Peluso G., Petillo O., Ranieri M., Santin M., Ambrosio L., Calabro D., Avallone B., Balsamo G. (1994) Chitosan-mediated stimulation of macrophage function, *Biomaterials*, 15 (15) 1215–1220.

Petkar K., Chavhan S., Agatonovik-Kustrin S., Sawant K. (2011) Nanostructured Materials in Drug and Gene Delivery: A Review of the State of the Art, *Critical Reviews™ in Therapeutic Drug Carrier Systems*, 28(2), 101–164.

Praveen S., Sahoo S.K. (2011) Long circulating chitosan/PEG blended PLGA nanoparticle for tumor drug delivery, *European Journal of Pharmacology*, 670, 2–3, 372–383.

Salamanca A.E., Diebold Y., Calonge M., Garcí a-Vazquez C., Callejo S., Vila A., Alonso M.J. (2006) Chitosan Nanoparticles as a Potential Drug Delivery System for the Ocular Surface: Toxicity, Uptake Mechanism and In Vivo Tolerance, *Investigative Ophthalmology & Visual Science*, 47, 4.

Schroder U., Svenson S. (2001) Tuberculosis vaccine formulation comprising monoglycerides or fatty acids as adjuvant. EP 1154792.

Shahiwala A., Vyas T.K., Amiji M.M. (2007) Nanocarriers for systemic and mucosal vaccine delivery. *Recent patents on drug delivery and formulation*, 1, 1-9.

Shegokar R., Shaal L., Mitri K. (2011) Present Status of Nanoparticle Research for Treatment of Tuberculosis, *J Pharm Pharmaceut Sci.*, 14(1), 100-116.

Suh JKF., Matthew HWT. (2000) Application of chitosan-based polysaccharide biomaterials in cartilage tissue engineering: a review. *Biomaterials*, 21,2589–98.

Tanghe A., D'souza S., Rosseels V., Denis O., Ottenhoff T.H.M., Dalemans W., Wheeler C., Huygen K. (2001) Improved Immunogenicity and Protective Efficacy of a Tuberculosis DNA Vaccine Encoding Ag85 by Protein Boosting, *Infection And Immunity*, 69, 5, 3041–3047.

Tien CL., Lacroix M., Ispas-Szabo P., Mateescu M-A. (2003) N-acylated chitosan: hydrophobic matrices for controlled drug release. *J Control Rel.* 93, 1-13.

Vehring R. (2008) Pharmaceutical Particle Engineering via Spray Drying, *Pharmaceutical Research*, 25, 5, 999-1022.

Vyas S.P., Kannan M.E., Jain S., Mishra V., Singh P. (2004) Design of liposomal aerosols for improved delivery of rifampicin to alveolar macrophages *International Journal of Pharmaceutics*, 269, 1, 37-49.

Yang Y., Bajaj N., Xu P., Ohn K., Tsifansky MD., Yeo Y. (2009) Development of highly porous large PLGA microparticles for pulmonary drug delivery. *Biomaterials*. 30(10), 1947-53.

Yeboah K., D'souza M. (2008) Induction of mucosal immune response to M. Tuberculosis using microparticle encapsulated dead cell antigens, *AAPS PharmSciTech*.

Yu F., Wang J., Dou J., Yang H., He X., Xu W., Zhang Y., Hu K., Gu N. (2012) Nanoparticle-based adjuvant for enhanced protective efficacy of DNA vaccine Ag85A-ESAT-6-IL-21 against *Mycobacterium tuberculosis* infection, *Nanomedicine: Nanotechnology, Biology and Medicine*, 8(8), 1337-1344.

## **2.0 Literature Review on Tuberculosis**

### **2.1 History and Epidemiology of TB**

Tuberculosis (TB) is known to mankind since ancient times and has been recognized as one of the most deadly disease since the time of antediluvian ayurvedic system practiced by Sushruta, Samhita and Charaka in around 2500 BC. Historically this disease is known by variety of names such as consumption (due to severe weight loss, which appeared to “consume” the patient), phthisis pulmonaris and the white plague (because of the extreme pallor observed among the infected patients). Primitive literature indicated that the disease could be due to imbalance in the homeostasis, referable to variation in the Vata (combination of Earth and Air), Pitta (Fire) and Kapha (combination of Water and Earth). Until mid-1800, TB was regarded as hereditary disease. But in the year 1865, Jean Antoine-Villemin confirmed that TB was contagious and finally Robert Koch isolated the causative organism for TB (*M. Tb*) in 1882. Later on, various species of Mycobacterium were identified (*M. bovis*, *M. avium* and *M. leprae*), but the discovery of Koch directed the scientific community to think intelligently about prevention and cure of this disease. Subsequently, German chemists, Franz Ritter von Soxhlet adapted the pasteurization techniques for the preservation of milk (Prescott 1999c) which resulted in the reduction of milk-transmittable diseases, including TB (*M. bovis*). Afterwards, first vaccine against TB was developed by Albert Calmette and Camille Guerin which was administered for the first time in the year 1921 as BCG vaccine and first antibiotic, streptomycin was discovered by Albert Schatz in the year 1943 (under supervision of Selman Waksman) for the effective treatment of TB (<http://www.albertschatzphd.com>). Figure 2.1 represents the overall TB history since the confirmation of TB’s nature as contagious. With such efforts, mortality rate of TB was declined significantly in all developed countries. Hence, with the public awareness programs and the use of available therapy, it was believed that the TB disease would be completely wiped out within a short period of time. However, throughout recorded history, the epidemiology of TB was never constant and has grown up and fallen down following the concept “herd immunity”, where those who gets infected either died or developed immunity.

Until today, TB remains a major global health problem causing ill-health among millions of people each year. It ranks as the second leading cause of death from an infectious disease worldwide, after the human immunodeficiency virus (HIV). The latest estimate by the WHO indicated that there were almost 9 million new cases in 2011 (Figure 2.2) (out of which 13% were co-infected with HIV) and 1.4 million TB deaths including 9,90,000 among HIV

negative people and 4,30,000 cases amidst people who had HIV-associated TB. Geographically, WHO reported that the burden of TB is highest in Asia and Africa. India and China together contribute almost 40% of the world's TB cases; whereas South-East Asia and Western Pacific Regions contributes 60% of cases (Who Global Tuberculosis Report, 2012). Tuberculosis associated with HIV infection which is referred to as double trouble has increased the mortality and is considered to be the leading cause of death among HIV-infected persons worldwide. It is developed in one of the two ways, when the patients with LTBI becomes HIV positive resulting in loss of immunity and progression of LTBI into TB disease or HIV patients may get infected with *M. TB*. Of the estimated 33.4 million people living with HIV in 2008, nearly 30% were estimated to have latent or active TB infection.

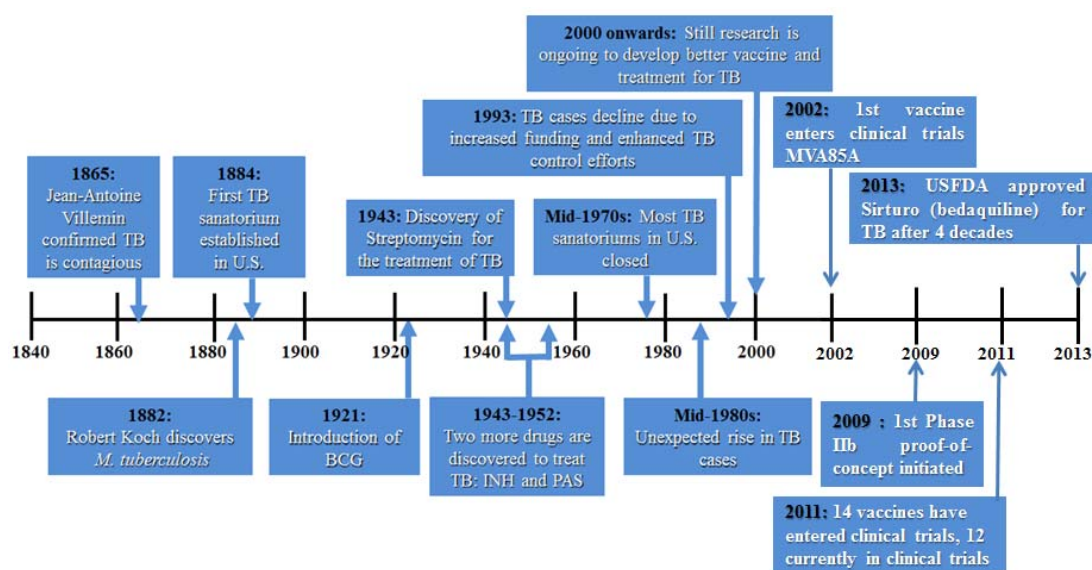


**Figure 2.1: History Timeline of TB**

In addition, the rapid spread of drug resistance, including multi-drug resistant tuberculosis (MDR-TB) and recently, extensively drug resistant tuberculosis (XDR-TB) contributed to the worsening treatment outcomes of tuberculosis. Drug resistance by *MTB* results from the mutations caused due to nucleotide substitutions, insertions or deletions in specific resistance-determining regions of the genetic targets or by activating enzymes of anti-TB chemotherapeutic agents (Jain et al., 2008). In 2011, there were almost 630000 cases of MDR-TB globally among the world's 12 million prevalent cases of TB, out of which almost 60% cases were observed in India, China and Russian federation. Similarly, XDR-TB cases have been identified in 84 countries and the average proportion of MDR-TB cases with XDR-TB was found to be 9.0% (6.7–11.2%) (Who Global Tuberculosis Report, 2012). Currently, the incidence of TB in HIV-infected persons is 100 times greater than that of the general population. Likewise, HIV infected persons are at greater risk for MDR-TB and

XDR-TB (Kwan et.al., 2011). Thus, despite the availability of treatment that proved impressive results and remarkable accomplishments, TB continued to be a major public health problem ascribable to its complicated drug therapy, drug resistance, double trouble due to HIV and less efficacious BCG vaccine leading to low cure and prevention rates (Who Global Tuberculosis Report, 2012). Hence, there is a still need to further improve on vaccine and drug delivery research and development to combat deadly tuberculosis to provide complete protection, especially in developing nations where resources are inadequate to identify and treat all cases.

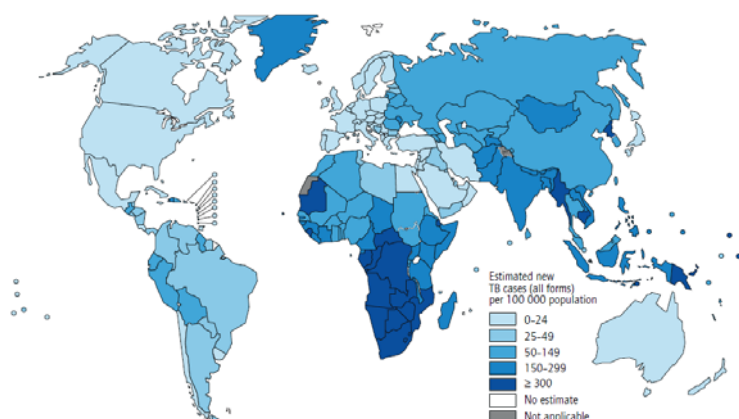


**Figure 2.2: Estimated TB incidence rate in the year 2011**  
(Source: Who Global Tuberculosis Report, 2012)

## 2.2 Pathogen, Pathogenesis and Progression of TB

*M. tuberculosis* (*MTB*) is an airborne disease caused due to inhalation of tiny droplets (particles) generated through exhalation (while coughing, sneezing, shouting, or singing) by the infected person who have pulmonary or laryngeal TB disease. Humans are a reservoir of this bacillus. *MTB* bacilli are nonmotile, rod-shaped having length of around 1-5  $\mu\text{m}$  and width of 0.2-0.3  $\mu\text{m}$ , which depending upon the environment may remain suspended in the air for several hours. *MTB* bacterium is facultative intracellular parasites usually appear in the well-aerated upper lobes of the lungs due to their obligatory aerobic nature (Todar's online Textbook of Bacteriology). Transmission occurs when a person inhales droplet nuclei containing *MTB*, subsequently they traverse the mouth or nasal passages, upper respiratory tract, and bronchi to reach the alveoli of the lungs, where they occupy compartment vesicles of macrophages (Tuberculosis, Centre for Disease control and prevention (<http://www.cdc.gov/tb/topic/basics/default.htm>)).

Among prokaryotes, *MTB* possesses a unique cell wall structure, which is considered as a major determinant of virulence for the bacterium. The cell wall of the bacterium is made up of around 60 % of complex lipids including mycolic acids, cord factor & wax-D and peptidoglycan. ***Mycolic acid*** contributes up to 50% of the dry weight of the mycobacterial cell wall envelope and is strong hydrophobic molecules that form a lipid shell around the organism, affecting its permeability properties at the cell surface. They are thought to be a significant determinant of virulence in *MTB* which helps preventing attacks by cationic proteins, lysozyme, and oxygen radicals in the phagocytic granule. ***Cord Factor*** is responsible for the serpentine cording (in-vitro cultures often form serpentine cord) and toxic to mammalian cells, which also inhibits polymonocytes (PMN) migration. Finally, ***Wax-D*** present in the cell envelope is a major component of Freund's complete adjuvant (FCA). Thus, high percentage of lipids in the cell wall of *MTB* is believed to be responsible for the development of resistance to many antibiotics. Moreover, it shows impermeability to stains and dyes, resistance to killing by acidic and alkaline compounds, resistance to osmotic lysis via complement deposition and resistance to lethal oxidations contributing to safe existence of bacterium inside macrophages (Todar's online Textbook of Bacteriology).

Pulmonary TB often begins when the tubercle bacilli are inhaled and reached to the alveoli. Once the organisms have made their entry into lung, they show four potential fates. 1) They are ingested by alveolar macrophages and presented to other white blood cells. This triggers initial host immune response in which white blood cells completely kill or encapsulate most of the bacilli, leading to the formation of a granuloma and thus majority of these bacilli are kept under control by the immune system of the person (bacilli are either destroyed or inhibited) in such a way that there is no chance of developing tuberculosis at any time point in the future; 2) The organisms can begin to multiply and grow immediately after infection, causing clinical disease known as primary tuberculosis; 3) Bacilli may become dormant and never cause disease at all, this form of infection is denoted as Latent TB Infection (LTBI), manifest only by a positive tuberculin skin test; or 4) the latent organisms can eventually begin to multiply intracellularly and are released when the immune systems grip over bacilli is loosened (generally macrophages die) leading to development of clinical disease, known as reactivation tuberculosis. Alive bacilli spread throughout the body by way of lymphatic channels or through the bloodstream to more distant tissues and organs such as regional lymph nodes, apex of the lung, kidneys, brain, and bone etc. which further leads to the progression of TB disease. In broad way, TB has been categorized as latent tuberculosis

infection (LTBI) and TB disease. Figure 2.3 depicts the pathogenesis of LTBI and TB disease. (Tuberculosis, Centre for Disease control and prevention, <http://www.cdc.gov/tb/publications/slidesets/selfstudymodules/module1/pathogenesis.htm>) Date Accessed, March 2013.

LTBI is a form of infection where, *MTB* bacilli remain in the body of infected person, but are not recognized to have TB disease due to their inability to spread the infection to other people and therefore a person with LTBI is not considered as an active case of TB. LTBI may be detected by using the Mantoux tuberculin skin test (TST) or blood test such as interferon-gamma release assay (IGRA). It takes around 2 to 8 weeks (after the initial infection of TB) for the body's immune system to react to tuberculin and to get detected by the TST or IGRA. After infection, the immune system arrests the multiplication of tubercle bacilli thereby preventing further progression of TB. In certain cases, the immune system remains ineffective to control the tubercle bacilli, which leads to multiplication of bacilli, resulting in progression of TB from LTBI to TB disease which is usually infectious. The progression from LTBI to TB disease can occur at any time after infection, may be during early days of infection or even take years after infection. But it was noted that the risk of developing TB disease is highest after 2 years of tubercle bacilli infection. Collection of body fluid or tissue from the disease site for acid fast bacilli (AFB) smear and culture is helpful for the diagnosis of TB (positive culture for *M. tuberculosis* confirms the diagnosis of TB disease). Figure 2.4 describes the progression of TB after exposure of persons to tubercle bacilli.

### 2.3 Macrophage activation and immune response

After deposition of tubercle bacilli in the lungs, they are phagocytosed by resident alveolar macrophages through the specific Toll like receptors involved in the uptake of pathogens. These includes, macrophage mannose receptor (MMR) and complement receptors (CR1, 3 & 4) (Ernst, 1998 ; Schluger et.al., 1998). Phagocytosis of *MTB* by macrophages induces release of IL-12 leading to development of cell-mediated immunity (CMI) which is important in protection from *MTB* infection (Ernst, 1998 ; Schluger et.al., 1998). CD4 Th1 cells are of primary importance in this protection from initial infection. *MTB* resides primarily in a vacuole within the macrophage, resulting in MHC class II presentation of mycobacterial antigen to CD4 T cells. The primary effector function of CD4 T cells is believed to be the production of IFN- $\gamma$  and other cytokines in order to activate macrophages.

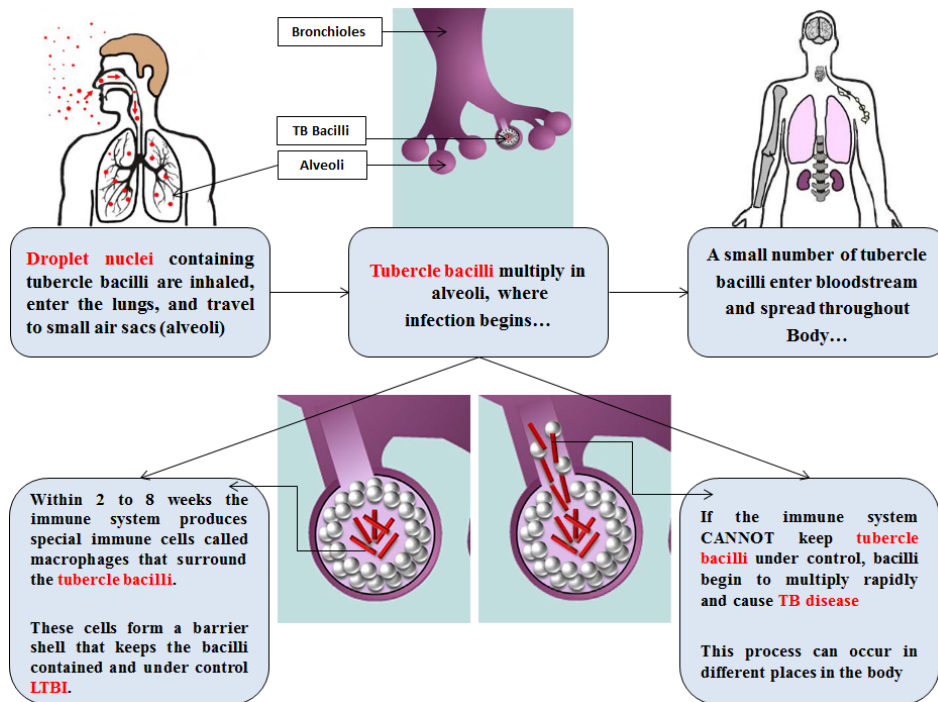


Figure 2.3: Pathogenesis of LTBI and TB disease.

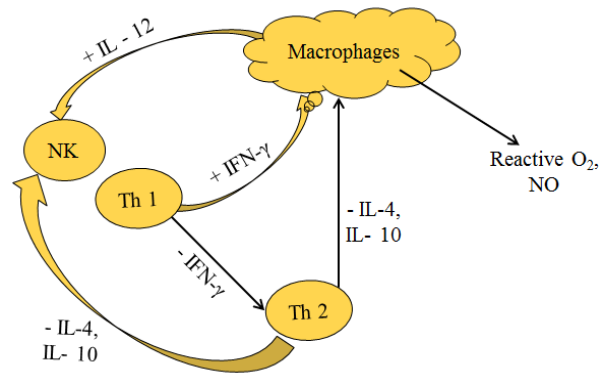
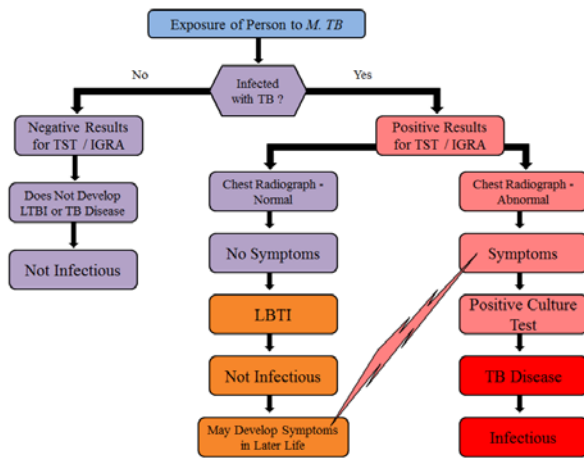


Figure 2.4: Progression of LTBI and active TB. Figure 2.5: Macrophage-Lymphocyte Interaction in TB.

The *MTB* bacilli within the vacuoles may have access to the cytoplasm (Teitelbaum, Cammer and Maitland, 1999). The antigen epitope - MHC class I complex can be recognized by CD8 T cells, which then produce cytokines IFN- $\gamma$  and TNF- $\alpha$  and act as cytotoxic cells. IFN- $\gamma$  is the key activating agent that triggers antimycobacterial effects of macrophages (Flesch and Kaufmann, 1987). It improves or augments the antigen presentation in macrophages, leading to a recruitment of more CD4+ T lymphocytes and cytotoxic T-lymphocytes (CTL) (Flesch, 1993)]. TNF- $\alpha$ , which is secreted by macrophages, dendritic cells and T cells, induces

chemokine production from macrophages and endothelial cells and also up-regulates adhesion molecules on vascular endothelial cells, resulting in cellular influx of further inflammatory cells (Hartmann and Plum, 1999). TNF- $\alpha$ , in collaboration with IFN- $\gamma$ , induces the production of nitric oxide and related nitrogen intermediates (RNIs) by macrophages via the action of the inducible form of nitric oxide synthase (NOS). Type 1 CD4+ T lymphocytes (Th1) and natural killer T lymphocytes (NK) secrete IFN- $\gamma$ , which activates alveolar macrophages to produce variety of substances, including reactive oxygen and nitrogen species, which are involved in growth inhibition and killing of mycobacteria. Macrophages also secrete IL-12 in a positive feedback loop to amplify this pathway. Although IL-4 and 10 inhibits macrophage function.

The success of MTB as pathogen is mostly due to its ability to survive and persist inside the host phagocytic cells called macrophages for long period of time. These pathogens protect themselves from the antimicrobial mechanisms of macrophages, which are designed to destroy any incoming microbe. Pathogenic mycobacteria have developed different strategies to exist within macrophages by getting protection from the cell wall of the bacteria and promoting their persistence in the host environment by preventing phagosome-lysosome fusion. *MTB* does this firstly, by stopping the normal maturation process of phagosomes to phago-lysosome by changing the endosomal pH and inhibit the acidification of the early phagosome. Secondly, *MTB* produces chemicals such as superoxide, by the action of the enzyme superoxide dismutase (SOD), which inhibits host defenses by interfering with host apoptosis. *MTB* avoids the development of a localized, productive immune response that could activate the macrophages leading to the destruction of the intracellular pathogens (Girard et.al., 2005 ; Dongmei 2007).

### 2.4 Current status of TB vaccine development

#### 2.4.1 BCG vaccine

Calmette, a physician, and Guérin, a veterinarian, developed live attenuated (weakened) strain of *M. bovis* by culturing a *M. bovis* isolate from a cow and subsequently sub-culturing it every three weeks over a period of 13 years (with a total of around 231 passages) at Institute of Pasteur in Paris. After 13 years, they obtained a strain with the less virulence, this altered organism was called BCG. After extensive tests in animals, BCG was first used as oral vaccine in infants in the year 1921. Later on, new routes of administration were innovated, such as intradermal, multiple puncture, and scarification (Girard et. al., 2005;

[www.who.int/vaccine](http://www.who.int/vaccine)). BCG vaccination has been included in the WHO Expanded Program on Immunization since 1974. Today it is estimated that more than four billion people have received BCG ([www.who.int/vaccine](http://www.who.int/vaccine)).

The safety record of BCG vaccine after such huge administration is impressive. It has not shown any serious issue until recently, except little concern in immune compromised persons where BCG itself may cause an infection and in immune competent persons who show local reactions, (including ulceration at the site of vaccination) resulting in shedding of live organisms which could infect others who are immune compromised ([www.who.int/vaccine](http://www.who.int/vaccine)). However, studies have shown that BCG has been the most controversial vaccine presently available in the market due to variation in its ability to confer excellent to no protection against TB (Kaufmann et.al., 2010 ; Fine et. al., 1995). It is demonstrated that BCG vaccines bestow excellent protection against severe forms of TB (such as meningitis and disseminated TB), than moderate forms. Reports indicated that, the efficacy of BCG vaccination in children wanes with age (82% in children less than 15 years of age to 67% in the 15–24-year-old group, and to only 20% in persons over 25) (Kaufmann et.al., 2010). Figure 2.6, represents the inefficiency of BCG vaccine over 25 years of age. Variation in efficacy of BCG vaccine in young children ranges from 46–100%, while, its efficacy against pulmonary TB (more prevalent in adolescents and adults) ranges from 0–80%. Moreover, geographic latitude has also been a cause to vary efficacy of BCG vaccine - the farther from the equator, the more efficacious the vaccine. It is presumed that, exposure to environmental nonpathogenic mycobacteria, which is more in warm climates, induces a degree of protective immunity in exposed populations, thus interfering with BCG and masking potential protection from BCG (*Girard et. al., 2005*). In sum, variation in the efficacy of BCG are mainly caused due to - 1) differences among BCG vaccine sub-strains; and phenotypic changes in the vaccine during sub-culturing of original cultures and manufacturing process; 2) the deletion of protective antigens from BCG; 3) variability in age, dose, mode of administration; 4) genetic differences among vaccinees; 5) lyophilization of the vaccine; 5) interference with the immune response to BCG caused by previous exposure to environmental mycobacteria (*Girard et. al., 2005*).

Despite the drawbacks, currently BCG is the only vaccine used worldwide for the prevention of TB due to its efficacy in preventing life-threatening forms of TB in infants and young children. Moreover, it is inexpensive, requires only one encounter with the baby, and less side

effects. However, BCG is unsuccessful to control the increased new TB cases in adults worldwide due to inefficacy in adults, variation in efficacy, association of HIV and also reactivation. Moreover, a major limitation associated with BCG may be its inability to induce an effective CD8<sup>+</sup> T cell immune response, which plays a vital role in the immunity against *MTB* (Delogu et.al., 2009). Therefore, to reduce the global burden of disease, there is an urgent need to develop better TB vaccines or new vaccination strategies against tuberculosis to induce a more efficient immunity than that achieved with BCG vaccine, not only in infants but also in adolescents and adults. In response to this, large numbers of scientific organizations are involved in the investigation of new and more potent vaccine candidate against TB either by improving existing BCG vaccine, developing new live attenuated TB vaccine, DNA vaccines and subunit vaccines or by developing prime boost (post exposure) vaccination strategies to target dormant *MTB* for the prevention of reactivation (in regions with high prevalence of TB). Certain post-exposure vaccination strategies are summarized in Figure 2.6. (Kaufmann et.al., 2010). Among all these groups, large numbers of TB vaccine candidates have been investigated and demonstrated their suitability with the improved efficacy through preclinical and clinical studies (Table 2.1).

### ***2.4.2 Live and attenuated mycobacterial vaccines:***

Live mycobacterial vaccines have been developed by improving existing BCG vaccine either by addition/deletion of relevant genes or an attenuation of *M tuberculosis* through removal of genes responsible for virulence. The first attempt to develop improved BCG vaccines was made by Horwitz et al., who over-expressed Ag85B in BCG, called rBCG30. Results from the study demonstrated improved protection against TB in animal models, and found to be immunogenic in humans (Ottenhoff et.al., 2012). More recent studies reported a recombinant BCG strain to over-express Ag85A, Ag85B, and TB10.4 (Ottenhoff et.al., 2012). Another strategy to improve BCG involves the expression of listeriolysin and deleting expression of ureC in BCG (rBCG $\Delta$ ureC:Hly - VPM1002). rBCG $\Delta$ ureC:Hly (VPM1002), is a recombinant strain that secretes listeriolysin produced by *Listeria monocytogenes*, which helps to sustain an acidic phagosomal pH for optimum listeriolysin activity. It is believed that it creates perforation on the phagosomal membrane which probably promotes antigen translocation into the cytoplasm and facilitates cross-priming and stimulation of Th17 cells through increased apoptosis (Grode et.al., 2005 ; Sun et.al., 2009). Results of preclinical studies demonstrated that both the vaccines were more potent and safer than the currently used BCG vaccine. Other promising attenuated vaccine candidates includes, MTBVAC01

vaccine, constructed by disruption of the transcriptional regulator gene *PboP* (which is associated with expression of many genes including *M tuberculosis* virulence gene) and the *fadD26* genes (which is involved in the synthesis of the cell wall lipid phthiocerol dimycocerosate (PDIM)) (Martin et. al., 2006). This strain is called as  $\Delta$ PhoP $\Delta$ fad *Mtb* strain (*MTB H37Ra*). Martin et al., accounted superior level of protection upon aerosol challenge as compared to BCG vaccination. Another attenuated *MTB* vaccine candidate is *MTB*  $\Delta$ RD1  $\Delta$ panCD. Authors reported the construction and characterization of an unlinked double deletion mutant of *MTB H37Rv* by deleting both the primary attenuating mutation of BCG ( $\Delta$ RD1) and two genes required for the synthesis of pantothenate ( $\Delta$ panCD). They found long-lived protective immune responses following immunization with the mc<sup>2</sup>6030 strain in wild type mice and CD4-deficient mice against an aerosol challenge with virulent *M. tuberculosis*. (Sambandamurthy et.al., 2006). Furthermore, two attenuated vaccine candidates are currently under phase III clinical studies, one is Mw [*M. indicus pranii* (MIP)], a whole cell saprophytic non-TB mycobacterium cells which is sponsored by Department of Biotechnology, (Ministry of Science and Technology), India and Cadila Pharmaceuticals Inc. (Brennan et.al., 2012) and another is *M. Vaccae* which is made up of an inactivated whole-cell strain of Mycobacterium vaccae and derived from rough variant of an environmental isolate. It was developed initially as a therapeutic TB vaccine candidate (sponsored by National Institute of Health and Immunology) ([http://www.who.int/vaccine\\_research/documents/se05Hawkridge.pdf](http://www.who.int/vaccine_research/documents/se05Hawkridge.pdf)).

Despite the developments, safety concerns as well as technical challenges in the manufacturing and reproducibility associated with live mycobacterial vaccines (particularly in immunocompromised persons) make them unsuitable candidates for most vaccine manufacturers. Therefore, the development of new TB vaccine approaches are riveted on recombinant DNA vaccines, subunit vaccines (protein adjuvant and viral vector based) and attenuated vaccines which prominently expresses required mycobacterial antigens exhibiting protective or therapeutic efficacy.

### **2.4.3 DNA vaccines:**

DNA vaccination presents many advantages such as, easy manipulation, safety, and ease in storage and transportation and most importantly its ability to induce both humoral and cellular immune responses. It can be constructed together with immunostimulatory molecules such as cytokine genes and immunostimulatory DNA sequences, like the CpG sequences, to

enhance its immunogenicity. In addition, inherent ability of plasmid DNA to multiply causes endogenous expression of antigen over prolonged period of time and thus efficient presentation of antigen on the MHC class I molecules leading to activation of cytotoxic T lymphocytes (CTL) and thus enhancing immune response against MTB (Nor et.al., 2004).

First DNA vaccine against tuberculosis sprang up serendipitously when Lowrie et. al., were researching on the basic immunobiology of a dominant mycobacterial antigen (heat shock protein 65 - hsp65) in adult Balb/c mice, which resulted in substantial cell-mediated protection against challenge with *MTB* (Lowrie et.al., 1994). In another research, they studied intramuscular injection of plasmid DNA expressing the antigen hsp 65 (from viral and murine promoter) and reported equivalent protection against TB in comparison to BCG. They also studied plasmids encoding mycobacterial antigens such as hsp70, 36 kDa and 6 kDa, and suggested their effectiveness, hypothesizing birth of a new potent vaccine (Lowrie et.al., 1997). Thus, as illustrated by Lowrie et. al., DNA vaccines have provided tantamount protection to that provided by the standard BCG vaccine. Thenceforward, many researchers reported DNA vaccines encoding various antigens (either alone or in combination) with effective protection against virulent *MTB* in a range of animals (Lowrie et.al., 1997 ; Wang et.al., 2004 ; Vipond et.al., 2006 ; Gupta et.al., 2007 ; Okada et.al., 2007 ; Daniella et.al., 2009). Although protection is not always strong with these prototype vaccines and therefore heterologous prime/boost approach with BCG vaccine was devised and currently post exposure vaccination seems to be effective in protection against TB (Lowrie 2006). More recently, Cervantes-Villagrana et.al., investigated prime-boost BCG vaccination with DNA vaccines based in  $\beta$ -defensin-2 & mycobacterial antigens ESAT6 or Ag85B and reported improvement in the protection against tuberculosis experimental model (Cervantes-Villagrana et.al., 2013). In a study, Meerak et.al., demonstrated autophagy induced immune response of DNA vaccine against TB. They encapsulated plasmid DNA (encoding MTB Antigen 85B (Ag85B) into low molecular weight chitosan, administered along with an autophagy-inducing element and concluded improved immune response based on the enhanced proliferation of CD4+ T cells from experiments on mice (Meerak et.al., 2013). These results confirm the potential application of plasmid DNA vaccination strategy against TB. However, safety issues of DNA vaccine in terms of their integrity into the host genome or their ability to cause autoimmune disease still exist.

### ***2.4.4 Subunit vaccines:***

This strategy involves the delivery of immunodominant mycobacterial antigens to the immune system, using viral vectors or polymeric vehicles along with protein adjuvant system to improve the efficacy of BCG. Subunit vaccines are made up of only antigen or epitope (the very specific parts of the antigen that antibodies or T cells recognize and bind to) that best stimulate the immune system in lieu of entire microbe. Because subunit vaccines contain only the essential antigens, the chances of adverse reactions to the vaccine are lower and thus safer as compared to live and DNA vaccines. However, they are expensive to manufacturer, less immunogenic and often requires adjuvant to enhance immune response (Nor et.al., 2004). As subunit vaccines is a mixture of 1 to 20 or more antigens, identifying antigens which best stimulate the immune system is difficult and time-consuming process. But, once it is done, subunit vaccines can be prepared either by growing the microbe in the laboratory and breaking them apart chemically to get the important antigens or by manufacturing the antigen molecules from the microbe using recombinant DNA technology (recombinant subunit vaccines).

(<http://www.niaid.nih.gov/topics/vaccines/understanding/pages/typesvaccines.aspx>). The development of subunit a vaccine has opened a new era in vaccinology and has become the current trend in vaccine development.

Subunit vaccines for TB are mainly developed either by BCG antigens and live viral vectors that express one or several mycobacterial proteins or recombinant proteins and fusion proteins consisting of two or more dominant *MTB* antigens. They are predominantly used in a prime-boost strategy to complement the immune response induced by BCG (figure 2.6) (Kaufmann et. al., 2010). Large numbers of antigens have been isolated from whole bacteria, or bacterial short-term culture filtrates. These includes, ESAT-6, group of mycolyltransferases proteins (Ag85A, Ag85B and Ag85C) (Gupta et.al., 2007), CFP 10, MTP64, hsp60, R8307 protein, a 36 kDa proline-rich mycobacterial antigen, or the 19 kDa and 45 kDa proteins etc. when combined with a strong Th1 inducing adjuvant showed similar protection levels to that obtained with BCG in mice (Girard et.al., 2005). Early secreted protein antigen, ESAT-6 of size 9.8 kDa is strongly recognized by T cells of *MTB* -infected individuals and in animal models of TB. This protein has been found to be immunodominant, inducing IFN- $\gamma$  production by T cells from infected mice (Andersen et.al., 1995; Sorensen et.al., 1995). ESAT-6 induced protection (either as a subunit vaccine or as a DNA

vaccine) was found to be good as that of the BCG. Likewise, various antigens tested (as mentioned above) indicated good immune response.

Other major protein secreted by MTB belongs to a group of mycolyltransferase proteins consisting of three closely related mycolyltransferases Ag85A, Ag85B and Ag85C. Amongst, Ag85A and Ag85B have been found to be the most potent antigens and major targets of human T cell responses to *MTB*. These proteins have also been extensively researched and reported to be the leading vaccine candidates by number of workers (Ohara et. al., 2001; Ronning et.al., 2004 ; Hajizadeh et.al., 2007; Geluk et.al., 2012). Currently, the MVA85A single dose booster vaccine candidate is under phase IIb clinical trials. The vaccine is delivered using an attenuated modified vaccinia virus Ankara (MVA) and is the most clinically-advanced single dose, next generation TB vaccine candidate in the world. Developed as a booster vaccine, MVA85A is intended to increase the immune response in individuals who have previously been vaccinated with BCG (<http://www.aeras.org/portfolio/clinical-trials.php?id=20>) (Table 2.1). Co-administration of DNA with the protein Ag85B, ESAT6 or MPT65 has been shown to provide better protection as compared to the one which is induced by any single DNA vaccine (Kamath *et al.*, 2000). Recently, Ag85 purified protein from the avirulent H37Ra strain have shown protection against MTB (Yadav et.al., 2001), and reports indicated that delivery vehicles such as liposomes and microspheres could be used to deliver Ag85 and protect mice from a high dose intravenous challenge (Orme, 2006).

Currently molecular biologist's major area of interest is the construction of fusion proteins, or polyproteins by recombinant engineering. One such example is recombinant fusion protein molecule, Ag85B-ESAT-6 (H1) vaccine designed with a strong Th1 adjuvant, IC31 (Intercell, Vienna, Austria) (a mixture of oligodeoxynucleotides and polycationic aminoacids). The success in the preclinical studies made it possible to be assessed in two phase 1 clinical trials, progressive efficacy led to the phase II clinical studies ([http://www.who.int/vaccine\\_research/documents/se05Hawkridge.pdf](http://www.who.int/vaccine_research/documents/se05Hawkridge.pdf)). It was found to be well tolerated, without any serious adverse reactions, and highly immunogenic in human beings (Olsen et. al., 2001). Nevertheless, risks associated with ESAT-6 were identified due to its interference in ESAT-6-based diagnostic assay and therefore, another fusion protein Ag85B-TB-10.4 (H4, AERAS-404) was developed as an alternative to Ag85B-ESAT-6. It has been shown that a fusion of TB10.4 peptide and Ag85B is also very protective in mice

(Kaufmann et.al., 2010). Continued progress in the past decade has shown that it is possible that at least one new vaccine could be licensed by 2025. Various strategies of post exposure vaccinations are depicted in figure 2.6 and vaccine candidates under clinical trials are presented in figure 2.7.

Among the various protein identified, Ag85 complex protein (including Ag85A, B and C) has presented promising characteristics due to its ability to bind fibronectin and promote their adherence to mucosal surfaces thereby facilitating their entry into host cells. Moreover, Ag85 complex interacts with the immune system at an early stage of the infectious process and induces both humoral and cell-mediated immune responses in *MTB*-infected patients and animal models (Lu D, 2007). The early-stage antigens would be most useful in a preventive vaccine. A mycolyl-transferase member, Ag85A is well characterized antigen 85 complex of *MTB* and is a promising vaccine candidate which has shown to induces strong protective responses in experimental animal models (Tanghe et.al., 2001). Thus, Ag85A is the most investigated protein and examined at preclinical and clinical level. However, as discussed earlier, a major drawback of protein vaccine is low immunogenicity especially by mucosal routes, therefore adjuvant co-administration is often advised and currently research is still under progress to increase the immunogenicity of subunit protein vaccines using various adjuvants with due concerns to its safety. Till date, there is no effective vaccine to prevent TB and pulmonary TB in adults. Because *MTB* uses the respiratory tract as port of entry into the body, pulmonary vaccination could be the best way to induce a specific immunity in the lungs and to protect against the disease. Pulmonary vaccination has the advantage to be needle free and to generate a mucosal as well as systemic immunity. Considering these fact, Ag85A (proteins) was utilized in this research work.

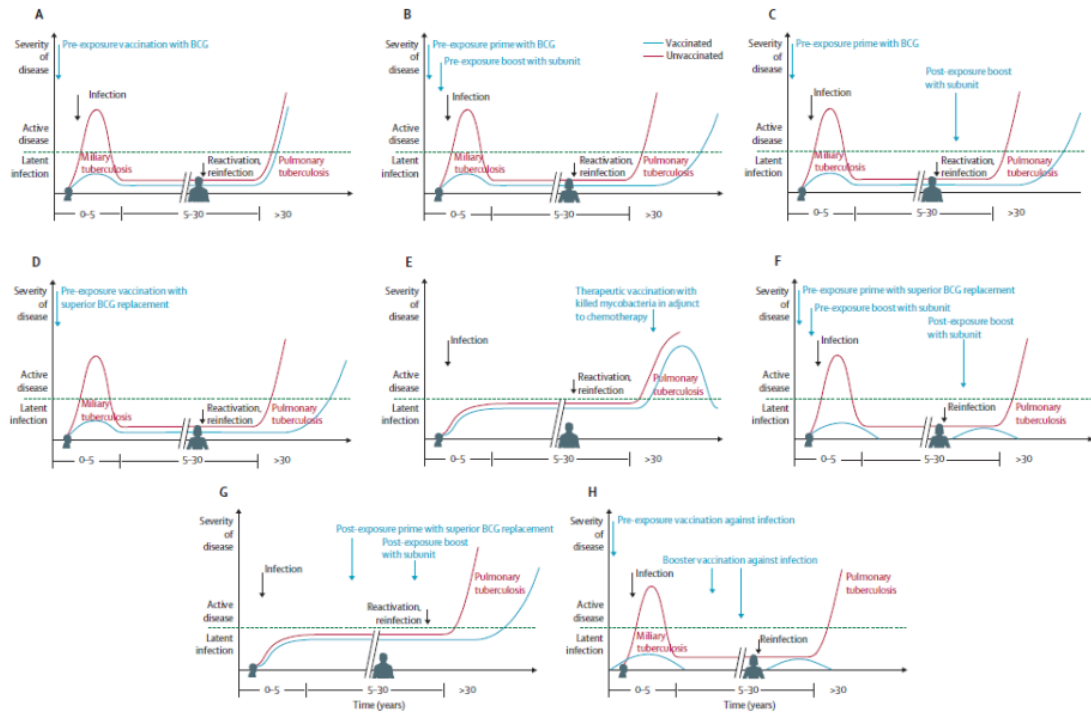


**Figure 2.6: Various strategies for post exposure TB vaccination (Reproduced from Source: Stefan et. al., 2010)**

**Current strategy:** (A) pre-exposure vaccination with BCG to protect early childhood tuberculosis (which does not eradicate *MTB* and reactivates in adulthood).

**Vaccination strategies under research:** (B) pre-exposure boost (subunit vaccine) in children primed with BCG to prevent tuberculosis in early childhood (it delays tuberculosis disease outbreak in adults); (C) post-exposure boost (subunit vaccine) in adults those are primed with BCG during early childhood (to delay tuberculosis disease outbreak in adults); (D) pre-exposure vaccination with superior BCG replacement to prevent tuberculosis in early childhood and to delay tuberculosis disease outbreak in adults; (E) therapeutic vaccination (vaccine+chemotherapy) to kill *MTB* in patients with active tuberculosis; (F) heterologous prime-boost vaccination with superior BCG replacement and subunit vaccine, to eradicate *MTB*; (G) post exposure prime-boost vaccination in individuals with LTBI (prime with superior BCG replacement and boost with subunit vaccine) to delay and prevent tuberculosis disease outbreak; and (H) pre-exposure vaccination to prevent stable infection with *MTB*.

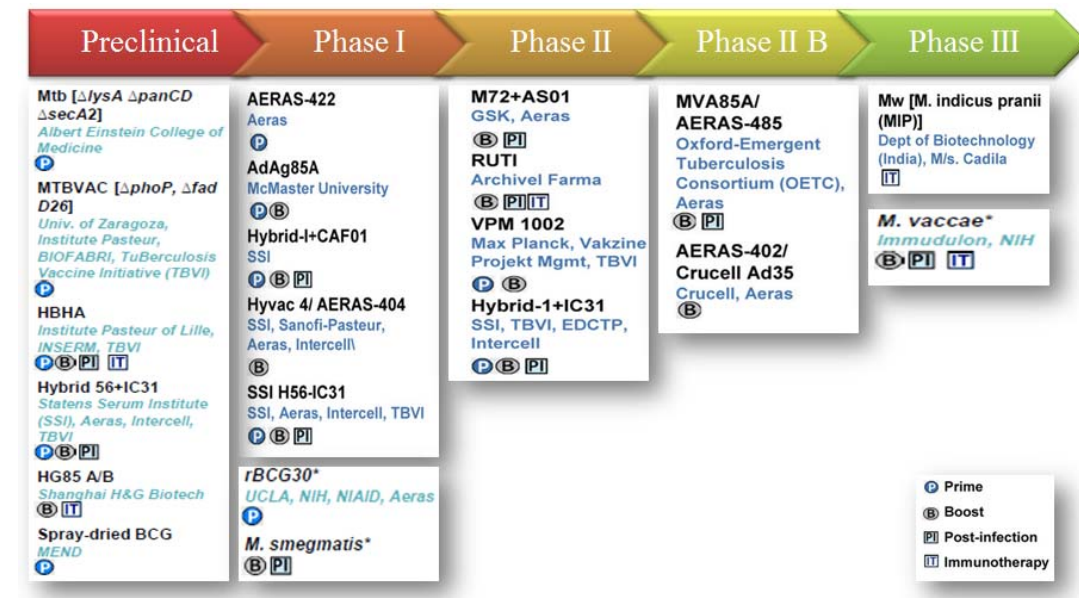


Figure 2.7: Vaccines in preclinical and clinical trials

\* Indicates candidates that have been in clinical trials in the past, but are not currently being tested in clinical trials

**Preclinical vaccine candidates** - manufactured under Good Manufacturing Practice (GMP) for clinical use and have undergone preclinical testing that meets regulatory standards (Source: *Tuberculosis Vaccine Candidates – 2012; Stop TB Partnership Working Group on New TB Vaccines*)



Table 2.1: Various vaccine candidates and their current research status

Strategy of TB Vaccination	Name of Product	Description	Status	Sponsor	Reference
<b>Live mycobacterial and Improved BCG vaccines:</b> The rationale for novel live-attenuated mycobacterial vaccines is to improve the efficacy of BCG against systemic disease and also identifying reasons for its limited efficacy against pulmonary TB					
BCG overexpressing antigens/reengineering BCG	rBCG30	rBCG30 engineered to overexpresses Ag85B and induces increased protection compared with BCG strain in animal challenge studies.	Completed - Phase I trial Prime	UCLA, NIH, NIAID, Aeras	Brennan et.al., 2012
	AERAS 422	Recombinant BCG expressing mutated PfoA and overexpressing antigens 85A, 85B, and Rv3407	Ongoing - Phase I clinical trial	Aeras	<a href="http://www.who.int/vaccine_research/documents/se05Hawkridge.pdf">http://www.who.int/vaccine_research/documents/se05Hawkridge.pdf</a>
BCG with the ability to escape endosome	VPM 1001 - rBCG $\Delta$ ureC::hly::hyg	Listeria monocytogenes Hly (listeriolysin) is a sulphhydryl-activated cytolysin that forms pores in the membrane of the early phagosome. rBCG vaccine excretes Hly to induce holes in the endosome, allowing leakage of BCG to cytosol and thus increase response of CD8+ T cells.	Ongoing – Phase II studies, B, PII	Max Plank Vakzine, Project Management TBVI	
Reducing BCG interference with Immunity	---	Host superoxides produced by macrophages kill MTB and can amplify host T-cell recruiting signals. Secretion of superoxide dismutase (SOD) by MTB, to inactivate superoxides promotes granuloma formation & contributes to inhibition of host defenses and persistence of the organism. rBCG with reduced secretion of functional SOD is more potent than the parent strain. Deletion of nlaA genes, which inhibit apoptosis of infected cells, might lead also to a superior vaccine.	Preclinical, GMP	Albert Einstein Coll of Med. NIH	Kernodle & Bochan, 2012; Sambandamurthy et.al., 2005

Reintroduction of deleted genes	BCG:RDI	Reintroduces regional domain (RD) 1 locus encoding immunodominant and protective ESAT-6 and CFP-10 proteins which were deleted during BCG attenuation	Preclinical, GMP	Institute Pasteur, Paris, France	Pym et.al., 2003
	BCG:RDI	Same as above, expression of ESAT-6 and Ag85A proteins.	Preclinical, GMP	Institute Pasteur, Paris, France	Pym et.al., 2003
	MTB mc <sup>2</sup> 6030	MTB H37Rv with deletion of pantothenate (panCD) and RD-1 locus	Preclinical, GMP	Albert Einstein Coll of Med. NIH	Sambandamurthy et.al., 2006
	MTB mc <sup>2</sup> 6020	MTB H37Rv with deletion of the lysA and the panCD locus	Preclinical, GMP	Albert Einstein Coll of Med. NIH	Sambandamurthy et.al., 2006
	BCG:PhoP	Inactivation of PhoP, regulates expression of selective MTB proteins (attenuate MTB virulence) to maintain immune responses associated with parental MTB strain.	Preclinical, GMP	Uni of Zaragoza, Institute Pasteur, BIOFABRI, TB VI	Martin et.al., 2006
<b>Attenuated TB vaccine:</b> This strategy involves production of auxotrophic MTB strains or less virulent mycobacteria such as <i>M. microti</i> , <i>M. vaccae</i> , or <i>M. smegmatis</i> that overproduce immunogenic antigens of MTB					
	<i>M. Vaccae</i>	Inactivated whole-cell strain of Mycobacterium vaccae. Derived from rough variant of an environmental isolate. Developed as a therapeutic TB vaccine candidate.	Completed-Phase III clinical trials, B to BCG in HIV	NIH, Immodulon	<a href="http://www.who.int/vaccine_research/documents/se05Hawkridge.pdf">http://www.who.int/vaccine_research/documents/se05Hawkridge.pdf</a>
	Mw [ <i>M. indicus pranii</i> (MIP)]	Whole cell saprophytic non-TB mycobacterium	Ongoing: Phase III clinical trials Immunotherapy	Dept of Biotech. (Min of Sci & Tech, GOI), Cadila Pharma Ltd.	Brennan et.al., 2012

	RUTI®	RUTI, a therapeutic vaccine made of detoxified, fragmented Mycobacterium tuberculosis cells, delivered in liposomes, was used to assess its effectiveness in a short period of chemotherapy (1 month). Target subject with latent TB infection	Ongoing – Phase II studies, B, PII	Archival Pharma	<a href="#">Cardona</a> , 2006
<b>DNA Vaccine:</b> This approach involves direct injection of plasmid DNA encoding specific antigens or epitopes that can lead to protective immunity					
	DNA vaccine	DNA vaccines by the fusion of the gene encoding $\beta$ -defensin-2 and antigens ESAT6 (pDE) and 85B (pDA)	Preclinical, B	Med Res. Unit-Zacatecas, Mexican Institute of Social Security IMSS, Zacatecas, Mexico	Cervantes-Villagrana et.al., 2013
	HG85 A/B	Chimeric DNA vaccines—Ag85A/Ag85B	Preclinical studies, B	Shanghai H&G Biotech	<a href="http://www.aeras.org/newscenter/publications_scientific.php">http://www.aeras.org/newscenter/publications_scientific.php</a>
	HVJ-Envelope /HSP65 DNA+IL-12 DNA	Combination of DNA vaccines expressing mycobacterial heat-shock protein 65 & IL-12	Preclinical studies, B, PII	Osaka University	
	pUMVC6/7 DNA	DNA vaccine plasmid vectors pUMVC6 or pUMVC7 expressing Rv3872, Rv3873, Rv3874, Rv3875 or Rv3619c	Preclinical studies, P	Kuwait University	
	TBVax	T cell epitope-based DNA-prime/peptide boost vaccine	Preclinical studies, B, PII	EpiVax , Inc.	
	Hsp DNA vaccine	Codon-optimized heat shock protein from <i>M. leprae</i> , a CpG island	Preclinical studies, B	Cardiff Uni., Sequella	

	HVJ-Envelope /HSP65 DNA+IL-12 DNA	Combination of DNA vaccines expressing mycobacterial heat-shock protein 65 & IL-12	Preclinical studies, B, PII	Osaka University	
<b>Subunit Vaccine:</b> This strategy involves the delivery of immunodominant mycobacterial antigens to the immune system, using viral vectors or protein –adjuvant system to improve the efficacy of BCG.					
<b>Viral Vectored Vaccine</b>	MVA85A	The MVA85A single dose booster vaccine candidate. Originally developed at the University of Oxford. It is the most clinically-advanced single dose, next generation TB vaccine candidate in the world. MVA85A is intended to increase the immune response in individuals who have previously been vaccinated with BCG. The vaccine is delivered using an attenuated modified vaccinia virus Ankara (MVA).	Completed - Phase IIb Infants, Prior BCG Vaccination. Ongoing - Phase IIb Adults, HIV infected	Oxford Emergent Tuberculosis Consortium (OETC), Aeras	<a href="http://www.aeras.org/portfolio/clinical-trials.php?id=20">http://www.aeras.org/portfolio/clinical-trials.php?id=20</a>
	AERAS-402/ Crucell Ad35	This adenovirus delivery system uses a replication-deficient adenovirus. Ad35 contains <i>M. tuberculosis</i> antigens 85A, 85B, and TB10.4 and adeno vectored vaccines consistently induced high levels of CD8+ T cell responses, which are essential for an effective new TB vaccine.	Ongoing - Phase IIb Adults, HIV-infected, Latent TB, Prior BCG Vaccination. Phase IIb Infants, BCG vaccinated.	Crucell, Aeras	Hoft et.al., 2012
	GSK M72	An immunogenic fusion protein developed by GSK, recombining two proteins. Also uses GSK proprietary adjuvants. It is the only candidate in a BCG prime-boost regimen thus far to show	Completed - Phase II Adolescents, Prior BCG	GSK	<a href="#">Leroux-Roels et.al., 2012</a>

		protection better than BCG in the long-term non-human primate (NHP) challenge model.	Vaccination. Ongoing - Phase II Infants, Prior BCG vaccination		
	Ad Ag85A	Recombinant Adenovirus vectored Ag85A. Canada's first TB vaccine.	Ongoing – Phase I trials, P, B	McMaster university	Xing et.al., 2009
<b>Protein-Adjuvant Vaccines</b>	Hybrid 1-IC31	Recombinant protein (Ag85B plus ESAT 6) fusion molecule with adjuvant (IC31)	Ongoing – Phase II clinical trial, P, B, PII	SSI, TBVI, Intercell	<a href="http://www.who.int/vaccine_research/documents/se05Hawkridge.pdf">http://www.who.int/vaccine_research/documents/se05Hawkridge.pdf</a>
	H4-IC31®	It is a fusion protein of 85B and TB10.4, combined with Intercell's IC31® adjuvant to stimulate T cell-mediated immunity. This candidate vaccine has induced more protection in a BCG prime-boost regimen than any other vaccine tested in the long-term guinea pig challenge model.	Completed - Phase I Adults, Prior BCG vaccination. Adult. P, B	Statens Serum Institut (SSI), Intercell and AERAS	<a href="http://www.aeras.org/portfolio/clinical-trials.php?id=20">http://www.aeras.org/portfolio/clinical-trials.php?id=20</a>
	H56-IC31	It is a subunit vaccine containing recombinant TB proteins formulated in a proprietary adjuvant IC31® from Intercell	Ongoing - Phase I Adults, including exposed to TB	Statens Serum Institut (SSI), Intercell and AERAS	Lin et.al., 2012
	ID93/GLA-SE	ID93/GLA-SE composed of an recombinant fusion-protein antigen plus IDRI's proprietary adjuvant, GLA. The vaccine candidate targets both active tuberculosis and latent TB.	Ongoing – Phase I Adults	Infectious Disease Research Institute (IDRI), AERAS	<a href="http://www.aeras.org/portfolio/clinical-trials.php?id=20">http://www.aeras.org/portfolio/clinical-trials.php?id=20</a>

	Hyvac 4, Aeras 404	This vaccine (HyVac4), adjuvanted with MPL. HyVac4 formulated in IC31 and given in a prime–boost regimen with BCG was immunogenic and offered enhanced protection to <i>M. tuberculosis</i> aerosol challenge over BCG in guinea pigs	Ongoing – Phase I clinical trial, B	Statens Serum Institut (SSI), Sanofi Pasteur, Intercell and AERAS	Rowland and McShane 2012
	Hybrid 1-IC A F01	Recombinant protein	Ongoing – Phase I clinical trial, P, B, PII	SSI	Brennan et.al., 2012

**Source:** *Tuberculosis Vaccine Candidates – 2012; Stop TB Partnership Working Group on New TB Vaccines* (stop TB blue print, TB vaccine in pipeline).

**Prime – P; Boost – B; Post infection immunotherapy - PII**

**Preclinical vaccine candidates** - manufactured under Good Manufacturing Practice (GMP) for clinical use and have undergone preclinical testing as per regulatory standards.

### **2.5 Evolution and current status of TB chemotherapy**

The chemotherapy of infectious diseases was afoot using antibiotics, sulfonamide and penicillin for several years, but these molecules were found to be ineffective against *MTB*. Selman A. Waksman had been systematically screening soil bacteria and fungi since 1914 and discovered marked inhibitory effect of fungi (actinomycetes) on bacterial growth in 1939. In a subsequent year, he and his team members isolated an effective anti-TB antibiotic, actinomycin. However, soon the toxicity associated with this drug restricted its use in animals and humans. Continued screening of soil bacteria in Selman Waksman's laboratory led to the discovery of streptomycin (SM - purified from *Streptomyces griseus*) in 1943. Animal studies confirmed maximal inhibition of *MTB* with relatively low toxicity. Later on, it was November 20, 1944, when this antibiotic was administered for the first time to a critically ill TB patient. The effects were impressive, patients advanced disease was visibly arrested, the bacteria disappeared from his sputum, and he made a rapid recovery. However, a few months after healing, the patients' again showed lesion, which was later, discovered that bacteria had developed mutant strains resistant to antibiotic action. Moreover, it was also found to have side effects on the vestibular portion of cranial nerve VIII (the vestibulocochlear nerve) and nephrons. Nevertheless, SM was a ray hope due to the fact that *MTB* could be circumvented within the human body (<http://www.umdj.edu/ntbc/tbhistory.htm>).

Afterwards, Jorgen Lehman synthesised the para-amino salt of salicylic acid (PAS) with recognizable activity against clinical TB. Fortunately British Medical Research Council (BMRC) discovered the effectiveness of SM and PAS in combination, to prevent and cure acquired drug resistance, while performing one of the first randomised clinical trials comparing PAS or SM (alone and with the combination of both agents) during scarcity of SM. (Iseman, 2002). Subsequently, Lehman discovered iso-nicotinic acid hydrazide (isoniazid - INH) and its anti-TB activity (1952). Co-administration of INH with the combination of PAS and SM (triple therapy) showed predictable cures in 90–95% of patients (Iseman, 2002), solved the problem of resistance and finally accomplished a long-cherished goal of finding chemotherapeutic treatment to cure all the cases and visceral regions of tuberculosis. Notwithstanding, patient non-compliance due to a prolong administration of drugs for 12-24 months was a serious inconvenience to the effectiveness of the treatment regimen. Thereafter, ethambutol (EMB) was discovered (1962), which replaced PAS (from triple therapy) due to additional benefits of better tolerance than PAS and reduction in the

duration of treatment to 18 months. Then, major advancement in therapy of TB occurred with the introduction of rifampicin (RIF) (derived from *Streptomyces mediterranei*) in the year 1963. Extensive studies on RIF evidenced that addition of RIF to the combinations of INH, SM, EMB could give rise to predictable cures in 95% of cases with reduction in duration of therapy to just 8–9 months. This effect was found to be due to the ability of RIF to kill mycobacteria undergoing sporadic metabolism, the so-called "sterilizing effect". Later on, co-administration of pyrazinamide (PZA) with INH and RIF further helped to reduce the duration of therapy to 6 months with cure rates of almost 95 % (Iseman, 2002). Subsequently, various anti-TB drugs were discovered including cycloserine (1955), aminoglycosides such as capreomycin, viomycin, kanamycin and amikacin, and the newer quinolones (e.g. ofloxacin, ciprofloxacin, moxifloxacin, gatifloxacin) which were used only in drug resistance situations. Although, duration of TB therapy required for cure was reduced from 24 to 6 months, noncompliance or abandonment of treatment remained the prominent obstruction in the effectiveness of therapy. Since the major advancement in TB treatment, not much success was achieved in discovering new effective molecule for the betterment of TB therapy. Instead research was mainly focused on employing different strategies mostly involving manipulation in combination of drugs to reduce duration of therapy and associated side effects for better treatment of deadly TB.

During this period, India has also excellently contributed towards TB research in controlling TB globally. India was responsible for unraveling the essential principles of directly observed therapy (DOT) globally and its establishment in India. The principle behind this program was to avoid hospitalization of TB patients, which changed the management and care of TB patient's worldwide (Tyagi et. al., 2011). Globally, World Health Organization (WHO) endorsed DOT in a modified model called "DOTS" (directly observed therapy short course) which was launched in 1995. WHO specified five elements to Pursue high -quality DOTS expansion and enhancement program for the effective treatment, this includes: 1) Secure political commitment, with adequate and sustained financing; 2) Ensure early case detection, and diagnosis through quality-assured bacteriology; 3) Provide standardized treatment with supervision, and patient support; 4) Ensure effective drug supply and management; and 5) Monitor and evaluate performance and impact (WHO Global Tuberculosis Report, 2012). The strategy is based around short course treatment regimens for a minimum of six months. Patients are considered cured if they finish the treatment with negative sputum bacteriology.

Despite being assessed as cured, patients have been observed to develop recurrent disease. This was thought to result from relapse of the same infection and reinfection with a different strain of MTB (Cox et.al., 2008). There is abundant evidence that, when all the recommended procedures are in place, chemotherapy under DOTS can achieve cure rates of 90% or more, and prevent the emergence of resistance to first-line drugs (WHO Global Tuberculosis Report, 2012). Most recent progress in the TB therapy includes, USFDAs (U.S. Food and Drug Administration) approval to Sirturo (bedaquiline) on Dec. 28, 2013 as part of combination therapy to treat adults with multi-drug resistant pulmonary tuberculosis (TB) when other alternatives are not available

(<http://www.fda.gov/NewsEvents/Newsroom/PressAnnouncements/ucm333695.htm>). The overall journey of tuberculosis treatment using different antibiotics and their combination is tabulated in chronological order in Table 2.2. Moreover, reports from WHO indicated that various anti-TB drugs are under clinical trials and have been evaluated to boost the effectiveness of MDR-TB regimens (Table 2.3) (WHO Global Tuberculosis Report, 2012). A novel regimen that could be used to treat both drug-sensitive TB and MDR-TB and shortened duration of treatment has shown encouraging results in clinical trials and may help to reduce the burden of TB in the years to come.

**Table 2.2: Progress in Tuberculosis (TB) chemotherapy**

Year	TB Chemotherapeutic Progress	Duration of therapy
1944	Streptomycin (SM) and para-amino salicylic acid (PAS)	
1948	Randomised trial, SM versus PAS versus SM/PAS	
1952	Triple therapy, isoniazid (INH)/SM/PAS,	24 months
1960s	Ethambutol (EMB) replaces PAS - INH/PAS/SM	18 months
1970s	Rifampicin (RIF) added to INH/EMB/SM-RIF/ INH/EMB/SM	9 months
1980s	Pyrazinamide (PZA) added to INH/RIF - INH/RIF/PZA	6 months
Current Therapy - WHO DOTS	Cocktail of 4 first line agents - INH, RIF, PZA and EMB or SM. <i>Initially for 2 months for destruction of bacteria in all growing stage and then continuation with <b>INH and RIF</b> for 4 months to eliminate any residual bacteria</i>	6 months, MDR-TB requires 20 months course
	If above cocktail fails, second-line drugs, such as PAS, kanamycin, fluoroquinolones, capreomycin, ethionamide and cycloserine are used	
2013	USFDA approved, Sirturo (bedaquiline) as part of combination therapy to treat adults with multi-drug resistant pulmonary tuberculosis (TB) when other alternatives are not available.	NA

Despite the availability of an effective therapeutic regimen for TB, even today global burden of TB is not reduced, of which the credit goes to various shortcomings in the TB therapy such as: high dose, patient non-compliance (due to *frequent dosing regimens* of drugs, daily or several times a week) leading to emergence of multi drug resistance (MDR) and extensive drug resistance (XDR), costly treatment for MDR-TB, serious adverse effects and in certain cases reactivation of the infection and reinfection causing unsuccessful treatment of tuberculosis. Therefore, in the view of slow progress in drug discovery, an alternative formulation strategy of existing drugs play an important role in overcoming various drawbacks linked up with the current TB therapy.

If we look at all the drugs which are currently used for the treatment of TB, it can be clearly identified that, two (RIF and INH) of the four first-line drugs recommended for TB chemotherapy have been most widely investigated and therefore, RIF is selected for the current investigation (Esmaceli et.al., 2007). RIF is also associated with the drawbacks, which are mentioned in the above paragraph. In addition, less macrophage uptake, causing less concentration to reach at macrophages (where TB bacilli resides) and its non-localized delivery are another concerns with the current rifampicin therapy (Kumar et al., 2006). As rifampicin is a first line drug for the treatment of TB, many research groups have addressed these challenges by reporting different formulation strategies such as encapsulation of rifampicin in polymeric microparticles, nanoparticles and liposomes etc. where sustained release, improved intracellular delivery and high drug loading can be achieved (Booyesen et.al., 2013; Doan et.al., 2011 ; Esmaceli et.al., 2007 ; Pandey et.al., 2003 ; Vyas et.al., 2004). These systems are known to manipulate dose, dosing frequency, minimizing first pass metabolism by protecting drug inside the polymeric shell (Couvreur and Vauthier, 2006) and contributing toward protein binding, biodistribution, cellular uptake and immune response due to their various physicochemical properties. However, research is still underway to accomplish bountiful delivery system, using alternative route of administration. Thus, there is a therapeutic rationale for delivering RIF in suitable pulmonary mucosal delivery system to passively target alveolar macrophages, where a large number of tubercule bacilli harbor. Hence, we have chosen rifampicin to address the challenges associated with its current therapy. In "Doctors Dilemma", 'Bernard Shaws' has written that, "there is at bottom only one genuinely scientific treatment for all diseases, and that is to "Stimulate the phagocytes". "Drugs are a delusion." Likewise the current research was also focused on improving TB chemotherapy using RIF (drug) and immunomodulation using protein antigen (Ag85A) to stimulate phagocyte.

Table 2.3: New Anti-TB molecules in Preclinical and clinical trials

Compound	Target	Resistance mechanisms	Mechanism of action	Potential to shorten Treatment	Active against Latent TB	Active against MDR-TB	Useful in HIV infected with TB	Phase
<b>Fluoroquinolones</b>								
Moxifloxacin	DNA gyrase	Inhibition of DNA biosynthesis	<i>gyrA</i> mutations	Yes	Yes <sup>a</sup>	Yes	Yes	III
Gatifloxacin	DNA gyrase	Inhibition of DNA biosynthesis	<i>gyrA</i> mutations	Yes	Unknown	Yes	Yes	III
<b>Semisynthetic, derived from <i>Streptomyces mediterranei</i></b>								
High dose rifampin	$\beta$ -subunit of the RNA polymerase	Mutations in the <i>rpoB</i> gene that codes for the $\beta$ -subunit of the RNA polymerase	Inhibits $\beta$ -subunit of the RNA polymerase, a multisubunit enzyme that transcribes bacterial RNA	Yes	Yes but not first choice	Limited	Yes but not co-administered with protease inhibitors	II
High dose rifapentin	$\beta$ -subunit of the RNA polymerase	Mutations in the <i>rpoB</i> gene that codes for the $\beta$ -subunit of the RNA polymerase	Inhibits $\beta$ -subunit of the RNA polymerase, a multisubunit enzyme that transcribes bacterial RNA	Yes <sup>a</sup>	Yes	Limited	To be established	II
<b>Nitroimidazoxacines</b>								
PA-824	F420 dependent nitroreductase	Inhibition of proteins and cell wall biosynthesis	Rv0407, Rv3547, Rv3261 and Rv3262 mutations	Doubtful	Yes <sup>a</sup>	Yes	Unknown	II
OPC-67683	Nitroreductase	Inhibition of mycolic acid & cell wall biosynthesis	Rv3547 mutations	Yes <sup>a</sup>	Yes	Yes	Unknown	II

<b><i>Diarilquinolines</i></b>								
TMC207	ATP sintetase	Inhibition of ATP synthesis and disruption of membrane potential	<i>atp</i> E mutations	Yes <sup>a</sup>	Unknown	Yes	Unknown	II
<b><i>Dietilamins</i></b>								
SQ109	Unknown	Inhibition of cell wall biosynthesis	Unknown	Yes <sup>a</sup>	Unknown	Yes	Unknown	I/II
<b><i>Pyrrols</i></b>								
LL3858 (sudoterb)	Unknown	Unknown	Unknown	Yes <sup>a</sup>	Unknown	Yes	Unknown	I
<b><i>Oxazolidinediones</i></b>								
Linezolid	50s Ribosomal subunit	Inhibition of protein synthesis	23 rRNA mutation	Unknown	Unknown	Under research	Unknown	Lead optimization
<b><i>Other Molecules</i></b> – There are various other molecules those are in clinical or pre-clinical trials, although there is limited information available								
OPC-37306	Active against drug susceptible and resistant MTB strains, and appears to be more potent than RIF in mouse models							Pre clinical Stage
FAS20013	Claims that it can eliminate more than 99% of MTB (including latent bacilli) within 24 h. No resistant strains observed so far and a showed good pharmacokinetic profile.							
SQ-609	Interferes with cell wall synthesis but whose precise target has not been identified and							
SQ641	Inhibitor of translocase I, an enzyme required for cell wall peptidoglycan synthesis							

(**Source:** Janin et.al., 2007 ; Rivers and Mancera et.al., 2008 ; Boogaard et.al., 2009 ; Shi and Sugawara 2010; Bocanegra-Garcia et. al., 2011)

<sup>a</sup> from preclinical data).

## **2.6 Pulmonary mucosal delivery of vaccines and drugs - an alternative route**

### ***2.6.1 Anatomy of Lung***

The normal human lung weigh about 1 kg containing 40% to 50% of blood and is made up of nearly 50 distinct types of cells, of which at least 12 can be found in the airways. It is usually separated into three lobes on the right and two lobes on the left by pleural membranes. Traditionally, respiratory tract has been divided into the nasal cavities, oral airway (mouth to trachea), the tracheobronchial tree (typically Generations 0–3 or 6) and part of the alveolar region ranging from single alveolar cells to alveolar ducts. Whereas, functionally, it is divided into two zones viz. conducting zone (Generations 0-16) and the respiratory zone (Generation 17-23) for the exchange of gases (Effros 2006). Once air is inhaled, it passes through the "airways," (the nose and mouth) from the larynx to trachea, which then flows through dividing series of nearly 16 generations of conductive bronchi and bronchioles. Thereafter, alveoli begin to appear in the walls from 17<sup>th</sup> generation of bronchioles which are called as respiratory bronchioles, whereas, alveolar ducts (the entire walls of airways composed of alveoli) comes along by the 20<sup>th</sup> generation of airways, which are then end up at about 23<sup>rd</sup> generation in blind sacs. These blind sacs are lined with the alveoli and therefore are referred to as alveolar sacs. It is approximated that human lung consists of around 300 million alveoli with the surface area of almost 90 m<sup>2</sup> (Figure 2.8) (Effros 2006 ; Kleinstreuer et.al., 2008).

The pulmonary capillaries are separated from the alveolar air by a barrier constituting endothelial cells, interstitial space, and pulmonary epithelial cells (pneumocytes or alveolar cells). There are two types of alveolar cells, type I cells are very flat, with 0.2  $\mu$ m diameter over much of their surface and cover most of the alveolar surface, whereas type II cells are large, cuboidal shaped and contains lamellar bodies and microvilli, whose main function is to secrete surfactant. The type I and type II cells are able to further divide and produce more number of respective cells (Effros 2006). Moreover, airway membrane consisting of bronchial surface carries sub-mucosal glands and goblet cells, which are responsible for the secretion of mucous onto bronchial surface. Submucosal cells create a thin layer of electrolyte solution onto which a thick mucous layer rests. In addition, the presence cilia on top of the ciliated columnar cells in the airway membrane, helps in transporting mucous covering airway membrane towards mouth, where it is then swallowed. This process is called

as ‘mucociliary elevator’, which is mainly responsible for removal of foreign materials, those lands on the bronchial surfaces.

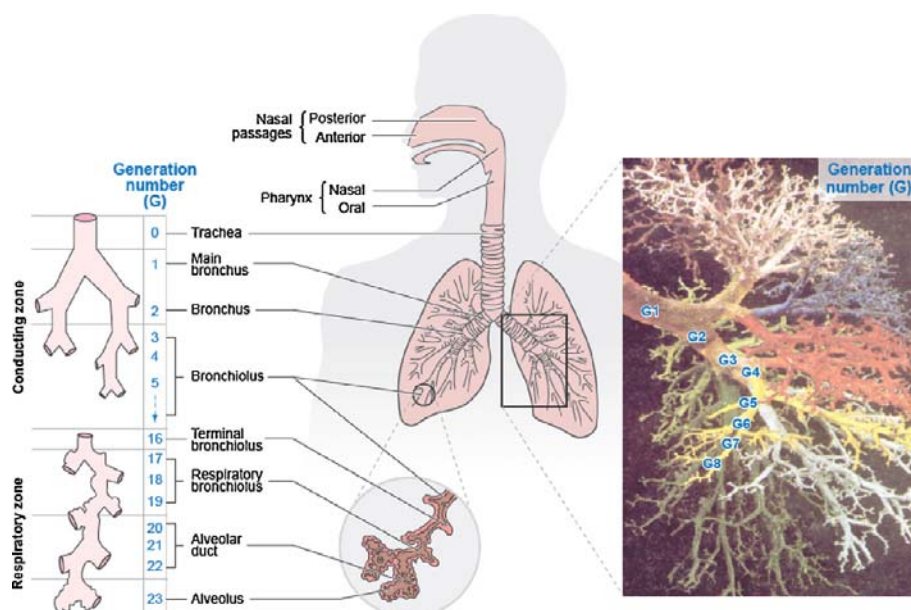


**Figure 2.8: Anatomy Human Lung (Reproduced from: Kleinstreuer et. al., 2008)**

### 2.6.2 Rational behind delivery of drug and vaccines to lungs

Advantages offered by the lungs makes it splendid alternative as noninvasive route of administration and therefore has achieved much attention of the pharmaceutical research community in the recent years. Advantages include : 1) large and highly absorptive surface area of the lung (80–120 m<sup>2</sup>), 2) suitable for a wide variety of substances from small molecules to very large proteins, 3) deliver high drug concentrations directly to the disease site, thus minimal risk of systemic toxicity, 4) extensively vascularized tissue, 5) thin alveolar epithelium, 6) speedy absorption of drug into the bloodstream causing rapid onset of pharmacological action, 5) avoidance of gastrointestinal degradation, 7) bypassing first-pass metabolism and 8) significant proteolytic activity of the lungs (Kammona et.al., 2012). Nevertheless, there are certain factors which obstruct the penetration of drugs into circulation, such as: thick lung surfactant layer in the air-blood barrier, a surface lining fluid, the epithelium cell monolayer, the interstitium and basement membrane and the vascular endothelium cell monolayer (Kammona et.al., 2012). Yet, advantages overweigh the drawbacks and therefore currently it is widely employed route for local (mucosal) delivery of vaccines and drugs.

Mucosal immunity is the primary defense mechanism against pathogens entering the body via mucosal surfaces. Mucosal immune system primarily functions - to protect the mucous membranes from potentially dangerous pathogen and their colonization, to prevent uptake of undegraded antigens (including proteins derived from ingested food, airborne particles and commensal microorganism) and thereby harmful immune responses generated due to them (Holmgren and Czerkinsky, 2005). The mucosal system consists of phenotypically and functionally distinct B-cells, T-cells and accessory cell sub-populations similar to that of systemic lymphoid tissues (Gallichan et.al., 1996 ; Belyakov et.al., 1999). Exposure to antigen or infection induces B cells in mucosal tissues, resulting the migration of B lymphocytes to the blood stream and other mucosal effector sites via regional lymph nodes and thoracic duct. This migration ensures the maintenance of secretory IgA production at other mucosal sites of mucosa associated lymphoid tissues (MALT - gut, nasal and genitourinary-associated lymphoid tissues etc.), which is denoted as the 'common mucosal immune system' (CMIS) (Mestecky J. 1987; Gallichan et.al., 1996; Holmgren and Czerkinsky, 2005). However, this migration appeared to have organ selectivity as enhanced memory was observed at the site of mucosal priming compared to that of distant mucosal sites. Figure 2.9 depicts immunization study carried out in humans using cholera toxin B subunit by different mucosal routes. Results indicated strongest response at the directly vaccine-exposed mucosa, whereas adjacent mucosae or specifically interconnected inductive-expression mucosa showed second-best responses (Bergquist et.al., 1997; Holmgren and Czerkinsky, 2005). These observations indicate the presence of CMIS, where immunological responses generated at one site may migrate immunity to other mucosal tissues rather than to systemic sites.

Moreover, T cell-mediated cytotoxicity in mucosa-associated tissues (T cell-mediated immunity) is also a critical component for protection against mucosal pathogens via clearance of virus at mucosal surfaces leading to reduced virus-related pathology (Gallichan and Rosenthal, 1996). It is believed that induction of general systemic immunity is another attractive feature of mucosal immunization, where the generation of secretory IgA as well as transudated IgG antibodies crosses epithelial membranes and prevents further entry of pathogens through the mucosal site (comparison of systemic and mucosal immunity is presented in Table 2.4). Gallichan and Rosenthal also reported long-lived cytotoxic T memory lymphocytes upon mucosal immunization than systemic one (Gallichan and Rosenthal, 1996). Hence, denseness of antigen presenting cells (APCs) like alveolar

macrophages (AMs), dendritic cells (DCs), B cells and bronchus associated lymphoid tissues makes lung an ideal site for induction of strong mucosal and systemic immune response and thus confirms the suitability of pulmonary mucosal vaccination. Therefore, there is a strong rationale in delivery of vaccine to the lungs.

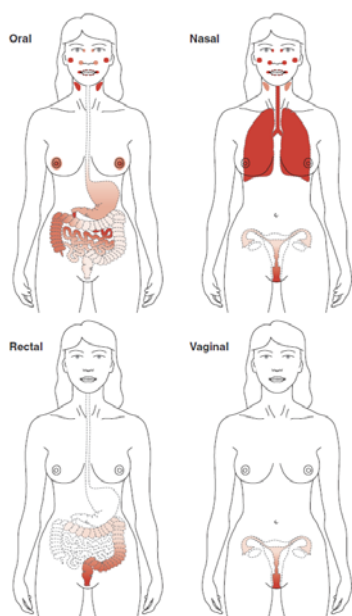


**Figure 2.9: Depiction of Common Mucosal Immune System**

Expression of mucosal IgA immune responses after different routes of vaccination.

**Oral** - gut mammary gland in lactating women ;  
**Nasal** - Nasal, Pulmonary and genito-vaginal ;  
**Rectal** - Rectal ; **Vaginal** – Vaginal.

*(Reproduced from Source:  
 Holmgren and Czerkinsky, 2005)*

**Table No. 2.4: Comparison of Systemic and Mucosal Immunity**

Systemic Immunity (Internal)	Mucosal Immunity (External)
<ul style="list-style-type: none"> <li>✓ Production of IgG and IgM</li> <li>✓ Invasive</li> <li>✓ Only systemic immune response</li> <li>✓ Boosts mucosal response</li> <li>✓ Small amount of antigen is enough</li> <li>✓ Sensitive to complex microbial antigen</li> </ul>	<ul style="list-style-type: none"> <li>✓ Production of IgA</li> <li>✓ Non-invasive</li> <li>✓ Both local as well as systemic immunity</li> <li>✓ Enhanced by parenteral priming</li> <li>✓ Needs more antigen to induce response</li> <li>✓ Mucosal adhesion is critical property</li> </ul>

Numerous pathogens (including respiratory, gastrointestinal, sexually transmitted agents e.g HSV and HIV) enter the body via various mucous membranes such as gastrointestinal tract, nose, lungs, eyes, urogenital tract, inner ear, and ducts of exocrine glands and initiate infection at mucosal surfaces. Of which 80 % of immunocytes are contributed by pulmonary, nasal and oral mucosal membranes. Among various infections, respiratory infections top's the list of 10 leading causes of death in low income countries (<http://who.int/mediacentre/factsheets/fs310/en/>). Likewise, TB is also an airborne disease

caused due to inhalation of tiny droplets (particles) generated by the infected person who have pulmonary or laryngeal TB disease. After infection, MTB traverse the mouth or nasal passages, upper respiratory tract, and bronchi to reach the alveoli of the lungs, where they occupy compartment vesicles of macrophages (Tuberculosis, Centre for Disease control and prevention, <http://www.cdc.gov/tb/topic/basics/default.htm>). In the view of involvement of lung, since initial entry of MTB to its localization in the macrophages and initiation of mucosal immune response, pulmonary delivery of vaccines & drugs would be most thoughtful option to combat the infection either by protective or therapeutic means (Holmgren and Czerkinsky, 2005). Hence, current research was envisaged to deliver drug and vaccine via pulmonary route of administration.

### ***2.6.3 Advances in pulmonary drug and vaccine delivery***

The lung has been recognized as a route of administration before thousands of years and inhalation was practiced in many parts of the world. The earliest recording of inhalation therapy is from ancient Egypt in 1554 BC, when Ebers Papyrys discovered inhalation of black henbane vapors for the treatment of breathlessness (Labiris & Dolovich 2003 ; Sanders 2008; Sanders 2011). He used to throw leaves of henbane onto hot bricks, causing henbane to vaporize alkaloid for the inhalation (without any device) by patient (Sanders 2011). Inhalation therapy was also practiced in India around 4000 years ago, in fact the Indians were the pioneer users of burnt Indian hemp (*Cannabis Indica*) for refreshment and sedation. Moreover, Indians were also used to smoke the leaves of the *Atropa belladonna* plant for suppression of cough. Afterward in the 19<sup>th</sup> and early 20<sup>th</sup> century, asthmatic people started smoking cigarettes containing stramonium powder mixed with tobacco (asthma cigarettes) to palliate the symptoms associated with their disease. However, the term inhaler was first used by the English physician Christopher Benet in 1654. Subsequently, immense research in the field led to the invention of first powered (pressurized) inhaler in France by Sales-Girons (1858) and later, Newton patented first apparatus for delivery of dry powder in 1864 in London. Since then tremendous progress has been made to develop various devices such as nebulizers, metered dose inhalers (MDI) and dry powder inhaler (DPIs) for delivery of therapeutics agents to lung (Chow et.al., 2007; Sanders 2008; Sanders 2011). Table 2.5 summarizes advancement along with the advantages and disadvantages of various inhalers.

Table 2.5: Advantages and Disadvantages and Advancements in different inhalers

Inhaler type →	Nebulizers (jet, ultrasonic)	Pressurized metered dose Compact inhalers (pMDI)	Dry powder inhalers (DPI)
<b>Advantages</b>	<ul style="list-style-type: none"> <li>▪ No specific inhalation technique or co-ordination required</li> <li>▪ Aerosolizes most drug solutions</li> <li>▪ Delivers large doses</li> <li>▪ Suitable for pediatric, geriatric, &amp; physically sick patients (those can't use other devices)</li> </ul>	<ul style="list-style-type: none"> <li>▪ Compact</li> <li>▪ Portable</li> <li>▪ Multidose (approximately 200 doses)</li> <li>▪ Inexpensive</li> <li>▪ Sealed environment (no degradation of drug)</li> <li>▪ Reproducible dosing</li> </ul>	<ul style="list-style-type: none"> <li>▪ Compact</li> <li>▪ Portable</li> <li>▪ Breath actuated</li> <li>▪ Easy to use</li> <li>▪ No hand-mouth co-ordination required</li> </ul>
<b>Disadvantage</b>	<ul style="list-style-type: none"> <li>▪ Time consuming</li> <li>▪ Bulky</li> <li>▪ Nonportable</li> <li>▪ Content contamination</li> <li>▪ Expensive</li> <li>▪ Poor delivery efficiency</li> <li>▪ Drug wastage</li> <li>▪ Wide performance variation between different models and operating conditions</li> </ul>	<ul style="list-style-type: none"> <li>▪ Special inhalation technique</li> <li>▪ patient co-ordination required</li> <li>▪ High oral deposition</li> <li>▪ Maximum dose of 5 mg</li> <li>▪ Suitable for limited range of drugs</li> </ul>	<ul style="list-style-type: none"> <li>▪ Respirable dose dependent on inspiratory flow rate</li> <li>▪ Humidity may cause powders to aggregate and capsules to soften</li> <li>▪ Dose loss if patient inadvertently exhales into DPI</li> </ul>
<b>Advanced Nebulizers</b>			
<ul style="list-style-type: none"> <li>▪ <b>Pari LC Star</b> (<i>Pari, Germany</i>): Reduce waste and improve delivery efficiency.</li> <li>▪ <b>Breath-actuated nebulizers e.g. AeroEclipse</b> (<i>Trudell Medical International, London, ON, Canada</i>): controls an actuator piston to produce aerosol in inspiration and at rest position in patient's expiration.</li> <li>▪ <b>Halolite</b> (<i>Medic-Aid Limited, West Sussex, UK</i>): Monitors a patient's breathing pattern in the first three breaths and then targets the aerosol delivery into the first 50% of each inhalation.</li> </ul>			
<b>Advanced Pressurized Metered Dose Compact Inhalers (pMDI)</b>			
<ul style="list-style-type: none"> <li>▪ <b>The Autohaler</b> (<i>3M Pharmaceuticals, Minnesota, USA</i>): Increased lung deposition from 7.2% with a conventional MDI to 20.8% of the dose using the breath activated pMDI.</li> <li>▪ <b>MD Turbo</b> (<i>Accentia Biopharmaceuticals, Tampa, Florida</i>): A new breath-activated, dose-counting inhaler: Helps to coordinate the press-and-breathe action needed for proper use of an inhaler apart from counting the remaining doses in the inhaler.</li> </ul>			
<b>Advanced Dry Powder Inhalers (DPI)</b>			
<ul style="list-style-type: none"> <li>▪ <b>Aspirair</b> (<i>Vectura, Wiltshire, UK</i>): Triggered by the patient's inhalation. It generates an aerosol plume significantly slower than most inhalers currently available. Aspirair reduces the amount of drug that is unintentionally deposited in the mouth and throat (leading to swallowing rather than reaching the lungs).</li> <li>▪ <b>Spiros</b> (<i>Dura pharmaceuticals, San Diego, CA</i>): A battery-driven propeller aids in the dispersion of powders.</li> <li>▪ <b>Inhance Pulmonary Delivery System</b> (<i>Nektar, San Carlos, CA</i>): A compressed air is being used to aerosolize the powder and then converts it into a standing cloud in a holding chamber, leading to generation of aerosol independent of patients' inspiratory effort.</li> </ul>			
<b>Reference: Lu D., 2008</b>			

While advancing inhalable pulmonary delivery of drugs, the potential of aerogenic vaccination with single or combined live vaccines for immunization in humans was uncovered in the Soviet Union (Aleksandrov and Gefen, 1958) and the United States (Eigelsbach, Tigertt, Saslaw *et al.*, 1962) around forty years ago, which was otherwise administered by parenteral routes such as subcutaneous and intramuscular (Hornick *et al.*, 1966; Lu D, 2008). The Russian investigators utilized live vegetative cells or spores of attenuated strains in a dry vaccine formulation for immunization in human and demonstrated the comparable effectiveness of aerogenic vaccination to that of subcutaneous vaccination against plague, tularemia, brucellosis and anthrax (Aleksandrov *et al.*, 1958; Aleksandrov and Gefen, 1959; Eigelsbach *et al.*, 1962; Cuts *et al.*, 1997). In 1968 at University of Illinois, Rosenthal *et al.*, nebulized BCGs to different age groups of people and reported useful information about aerosol vaccination & animal models and concluded that TB pathology in human beings was similar to that of guinea pigs rather than mice or rabbits (Rosenthal *et al.*, 1968).

All these years, immense research in the field of pulmonary delivery for the vaccination was carried out to identify its advantages and potential (Goonetilleke *et al.*, 2003 ; Kamath *et al.*, 2004 ; Zammit *et al.*, 2005; Zammit *et al.*, 2006; Lighter *et al.*, 2012). It is considered that antigen-specific CD8<sup>+</sup> T cells are important for vaccine-induced immunity, and therefore, many vaccine strategies have been developed to potentially evoke CD8<sup>+</sup> T cells. However, the scarcity of defined human and murine epitopes generated from vaccine candidates and their recognition by MHC class I-restricted CD8<sup>+</sup> T cells impaired their immunological evaluation (Kamath *et al.*, 2004). In a study, Santosuosso *et al.*, studied intranasal (IN) and intramuscular (IM) administration of AdAg85A in mice and found high numbers of Ag-specific CD4 and CD8 T cells in the airway lumen that were capable of IFN- $\gamma$  production and cytolytic activities after IN administration, these results were in contrast to the results obtained after IM dosing which resulted in activation of T cells (specifically, CD8 T cells), in the spleen and, to a lesser extent, in the lung interstitium. This indicated, T cell population in the airway lumen plays an important role in immune protection against pulmonary TB (Santosuosso *et al.*, 2005). Zammit *et al.*, also demonstrated localization of immune cells in an influenza murine model and claimed very less systemic migration of B cells and T cells (Lighter *et al.*, 2012; Zammit *et al.*, 2005; Zammit *et al.*, 2006). They reported localization of influenza-specific CD8-T cells within the respiratory tract due to cycling phenomenon

between the respiratory mucosa and the local lymph nodes and thus scarcely reaching the bloodstream or the peripheral lymphoid tissue, which may be credited to special anatomy of the lung lymphatic drainage (Zammit et.al., 2006 ; Zammit et.al., 2005). From the local pulmonary nodes, cells enter into the thoracic duct, which move along the pulmonary arterial blood to lung, due to their (triggered cells) ability to adhere to the vascular endothelium (which makes them to move back into the lung). Thus, cells remain localized at the site of infection, while, certain cells may reach to the systemic circulation. Thereafter, cells again move to the local nodes where they re-encounter antigen (Kamath et. al., 2004 ; Santosuosso et.al., 2005). This phenomenon suggested the localization of therapeutic molecule upon administration via pulmonary route.

The first successful clinical evaluation of pulmonary vaccination with aerosol device technology is a pulmonary measles immunization study conducted in Mexico on school children. Roughly 4 million children were exposed to aerosolic measles vaccine, achieving high level of successful prevention (Cutts et.al., 1997). The custom made Classical Mexican Device, (International Product Inc. - IPI jet nebulizer) driven by an Evans industrial air compressor and aerosols of the reconstituted Edmonston Zagreb strain of attenuated measles vaccine virus were delivered. The seroconversion produced using pulmonary delivery system was found to be higher (52-64%) as compared to subcutaneous administration (4-23% seroconversion) (Bennett *et al.*, 2002). Many children received a much higher dose for immunization than required without any side effects. Thereafter, WHO identified three nebulization devices manufactured by Omron, Trudell and Aerogen (meeting the desired performance criteria) to replace the classical Mexican device (Laube, 2005). Stability problems associated with reconstituted vaccines led to the emergence of pulmonary dry powder aerosol formulations which maintains physicochemical stability, as well as biological stability of measles vaccine formulation. Hence, vaccines and vaccine candidates ranging from whole bacilli to DNA sequences required some type of compounding or formulation in order to administer them to the airways.

Considering these facts, various researchers focused on the fabricating suitable delivery systems for a TB vaccine to successfully evoke localized protective immune response in the pulmonary and respiratory mucosal system by directly stimulating the antigen-presenting cells

in the respiratory epithelium and also achieving high local drug concentration by delivery them at the site of infection.

Advancements in pulmonary delivery devices and recombinant protein technology led to development of first DPI formulation containing peptide (Exubera) by Nektar/Pfizer, which was approved and released into the market in January 2006. However, it was immediately withdrawn from the market due to several reasons (bulky device, complex administration, contraindication in smokers and insufficient evidence with regulatory bodies regarding the patients preference of Exubera (inhaled dosage form) compared to other dosage forms) (Mark, 2007). Rigorous investigations by the pharmaceutical industry helped developing few more systems such as the AIR system (Alkermes/Eli Lilly), the Technosphere system (Mannkind) and Kos inhaled insulin (Kos Pharm/Abbott) for Type I/II diabetes, and Granulocyte-colony-stimulating factor (G-CSF) for Neutropenia (Amgen) (Kunda et.al., 2012). However, there is still need to further strengthen the research in pulmonary delivery of biopharmaceuticals, and thus many researchers are accomplishing this by delivering vaccine candidate and drug directly to the pulmonary and mucosal interface employing various novel delivery systems, formulation strategies and aerosol technologies.

### ***2.6.4 Polymeric carrier based delivery systems***

Difficulties in the delivery of drugs and antigens has motivated the development of micro and nanocarrier-based drug delivery systems, which are capable of maintaining therapeutic drug levels without side effects, give uniform dose distribution (among the alveoli in case of pulmonary delivery), delay drug residence time in the tissue to control its release, passing through the deleterious mucosal environment, and achieving mucosal immunity. Moreover, large surface area and increased saturation solubility favors their application in the field of drug and vaccine delivery. Generally **nanoparticles** (NPs) are referred to as particles having size range of 1-100 nm, however, NPs larger than 100 nm is prerequisite for delivery of therapeutic agents in order to achieve effective loading of active molecule (Sung et al., 2007). Employment of a several methods like encapsulation, dissolution, surface adsorption or chemical conjugation is currently being adopted for the nanoparticulate mucosal delivery of drugs and antigens.

In connection to the pulmonary delivery of NPs by inhalation, inhaled particles are carried with the tidal air through the respiratory system under the control of several mechanical forces (gravity, inertia, and impulse) and thus follow different trajectories from that of air stream lines. Hence, deposition of NPs in the airway occurs through - ***inertial impaction*** (particles do not change their path and with the change in airflow & bifurcations they gets impacted on the airway surface. Highly dependent on the aerodynamic properties of the particles, mostly happens with large particles), ***sedimentation*** (This means settling down of the delivered particles, which is generally observed in the bronchioles and alveoli), ***Interception*** (particles interact with the airway surface and is experienced when the particles are close to the airway wall. Mostly occurs due to particles size and shape,) and ***diffusion*** (particle transportation from a region of higher concentration to lower concentration. It is observed for particles less than 0.5  $\mu\text{m}$  in diameter and occurs in the regions where the airflow is low. Thus, highly dependent on the geometric diameter of the particles). In sum, overall movement of the particles in the airway depends on particle size, density, airflow, breathing rate, respiratory volume and the health of the individual (Heyder et.al., 2004, Kunda et.al., 2013). However, the particle deposition in the lungs is characterized by aerodynamic particle size, which is defined by the following equation -

$$da = dg \sqrt{\frac{\rho}{\rho_a}}$$

Where,  $da$  is the particle size,  $dg$  is geometric diameter,  $\rho$  is the mass density of the particle,  $\rho_a$  is the unit density ( $1 \text{ g/cm}^3$ ). It is postulated that, larger particles with the size more than  $10 \mu\text{m}$  are deposited by inertial impaction in the mouth, throat or sedimented in the bronchial region, smaller particles in the size range of 1 to  $5 \mu\text{m}$  ( $da$ ) also utilizes inertial impaction and sedimentation mechanism for deposition, however in this case they gets deposited in the respirable airways and the periphery of the lung & avoids throat, whereas very small particles less than  $1 \mu\text{m}$  ( $da$ ) are driven by diffusion, mostly remain suspended in the airways and are exhaled, thus no deposition occurs in the alveolar region (Sung et. al., 2007). Particles having diameter of less than  $100 \text{ nm}$  are able to deposit in the alveolar region of the lungs by diffusion mechanism, however, such delivery systems is difficult due to large amounts of energy required during production and tend to aggregate upon long storage because of high particle-particle interactions. Therefore, particles with aerodynamic diameter of 1 to  $5 \mu\text{m}$  have been shown to deposit optimally in the alveolar region of the lungs (Sung

et. al., 2007). In the recent years, various techniques of micro and nanoparticle preparation employing variety of polymers have been extensively investigated as vaccine delivery systems due to their enhanced phagocytosis leading to facilitated internalization and presentation of antigen in DCs and even as delivery systems to intelligently deliver drugs.

Over the past decades, large numbers of biodegradable materials of natural and synthetic origin have been utilized in controlled drug delivery for the formulation of micro and nanoparticles. They are either hydrophobic polymers synthesized chemically or amphiphilic macromolecules obtained from natural sources. The most widely investigated synthetic polymers include poly(lactic-co-glycolic acid), (PLGA), poly(alkylcyanoacrylate) (PACA), poly(butylcyanoacrylate) (PBCA), poly(ethylcyanoacrylate) (PECA), poly(caprolactone) (PCL), poly(lactic acid) (PLA), and poly(methacrylic acid-coethylacrylate) block co-polymer, whereas, albumin, chitosan, hyaluronan, gelatin, alginates and inorganic material like hydroxyapatite are categorized as natural polymers (Makadia et.al., 2011). Both the types of polymers present their own advantages and drawbacks. A detailed review on this is recently discussed (Hans et.al., 2002; Nair et al., 2007; Petkar et al., 2011). Amidst, chitosan and PLGA are most abundantly employed polymers in the vaccine and drug delivery systems, as both polymers are inert, biodegradable, biocompatible and non-toxic in nature and present unique characteristics for the formulation of vaccine and drug delivery systems.

### ***2.6.5 PLGA and Chitosan for pulmonary vaccine and drug delivery systems***

#### ***2.6.5.1 PLGA***

PLGA is a copolymer of poly lactic acid (PLA) and poly glycolic acid (PGA) and it is the best copolymeric elastomer available to date for vaccine and drug delivery with respect to design and performance of delivery systems (Makadia et.al., 2011). It is approved by the US FDA and European Medicine Agency (EMA) in various drug delivery systems in humans owing to its biodegradability, biocompatibility and safety. In addition, ease of preparation of micro/nanoparticles, drug-polymer compatibility, predictable drug release behavior, targeting ability make it widely acceptable material in vaccine and drug delivery (Petkar et al., 2011). Nevertheless, limitation in the application of synthetic polymers like PLGA (in the context of DNA/RNA and protein delivery), lies primarily in their negative charge, which confines the interaction with the negatively charged DNA, RNA and proteins (Merdan et.al., 2002; Luten et.al., 2008). Therefore, surface modification of PLGA using various poly-cations (including

chitosan) has been used to overcome this disadvantage, owing to the unique properties of chitosan.

Several studies have proved the application of PLGA in drug and vaccine delivery. Manca et.al., formulated PLGA, chitosan and PLGA/Chitosan microparticles (MPs) by emulsion or precipitation techniques, they observed best nebulization ability and stability from the formulation containing PLGA and chitosan (Manca et.al., 2008). Booysen et.al., developed rifampicin loaded PLGA nanoparticles using double emulsion solvent evaporation spray-drying technique and coated with 1% v/v polyethylene glycol (PEG) and concluded potential of the said delivery system for the improved of tuberculosis chemotherapy (Booyesen et.al., 2013). In an attempt to deliver vaccines to the lungs, Bivas-Benita et. al., evaluated the immunogenicity of a DNA vaccine encoding Rv1733c (*MTB* antigen) and explored the effect of pulmonary delivery and co-formulation with poly (D,L-lactide-co-glycolide) (PLGA)–polyethyleneimine (PEI) nanoparticles (NP) on host immunity. They ascertained that pulmonary priming with NP-adsorbed Rv1733c DNA followed by boosting with Rv1733c protein produced strongest immunogenicity, which indicated efficiency of PLGA–PEI NP as DNA vaccine delivery system to enhance T cell responses through pulmonary delivery in a DNA prime/protein boost vaccine regimen (Bivas-Benita et. al., 2009). Thus, increased immunity as measured by antibody and cytokine production confirmed the suitability of nanoparticulate carriers for the induction of immunity. Hence, considering the advantages of PLGA and its wide utility as delivery vehicle, the present research was undertaken using PLGA as a carrier system to encapsulate a model antigen Ag85A for pulmonary vaccine delivery in the TB.

### **2.6.5.2 Chitosan**

Chitosan, one of the most widely used natural polymer (polysaccharide) after cellulose, having similar structure to that of cellulose, as both are made up of linear  $\beta$ - (1 to 4)-linked monosaccharides. However, chitosan is different to that of cellulose due to presence of 2-amino-2-deoxy- $\beta$ -d-glucan combined with glycosidic linkages. From a regulatory perspective, it is important to state that chitosan received FDA GRAS status (Food and Drug Administration – Generally regarded as safe) to use as a common dietary supplement for preventing fat absorption and also in wound dressings (Hu et.al., 2013). The primary amine groups and primary as well as a secondary hydroxyl groups in its monomers affords chemical

modification of this polymer (Figure 2.10), which furnishes very special properties and makes it extensively used polymer in biomedical and pharmaceutical (including drug delivery) applications among all natural polymers. Unusual combination of biological activities plus mechanical and physical properties including presence of primary amine groups, positive charge, mucoadhesive nature and its ability to efficiently permeate across absorptive epithelia makes it more suitable in sustained and targeted drug delivery (Maurya et.al., 2008 ; Nafee et.al., 2007; Praveen et.al., 2011; Cho et.al., 2012; Agnihotri et. al., 2004). It has been also reported that chitosan particles interact with the mannose receptors of macrophages, which results in the phagocytosis of the particles in macrophages followed by the degradation of lysozymes and N-acetyl- $\beta$ -d-glucosaminidase in phagosomes, thus presenting inherent immunoadjuvant activity (Bianco et.al., 2000; Suh et al., 2000 ; Peluso et.al., 1994; Wen et.al., 2011).

Notwithstanding, one of the serious disadvantages of the chitosan is its poor water and organic solubility due to its crystalline structure leading to limited use in pharmaceutical and biomedical industry. Weakly basic nature of chitosan requires some amount of acid for the conversion of glucosamine units into the positively charged, water-soluble form. At neutral pH, chitosan molecules lose their charge and studies have shown that only protonated, soluble chitosan can open the tight junctions and augment the paracellular transport of hydrophilic mannitol (Kotze' et al., 1998a). Furthermore, solubility of chitosan in acidic environment demonstrates another limitation due to harmful effects of acid, while delivering bioactive materials like protein/peptides, DNA/RNA and anticancer drugs (Jang et. al., 2001). In addition, cumbersome methods of nanoparticle preparation (e.g. complexation-coacervation methods) usually involving crosslinking agent (e.g. tri-polyphosphate – TPP. Calcium chloride) poses another problem in the preparation of delivery systems (Agnihotri et. al., 2004 ; Bivas-Benita et.al., 2004; Salamanca et. al., 2006; Hu et.al., 2013).

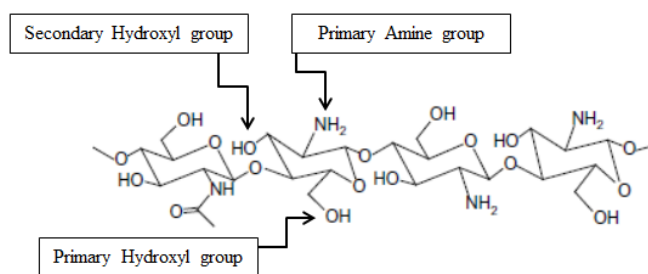


**Figure 2.10: Structure of chitosan**

In order to overcome these problems and avail the important features of chitosan, many studies have been undertaken either to enhance the solubility of chitosan in organic solvents and water by its chemical modification (as it would bring new and improved properties to chitosan without changing its basic skeleton and physicochemical and biochemical properties) (Maurya et.al., 2008 ; Jang et. al., 2001; Huang Y., et.al., 2010) or surface modification of synthetic polymers using chitosan and thus presenting characteristics of chitosan onto synthetic polymers for their improved application in vaccine and drug delivery (Danhier et.al., 2012). There are several chemically modified chitosan derivatives reported in the literature, these includes – Quaternized chitosan and N-alkyl chitosan, N-acyl chitosan, O-acyl chitosan, highly cationic derivative, hydroxyalkyl chitosan, carboxyalkyl chitosan, thiolated chitosan and sulfated chitosan, while certain miscellaneous modifications like sugar, cyclodextrin, dendrimers and crown ethers modified chitosan have been able to produce multifunctional chitosan (Holme et.al., 1997 ; Maurya et.al., 2008 ; Jang et. al., 2001; Huang Y., et.al., 2010). Such chemical modification give rise to wide range of chitosan derivatives leading to modified properties with applications in diversified areas of pharmaceutical, biomedical fields. Recently, Maurya et.al., have most beautifully elaborated modifications and applications of chitosan in their review (Maurya et.al., 2008). During these years, the potential applications of chitosan nanocarriers have been reported for varied areas including vaccine (vaccination-immunization) and drug delivery employing several routes of administration.

Several reports can be found in the literature stating application of chitosan nanoparticles in vaccine and drug delivery (Zhu et.al., 2008 ; ). Zhu et. al., developed biodegradable chitosan microspheres as novel delivery system for TB subunit vaccine to deliver a fusion protein made from three MTB genes (Ag85B–MPT64190–198–Mtb8.4 - AMM), and reported that fusion protein AMM incorporated in chitosan microspheres could elicit strong humoral and cell-mediated immune responses (Zhu et.al., 2008). Bivas-Benita et.al., formulated chitosan nanoparticles incorporating DNA plasmid encoding eight HLA-A\*0201-restricted T-cell epitopes and observed maturation of dendritic cells (DCs) and increased levels of IFN- $\gamma$  compared to pulmonary delivery of plasmid in solution (Bivas-Benita et. al., 2004).

Among the chitosan derivatives, quaternized chitosan derivative (N-Trimethylene chloride chitosan – TMC) has been extensively investigated for drug and vaccine delivery (Kotze' et al., 1999; Sayina et.al., 2009). In a study by Kotze' et al., they synthesized partially

quaternized derivative of chitosan with different degrees of quaternization [12.6% quaternized (TMC-Low) and 19.9% quaternized (TMC-High)] for enhanced water solubility. They reported more than 50 % enhancement in permeability (without any deleterious effect on cells) by opening tight junctions of intestinal epithelial cells to allow paracellular transport of hydrophilic molecule (Kotze' et al., 1999). In a study by Sayina et. al., they demonstrated suitability of (N-trimethyl chitosan–mono-N-carboxymethyl chitosan) TMC/MCC complex nanoparticles for nasal administration of tetanus toxoid (TT) and also evaluated its adjuvant property for the first time. TMC/MCC complex nanoparticles were shown to induce both the mucosal and systemic immune response indicating the potential of this newly developed system for mucosal immunization (Sayina et.al., 2009). In an attempt to synthesize hydrophobic chitosan derivative, Tien et.al., performed N-acylation of chitosan using various fatty acid (C6–C16) chlorides and noted some important changes in its structural features. They observed high stability of the monolithic tablets prepared using modified chitosan, which may be attributed to hydrophobic interactions between side chains. Moreover, they observed longer drug release times using chitosan with higher degrees of fatty chloride functionalization, suggesting application of palmitoyl chitosan as an excipients for controlled drug delivery system (Tien et.al., 2003). Likewise during the years, several research groups have focused on the modification of chitosan for better and useful properties in order to find out suitable chitosan derivative for drug and vaccine delivery (Jang et. al., 2001; Jiang et.al., 2006; Huang Y., et.al., 2010; Sonia et.al., 2011; Layek and Singh, 2012). Recently, Prabakaran and Mano have reviewed application of chitosan and its derivatives as controlled delivery systems (Prabakaran and Mano 2005).

Considering the reports available in the literature regarding benefits and limitations associated with the chitosan, we choose to work upon the modification of chitosan through acylation, its application in the preparation of nanoparticles for vaccine and drug delivery via pulmonary route of administration. Table 2.6, tabulates chitosan derivatives alongwith their recent application in drug/vaccine delivery systems. Thus, overall research work was undertaken to develop nanoparticulate delivery system for Ag85A and rifampicin for pulmonary delivery using modified chitosan and PLGA for better protective and therapeutic effect.

### ***2.7 Formulation Development of Nanoparticles***

As we discussed in the previous sections, formulation is an important part in determining the stability of vaccines (DNA, subunit antigens or live attenuated/inactivated vaccine strains) and drugs. Various formulation strategies have been developed to modulate and meet the required physicochemical properties so as to achieve desirable properties for pulmonary delivery. Such formulations (for drug and vaccine delivery) are made up of variety of components, which are prerequisite to exhibit better physicochemical characteristics and achieve better therapeutic profile. Nanoparticulate formulations in particular require drug or vaccine, polymer, adjuvants (for vaccine delivery) and stability excipients. **Adjuvants** are molecules, compounds or macromolecular complexes that boost the potency and longevity of specific immune response to antigens, but cause minimal toxicity & long lasting immunogenicity on their own and are often included in the vaccine preparation to evoke immune responses of poor immunogens. Broadly, adjuvants have been grouped into two classes, 'immunostimulatory adjuvant' and 'vaccine delivery systems'. Several adjuvants are reported in the literature including immunostimulant complexes (ISCOM), emulsions, oil adjuvants (Freund's complete/incomplete adjuvant), immunomodulation by modifying cytokine networks (lipopolysaccharide - LPS), monophosphoryl lipid A (MPL), lipopeptides, CpG motif, muramyl dipeptide (MDP), and delivery vehicles (liposomes, biodegradable polymer microparticles), which are intended to carry antigens for targeting APCs. The only approved adjuvant for humans is alum (potassium aluminum sulfate, aluminium hydroxide or aluminium phosphate gels) and hence, for the last many years, alum has been used as an adjuvant in several licensed vaccines (Pulendran et. al., 2010), which eliminate many cytotoxic properties of Incomplete Freund's adjuvant (IFA). Nevertheless, certain drawbacks like instability to freezing and drying, inconsistent and weak humoral immunity and certain safety concerns are questioning its efficacy as immunostimulator (Pulendran et. al., 2010). Therefore, micro or nano scaled vaccine delivery systems using polymers are under extensive research so as to replace existing adjuvants. Large numbers of natural and synthetic polymers have been widely investigated in the preparation of delivery systems for vaccines. Among them, PLGA and chitosan (including derivatives) have been recruited in the preparation of hundreds of micro or nanoparticle (NPs) formulations as a vehicle for myriad of vaccine candidates (discussed in the earlier section) (Peluso et.al., 1994). In addition, NPs offer an advantage for vaccine delivery systems by acting as adjuvants and aiding in activating both cellular and humoral immune responses.

Table 2.6: Nanoparticles prepared using modified chitosan derivatives

Chitosan Derivatives	Examples of Derivative (Application)	Formulation Example	Method of NP preparation	Model drug/vaccine	References
<b>Quaternized chitosan, alkyl chitosan</b>	Trimethyl chitosan chloride (TMC), N-propyl-N,N-dimethyl chitosan and N-furfuryl-N,N-dimethyl chitosan N-diethylmethylamino chitosan	TMC nanoparticles	Ionic gelation (Crosslinking using TPP)	monovalent influenza A subunit H3N2/surface antigen	Amidi et.al., 2007/ Subbiaha et.al., 2012
<b>N-acylchitosans</b>	Formyl, acetyl, propionyl, butyryl, hexanoyl, octanoyl, decanoyl, dodecanoyl, tetradecanoyl, lauroyl, myristoyl, palmitoyl, stearyl, benzoyl, monochloroacetyl, dichloroacetyl, trifluoroacetyl, carbamoyl, succinyl, acetoxycarbonyl (aspirin) (textiles, membranes, & med. aids)	N-acyl chitosan nanoparticles	self-aggregation	BSA as model protein	Cho et.al., 2012
<b>N-Carboxyalkyl / (aryl) chitosans</b>	N-Carboxymethyl chitosan (glycine glucan), N-carboxypropyl chitosan, N-carboxybenzyl, alanine glucan, phenylalanine glucan, tyrosine glucan, serine glucan, glutamic acid glucan, methionine glucan, leucine glucan (chromatographic media and metal ion collection)	TMC/MCC complex nanoparticles	Ionic gelation method	Tetanus toxoid (TT)	Sayina et.al., 2009
<b>O-Carboxyalkyl</b>	O-Carboxymethyl chitosan (OCMC), cross-linked O-carboxymethyl chitosans (molecular sieves, viscosity builders, and metal ion collection)	O-CMC nanoparticles	Ionic gelation method	Tetracycline	Maya et.al., 2012
<b>N-Carboxyacyl-chitosan</b>	From anhydrides such as maleic, succinic, itaconic, glutaric, trimellitic, pyromellitic, thiosuccinic, phthalic,	Oleoyl-carboxymethyl	Self-aggregation	Rifampicin	Li et.al., 2011

	cis-1,2,3,6-tetrahydrophthalic; 5-norbornyl-endo-2,3-dicarboxylic, acetylthiosuccinic, cyclohexane 1,2-dicarboxylic, diphenic, salicyl	chitosan NPs	and o/w emulsification using TPP		
<b>Thiolated chitosan</b>	Chitosan–cysteine conjugate, chitosan–thioglycolic acid (TGA), chitosan–4-thio-butylamidine, chitosan–2-iminothiolane conjugate	Thiolated chitosan NPs using TGA	Crosslinking using TPP	Theophylline	Lee et.al., 2006
<b>Sugar derivatives</b>	1-Deoxygalactac-1-yl-, 1-deoxyglucit-1-yl-, 1-deoxymelibit-1-yl-, 1-deoxylactit-1-yl-, 1-deoxylactit-1-yl-4-(2,2,6,6 tetramethylpiperidine-1-oxyl)-, 1-deoxy-60-aldehydolactit-1-yl-, 1-deoxy-60-aldehydomelibit-1-yl-, cellobiit-1-yl chitosans, products obtained from ascorbic acid	Chitosan-zinc sulphide:Mn nose (C:ZnS:Mn) nanocrystals	synthesis of C-ZnS nanocrystals (C-ZnS NCs) and mannosylation of the NCs	Carrier useful in targeting cancer cells	Jayasree et.al., 2011
<b>Metal ion</b>	chelates Palladium, copper, silver, iodine (catalyst, photography, health products, and insecticides)	Metal–chitosan nanocomposites	Chemical reduction of metal salts to yield the corresponding zero valent metal NPs with NaBH <sub>4</sub>	Silver (Ag), Gold (Au), Platinum (Pt), and Palladium (Pd)	Huang et.al., 2004
<b>Semisynthetic resins of chitosan</b>	Copolymer of chitosan with methyl methacrylate (CMM), resins of polyurea–urethane, poly(amide ester), chitosan acrylamide– maleic anhydride	CMM nanoparticles	Free radical polymerization of chitosan and methyl	Model protein - Insulin	Qian et.al., 2006

			methacrylate		
<b>Natural chitosan</b>	Glucans from various organisms (flocculation and metal ion polysaccharide chelation complexes)	Chitosan-DNA NPs	Complexation-coacervation method	pDNA encoding HLA-A*0201-restricted T-cell epitopes from <i>MTB</i>	Bivas-Benita et.al., 2004
<b>Miscellaneous</b>	<ul style="list-style-type: none"> <li>• Cyanoethyl chitosan (desalting, filtration, dialysis, and insulating papers).</li> <li>• Glycol chitosan (enzymology, dialysis, and special papers) Glutaraldehyde chitosan (enzyme immobilization).</li> <li>• Linoelic acid–chitosan complex (food additive and anticholesterolemic).</li> <li>• Uracylchitosan, theophylline chitosan, adenine chitosan, chitosan salts of acid polysaccharides, chitosan–streptomycin, N-cyclohexane chitosan, 2-amido-2,6-diaminoheptanoic acid chitosan Hydroxyalkyl chitosans, cyanoethyl chitosan Chitosan ascorbate ketimine and its reduced form (used to treat parodontopathies).</li> <li>• Imidazole chitosan (proposed for treatment of bone lesions).</li> <li>• Chemically cross-linked glycine glucan (suitable for collection of carrier-free radioisotopes).</li> <li>• <b>Sulfated chitosan (hemostatic).</b></li> <li>• Phosphorylated chitosan (metal chelation).</li> </ul>	Glycyrrhetic acid-modified sulfated chitosan NPs	Dialysis method for micelle formation	Doxorubicin	Tian et.al., 2012
<i>(Source: Modified and reproduced from the original source: Mourya et. al., 2008)</i>					

For the brevity of topic, nanoparticles preparation and characterization is discussed herein briefly. Different methods for the preparation of polymeric NPs have been employed depending upon its application and type of drug & vaccine candidate, wherein drug or vaccine candidates can either be encapsulated or surface adsorbed (Vauthier and Bouchemal, 2009). In brief, two main steps are involved in the preparation of nanoparticles. An emulsified system is prepared in the first step, while second step involves the formation of nanoparticle, which can be achieved by precipitation or the gelation of a polymer or by polymerization of monomer. In case of emulsions, mini-emulsions, nano-emulsions and microemulsions, NPs form at the same time while forming emulsified system. Whereas, other methods rely on precipitation of polymer (while formation of spontaneous dispersion) or self-assembly of macromolecules to form nanogels or polyelectrolyte complexes from a polymer solution (requires just a single step for the formation of NPs) (Vauthier and Bouchemal, 2009). In broad terms, NPs are prepared either by polymerization of monomer (emulsion polymerization and interfacial polymerization) or from preformed polymers (emulsification/solvent evaporation, solvent displacement and interfacial deposition, emulsification/solvent diffusion, salting out with synthetic polymers, nanoprecipitation of a polymer, gelation of the emulsion droplets, formation of polyelectrolyte complexes, nanoparticles from neutral nanogels and ionic gelation method) (Reis et.al., 2006 ; Vauthier and Bouchemal, 2009; Kumari et.al., 2010). More details on polymeric nanoparticles (methods of preparation, application and analysis) are reviewed elsewhere (Reis et.al., 2006 ; Vauthier and Bouchemal, 2009; Kumari et.al., 2010). In case of chitosan nanoparticles, literature suggests at least four methods for its preparation such as ionotropic gelation, microemulsion, emulsification solvent diffusion and polyelectrolyte complex (Tiyaboonchai, 2003). Table 2.8 enlists some of the advantages and disadvantages of each method. However, in the present research work, double emulsification solvent evaporation method was employed for the preparation of nanoparticles from modified chitosan and PLGA.

### ***2.8 Techniques for the preparation of Dry powders***

Usually NPs are obtained in the form of suspension, which is often associated with the problems related to aggregation and sedimentation of NPs leading to physicochemical instability, decreased or loss of biological activity of the drug, contamination, and degradation of the polymer due to hydrolysis. Therefore, conversion of NPs into dry powder form is a prerequisite for ease in storage and transportation of nanoparticulate formulations. In addition, it present potential benefits in - increasing stability during administration and safety by removing risk of

contamination and improved cost-effectiveness. Suspension of NPs can be transformed into dry powders using various commonly used methods such as freeze-drying, spray-drying (including nano spray drying), spray-freeze-drying and the super critical fluid technologies (Abdelwahed et.al., 2006; Byrappa et.al., 2008; Lee et.al., 2011; Kunda et.al., 2012). Table 2.9 highlights different methods for the preparation of dry powder along with their advantages and disadvantages.

### ***2.9 Characterization of Nanoparticulate formulations***

Characterization of the nanoparticulate drug/vaccine carrier systems is important to thoroughly understand the essential properties before launching it for particular pharmaceutical application. Characterization of nanoparticles can be done at two levels - 1) Physicochemical characterization (particle size (including aerodynamic particle size), size distribution, and surface properties - composition, charge, hydrophobicity) of the nanoparticles & 2) Biopharmaceutical characterization (drug encapsulation, in vitro drug/antigen release rates, *in-vitro* cell line studies and *in-vivo* studies revealing biodistribution, bioavailability, and efficacy of the drug/vaccine). The major techniques for the characterization of nanoparticulate delivery systems are summarized in Table 2.10.

Table 2.7: Methods of NP preparation and their advantages and disadvantages

Nanoparticles obtained by in-situ polymerization of a monomer
<p><b>Emulsion polymerization:</b></p> <p><i>Advantages:</i> i) Easy to obtain core-shell NPs. ii) Control the size of the NPs by surfactant. iii) Easily scalable</p> <p><i>Disadvantages:</i> i) Possible reaction between the drug and Ce VI in the case of radical emulsion polymerization. ii) Purification is needed</p>
<p><b>Interfacial polymerization :</b></p> <p><i>Advantages:</i> i) Low concentrations of surfactants. ii) Modulation of the nanocapsule thickness by varying the monomer concentration</p> <p><i>Disadvantages:</i> i) Limited to the encapsulation of lipophilic drugs. ii) Purification is needed</p>
NPs by Synthetic preformed polymers
<p><b>Emulsification/solvent evaporation:</b></p> <p><i>Advantages:</i> i) Encapsulate both hydrophilic and lipophilic drugs. <b>Disadvantages: i)</b> Coalescence of the nanodroplets during evaporation.</p>
<p><b>Solvent displacement and interfacial deposition:</b></p> <p><i>Advantages: i)</i> Simple technique. ii) High loading efficiencies (reported for lipophilic drugs).</p> <p><i>Disadvantages: i)</i> Limited to water-miscible solvents. ii) Applicable to lipophilic drugs only.</p>
<p><b>Emulsification/solvent diffusion:</b></p> <p><i>Advantages: i)</i> Possibility to control the size of the nanoparticles. ii) Easy to scale-up</p> <p><i>Disadvantages: i)</i> Leakage of water-soluble drug into the saturated-aqueous external phase. ii) High volumes of water to be eliminated</p>
<p><b>Salting out with synthetic polymers:</b></p> <p><i>Advantages: i)</i> Sensitive drugs can be used. ii) High loading efficiency. iii) Easy to scale-up.</p>

**Disadvantages:** i) Incompatibility between the salts and the drugs. ii) Purification is required to remove excess electrolytes.

#### Nano-precipitation of a polymer:

**Advantages:** i) Simple, fast & reproducible. ii) Requires less concentrations of surfactants. iii) Easy to scale-up

**Disadvantages:** i) Low polymer concentration in the organic phase.

#### Nanoparticles by gelation of the emulsion droplets:

**Advantages:** i) Natural macromolecules & hydrophilic drugs can be used. **Disadvantages:** i) Limited to hydrophilic drugs.

#### Polyelectrolyte complexes, self-aggregation:

**Advantages:** i) Easy to achieve. ii) Positively or negatively charged NPs can be synthesized based on nature of the polyelectrolyte. **Disadvantages:**

i) Need to optimize the ratio between negatively and positively charged molecules

#### Nanoparticles from neutral nanogels:

**Advantages:** i) No need of organic solvent. ii) Controlled release of the drug. **Disadvantages:** i) not yet applicable to hydrophilic drugs

#### Ionic gelation (one step):

**Advantages:** i) No need of organic solvent. ii) Action of a pH or variation in ion concentration may control the release of a drug. **Disadvantages:**

i) Possible particle disintegration due to weakness of the ionic interactions.

*(Compiled from Sources: Tiyaboonchai, 2003; Reis et.al., 2006 ; Vauthier and Bouchemal, 2009; Kumari et.al., 2010)*

Table 2.8: Methods for the preparation of dry powder formulations

Different Methods for the preparation of dry powder formulations	
Advantages	Disadvantages
<p><b>Freeze drying:</b> Removal of water from a frozen sample by sublimation and desorption under vacuum.  <b>Process:</b> 1) Freezing (solidification), 2) Primary drying (ice sublimation) and 3) Secondary drying (desorption of unfrozen water) (Abdelwahed et. al., 2006).</p>	
1) Preservation of primary physical and chemical characteristics of the product (elegant cake, short reconstitution time, low particle size distribution, unchanged activity of encapsulated drug), and 2) Long-term stability. 3) Oxidation is minimized due to high vacuum.	1) Slow and very expensive process. 2) Generates stress on products during freezing & drying. 3) Cryo-protectants required stabilizing the products to avoid aggregation and to ensure acceptable tonicity and reconstitution. 4) Hygroscopicity of the product.
<p><b>Spray-Drying:</b> Converts liquid feed (solution, suspension or colloidal dispersion) into dry particles by heating.  <b>Process:</b> 1) Atomization [rotary atomizers (centrifugal energy) and pressure nozzles (pressure energy) or two-fluid nozzle (kinetic energy)], 2) Spray-air contact (break the liquid into droplets and this spray comes into contact with a hot gas), 3) drying (rapid evaporation of the droplets to form dry particles) and 4) separation (dry particles are then separated from the hot gas with the help of a cyclone separator). (Kunda et.al., 2012; Lee et.al., 2011)</p>	
1) One-step process. 2) Simple, easily scalable & cost-effective. 3) suitable for heat sensitive products & 4) enables high drug loading	1) Degradation of macromolecules due to high shear stress in the nozzle and thermal stress while drying. 2) Bulky instrumentation
<p><b>Nano Spray Drying (NSD):</b> Nano Spray Dryer B-90 is 4<sup>th</sup> generation of laboratory scale spray dryer. Utilizes vibrating mesh technology for forming the droplets (spray meshes of 4<math>\mu</math>m, 5.5<math>\mu</math>m or 7<math>\mu</math>m).  <b>Process:</b> 1) Atomization (piezoelectric actuator), 2) Spray-air contact (break the liquid into droplets and this spray form comes into contact with a hot gas which works on a laminar flow principle), 3) drying (rapid evaporation of the droplets to form dry particles) and 4) separation (dry particles are then separated from the hot gas with the help of electrostatic precipitator). 5) Collection of fine particles with high efficiency is achieved with the novel electrostatic particle collector consisting of a cathode and anode (Lee et.al., 2011)</p>	
1) Needs less sample. 2) High yield. 3) generates particle size ranging from 300 nm to 5 $\mu$ m. 4) suitable for heat sensitive materials	1) Degradation of macromolecules during the process due to high shear stress in the nozzle. 2) Thermal stress while drying.

**Spray-freeze-drying (SFD):** Liquid feed is sprayed into a chamber containing cryogenic liquid such as nitrogen, oxygen or argon, which causes instant freezing of the droplets due to low boiling temperatures of cryogenic liquid, which are then collected and lyophilized to obtain dry particles.

**Process:** 1) Atomization. 2) Rapid freezing and 3) Lyophilisation. (Kunda et.al., 2012)

1) Produce particles with adjustable sizes as it is conducted at sub-ambient temperature. 2) Thermolabile polymers and highly potent biopharmaceuticals can be formulated into dry powder products

1) Stresses due to freezing and drying, cause irreversible damage to proteins (aggregation and loss of biological activity upon rehydration). 2) Loss of stability (unfolding and aggregation). 4) low efficacy, time consuming, and expensive process

**Supercritical fluids (SCF) Technology:** SCFs are compressed gases or liquids above their critical temperatures ( $T_c$ ) and pressures ( $P_c$ ).

**Process:** Two principals for particle formation, first employs SCF as a *solvent and other antisolvent*. **1) Drug is solubilized in SCF** & sudden decompression, passing the solution through an orifice and rapid expansion at low pressure leads to particle formation. **Method:** Rapid Expansion of a Supercritical Solution (RESS). **2) Drug is insoluble in SCF**, hence it is dissolved in an organic solvent and then precipitated by the SCF (antisolvent) (SCF is absorbed by the organic solvent, then expansion of the liquid phase and a decrease in the solvation power leads to particle formation. **Method:** Gas Anti-Solvent (GAS), Aerosol Solvent Extraction System (ASES), Supercritical Fluid Antisolvent (SAS), Precipitation with Compressed Antisolvent (PCA), Solution Enhanced Dispersion by Supercritical Fluids (SEDS), and supercritical fluid extraction of emulsion (SFEE). (Byrappa et.al., 2008)

1) Suitable for handling heat-labile & physically unstable drugs. 2) Particles formed in well-ordered fashion to achieve the desired morphology. 3) Negative effects on the macromolecules can be minimized. 4) Uniformity in terms of crystallinity, morphology, particle-size distribution and shape than jet milled particles.

1) Low yield. 2) Scale up operation may be troublesome. 3) Processing and maintenance of operating conditions are difficult due involvement of high pressures.



**Table 2.9: Major Techniques used for the Characterization of Nanoparticulate Drug/Vaccine Delivery System**

(Modified from Source: Petkar et. al., 2011)

Parameter	Techniques
Particle size	Photon correlation spectroscopy, scanning electron microscopy, transmission electron microscopy, small-angle X-ray scattering
Morphology	Scanning electron microscopy, transmission electron microscopy, electron spectroscopy for chemical analysis, secondary ion mass spectrometry, small-angle X-ray scattering, atomic force and scanning tunneling microscopy
Surface characteristics Charge	Laser doppler anemometry, electrophoresis, dielectricity. Hydrophobicity: hydrophobic interaction chromatography, contact angle
Physical state of the drug and polymer	Differential thermal analysis, differential scanning calorimetry, X-ray diffraction Molecular weight Gel-permeation chromatography
Drug loading	Classical analytical methods (UV, HPLC) after ultracentrifugation, ultrafiltration, gel filtration, or centrifugal ultrafiltration
Particle deposition in lung	Glass Twin Impinger, Cascade Impactor, Andersen Cascade Impactor, Next Generation Impactor, Multi Stage Liquid Impinger
Drug release	Dialysis, direct dilution + ultracentrifugation, ultrafiltration, or centrifugal ultrafiltration
Miscellaneous	Electron spectroscopy for chemical analysis, secondary in mass spectroscopy, dielectric measurements, small-angle X-ray scattering experiments, surface hydrophobicity, advanced microscopic techniques
In-vitro studies	Cell line cytotoxicity, Macrophage uptake studies etc.
Bioavailability, biodistribution, immunization	<b>Preclinical - Animal models</b> – Mice, Guinea Pigs, Rabbit, Non human primate & cattle. <b>Clinical</b> - Humans

(Ref: Cryan et.al., 2007; Copley Scientific, Quality solution for inhaler testing, 2012)

**References**

- Abdelwahed W., Degobert G., Stainmesse S., Fessi H. (2006) Freeze-drying of nanoparticles: Formulation, process and storage considerations, *Adv. Drug Delivery Rev.*, 58, 1688–1713.
- Aleksandrov N.I. and Gefen N.Y. (1958). A method of aerogenic (inhalation) immunization and possibilities of improving it. *VoyennoMeditsinsky Zh.*, 11.
- Aleksandrov N.I., Gefen N.E., Garin N.S., Gapochko K.G., Sergeev V.M., Smirnov M.S., Tamarin A.L. and Shliakhov E.N. (1959) Experiment of mass aerogenic vaccination of people against anthrax. *voenno-Med. Zhur.*, 8, 27-32.
- Amidi M., Romeijn S.G., Verhoef J.C., Junginger H.E., Bungener L., Huckriede A., Crommelin D.J., Jiskoot W. (2007) N-trimethyl chitosan (TMC) nanoparticles loaded with influenza subunit antigen for intranasal vaccination: biological properties and immunogenicity in a mouse model, *Vaccine*. 25, 1, 144-53.
- Andersen P., Andersen A.B., Sorensen A.L., Nagai S. (1995) Recall of longlived immunity to *Mycobacterium tuberculosis* infection in mice. *J Immunol*, 154, 3359–72.
- Bandermann S., Smith D., Bancroft G.J., Reyrat J-M., Soolingen D.V., Raupach B., Kaufmann S.H.E. (2005) Increased vaccine efficacy against tuberculosis of recombinant *Mycobacterium bovis* bacille Calmette-Guérin mutants that secrete listeriolysin, *J Clin Invest*. 115, 9, 2472–2479.
- Belyakov I.M., Moss B., Strober W., Berzofsky J.A., (1999). Mucosal vaccination overcomes the barrier to recombinant vaccinia immunization caused by pre-existing poxvirus immunity. *Proc Natl Acad Sci.*, 96(8), 4512-4517.
- Bergquist C., Johansson E-L., Lagergård T., Holmgren J., and Rudin A. (1997) Intranasal Vaccination of Humans with Recombinant Cholera Toxin B Subunit Induces Systemic and Local Antibody Responses in the Upper Respiratory Tract and the Vagina, *Infection and Immunity*, 65, 7, 2676–2684.
- Bivas-Benita M., Meijgaarden<sup>b</sup>, Meijgaarden K.E.V., Franken K.L.M.C., Borchard G., Ottenhoff T.M.H. and Annemieke G. (2004) Pulmonary delivery of chitosan-DNA nanoparticles enhances the immunogenicity of a DNA vaccine encoding HLA-A\*0201-restricted T-cell epitopes of *Mycobacterium tuberculosis*, *Vaccine*, 22, 13-14, 1609-1615.
- Bivas-Benita M., Lin M.Y., Bal S.M., Meijgaarden K.E.V., Franken K.L.M.C., Friggen A.H., Junginger H.E., Borchard G., Klein M.R., Ottenhoff T.M.H. (2009) Pulmonary delivery of DNA encoding *Mycobacterium tuberculosis* latency antigen Rv1733c associated to PLGA–PEI nanoparticles enhances T cell responses in a DNA prime/protein boost vaccination regimen in mice, *Vaccine*, 27, 30, 4010-4017.
- Bocanegra-García V., García A., Palma-Nicolás J.S., Palos I., and Rivera G. (2011). Antitubercular Drugs Development: Recent Advances in Selected Therapeutic Targets and Rational Drug Design, *Drug Development - A Case Study Based Insight into Modern Strategies*.

Dr. Chris Rundfeldt (Ed.), ISBN: 978-953-307-257-9, InTech, DOI: 10.5772/27735. Available from: <http://www.intechopen.com/books/drug-development-a-case-study-based-insight-into-modern-strategies/antitubercular-drugs-development-recent-advances-in-selected-therapeutic-targets-and-rational-drug-d> (Date Accessed March 2013).

Boogaard J.V.D., Kibiki G.S., Kisanga E.R., Boeree M.J. and Aarnoutse R.E. (2009) Problems, Progress, and Evaluation of Agents in Clinical Development, *Antimicrob. Agents Chemother.* 53,3, 849.

Booyesen L.L.I.J., Kalombo L., Brooks E., Hansen R., Gilliland J., Gruppo V., Lungenhofer P., Semete-Makokotlela B., Swai H.S., Kotze A.F., Lenaerts A., Plessis L.H. (2013) In vivo/in vitro pharmacokinetic and pharmacodynamic study of spray-dried poly-(dl-lactic-co-glycolic) acid nanoparticles encapsulating rifampicin and isoniazid, *International Journal of Pharmaceutics*, In Press.

Brennan M.J., Thole J. (2012) Tuberculosis Vaccines: A Strategic Blueprint for the Next Decade, *Tuberculosis*, 92S1, S6–S13.

Byrappa K., Ohara S., Adschiri T. (2008) Nanoparticles synthesis using supercritical fluid technology - towards biomedical applications, *Adv. Drug Delivery Reviews*, 60, 299-327.

Cardona P.J. (2006) RUTI: a new chance to shorten the treatment of latent tuberculosis infection. *Tuberculosis*, 86 (3-4), 273-89.

Cervantes-Villagrana A.R., Hernández-Pando R., Biragyn A. (2013) Prime-boost BCG vaccination with DNA vaccines based in  $\alpha$ -defensin-2 and mycobacterial antigens ESAT6 or Ag85B improve protection in a tuberculosis experimental model, *Vaccine*, 31, 676– 684.

Cho Y., Kim J.T., and Park H.J. (2012) Preparation, characterization, and protein loading properties of N-acyl chitosan nanoparticles, *J. of Applied Polymer Science*, 124,2, 1366-1372.

Chow A.H.L., Tong H.N.Y., Chattopadhyay P., and Shekunov B.Y. (2007) Particle Engineering for Pulmonary Drug Delivery, *Pharm. Res.* 24, 3, 411-437

Couvreur P., Vauthier C. (2006). Nanotechnology: intelligent design to treat complex 615 disease. *Pharm. Res.* 23, 1417–1450.

Cox H.S., Morrow M., Deutschmann P.W. (2008) Long term efficacy of DOTS regimens for tuberculosis: systematic review, *BMJ*, 336, 484-7.

Cryan S., Sivadas N., Garcia-Contreras L. (2007) In vivo animal models for drug delivery across the lung mucosal barrier, *Adv. Drug Delivery Rev.* 59 (2007) 1133–1151.

Cutts F.T., Clements C.J., and Bennett J. V. (1997) Alternative Routes of Measles Immunization: a Review, *Biologicals*, 25, 323–338.

Daniella de Souza Silva B., Batista da Silva E., Pereira do Nascimento I., Guerreiro dos Reis M.C., Kipnis A., Junqueira-Kipnis A.P. (2009) MPT-51/CpG DNA vaccine protects mice against *Mycobacterium tuberculosis*, *Vaccine* 27 (2009) 4402–4407.

Delogu G., and Fadda G. (2009) The Quest for a New Vaccine Against Tuberculosis, *J Infect Developing Countries*, 3(1), 5-15.

Doan T.V.P., Couet W., Olivier J.C. (2011) Formulation and in vitro characterization of inhalable rifampicin-loaded PLGA microspheres for sustained lung delivery, *International Journal of Pharmaceutics* 414, 112– 117.

Effros R.M. (2006) Anatomy, development, and physiology of the lungs, *GI Motility online* (2006) doi:10.1038/gimo73, Published 16 May 2006.  
<http://www.nature.com/gimo/contents/pt1/full/gimo73.html> (Date Accessed April 2013)

Eigelsbach H. T., Tulis J. J., Mcgavran M. H., White J. D. (1962) Live Tularemia Vaccine I. Host-Parasite Relationship In Monkeys Vaccinated Intracutaneously or Aerogenically, *J. Bacteriol.*, 84, 1020-1027.

Ernst J.D. (1998) Macrophage Receptors for *Mycobacterium Tuberculosis*, *Infection and Immunity*, 66, 4, 1277–1281.

Fine P.E. (1995) Variation in protection by BCG: implications of and for heterologous immunity, *Lancet*, 346, 8986, 1339–45.

Gallichan W.S., Rosenthal K.L. (1996). Long lived cytotoxic T lymphocytes memory in mucosal tissues after mucosal but not systemic immunization. *J.Exp.Med.*, 184(5),1879-1890.

Ge H., and Luo D. (2005) Preparation of carboxymethyl chitosan in aqueous solution under microwave irradiation, *Carbohydrate Research*, 340, 1351–1356.

Geluk A., Eeden V.S.J.F., Meijgaarden K.S.E., Dijkman K., Franken K.L.M.C., Ottenhoff T.H.M. (2012) A multistage-polyepitope vaccine protects against *Mycobacterium tuberculosis* infection in HLA-DR3 transgenic mice, *Vaccine*, 30, 52, 7513-7521.

George Bernard Shaw (1906) *The Doctor's Dilemma*, the Pennsylvania State University, Electronic Classics Series, Jim Manis, Faculty Editor, Hazleton, PA 18202-1291. Pp. 23.

Girard M.P., Fruth U., Kieny M.P. (2005) A review of vaccine research and development: Tuberculosis, *Vaccine*, 23, 5725–5731.

Goonetilleke N.P., McShane H., Hannan C.M., Anderson R.J., Brookes R.H., and Hill A.V.S. (2003) Enhanced Immunogenicity and Protective Efficacy Against *Mycobacterium tuberculosis* of Bacille Calmette Gue´rin Vaccine Using Mucosal Administration and Boosting with a Recombinant Modified Vaccinia Virus Ankara, *The Journal of Immunology*, 171, 1602–1609.

Grode L., Seiler P., Baumann S., Hess J., Brinkmann V., Eddine A.N., Mann P., Goosmann C., Gupta U.D., Katoch V.M., McMurray D.N. (2007) Current status of TB vaccines, *Vaccine*, 25, 3742–3751.

Gupta U.D. & Katoch V.M. (2009) Animal models of tuberculosis for vaccine development, *Indian J Med Res*, 129, 11-18.

Hajizadeh R., Sato H., Carlisle J., Nadaf M.T., Evans W., Shepherd B.E., Miller R.F., Kalams S.A., and Drake W.P. (2007) *Mycobacterium tuberculosis* Antigen 85A Induces Th-1 Immune Responses in Systemic Sarcoidosis, *Journal of Clinical Immunology*, 27, 4, 445.

Heyder J. (2004) Deposition of Inhaled Particles in the Human Respiratory Tract and Consequences for Regional Targeting in Respiratory Drug Delivery, *Proc Am Thorac Soc.*, 1, 1, 315–320.

Hoft D.F., Blazevic A., Stanley J., et.al. (2012) A recombinant adenovirus expressing immunodominant TB antigens can significantly enhance BCG-induced human immunity, *Vaccine*, 30, 2098–2108.

Holme K.R., Perlin A.S. (1997) Chitosan N-sulfate. A water-soluble polyelectrolyte, *Carbohydrate Research*, 302, 7-12.

Holmgren J., & Czerkinsky C. (2005). Mucosal Immunity and Vaccine. *Nat. Med.*, 11, S45-S53.

Hornick R.B., and Eigelsbach H.T.. (1966) Aerogenic Immunization of Man with Live Tularemia Vaccine, *Bacteriological Reviews*, 30, 3, 532-538.

Hu L., Sun Y., and Wu Y. (2013) Advances in chitosan-based drug delivery vehicles, *Nanoscale*, 2013, 5, 3103.

Huang H., Yuan Q., Yang X. (2004) Preparation and characterization of metal–chitosan nanocomposites, *Colloids and Surfaces B: Biointerfaces*, 39, 31–37.

Huang Y., Yu H., Guo L., Huang Q. (2010) Structure and Self-Assembly Properties of a New Chitosan-Based Amphiphile, *J. Phys. Chem. B*, 114, 7719-7726.

Iseman M.D. (2002) Tuberculosis therapy: past, present and future, *Eur Respir J*, 20, Suppl. 36, 87s–94s.

Jain A., Dixit P. (2008) Multidrug resistant to extensively drug resistant tuberculosis: What is next? *J. Biosci.* 33(4), 605–616.

Janin Y.L. (2007) Antituberculosis drugs: Ten years of research, *Bioorganic & Medicinal Chemistry*, 15, 2479–2513.

Jayasree A., Sasidharan S., Koyakutty M., Nair S., Menon D. (2011) Mannosylated chitosan-zinc sulphide nanocrystals as fluorescent bioprobes for targeted cancer imaging, *Carbohydrate Polymers*, 85, 37–43.

Jiang G., Quan D., Liao K., Wang H. (2006) Preparation of polymeric micelles based on chitosan bearing a small amount of highly hydrophobic groups, *Carbohydrate Polymers*, 66, 514–520.

Kamath, A.T., Groat, N.L., Bean, A.G. and Britton, W.J. (2000). Protective effect of DNA immunization against mycobacterial infection is associated with the early emergence of interferon-gamma-secreting lymphocytes. *Clin. Exp. Immunol.*, 120(3), 476-82.

Kamath, A. B., J. Woodworth, X. Xiong, C. Taylor, Y. Weng, S. M. Behar. (2004). Cytolytic CD8<sup>+</sup> T cells recognizing CFP10 are recruited to the lung after *Mycobacterium tuberculosis* infection. *J. Exp. Med.* 200: 1479-1489.

Kammona O., Kiparissides C. (2012) Recent advances in nanocarrier-based mucosal delivery of biomolecules, *Journal of Controlled Release*, 161, 781–794.

Kaufmann S.H.E, Hussey G., Lambert P-H. (2010) New vaccines for tuberculosis, *The Lancet*, 375, 2110-2119.

Kellaway I.W. and Farr S.J. (1990) Liposomes as drug delivery systems to the, *Advanced Drug Delivery Reviews*, 5, 149, 149-161.

Kernodle S.D. and Bochan R.M. (2012) Pro-apoptotic bacterial vaccines to enhance cellular immune responses, *European Patent 1361794 B1*, Jan 25.

Kleinstreuer C., Zhang Z., Li Z. (2008) Modeling airflow and particle transport/deposition in pulmonary airways, *Respiratory Physiology & Neurobiology*, 163, 128–138.

Kotze' A.F., Thanou M.M., Luessen H.L., De Boer B.G., Verhoef J.C., Junginger H.E. (1999). Effect of the degree of quaternization of N-trimethyl chitosan chloride on the permeability of intestinal epithelial cells (Caco-2). *Eur. J. Pharm. Biopharm*, 47,3, 269–274.

Kotze', A.F., Luessen, H.L., De Boer, A.G., Verhoef, J.C., Junginger, H.E. (1998a). Chitosan for enhanced intestinal permeability: prospects for derivatives soluble in neutral and basic environment. *Eur. J. Pharm. Sci*, 7, 145–151.

Kumar P.V., Asthana A., Dutta T., Jain N.K. (2006) Intracellular macrophage uptake of rifampicin loaded mannosylated Dendrimers, *J Drug Targeting*, 14 (8) 546-556.

Kumari A., Yadav S.K., Yadav S.C. (2010) Biodegradable polymeric nanoparticles based drug delivery systems, *Colloids and Surfaces B: Biointerfaces*, 75, 1–18.

Kunda N.K., Somavarapu S., Gordon S.B., Hutcheon G.A., Saleem I.Y. (2013) Nanocarriers Targeting Dendritic Cells for Pulmonary Vaccine Delivery, *Pharm Res.*, 30,325–341.

Kwan C.K., and Ernst J.D. (2011) HIV and Tuberculosis: a Deadly Human Syndemic, *Clin Microbiol Rev.* 24(2), 351–376.

Labiris N. R., & Dolovich M. B. (2003) Pulmonary drug delivery. Part II: The role of inhalant delivery devices and drug formulations in therapeutic effectiveness of aerosolized medications, *Br J Clin Pharmacol* 56, 600–612.

Layek B., Singh J. (2012) N-hexanoyl, N-octanoyl and N-decanoyl chitosans: Binding affinity, cell uptake, and transfection, *Carbohydrate Polymers*, 89, 403– 410.

Lee D., Shirley S.A., Lockey R.F., and Mohapatra S.S. (2006) Thiolated chitosan nanoparticles enhance anti-inflammatory effects of intranasally delivered theophylline, *Respiratory Research*, 2006, 7, 112.

Lee S.H., Heng D., Ng W.K., Chan H., Tan R.B.H. (2011) Nano spray drying: A novel method for preparing protein nanoparticles for protein therapy, *International Journal of Pharmaceutics*, 403, 192–200.

Leroux-Roels I., Forgue S., Boever F.D. (2013) Improved CD4<sup>+</sup> T cell responses to *Mycobacterium tuberculosis* in PPD-negative adults by M72/AS01 as compared to the M72/AS02 and Mtb72F/AS02 tuberculosis candidate vaccine formulations: A randomized trial, *Vaccine*, 19, 31, 2196-206.

Li Y., Zhanga S., Menga X., Chenb X., Rena G. (2011) The preparation and characterization of a novel amphiphilic oleoyl-carboxymethyl chitosan self-assembled nanoparticles, *Carbohydrate Polymers*, 83, 130–136.

Lighter J., and Fisher J. (2013) Tuberculosis vaccine and method of using same US Patent Number 8394389 B2.

Lin P. L., Dietrich J., Tan E. (2012) The multistage vaccine H56 boosts the effects of BCG to protect cynomolgus macaques against active tuberculosis and reactivation of latent *Mycobacterium tuberculosis* infection, *J. Clin Invest.* 122(1), 303–314.

Lowrie D.B., Tascon R.E., Colston M.J., and Silva C.L. (1994) Towards a DNA vaccine against tuberculosis, *Vaccine*, 12, 1537.

Lowrie D.B., Silva C.L., Colston M.J., Ragno S., and Tascon R.E. (1997) Protection against tuberculosis by a plasmid DNA vaccine, *Vaccine*, 15, 834.

Lowrie D.B. (2006) DNA vaccines for therapy of tuberculosis: Where are we now? *Vaccine*, 24, 1983–1989.

Lu D. (2007) Aerosol Delivery of Recombinant Antigen 85B in Microparticle Vaccine Systems for Protection against Tuberculosis, Chapel Hill, NC. PhD Dissertation.

Mack G.S. (2007) Pfizer dumps Exubera. *Nat Biotech.*, 25, 1331–2.

Martin C., Williams A., Hernandez-Pando R., Cardona P.J., Gormley E., Bordat Y., Soto C.Y., Clark S.O., Hatch G.J., Aguilar D., Ausina V., Gicquel B. (2006) The live *Mycobacterium tuberculosis phoP* mutant strain is more attenuated than BCG and confers protective immunity against tuberculosis in mice and guinea pigs, *Vaccine*, 24, 3408–3419.

Maya S., Indulekha<sup>1</sup> S., Sukhithasri V., Smitha K.T., Nair S.V., Jayakumar R., Biswas R. (2012) Efficacy of tetracycline encapsulated O-carboxymethyl chitosan nanoparticles against intracellular infections of *Staphylococcus aureus*, *International Journal of Biological Macromolecules*, 51, 392– 399.

Meerak M., Wanichwecharungruang S.P., Palaga T. (2013) Enhancement of immune response to a DNA vaccine against *Mycobacterium tuberculosis* Ag85B by incorporation of an autophagy inducing system, *Vaccine*, 31, 784– 790.

Mestecky J. (1987) The common mucosal immune system and current strategies for induction of immune responses in external secretions, *J Clin Immunol.* 7, 4, 265-76.

Nor N.M., Musa M. (2004) Approaches towards the development of a vaccine against tuberculosis: recombinant BCG and DNA vaccine, *Tuberculosis*, 84, 102–109.

Ohara N., Matsuoka M., Nomaguchi H., Naito M., Yamada T. (2001) Protective responses against experimental *Mycobacterium leprae* infection in mice induced by recombinant *Bacillus Calmette-Guérin* over-producing three putative protective antigen candidates, *Vaccine*, 19, 15–16, 1906-1910.

Okada M., Kita Y., Nakajima T. et.al., (2007) Evaluation of a novel vaccine (HVJ-liposome/HSP65 DNA+ IL-12 DNA) against tuberculosis using the cynomolgus monkey model of TB, *Vaccine*, 25, 2990–2993.

Olsen AW, van Pinxteren L, Okkels LM, Rasmussen PB, Andersen P. (2001) Protection of mice with a tuberculosis subunit vaccine based on a fusion protein of Antigen 85B and ESAT-6. *Infect Immun*, 69, 2773–8.

Orme I.M. (2006) Preclinical testing of new vaccines for tuberculosis: A comprehensive review, *Vaccine*, 24, 2–19.

Ottenhoff T.H.M., Kaufmann S.H.E. (2012) Vaccines against Tuberculosis: Where Are We and Where Do We Need to Go? *PLoS Pathog* 8(5): e1002607.

Pandey R., Zahoor A., Sharma S., Khuller G.K. (2003) Nanoparticle encapsulated antitubercular drugs as a potential oral drug delivery system against murine tuberculosis, *Tuberculosis*, 83, 373–378.

Peluso G., Petillo O., Ranieri M., Santin M., Ambrosio L., Calabro D., Avallone B., Balsamo G. (1994) Chitosan-mediated stimulation of macrophage function, *Biomaterials*, 15 (15) 1215–1220.

Prabaharan M. and Mano J. F. (2005) Chitosan-Based Particles as Controlled Drug Delivery Systems, *Drug Delivery*, 12, 41–57.

Prescott, L.M., Harley J.P., Klein, D.A. (1999c). *Microbiology*, 4<sup>th</sup> edition. WGB/McGraw-Hill, Boston, p 141.

Pulendran B., Powell J., Flavell R.A. (2010) Modulating Vaccine Responses with Innate Immunity: In: Levine MM, editor. *New generation vaccines*, 4<sup>th</sup> Edition, NY, USA, Informa Healthcare, p. 183-190.

Pym, A.S., Brodin, P., Majlessi, L., Brosch, R., Demangel, C., Williams, A., Griffiths, K.E., Marchal, G., Leclerc, C. and Cole, S.T. (2003) Recombinant BCG exporting ESAT-6 confers enhanced protection against tuberculosis, *Nat Med.*, 9,5, 533-9.

Qian F., Cui F., Ding J., Tang C., and Yin C. (2006) Chitosan Graft Copolymer Nanoparticles for Oral Protein Drug Delivery: Preparation and Characterization, *Biomacromolecules*, 7, 2722 – 2727.

Reis C., Neufeld R.J., Ribeiro A.J., Veiga F. (2006) Nanoencapsulation I. Methods for preparation of drug-loaded polymeric nanoparticles, *Nanomedicine: Nanotechnology, Biology, and Medicine*, 2, 8– 21.

Rivers E.C. and Mancera R.L. (2008) New anti-tuberculosis drugs in clinical trials with novel mechanisms of action, *Drug Discovery Today*, 13, 23/24, 1090-1098.

Ronning D.R., Vissa V., Besra G.S., Belisle J.T., Sacchettini J.C. (2004) *Mycobacterium tuberculosis* Antigen 85A and 85C Structures Confirm Binding Orientation and Conserved Substrate Specificity, *The Journal of Biological Chemistry*, 279, 35, 36771–36777.

Rosenthal S.R., McEnery J.T. and Raisys N. (1968). Aerogenic BCG vaccination against tuberculosis in animal and human subjects. *J Asthma Res.*, 5, 4, 309-23.

Rowland R., and McShane M. (2012) Tuberculosis vaccines in clinical trials, *Expert Rev Vaccines*, 10(5), 645–658.

Sambandamurthy V.K. and Jacobs W.R. Jr. (2005) Live attenuated mutants of *Mycobacterium tuberculosis* as candidate vaccines against tuberculosis, *Microbes and Infection*, 7, 955–961.

Sambandamurthy V.K., Derrick S.C., Hsu T., et al. (2006) *Mycobacterium tuberculosis* Delta RD1 Delta pan CD: a safe and limited replicating mutant strain that protects immunocompetent and immunocompromised mice against experimental tuberculosis. *Vaccine*, 24, 6309–20.

Sanders M. (2007) Inhalation therapy: an historical overview, *Primary Care Respiratory Journal*, 16, 2, 71-81.

Santosuosso, M., X. Zhang, S. McCormick, J. Wang, M. Hitt, Z. Xing. (2005). Mechanisms of mucosal and parenteral tuberculosis vaccinations: adenoviral-based mucosal immunization preferentially elicits sustained accumulation of immune protective CD4 and CD8 T cells within the airway lumen. *J. Immunol.*, 174, 7986-7994.

Sayina B., Somavarapu S., Li X., Sesardic D., Senela S., Alpar O.H. (2009) TMC–MCC (N-trimethyl chitosan–mono-N-carboxymethyl chitosan) nanocomplexes for mucosal delivery of vaccines, *European Journal of Pharmaceutical Sciences*, 38, 362–369.

Schluger N.W., and Rom W.N. (1998) The Host Immune Response to Tuberculosis, *Am J Respir Crit Care Med*, 157, 679–691.

Shi R., Sugawara I. (2010) Development of new anti-tuberculosis drug candidates, *Tohoku J Exp Med.*, 221, 2, 97-106.

Smyth H.D.C. and Hickey A.J. (Eds) Controlled pulmonary drug delivery In *Advances in delivery science and Technology*. Controlled Release Society, pp. 51.

Sonia T. A., Rekha M. R., Sharma C.P. (2011) Bioadhesive Hydrophobic Chitosan Microparticles for Oral Delivery of Insulin: In Vitro Characterization and In Vivo Uptake Studies, *Journal of Applied Polymer Science*, 119, 2902–2910.

Sorensen A.L., Nagai S., Houeu G., Andersen P. (1995) Purification. Characterization a low molecular mass T-cell antigen secreted by *Mycobacterium tuberculosis*. *Infect Immun.*, 63, 1710-7.

Subbiaha R., Ramalingam P., Ramasundaram S., Kimb D.Y., Parkb K., Ramasamy M.K., Choid K.J. (2012) N,N,N-Trimethyl chitosan nanoparticles for controlled intranasal delivery of HBV surface antigen, *Carbohydrate Polymers*, 89, 1289– 1297.

Sun R., Skeiky Y.A.W., Izzo A. et.al., (2009) Novel recombinant BCG expressing perfringolysin O and the over-expression of key immunodominant antigens; pre-clinical characterization, safety and protection against challenge with *Mycobacterium tuberculosis*, *Vaccine*, 27, 4412–4423.

Sung J.C., Pulliam B.L., Edwards D.A. (2007) Nanoparticles for drug delivery to the Lungs, *TRENDS in Biotechnology*, 25,12, 563-570.

Tanghe A., D'souza S., Rosseels V., Denis O., Ottenhoff T.H.M., Dalemans W., Wheeler C., Huygen K. (2001) Improved Immunogenicity and Protective Efficacy of a Tuberculosis DNA Vaccine Encoding Ag85 by Protein Boosting, *Infection And Immunity*, 69, 5, 3041–3047.

Tian Q., Wang X., Wang W., Zhang C., Wang P., Yuan Z., (2012) Self-assembly and liver targeting of sulfated chitosan nanoparticles functionalized with glycyrrhetic acid, *Nanomedicine: Nanotechnology, Biology, and Medicine*, 8, 870–879.

Tien C.L., Lacroix M., Ispas-Szabo P., Mateescu M. (2003) N-acylated chitosan: hydrophobic matrices for controlled drug release, *Journal of Controlled Release*, 93, 1– 13.

Tiyaboonchai W. (2003) Chitosan Nanoparticles: A Promising System for Drug Delivery, *Naresuan University Journal*, 11, 3, 51-66 51.

Tyagi A.K., Nangpal P., Satchidanandam V. (2011) Development of vaccines against tuberculosis, *Tuberculosis*, 91, 469e478.

Vauthier C., and Bouchemal K. (2009), Methods for the Preparation and Manufacture of Polymeric Nanoparticles, *Pharm Res.*, 26,5,1025-1058.

Vipond J., Vipond R., Allen-Vercoe E., Clark S.O., Hatch G.J., Gooch K.E., Bacon J., Hampshire T., Shuttleworth H., Minton N.P., Blake K., Williams A., Marsh P.D. (2006) Selection of novel TB vaccine candidates and their evaluation as DNA vaccines against aerosol challenge, *Vaccine*, 24, 6340–6350.

Vyas S.P., Kannan M.E., Jain S., Mishra V., Singh P. (2004) Design of liposomal aerosols for improved delivery of rifampicin to alveolar macrophages *International Journal of Pharmaceutics*, 269, 1, 37-49.

Wang Q., Sun S., Hu Z., Yin M., Xiao C., Zhang J. (2004) Improved immunogenicity of a tuberculosis DNA vaccine encoding ESAT6 by DNA priming and protein boosting, *Vaccine*, 22, 3622–3627.

Wen Z., Xu Y., Zou X., Xu Z. (2011) Chitosan Nanoparticles Act as an Adjuvant to Promote both Th1 and Th2 Immune Responses Induced by Ovalbumin in Mice, *Mar. Drugs*,9, 1038-1055.

Xing Z., McFarland C.T., Sallenave J-M. (2009) Intranasal Mucosal Boosting with an Adenovirus-Vectored Vaccine Markedly Enhances the Protection of BCG-Primed Guinea Pigs against Pulmonary Tuberculosis, *PLoS ONE*. 2009; 4(6): e5856.

Yadav D., Khuller G.K. (2001) Evaluation of immune responses directed against 30 kDa secretory protein of *Mycobacterium tuberculosis* H37Ra complexed in different adjuvants. *Indian J Exp Biol*, 39,12, 1227–34.

Zammit D.J., Cauley L.S., Pham Q-M., and Lefrançois L. (2005) Dendritic Cells Maximize the Memory CD8 T Cell Response to Infection. *Immunity*, 22, 5, 561–57.

Zammit D.J., Turner D.L., Klonowski K.D., Lefrançois L., and Cauley L.S. (2006) Residual Antigen Presentation after Influenza Virus Infection Affects CD8 T Cell Activation and Migration, *Immunity*. 24, 4, 439–449.

Zhu B., Qie Y., Wang J., Zhang Y., Wang Q., Xu Y., Wang H. (2008) Chitosan microspheres enhance the immunogenicity of an Ag85B-based fusion protein containing multiple T-cell epitopes of *Mycobacterium tuberculosis*, *European Journal of Pharmaceutics and Biopharmaceutics*, 66, 318–326.

### Internet Resources:

Copley Scientific, Quality solution for inhaler testing, (2012)

<http://www.copleyscientific.com/documents/ww/Inhaler%20Brochure%202012%20%28Low%20Res%29.pdf> (Date Accessed, April 2013).

FDA News Release, (Dec. 2012)

<http://www.fda.gov/NewsEvents/Newsroom/PressAnnouncements/ucm333695.htm> (Date Accessed, March 2013).

Portfolio of candidates under clinical trials, <http://www.aeras.org/portfolio/clinical-trials.php?id=20>. (Date Accessed March 2013)

Stop TB blue print and TB vaccine in pipeline. (2010) DNA Vaccine,

[http://www.aeras.org/newscenter/publications\\_scientific.php](http://www.aeras.org/newscenter/publications_scientific.php) (Date Accessed March 2013)

The top 10 causes of death, (2008) <http://who.int/mediacentre/factsheets/fs310/en/> (Date accessed April 2013)

Todar K. (2012) Online Textbook of Bacteriology, Madison, Wisconsin.

<http://textbookofbacteriology.net/tuberculosis.html> (Date Accessed, March 2013).

Tuberculosis, Centre for Disease control and prevention,

<http://www.cdc.gov/tb/publications/slidesets/selfstudymodules/module1/pathogenesis.htm> (Date Accessed, March 2013).

Vaccine Research,

[http://www.who.int/vaccine\\_research/diseases/tb/vaccine\\_development/bcg/en/](http://www.who.int/vaccine_research/diseases/tb/vaccine_development/bcg/en/) (Date Accessed March 2013)

Vaccine Research, [http://www.who.int/vaccine\\_research/documents/se05Hawkridge.pdf](http://www.who.int/vaccine_research/documents/se05Hawkridge.pdf) (Date Accessed March 2013)

World Health Organization. (2012) Global TB control - epidemiology, strategy, financing. Programs and Projects: WHO Global Tuberculosis Report - 2012.

([http://www.who.int/tb/publications/global\\_report/en/](http://www.who.int/tb/publications/global_report/en/)) (Date accessed March 2013).

### 3.0 Analytical Methods

#### 3.1 Materials

Bovine serum Albumin and Rifampicin was purchased from Sigma-Aldrich (St-Louis, USA). Chitosan (MW 1K) was supplied by Kitto Life (KYONGKI-DO, KOREA). Tri-nitro benzene sulfonic acid (TNBS), Fluorescein isothiocyanate (FITC) was purchased from Sigma-Aldrich (St-Louis, USA). Calcium chloride dehydrate, magnesium chloride, potassium chloride, sodium acetate, sodium bicarbonate, sodium chloride, sodium citrate, sodium dihydrogen phosphate, sodium dodecyl sulfate (SDS), sodium hydroxide, sodium phosphate monobasic monohydrate, sodium sulfate were purchased from Sigma-Aldrich (St-Louis, USA). Ethanol, Methanol, hydrochloric acid (HCl), Tetrahydrofuran (THF) etc. and all other HPLC grade solvents were obtained from Sigma-Aldrich (St-Louis, USA).

#### 3.2 Trinitrobenzene sulfonic acid (TNBS) Assay for determination of degree of substitution (acylation) in octanoyl chitosan

TNBS Reagent is a 5% solution of trinitrobenzene sulfonic acid in methanol that reacts with primary amines (peptides or amino acids) to yield a soluble colored product, a property useful for various assay methods. Therefore, we are utilizing TNBS assay to determine degree of acyl groups conjugation to chitosan (Loretz et. al., 2006).

##### 3.2.1 Stock solution

Standard stock solution of 5 mg /ml chitosan was prepared in water (Chae et. al., 2005; Jang et.al., 2001).

##### 3.2.2 Calibration curve in water

Stock solution of 1 mg/ml was prepared from the standard stock solution of chitosan (5mg/ml) in water. From the stock solution, dilutions were made and calibration curve was plotted between 40 and 200 µg/ml. In brief, from the standard dilutions (40 and 200 µg/ml), 300 µl of sample was taken, 300 µl of 4 % sodium bicarbonate and 0.2 % TNBS was added to it and incubated at 37° C for two hours. Finally, 2 N HCl was added to it, mixed well and absorbance was measured using UV/Vis spectrophotometer at 344 nm (Jenway UV/Vis Spectrophotometer, Staffordshire, UK). (Sonia et. al., 2011)

**Table 3.1: Protocol for TNBS assay**

Sr. No.	Standard final Conc. (µg/ml)	Standard Vol. (µl)	4 % Sodium Bicarbonate (µl)	0.2 % TNBS (µl)	Incubation at 37° C for 2 Hrs	2 N HCl (µl)	Measurement of Absorbance
1	40	300	300	300		300	
2	80	300	300	300		300	
3	120	300	300	300		300	
4	160	300	300	300		300	
5	200	300	300	300		300	

### 3.3 Estimation of FITC using Fluorometric method of analysis (Wang et.al., 2012)

#### 3.3.1 Stock solution

Standard stock solution (100 µg/ml) was prepared from the stock solution of 1mg /ml FITC in Methanol:water (7:3).

#### 3.3.2 Calibration curve in water

Spectrofluorometric method of analysis for FITC in deionized water was carried out by the modification of method reported by Jia et. al., (Jia et. al., 2009). Accordingly, solution of FITC (1 µg/ml) was first scanned between 370 to 600 nm to determine its excitation and emission wavelength ( $\lambda_{max}$ ). Further dilutions were made and calibration curve was plotted between 0.01 and 2 µg/ml by measuring the absorbances at excitation and emission  $\lambda_{max}$  using spectrofluorometer (LS 55 Fluorescence Spectrometer, Perkin–Elmer, UK).

### 3.4 Estimation of BSA using QuantiPro™ bicinchoninic acid (BCA) protein assay kit by Visible Spectroscopy

#### Principle

The principle of the BCA assay is similar to the Lowry method of protein estimation in that both rely on the formation of Cu-protein complex under alkaline conditions, followed by reduction on the  $Cu^{2+}$  to  $Cu^{1+}$ . The amount of reduction is proportional to protein present. It has been shown that certain amine groups and peptide bonds present in the protein are responsible to reduce  $Cu^{2+}$  to  $Cu^{1+}$ . BCA forms purple blue complex with  $Cu^{1+}$  in alkaline conditions, which provides indication to the reduction of alkaline  $Cu^{2+}$  by proteins. (Product information, Sigma-aldrich, Saint Louis, Missouri, USA)

#### Preparation of working reagent from QuantiPro™ BCA protein assay kit

Volume of working reagent was prepared depending upon the number of blanks, protein standards and unknown samples are to be assayed. According to the values given in the table 3.2, volume of QA, QB and QC was varied and working reagent was prepared.

Table 3.2: Working reagent preparation for BSA estimation

Number of Assays	Amount of each reagent used			Total amount of working reagent (ml)
	QA (ml)	QB (ml)	QC (ml)	
1	0.5	0.5	0.02	1.02
5	2.5	2.5	0.1	5.1
10	5.0	5.0	0.2	10.2
15	7.75	7.75	0.31	15.81

#### 3.4.1 Calibration curve of BSA in water using QuantiPro™ BCA assay kit

##### Preparation of stock solution and calibration curve

A working stock solution of 50µg/ml was prepared in deionized water from the standard stock solution of 2mg/ml BSA in water.

BSA protein estimation was carried out as per the manufacturer's protocol (Sigma Aldrich, St. Louis, USA).

Spectrophotometric method for the analysis of standard protein BSA (in water) using QuantiPro™ BCA assay kit was done by first scanning solution of BSA (10µg/ml) in the visible range and determining its  $\lambda_{max}$ . Suitable aliquots from the stock solution of BSA were pipetted out in eppendorrf and the volume was made upto 1 ml with deionized water to give final concentrations ranging from 0.5-30 µg/ml. To this, 1 ml of BCA working reagent was added, solutions were mixed using vortex mixer and incubated at 37°C for 2 hrs. Their absorbance were measured at  $\lambda_{max}$  of 562 nm using water as blank on Jenway UV/Vis Spectrophotometer and calibration curve was plotted (Table 3.3). The above procedure was performed in triplicate.

**Table 3.3: Sample preparation for standard protein (BSA) estimation in water**

Sr. No.	Sample Buffer (water)(µl)	Protein Standard Solution (µl) (50µg/ml)	Protein Concentration (µg/ml)	BCA working reagent (µl)	Incubation at 37°C	Measurement of Absorbance at 562 nm
1	1000	---	0	1000		
2	990	10	0.5	1000		
3	900	100	5	1000		
4	800	200	10	1000		
5	600	400	20	1000		
6	400	600	30	1000		

#### **3.4.2. Calibration curve of BSA in SDS/NaOH solution using QuantiPro™ BCA assay kit**

##### ***Preparation of stock solution and calibration curve***

A stock solution of 50µg/ml was prepared in SDS/NaOH solution from the standard stock solution of 2mg/ml BSA in SDS/NaOH.

SDS/NaOH solution – 5 % SDS prepared in 0.1 M NaOH.

BSA protein estimation was carried out as per the manufacturer's protocol.

Spectrophotometric method for the analysis of standard protein BSA (in SDS/NaOH) using QuantiPro™ BCA assay kit was performed by first scanning solution of BSA (10µg/ml) in the visible range and determining its  $\lambda_{max}$ . Suitable aliquots from the stock solution of BSA were pipetted out into vial and the volume was made upto 1 ml with SDS/NaOH solution to give final concentrations ranging from 0.5-30 µg/ml. To this, 1 ml of BCA working reagent was added, solutions were mixed using vortex mixer and incubated in water bath at 37°C for 2 hrs. Absorbance was measured at determined  $\lambda_{max}$  of 562 nm using SDS/NaOH solution as blank on Jenway UV/Vis Spectrophotometer and calibration curve was plotted (Table 3.4). The experiment was carried out in triplicate.

**Table 3.4: Sample preparation for protein estimation in NaOH/SDS solution**

Sr. No.	Sample Buffer (NaOH/SDS) ( $\mu\text{l}$ )	Protein Standard Solution ( $\mu\text{l}$ ) (50 $\mu\text{g}/\text{ml}$ )	Protein Concentration ( $\mu\text{g}/\text{ml}$ )	BCA working reagent ( $\mu\text{l}$ )	Incubation at 37°C	Measurement of Absorbance 562 nm
1	1000	---	0	1000		
2	990	10	0.5	1000		
3	900	100	5	1000		
4	800	200	10	1000		
5	600	400	20	1000		
6	400	600	30	1000		

### 3.4.3 Calibration curve of BSA in Simulated Lung Fluid (SLF) using QuantiPro™ BCA assay kit

#### Preparation of stock solution and Calibration curve

A stock solution of 50 $\mu\text{g}/\text{ml}$  was prepared in SDS/NaOH solution from the standard stock solution of 2mg/ml BSA in SDS/NaOH (Marques et.al., 2011).

#### Composition of SLF, pH 7.4

Ingredient	Quantity (g/L)
Magnesium Chloride hexahydrate	0.2033
Sodium Chloride	6.0193
Potassium Chloride	0.2982
Sodium sulfate anhydrous	0.0710
Calcium Chloride dihydrate	0.3676
Sodium Acetate trihydrate	0.9526
Sodium Hydrogen carbonate	2.6043
Sodium citrate dihydrate	0.0970
Sodium phosphate monobasic monohydrate	0.1420

BSA protein estimation was carried out as per the manufacturer's protocol.

Spectrophotometric method for the analysis of standard protein, BSA (in SLF) using QuantiPro™ BCA assay kit was executed by first scanning solution of BSA (10 $\mu\text{g}/\text{ml}$ ) in the visible range and determining its  $\lambda_{\text{max}}$ . Suitable aliquots from the stock solution of BSA were pipetted out in an eppendorff tube and the volume was made upto 1 ml with SLF to give final concentrations ranging from 0.5-30  $\mu\text{g}/\text{ml}$ . To this, 1 ml of BCA working reagent was added, solutions were mixed using vortex mixer and incubated in water bath at 37°C for 2 hrs. Absorbance values were measured at  $\lambda_{\text{max}}$  of 562 nm using SLF as blank on Jenway UV/Vis Spectrophotometer and calibration curve was plotted (Table 3.5). The experiment was run in triplicate.

**Table 3.5: Sample preparation for protein estimation in SLF**

Sr. No.	Sample Buffer (SLF)( $\mu$ l)	Protein Standard Solution ( $\mu$ l) (50 $\mu$ g/ml)	Protein Concentration ( $\mu$ g/ml)	BCA working reagent ( $\mu$ l)	Incubation at 37°C	Measurement of Absorbance 562 nm
1	1000	---	0	1000		
2	990	10	0.5	1000		
3	900	100	5	1000		
4	800	200	10	1000		
5	600	400	20	1000		
6	400	600	30	1000		

### 3.5 Results and Discussion

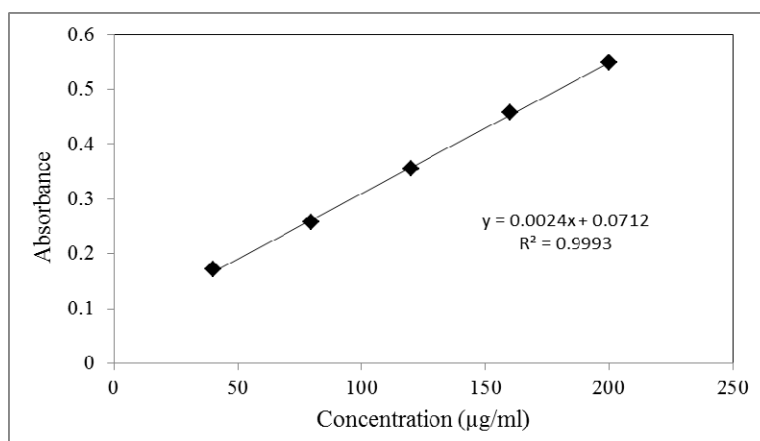
#### 3.5.1 Calibration curve of chitosan using TNBS assay

Reaction between primary amine groups in the chitosan and TNBS reagent yielded soluble colored product and showed absorption maximum at 344 nm and this wavelength was selected as analytical wavelength for further measurements of chitosan. Beer's Lambert's law was obeyed between 40 and 200  $\mu$ g/ml (Table 3.6). Regression equation for standard curve was found to be  $y = 0.0024x + 0.0712$  (Fig. 3.1). Correlation coefficient was noted as 0.9993 signifying the existence of linear relationship between absorbance and concentration of the chitosan. Parameters indicating linearity for the spectrophotometric method of analysis for estimation of chitosan are shown in Table 3.7.

**Table 3.6: Calibration data for chitosan using TNBS assay**

Sr. No	Concentration ( $\mu$ g/ml)	Mean Absorbance* $\pm$ SD
1	40	0.171 $\pm$ 0.007
2	80	0.257 $\pm$ 0.020
3	120	0.355 $\pm$ 0.007
4	160	0.457 $\pm$ 0.035
5	200	0.549 $\pm$ 0.007

\*Average of 3 determinations

**Fig. 3.1** Calibration curve for chitosan using TNBS assay

**Table 3.7** Parameters for TNBS assay of chitosan

Parameters	Results
$\lambda_{\text{max}}$	344 nm
Linearity range	40-200 $\mu\text{g/ml}$
Regression equation	$y = 0.0024x + 0.0712$
Correlation coefficient	0.9993

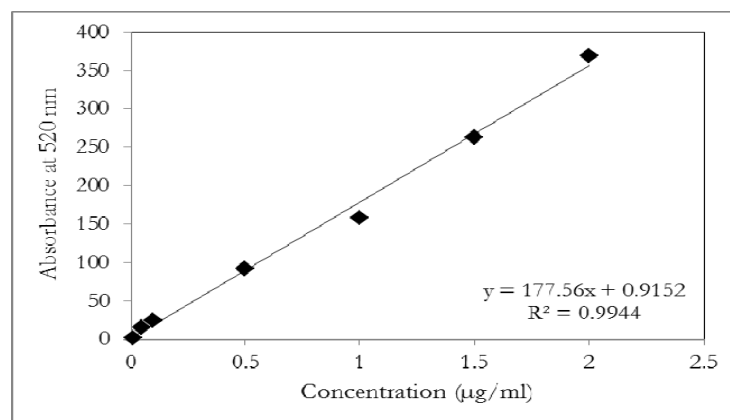
### 3.5.2 Calibration curve of FITC using spectrofluorometer

FITC in water showed emission absorption maximum at 520 nm and excitation absorption maximum at 490 nm. Both these wavelengths were selected as analytical wavelength for the measurement of FITC standard solutions. Beer's Lambert's law was obeyed between 0.01 and 2  $\mu\text{g/ml}$  (Table 3.8 to 3.11). Regression equation for calibration curve at 520 and 490 was found to be  $y = 178.97x + 0.6281$  and  $y = 177.86x + 1.572$  respectively (Fig. 3.2 and 3.3). Correlation coefficients for these methods were found to be 0.9935 for emission absorbance maxima and 0.9947 for excitation absorbance maxima suggesting the existence of linear relationship between the absorbance and concentration of FITC. Parameters showing linearity for the spectrofluorometric method of analysis for FITC estimation are shown in Table 3.8 to 3.11.

**Table 3.8** Calibration data for FITC at emission wavelength (520 nm)

Sr. No	Concentration ( $\mu\text{g/ml}$ )	Mean fluorescence* $\pm$ SD
1	0.01	$2.053 \pm 0.050$
2	0.05	$15.527 \pm 0.163$
3	0.1	$24.080 \pm 0.020$
4	0.5	$91.327 \pm 0.168$
5	1	$158.167 \pm 0.206$
6	1.5	$262.627 \pm 0.546$
7	2	$368.86 \pm 0.087$

\*Average of 3 determinations

**Fig. 3.2** Calibration Curve of FITC at emission wavelength (520 nm)

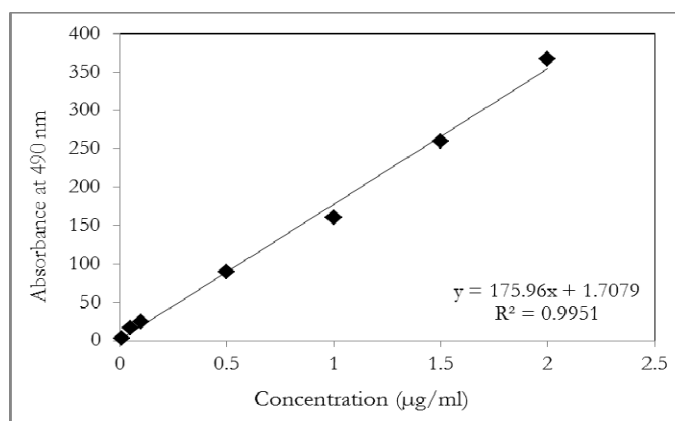
**Table 3.9** Parameters for FITC at emission wavelength 520 nm

Parameters	Results
$\lambda_{\text{max}}$	520 nm
Linearity range	0.01-2 $\mu\text{g/ml}$
Regression equation	$y = 177.56x + 0.9152$
Correlation coefficient	0.9944

**Table 3.10** Calibration data of FITC at excitation wavelength (490 nm)

Sr. No	Concentration ( $\mu\text{g/ml}$ )	Mean fluorescence * $\pm$ SD
1	0.01	1.947 $\pm$ 0.045
2	0.05	16.733 $\pm$ 0.158
3	0.1	24.417 $\pm$ 0.297
4	0.5	90.033 $\pm$ 0.124
5	1	160.39 $\pm$ 0.052
6	1.5	259.473 $\pm$ 0.231
7	2	366.41 $\pm$ 0.364

\*Average of 3 determinations

**Fig. 3.3** Calibration Curve of FITC at excitation wavelength of 490 nm**Table 3.11** Parameters for FITC at excitation wavelength of 490 nm

Parameters	Results
$\lambda_{\text{max}}$	490 nm
Linearity range	0.01-2 $\mu\text{g/ml}$
Regression equation	$y = 175.96x + 1.7079$
Correlation coefficient	0.9951

### 3.5.3 Calibration curve of standard protein (BSA) in water using QuantiPro™ BCA assay kit

Purple blue complex formed between BCA and  $\text{Cu}^{+1}$  in presence of BSA in water demonstrated absorption maximum at 562 nm and this wavelength was selected as analytical wavelength for the measurement of standard protein. Beer's Lambert's law was obeyed

between 0.5 and 30 µg/ml (Table 3.12). Regression analysis was executed on the experimental data. Regression equation for standard curve was established to be  $y = 0.0191x + 0.0167$  (Fig. 3.4). Correlation coefficient for the method was 0.9991 signifying that a linear relationship existed between absorbance and concentration of the protein (BSA). Parameters of linearity for the visible spectrometric method of analysis for protein are shown in Table 3.13.

**Table 3.12** Calibration data for BSA in water by visible spectroscopy

Sr. No	Concentration (µg/ml)	Mean Absorbance* ± SD
1	0.5	0.024 ± 0.023
2	5	0.111 ± 0.015
3	10	0.206 ± 0.007
4	20	0.409 ± 0.003
5	30	0.582 ± 0.013

\*Average of 3 determinations

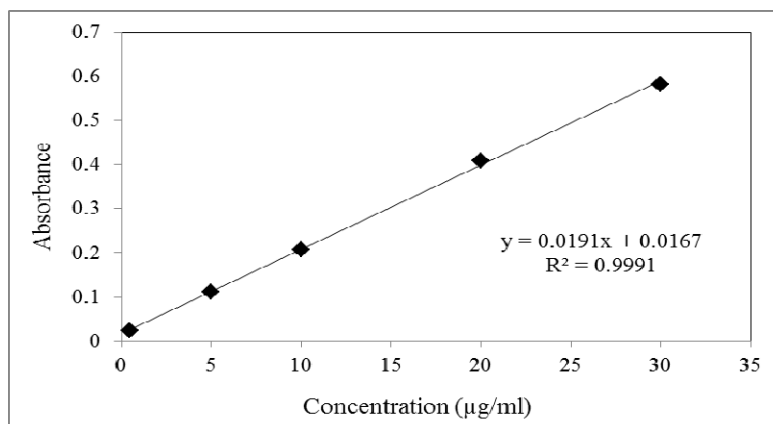


**Fig. 3.4** Calibration Curve of BSA in water by visible spectroscopy

**Table 3.13** Parameters for BSA estimation using QuantiPro™ BCA assay kit in water

Parameters	Results
λ <sub>max</sub>	556 nm
Linearity range	0.5-30 µg/ml
Regression equation	$y = 0.0191x + 0.0167$
Correlation coefficient	0.9991

#### 3.5.4 Calibration curve of BSA in 5% SDS (w/v) in 0.1 M sodium hydroxide (NaOH/SDS) solution using QuantiPro™ BCA assay kit

A characteristic spectrum of purple blue complex formed between BCA and Cu<sup>+1</sup> in presence of BSA in NaOH/SDS solution was observed when scanned in the visible range. The scan exhibited absorption maximum at 562 nm and this wavelength was selected as analytical wavelength for the measurement of standard protein. Beer's Lambert's law was obeyed between 0.5 and 30 µg/ml (Table 3.14). Regression equation for calibration curve was determined as  $y = 0.012x - 0.013$  (Fig.3.5). Correlation coefficient for this analytical

method was found to be 0.9994, standing for a linear relationship between absorbance and BSA concentration. Parameters evidencing linearity for the method of analysis for BSA are shown in Table 3.15.

**Table 3.14 Calibration data for BSA in NaOH/SDS solution**

Sr. No	Concentration ( $\mu\text{g/ml}$ )	Mean Absorbance* $\pm$ SD
1	0.5	0.018 $\pm$ 0.006
2	5	0.074 $\pm$ 0.008
3	10	0.130 $\pm$ 0.004
4	20	0.258 $\pm$ 0.003
5	30	0.369 $\pm$ 0.008

\*Average of 3 determinations

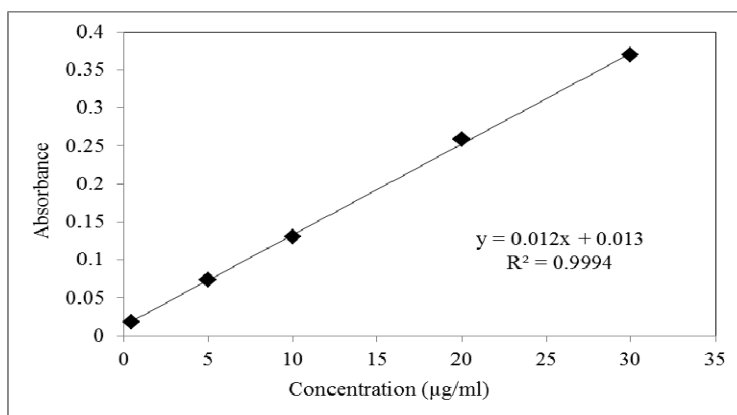


**Fig. 3.5** Calibration Curve of BSA in NaOH/SDS solution by visible spectroscopy

**Table 3.15** Parameters for BSA protein estimation using QuantiPro™ BCA assay kit in NaOH/SDS solution

Parameters	Results
$\lambda_{\text{max}}$	556 nm
Linearity range	0.5-30 $\mu\text{g/ml}$
Regression equation	$y = 0.012x + 0.013$
Correlation coefficient	0.9994

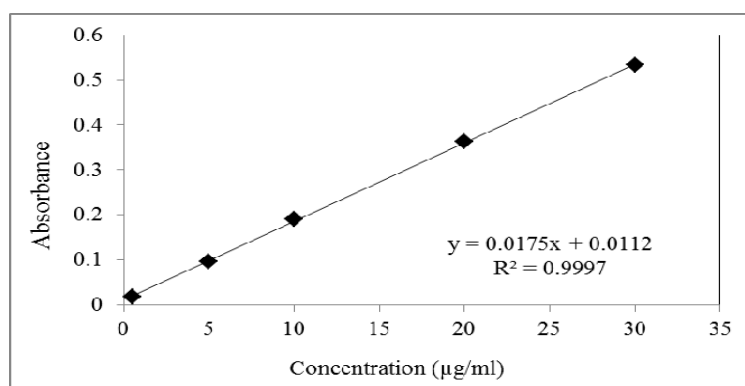
### 3.5.5 Calibration curve of BSA in SLF using QuantiPro™ BCA assay kit

Purple blue colored complex of BCA- $\text{Cu}^{+1}$  showed a characteristic spectrum in SLF in the visible range and displayed absorption maximum at 562 nm. This wavelength was chosen as analytical wavelength for the measurement of standard protein. Beer's Lambert's law was obeyed between 0.5 and 30  $\mu\text{g/ml}$  (Table 3.16). Regression equation for calibration curve was found to be  $y = 0.0175x - 0.0112$  (Fig.3.6). Correlation coefficient for this analytical method was noted as 0.9997, denoting a linear relationship between absorbance and concentration of the BSA. Linearity parameters for the method of analysis for BSA are shown in Table 3.17.

**Table 3.16** Calibration data for standard protein (BSA) in SLF

Sr. No	Concentration ( $\mu\text{g/ml}$ )	Mean Absorbance* $\pm$ SD
1	0.5	0.018 $\pm$ 0.006
2	5	0.096 $\pm$ 0.023
3	10	0.191 $\pm$ 0.016
4	20	0.363 $\pm$ 0.027
5	30	0.533 $\pm$ 0.027

\*Average of 3 determinations

**Fig. 3.6** Calibration Curve of standard protein (BSA) in SLF by visible spectroscopy**Table 3.17** Parameters for standard protein (BSA) estimation using QuantiPro™ BCA assay kit in SLF

Parameters	Results
$\lambda_{\text{max}}$	556 nm
Linearity range	0.5-30 $\mu\text{g/ml}$
Regression equation	$y = 0.0175x + 0.0112$
Correlation coefficient	0.9997

**3.6 Estimation of Rifampicin by Ultraviolet Spectroscopy (UV)** (Benetton et.al., 1998; IP, 1996)

### 3.6.1 Calibration curve in water

Standard stock solution (1 mg/ml) was prepared by dissolving 10 mg of rifampicin in 10 ml of methanol. Then aliquot was withdrawn, volume was made up with double distilled water (DDW) and UV spectrophotometric method of analysis was carried out by first scanning rifampicin solution of concentration 10  $\mu\text{g/ml}$  in the visible range between 400 and 600 nm to determine its  $\lambda_{\text{max}}$ . Later on, suitable aliquots of the stock solution of rifampicin were pipetted out into 10 ml volumetric flasks and the volume was made upto 10 ml with DDW to give final concentrations ranging from 5-60  $\mu\text{g/ml}$ . The solutions were mixed using vortex mixer and the absorbance was measured at  $\lambda_{\text{max}}$  using water as blank on Shimadzu 1700 UV-Visible Spectrophotometer and calibration curve was plotted. The experiment was performed in triplicate. Standard concentration of 3.0, 7.0, and 15.0  $\mu\text{g/ml}$  were prepared for interday and intraday analysis to estimate accuracy and precision of the said method.

### 3.6.2 Calibration curve in SLF (pH 7.4)

Standard stock solution (1 mg/ml) was prepared by dissolving 10 mg of rifampicin in 10 ml of methanol. Aliquot was withdrawn, volume was made up with simulated lung fluid (SLF) and UV spectrophotometric method of analysis was carried out by first scanning rifampicin solution of concentration 10 µg/ml in the visible range between 400 and 600 nm to determine its  $\lambda_{\text{max}}$ . Further, suitable aliquots of the stock solution of rifampicin were pipetted out into 10 ml volumetric flasks and the volume was made upto 10 ml with SLF to give final concentrations ranging from 5-60 µg/ml. The solutions were mixed using vortex mixer and their absorbance values were measured at  $\lambda_{\text{max}}$  using SLF as blank on Shimadzu 1700 UV-Visible Spectrophotometer and calibration curve was plotted. The experiment was performed in triplicate. Standard concentration of 3.0, 7.0, and 15.0 µg/ml were prepared and subjected to interday and intraday analysis to determine the accuracy and precision of said method.

### 3.6.3 Analytical method validation

Analytical methods of estimation for rifampicin were validated for linearity, accuracy and precision.

#### 3.6.3.1 Linearity

The linearity of an analytical method is its ability to obtain results directly proportional to the concentrations (quantities) of the analyte in the sample within a definite range (Hubert et al., 2003). Linearity of a light absorption determination should be examined to ensure that Beer's-Lambert's law operates over the range of interest.

For evaluation of the linearity of the UV method of rifampicin, the standard solutions were prepared at 5, 10, 20, 30, 40, 50 and 60 µg/ml concentrations ( $n = 3$ ) and absorbance values were noted at 475 nm. The method was said to be linear for estimation of rifampicin if  $R^2$  value was near to 1. Least square regression method was used to determine the regression coefficient,  $r$  and the equation for the best fitting line.

#### 3.6.3.2 Accuracy

Accuracy refers to the closeness of an individual observation or mean of the observations to true value (Bolton, 1990). The "true" value is the result which would be observed in absence of error. Accuracy of the assay is defined as the percentage of the agreement between the measured value and the true value as follows (Merodia et al, 2000). The accuracy is calculated by using following formula:

$$\text{Accuracy} = \frac{\text{True Value} - \text{Measured Value}}{\text{True Value}} \times 100$$

#### 3.6.3.3 Precision

Precision refers to the extent of variability of a group of measurements observed under similar conditions. Precision provides an indication of random errors and is generally subdivided into - repeatability and reproducibility, which are determined by calculating Relative standard deviation (RSD) or Coefficient of variation (CV) of inter-day and intra-day

determinations. One of the common ways of expressing the variability, which takes into account its relative magnitude, is the ratio of the standard deviation (SD) to the mean, (SD/Mean). This ratio, often expressed as a percentage and is called as RSD or CV. The variability in chemical and instrumental analysis of drugs is usually small as compared to the one tested in biological samples (Bolton, 1990).

### 3.7 Results and Discussion

#### 3.7.1 Calibration curve of rifampicin in water

A characteristic spectrum of rifampicin was observed in water, when scanned in the visible range between 400 and 600 nm. The scan depicted absorption maximum 475 nm and this wavelength was chosen as the analytical wavelength. Beer's Lambert's law was obeyed between 5 and 60  $\mu\text{g/ml}$  (Table 3.18). Regression analysis was performed on the experimental data. Regression equation for standard curve was found to be  $y = 0.0144x - 0.022$  (Fig. 3.7). Correlation coefficient for the method was noted to be 0.9987 signifying existence of a linear relationship between absorbance and concentration of the drug. Parameters determining linearity for the UV spectrometric method of analysis for rifampicin are shown in Table 3.19.

**Table 3.18** Calibration data for Rifampicin in water

Sr. No	Concentration ( $\mu\text{g/ml}$ )	Mean Absorbance $\pm$ SD
1	5	0.101 $\pm$ 0.001
2	10	0.159 $\pm$ 0.019
3	20	0.297 $\pm$ 0.002
4	30	0.457 $\pm$ 0.006
5	40	0.617 $\pm$ 0.031
6	50	0.739 $\pm$ 0.002
7	60	0.878 $\pm$ 0.007

\*Average of 3 determinations

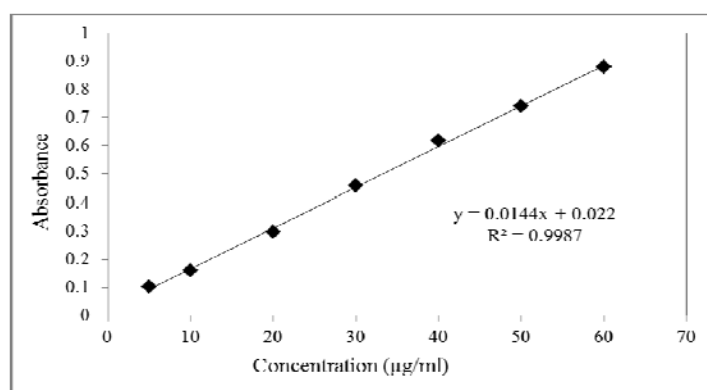


**Fig. 3.7** Standard Curve of Rifampicin in water

**Table 3.19** Parameters for UV spectrometric method of analysis for Rifampicin in water

Parameters	Results
$\lambda_{\max}$	475 nm
Linearity range	5-60 $\mu\text{g/ml}$
Regression equation	$y = 0.0144x + 0.022$
Correlation coefficient	0.9987

Intraday and interday precision and accuracy for the rifampicin assay by UV spectroscopy was accessed. The low % CV values as presented in Table 3.20 and 3.21 confirm the precision of method. No significant difference between the amount of drug added (actual) and observed concentration was noticed indicating accuracy of the method.

**Table 3.20** Intraday precision and accuracy for rifampicin assay in water by UV spectroscopy.

Standard Concentration ( $\mu\text{g/ml}$ )		Precision (%) <sup>a</sup>	Accuracy (%) <sup>b</sup>
Actual	Observed		
7	$7.12 \pm 0.093$	1.309	101.775
15	$15.1 \pm 0.095$	0.630	100.707
25	$25.12 \pm 0.089$	0.355	100.48

<sup>a</sup> Expressed as relative standard deviation, RSD

$$\text{RSD} = (\text{standard deviation}/\text{mean concentration}) \times 100$$

<sup>b</sup> Expressed as (mean observed concentration/actual concentration)  $\times$  100

**Table 3.21** Interday precision and accuracy for rifampicin assay in water by UV spectroscopy.

Standard Concentration ( $\mu\text{g/ml}$ )		Precision (%) <sup>a</sup>	Accuracy (%) <sup>b</sup>
Actual	Observed		
7	$7.14 \pm 0.11$	1.49	102.011
15	$15.3 \pm 0.22$	1.41	101.910
25	$25.02 \pm 0.09$	0.38	100.08

<sup>a</sup> Expressed as relative standard deviation, RSD

$$\text{RSD} = (\text{standard deviation}/\text{mean concentration}) \times 100$$

<sup>b</sup> Expressed as (mean observed concentration/actual concentration)  $\times$  100

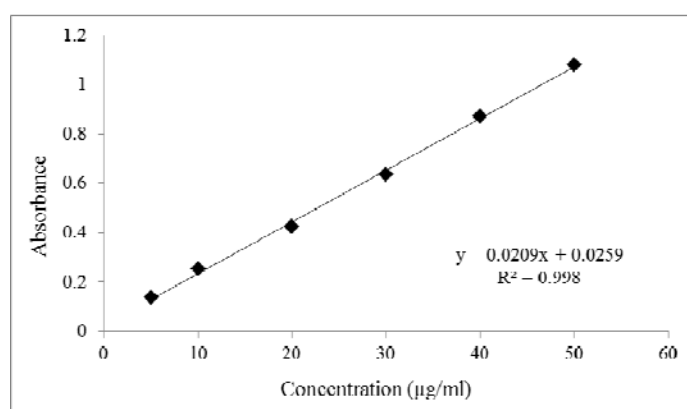
### 3.7.2 Calibration curve of rifampicin in SLF

Rifampicin in SLF showed a characteristic spectrum, when scanned in the visible range between 400 and 600 nm. The scan showed absorption maximum 475 nm and this wavelength was chosen as analytical wavelength. Beer's Lambert's law was obeyed between 5 and 50  $\mu\text{g/ml}$  (Table 3.22). Regression analysis was performed on the experimental data. Regression equation for standard curve was  $y = 0.0209x - 0.0259$  (Fig. 3.8). Correlation coefficient for the method was found to be 0.9980 suggesting a linear relationship between absorbance and concentration of the drug. Parameters signaling linearity for UV spectrometric method of analysis for rifampicin are shown in Table 3.23.

**Table 3.22** Calibration data for Rifampicin in SLF

Sr. No	Concentration ( $\mu\text{g/ml}$ )	Mean Absorbance $\pm$ SD
1	5	0.135 $\pm$ 0.014
2	10	0.253 $\pm$ 0.009
3	20	0.422 $\pm$ 0.012
4	30	0.635 $\pm$ 0.004
5	40	0.870 $\pm$ 0.018
6	50	1.081 $\pm$ 0.028

\*Average of 3 determinations

**Fig. 3.8** Standard Curve of Rifampicin in SLF**Table 3.23** Parameters for UV spectrometric method of analysis for Rifampicin in SLF

Parameters	Results
$\lambda_{\text{max}}$	475 nm
Linearity range	5-60 $\mu\text{g/ml}$
Regression equation	$y = 0.0209x + 0.0259$
Correlation coefficient	0.998

Table 3.24 and 3.25 tabulates intraday and interday precision and accuracy for the rifampicin assay in SLF by UV spectroscopy. The low % CV in Table 3.24 and 3.25 values indicate precision of the method. No significant difference between the actual amount of drug added and observed concentration was noticed justifying accuracy of the method. Interference studies with the polymers and excipients showed no difference in absorbance at 475 nm confirming the suitability of method in the presence of excipients.

**Table 3.24** Intraday precision and accuracy for rifampicin assay in SLF by UV spectroscopy.

Standard Concentration ( $\mu\text{g/ml}$ )		Precision (%) <sup>a</sup>	Accuracy (%) <sup>b</sup>
Actual	Observed		
7	$6.98 \pm 0.04$	0.624	99.717
15	$15.11 \pm 0.24$	1.573	100.764
25	$24.75 \pm 0.64$	0.84	98.88

<sup>a</sup> Expressed as relative standard deviation, RSD;

RSD = (standard deviation/mean concentration) x 100;

<sup>b</sup> Expressed as (mean observed concentration/actual concentration)  $\times$  100

**Table 3.25** Interday precision and accuracy for rifampicin assay in SLF by UV spectroscopy.

Standard Concentration ( $\mu\text{g/ml}$ )		Precision (%) <sup>a</sup>	Accuracy (%) <sup>b</sup>
Actual	Observed		
7	$7.13 \pm 0.14$	2.02	101.88
15	$15.2 \pm 0.26$	1.74	101.207
25	$24.91 \pm 0.92$	0.66	99.64

<sup>a</sup> Expressed as relative standard deviation, RSD;

RSD = (standard deviation/mean concentration) x 100;

<sup>b</sup> Expressed as (mean observed concentration/actual concentration)  $\times$  100

### 3.8 Estimation of rifampicin in DDW and SLF by high performance liquid chromatography (HPLC) (Tatarczak et.al., 2005)

High performance liquid chromatography (HPLC) UV was carried out on Agilent Technologies 1200 series with the use of a C18 column. The mobile phase consisted of 30 % (v/v) tetrahydrofuran (THF) and 70 % (v/v) Phosphate buffer ( $\text{KH}_2\text{PO}_4$ , 0.05M, pH 4.5). After preparation of the mobile phase, it was degassed and filtered through 0.45  $\mu$  inorganic filter. The required parameters were programmed using software. Injection volume was 10  $\mu$ l and the flow was set to 1.0 mL/min. and column thermostat was set on 40°C. Compound eluted was recorded by UV detector at 335nm.

Standard stock solution of 10.00 mg of rifampicin in 100.0mL water:methanol (8:2, v:v) was prepared. From this stock solution, solutions with a concentration of 5, 10, 25, 50, 60 and 80  $\mu\text{g/mL}$  were prepared in volumetric flask using water as diluent and experiment was run and calibration curve was drawn by plotting peak area of curve observed vs drug concentration. The method was validated for linearity, accuracy and precision. Following gradient composition of mobile phase was used for the method (Table 3.26).

Similar method was used to prepare samples in SLF, by replacing water with SLF (SLF:Methanol – 8:2 v/v) and calibration curve was plotted as peak area vs drug concentration.

**Table 3.26: Concentration of THF in mobile phase reached at a given time during one run**

Time (min)	Phosphate Buffer (% v/v)	THF (% v/v)
0	70	30
10	70	30
20	40	60
25	40	60
26	70	30
32	70	30

**3.8.1 Validation**

Analytical method was validated for linearity, precision, and accuracy as described in section 3.6.3.

**3.9 Results and Discussions**

The peak for rifampicin was eluted at around 3.5 min. The standard plot for rifampicin is shown in Fig. 3.9 and data is presented in Table 3.27.

**3.9.1 Calibration curve in water****3.9.1.1 Linearity:**

The data for calibration curve of rifampicin in water by HPLC was fitted into a linear equation ( $y = 1.4519x + 1.063$ ) with correlation coefficient of  $R^2=0.9993$ , indicating linearity of the curve (Table 3.28).

**3.9.1.2 Precision:**

Precision of the method was assessed by analyzing the rifampicin at different concentrations of 5, 25 and 50  $\mu\text{g/ml}$ . Three replicate of each concentration was analyzed and results are tabulated in Table 3.29 and 3.30. To evaluate precision, the mean values and the % RSD values were calculated for each concentration. The % RSD values for intraday and interday assay precision are presented in Table 3.29 and 3.30. The low % CV values indicate precision of the method.

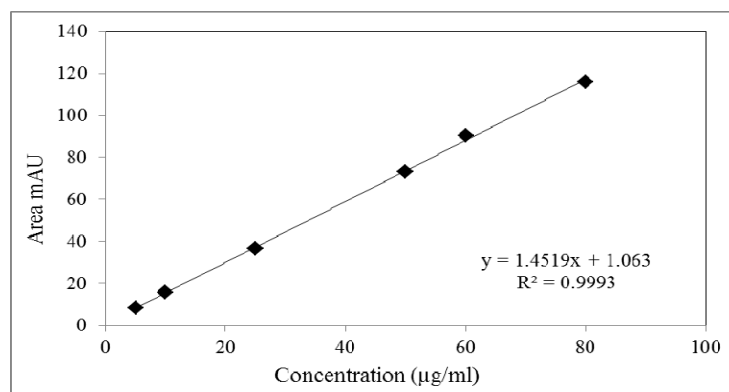
**3.9.1.3 Accuracy:**

The accuracy is expressed as % bias or % relative error (difference from added concentration) and it takes into account the total error, i.e. systematic and random errors, related to the test result (Hubert et al, 2003). The tolerance limits for intraday assay and interday assay samples are presented in Table 3.29 and 3.30 as a function of the introduced concentrations. No significant difference between the amount of rifampicin added (actual) and observed concentration was noticed at all the concentration levels tested, indicating accuracy of the method (Boulanger et al, 2003; Guidance for industry, 2001).

**Table 3.27** Calibration data for rifampicin in water

Sr. No.	Concentration ( $\mu\text{g/ml}$ )	Area under curve (mAU)
1	5	$8.3 \pm 0.283$
2	10	$15.67 \pm 0.0424$
3	25	$36.8 \pm 0.000$
4	50	$73.05 \pm 0.417$
5	60	$90.42 \pm 1.301$
6	80	$116.09 \pm 2.539$

\*Average of 3 determinations

**Fig. 3.9** Calibration Curve of rifampicin in water by HPLC**Table 3.28** Parameters for method of analysis of Rifampicin by HPLC

Parameters	Results
$\lambda_{\text{max}}$	315 nm
Linearity range	5-80 $\mu\text{g/ml}$
Regression equation	$y = 1.4519x + 1.063$
Correlation coefficient	0.9993
Retention Time	3.5 min

**Table 3.29** Intraday precision and accuracy for rifampicin assay in water by HPLC.

Standard Concentration ( $\mu\text{g/ml}$ )		Precision (%) <sup>a</sup>	Accuracy (%) <sup>b</sup>
Actual	Observed		
5	$4.905 \pm 0.16$	3.25	98.096
25	$24.33 \pm 1.11$	4.55	97.155
50	$50.251 \pm 2.74$	5.45	100.502

<sup>a</sup> Expressed as relative standard deviation, RSDRSD = (standard deviation/mean concentration)  $\times$  100<sup>b</sup> Expressed as (mean observed concentration/actual concentration)  $\times$  100

**Table 3.30** Interday precision and accuracy for rifampicin assay in water by HPLC.

Standard Concentration ( $\mu\text{g/ml}$ )		Precision (%) <sup>a</sup>	Accuracy (%) <sup>b</sup>
Actual	Observed		
5	4.983 $\pm$ 0.133	2.67	99.667
25	24.583 $\pm$ 0.93	3.78	98.332
50	50.86 $\pm$ 1.51	2.96	101.711

<sup>a</sup> Expressed as relative standard deviation, RSD

RSD = (standard deviation/mean concentration)  $\times$  100

<sup>b</sup> Expressed as (mean observed concentration/actual concentration)  $\times$  100

### 3.9.2 Calibration curve in SLF

#### 3.9.2.1 Linearity:

The data for calibration curve of rifampicin in water by HPLC was fitted into a linear equation ( $y = 1.6217x + 2.2834$ ) with correlation coefficient of  $R^2=0.9993$ , indicating linearity of the curve (Table 3.32).

#### 3.9.2.2 Precision:

Precision of the method was assessed by analyzing the rifampicin at different concentrations of 5, 25 and 50  $\mu\text{g/ml}$ . Three replicate of each concentration was analyzed and results are tabulated in Table 3.33 and 3.34. To evaluate precision, the mean values and the % RSD values were calculated for each concentration. The % RSD values for intraday and interday assay precision are presented in Table 3.33 and 3.34. The low % CV values indicate precision of the method.

#### 3.9.2.3 Accuracy:

The accuracy is expressed as % bias or % relative error (difference from added concentration) and it takes into account the total error, i.e. systematic and random errors, related to the test result (Hubert et al, 2003). The tolerance limits for intraday assay and interday assay samples are presented in Table 3.29 and 3.30 as a function of the introduced concentrations. No significant difference between the amount of rifampicin added (actual) and observed concentration was noticed at all the concentration levels tested, indicating accuracy of the method (Boulanger et al, 2003; Guidance for industry, 2001).

**Table 3.31** Calibration data for rifampicin in water

Sr. No.	Concentration ( $\mu\text{g/ml}$ )	Area under curve (mAU)
1	5	11.29 $\pm$ 0.375
2	10	19.21 $\pm$ 0.671
3	25	41.29 $\pm$ 1.358
4	50	81.54 $\pm$ 1.893
5	60	100.66 $\pm$ 0.731
6	80	132.68 $\pm$ 0.640

\*Average of 3 determinations

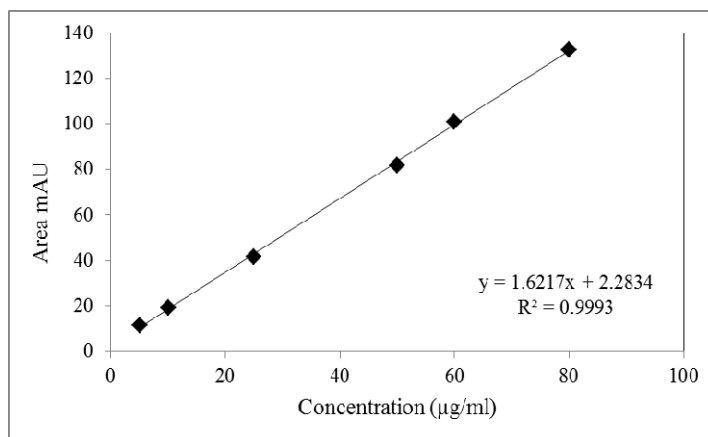


Fig. 3.10 Calibration Curve of rifampicin in SLF by HPLC

Table 3.32 Parameters for method of analysis of Rifampicin by HPLC

Parameters	Results
$\lambda_{\max}$	315 nm
Linearity range	5-80 µg/ml
Regression equation	$y = 1.6217x + 2.2834$
Correlation coefficient	0.9993
Retention Time	3.5 min

Table 3.33 Intraday precision and accuracy for rifampicin assay in SLF by HPLC.

Standard Concentration (µg/ml)		Precision (%) <sup>a</sup>	Accuracy (%) <sup>b</sup>
Actual	Observed		
5	5.25 ± 0.19	3.597	105.08
25	24.54 ± 0.74	2.998	98.16
50	49.13 ± 1.39	2.829	98.25

<sup>a</sup> Expressed as relative standard deviation, RSD

RSD = (standard deviation/mean concentration) × 100

<sup>b</sup> Expressed as (mean observed concentration/actual concentration) × 100

Table 3.34 Interday precision and accuracy for rifampicin assay in SLF by HPLC.

Standard Concentration (µg/ml)		Precision (%) <sup>a</sup>	Accuracy (%) <sup>b</sup>
Actual	Observed		
5	5.25 ± 0.15	2.83	104.98
25	24.45 ± 0.83	3.39	97.80
50	49.438 ± 1.07	2.16	98.88

<sup>a</sup> Expressed as relative standard deviation, RSD

RSD = (standard deviation/mean concentration) × 100

<sup>b</sup> Expressed as (mean observed concentration/actual concentration) × 100

### References

- Benetton S.A., Kedor-Hackmann E.R.M., Santoro M.I.R.M., Borges V.M. (1998) Visible spectrophotometric and first-derivative UV spectrophotometric determination of rifampicin and isoniazid in pharmaceutical preparations, *Talanta*, 47,3, 639–643
- Bolton S, Swarbrick J. (1990) Basic definitions and concepts In: *Pharmaceutical statistics: Practical and clinical applications*. 3rd Ed., Marcel Dekker, New York, pp 24.
- Boulanger B, Dewe W, Chiap P, Crommen J, Hubert PH. (2003) An analysis of the SFSTP guide on validation of bioanalytical methods: progress and limitations. *J Pharm Biomed Anal.* 32, 753-765.
- Chae S.Y., Jang Mi-K., Nah Jae-Woon. (2005) Influence of molecular weight on oral absorption of water soluble chitosans, *Journal of Controlled Release*, 102, 383–394;
- Guidance for industry: Bioanalytical Method Validation, U.S. Department of Health and Human Services, Food and Drug Administration, Center for Drug Evaluation and Research (CDER), Center for Biologics Evaluation and Research (CBER), May 2001.
- Hubert PH, Chiap P, Crommen J, Boulanger B, Chapuzet E, Mercier N, Bervoas MS, Chevalier P, Grandjean D, Lagorce P, Lallier M, Laparra MC, Laurentie M, Nivet JC. (2003) Validation of the quantitative analytical procedures. Harmonization of the steps. *STP Pharma practice* 13, 101-138.
- Jang M., and Nah J. (2001) The synthesis of LMWSC for pharmaceutical application, *Applied Chemistry*, 6(2), 611-614
- Jia X., Chen X., Xu Y., Han X., Xu Z. (2009) Tracing transport of chitosan nanoparticles and molecules in Caco-2 cells by fluorescent labeling, *Carbohydrate Polymers* 78, 323–329
- Loretz B., and Bernkop-Schnürch A. (2006) In Vitro Evaluation of Chitosan-EDTA Conjugate Polyplexes as a Nanoparticulate Gene Delivery System, *The AAPS Journal*, 8 (4) Article 85
- Marques M.R.C., Loebenberg R., and Almukainzi M. (2011) Simulated Biological Fluids with Possible Application in Dissolution Testing, *Dissolution Technologies*, Aug.
- Merodia M, Mirshahi T, Mirshahi M. (2000) Development of a sensitive method for the determination of ganciclovir by reversed phase high-performance liquid chromatography. *J Chromatogr.* 870, 159-167
- QuantiPro™ BCA Assay Kit, Product information, Sigma-aldrich, Saint Louis, Missouri, USA
- Rifampicin Monograph, Indian Pharmacopoeia, Government of India, Ministry of Health and Family Welfare, 1996, Published by – Controller of Publication, New Delhi, pp. 666.
- Sonia T. A., Rekha M. R., Sharma C.P. (2011) Bioadhesive hydrophobic chitosan microparticles for oral delivery of insulin: *In vitro* characterization and *in vivo* uptake studies *Journal of Applied Polymer Science*, 119, 5, 2902–2910.
- Tatarczak M, Flieger J., and Szumilo H. (2005), High-Performance Liquid-Chromatographic Determination Of Rifampicin In Complex Pharmaceutical Preparation And In Serum Mycobacterium Tuberculosis-Infected Patients, *Acta Poloniae Pharmaceutica - Drug Research*, 62, 4, 251-256.
- Wang C., Ouyang J., Ye D.K., Xu J.J., Chen H.Y., Xia X.H. (2012) Rapid protein concentration, efficient fluorescence labeling and purification on a micro/nanofluidics chip, *12(15)*, 2664-71.

### 4.0 Vaccine preparation, extraction and purification

#### 4.1 Materials

PMRLB41/Rv3804/Ag85A in pET 15b pDNA, recombinant Ag85A protein and anti-Ag85 rabbit polyclonal antibody was obtained as a gift sample from Colorado State University (TBVRAM), (Colorado, USA). *E. Coli* DH5 $\alpha$  and BL21 DE3 pLysS cultures were obtained as a gift from Dr. Jayashree Pohnerkar's Lab, Department of Biochemistry, The M. S. University (Baroda, India). Agar and Luria broth (LB) were purchased from HiMedia Pvt. Ltd. (Mumbai, India). QuantiPro™ BCA protein assay kit, Bovine Serum Albumin was purchased from Sigma-Aldrich (St-Louis, USA). Minigel gel electrophoresis unit with power cable and BCA assay kit and Isopropyl  $\beta$ -D-1-thiogalactopyranoside (IPTG) were supplied by Bangalore Genei Pvt. Ltd. (Bangalore, India). Protease Inhibitor Cocktail, agarose, ethidium bromide, bromophenol blue were purchased from Sigma-Aldrich (St-Louis, USA). Digestion enzyme Xho I and digestion buffer 'O' was supplied from Fermentas International Inc., (Canada). HIS-Bind spin column were purchased from Sigma-Aldrich (St-Louis, USA). Cellulose dialysis tubing (Molecular weight cut of 12-14000 Da) were purchased from HiMedia Pvt. Ltd. (Mumbai, India). 96 well plates (Maxisorp) were purchased from Nunc (Denmark). Goat anti- rabbit IgG-pNPP (secondary anti-antibody) was purchased from Santa Cruz Biotechnology, Inc. (USA). Ammonium bicarbonate, calcium chloride, magnesium chloride, sodium dodecyl sulphate (SDS), glucose, EDTA, Tris.chloride, sodium hydroxide, potassium acetate, sodium acetate, sodium bicarbonate, sodium carbonate, glycerol, glacial acetic acid, urea were of molecular biology grade and purchased from Sigma-Aldrich (St-Louis, USA), Ethanol, methanol, hydrochloric acid (HCl) etc. and all other HPLC or molecular biology grade solvents were obtained from Sigma-Aldrich (St-Louis, USA).

#### 4.2 Transformation of pDNA into *E. Coli* DH5 $\alpha$ and BL21 DE3 pLysS

Methods for bacterial transformations are based on the work carried out by Mandel and Higa (1970). They demonstrated that, treatment of bacterial cells with chilled solution of calcium chloride and subsequent heat shock could cause transfection with bacetriophage-  $\lambda$  DNA. The same method was further used to transform bacteria with plasmid DNA and *E.Coli* chromosomal DNA (Cohen 1972). It was observed that, chilling cells in the presence of divalent cations such as Ca<sup>2+</sup> helps cell membrane to become permeable to plasmid DNA. Apparently, the treatment induces a transitory state of competence in the recipient bacteria, during which they are able to take up pDNAs derived from a variety of sources. In the current research work, similar method of transformation was utilized for the transfection of PMRL B41/Rv3804/Ag85A in *E. Coli* cells for pDNA isolation and protein expression. In this experiment, Ag85A was transformed into *E. Coli* DH5 $\alpha$  and BL21 DE3 pLysS for identification of Ag85A and expression of protein respectively as *E. Coli* DH5 $\alpha$  is known for its suitability in pDNA isolation and BL21 DE3 pLysS for protein expression.

##### 4.2.1 Transformation of PMRL B41/Rv3804/Ag85A (pDNA) into *E. Coli* DH5 $\alpha$ and BL21 DE3 pLysS by CaCl<sub>2</sub> method

Freshly autoclave sterilized Luria broth (LB) medium (5-10 ml) was inoculated with *E. coli* DH5 $\alpha$  and incubated overnight on shaker incubator at 30°C. Newly grown bacterial culture

was used to inoculate 50 ml of sterilized LB and incubated on shaker incubator for 3-4 hrs to grow upto mid log phase. After 3-4 hrs, mid log phase grown culture was centrifuged at 4000 rpm for 4 min at 4°C. Resultant pellet was treated with 1 ml of chilled 0.1 M MgCl<sub>2</sub> kept aside for 10 min and again centrifuged at 4000 rpm for 4 min at 4°C. Supernatant was discarded and pellet was suspended in last drop of supernatant (Caution !!! never vortex mixture at this stage). Thereafter, 1 ml of chilled 0.1 M CaCl<sub>2</sub> was added to it and allowed to react for 10 min. Suspension was centrifuged at 4000 rpm, 4°C for 4 min and the culture was maintained in 100 µl of 0.1 M CaCl<sub>2</sub> in ice bath for 45 min. pDNA was added to it and resultant composition was incubated in ice bath for 45 min. CaCl<sub>2</sub> treated pDNA was then subjected to heat shock at 42°C for 90 sec. and preserved in ice for 2 min. Thereafter, 1 ml of LB was added and incubated for 1 hr at 30°C. Suspension was centrifuged and pellet was suspended in 100 µl of LB, mixed well and the content was streaked on antibiotic containing LB-agar medium (to allow identification of plasmid-containing colonies) with the help of sterile streaking loop. Plates were incubated overnight at 37°C and single colony from the streaked plate was picked up and streaked again on the antibiotic-containing LB-agar medium so as to get the purified form of Ag85A transformed cells. This single colony was further grown in liquid media to collect pDNA.

Similar protocol was followed for the transformation of Ag85A in E. coli BL21 DE3pLysS by using BL21 DE3pLysS strain instead of DH5α.

### 4.3 Plasmid preparation using Alkaline Lysis method for isolation of pDNA

(Sambrooke, 2001)

#### 4.3.1 Preparation of reagents

Following reagents were prepared for the isolation of pDNA.

**Table 4.1: Composition of Different Alkaline Lysis solutions**

Alkaline Lysis I (GTE)	Alkaline Lysis II	Alkaline Lysis III (ml)
50 mM glucose	0.2 N NaOH	5M Potassium Acetate (60)
25 mM Tris.Cl (pH = 8.0)	1% SDS	Glacial Acetic Acid (11.5)
10mM EDTA (pH = 8.0)		Water (28.5)

#### ➤ Stock Solutions for Alkaline Lysis I (GTE)

- **Preparation of 1 M Glucose**

18.02 gms of glucose was weighed accurately and dissolved in 80 mL water, the final volume was made to 100 mL.

- **Preparation of 1M Tris Cl**

12.11 gm of Tris base was dissolved in 80 ml of water, pH was adjusted to the desired value using concentrated HCl and final vlume was made upto 100 ml using deionized water. (e.g. for pH 8, 42 ml of concentrated HCl was required for 1000 ml).

- **Preparation of 0.5 M Di-Sodium Ethylene Diaminetetraacetate (EDTA) (pH 8.0)**  
18.68 gm of EDTA · 2H<sub>2</sub>O was suspended in 80 ml of water and stirred vigorously on magnetic stirrer. pH of the solution was adjusted to 8.0 using sodium hydroxide to solubilize EDTA. It was then dispensed into aliquots and sterilized by autoclaving.

Solution I was prepared by adding required quantity of above mentioned reagents to give concentration of individual components as mentioned in the formula (Table 4.1). Solution I was prepared in batches of approximately 100 ml, autoclaved for 15-20 minutes at 15 PSI and stored at 4°C.

➤ **Stock Solutions for Alkaline Lysis II**

For preparation of alkaline lysis solution II, stock solutions of 0.2 N NaOH and 1% SDS were prepared and mixed just before its use.

➤ **Stock Solutions for Alkaline Lysis III**

- **Preparation of 5 M Potassium Acetate**

Potassium acetate (9.815 gms) was dissolved in 80 mL of milli Q water and final volume was made upto 100 mL. It was then sterilized by Autoclaving.

The resulting solution was 3 M with respect to potassium and 5M with respect to acetate.

➤ **Preparation of RNase stock solution**

Pancreatic RNase at a concentration of 10 mg/ml was added in 0.01 M potassium acetate (pH 5.2). This mixture was heated to 100°C for 15 minutes and allowed to cool slowly to room temperature (RT). pH of the solution was adjusted using 1M Tris Cl (pH 7.4) and dispensed into aliquots. Aliquots were stored at -20°C.

➤ **Preparation of Luria Broth (LB) medium**

20 gm of LB was added in 1000 mL deionized water and sterilized by autoclaving. After cooling to RT, calculated quantity of Ampicillin was added aseptically and resultant Amp-LB medium was dispensed as 5 ml aliquots in 25 mL conical flasks and stored them at RT.

➤ **Preparation of LB agar plates**

20 gm of LB and 10 gm of nutrient agar was added in 800 mL of deionized water, final volume was made to 1000 mL and LB medium was sterilized by autoclaving. Mixture was then cooled to around 50 °C (when it's bearable temperature to hold the flask) and calculated quantity of Ampicillin was added to it aseptically. Required volume of medium was transferred to sterile petri-plates aseptically and allowed to solidify. Plates were then sealed with parafilm and stored at 4 °C until used.

➤ **Preparation of Ampicillin antibiotic solution**

The stock solution of ampicillin (50 mg/mL in autoclaved water) was prepared and sterilized by filtration using 0.22 µ membrane filter. Stock solution was then stored at -20° C. Amount

of ampicillin required was transferred in a way to give final concentration of 100µg/mL depending upon the volume of LB medium and LB-agar medium.

#### 4.3.2 Plasmid (pDNA) isolation using alkaline lysis method

LB medium was inoculated with PMRL B41/Rv3804/Ag85A containing *E. coli* DH 5α and incubated overnight at 37 °C. Overnight grown culture was centrifuged for 5 min at 5000 rpm and pellet obtained was washed using 500 µl of Lysis I solution, mixed properly and centrifuged at 5000 rpm for 5 min. Pellet obtained was suspended in 100 µl of Lysis I solution, mixed properly and incubated for 5 min on ice. After the incubation period, 200 µl of freshly prepared Lysis II or Alkaline SDS solution was added, mixed gently and allowed to stand for 1-2 min. (Note: Close the tube tightly and mix the contents by inverting the tube rapidly five times. Make sure that the entire surface of tubes comes in contact with solution II. Do not VORTEX. Do not TAPE). Thereafter, 150 µl of Lysis III solution was added and vortexed in inverted position for 10 seconds to disperse solution III throughout the viscous bacterial lysate and incubated for 15-20 min in ice or in the freezer. The mixture was subjected to centrifugation for 5 min at 20000 rpm, supernatant was collected in a fresh tube, discarding cellular debris. To the supernatant, equal volume of phenol:chloroform was added, vortexed and centrifuged at 20000 rpm for 5 min. Upper phase containing supernatant was removed and equal volume of chloroform was added to it, again vortexed and centrifuged for 5 min at 2000 rpm. To the supernatant, 0.8 volume of isopropyl alcohol (IPA) was added and incubated for 20 min in ice or freezer to allow precipitation of pDNA. Resultant solution was centrifuged and pellet was air dried. 20 µl of TDW was added to dissolve the pellet and analyzed by 1 % gel electrophoresis using 2-5 µl of pDNA.

#### 4.4 Restriction analysis of small-scale preparations of plasmid DNA (PMRL B41/Rv3804c/Ag85A in pET15b) in *E. coli* DH-5α by Xho I Digestion

There are four commonly used methods to identify bacterial colonies containing recombinant plasmids viz. 1) Restriction analysis of small-scale preparations of plasmid DNA ; 2) A- complementation; 3) Insertional inactivation; 4) Screening by hybridization.

Out of these methods, restriction analysis was carried in the current research work. Following restriction enzymes can be used to determine pMRLB41/Rv3804c/Ag85A leading to different sizes of fragments as shown in table 4.2. In the given experiment, single digestion studies using Xho I RE were performed to determine the size of linearized plasmid (Colorado State University, Recombinant Protein production and quality record for TBRMVT contract HHSN266200400091C).

**Table 4.2: Fragment size and Res for Rv3804c**

Fragment (size)	REs
Vector- (5.69 kb pET 15b)	Nde I + Bam HI
Insert (0.893 kb RV 3804 C)	Nde I + Bam HI
Other 6.58 kb linearized plasmid	Nde I, Bam HI, Xho I single digest

In this method, a number of independently transformed bacterial colonies were picked up and grown in small-scale cultures. Plasmid DNA was isolated and purified as explained in the section 4.3.2 and pDNA obtained was analysed by restriction enzyme (RE) digestion studies using Xho I RE. Identification of Ag85A was carried out on agarose gel (1 %) electrophoresis. (Cohen, 1973, Sambrooke, 2001).

The system for the digestion was prepared as per the formula shown in table 4.3 and the total system was incubated at 37° C in water bath for 3 hrs. After the conditioned time, total amount of the digested pDNA was analysed on 1 % agarose gel electrophoresis in comparison with the λDNA ladder.

**Table 4.3: Composition of Restriction enzyme digestion studies**

Component	Quantity (µl)
Digestion Buffer	2
BSA	2
pDNA (Ag85A)	2
TDW	17.5
RE Xho I	0.5
<b>Total system</b>	<b>20.0</b>

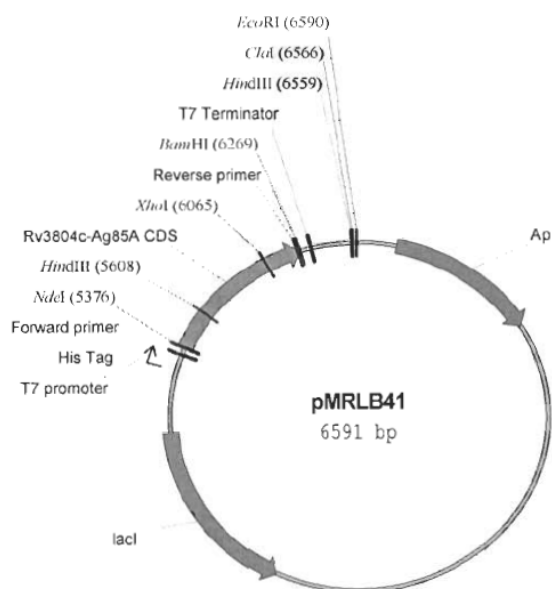


**Figure 4.1: pMRLB.41 – Rv 3804c – Ag85A in pET15b**

#### 4.5 Agarose Gel Electrophoresis (AGE)

Agarose gel electrophoresis is a common method used in molecular biology research so as to separate DNA or RNA molecules according to their sizes. It is based on the principle that, negatively charged nucleic acid molecules move through an agarose matrix when an electric field (electrophoresis) is applied. Shorter molecules move faster and migrate farther than

longer ones. Thus, the process allows the separation of large and small fragments of pDNA with the help of a molecular weight marker which is a mixture of known molecular weight DNAs alongside the purified plasmid DNA. This helps to estimate size of DNA fragment. Various proportion of agarose can be prepared for effective size separation of DNA molecules. Table 4.4 shows the different amount of agarose added in preparation of gel agarose electrophoresis for efficient separation of linear DNA molecules. (Brody 1972, Sambrooke 2001)

**Table 4.4 Percentage of agarose in gel for effective separation of linear pDNA**

<b>Amount of Agarose in Gel (%)</b>	<b>Effective range of resolution of linear DNA fragment (kb)</b>
0.5	1-30
0.7	0.8-12
1.0	0.5-10
1.2	0.4-7
1.5	0.2-3

#### 4.5.1 Preparation of reagents

Following composition of reagents were prepared for the agarose gel electrophoresis (AGE) (Table 4.5) and used in the given experiment.

**Table 4.5: Reagents for AGE**

<b>Buffer</b>	<b>Concentrated Stock Solution per Liter</b>	<b>Working Solution</b>
<b>50 x Tris- Acetate (TAE) – electrophoresis buffer</b>	<b>50x stock solution:</b> 242 gm Tris Base, 57.1 mL glacial acetic acid, 37.2 g EDTA (pH = 8) in 1000 ml water	<b>1x working reagent :</b> 40 mM Tris acetate ; 2 mM EDTA
<b>6x Buffer -gel loading buffer</b>	0.25% (w/v) bromophenol blue + 0.25% (w/v) xylene cyanol + 30% (v/v) glycerol was prepared in autoclaved deionized water. Stored at 4°C	
<b>Ethidium bromide solution</b>	<b>1000x stock:</b> 50 mg in 100 ml water	0.5 µg/ml

#### 4.5.2 Protocol for Agarose Gel Electrophoresis (Sambrooke, 2001)

A clean, dry agarose gel cast was sealed from the open end with cello tape to form a mold. A comb was placed in the notches provided so that a complete well was formed when poured agarose gets solidified. A known volume of 1 X TAE (electrophoresis buffer) was prepared, required quantity of agarose was weighed and dissolved in required volume of 1 X TAE to make 1 % of agarose gel. The neck of the flask was loosely packed with cotton plug and the slurry was heated in a microwave oven for a time required to allow all of the agarose grains to dissolve. The flask was shaken periodically to make sure that any grains sticking to the

walls enter the solution. Care was taken to avoid overheating of agarose solution, as it may cause higher evaporation of water during boiling and may change the percentage of agarose. Prepared agarose gel was preserved at RT for further use. Whenever needed, solid mass of agarose gel was melted in microwave oven, amount required to fill gel cast so as to form a gel thickness of around 3-5 mm was measured, ethidium bromide (from stock solution of 10 mg/mL in water to a final concentration of 0.5 $\mu$ g/mL and mix thoroughly) was added to it and molten mass was then poured into gel cast.

After complete solidification of gel (30-45 minutes at RT), the comb and autoclave tapes were removed carefully and the gel was placed in the electrophoresis tank. Electrophoresis tank was filled with the TAE buffer to cover the gel. A small quantity of pDNA (2-5 $\mu$ l) was mixed with the equal amount of gel loading buffer on parafilm using pipette and the mixture was slowly loaded into wells of the gel.

The electrophoresis unit was then closed with the lid and electrical Voltage of 1-5 v/cm (measured as the distance between the electrodes) was applied so that the DNA will migrate toward the anode (red lead). (**Observation:** If the leads have been attached correctly, bubbles should be generated at the anode and cathode (due to electrolysis) and within few minutes, the bromophenol blue should start migrating from the wells into the body of the gel). The gel was run until the bromophenol blue migrated the appropriate distance through the gel. (Note: During electrophoresis the ethidium bromide migrates towards the cathode in the direction opposite to that of DNA). Once the marker color was seen near the end of the gel (may be around 5 mm before the end of gel), the electric current was turned off and lead was removed. The gel was taken from the electrophoresis tank, examined under transilluminator (UVP, Cambridge, UK) and picture was captured using gel documentation system (UVP, Cambridge, UK).

### 4.6 Protein expression - induction, isolation and purification from Ag85A pDNA containing *E. Coli* BL 21 DE3 pLysS

**Protein expression** refers to the way in which proteins are synthesized, modified and regulated in living organisms. It is a subcomponent of gene expression consisting of the stages after DNA has been translated into poly peptide chains, which gets folded into proteins (Figure 4.3). Protein expression is very common phenomenon used in the biomedical research to measure the presence and copiousness of one or more proteins in a particular cell or tissue. It is usually done in living host systems such as Escherichia coli (*E. coli*), which is one of the most widely used bacterial host system for the production of heterologous proteins. The credit for its widespread use goes to its advantages like - availability of simple techniques to express usable amounts of protein, requirement of very short time to generate an overexpressing strain, cheap to grow and far better characterization of its genetics and physiology, which made it possible to think intelligently. Hence, *E. coli* is a choice of living host to begin with pilot expression experiments and for expression of commercially important proteins (Sambrook, 2001). Recent progress in the fundamental understanding of transcription, translation, and protein folding in *E. coli*, together with

availability of improved genetic tools are making this bacterium more valuable than ever for the expression of complex eukaryotic proteins. Proteins are normally expressed in their soluble form. However, many times, they are also present in the form of insoluble recombinant proteins and are called as inclusion bodies.

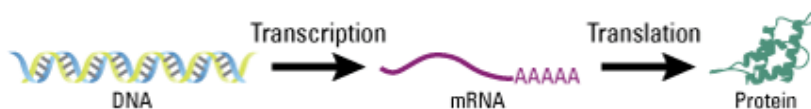


**Fig 4.2:** Schematic representation of protein synthesis

**Insoluble recombinant proteins (inclusion bodies):** Recombinant proteins are sometimes expressed (usually in *Escherichia coli*) in their insoluble form are called as inclusion bodies. Inclusion bodies are dense aggregates found inside cells consisting of a desired recombinant product in a nonnative state. The formation of inclusion bodies may be due to variety of reasons such as insolubility of the product at the concentrations being produced, inability to fold correctly in the bacterial environment, or inability to form correct, or any, disulfide bonds in the reducing intracellular environment. Their purification is simple, as they can be easily separated by centrifugation process from other cellular constituents leading to pure product. However, the protein obtained from inclusion bodies is not in its native state (occur in insoluble form). Palmer and Wingfield described methods for obtaining an active product from inclusion bodies (Palmer and Wingfield, 1995). One of them is to solubilize the protein using denaturing agents such as urea and refolding of the protein by slowly removing denaturing agent at controlled temperature (Sambrook, 2001; Kulshrestha et.al., 2005).

**Isopropyl  $\beta$ -D-1-thiogalactopyranoside (IPTG)** (Chemical formula:  $C_9H_{18}O_5S$ , Mol Wt: 238.3) is a molecular biology reagent, used as a molecular mimic of allolactose, a lactose metabolites that triggers transcription of the *lac operon*. Unlike allolactose, the sulphur (S) atom creates a chemical bond which is non-hydrolyzable by the cell, preventing the cell from "eating up" or degrading the inductant; therefore the IPTG concentration remains constant. IPTG induces the transcription of the gene coding for  $\beta$ -galactosidase, an enzyme that promotes lactose utilization, by binding and inhibiting the Lac 1 repressor. In cloning experiments, the *lacZ* gene is replaced with the gene of interest and IPTG is then used to induce gene expression. Many regulatory elements of the *lac* operon are used in inducible recombinant protein systems; IPTG is an effective inducer in the concentration range of 100  $\mu$ M to 1.5 mM.

**Protease Inhibitors:** Crude cell extracts contain a number of endogenous enzymes, such as proteases and phosphatases, which are capable of degrading the proteins present in the extract. The best way to improve the yield of intact proteins is to add inhibitors of those enzymes known to be present in the cell lysate and are called as protease inhibitors. Thus, Protease inhibitors are the substances used to prevent breakdown of protein into small fragments. This substance is added after induction and before cell lysis to prevent protein fragmentations. In this experiment protease inhibitor cocktail was used, which is a mixture of protease inhibitors with a broad specificity for the inhibition of serine, cysteine, acid and

thermolysin like proteases and aminopeptidases. One ml of cocktail solution is recommended for the inhibition of endogenous enzymes found in 100 ml lysate from 20 g (wet weight) of E. coli cells. (Product information, protease Inhibitor Cocktail for use in purification of Histidine-tagged proteins, Sigma Aldrich, st Louis, USA).

**4.6.1 Preparation of reagents**

***Preparation of separating (resolving) and stacking gel***

Stacking and separating gels were prepared as per the compositions given in the table 4.6. Plates were assembled for the preparation of SDS PAGE. All the ingredients required for the preparation of stacking and separating gel were mixed properly (Table 4.6). Just prior to pouring into the plates, TEMED was added into this mixture, vortexed and poured into the plates. Plates filled with the respective gels were kept aside for the polymerization of gel to form a firm gel.

**Table 4.6: Composition of Separating (Resolving) Gel and stacking Gel**

Chemicals	Separating Gel (10 ml)					Stacking Gel (5 %)	
	6%	8%	10%	12%	15%	4 ml	2 ml
Water	5.3	4.6	4	3.3	2.3	2.4	1.22
Acryl-bisacrylamide (30 %)	2.0	2.7	3.3	4.0	5.0	0.532	0.266
Tris Cl pH 8.8 (1.5 M)	2.5	2.5	2.5	2.5	2.5	--	--
Tris Cl pH 6.8 (1.5 M)	--	--	--	--	--	1.0	0.5
SDS (10 %)	0.1	0.1	0.1	0.1	0.1	0.04	0.02
APS (10 %)	0.1	0.1	0.1	0.1	0.1	0.04	0.02
TEMED	0.004	0.004	0.004	0.004	0.004	0.002	0.002

***Preparation of various solutions, buffers and reagents***

Various solutions, buffers and reagents which are useful for the protein expression and purification experiments were prepared as per the composition given in the table 4.7 and used for the experiments during the course of protein expression, induction and purification.

**Table 4.7: Compositions of buffers and reagents for expression & purification studies**

Name of Solution	Procedure
<b>10 % SDS</b>	10% stock was prepared in de-ionized water and stored at RT
<b>IPTG 100 mM Solution</b>	0.238gm of IPTG was dissolved in 10 mL milli Q water and sterilized by 0.22 µm disposable filter unit in a sterile tube under aseptic condition. Dispensed in 1 ml eppendorf and stored at -20°C
<b>1M Imidazole</b>	Accurately weighed 6.81 g of imidazole was dissolved in 100ml of deionized water.

## Chapter 4 - Vaccine Preparation, Extraction and Purification

<b>1M Sodium Chloride</b>	5.85 g sodium chloride was dissolved in 100 ml of deionised water
<b>200 mM Tris.HCl</b>	1.211 g of Tris base was dissolved in 50 mL of deionised water
<b>Tris Glycine Electrophoresis Buffer/ (5x Tank Buffer)</b>	3.02 g of Tris base (25mM) and 14.4 gms of glycine (192mM) was dissolved in 900 mL of de-ionized water. 10 mL of SDS solution (10% w/v) was added and final volume was adjusted to 1000 mL with de-ionized water.
<b>2x SDS-PAGE sample loading buffer</b>	Tris Cl (pH 6.8) – 25 ml, β-mercaptoethanol - 2 ml (0.2% final), SDS (electrophoresis grade) – 4 g (4 % final), Bromophenol blue – 1 mg (0.001 % final), Glycerol – 20 ml (20% final) were dissolved in deionized water and volume was made upto 100 ml. Stored in 1 ml aliquots at –70°C
<b>Preparation of 30% Acrylamide solution</b>	A stock solution containing 29% w/v acrylamide and 1% w/v N, N' methylene bisacrylamide was prepared in deionized warm water (to assist the dissolution of bisacrylamide) and stored at 2-8°C.
<b>10% Ammonium per Sulphate (APS)</b>	10 g of APS was transferred to 80 mL of de-ionized water and the final volume was made to 100 ml.
<b>1.5 M Tris Cl, pH 8.8</b>	18.15 g of Tris Cl was added in 80 mL of water, pH was adjusted to 8.8 by adding HCl and the volume was made to 100 ml with de-ionized water.
<b>1.5 M Tris Cl, pH 6.8</b>	6.05 g of Tris Cl was added in 80 mL of water, pH was adjusted to 6.8 by adding HCL and final volume was made to 100 ml with de-ionized water.
<b>Staining solution (Coomassie Brilliant Blue)</b>	0.025 g of Coomassie Brilliant Blue R-250 was dissolved in 100 ml of the methanol:acetic acid:water mixture (40:10:50 ) by stirring on a magnetic stirrer for about 3 hours and solution was filtered through whatman filter to remove any particulate matter.
<b>Destaining Solution I</b>	Methanol:Acetic acid:water (50: 10: 40 v/v)
<b>Destaining Solution II</b>	Methanol:Acetic acid:water (5: 7: 82 v/v)
<b>Equilibration Buffer for purification</b>	50 mM sodium phosphate with 0.3 M sodium chloride, pH 8.0
<b>Wash Buffer for purification</b>	50 mM sodium phosphate with 0.3 M sodium chloride and 5 mM imidazole, pH 8.0
<b>Elution Buffer for purification</b>	50 mM sodium phosphate with 0.3 M sodium chloride and 250 mM imidazole, pH 8.0
<b>Binding Buffer</b>	20mM Tris HCl, 250 mM NaCl, 5 mM Imizadole
<b>Lysozyme stock solution</b>	100 mg/ml in water
<b>Wash buffer for inclusion bodies</b>	50mM Tris.HCl ; 10 mM EDTA ; 0.5 % Triton X 100, pH 8.0 ; 100 mM sodium chloride
<b>Solubilisation buffer for inclusion bodies</b>	6M Urea, 10 mM Tris.HCl, pH 7.4
<b>Ammonium bicarbonate buffer pH 7.0 (ABB)</b>	1.582 g of ammonium bicarbonate was dissolved in 2000 ml of deionized water and filtered using whatman filter paper.
<b>Urea 6 M in ABB</b>	72.07 g of urea was dissolved in 200 ml of ABB.

## Chapter 4 - Vaccine Preparation, Extraction and Purification

<b>Triton x 100</b>	1% stock was prepared in deionised water.
<b>DNase stock</b>	5 µg/ml stock solution was prepared in deionised water
<b>RNase stock</b>	1 mg/ml stock solution was prepared in deionised water
<b>Saline solution</b>	0.9 % sodium chloride in deionised water

### 4.6.2 Transformation of pMRLB41/Rv3804c/Ag85A in E.coli BL21 DE3 pLysS

Transformation of pMRLB41/Rv3804c/Ag85A in E. coli BL21 DE3 pLysS was carried out using CaCl<sub>2</sub> method as per the protocol given in the section 4.2.1.

### 4.6.3 Induction of Protein Expression (Sambrooke, 2001)

Single bacterial colony (transformed) was transferred in to 5 mL of LB containing antibiotic (Ampicillin 100 µg/ mL) in loosely capped (cotton plug) 25 mL conical flask. The culture was incubated overnight at 37°C with vigorous shaking. Two flasks containing 5 mL of LB-antibiotic medium was inoculated with 1% of the primary inoculum. It was then incubated at 30°C for 3- 5 hours till it reached to optical density~0.6 at 600 nm. In one of the flask, sterile 0.5 mM IPTG was added aseptically (induced) and another kept blank without IPTG (uninduced). For Ag85A, induction was carried out at 20°C for 5-7 hours. Culture was pelleted down, washed with saline solution and lysate was prepared for further studies.

After confirmation of protein induction in a small batch, protein was expressed on large scale using 1 Liter bacterial culture and processed in a similar way to get purified protein for further use.

### 4.6.4 Cell Lysate Preparation and Extraction of Protein

#### 4.6.4.1 Cell Lysate Preparation

After expression studies (growing E. coli containing Ag85A = with and without IPTG), samples were pelleted down at 5000 rpm. Pellet was washed with saline thrice and final volume was made upto 0.5 ml using saline.

50-100 µl of uninduced and induced lysate was taken in test tube and volume was made upto 1-2 ml with saline. Optical density of both the solutions was matched to 0.6 OD by dilution and this cell lysate was used for the analysis of protein using SDS PAGE.

#### 4.6.4.2 Protein extraction from cell lysate

- 1) Remaining bulk sample of uninduced and induced protein cell lysate was subjected to sonication (2 pulses of 10 sec with 10 sec interval) until sample became clear.
- 2) After sonication, sample was centrifuged at highest speed for 30 min.
- 3) Supernatant was collected and checked for protein content using BCA protein assay kit.
- 4) Pellet was also suspended in saline and assessed for the protein content.
- 5) After this, uninduced and induced samples were collected from cell suspension, supernatant after sonication and remaining pellet after sonication.
- 6) Samples were taken in small eppendorf tubes, treated with SDS loading buffer and boiled at 90 °C for 10 min.

- 7) Samples were loaded in the well of SDS PAGE and electrophoresis was started at 100 mA
- 8) After 3-4 hrs, SDS PAGE unit was turned off and gel was carefully removed and washed using deionized water. Gel was then stained using staining solution, destained and observed and photographed using gel documentation system.

### ***4.6.4.3 Protein extraction from inclusion bodies***

After extraction of protein from cell lysate by sonication, remaining cell pellet was also analyzed using SDS-PAGE for possibility of protein present in it. The extraction of protein from cell pellet was carried out by suspending the pellet in binding buffer and denaturing agent (6M urea). Resultant mixture was subjected to shaking for 4 hrs at RT to solubilize any protein present. After 4 hrs, suspension was centrifuged at 20K for 40 min and supernatant collected was analyzed using SDS-PAGE. The protein present in the form of inclusion was solubilized using urea as denaturing agent and refolded by slowly removing urea (this was accomplished by gradient dialysis method) under controlled temperature.

### ***4.6.4.4 Renaturation/refolding of protein obtained from inclusion bodies***

Optimum solubilization of inclusion bodies was carried out using denaturing agent (urea) solution. The protein in the form of inclusion bodies was solubilized in a series of urea solutions from 1 M to 6 M and concentration of urea required to solubilize protein was selected based on the highest quantity of protein solubilized in it. Once this was determined, refolding of the protein obtained from inclusion bodies (solubilized using urea) was done by slowly removing denaturing agent using gradient dialysis method. Table 4.8 shows the entire protocol for the refolding experiment. In brief, protein inclusion bodies were solubilized in a small amount of 6M urea and transferred to dialysis bag of which one end was tied with the help of thread. After transferring protein solution, another end of dialysis bag was tied making sure that no protein solution was leaking from the dialysis bag. Bag was immersed in 200 ml of 6 M urea solution (in ABB) and incubated under stirring at 4°C. Concentration of urea was slowly decreased by adding fresh ABB and was finally reduced to 00 M of urea (Table 4.8). Dialysis was continued for a day in fresh ABB without urea (Observation: no sign of precipitation in the dialysis bag indicated successful refolding of protein). Refolded protein was analyzed using BCA protein assay kit and SDS PAGE.

Table 4.8: Protocol for refolding of the denatured protein

Time (Hr)	6 M Urea in ABB (ml)	ABB added (ml)	Total Vol (ml)	Concentration Urea (M)
0	200	Dialysis started		6M
2		33	233	5 M
4		66	299	4 M
6		100	399	3 M
8 & kept Overnight		133	532	2 M
Next day		Removed 282 ml and added 250 ml of fresh buffer	500	1 M
After 4 hrs		Removed 250 ml and added 250 ml of fresh buffer	500	0.5 M
After 8 hrs, contd. dialysis for a day		Replaced entire volume and added fresh buffer	500	00 M
Next day		Collected refolded protein from dialysis bag and analyzed by BCA protein assay kit		

#### 4.6.5 Sodium Dodecyl Sulfate Poly Acrylamide Gel Electrophoresis (SDS PAGE)

Electrophoresis is used to separate complex mixtures of proteins (e.g., from cells, subcellular fractions, column fractions, or immunoprecipitates), to investigate subunit compositions, and to verify homogeneity of protein samples. Almost all analytical electrophoresis of protein is carried out using poly acrylamide gels under conditions that ensure dissociation of the proteins into their individual poly peptide sub-units and that minimize aggregation. Most commonly, the stronger anionic detergent SDS in combination with a reducing agent and heat is used to dissociate the proteins before they are loaded onto the gel. The denatured poly-peptides bind to SDS and become negatively charged. Because the amount of SDS bound is always proportional to the molecular weight of poly peptide and is independent of its sequence, SDS-poly-peptide complex migrate through poly acrylamide gels in accordance with the size of poly peptide. In polyacrylamide gel electrophoresis, proteins migrate in response to an electrical field through pores in the gel matrix; pore size decreases with higher acrylamide concentrations. The combination of gel pore size and protein charge, size, and shape determines the migration rate of the protein. At saturation, approximately 1.4 g of SDS is bound per gram of poly peptide. By using marker of known molecular weight protein, it is therefore possible to estimate the molecular weight of the polypeptide chain (Sambrooke 2001).

In most cases, SDS-PAGE is carried out with discontinuous buffer system in which the buffer in the reservoir is of a different pH and ionic strength than the buffer used to cast gel. The SDS-poly peptide complexes in the sample that is applied to the gel are swept along by a moving boundary created when electric current is passed between electrodes. After migrating through a stacking gel of high porosity, the complexes are deposited in a low porosity zone of the resolving gel. The ability of discontinuous buffer systems to concentrate the entire sample into a very small volume greatly increases the resolution of SDS-polyacrylamide gels.

Discontinuous buffer system that is most widely used was originally devised by Ornstein (1964). The sample and stacking gel is made up of Tris.Cl buffer (pH 6.8), whereas resolving gel contains Tris. Cl (pH 8.8). Reservoir buffer contain Tris-glycine of pH 8.3, which is used to fill upper and lower chamber of the SDS PAGE unit. All components of the system contain 0.1% SDS. The chloride ions in the sample and stacking gel form the leading edge of the moving boundary, and the trailing edge is composed of glycine molecules. Between leading and trailing edges of boundary is a zone of lower conductivity and steeper voltage of gradient which sweeps the poly peptides from the sample and deposits them on the surface of the resolving gel. There, the higher pH of the resolving gel favours the ionization of glycine, and the resulting glycine ions migrate through the stacked poly peptides and travel through the resolving gel immediately behind chloride ions. Freed from the resolving boundary, the SDS-poly peptide complexes move through the resolving gel in a zone of uniform voltage and pH and are separated according to size by sieving across the resolving gel.

Polyacrylamide gels are composed of chains of polymerized acrylamide that are cross linked by a bifunctional agent such as N, N' – methylenebisacrylamide. The effective range of separation of SDS-PAGE depends on the concentration of polyacrylamide used to cast the gel and on the amount of cross linking. Polymerization of acrylamide in the absence of cross linking agents generates viscous solutions having no practical value in the preparation of gels. Cross linking between acrylamide and bisacrylamide add rigidity and tensile strength to the gel and form pores through which the SDS-polypeptide complex passes. The size of these pores decreases as the bisacrylamide:acrylamide ratio increases, reaching a minimum when the ratio is approximately 1:20. Most SDS- polyacrylamide gels are cast with a molar ratio of bisacrylamide: acrylamide of 1:29 which has been shown empirically to be capable of resolving poly peptide that differ in size by as little as 3%. Thus, sieving properties of the gels are determined by the size of the pores which is a function of the absolute concentration of acrylamide and bisacrylamide used to cast the gel.

### 4.6.5.1 Procedure for SDS-PAGE

Two plates (one notched and other continuous) were assembled, a spacer was placed between two plates and plates were tightened with the help of clips at both the ends. The bottom of the plates was sealed with agarose solution. Assembled plates were kept vertically in the SDS-PAGE unit. Resolving and stacking solution were prepared as per the composition and quantities in the table 4.6. TEMED was added just before pouring the gel (as polymerization starts as soon as TEMED is added). Resolving gel solution was poured between the gap of the plates and a small amount of butanol was also poured over it to ensure even layer and was then allowed to polymerize for around 30 minutes. After polymerization, the upper layer of the resolving gel was cleaned by washing with water and stacking gel solution was poured directly onto its surface. Immediately, a clean Teflon comb was inserted into stacking gel solution, taking care to avoid any air bubbles. More stacking gel solution was added to fill the spaces of the comb completely. Finally, the gel was kept vertical at RT to allow polymerization of stacking gel solution. Meanwhile, protein (Ag85A) samples

were prepared by heating them to 100 °C for 3 minutes in 2x SDS-PAGE loading buffer (table 4.7) to denature proteins.

After complete polymerization of the stacking layer, teflon comb was removed carefully. Wells were washed with deionized water to remove any un-polymerized acrylamide and the gel was mounted in the electrophoresis apparatus. Tris-glycine electrophoresis running buffer was added to the top and bottom reservoir. The composition of gel running buffer is as shown in table 4.7. 30 µL of each sample was loaded in a pre-determined order into wells and the electrophoresis apparatus was attached to an electric power supply with the voltage of 50 mV. The gel was run until bromophenol blue moved into resolving gel and the voltage was increased to 120 mV and run until bromophenol blue reached the bottom of the resolving gel (it took about 4 hours). The power was turned off, glass plates were removed from the electrophoresis apparatus and placed on a paper towel to soak any of the liquid. The plates were separated by applying gentle pressure with spatula. The orientation of the gel was marked by cutting a corner from the bottom of the gel that was close to the leftmost well. (Note: do not cut the corner from gels that are to be used for western blotting).

The gel was then stained with Coomassie brilliant blue staining solution. In brief, the gel was immersed in at least 5 volumes of staining solution and placed on a rocking platform (rocker) for minimum 4 hours at RT. After 4-5 hrs, gel was removed from the staining solution and immersed in the de-staining solution for 3-4 times. (Note: The more thoroughly the gel is de-stained, the smaller the amount of protein that can be detected by staining with Coomassie Brilliant blue. De-staining for 24 hours usually allows as little as 0.1µg of protein to be detected in a single band). After de-staining, gel was scanned for permanent records (Note: gel may be stored indefinitely in water in a sealed plastic container without any diminution in the intensity of staining. Stained gels should not be stored in de-staining buffer which will cause the stained protein bands to fade).

### 4.6.6 Protein Purification using HIS-Select™ spin column (Product information, Sigma Aldrich)

The HIS-Select Spin Column is an immobilized metal-ion affinity chromatography (IMAC) product that allows rapid purification of small-scale crude cell extracts containing histidine tagged proteins. The HIS-Select Spin Column contains 20 mm, spherical silica particles (100 nm pore size) with a hydrophilic layer. The silica is derivatized with a proprietary quadridentate chelate charged with nickel. HIS-Select Spin Columns are selective for recombinant proteins with histidine tags and exhibit very low non-specific binding of other proteins. The selectivity can be modulated with the inclusion of imidazole during chromatography. The binding capacity of a HIS-Select Spin Column is >500 µg per column as determined with an ~30 kDa histidine tagged protein recovered under high levels of protein expression. Protein purification was carried out using HIS-Select™ spin column as per manufacturer's protocol (HIS-Select™ spin column, H 7787, Sigma Aldrich, St. Louis, USA). The Equilibration and wash buffer were supplemented with 1–10 mM imidazole and 0.15–0.5 M sodium chloride to reduce non-specific protein binding. Due to the unique

selectivity of the chelate, 5 mM imidazole in the Wash Buffer is sufficient to obtain high purity samples.

**4.6.6.1 Protocol for protein purification**

Protein purification was performed as per manufacturer’s protocol (HIS-Select™ spin column, H 7787, Sigma Aldrich, St. Louis, USA) as given below.

- 1) HIS-Select Spin Columns and collection tubes were removed from bag.
- 2) 600 µl of equilibration buffer was added to the spin columns and were closed with the help of collection tube lid.
- 3) Tubes were subjected to centrifugation at 2,000–5,000 rpm (325–2,040 g) at room temperature for ~2 minutes. Note: HIS-Select Spin Columns may also be used with an appropriate vacuum manifold in place of the centrifugation step.
- 4) Spin columns were removed from collection tube.
- 5) Collection tubes were emptied and spin column was placed back in the same collection tube.
- 6) The prepared cell extract was loaded on the column (The column capacity up to 600 µl of extract at one time) and centrifuged as given in step 3.
- 7) Spin columns were removed from collection tubes and the flow-through was saved for later analysis.
- 8) Using a new collection tube, unbound protein was washed from the spin column using 600 µl of wash buffer with centrifugation. Collection tubes were emptied and samples were collected.
- 9) Washing step was repeated three times with 600 µl of wash buffer.
- 10) Using new collection tube, the targeted protein was eluted using up to 500 µl of elution buffer by using centrifugation as given in the step 3.
- 11) Samples were collected and analyzed for protein using BCA protein assay kit, QuantiPro BCA Reagent and SDS-PAGE.

**4.7 ELISA (criss cross) assay to optimize reagent concentration and Ag85A activity**  
(Sambrooke 2001)

**4.7.1 Preparation of reagents**

Following reagents were prepared for their application in ELISA assay (Table 4.9).

**Table 4.9: Reagents for ELISA assay**

Reagent	Procedure
<b>Carbonate buffer, (0.1M, pH 9.2) (Coating buffer)</b>	1.36 g of sodium carbonate and 7.35 g of sodium bicarbonate was dissolved in 800 ml of deionized water and pH was adjusted with 1M HCl or 1M NaOH if necessary & volume was made upto 1000 ml
<b>10x Phosphate buffer saline (PBS) pH 7.5</b>	80 g of sodium chloride, 2 g of potassium chloride, 11.5 g of disodium hydrogen phosphate, and 2 g of potassium dihydrogen phosphate were dissolved in 800 ml of deionized water, pH was adjusted & volume was made upto 1000 ml
<b>Blocking buffer (1x)</b>	0.02 % sodium azide + 0.5% BSA was prepared in 1x PBS

<b>PBS)</b>	
<b>1x PBS</b>	0.02 % sodium azide was prepared in 1x PBS
<b>1x PBST</b>	0.05% tween 20 was prepared in 1x PBS
<b>Diethanolamine buffer</b>	10mM Diethanolamine + 0.5% magnesium chloride in water
<b>Antigen solution</b>	Required amount of antigen was prepared in coating buffer solution
<b>Primary antibody (1:200; 1:1000; 1:5000)</b>	Required dilution was prepared in blocking buffer
<b>Secondary antibody-alkaline phosphatase (ALP) (1:500; 1:1000; 1:5000)</b>	Required dilution was prepared in blocking buffer
<b>p-nitrophenyl phosphate (pNPP) substrate</b>	1mg/ml stock solution was prepared in diethanolamine buffer

#### 4.7.2 Procedure for criss cross ELISA

A slight modification of criss cross analyses was performed to determine optimal concentrations of reagents to be used in ELISA assay (Sambrook, 2001). Reagents tested included, antigen, primary antibody and secondary antibody. All three reactants, a primary solid-phase coating reagent (antigen Ag85A), a secondary reagent (primary antibody) that binds the primary reagent and secondary reagent (secondary antibody) were diluted and analyzed by a criss-cross matrix analysis (Table 4.10). Antigen Ag85A concentration was varied from 0-1 µg, primary antibody was serially diluted (two fold dilution) and secondary antibody was varied from 1:500-1:5000. The concentration of three reagents was considered optimum, where OD ~ 1 was obtained. Once the optimal concentrations of reagents to be used for ELISA assay were determined, these variables were kept constant and antigen concentration was determined in comparison to the standard antigen provided by Colorado State University.

100 µL solution of Ag85A in 100 mM coating buffer (carbonate buffer, pH 9.2) was transferred to 96 well plates. The plate was incubated overnight (about 14-16 hours) at 2-8°C to coat the antigen to wells of the plate. The antigen solution was withdrawn from the wells and blocked with 200 µl of blocking buffer (1X PBS containing 0.5% BSA+ 0.02% sodium azide). The plate was left aside for about 3-4 hours at RT to allow antigen bind with surface of well. The content was discarded and washed once with 1X PBS solution (1X PBS containing + 0.02% sodium azide). 100 µL of primary antibody was transferred to proteins Ag85A coated wells as shown in table 4.10 and incubated at RT for 4 hrs. After the incubation period, wells were washed thrice with PBST (1X PBS+ 0.05% Tween 20, pH 7.4) and 100 µl of previously diluted secondary antibody-ALP (attached to alkaline phosphatase) was added to each well as shown in table 4.10. Plates were then kept aside for 1 hr at RT. Again wells were washed 3 times with PBST with the interval of three minutes and 100 µl of pNPP substrate was added to each well and incubated at RT for 20 min. Hydrolysis was monitored qualitatively by visual inspection (development of yellow colour) and quantitatively with a microtiter plate reader. Hydrolysis was stopped by adding 100 µL 0.1M

EDTA and the absorbance was measured at 405 nm using ELISA plate reader (680XR, Bio-rad, France).

**Table 4.10: Criss Cross analysis to determine optimal reagent concentration**

Ag(ng)	1	2	3	4	5	6	7	8	9	10	11	12	
A	0	100	500	1000	0	100	500	1000	0	100	500	1000	2°Ab, 1:
B	0	100	500	1000	0	100	500	1000	0	100	500	1000	500
C	0	100	500	1000	0	100	500	1000	0	100	500	1000	500
D	0	100	500	1000	0	100	500	1000	0	100	500	1000	1000
E	0	100	500	1000	0	100	500	1000	0	100	500	1000	1000
F	0	100	500	1000	0	100	500	1000	0	100	500	1000	5000
G	--	--	--	--	--	--	--	--	--	--	--	--	5000
H	--	--	--	--	--	--	--	--	--	--	--	--	
1°Ab,1 : :	20 0	200	200	200	100 0	100 0	100 0	1000	50 00	500 0	500 0	5000	

Coloured area denotes 96 wells of the plate; 1° Ab – Primary antibody (1: respective concentration, e.g. 1:200); 2° Ab – Secondary antibody (1: respective concentration, e.g. 1:500)

#### 4.7.3 Determination of Ag85A Activity

The purified protein Ag85A was subjected to ELISA assay to estimate its antigenicity. The comparison of Ag85A activity was made with the standard Ag85A proteins provided by Colorado State University (USA). The optimized concentrations of primary antibody and ALP conjugated secondary antibody were taken and the quantity of Ag85A was determined.

100 µL solution of Ag85A in 100 mM coating buffer (carbonate buffer, pH 9.2) was transferred to 96 well plates. The plate was incubated overnight (about 14-16 hours) at 2-8°C. The antigen solution was withdrawn from the wells and blocked with 200 µl of blocking buffer (1X PBS containing 0.5% BSA+ 0.02% sodium azide). The plate was left aside for about 3-4 hours at RT to allow antigen bind with surface of well. The content was discarded and washed once with 1X PBS solution (1X PBS containing + 0.02% sodium azide). 100 µL of primary antibody was transferred to proteins Ag85A coated wells (as shown in table 4.10) and incubated at RT for 4 hrs. After the incubation period, wells were washed thrice with PBST (1X PBS+ 0.05% tween 20, pH 7.4) and 100 µl of previously diluted secondary antibody was added to each well as shown in table 4.10. Plates were then kept aside for 1 hr at RT and were again washed 3 times with PBST at interval of three minutes. 100 µl of pNPP substrate was added to each well and incubated at RT for 20 min. Hydrolysis of phosphate group from substrate molecule (ALP) was monitored qualitatively by visual inspection through development of yellow coloured complex and quantitatively with a microtiter plate reader. Hydrolysis reaction was stopped by adding 100 µL 0.1M EDTA (as soon as the color development reached OD 1) and the absorbance was measured at 405 nm using ELISA plate reader (680XR, Bio-rad, France).

#### 4.8 Fluorometric analysis of Tryptophan, BSA, native, urea-denatured and refolded Ag85A

Nature of urea-denatured and refolded protein was examined by means of fluorescence emission spectra (Ostrowski et.al., 1993). Samples were prepared by dissolving proteins (tryptophan, BSA, native Ag85A, refolded Ag85A, denatured Ag85A) in water (pH 7.0) to make a concentration of 0.05µg/ml and emission spectra for all samples were recorded using fluorometer (RF-530, Shimadzu, USA).

#### 4.9 Results and Discussion

##### 4.9.1 Transformation and pDNA isolation

Transformation of Ag85A was successfully carried out in E. Coli DH5α (for determination of pDNA) and BL 21DE3 pLysS (for protein expression). When transformed cells were subjected to single colony purification, easily identifiable single colonies of Ag85A transformed cells were observed on antibiotic containing LB-Agar medium. pDNA was successfully transformed and carefully isolated from the transformed cells using alkaline lysis method. Purified pDNA was further confirmed by the restriction enzyme digestion studies.

After single digestion studies, a single band of 6591 base pairs was observed on the agarose gel indicating that the DNA was cut using Xho I and digested the pMRLB.41 (Rv3804c/ Ag 85 A in pET15b) leading to linear fragment of the said pDNA. Fig 4.3 shows the results of Xho I single digestion of pDNA in comparison to molecular marker λ-H (1:10).



**Fig 4.3 - Ag85A by Xho I digestion**  
**Lane 1 – Ag85A; Lane 2 – Ag85 A ; Lane 3 – Marker ladder**

The relative distance travelled by linearized plasmid DNA after digestion studies was compared with standard DNA ladder and results of the AGE confirmed that the size of linearized plasmid DNA under study was 6591 bp.

##### 4.9.2 Protein Expression and Purification

Transformation of Ag85A was successfully carried out in E. Coli BL21DE3 pLysS (for protein expression). Transformed cells were subjected to single colony purification and easily identifiable single colonies of Ag85A transformed cells were observed on antibiotic containing LB-Agar medium. pDNA was carefully isolated from the transformed cells using alkaline lysis method. After alkaline lysis experiment, pDNA obtained was further used for protein expression studies.

Protein expression study was successfully carried out in *E. coli* BL21 DE3 pLysS strain. Expression of Ag85A was clearly observed after induction of Ag85A using IPTG (Figure 4.4). Initially, induction was carried out at room temperature. However, no induction was noted. Therefore, temperature and time after adding IPTG was changed to 20 °C. The samples were incubated on shaker incubator at 20°C for 14-16 hours for induction. The culture was pelleted down and processed further for SDS-PAGE analysis. Results of the SDS PAGE studies clearly indicated induction of Ag85A in the cell lysate under the conditions optimized (Fig 4.4). Lane 2 shows highly expressed band of Ag85A at 32 kDa (when compared to protein marker (PM). A band of 32 kDa was observed just above the PM band of 29 kDa. However, no induction of expression was seen in uninduced Ag85A (Lane 1). This indicated that IPTG was helpful to induce the expression of 32 kDa protein Ag85A.

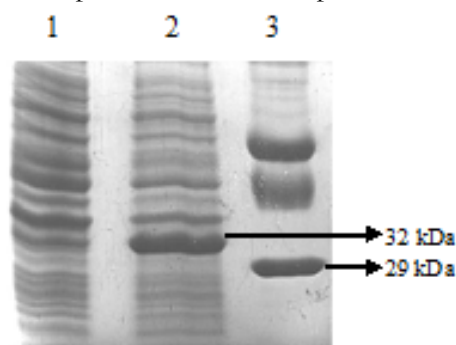


**Figure 4.4: Protein expression in cell lysate**

**Lane 1** – Ag85A uninduced (without IPTG); **Lane 2** –Ag85A induced (with IPTG);  
**Lane 3**- Protein Marker

Sonication was used to break the cells and release the protein from cells. After sonication, supernatant and pellet was collected and analyzed by SDS-PAGE. Results of the SDS PAGE analysis confirmed the presence of 32 kDa protein Ag85A in the supernatant. However, a band of 32 kDa protein (Ag85A) was also observed in the pellet as inclusion bodies on the gel. Therefore, pellet was also processed to extract Ag85A from inclusion bodies. Results of the SDS-PAGE after sonication of cell lysate are shown in figure 4.5. Lane 1 clearly indicates the presence of 32 kDa protein Ag85A in the supernatant (Ind - S). Similarly, Ag85A was also found in insoluble form indicating accumulation of protein as inclusion bodies, as shown in Fig 4.5, Lane 4 (Ind - P). In comparison to the protein marker (PM) of 42 kDa protein, both the Lanes, 1 and 4 were found to show a band of 32 kDa Ag85A. The presence of Ag85A in the form of inclusion bodies (Lane 4) was found to be pure than the one present in soluble form (Lane 1). This result is in compliance with the general reports on protein expression (Sambrook, 2001).

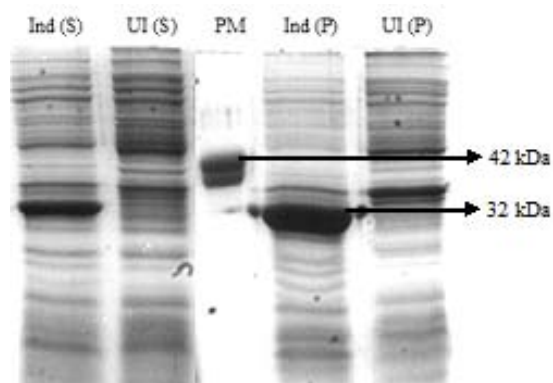


**Figure 4.5: Protein expression in cell suspension and pellet**

**Lane 1 (Ind(S))** - Ag85A induced (with IPTG); **Lane 2 (UI (S))** - Ag85A uninduced (without IPTG) ; **Lane 3 – PM (42 kDa)**; **Lane 4 (Ind(P))** - Ag85A induced (with IPTG); **Lane 5 (UI(P))**- Ag85A uninduced (without IPTG)

After determining the presence of 32 kDa protein Ag85A in inclusion bodies, Ag85A solubilization was standardized using different molar concentrations of denaturing agent urea (fig 4.6). In brief, pellet containing inclusion bodies obtained after sonication was subjected to solubilization using denaturing agent urea by shaking for around 4-5 hrs in shaker incubator at 20°C. After 4-5 hrs, suspension was centrifuged and supernatant obtained was collected and analyzed by SDS PAGE. Concentration of urea by which higher amount of Ag85A was extracted was selected to isolate Ag85A from inclusion bodies. Results of the standardization of protein solubilization indicated that 6 M urea was able to extract higher amount of protein from the inclusion bodies (Fig 4.6, Lane 7) and therefore it was selected for further extraction of protein. Figure 4.6, Lane 7 indicated the presence of Ag85A in its soluble form due to denaturing agent (urea) and was found to be pure than the one obtained from initial cell lysate supernatant (fig 4.5, Lane 1, Ind-S). The band presented in the lane 7 was compared with the band of protein marker (PM) (Lane 8) and concluded that, the band in Lane 7 should be of 32 kDa, as its occurrence was just below the band of 42 kDa protein in the lane 8. SDS PAGE analysis of remaining pellet after solubilization of protein in urea was also done. Results displayed in figure 4.7 showed the presence of Ag85A in lane 4 (urea solubilized). However, nothing was observed in the Lanes 1 to 3, suggesting complete solubilization of Ag85A in denaturing agent (urea).

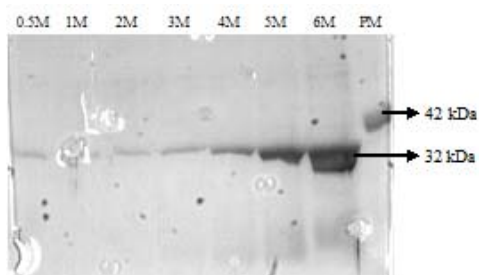


**Figure 4.6: Standardization of inclusion bodies solubilization using different molar urea**

**Lane 1** – 0.5M urea ; **Lane 2** - 1M urea; **Lane 3** – 2 M urea; **Lane 4** – 3 M urea ; **Lane 5** – 4 M urea; **Lane 6** - 5 M urea; **Lane 7**- 6 M urea; **Lane 8** - PM (42 kDa)

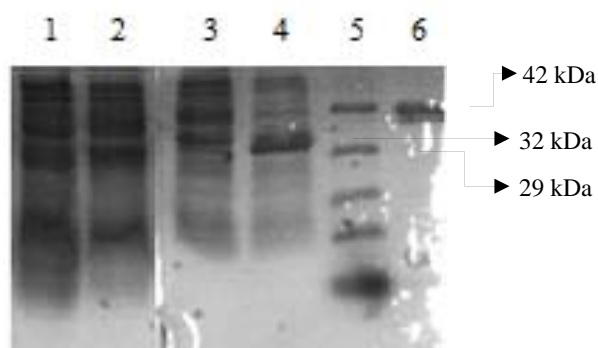


**Figure 4.7: Protein expression in inclusion bodies after urea solubilisation**

**Lane 1 (UI (P))** - Ag85A uninduced (without IPTG); **Lane 2 (Ind (P))** - Ag85A induced (with IPTG) ; **Lane 3 (UI (S))** - Ag85A uninduced (without IPTG); **Lane 4 (Ind (S))**- Ag85A induced (with IPTG); **Lane 5** – PM ; **Lane 6** : PM (42 kDa)

The protein obtained in its insoluble form as inclusion bodies was further refolded by slow removal of denaturing agent at 4°C. After complete refolding, protein Ag85A was separated and detected on SDS PAGE. Figure 4.8 depicts the image of refolded Ag85A and it can be distinctly seen in lane 2 and 3 in comparison to the protein marker in lane 1.

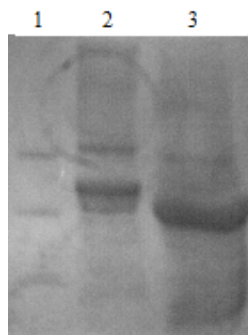


**Figure 4.8: Refolded protein on SDS PAGE**

**Lane 1** – PM; **Lane 2** – Refolded Ag85A; **Lane 3** – Refolded Ag85A

Thus, the overall experiment yielded two types of Ag85A, native Ag85A (Protein 1) and refolded Ag85A (Protein R1), both of which found to be in soluble form. These proteins were then successfully purified using His-tag Spin Columns™. Figure 4.9 and 4.10 represents the SDS PAGE image of purified protein 1 and R1 respectively. Bands of Ag85A, 32 kDa purified protein 1 (Fig 4.9, Lane 5) and R1 (Fig 4.10, Lane 4) can be distinctly seen on SDS PAGE. Purified Ag85A 1 was quantified by using BCA protein assay kit and the yield of the protein was found to be 1817µg/ml from 5 liter bacterial culture. Similarly Ag85A R1 was also quantified and its concentration was found to be 209.2 µg/ml of Ag85A R1 from 1 liter bacterial culture.

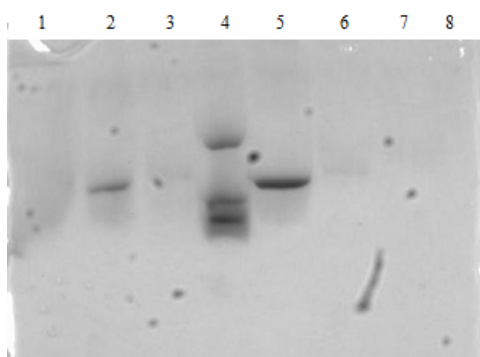


**Figure 4.9: Purified protein 1 (Ag85A)**

**Lane 1** - Flow through (FT); **Lane 2** – Wash 1 (W1) ; **Lane 3** - Wash 2 (W2) ;  
**Lane 4** - Protein Marker (PM); **Lane 5** - Elute 1(E1); **Lane 6** - Elute 2 (E2);  
**Lane 7** - Elute 3 (E3); **Lane 8**- Elute 4 (E4)

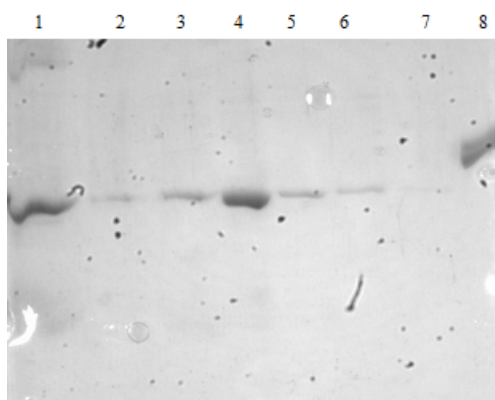


**Figure 4.10: Purified protein R1 (Refolded Ag85A)**

**Lane 1** - Flow through (FT1); **Lane 2** – Flow through (FT2); **Lane 3** - Wash 2 (W2) ; **Lane 4** - Elute 1(E1); **Lane 5** - Elute 2 (E2); **Lane 6** - Elute 3 (E3);  
**Lane 7** - Elute 4 (E4); **Lane 8**- Protein Marker (PM)

### 4.9.3 ELISA assay

Criss cross ELISA assay was performed to determine optimum concentrations of antigen Ag85A, primary antibody, and secondary antibody so as to get the proper concentrations of each reactant for optimum colour development to confirm the presence of Ag85A. Table 4.11 shows the results of optimization of reagents tested. Absorbance values near to one

were obtained from the combination of 500 ng of Ag85A, 1:1000 dilution of primary antibody and 1:5000 dilution of secondary antibody. Table 4.12 represents the optimized parameters for ELISA assay. Absorbance values obtained from the combination of reagents were subtracted from the blank absorbance (with no=0 antigen). Absorbance in the wells with no antigen could be due to non-specific binding of antibody. Finally, the concentration of reagents where absorbance value equals to one was noted and considered as optimized concentration of each reagent under test (Table 4.11).

**Table 4.11: Criss Cross analysis to determine optimal reagent concentration**

Ag(ng)	0	100	500	1000	0	100	500	1000	0	100	500	1000	2°Ab
	1	2	3	4	5	6	7	8	9	10	11	12	-1:
A	0.466	2.415	Over	Over	0.425	0.977	2.3	2.821	0.142	0.265	0.714	0.866	500
B	0.320	2.005	Over	3.375	0.245	1.053	2.512	2.384	0.132	0.325	0.891	1.148	500
C	0.274	1.901	3.262	2.638	0.273	0.883	1.427	2.13	0.12	0.196	0.521	0.533	1000
D	0.272	1.874	3.309	3.088	0.258	0.824	1.396	2.278	0.124	0.234	0.690	0.535	1000
E	0.219	1.555	2.255	2.218	<b>0.205</b>	0.522	<b>1.216</b>	1.740	0.111	0.175	0.491	0.400	<b>5000</b>
F	0.046	1.736	2.441	2.012	<b>0.176</b>	0.66	<b>1.204</b>	1.881	0.111	0.207	0.518	0.645	<b>5000</b>
G					<b>C Ab</b>		<b>1.011</b>						
H					<b>C Ab</b>		<b>1.027</b>						
1°Ab,1:	200	200	200	200	1000	1000	<b>1000</b>	1000	5000	5000	5000	5000	

*C Ab* – corrected absorbance (shown in bold letters); Blue colored area denotes total well of the plate (96 wells) under study; Purple coloured blocks indicated reagents under study; Olive green block means blank absorbance; Orange coloured blocks stands for optimized concentration of respective reagent.

**Table 4.12: Optimized parameters for ELISA**

Sr. No.	Parameters	Optimized Values
1	Antigen Concentration	500 ng
2	Primary Antibody dilution	1:1000
3	Secondary Antibody dilution	1:5000
4	Incubation time for coating	overnight (14-16 hrs) at 4°C
5	Incubation time for primary antibody	4 hrs at RT
6	Incubation time for secondary antibody	1 hr at RT
7	Incubation time for substrate	20 min at RT

The antigenicity of each protein Ag85A 1 and Ag-85A R1 was compared with the standard proteins provided by Colorado State University (USA). 0.5 µg of each protein was coated on Nunc Maxisorb ELISA plates in triplicate. Similarly, standard protein was also coated. The protein activity was determined by ELISA as explained in the section 4.8. Average values of absorbance were noted and percentage of protein activity was calculated with respect to values obtained with standard protein. The antigenicity of Ag85A protein synthesized in our laboratory was found to be 98.33 % for Ag85A 1 and 91.66 % for Ag 85 A R1.

#### 4.9.4 Fluorometric analysis of Tryptophan, BSA, native Ag85A, urea-denatured Ag85A & refolded Ag85A

Nature of urea-denatured and refolded protein was examined by means of fluorescence emission spectroscopy. The native protein (pH 7.0), when excited at 227 nm, showed an emission maximum at 340 nm. Similarly, the emission maximum of free tryptophan was at 360 nm upon excitation at 280 nm. After denaturation of Ag85A inclusion bodies with 6 M urea at 20°C, the emission maximum of the denatured Ag85A was found to be 350 nm indicating slight shift in the spectrum by 10 nm towards higher wavelength. When the urea denatured protein (UDP) was refolded by using gradient dialysis at 4 °C, the emission spectra of re-natured protein shifted back to 340 nm (figure 4.11).

Refolded Ag85A showed the same characteristics to that of the native Ag85A by spectral shift, when it was renatured using gradient dialysis at 4°C. These results suggested that refolded Ag85A does not differ a lot from that of the native one. But, there could be apparent difference in the conformation of Ag85A in the refolded state as compared to its native form. These results are in accordance with the results reported by the Ostrowski et.al., (1993).

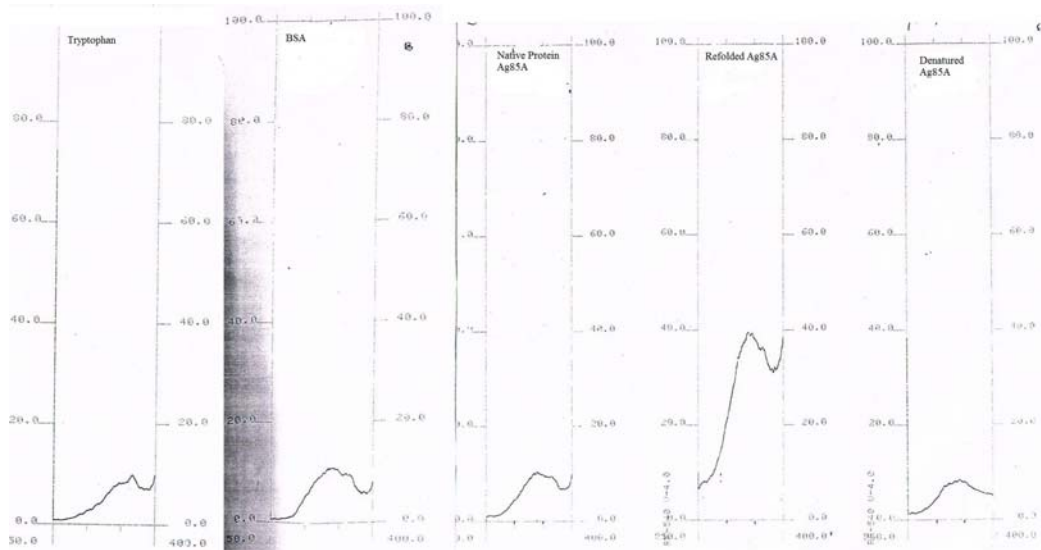


**Figure 4.11: Fluorimetric Emission Spectra of Tryptophan, BSA, native Ag85A, refolded Ag85A and denatured Ag85A.**

Taking into account the fact that the protein activity was almost regained in the refolded protein (91.66 %) as compared to native Ag85A (98.33 %), it is considered that the conformation of the active site might have re-established during refolding, but the exact structure of the refolded protein could be different from that of the native Ag85A. Extensive studies are required to confirm the nature of refolded Ag85A which is out of scope of this thesis.

### References

- Cohen, S.N., Chang, A.C. (1972). Nonchromosomal antibiotic resistance in bacteria: genetic transformation of *E. Coli* by R-factor DNA. *Proc Natl Acad Sci USA*, 69(8), 2110-2114.
- Brody, J.R. and Kern S.E. (2004). History and principles of conductive media for standard DNA electrophoresis. *Anal Biochem*, 333, 1-13.
- Kulshrestha A., Gupta A., Verma N., Sharma S.K., Tyagi A.K., Chaudhary V.K. (2005) Expression and purification of recombinant antigens of *Mycobacterium tuberculosis* for application in serodiagnosis, *Protein Expression and Purification*, 44, 75–85
- Mandel, M. and Higa, A. (1992). Calcium-dependent bacteriophage DNA infection. *Biotechnology*, 24, 198-201.
- Ostrowski W.S., Kuciel R., Tanaka F., and Yagi K. (1993) Fluorometric analysis of native, urea-denatured and refolded human prostatic acid phosphatase, *Biochimica et Biophysica Acta*, 1164, 319-326.
- Palmer I. and Wingfield P.T. (1995) Preparation and extraction of insoluble (inclusion-body) proteins from *Escherichia coli*. In *Current Protocols in Protein Science* (Coligan J.E., Dunn B.M., Ploegh H.L., Speicher D.W., and Wingfield P.T., eds.) pp. 6.3.1-6.3.15. John Wiley & Sons, New York.
- Product information, protease Inhibitor Cocktail for use in purification of Histidine-tagged proteins, Sigma Aldrich, St Louis, USA
- Product information, HIS-Select™ spin column for purification of Histidine-tagged proteins, H 7787, Sigma Aldrich, St. Louis, USA
- Sambrook J., Russell D. W. (2001) *Molecular Cloning: A Laboratory Manual*, the Third edition (Cold Spring Harbor Laboratory Press, Cold Spring Harbor, New York, A1.27, 1.124-1.125.

## 5.0 Synthesis & Characterization of hydrophobic chitosan derivative (HCD)

### 5.1 Materials

Rifampicin was purchased from Sigma-Aldrich (St-Louis, USA). Chitosan oligosaccharide (MW > 5kDa; degree of deacetylation (DDA) 80-90%) was supplied by Kitto Life Co. Ltd. (Kyongki-Do, Seol Korea). Octanoyl chloride, methane sulfonic acid, sodium bicarbonate were purchased from Sigma-Aldrich (St-Louis, USA). Cellulose dialysis tubing (Molecular weight cut of 12-14000 Da, 5000 Da) were purchased from Medicell international Ltd., (London, UK). Dimethyl sulfoxide (DMSO, anhydrous), Deuterated chloroform (CDCl<sub>3</sub>), and Deuterium oxide (D<sub>2</sub>O) were obtained from Sigma-Aldrich (St-Louis, USA). Acetonitrile, methanol, ethanol, chloroform, dichloromethane (DCM), acetone etc. and all other HPLC grade solvents were obtained from Sigma-Aldrich (St-Louis, USA).

### 5.2 Equipment

1. High speed magnetic stirrer (FisherBrand, Loughborough, UK)
2. Fourier Transform Infra-red spectrophotometer (FTIR) (Perkin Elmer, MA, USA)
3. Differential Scanning Calorimeter DSC Q 2000, (TA Instruments, New Castle, UK)
4. Nuclear Magnetic Resonance (Bruker, Karlsruhe, Germany)
5. X-Ray Diffractometer (Oxford Diffraction Xcalibur NovaT, UK)
6. Rotary Evaporator (Hei-VAP Advantage, Heidolph, Schwabach, Germany)
7. Vaccume pump (KNF Laboport, KNF Neuberger, Freiburg, Germany)

### 5.3 Methods

#### 5.3.1 Synthesis of hydrophobic chitosan derivative (HCD)

O-octanoyl-chitosan was prepared as described by Huang et al. (Huang et.al., 2010). In brief, chitosan was added to dissolve in methane-sulfonic acid at room temperature for 1 hr and octanoyl chloride was then added drop-wise under stirring with the molar ratio of repeating unit of chitosan to octanoyl chloride equal to 1:3. The reaction was allowed to continue overnight at ambient temperature. The reaction was then stopped by the addition of crushed ice. Precipitation of octanoyl chitosan was observed. Sodium bicarbonate was added to it to neutralize the acid. The resultant composition was heated at 40°C to accelerate the neutralization of acid. Excess sodium bicarbonate was removed by repeated washings of precipitate with water. Solid material obtained was collected, suspended in water and dialyzed (Molecular weight cut of 5000 Da) against water for 1-2 days to remove the remaining acid and traces of sodium bicarbonate. After dialysis, resultant solid material was dissolved in the mixture of dichloromethane/chloroform (DCM/Chloroform, 2:8) to check its solubility. Soluble fraction was decanted and solvent was evaporated (Rotary Evaporator, Hei-VAP Advantage, Heidolph, Schwabach, Germany) to get the product. The product was treated with glacial acetic acid (1 ml) and washed with water several times to remove acid. Final product was vacuum dried and used for further analysis and experiments.

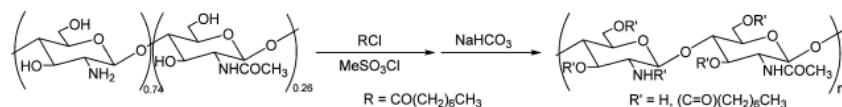


Figure 5.1: Scheme for synthesis of HCD

### 5.4 Solubility Study

Solubility of chitosan and HCD was carried out in water and several organic solvents by visual observation according to the method reported by Haung et.al., and Hu et.al., (Haung et.al., 2010; Hu et.al., 2005). Samples (5mg/ml) were suspended in water, ethanol, methanol, acetone, chloroform, dichloromethane (DCM), ethyl acetate (EtoAc), tetrahydrofuran (THF) at RT under stirring and was observed to ascertain the solubility after 24 hr.

### 5.5 Degree of Substitution (DS) by FTIR

The degree of substitution was evaluated by FT-IR spectrophotometer (Spectrum 100, Perkin Elmer, MA, USA) based on the ratio of absorbance at 1560 cm<sup>-1</sup> (ascribed to amide I band, NH bending) and 897 cm<sup>-1</sup>, applying the equation proposed by Moore and Roberts (Moore et.al., 1980; Miya et.al., 1985; Shigemasa et.al., 1996; Tien et al., 2003; Kjartansson, 2008;) -

$$DS (\%) = [(A_{1560}/A_{897}) - 0.12] \times 100$$

Here, DS represents degree of substitution and the value 0.12 indicates the acetyl groups specified in native chitosan. Powdered sample (app 5-10 mg) was taken and FT-IR spectra was recorded using Perkin Elmer Spectrum 100 FT-IR spectrophotometer (Perkin Elmer, MA, USA). Each measurement was done in triplicate at room temperature in a range of 400 to 4000 cm<sup>-1</sup> at a resolution of 4 cm<sup>-1</sup>. Data obtained was analyzed utilizing Perkin Elmer Spectrum Express software (Perkin Elmer, MA, USA).

### 5.6 Structural analysis of HCD

#### 5.6.1 *Fourier Transform Infrared Spectroscopy (FTIR)*

The IR spectrum of chitosan and HCD was recorded on a Perkin Elmer Spectrum 100 FT-IR spectrophotometer (Perkin Elmer, MA, USA) at room temperature in the range of 400 to 4000 cm<sup>-1</sup> at a resolution of 4 cm<sup>-1</sup>. Data analysis was performed using the Perkin Elmer Spectrum Express software (Perkin Elmer, MA, USA).

#### 5.6.2 *Nuclear magnetic resonance (<sup>1</sup>H-NMR) spectroscopy*

High resolution <sup>1</sup>H-NMR spectroscopy was executed on a 600 MHz spectrometer (Bruker, Karlsruhe, Germany). Samples (chitosan and HCD) were prepared by dissolving in deuterated water and chloroform respectively at a concentration of 5mg/ml.

#### 5.6.3 *Differential Scanning Calorimetry (DSC)*

Differential Scanning Calorimetry (DSC) (DSC Q2000 module, TA Instruments, LLC, USA) was carried out to determine the thermal characteristics of chitosan and octanoyl chitosan. Samples of approximately 5 mg were sealed in aluminium hermetic pans (TA Instruments, New Castle, UK) and heated from 20-300°C with a heating rate of 10°C/min. After first cycle, samples were quenched to 0°C at a cooling rate of 10°C/min under liquid nitrogen. This step was followed by a second heating cycle at the similar parameters (heating from 20-300°C with a heating rate of 10°C/min) which were used for first cycle. The measurements were performed under nitrogen atmosphere at a flow rate of 50 mL/min.

### 5.6.4 X-Ray diffractometry (XRD)

XRD pattern of native chitosan and HCD were recorded using X-ray diffractometer (Oxford Diffraction Xcalibur novaT X-ray diffractometer) which utilizes Cu K $\alpha$  radiation (The data was collected at room temperature and scanned with a step size of 10 $^{\circ}$ 2-theta). The data obtained was processed and scaled using CrysAlisPro (Oxford Diffraction).

### 5.7 Results and Discussion

In spite of advantages offered by chitosan, its poor solubility in water and common organic solvents due to its rigid crystalline structure has restricted its widespread application. Therefore, conversion of chitosan into such a derivative which is either water or organic solvent-soluble to enhance its utility in pharmaceutical and biomedical fields is prerequisite. Hence, an attempt was made to convert chitosan into hydrophobic derivative keeping its inherent surface charge intact.

As hydroxyl groups are less reactive than amino groups, amino groups are to be blocked prior to O-acylation. The reaction of chitosan with acid chlorides (e.g. octanoyl chloride) in methanesulfonic acid helps to achieve O-acylation of chitosan by protecting the amino group of chitosan molecules from acylation reaction. In this case, methanesulfonic acid used in the reaction protonates amino groups and thus becomes inactive in the nucleophilic substitution reaction. Later on, they are unblocked to confer positive charge onto acylated chitosan molecule (Chu et.al., 2011; Huang et.al., 2010; Mourya and Inamdar, 2008).

#### 5.7.1 Solubility and Degree of Substitution

Chitosan (in general) is insoluble in water and organic solvents due to strong and extensive interaction between inter- and intra-molecular hydrogen bonds. In the present investigation, water soluble chitosan was used for the synthesis of HCD. HCD showed solubility in range of organic solvents, whereas it was found to be insoluble in water, which may be due to introduction of hydrophobic octanoyl groups to the parent chitosan. Table 5.1 presents the solubility data of chitosan and its derivative (HCD).

Degree of substitution of acyl groups (DS) for HCD was found to be  $44.05 \pm 1.75$  %, which was almost double in comparison to the parent chitosan ( $20.14 \pm 2.5$ %). It is reported that the solubility of HCD in organic solvents increases with increase in the DS value (Chen et. al., 2013). This may be due to replacement of hydrophilic amino and hydroxyl groups present in the parent chitosan by hydrophobic benzene groups and carbon chains. This phenomenon ultimately causes increased hydrophobic benzene groups and carbon chains into chitosan and thereby prevents the formation of intra- and inter-molecular hydrogen bonding interaction between the amino and hydroxyl groups of chitosan leading to improved solubility of the associated chitosan in common organic solvents (Chen et. al., 2013). In accordance with these results, DS for HCD was found to more as compared to parent and hence showed insolubility in water. However, it was soluble in range of organic solvents. Among various organic solvents tested, best solvents were noted to be DCM, THF and chloroform in which HCD was found to be easily soluble as compared to other solvents.

Table 5.1: Solubility of Chitosan and HCD

Sample	Solvents							
	Water	Ethanol	Methanol	Acetone	DCM	Chloroform	EtOAc	THF
Chitosan	√	x	x	x	x	x	x	x
HCD	x	√	√	√	√	√	√	√
<b>Sample</b>	<b>% DS</b>	DS – Degree of Substitution ; DCM – Dichloromethane; EtOAc – Ethyl Acetate; THF – Tetrahydrofuran; Soluble - √ ; Insoluble - x						
Chitosan	20.14±2.5							
HCD	44.05±1.75							

### 5.7.2 Characterization of HCD powder

#### 5.7.2.1 FTIR and <sup>1</sup>H NMR analysis

FTIR spectra of chitosan and its acylated derivative HCD (synthesized using octanoyl chloride (OC)) is presented in figure 5.2. Chitosan is characterized by various absorption bands in its FTIR spectra, including – 1) absorption band between 3000 to 4000 cm<sup>-1</sup> (which is attributed to the axial stretching of O–H and N–H bonds). (2) a band near 2910 cm<sup>-1</sup> corresponding to the axial stretching of C–H bonds; (3) bands at 1653 and 1580 cm<sup>-1</sup>, assigned as amide I and amide II vibrations, respectively; (4) bands at 1417 & 1377 cm<sup>-1</sup> resulting from the coupling of C–N axial stretching and N–H angular deformation; and (5) the bands in the range 1153–897 cm<sup>-1</sup>, which is attributed to polysaccharide skeleton (glycosidic bonds, C–O and C–O–C stretching) (Britto et.al., 2007).

Results of FTIR spectra of chitosan have also indicated absorption bands at - 1) 3275 cm<sup>-1</sup> (stretching of O–H and N–H bonds). (2) 2873 cm<sup>-1</sup> (axial stretching of C–H bonds); (3) 1647 and 1580 cm<sup>-1</sup>, (as amide I and amide II vibrations, respectively); (4) 1417 & 1316 cm<sup>-1</sup> (may be due to coupling of C–N axial stretching and N–H angular deformation); and (5) between 1153–897 cm<sup>-1</sup>, (polysaccharide skeleton - glycosidic bonds, C–O and C–O–C stretching) (Britto et.al., 2007). In case of HCD, following new bands corresponding to particular functional group were identified in FTIR spectra - 2850-2920 cm<sup>-1</sup> : (C–H stretching of CH<sub>2</sub> and CH<sub>3</sub> groups of the alkyl substituent); 1738.58 cm<sup>-1</sup>: Octanoyl groups ; 1659.42 cm<sup>-1</sup>: Amide I band (C=O stretching) 1531.20 cm<sup>-1</sup> : Amide II band (N-H bending vibrations) ; 1570: Primary amine band.

The presence of new absorption bands in the FTIR spectra of HCD at ~ 1740 cm<sup>-1</sup> corresponding to reaction between octanoyl and amine and hydroxyl groups of the chitosan confirmed the substitution of octanoyl groups on chitosan. The absorption peaks at ~ 1655 cm<sup>-1</sup>, which can be assigned to the carbonyl stretching of amide band I (secondary amides) and ~1555 cm<sup>-1</sup> correlates to the N-H bending vibrations of the amide band II in OC, whereas N-H bending vibrations of primary amines in parent chitosan found at ~ 1570 cm<sup>-1</sup> (Tien et.al., 2003). Moreover, significant decrease in the relative intensity of the broad peak at 3275 cm<sup>-1</sup> was observed in the HCD, which is corresponding to the inter and intra molecular hydrogen bonding of hydroxyl and amine groups in the chitosan. In addition, a

sharp increase in the intensity of the bands near 2810–2980  $\text{cm}^{-1}$  in the FTIR spectra of HCD clearly evidenced the introduction of alkyl substituent at the amino sites of chitosan. According to earlier report, FTIR spectra of acylated or quaternized chitosan (in this case HCD) can also be differentiated based on the decreased band intensity at 1593  $\text{cm}^{-1}$  and appearance of a new band at 1469  $\text{cm}^{-1}$  (Britto et.al., 2007). In compliance to this, our results clearly indicated complete absence of a band at 1593  $\text{cm}^{-1}$  and introduction of a new band at 1457  $\text{cm}^{-1}$  may be due to angular deformation of C–H. The relative intensities of the transmission of COO– group (1740  $\text{cm}^{-1}$ ) depended upon the degree of substitution (DS) values. In this experiment, higher intensity of transmission for this group was observed indicating higher degree of substitution conferring higher hydrophobic nature to HCD. These results confirmed that octanoyl groups were grafted onto the monosaccharide structure of chitosan (comprising hydroxyl and amino groups) to form octanoyl chitosan (named as hydrophobic chitosan derivative - HCD).

Additional information on substitution of octanoyl group on chitosan forming acylated chitosan or hydrophobic chitosan derivative (HCD) was obtained from the  $^1\text{H-NMR}$  analysis. The peaks of parent chitosan were observed between 1.7 to 5.1 ppm (as shown in figure 5.3), whereas,  $^1\text{H-NMR}$  analysis of HCD showed new peaks at 0.75, 1.15, 1.48 and 2.20 ppm. These peaks were mainly due to alkyl proton of chitosan upon reaction with octanoyl chloride. Presence of these peaks indicated the conjugation of octanoyl groups to the parent chitosan leading to formation of HCD.

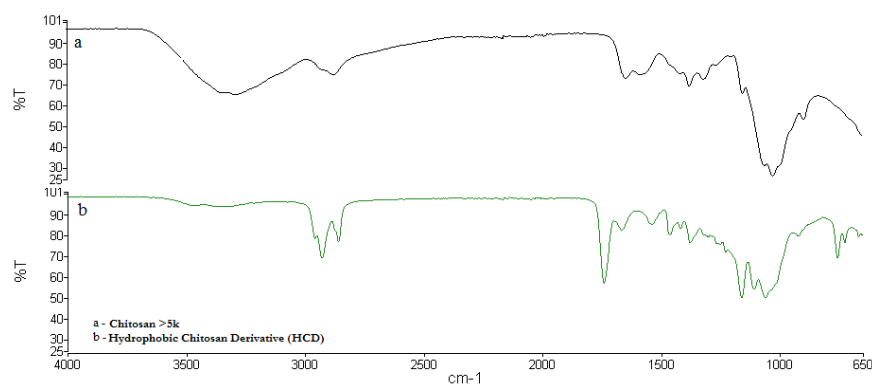


**Figure 5.2:** FTIR Spectra of – a) Chitosan; and b) HCD

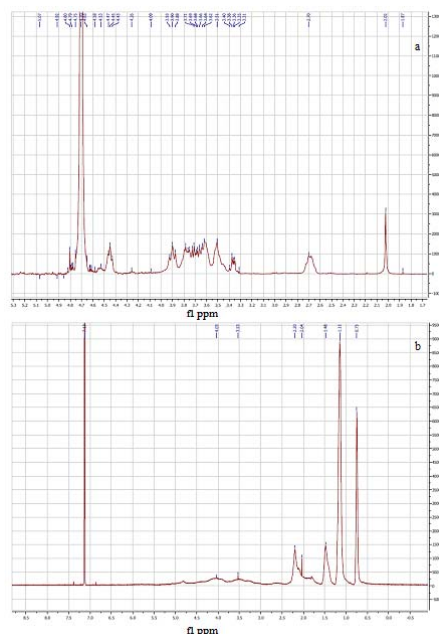


Figure 5.3: NMR spectra of – Chitosan (a) and HCD (b)

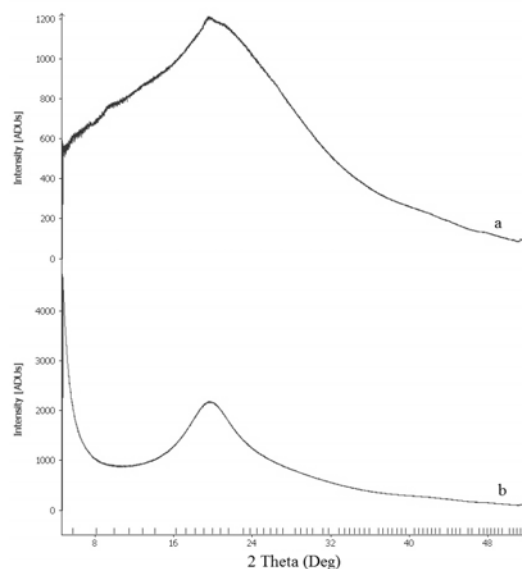


Figure 5.4: X-Ray Diffratograms of – a) Chitosan and b) HCD

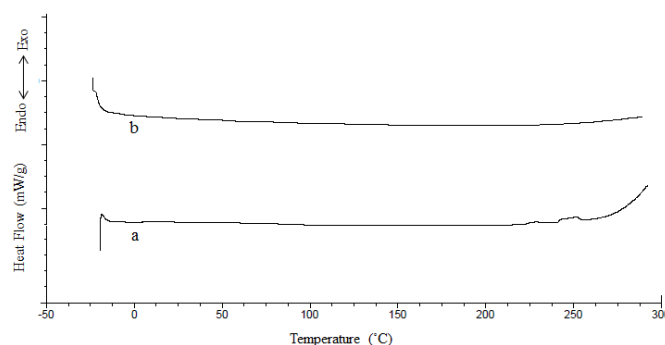
### 5.7.2.2 X-Ray Diffraction studies

Figure 5.4 represents the X-ray diffractograms of parent chitosan and HCD. It was observed that parent chitosan showed a peak of moderately low intensity and broader than that of HCD. It can be noted from the diffractogram, that HCD showed more intense peak as compared to parent chitosan. In addition HCD also showed a new peak below 2 theta value of 8, which indicates the more crystalline nature of HCD than parent chitosan. As per Tien et al., the major change at 19.4 Å which comes below 2 theta value of 8, corresponds to more crystalline and stable organization of HCD than the parent chitosan (Tien et. al., 2003). In a

study using octanoyl chitosan, myristoyl chitosan and caproyl chitosan, authors reported that longer acyl chains length (C8–C14) is responsible for sharper peak. In compliance to this, XRD results of HCD also showed a peak resembling to parent chitosan with high intensity and a new peak below 2 theta value of 8. This important change suggested a more crystalline nature of HCD, which is induced by the hydrophobic side chains.

### 5.7.2.3 Differential Scanning Calorimetry (DSC)

DSC thermograms of chitosan and HCD (acylated chitosan) are shown in figure 5.5. It is known that chitosan shows two weight loss stages, in first stage, a broad endothermic peak at 100 °C corresponds to moisture absorption due to loss of residual water from the sample (Haung et.al., 2010) and second peak at around 300 - 320°C is attributed to thermal decomposition of chitosan. Hence, two cycles of heating and cooling runs were employed in the experiment. In this study, investigations with chitosan showed a broad endothermic peak at around 100 °C ascribed to the vaporization of the water (Haung et.al., 2010). However, no exothermic peak was observed, but it can be expected beyond 300°C owing to the onset of curvature from 260 °C in the DSC thermogram of chitosan. This curvature may be corresponding to the beginning of monomer dehydration, glycoside bond cleavage and decomposition of the acetyl and deacetylated units of chitosan. In case of HCD, DSC thermogram neither exhibited endothermic nor exothermic peak between 20 to 300 °C. In addition, no obvious glass transition (T<sub>g</sub>) was observed in both chitosan and HCD. These results are in line with the reports published by Zong et. al. and Ma et. al., (Zong et. al. 2000; Ma et. al., 2008).



**Fig. 5.5. DSC Thermograms of Chitosan (a) and HCD (b)**

In a study by Choi et. al., they reported chitosan fibers with the strong exothermal peak within the temperature range of 280–320 °C. However, they observed endothermal depression for *N*-acyl chitosan fibers within the temperature range of 320–390 °C and they also reported stronger depression in acylated chitosan with respect to the length of acyl chains due to decomposition of crystalline regions. Longer the acyl chain length, deeper peak was reported, due to higher crystallinity for a longer acyl chain length (Choi et al. 2007).

In contrast to the results shown by Choi et. al., we did not observe any endothermic or exothermic peak between 20 to 300 °C for chitosan and HCD. However, if we look at the thermogram of chitosan carefully, the presence of slight curvature in the chitosan

thermograph was observed indicating onset of chitosan decomposition, which may lead to an exothermic peak beyond 300 °C. However, no such curvature was noted in HCD, which may indicate shifting of the peak to higher temperature suggesting highly stable nature of HCD due to enhanced thermal stability with the substitution of acyl groups. Based on these results, it can be concluded that there could be improved thermal stability of HCD as compared to native chitosan.

It is reported that the determination of the thermal properties of chitosan is difficult, due to the problems associated with the sample preparation and its hygroscopicity. Chitosan have the ability to absorb water leading to creation of large number of inter and intrachain hydrogen bonds, which affect its thermal and mechanical properties (Ferreira et. al., 2006). This phenomenon results in a substantial influence on the Tg due to degradation of chitosan before attaining their glass transition temperature. Hence, Tg of chitosan and chitin is yet to be precisely characterized (Britto et. al., 2005). In connection to this, various authors have reported variable Tg for chitosan. Ratto et. al. reported glass transition temperature of chitosan at 30 °C for water content ranging from 8 to 30%, whereas Lazaridou et. al., observed Tg ranging from -23 ° to 67 °C based on their water content suggesting plasticizing effect of water in both cases (Ratto et.al., 1995; Lazaridou et. al., 2002). In another study, Sakurai et. al., detected Tg of chitosan at 203 °C, while Kittur et. al; Zong et. al. and Ma et. al., accounted no evidence for Tg (Sakuri et.al., 2000; Kittur et.al., 2002; Zong et. al. 2000; Ma et. al., 2008 ). Hence, they suggested that Tg for chitosan may be located somewhere at higher temperature, where degradation prevents its determination. In support with these reports, no Tg was observed in our study, indicating that Tg may lie at higher temperature.

Overall results as obtained after characterization of HCD indicated the formation of hydrophobic chitosan derivative by substitution of Octanoyl onto the parent Chitosan moiety. Hydrophobic nature of the chitosan derivative was clearly evidenced from the solubility studies and high degree of substitution.

## References

## Chapter 5 - Synthesis of Hydrophobic Chitosan Derivative

---

Britto D., Campana-Filho S.P., Assis O.B.G. (2005) Mechanical Properties of N,N,N-trimethylchitosan Chloride Films, *Polímeros: Ciência e Tecnologia*, 15 (2), 142-145,

Britto D., Assis O.B. (2007) Synthesis and mechanical properties of quaternary salts of chitosan-based films for food application. *International Journal of Biological Macromolecules*. 41, 198–203

Chen C., Tao S., Qiu X., Ren X., Hu S. (2013) Long-alkane-chain modified N-phthaloyl chitosan membranes with controlled permeability. *Carbohydrate Polymers*, 91, 269– 276

Choi C.Y., Kim S.B., Pak P.K., Yoo D.I., Chung Y.S. (2007) Effect of N-acylation on structure and properties of chitosan fibers. *Carbohydrate Polymers*, 68, 122–127

Chu C-C., Zhong C. (2011) Organo soluble chitosan salts and chitosan derived biomaterials prepared thereof. US Patent. US2011/0150999 A1.

Ferreira P. (2006) Thermal Characterization of Chitosan-Grafted Membranes to be Used as Wound Dressings, *Journal of Carbohydrate Chemistry*, 25, 233–251.

Grant S., Blair H.S., McKay G. (1990) determination of degree of acetylation of chitin and chitosan by thermal analysis. *Polym Commun*. 31, 267

Huang Y., Yu H., Guo L., Huang Q. (2010) Structure and Self-Assembly Properties of a New Chitosan-Based Amphiphile, *J.Phys.Chem. B*, 114, 7719-7726

Hu Y., Jiang H., Xu C., Wang Y., Zhu K. (2005) Preparation and characterization of poly(ethylene glycol)-g-chitosan with water- and organosolubility, *Carbohydrate Polymers*, 61, 472–479

Kittur F, Prashanth K, Uday Sanka K, Tharanathan R. (2002) Characterization of chitin, chitosan and their carboxymethyl derivatives by differential scanning calorimetry, *Carbohydr. Polymer*, 49, 185-193

Kjartansson G.T. (2008) Extraction of functional properties of ultrasonicated chitin and chitosan from Crustacean byproducts. A PhD thesis submitted to University of Massachusetts, Amherst, USA.

Lazaridou A, Biliaderis C. (2002) Thermophysical properties of chitosan, chitosan–starch and chitosan–pullulan films near the glass transition, *Carbohydr. Polym*; 2002, 48, 179-190

Ma G., Yang D., Zhou Y., Xiao M., Kennedy J.F., Nie J. (2008) Preparation and characterization of water-soluble N-alkylated chitosan. *Carbohydrate Polymers*. 74, 121–126

## Chapter 5 - Synthesis of Hydrophobic Chitosan Derivative

---

Miya M., Iwamoto E., Ohta O., Mima S. (1985) N-Acetylation of Chitosan Films, *Kobunshi Ronbunshu*, 42, 3, 181-189.

Moore G.K. and Roberts G.A.F. (1980) Determination of the degree of N-acetylation of chitosan, *Int. J. Biol. Macromol.*, 2, 115-116.

Mourya V.K., Inamdar N.N. (2008) Chitosan modifications and application: opportunities galore. *Reactive and functional polymers*, 68, 1013-1051.

Ratto J, Hatakeyama T. (1995) Differential scanning calorimetry investigation of phase transitions in water/ chitosan systems, *Polymer*, 36, 2915-2919.

Sakurai K., Maegawa T., Takahashi T. (2000) Glass transition temperature of chitosan and miscibility of chitosan/poly(N-vinyl pyrrolidone) blends, *Polymer*, 41(19), 7051-7056

Shigemasa Y., Matsuura H., Sashiwa H., Saimoto H. (1996) Evaluation of different absorbance ratios from infrared spectroscopy for analyzing the degree of deacetylation in chitin. *International Journal of Biological Macromolecules*, 18, 237-242.

Tien C.L., Lacroix M., Ispas-Szabo P., Mateescu M. (2003) N-acylated chitosan: hydrophobic matrices for controlled drug release, *Journal of Controlled Release*, 93, 1, 1-13.

Zong Z., Kimura Y., Takahashi M., Yamane H. (2000) Characterization of chemical and solid state structures of acylated Chitosans. *Polymer*. 41, 899–906.

## 6.0 Synthesis and Characterization of modified chitosan derivative (MCD)

### 6.1 Materials

Rifampicin was purchased from Sigma-Aldrich (St-Louis, USA). Chitosan oligosaccharide (MW 1k; degree of deacetylation (DDA) 80-90%) was supplied by Kitto Life Co. Ltd. (Kyongki-Do, Seol Korea). Octanoyl chloride, methane sulfonic acid, sodium bicarbonate were purchased from Sigma-Aldrich (St-Louis, USA). Cellulose dialysis tubing (Molecular weight cut of 12-14000 Da, 5000 Da) was purchased from Medicell international Ltd., (London, UK). Dimethyl sulfoxide (DMSO, anhydrous), Deuterium oxide (D<sub>2</sub>O) were obtained from Sigma-Aldrich (St-Louis, USA). Acetonitrile, methanol, ethanol, chloroform, dichloromethane (DCM), acetone etc. and all other HPLC grade solvents were obtained from Sigma-Aldrich (St-Louis, USA).

### 6.2 Equipment

1. High speed magnetic stirrer (FisherBrand, Loughborough, UK)
2. UV-VIS Spectrophotometer (Jenway UV/Vis Spectrophotometer, Staffordshire, UK)
3. Fourier Transform Infra-red spectrophotometer (FTIR) (Perkin Elmer, MA, USA)
4. Differential Scanning Calorimeter DSC Q 2000, (TA Instruments, New Castle, UK)
5. Nuclear Magnetic Resonance (NMR) (Bruker, Karlsruhe, Germany)
6. X-Ray Diffractometer (Oxford Diffraction Xcalibur novaT, UK)

### 6.3 Methods

#### 6.3.1 Synthesis of modified chitosan derivative (MCD)

The method for the synthesis of MCD was based on previous publications and patents (Haung et.al., 2010; Chu et.al., 2011). In brief, chitosan (10 g) was dissolved in 100 ml of distilled water (DDW). To it, 30 ml of octanoyl chloride diluted in 100 ml of acetone was slowly added drop-wise for half an hour under stirring. Resultant mixture was heated on water bath for half an hour at 90 C°. Two layers were observed, i) clear colourless layer, which indicated absence of chitosan ; & ii) brown coloured layer which was identified as chitosan containing layer due to colour of chitosan. The coloured layer was collected and octanoyl chitosan was precipitated by drop wise addition of acetone. Precipitate was separated by decanting the supernatant and remaining solid part was dissolved in methanol. This procedure was repeated several times to remove unreacted octanoyl chloride. After 2-3 washings with acetone, precipitate of octanoyl chitosan was dissolved in methanol, transferred to round bottom flask and solvent was evaporated (Rotary Evaporator, Hei-VAP Advantage, Heidolph, Schwabach, Germany). This product was collected and used for further analysis.

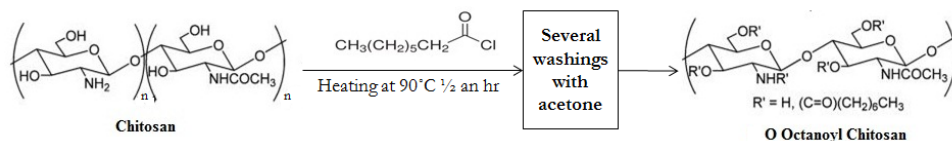


Figure 6.1: Scheme for synthesis of MCD

### 6.4 Solubility Study

Solubility of chitosan and MCD was determined in water and several organic solvents by visual observation. Samples (5mg/ml) were suspended in water, ethanol, methanol, DCM, chloroform, ethyl acetate and tetrahydrofuran at RT under stirring and the solubility after 24 hr was assessed by visual observation.

### 6.5 Degree of acylation by TNBS assay

TNBS Reagent is a 5% solution of trinitrobenzene sulfonic acid in methanol that reacts with primary amines (peptides or amino acids) to yield a soluble colored product, a property useful for various assay methods. Therefore, TNBS assay was utilized to determine degree of acyl groups conjugation to chitosan (Loretz et.al., 2006). In order to perform TNBS assay, Stock solution of 1 mg/ml was prepared from the standard stock solution of chitosan 1k (5mg/ml) in water. From the stock solution, standard dilutions of 40 and 200 µg/ml were made. From each standard dilutions (40 and 200 µg/ml), 300 µl of sample was taken, 300 µl of 4 % sodium bicarbonate and 0.2 % TNBS was added to it and incubated at 37° C for two hours. Finally, 2 N HCl was added to it, mixed well and absorbance was measured using UV/Vis spectrophotometer at λ<sub>max</sub> of 344 nm (Jenway UV/Vis Spectrophotometer, Staffordshire, UK) to plot calibration curve (Sonia et. al., 2011). Degree of acylation was determined using following formula.

$$\% \text{Acylation} = 1 - \frac{ABS_{cd}}{MASS_{cd}} \times \frac{ABS_c}{MASS_c}$$

Where, ABS stands for absorbance, Mass means total mass of chitosan derivative (cd) and native chitosan (c).

### 6.6 Structural analysis of MCD

#### 6.6.1 Fourier Transform Infrared Spectroscopy (FTIR)

The IR spectrum of chitosan and MCD was recorded on a Perkin Elmer Spectrum 100 FT-IR spectrophotometer (Perkin Elmer, MA, USA) at room temperature in a range of 400 to 4000 cm<sup>-1</sup> at a resolution of 4 cm<sup>-1</sup>. Data analysis was performed using the Perkin Elmer Spectrum Express software (Perkin Elmer, MA, USA).

#### 6.6.2 Nuclear magnetic resonance (<sup>1</sup>H-NMR) spectroscopy

Samples of chitosan and MCD were prepared by dissolving them in deuterated water at a concentration of 5mg/ml and high resolution <sup>1</sup>H-NMR spectroscopy was executed on a 600 MHz spectrometer (Bruker, Karlsruhe, Germany).

#### 6.6.3 Differential Scanning Calorimetry (DSC)

Thermal characteristization of chitosan and chitosan derivative was carried out by Differential Scanning Calorimetry (DSC) (DSC Q2000 module, TA Instruments, LLC, USA). Samples of approximately 5 mg were sealed in aluminium hermetic pans (TA Instruments, New Castle, UK) and heated from 20-300°C with a heating rate of 10°C/min. After first cycle, samples were quenched to 0°C at a cooling rate of 10°C/min under liquid nitrogen.

This step was followed by a second heating cycle at the similar parameters (heating from 20-300°C with a heating rate of 10°C/min) which were used for first cycle. The measurements were performed under nitrogen atmosphere at a flow rate of 50 mL/min.

#### 6.6.4 X-Ray diffractometry (XRD)

XRD pattern of native chitosan and MCD were recorded using X-ray diffractometer (Oxford Diffraction Xcalibur novaT X-ray diffractometer) which utilizes Cu K $\alpha$  radiation. The data obtained was processed and scaled using CrysAlisPro (Oxford Diffraction). The data was collected at room temperature and scanned with a step size of 10° 2-theta.

### 6.7 Results and Discussion

#### 6.7.1 Solubility and Degree of Acylation:

Chitosan (in general) is insoluble in water and organic solvents due to strong and extensive interaction between inter- and intra-molecular hydrogen bonds. In the present investigation, water soluble chitosan was used for the synthesis of MCD (O-octanoyl chitosan). Chitosan derivative (MCD) prepared in our laboratory showed solubility in water, methanol and ethanol, but it was found to be insoluble in many other organic solvents such as acetone, dichloromethane, chloroform, THF, EtOAc etc. which may be due to partial introduction of hydrophobic octanoyl groups to the parent chitosan (product was floating as observed visually). This data corresponds with the results of FTIR studies, which confirms the substitution at O position rather than N position (as confirmed by the peaks). Table 6.1 presents the solubility data of chitosan and its derivatives (MCD).

**Table 6.1: Solubility of Chitosan and MCD**

Sample	Solvents							
	Water	Ethanol	Methanol	Acetone	DCM	Chloroform	EtOAc	THF
Chitosan	√	x	x	x	x	x	x	x
HCD	√	√	√	x	x	x	x	x
<b>Sample</b>	<b>% DA</b>	DA – Degree of Acylation ; DCM – Dichloromethane; EtOAc – Ethyl Acetate; THF – Tetrahydrofuran; Soluble - √ ; Insoluble - x						
<b>MCD</b>	0.99±0.001							

Degree of acylation of octanoyl groups (DA) for MCD was found to be 0.99 ±0.001 %, which was very small as compared to HCD. It is reported that, the solubility of modified chitosan derivative in organic solvents is dependent on the DS. Thus, it increases with increase in the DS value (Chen et. al., 2013). This may be due to replacement of hydrophilic amino and hydroxyl groups present in the parent chitosan by introduction of hydrophobic benzene groups and carbon chains into chitosan. This phenomenon ultimately causes increased hydrophobic benzene groups and carbon chains into chitosan and thereby prevents the formation of intra- and inter-molecular hydrogen bonding interaction between the amino and hydroxyl groups of chitosan leading to improved solubility of the associated chitosan in common organic solvents (Chen et. al., 2013). In line with these reports, DS for MCD was

found to small and hence may have showed limited solubility in organic solvents, while retaining its solubility in water. This feature was found to be opposite to that of HCD.

### 6.7.2 FTIR studies

Figure 6.2 represents the FTIR spectra of chitosan and its acylated derivative (MCD - synthesized using octanoyl chloride). Chitosan can be characterized based on the various absorption bands in its FTIR spectra. These include – (a) absorption band region between 3000 to 4000  $\text{cm}^{-1}$ , which is attributed to the axial stretching of O–H and N–H bonds. (b) a band near 2910  $\text{cm}^{-1}$  corresponding to the axial stretching of C–H bonds; (c) bands at 1653 and 1580  $\text{cm}^{-1}$ , ascribed as amide I and amide II vibrations, respectively; (4) bands at 1417 & 1377  $\text{cm}^{-1}$  resulting from the coupling of C–N axial stretching and N–H angular deformation; and (5) the bands in the range 1153–897  $\text{cm}^{-1}$ , suggesting polysaccharide skeleton (glycosidic bonds, C–O and C–O–C stretching) (Britto et.al., 2007). In agreement with these, results of FTIR studies of chitosan (1 k) showed absorption bands at – 3292  $\text{cm}^{-1}$ ; 2859  $\text{cm}^{-1}$ ; 1589  $\text{cm}^{-1}$ ; 1373.84  $\text{cm}^{-1}$ ; and between 1152–894  $\text{cm}^{-1}$  assigning to the respective functional groups as mentioned above, whereas, MCD showed the presence of following bands in its FTIR spectra corresponding to particular functional group - 2887  $\text{cm}^{-1}$ : (C–H stretching of CH<sub>2</sub> and CH<sub>3</sub> groups of the alkyl substituent); exclusive new band at 1738.15  $\text{cm}^{-1}$ : Octanoyl groups; 1610.52  $\text{cm}^{-1}$ : Amide I band (C=O stretching) 1512.42  $\text{cm}^{-1}$ : Amide II band (N-H bending vibrations).

The incorporation of new absorption bands in the FTIR spectra of MCD at  $\sim 1738.15 \text{ cm}^{-1}$ , which is corresponding to the interaction between octanoyl and hydroxyl and amine groups suggests the substitution of octanoyl groups in chitosan. The absorption peaks at  $\sim 1610.52 \text{ cm}^{-1}$ , which can be assigned to the carbonyl stretching of amide band I (secondary amides) and  $\sim 1512.42 \text{ cm}^{-1}$  correlates to the N-H bending vibrations of the amide band II in MCD, whereas, N-H bending vibrations of primary amines in parent chitosan was found at  $\sim 1589 \text{ cm}^{-1}$ , which suggests the alkylation of chitosan and this was found to be in agreement with the Tien et.al., (Tien et.al., 2003). Very slight change in the relative intensity of the broad peak at 3292  $\text{cm}^{-1}$  of parent chitosan corresponding to the hydroxyl and amine groups in the chitosan was observed in MCD. However, a band at 2859  $\text{cm}^{-1}$  was found to be slightly shifted to 2887  $\text{cm}^{-1}$  in the FTIR spectra of MCD suggesting there may not be any introduction of alkyl substituent at the amino sites of chitosan. Hence, these results supported that octanoyl groups may have been grafted onto the monosaccharide structure of the chitosan (comprising hydroxyl groups) to form octanoyl chitosan leaving amine position devoid of substitution (named as chitosan derivative - MCD).

As discussed in the chapter 5, the relative intensities of the transmission of COO– group (1738  $\text{cm}^{-1}$ ) depends upon the degree of acylation (DA) values. In this experiment, lower intensity of transmission for this group suggested lower degree of acylation (which is determined by TNBS assay) conferring less hydrophobicity to MCD. Thus, in comparison to the HCD, MCD showed less DA values owing to low level of substitution of octanoyl groups on native chitosan. This may be the reason for the difference in the solubility of these

two chitosan derivatives (HCD and MCD). One (HCD) being highly hydrophobic, whereas other (MCD) less hydrophobic. However, without detailed studies, it would be difficult to state the site of acylation, whether O-, N-, or N, N – acylation.

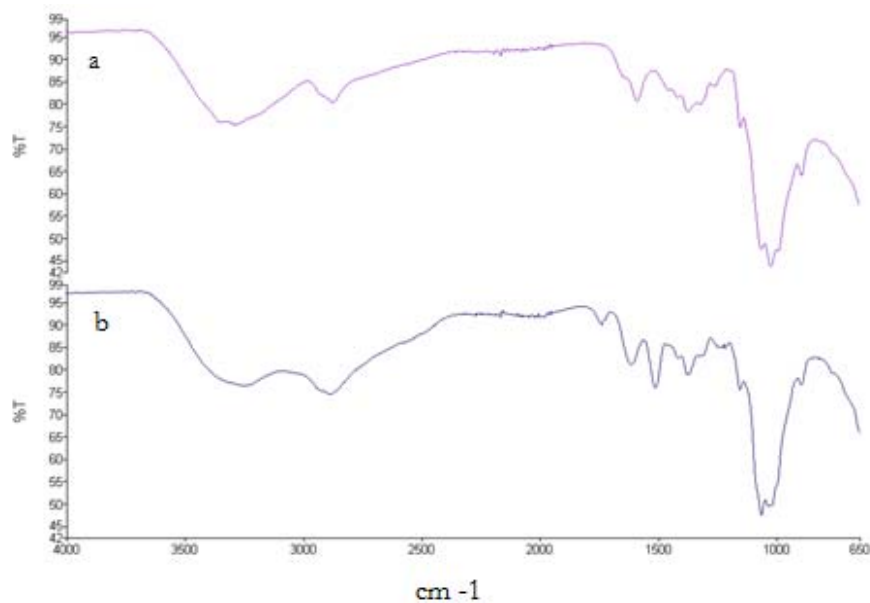


Figure 6.2: FTIR Spectra of – (a) Chitosan ; and (b) MCD

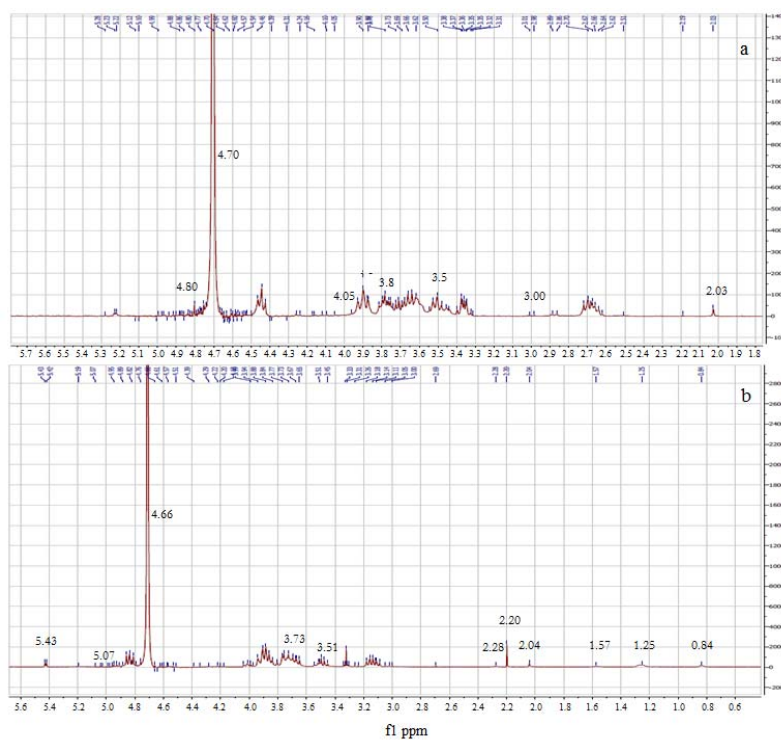


Figure 6.3: NMR spectra of – (a) Chitosan ; and (b) MCD

### 6.7.3 <sup>1</sup>H-NMR analysis

Additional information of the chitosan and MCD was obtained from the <sup>1</sup>H-NMR analysis. Fig. 6.3a and b represents the NMR spectra's of chitosan and MCD respectively. In case of chitosan, a small peak at 2.03 ppm was observed due to presence of –CH<sub>3</sub> of N-acetylglucosamine (GlcNAc) residue. A singlet at 3.31 ppm assigned to H<sub>2</sub> of glucosamine (GlcN) and N-alkylated GlcN, multiplets from 3.51 to 4.05 ppm may be corresponding to H<sub>3</sub>, H<sub>4</sub>, H<sub>5</sub> and H<sub>6</sub> of the methine protons of GlcN and GlcNAc. A small peak at 4.70 ppm may be attributed to H<sub>1</sub> of GlcN and GlcNAc. MCD showed that signals of newly formed at 5.07, 4.88 ppm attributed to H<sub>3</sub> and H<sub>4</sub> protons of the polysaccharide, respectively. Other new signals at 3.5 and 3.7 ppm assigned to H<sub>6</sub> and H<sub>5</sub> due to the protons of ring. Furthermore, the typical multiplet peak about at 2.28 ppm attributed to the H<sub>2</sub> and signal at 2.20 ppm was due to H<sub>a</sub>. New peaks 0.84, 1.25 and 1.57 ppm attributed to the –CH<sub>3</sub>, –CH<sub>2</sub>– and –CH<sub>2</sub>–(CO) groups of the octanoyl chloride chains. These peaks were mainly due to alkyl proton of the chitosan upon reaction with the octanoyl chloride. Presence of these peaks in the NMR spectra indicates the conjugation of major functional groups to the parent chitosan leading to formation of MCD, while retaining major functional groups of chitosan. These results are in agreement with the results reported by Tien et.al., Ma et.al., (Tien et.al., 2003; Ma et.al., 2008).

### 6.7.4 X-Ray Diffractometry (XRD)

X-ray diffractograms of chitosan and MCD is presented in Figure 6.4. Though peak in the XRD of MCD was found to be of moderately low intensity as compared to parent chitosan, the diffractograms of both MCD and parent chitosan showed intense peak. Unlike HCD, no sharp peak below 2 theta value of 8 was observed (chapter 6). However, a major change in the diffractogram of MCD below 2 theta value of 10 can be seen, which may be an indication of crystalline form of MCD. This important change may have been induced due to partial conjugation of hydrophobic side chains in chitosan due to substitution of octanoyl chloride, which is attributed to crystalline form of MCD leading to enhanced stability as compared to native chitosan. As per Tien et al., the major change at 19.4 Å which comes below 2 theta value of 8, corresponds to more crystalline and stable organization of MCD than the parent chitosan (Tien et.al., 2003). In a study using octanoyl chitosan, myristoyl chitosan and caproyl chitosan, he also reported that longer acyl chains length (C<sub>8</sub>–C<sub>14</sub>) is responsible for sharper peak. This study has utilized octanoyl groups with the acyl chain length of C<sub>8</sub>, may be the reason for shallow peak.

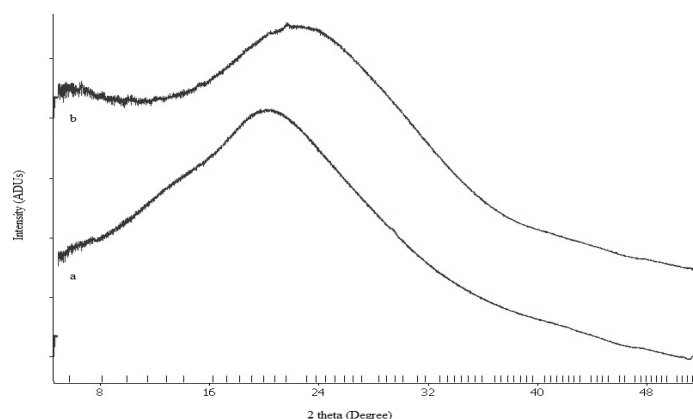
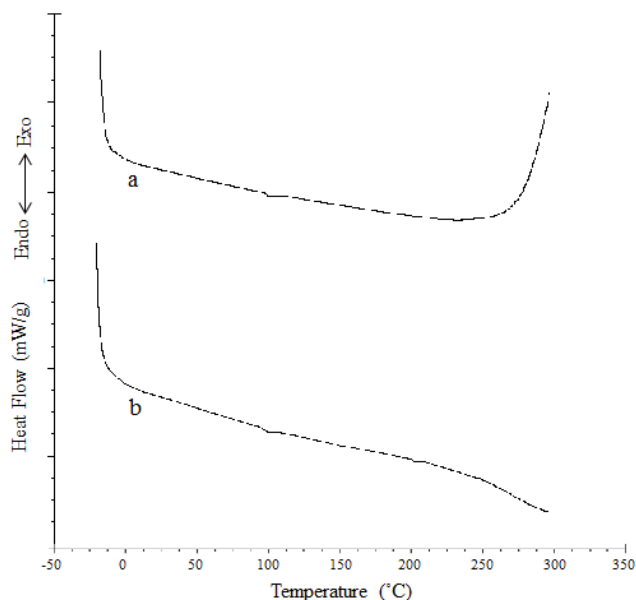


Figure 6.4: X-Ray Diffratograms of – a) Chitosan ; and b) MCD

#### 6.7.5 Differential Scanning Calorimetry (DSC)

Figure 6.5 presents DSC thermograms for native chitosan and MCD. As described in the chapter 5 and previous literature, chitosan exhibits two weight loss stages, i) a broad endothermic peak at 100 °C due to moisture absorption from the sample and ii) second peak corresponding to thermal decomposition of chitosan at 300 - 320°C (Haung et.al., 2010). Therefore, similar protocol for DSC studies was followed as elaborated in chapter 5. A broad endothermic peak due to moisture absorption was noted at 100 °C (data not shown). Unlike to HCD, an endothermic peak can be expected somewhere beyond 300°C, which may be attributed to decomposition of the acetyl and deacetylated units of chitosan. In addition, similar to the results obtained for HCD, no obvious glass transition was observed in both chitosan and MCD. Alike results are reported by Zong et al. where no glass transition was noted (Zong et al. 2000; Ma et.al., 2008).

According to the studies carried out by Grant et al. and Ma et.al., chitosan with a degree of deacetylation of 86.4% and its lauroyl derivative showed the decomposition peaks at 322 and 217°C, respectively. They suggested that the introduction of the acyl groups to chitosan (acylated chitosans) might have decreased the thermal stability of modified chitosan and hence they advised stability of modified chitosan below 225°C (Grant et.al., 1990; Ma et.al., 2008). In contrast to this, Choi et.al., (Choi et al. 2007) indicated similar results for chitosan fiber's with occurrence of a strong exothermal peak within the temperature range of 280–320 °C, whereas they noted endothermal depression within the temperature range of 320–390 °C for *N*-acyl chitosan fibers. They also reported direct dependability of this depression on the length of the acyl chains and observed stronger depression with the longer acyl chain length.



**Figure 6.5: DSC Thermograms of (a) Chitosan ; and (b) MCD (Octanoyl Chitosan)**

Investigations carried out on chitosan and MCD in this experiment did not show endothermic or exothermic peak until 300 °C for chitosan and MCD. However, the results could be considered in correlation with reports published Choi et. al., (Choi et.al., 2007). In accordance with the Choi et. al., results of DSC thermogram for chitosan may exhibit exothermic peak within 300 - 320 °C attributed to the exothermal reaction within the polymer, whereas depression phase with the endothermic peak can be expected beyond 300 °C for MCD, which is due to thermal decomposition of the crystalline regions in the polymer. In conformity with the reports of Choi et.al., results of the MCD thermograms are expected to show shifting of endothermic peak to higher temperature (Choi et.al., 2007), which may be due to longer octanoyl chain in the MCD presenting higher crystallinity. These results indicated improved thermal stability of MCD to that of the chitosan. However, extensive investigations with higher temperature range may be beneficial to understand exact thermal stability of MCD in comparison to parent chitosan.

### **Conclusions**

Results obtained after characterization of MCD indicated the formation of acylated chitosan derivative by substitution of Octanoyl onto the parent Chitosan moiety. Conversion of chitosan to octanoyl chitosan was evident from FTIR, NMR studies. Solubility of MCD in ethanol and methanol along with the water clearly demonstrated functionalization with small degree of acylation.

### References

- Britto D., Assis O.B. (2007) Synthesis and mechanical properties of quaternary salts of chitosan-based films for food application. *International Journal of Biological Macromolecules*. 41, 198–203
- Chen C., Tao S., Qiu X., Ren X., Hu S. (2013) Long-alkane-chain modified N-phthaloyl chitosan membranes with controlled permeability. *Carbohydrate Polymers*, 91, 269– 276
- Choi C.Y., Kim S.B., Pak P.K., Yoo D.I., Chung Y.S. (2007) Effect of N-acylation on structure and properties of chitosan fibers. *Carbohydrate Polymers*, 68, 122–127
- Chu C-C., Zhong C. (2011) Organo soluble chitosan salts and chitosan derived biomaterials prepared thereof. US Patent. US2011/0150999 A1.
- Grant S., Blair H.S., McKay G. (1990) determination of degree of acetylation of chitin and chitosan by thermal analysis. *Polym Commun*. 31, 267
- Huang Y., Yu H., Guo L., Huang Q. (2010) Structure and Self-Assembly Properties of a New Chitosan-Based Amphiphile, *J.Phys.Chem. B*, 114, 7719-7726
- Kjartansson G.T. (2008) Extraction of functional properties of ultrasonicated chitin and chitosan from Crustacean byproducts. A PhD thesis submitted to University of Massachusetts, Amherst, USA.
- Loretz B., and Bernkop-Schnürch A. (2006) In Vitro Evaluation of Chitosan-EDTA Conjugate Polyplexes as a Nanoparticulate Gene Delivery System, *The AAPS Journal*, 8 (4) Article 85
- Ma G., Yang D., Zhou Y., Xiao M., Kennedy J.F., Nie J. (2008) Preparation and characterization of water-soluble N-alkylated chitosan. *Carbohydrate Polymers*. 74, 121–126
- Miya M., Iwamoto E., Ohta O., Mima S. (1985) N-Acetylation of Chitosan Films, *Kobunshi Ronbunshu*, 42, 3, 181-189.
- Moore G.K. and Roberts G.A.F. (1980) Determination of the degree of N-acetylation of chitosan, *Int. J. Biol. Macromol.*, 2, 115-116.
- Shigemasa Y., Matsuura H., Sashiwa H., Saimoto H. (1996) Evaluation of different absorbance ratios from infrared spectroscopy for analyzing the degree of deacetylation in chitin. *International Journal of Biological Macromolecules*, 18, 237-242.
- Tien C.L., Lacroix M., Ispas-Szabo P., Mateescu M. (2003) N-acylated chitosan: hydrophobic matrices for controlled drug release, *Journal of Controlled Release*, 93, 1, 1-13.

## Chapter 6 - Synthesis of Modified Chitosan Derivative

---

Zong Z., Kimura Y., Takahashi M., Yamane H. (2000) Characterization of chemical and solid state structures of acylated Chitosans. *Polymer*. 41, 899–906.

### 7.0 Preparation and Characterization of PLGA-Ag85A Nanoparticles

#### 7.1 Materials

Ag85A was gifted by TB Vaccine Testing & Research Material Contract (TBVTRMC) Colorado State University, (Colorado, USA). PURASORB® PDLG 5002A 50/50 DL-lactide/glycolide copolymer was received as a gift sample from Purac Biomaterials, (Gorinchem, Netherland). Sodium bicarbonate were purchased from Sigma-Aldrich (St-Louis, USA). Cellulose dialysis tubing (Molecular weight cut of 12-14000 Da, 5000 Da) were purchased from Medicell international Ltd., (London, UK). Dimethyl sulfoxide (DMSO, anhydrous), sodium hydroxide was obtained from Sigma-Aldrich (St-Louis, USA). Methanol, ethanol, chloroform, dichloromethane (DCM), ethyl acetate etc. and all other HPLC grade solvents were obtained from Sigma-Aldrich (St-Louis, USA).

#### 7.2 Equipments

1. High speed magnetic stirrer (FisherBrand, UK)
2. Probe Sonicator (Labsonic® P, Sartorius Biotech GmbH, Germany)
3. UV-VIS Spectrophotometer (Jenway UV/Vis Spectrophotometer, UK)
4. Fourier Transform Infra-red spectrophotometer (FTIR) (Perkin Elmer, USA)
5. Differential Scanning Calorimeter DSC Q 2000, (TA Instruments, UK)
6. Zetasizer, Nanoseries Instrument (Nano 25, Malvern Instruments, UK)
7. High speed Centrifuge (Sigma 3K30, Germany & Sigma Laboratory Centrifuge, 3K30, UK)
8. Scanning Electron Microscope (FEI XL30 TMP, Philips, Netherlands)
9. X-Ray Diffractometer (Oxford Diffraction Xcalibur novaT, UK)
10. Twin Stage Impinger (Copley, UK)
11. Bath Sonicator, (Ultrawave Ltd, UK)
12. Transmission Electron Microscopy (TEM, Philips Electron Optics BV, Netherlands)
13. Lyophilizer (Benchtop, VirTis Co. Inc., UK)

#### 7.3 Preparation of nanoparticles

Double emulsion solvent evaporation technique was employed to prepare PLGA nanoparticles. In brief, PLGA (50 mg) was dissolved in 3.5 ml of DCM, deionised water (0.5 ml) containing specified amount of subunit protein ovalbumin (henceforth will be denoted as O-alb) was added to it and the resultant mixture was sonicated for 15 sec at 30 W to form primary w/o emulsion. This emulsion was then transferred to large aqueous phase (10 ml) consisting of 0.5 % PVA and sonicated for 30 sec at 45 W. This multiple emulsion was kept on magnetic stirrer (RO 10 power IKA WERKE, Staufen, Germany) at around 25-30°C for complete removal of organic solvent. The resultant nanoparticles were collected by centrifugation (21000 rpm for 30 min) (Sigma Laboratory Centrifuge, 3K30, UK) and washed thrice with fresh deionised water to remove any residual PVA and untrapped ova. The nanoparticles suspension was subjected to lyophilisation (VirTis Co. Inc., UK) using trehalose dehydrate as cryoprotectant (1 % w/v) as per the reports published by Holzer et. al., (Holzer et.al., 2009). Similar protocol was followed to prepare blank NPs without using O-alb.

### 7.3.1 Optimization of parameters

In preliminary optimization, the possible parameters influencing the formation of nanoparticles and size of nanoparticles were identified and optimized. The parameters studied were sonication time, sonication pulse, solvent selection and surfactant concentration.

#### 7.3.1.1 Selection of solvent

Dichloromethane, ethyl acetate and chloroform were chosen as solvents for the preparation of nanoparticles. Parameters as shown in Table 7.1 were kept constant and batches were prepared using multiple emulsion technique with the sonication pulse of 60. Particle size and PDI was measured to optimize solvent.

**Table 7.1. Composition of nanoparticles**

Component	Quantity
PLGA	50 (mg)
Vol. of organic phase	3.5 ml
Vol. of Internal Aqueous Phase	0.5 ml
Vol. of External Aqueous Phase	10 ml
Surfactant (PVA) concentration	1 % w/v

#### 7.3.1.2 Selection of Sonication time

Sonication was carried out for 15, 30 and 45 sec to study its effect on the formation of nanoparticles. Different batches of NPs were prepared varying the sonication time for primary and secondary emulsion in the preparation of nanoparticles. Particle size and PDI was measured. The surfactant used for the study was PVA at 1 % w/v concentration.

#### 7.3.1.3 Sonication Pulse

After optimization of sonication time, sonication pulse was optimized. Sonication was carried out at pulse rate of 40, 60 and 80 w to study their effect on the formation of nanoparticles. Nine batches of NPs were prepared varying the sonication pulse for primary and secondary emulsion to get desired size of nanoparticles. Particle size and PDI was measured. Rest other parameters as shown in formula (Table 7.1) were kept constant.

#### 7.3.1.4 Selection of surfactant concentration

Surfactant concentration was varied to study its effect on the nanoparticle formation. Total nine batches of NPs were prepared varying the concentration of surfactant (1, 2 & 3 % w/v) in secondary emulsion and keeping rest other parameters constant as shown in the formula (Table 7.1). Particle size and PDI was measured.

### 7.3.2 Optimization by Factorial design

Different variables can be simultaneously and most efficiently tested using systematic and detailed experimental design called factorial designs (Bolton and Bon, 2004). Factorial designs of experiments avoid large number of independent runs which are required while performing classical step-by-step methods. After preliminary parameter selection, 3<sup>2</sup>

## Chapter 7 - Preparation of PLGA-Ag85A Nanoparticles

randomized full factorial design was utilized to statistically optimize the formulation parameters and evaluate the main effects, interaction effects and quadratic effects of the formulation factors on the particle size (Y1) and encapsulation efficiency (Y2). In this design, two factors were evaluated, each at 3 levels, and experimental trials were performed at all 9 possible combinations with three replicates. The replicate experimental runs were carried out in complete randomized manner. Polymer concentration ( $X_1$ ) and concentration of ovalbumin ( $X_2$ ) were selected as independent variables and mean particle size (Y1) and EE (Y2) were chosen as dependent variables. A statistical model incorporating interactive and polynomial terms was used to evaluate the responses. The response surface curves and contour plots were prepared to study the effects of independent variables. All the statistical operations were carried out using Design Expert software (version 8.0.7.1) (Stat-Ease Inc, Minneapolis, USA), Statistica (Stat soft, Tulsa, USA) and Microsoft Excel 2010. For each factor, the experimental range was selected on the basis of the results of preliminary experiments and the feasibility of preparing the PLGA-O-alb at the extreme values. The value range of the variables was: amount of PLGA ( $X_1$ ): 50–100 mg, ovalbumin concentration ( $X_2$ ): 0.25–1.0 mg. Table 7.2 and Table 7.3 summarize experimental runs studied, their factor combinations, and the translation of the coded levels to the experimental units employed during the study.

**Table 7.2.** Factorial design parameters for optimization of nanoparticle formulation

Independent Factors	Levels used, Actual (coded)		
	Low (-1)	Medium (0)	High (+1)
$X_1$ - Polymer Concentration (mg)	50	75	100
$X_2$ - Concentration of O-alb ( $\mu$ g)	250	500	1000
Dependent Variables	Constraint		
Y1 = Particle Size nm	Minimize		
Y2 = % EE	Maximize		

**Table 7.3.** Formulation of the nanoparticles utilizing  $3^2$  factorial design (Coded values)

Batch No.	P1	P2	P3	P4	P5	P6	P7	P8	P9
$X_1$	-1	-1	-1	0	0	0	+1	+1	+1
$X_2$	-1	0	+1	-1	0	+1	-1	0	+1

### 7.3.3 Optimization Data Analysis

Response Surface Methodology (RSM) computations for the optimization study utilized in the current experiment was performed employing Design Expert® software (version 8.0.5.2, Stat-Ease Inc, Minneapolis, MN). Polynomial models including linear, interaction and quadratic terms were generated for the response variables using multiple regression analysis (MLRA) approach. The general form of MLRA model is represented in equation 1.

$$Y = b_0 + b_1X_1 + b_2X_2 + b_3X_1^2 + b_4X_2^2 + b_5X_1X_2 + b_6X_1^2X_2 + b_7X_1X_2^2 \text{-----(1)}$$

## Chapter 7 - Preparation of PLGA-Ag85A Nanoparticles

---

Where  $b_0$  is the intercept representing the arithmetic average of all quantitative outcomes of 9 runs;  $b_1$  to  $b_7$  are the coefficients calculated from the observed experimental values of  $Y$ ; and  $X_1$  and  $X_2$  are the coded levels of the independent variables. The terms  $X_1X_2$  represents interaction term, while  $X_i^2$  ( $i = 1$  to  $2$ ) denotes quadratic terms. The main effects ( $X_1$  and  $X_2$ ) represent the average result of changing one factor at a time from its low to high value. The interaction terms ( $X_1X_2$ ) indicate changes in the response parameters when two factors are simultaneously changed. The polynomial terms ( $X_1^2$  and  $X_2^2$ ) are included to investigate nonlinearity. The polynomial equation as mentioned above was used to conclude the results based on the values of magnitude of coefficients and the mathematical sign (positive or negative) it carries. A positive sign signifies a synergistic effect, whereas negative sign indicates antagonistic effect (Bolton S., 2004).

Statistical validity of the polynomials was determined on the basis of ANOVA provision in the Design Expert ® software and Microsoft Excel (I) (Gurgaon, India). Significance level was considered at  $P < 0.05$ . The best fitting mathematical model was selected based on the comparisons of several statistical parameters including the coefficient of variation (CV), the multiple correlation coefficient ( $R^2$ ), adjusted multiple correlation coefficient (Adj  $R^2$ ), and the predicted residual sum of squares (PRESS) provided by the software. Among them, PRESS indicates how well the model fits the data, and for the chosen model it should be small relative to the other models under consideration (Bolton S., 2004). Also, the 3-D response surface graphs and the 2-D contour plots were generated by the Design Expert® software.

### 7.3.4. Lyophilization of nanoparticles

The optimized batch of nanoparticle formulation was lyophilized using lyophilizer (Vitris Co. Inc., UK). Trehalose dehydrate was used as cryoprotectant at concentration of 1 % w/w (Holzer et.al., 2009). In brief, 1 % of cryoprotectant was dissolved in each batch, all sample containers were sealed by using parafilm, which was pricked to make holes and kept in the lyophilizer (Benchtop, VirTis Co. Inc., UK) for 38 hrs under vacuum. After specified time, vacuum was released, samples were withdrawn, tightly sealed and kept in desiccator until use.

After optimization of formula using O-alb loaded PLGA NPs. A batch of PLGA NPs incorporating Ag85A was prepared using the same optimized formula and process and characterized for following parameters.

## 7.4 Characterization of Nanoparticles

### 7.4.1 Particle size and zeta potential

The particle size and zeta potential of the particles was measured by dynamic light scattering (DLS) and laser doppler velocimetry (LDV) respectively using Zetasizer, Nanoseries Instrument (Nano 25, Malvern Instruments, Worcestershire, UK). The particles were redispersed in deionized water, sonicated in bath sonicator for 5 min. After sonication, particle size and zeta potential of the resultant sample was determined.

**7.4.2 Encapsulation efficiency (EE) & protein loading (PL)**

The protein (O-alb) entrapped in the PLGA NPs was determined by alkaline hydrolysis method using UV-VIS spectrophotometer. Known amount of O-alb loaded PLGA NPs were suspended in the mixture of SDS:NaOH and allowed to stand for 1 hr. Resultant suspension was centrifuged at 3000 rpm for 15 min and the concentration of O-alb in the supernatant was determined using BCA protein estimation kit by UV-VIS spectrophotometer (Jenway UV/Vis

Spectrophotometer, Staffordshire, UK) at 625 nm . Similar method was followed for estimation of Ag85A from optimized PLGA-Ag85A NPs. The analysis was carried out in triplicate in both the cases. The percent yield, entrapment efficiency and protein loading was calculated using following formulae:

$$\text{Yield (\%)} = \frac{\text{Weight of NPs recovered}}{\text{weight of protein+polymer+excipients}} \times 100 \text{-----(2)}$$

$$\text{Entrapment Efficiency (\%)} = \frac{\text{Weight of Protein in NPs}}{\text{weight of protein fed initially}} \times 100 \text{-----(3)}$$

$$\text{Protein Loading (\%)} = \frac{\text{Weight of protein in NPs}}{\text{weight of NP recovered}} \times 100 \text{-----(4)}$$

**7.4.3 Morphology**

Morphology of the lyophilized nanoparticle formulation was studied by Scanning Electron Microscopy (SEM) and Transmission Electron Microscopy (TEM). The samples were mounted onto the SEM sample holder and subjected to gold coating in a vacuum chamber and images were recorded at the required magnification at the acceleration voltage of 10 kV using FEI XL30 TMP SEM (FEI XL30 TMP, Philips, Netherlands). In case of TEM, a drop of nanoparticle suspension was stained with phototungstic acid and placed on a coated carbon grid and vacuum dried. The grid was then examined immediately under TEM (Philips Electron Optics BV, Netherlands) and electron micrographs were obtained.

**7.4.4 Differential scanning calorimetry (DSC) and X-Ray powder diffraction (XRD)**

The freeze dried nanoparticles were tested for crystallinity using DSC and XRD. Thermal property of the freeze-dried nanoparticles and plain protein (O-alb) was investigated with a DSC (DSC Q 2000, TA Instruments, USA). Accurately weighed samples (3-5 mg) were placed in hermetically closed aluminum pans and empty aluminum pan was used as a reference. Heating scans by heat runs for each sample was set from 10 °C to 300 °C at 10 °C min<sup>-1</sup> in a nitrogen atmosphere. The XRD patterns of pure PLGA, blank PLGA NPs and PLGA-Ag85A formulations were recorded using an X-ray diffractometer (Oxford Diffraction Xcalibur novaT, UK). The samples were mounted on a sample holder and X-RD patterns were recorded in the range of 5–50° at the speed of 5°per min.

**7.5 Antigen Integrity by SDS-PAGE Analysis**

After optimization of formula using O-alb loaded PLGA NPs. A batch of PLGA NPs incorporating Ag85A was prepared using the same optimized formula and process and tested for antigens integrity by SDS PAGE analysis. Briefly, 2 mg PLGA-Ag85A nanoparticles were

## Chapter 7 - Preparation of PLGA-Ag85A Nanoparticles

weighed immediately (after preparation and lyophilization) and after two-months of storage. NPs were dispersed in 200  $\mu$ L SDS sampling buffer (consisting of bromophenol blue) as the reducing agent, mixed well and boiled for 5 min to denature the protein. Resultant composition was centrifuged at 12,000 g for 10 min and 20  $\mu$ L of supernatant was loaded into wells of the 12% SDS-PAGE (Bio-Rad, Hercules, CA). Similar treatment was given to blank NPs and pure Ag85A and visualization of proteins was done by naked eye using Coomassie Blue staining.

### 7.6 In-vitro aerosolization & lung deposition using Twin Stage Impinger (TSI)

The aerosolization performance of the nanoparticle formulations was analysed using the twin stage impinger (Copley Scientific Ltd., Nottingham, UK) in accordance with the specifications of British Pharmacopoeia. PLGA-Ag85A NPs (40 mg) were dispersed in 5 mL of water and placed in a Pari LC Sprint nebulizer of which one end was connected to a TurboBoy N compressor (Pari GmbH, Germany) and mouth of nebulizer was placed in front of the “throat” of a twin impinger (Copley Instruments, Nottingham, UK) so that generated aerosol will directly enter into assembly of TSI. A flow rate of 60 L/min was adjusted using a vacuum pump (Copley Instruments, Nottingham, UK). The upper stages (stages 0 and 1) represent the upper airways, and the lower stage (stage 2) represents the lower respiratory airways. The flow rate of 60 L/min provides a cut-off aerodynamic diameter of 6.4  $\mu$ m (Hallworth and Westmorel, 1987; Nasr et.al., 2012). For the consideration of solubility of Ag85A from PLGA NPs, the upper and lower stages of the impinger were filled with 7 mL and 30 mL of 0.1 N NaOH (to hydrolyse PLGA) respectively. The nebulizer was operated until “dryness” (i.e. when aerosol generation completely ceased). The output was maximized by gentle tapping of the nebulizer wall during the sputtering period towards the end of nebulization. Each stage of TSI was rinsed with 0.1 N NaOH, samples were collected and the volume of the stages 0, 1 and 2 was made upto 3, 15 and 45 ml respectively. To each sample, 5% SDS was added for the extraction of protein from the NPs. The samples were taken from each stage (lower and upper stages) for analysis of Ag85A deposited in the different stages of the impinger and quantified by BCA protein estimation assay kit (Sigma Aldrich, USA) using UV-VIS spectrophotometer (Jenway UV/Vis Spectrophotometer, Staffordshire, UK). TSI studies were carried out in triplicate and the aerodynamic behaviour of the nanoparticles suspension was evaluated based on the parameters such as nebulization efficiency (NE) or aerosol output (total aerosolized mass of Ag85A detected in the nebulizer, throat, Stage 1 and Stage 2) (Desai et al., 2002) and respirable fraction (RF) (Matilainen et al., 2006) as calculated using equation 5 and 6. In addition, percent fine particle fraction (FPF) was calculated as the ratio of fine particle dose (FPD) i.e. protein mass deposited in stage 2 to recovered dose (RD), expressed as a percentage (Liu et.al., 2008; Li et.al., 2010).

$$NE (\%) = \frac{\text{Aerosolized Protein}}{\text{Protein Mass Loaded in nebulizer}} \times 100 \text{-----(5)}$$

$$RF (\%) = \frac{\text{Mass of Protein deposited in Stage 2 of TSI}}{\text{Protein Mass Loaded in nebulizer}} \times 100 \text{-----(6)}$$

### 7.7 In-vitro release studies

In-vitro release studies of Ag85A from PLGA-Ag85A nanoparticles was carried out in micro centrifuge tube using modified release technique (Marques et. al., 2011). Simulated lung fluid (SLF) (pH 7.4) was used as dissolution media. A known amount of Ag85A loaded lyophilized PLGA nanoparticles were taken in 2 ml of micro centrifuge tube, dispersed in 2 ml SLF and kept in water bath at 37°C under shaking. At selected time intervals, aliquots were withdrawn from the media, diluted as required and analyzed by QuantiPro™ BCA assay kit at 562 nm (Sigma Aldrich, St. Louis, USA). After the aliquots were withdrawn, media was replenished with the same amount of blank media (kept in water bath at 37°C) in order to maintain sink condition. A calibration curve was prepared prior to the start of dissolution using a SLF (correlation coefficient was 0.9993) as described in the analytical method section (chapter 3). The experiment was done in triplicate and the results reported as percent cumulative drug release *vs* time with  $\pm$  standard deviation.

### 7.8 Stability study

The stability study of lyophilized Ag85A-loaded PLGA nanoparticles was carried out by storing the samples in desiccator for 2 months at ambient temperature (10-15 °C). After two months, samples (2 mg) were withdrawn, rehydrated and the particle size & percentage of Ag85A remained in the nanoparticles were determined in order to assess storage stability. Integrity of Ag85A was also analyzed using SDS PAGE (section 7.5 of this chapter).

### 7.9 Statistical analysis

The experiments were performed in triplicate on separate occasions. The data collected in this study was expressed as the mean value  $\pm$  standard deviation.

## 7.10 Results and Discussion

### 7.10.1 Preparation of nanoparticles and characterization

The aim of the current study was to investigate the preparation of Ag85A incorporated PLGA nanoparticles (NPs) as vaccine delivery for TB. PLGA NPs were successfully prepared by double emulsion solvent evaporation method (DESE). The method for the preparation of NPs was found to be simple and efficient. Initially ovalbumin loaded PLGA NPs were prepared during the course of optimization. Ovalbumin as a model antigen during the optimization process was selected due to resemblance in the molecular weight of ovalbumin (45kDa) and Ag85A (32 kDa). Results of the parameters optimized during the course of formula optimization as given below.

### 7.10.2 Optimization of Parameters by preparing blank PLGA NPs

#### 7.10.2.1 Selection of solvent

In DESE method, emulsions are usually prepared using polymer solutions in volatile solvents. DCM, ethyl acetate and chloroform are widely used solvents for the preparation of NPs using DESE method. In this study, three batches were prepared by varying solvents (DCM, EtOAc and chloroform) and keeping rest other parameters constant. It was observed that EtOAc and DCM were found to be suitable solvents for the preparation of

## Chapter 7 - Preparation of PLGA-Ag85A Nanoparticles

NPs as compared to chloroform in terms of mean particle size. Ethyl acetate, which also presents a better toxicological profile (than DCM and chloroform) was found to produce smallest particle size as compared to DCM and chloroform. However, ethyl acetate required longer time for evaporation, which may be attributed to its high boiling point of 77.1°C and high water solubility (8.7%) leading to longer duration of contact of NPs with the external aqueous phase. This longer contact time may cause diffusion of protein molecules into the external aqueous phase from the particles during the course of evaporation, which in turn may affect entrapment efficiency (Meng et. al., 2003; Mainardes et.al., 2005). Therefore, ethyl acetate seemed unsuitable for the preparation of O-alb incorporated PLGA NPs. In case of chloroform, larger particles and aggregation was observed, as reported by Compton et.al., (Compton et.al., 2007), whereas DCM showed particle size of  $226.90 \pm 4.72$  nm and also required shorter time for evaporation in comparison to ethyl acetate. Shorter evaporation time of DCM may be attributed to its low boiling point (40.1°C) and less water solubility (1.60%). Therefore, DCM was chosen over ethyl acetate and chloroform

**Table 7.4. Selection of solvent for the preparation of PLGA NPs**

Batch	Solvent	MPS (nm)	PDI	Remark
1S	DCM	$226.90 \pm 4.72$	$0.248 \pm 0.068$	G
2S	Ethyl Acetate	$126.90 \pm 6.37$	$0.151 \pm 0.018$	G
3S	Chloroform	$475.13 \pm 23.39$	$0.579 \pm 0.135$	AG

n = 3;  $\pm$  Standard Deviation; G – Good; AG – Aggregate

**Table 7.5. Optimization of sonication time during primary and secondary emulsion**

Optimization of sonication time for primary emulsion					
Batch	Sonication time (Sec)		MPS (nm)	PDI	Remark
	Primary emulsion	Secondary emulsion			
1ST	15	45	$112.73 \pm 42.51$	$0.145 \pm 0.069$	AG
<b>2ST</b>	<b>30</b>	<b>45</b>	<b><math>144.27 \pm 21.34</math></b>	<b><math>0.195 \pm 0.062</math></b>	<b>G</b>
3ST	45	45	$175.43 \pm 43.39$	$0.189 \pm 0.075$	G
Optimization of sonication time for secondary emulsion					
1ST	30	15	$239.57 \pm 33.01$	$0.46 \pm 0.012$	AG
2ST	30	30	$216.67 \pm 12.42$	$0.39 \pm 0.023$	G
<b>3ST</b>	<b>30</b>	<b>45</b>	<b><math>120.90 \pm 6.37</math></b>	<b><math>0.17 \pm 0.044</math></b>	<b>G</b>

n = 3;  $\pm$  Standard Deviation; G – Good; AG – Aggregate; MPS – Mean particle size

### 7.10.2.2 Sonication Time

Sonication time of 15, 30, 45 sec. was used for the preparation of NPs during both the primary and secondary emulsion preparation. Mean particle size, PDI was determined and tabulated in Table 7.5. It was found that increase in the time of sonication for primary emulsification increased the particle size, whereas decrease in the particle size was observed with increase in sonication time during secondary emulsion. Lower sonication time of 15 sec for both primary and secondary emulsion showed improper formation of NPs characterized by lumps, which may be due to inefficient sonication of the polymer and hence sonication time of 15 sec. was considered unsuitable for the preparation of NPs. Sonication time of 30

and 45 sec. for primary emulsion and secondary emulsion preparation respectively yielded particle size of  $120.90 \pm 6.37$  and PDI of  $0.17 \pm 0.044$  without presence lumps. Therefore, the specified time of sonication was selected for the further preparation of NPs. The results of this study are in line with the reports published by Cohen-Sela et. al., where they reported reduction in particle size with the prolongation of sonication (Cohen-Sela et. al., 2009).

### **7.10.2.3 Sonication pulse**

Sonication pulse was varied and NPs were prepared to optimize it. Total of nine batches of nanoparticles were prepared varying sonication pulse at 40, 60 and 80 for both primary and secondary emulsion preparation. Mean particle size, PDI was determined and tabulated in Table 7.6. Increase in the particle size was obtained with decrease in the sonication pulse. When the medium pulse of 60 was applied to prepare NPs, MPS was found to be in the range of  $124.77 \pm 2.07$  to  $126.90 \pm 6.37$  nm, with the PDI values of  $0.151 \pm 0.018$  to  $0.173 \pm 0.009$ , whereas further decrease in sonication pulse to 40 led to formation of lumps in the batch of nanoparticles, indicating that the sonication pulse of 40 was unsuitable for the preparation of NPs. Increased sonication pulse (80) yielded smallest particle size ( $110.60 \pm 9.30$  to  $114.67 \pm 1.79$  nm). However no significant difference was observed in the particles size when pulse of 80 and 60 was used. Hence considering the presence of protein in the formulation, optimum pulse of 60 was selected as minimum possible pulse. Sonication time and intensity (pulse) of sonication is a very important for sensitive peptides or proteins. Therefore, smaller time and pulse was selected for the preparation of NPs. The main problem associated with the nanoparticulate protein formulation is the temperature generated during sonication, which is usually controlled by sonication of the samples in ice bath and using number of short pulses to re-establish a low temperature. Thus, chosen sonication parameters may promote retention of their chemical and physical stability and limit any potentially detrimental impact on the protein. These results are in the accordance with the reports published by the Bilati et. al., who suggested the use of minimum possible sonication time for the preparation of nanoparticles. (Bilati et. al., 2009)

### **7.10.2.4 Surfactant concentration**

Nine batches were prepared by varying surfactant concentration (1 - 3 % w/v) in external aqueous phase. Mean particle size of the NPs is a function of surfactant concentration in the external aqueous phase. Increase in the concentration of surfactant from 1 -3 % caused slight decrease in the particle size from  $114.67 \pm 1.79$  to  $110.60 \pm 9.30$  nm, when sonication pulse of 80 was used. Similarly, difference of only 3 nm ( $126.90 \pm 6.37$  to  $124.77 \pm 2.07$  nm) was noted, when surfactant concentration was increased from 1 -3 % using sonication pulse of 60. Thus, similar trend of decreasing particle size with increase in surfactant concentration was observed in all the three cases of sonication pulse. Number of studies have reported decrease in the particle size with increase in the surfactant concentration (Sahoo et.al., 2002; Zambaux et.al., 1998). This drop in the particle size could be attributed to increased viscosity due to increased concentration of surfactant leading to more stable and uniform sized particles with low polydispersity index. However, no significant decrease in the particles size was noted even after increasing the concentration of surfactant to 2 & 3 %. Our data showed smaller MPS of below 200 nm from all the batches of NPs (Table 7.6) indicating suitability

## Chapter 7 - Preparation of PLGA-Ag85A Nanoparticles

of all surfactant concentrations for the preparation of PLGA NPs. Sonication pulse of 60 and 1% surfactant concentration resulted mean particle size of  $126.90 \pm 6.37$  nm with the PDI values of  $0.151 \pm 0.018$ . It is reported that, higher surfactant concentration is not usually suggested due to its ability to hinder in-vivo degradation of NPs. In addition, removal of excess PVA (which is known to have carcinogenic potential) from the particle surface is difficult if higher concentration of PVA is utilized for the preparation of NPs. Hence, based on the results of this study and constraints with the PVA, 1 % of surfactant concentration was chosen for the preparation of final batches of NPs. Results of these studies are tabulated in Table 7.6, which are in line with the reports published by Ranjam et.al., (Ranjan et. al., 2012).

**Table 7.6. Optimization of Sonication pulse and Surfactant (PVA) concentration**

Batch	Sonication Pulse	Surf. Conc. %	Sonication time (Sec)	Average Particle Size	PDI	Zeta potential	Rem-ark
1SS	80	1	30 & 45	$114.67 \pm 1.79$	$0.151 \pm 0.015$	$-12.63 \pm 2.42$	G
2SS	80	2	30 & 45	$110.73 \pm 2.48$	$0.180 \pm 0.05$	$-12.30 \pm 2.10$	G
3SS	80	3	30 & 45	$110.60 \pm 9.30$	$0.205 \pm 0.015$	$-12.63 \pm 1.63$	G
<b>4SS</b>	<b>60</b>	<b>1</b>	<b>30 &amp; 45</b>	<b><math>126.90 \pm 6.37</math></b>	<b><math>0.151 \pm 0.018</math></b>	<b><math>-25.20 \pm 1.85</math></b>	<b>G</b>
5SS	60	2	30 & 45	$124.27 \pm 5.76$	$0.165 \pm 0.018$	$-24.86 \pm 3.39$	G
6SS	60	3	30 & 45	$124.77 \pm 2.07$	$0.173 \pm 0.009$	$-21.93 \pm 1.80$	G
7SS	40	1	30 & 45	$180.03 \pm 27.84$	$0.320 \pm 0.101$	$-25.30 \pm 0.95$	AG
8SS	40	2	30 & 45	$167.47 \pm 43.76$	$0.250 \pm 0.08$	$-24.81 \pm 5.44$	AG
9SS	40	3	30 & 45	$145.30 \pm 12.97$	$0.230 \pm 0.053$	$-21.74 \pm 4.26$	AG

G - Good; AG - Aggregate; n = 3;  $\pm$  Standard Deviation; (Sonication time for 1° & 2° emulsion respectively)

### 7.10.3 Optimization of formulation by Factorial design

From the investigation of preliminary parameters, various process parameters required for preparation of NPs were finalized to avoid design complexity and the effect of polymer and protein concentration on particle size and entrapment efficiency was studied. Optimized parameters were kept constant in factorial design studies: organic Phase (DCM) (3.5 ml); internal aqueous phase (0.5 ml); external aqueous phase (10 ml, 1% PVA); sonication pulse (60x0.6) and sonication time of 30 and 45 sec for primary and secondary emulsion respectively. Influence of important parameters such as polymer concentration ( $X_1$ ) and protein concentration ( $X_2$ ) was optimized by applying  $3^2$  factorial design. Nine formulations were prepared using  $3^2$  Factorial Design. Table 7.7 enlists the response parameters of all the nine formulations.

#### 7.10.3.1 Effect of formulation variables on the response parameters:

Data obtained from all 9 formulations prepared according to  $3^2$  factorial design was statistically analyzed using ANOVA (Microsoft Excel Corp, India) and Design Expert® 8.0 software by generating various polynomial equations, response surface and contour plots. The data obtained from the software is discussed in the following sections, depicting the effects of variables on the respective response parameters (Y1 and Y2).

**Table 7.7.** Response parameters for NPs prepared as per 3<sup>2</sup> factorial design.

Batch	PLGA (mg)	O-alb (µg)	Response (Y1) MPS (nm)	PDI	Response (Y2) EE (%)
<b>P1</b>	<b>50</b>	<b>250</b>	<b>250.2±5.77</b>	<b>0.481±0.084</b>	<b>80.88±0.78</b>
P2	50	500	215.3±6.27	0.551±0.003	67.90±2.56
P3	50	1000	297.5±21.07	0.696±0.044	52.13±1.95
P4	75	250	479.06±55.09	0.478±0.027	68.25±2.09
P5	75	500	399.97±22.25	0.588±0.17	55.86±2.25
P6	75	1000	481.2±91.54	0.673±0.07	47.28±6.02
P7	100	250	975.6±55.06	0.468±0.18	63.53±2.58
P8	100	500	951.067±75.95	0.588±0.09	53.64±1.26
P9	100	1000	1025.3±45.17	0.914±0.08	45.55±1.12

n = 3; ± Standard Deviation. O-alb – Ovalbumin; MPS – Mean particle size; PDI – Polydispersity index; EE – Entrapment Efficiency;

The responses obtained were fitted in simple linear equation (Eq. 7), interactive equation (Eq. 8) or quadratic model equation (Eq. 9) by carrying out multiple regression analysis and F-statistic to identify statistically significant terms.

$$Y = b_0 + b_1X_1 + b_2X_2 \tag{7}$$

$$Y = b_0 + b_1X_1 + b_2X_2 + b_{12}X_1X_2 \tag{8}$$

$$Y = b_0 + b_1X_1 + b_2X_2 + b_{11}X_{11} + b_{22}X_{22} + b_{12}X_1X_2 \tag{9}$$

From the multiple regressions, it was observed that factors X<sub>1</sub>, X<sub>11</sub> and X<sub>22</sub> had significant effect on the dependent variable MPS, whereas factors X<sub>1</sub>, X<sub>2</sub>, X<sub>11</sub> and X<sub>1</sub>X<sub>2</sub> showed significant effect on the EE based on the *p* values (*p* < 0.05). The multiple regression analysis suggested quadratic model as shown in equation 10 and 11.

**Table 7.8.** Evaluation parameters for NPs prepared as per 3<sup>2</sup> factorial design

Batch	Yield (%)	ZP (mV)	PL (%)
<b>P1</b>	<b>78.54±0.76</b>	<b>-11.37±0.38</b>	<b>0.173±0.004</b>
P2	78.12±1.67	-11.13±0.45	0.289±0.011
P3	78.31±2.39	-11.83±0.25	0.437±0.018
P4	79.29±0.85	-12.8±0.78	0.123±0.004
P5	79.72±2.17	-11.3±1.1	0.198±0.004
P6	80.85±6.02	-14.7±0.35	0.33±0.061
P7	81.49±1.697	-16.47±0.64	0.098±0.003
P8	82.17±3.627	-15.6±0.61	0.164±0.003
P9	80.59±3.246	-18.17±0.23	0.273±0.015

n = 3; ± Standard Deviation. PL – Drug loading; ZP – zeta potential

Nine batches of ovalbumin loaded PLGA NPs (PLGA-O-alb NPs) were prepared by DESE method based using 3<sup>2</sup> factorial design. The observed values and predicted values of MPS and EE for different batches of PLGA- O-alb NPs are shown in Table 7.9 and 7.10 respectively along with their residuals and percent relative error (%RE) values (calculated using equation 12).

## Chapter 7 - Preparation of PLGA-Ag85A Nanoparticles

$$Y1 = 411.57 + 364.83 X_1 + 16.49 X_2 + 165.82 X_{11} + 62.66 X_{22} - 0.6 X_1 X_2 \text{ -----(10)}$$

$$Y2 = 56.82 - 6.37 X_1 - 11.28 X_2 + 3.48 X_{11} + 0.47 X_{22} + 2.69 X_1 X_2 \text{ -----(11)}$$

$$\% \text{ Relative Error (RE)} = \frac{\text{Observed PS} - \text{Predicted PS}}{\text{Predicted PS}} \times 100 \text{ -----(12)}$$

The results of the regression output and response of full model of PLGA- O-alb NPs for both MPS and EE are presented in Table 7.11. The MPS (dependent variable) of PLGA-ova NPs obtained at various levels of two independent variables (X1 and X2) were subjected to multiple regression analysis to yield full model second order polynomial equation. The MPS values showed a wide variation ranging from 250.2±5.76 to 1025.3±163.5 nm, while values entrapment efficiency (EE) varied from 45.55±1.12 to 80.88±0.78 %. A substantially high EE was achieved in PLGA- O-alb NPs (80.88±0.78 %) at low levels (-1) of X1 (50mg) and X2 (250 µg) in batch 1. The responses in the equation Y1 and Y2 are the quantitative effect of the formulation components consisting of independent variables X1 and X2. The corresponding quadratic equations and regression coefficients for Y1 and Y2 (MPS and EE) are as follows:

The significance of each coefficient in equation (10) and (11) was determined based on the *p* values as tabulated in Table 7.11. Smaller the *p* value, the more significant is the corresponding coefficient, expressing that the amount of PLGA and ovalbumin is significant. The data for the MPS presented in the Table 7.11 confirms that the main effects of the independent variables (X<sub>1</sub>, X<sub>11</sub>, X<sub>22</sub>) were significant factors for prediction of MPS as their *p* values fall well below 0.05 (*p* < 0.05), while the interaction term X<sub>1</sub>X<sub>2</sub> has little predictive effect as their *p* values are above 0.05 (*p* > 0.05). In case of entrapment efficiency prediction, *p* values below 0.05 (*p* < 0.05) was observed from the independent variables X<sub>1</sub>, X<sub>2</sub>, X<sub>11</sub> and the interaction term X<sub>1</sub>X<sub>2</sub>, indicating that they are significant factors, whereas, X<sub>22</sub> showed little predictive effect due to higher *p* values (*p* > 0.05).

**Table 7.9.** Observed and Predicted values of response parameter – MPS (Y1)

Batch	Predicted Y1	Observed Y1	Residuals	RE	%RE
P1	259.33	250.2	-9.13	0.035	3.5
P2	212.56	215.3	2.74	0.013	1.3
P3	291.11	297.5	6.39	0.022	2.2
P4	457.74	479.06	21.32	0.047	4.7
P5	411.57	399.97	-11.59	0.029	2.9
P6	490.72	481.2	-9.72	0.019	1.9
P7	987.79	975.6	-12.19	0.012	1.2
P8	942.21	951.07	8.86	0.009	0.9
P9	1021.97	1025.3	3.33	0.003	0.3

RE - % Relative Error

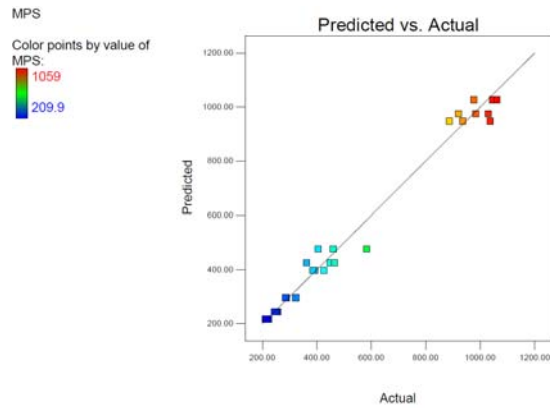


Figure 7.1: X-Y scatter plot showing the predicted vs actual values of MPS

Table 7.10. Observed and Predicted values of response parameter - EE (Y2)

Batch	Predicted Y2	Observed Y2	Residuals	RE	%RE
P1	81.11	80.88±0.78	-0.22	-0.0027	-0.272
P2	66.66	67.90±2.56	1.24	0.0186	1.863
P3	53.16	52.13±1.95	-1.02	-0.0192	-1.921
P4	68.57	68.25±2.09	-0.32	-0.0047	-0.471
P5	56.82	55.86±2.25	-0.95	-0.0168	-1.680
P6	46.01	47.28±6.02	1.28	0.0277	2.777
P7	62.99	63.53±2.58	0.54	0.0086	0.863
P8	53.93	53.64±1.26	-0.29	-0.0053	-0.533
P9	45.81	45.55±1.12	-0.26	-0.0055	-0.559

RE – relative error (%)

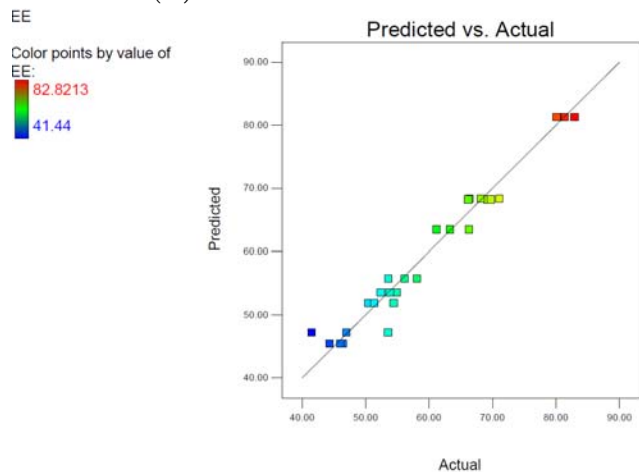


Figure 7.2 : X-Y scatter plot showing the predicted vs actual values of EE

**Table 7.11.** Response of full model of PLGA- O-alb NPs

	MPS		%EE	
	Coefficients	<i>p</i> -value	Coefficients	<i>p</i> -value
X1	364.828	2.02968E-05*	-6.37	0.00149*
X2	16.49	0.120063416	-11.28	0.00027*
X11	165.818	0.001099694*	3.476	0.0379*
X22	62.663	0.017914122*	0.472	0.6623
X1X2	0.6	0.952964808	2.694	0.0299*
Intercept	411.568	8.58178E-05#	56.82	1.311E-05#

\* Statistically significant ( $p < 0.05$ ). # Significance of F value.

The model F values for MPS and EE were found to be 491.65 and 113.13 respectively, while their corresponding calculated F values (F<sub>cal</sub>) were 0.005 and 0.00085 respectively. In addition, the goodness of fit of the model was checked by the correlation coefficient (R<sup>2</sup>). The correlation coefficient (R<sup>2</sup>) values of MPS (0.999) and EE (0.9946) indicated goodness of fit of the model. The values of adjusted correlation coefficient (adj R<sup>2</sup>) were also very high (0.997 for MPS and 0.9857 for EE) as obtained from the full model regression analysis. The predicted R<sup>2</sup> values of MPS and EE were found to be in reasonable agreement with the adj R<sup>2</sup> values, suggesting high significance of the model (R<sup>2</sup> value nearing to 1) and excellent correlation between the independent variables. Moreover, values of “probability > F” were found to be very less than 0.05, implying that the model terms viz. X<sub>1</sub> and X<sub>2</sub> are highly significant ( $p$  value < 0.05). Thus, all of the above considerations indicate that the model is highly significant and can effectively explain 99% variation around the mean value.

When the coefficients of the two independent variables in Eq. (10) were compared, the coefficient value for X<sub>1</sub> (b<sub>1</sub> = 364.83) was found to be maximum and hence it was considered to be a major contributing factor affecting the MPS of PLGA- O-alb NPs. Similarly, Eq. (11) indicated maximum coefficient values for independent variable X<sub>2</sub> (b<sub>1</sub> = -11.28) suggesting it as a major influencing variable for EE. Positive values of X<sub>1</sub> stands for synergistic influence of PLGA concentration on MPS, i.e. increase in the MPS with enhanced concentration of PLGA. However, significance of quadratic terms (X<sub>11</sub> and X<sub>22</sub>) suggested nonlinearity in the influence of independent variables (X<sub>1</sub> and X<sub>2</sub>) on MPS. In case of EE, negative values of variable X<sub>1</sub> and X<sub>2</sub> indicated their antagonistic influence on EE. Increasing the amount of PLGA and ovalbumin resulted in decrease in EE. The combined effect of factors X<sub>1</sub> and X<sub>2</sub> can be further elucidated with the help of response surface curve, contour plots and interaction plots as shown in fig. 3(a-c) and 4(a-c) respectively, which demonstrated that Y<sub>1</sub> and Y<sub>2</sub> varied as mentioned above with respect to PLGA and ovalbumin concentration.

The effects of independent variables X<sub>1</sub> and X<sub>2</sub> on dependent variables Y<sub>1</sub> and Y<sub>2</sub> are described with the help of contour plots, 3D response surface plot and interaction plots, which are presented in figure 7.3(a-c) and 7.3 (a-c). Increase in the value of X<sub>1</sub> from low (-1) to high (+1) level while keeping value of X<sub>2</sub> constant at low level (-1) resulted in significant

increase in MPS. Best (minimum) MPS was obtained at low level of  $X_2$ . Similarly, increase in value of  $X_2$  from low (-1) to high (+1) level, while keeping value of  $X_1$  constant at low level (-1) resulted in slight decrease in value of MPS initially, later on increase was noted at high level (+1) of  $X_2$ . Non linearity in the influence of  $X_2$  on the MPS was observed. However, no significant difference in MPS was noted, when the value of  $X_2$  varied from low (-1) to high (+1) level. Results indicated that at low level of  $X_1$  and low (-1) to high (+1) level of  $X_2$ , an optimum MPS can be obtained (Figure 7.3 a-c). In further analysis, it was observed that, medium (0) and high level (+1) of  $X_1$  yielded maximum value of MPS at all the 3 levels of  $X_2$  which indicated that interaction between  $X_1$  and  $X_2$  may have had significant synergistic effect on Y1. But the concentration of  $X_1$  have shown to increase value of MPS, which can be seen in the interaction plot as shown in figure 7.4 (c). This suggested that the effect of  $X_1$  on the MPS seems to be more pronounced as compared to that of  $X_2$ . The predicted and observed values of response parameters are shown in Table 7.9 and figure 7.1. Low percent relative error values (below 10 %) confirmed the reasonable agreement between predicted values and experimental values indicating suitability of the model. ANOVA results of MPS for full model are given in Table 7.12.

In addition, the Predicted Residual Sum of Squares (PRESS) values were also calculated. PRESS values indicate how well the model fits the data, and for the chosen model it should be small as compared to the other models under consideration (Shah et. al., 2008). In this experiment, the polynomial model with the lower PRESS value was selected to determine the fitness of data between full and reduced model. The value of PRESS for the polynomial full model for both Y1 (7842.55) and Y2 (5.72) was found to be low as compared to reduced model (10539.63 and 6.17). Hence, full model was selected due to goodness of fit.

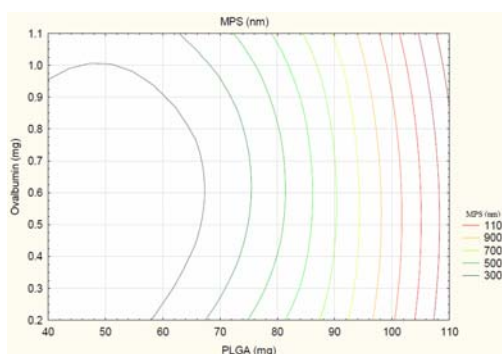


**Figure 7.3(a):** Contour plot showing the effect of independent factors on MPS

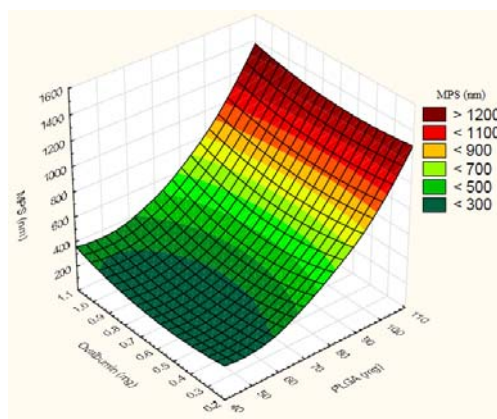


Figure 7.3(b): Response surface plot showing the effect of independent factors on MPS

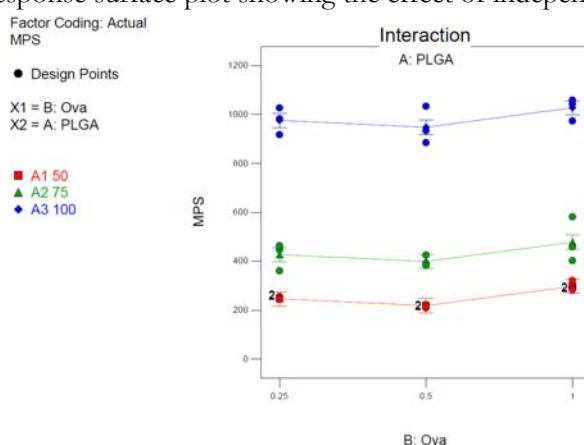


Figure 7.3(c): Interaction plot showing the interaction between PLGA and O-alb on MPS

Table 7.12. Analysis of variance (ANOVA) of MPS for full models of PLGA-O-alb NPs

	df	SS	MS	F	R <sup>2</sup>	Adj R <sup>2</sup>
Regression	5	863076.0634	172615.2127	491.6482382	0.9988	0.9967
Residual	3	1053.284844	351.0949481	--	--	--
Total	8	864129.3483	--	--	--	--

The results of the contour plots, 3D response surface plot and interaction plots for dependent variable Y2 (entrapment efficiency) are given in figure 7.4 (a-c). In this case, increase in value of X<sub>1</sub> from low (-1) to high (+1) level, while keeping value of X<sub>2</sub> constant at low level (-1) found to decrease EE of ovalbumin. Similar results were obtained at all the three levels of X<sub>2</sub>. Highest EE was noted at low level of X<sub>1</sub>. Likewise, when the value of X<sub>1</sub> was kept constant and X<sub>2</sub> varied from low (0.25 mg) to high level (1 mg), observation again revealed decrease in EE. Significantly different values of EE were observed in the experimental design. Results suggested that low level of X<sub>1</sub> (PLGA concentration) and X<sub>2</sub> (ovalbumin concentration) may give an optimum EE.

At medium (0) and High level (+1) of X<sub>1</sub> and X<sub>2</sub>, result obtained from all the 3 levels indicated that interaction between X<sub>1</sub> and X<sub>2</sub> might have resulted in significant antagonistic

## Chapter 7 - Preparation of PLGA-Ag85A Nanoparticles

effect of the two variables on Y2. However, careful observation of the surface response curve suggested strong antagonist effect of  $X_2$  on the EE as compared to that of  $X_1$  (figure 7.4-c). The predicted and observed values of response parameters are shown in Table 7.10 and Figure 7.2. Percent relative error values were found to be below 10 %, confirming suitability of the model. Results of ANOVA for full model of EE are tabulated in Table 7.13.

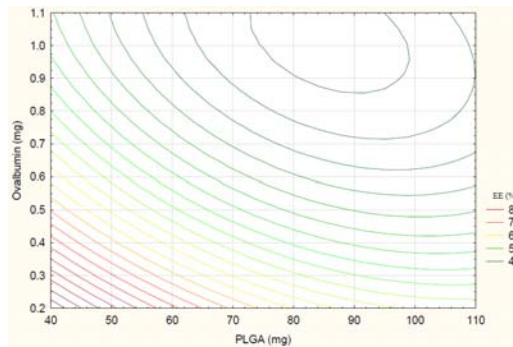


**Figure 7.4(a):** Contour plot showing the effect of independent factors on EE

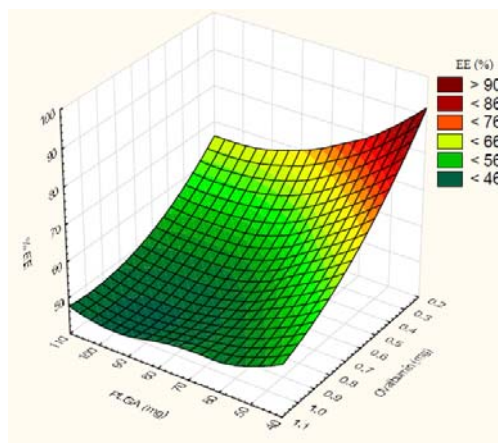


**Figure 7.4(b):** Contour plot showing the effect of independent factors on EE

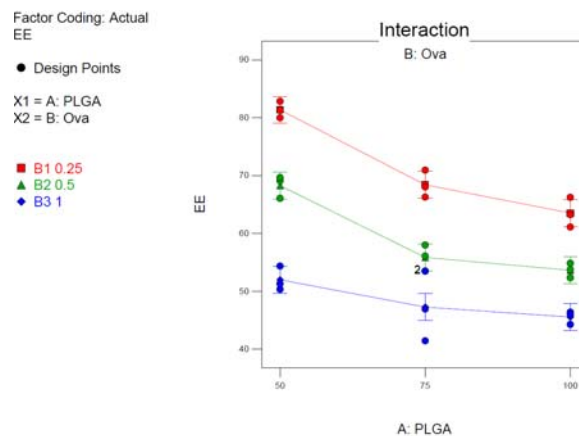


**Figure 7.4(c):** Interaction plot showing the interaction between PLGA and ova on EE

**Table 7.13.** Analysis of variance (ANOVA) of EE for full models of PLGA-O-alb NPs

	df	SS	MS	F	R <sup>2</sup>	Adj R <sup>2</sup>
Regression	5	1060.55631	212.111262	111.13013	0.9946	0.9857
Residual	3	5.72602	1.9087	--	--	--
Total	8	1066.28233	--	--	--	--

*df* degrees of freedom, *SS* sum of squares, *MS* mean of squares, *F* Fischer's ratio, *R*<sup>2</sup> regression coefficient

### 7.10.3.2 Effect of polymer concentration and theoretical protein loading (PL) on MPS and EE

Influence of the theoretical PL on the MPS was studied and a common trend was observed. At low theoretical PL of 250 µg, MPS of 250.2±5.76 nm was obtained, while MPS was found to be decreased to 215.3±6.27 nm when theoretical PL was increased to double (500 µg). Further increase in theoretical PL (1 mg) increased MPS to 297.5±21.07 nm. Similar trend was observed with respect to MPS and polymer concentration, upon increasing concentration of polymer to 75 and 100 mg. These results are correlating with the reports published by Conway and Alpar (Conway and Alpar 1996). However, increase in polymer concentration showed increased MPS. Polymer concentration of 75 mg almost doubled the MPS, whereas it was further increased with 100 mg of PLGA. This effect of the polymer concentration on mean particle size could be attributed to the increase in the viscosity of organic phase due to increased concentration of polymer leading to reduced efficiency of sonication and thus stirring of the medium. Significantly larger particles were produced, when 75 (479.06±55.09 nm) and 100 mg (975.6±55.06 nm) of polymer was used as compared with those produced by using 50 mg (250.2±5.76 nm) of polymer solution. These results are supported by the reports of Li et al. and Benoit et al., who suggested increased opportunities of the suspended nanoparticles to collide and merge leading to fusion of semiformed particles and thus enhancement in particle size (Li et. al., 1999; Murakami et.al., 1999).

In case of entrapment efficiency, increased polymer concentration causes high viscosity of the organic phase, which may lead to restricted migration of the internal aqueous phase containing ovalbumin to the external aqueous phase (Rafati et al. 1997). This contributes to reduced efficiency of emulsion, which may reduce ovalbumin entrapment (Kirby et.al., 2008). Results indicated that, polymer concentration of 50 mg yielded highest entrapment efficiency of 80.88±0.78 %, whereas 75 mg and 100 mg of polymer concentration showed 68.25±2.09 & 63.53±2.58 % of EE respectively. Thus, at low theoretical drug loading (250 µg), highest EE of 80.88±0.78 % was obtained. Enhancing the theoretical drug loading to double substantially decreased EE (67.90±2.56 %). Hence, lowest concentration of polymer (50 mg) was selected for the preparations of NPs. Nanoparticles with 50 mg of polymer exhibited smallest particle size with uniform size distribution as compared to the batches prepared with higher polymer concentration. Studies have shown that increased theoretical PL is associated with increased EE and MPS (Bilati et.al., 2009; Jeffery et al. 1993; Atkins and Peacock 1996;), similarly opposite results are also reported in the literature, where decreased EE was

observed with increase in theoretical PL (Bilati et.al., 2009; Alex and Bodmeier 1990; Conway and Alpar 1996; Yang et al. 2001). It is reported that, increase in theoretical PL to very high levels does not always yield high EE due to insufficiency of polymer to completely entrap the drug. Reports indicated that, most therapeutic peptides/proteins are active at low doses (Kirby et.al., 2008; Bilati et. al., 2009).

Once the NPs are formed, the particle population usually follows a multimodal size distribution. Therefore, PDI becomes a vital factor in order to understand variable particle size in a sample of particles. The PDI value close to 1 suggests wide size range and hence ideal value of PDI should be near to 0 (Ranjan et al. 2012). Results of this study showed that increasing amount of ovalbumin had positive effect on the polydispersity index. However, no significant effect of increasing polymer concentration on PDI was noticed (Table 7.6).

**7.10.3.3 Optimization of Responses Using Desirability Function (www.itl.nist.gov)**

The technique of optimization using desirability function is a way to overcome the difficulty of multiple and sometimes opposing responses. Each response is associated with its own partial desirability function. If the value of desirability function is 1, the response is considered optimum, while value zero completely outcast the result and is treated unacceptable. The desirability for each response can be calculated at a given response point in the experimental design. When the goal is to minimize the given response, formula 13 can be used to calculate individual desirability.

$$d_i(Y_i) = \frac{Y_i(mps) - U_i}{T_i - U_i} \text{-----13}$$

Where  $d_i$  is individual desirability,  $Y_i$  (mps) is experimental results of response MPS.  $U_i$  and  $T_i$  stands for maximum and target MPS. Similarly, to maximize the given response, individual desirability can be calculated using formula 14.

$$d_i(Y_i) = \frac{Y_i(ee) - L_i}{T_i - L_i} \text{-----14}$$

Where  $d_i$  is individual desirability,  $Y_i$  (e) is experimental results of response MPS.  $T_i$  and  $L_i$  stands for minimum and target EE respectively. Once we get this, we can calculate combined desirability (D) using equation 15, which involves multiplication of individual desirability.

$$D = \{(d_1(Y_1) \times d_2(Y_2) \times \dots \times d_n(Y_n))\}^{1/k} \text{-----15}$$

Where, k denotes total number of responses.

A numerical optimization technique by the desirability approach was utilized to generate the optimum parameters for the formulation. The process was optimized for the response parameter (Y1 and Y2) and the optimized formula was arrived by keeping the mean particle diameter in range of 200 to 300 nm and EE between 70 and 90%. Optimum formula with respect to the MPS and EE was found to be Batch P1 (containing low (-1) level of variable  $X_1$  and low level of variable  $X_2$ ). Individual desirability for MPS and EE and overall desirability was found to be 1, indicating acceptability of the model for the optimization of formula. Moreover, the result of the experimental and predicted values for MPS and EE

## Chapter 7 - Preparation of PLGA-Ag85A Nanoparticles

confirmed the practicability and validity of the model. Relative errors for both MPS and EE were found to be below 5 % indicating that the Response Surface Methodology (RSM) optimization technique was appropriate for optimization of PLGA-O-alb NPs.

### 7.10.3.4 Optimized Formulation:

Form these studies, optimum values of the independent variable were obtained. Thus, final formulation was prepared according to the optimized formula as shown in Table 7.14.

**Table 7.14.** Optimized formula for PLGA- O-alb NPs

Parameters	Value
PLGA (mg)	50
Organic Phase (ml)	3.5
Protein concentration ( $\mu\text{g}$ )	0.25
Vol. of internal aqueous Phase (ml)	0.5
Vol. of external aqueous Phase (EAP) (ml)	10
Surfactant in external aqueous phase	PVA
Concentration of surfactant (% w/v)	1

**Table 7.15.** The predicted and observed response variables of optimized PLGA-O-alb NPs

	Y1 (nm)	Y2 (%)
<b>Predicted</b>	240.77	81.61
<b>Observed</b>	250.2	81.36
<b>% RE</b>	3.5	0.31

After lyophilization of PLGA- O-alb NPs in the presence of trehalose as cryoprotective agent (1 % w/v), comparable results were achieved. The presence of 1% trehalose during freeze-drying did not show significant effect on the MPS. Initially MPS of PLGA- O-alb NPs was found to be  $242.87 \pm 9.6$  nm, which was slightly changed to  $250.2 \pm 5.77$  nm indicating the suitability of the trehalose as cryoprotectant during lyophilization (Table 7.15).

This optimized formula was utilized for the formulation of Ag85A loaded PLGA NPs. Parameters namely MPS, PDI, yield, EE and PL of PLGA-Ag85A NP were found to be  $240.03 \pm 3.33$  nm,  $0.34 \pm 0.015$ ,  $58.27 \pm 2.52$  %,  $76.45 \pm 5.58$  % and  $0.2183 \pm 0.0126$  % respectively. The EE of PLGA-Ag85A NPs was found to be in good agreement with the results of EE as obtained for PLGA- O-alb NPs (an optimized batch through design of experiment) with the standard deviation value of 3.47 (Table 7.16).

**Table 7.16.** Parameters for optimized formulation of PLGA-Ag85A NPs

Sr. No.	MPS (nm)	PDI	ZP (mV)	PL (%)	EE (%)	Yield (%)
A	$214.03 \pm 5.92$	$0.30 \pm 0.082$	$-12.1 \pm 2.234$	--	--	--
B	$240.03 \pm 3.33$	$0.34 \pm 0.015$	$-29.4 \pm 0.35$	$0.218 \pm 0.013$	$76.45 \pm 5.58$	$58.27 \pm 2.52$

A – before freeze drying (FD); B- after freeze drying; ZP - Zeta potential; PL - protein loading; EE - entrapment efficiency; PDI – polydispersity index.

### 7.11 Particle Characterization of PLGA-Ag85A nanoparticles

#### 7.11.1 Particle Size and zeta potential

The mean particle size of PLGA-Ag85A NP, prepared according to the optimized formula was found to be  $214.03.3 \pm 5.92$  nm with the PDI values of  $0.300 \pm 0.082$  before freeze drying. After freeze drying with the aid of trehalose as cryoprotectant in the concentration of 1 % yielded  $240.03 \pm 3.33$  and  $0.34 \pm 0.015$  of particle size and PDI respectively (Table 7.16). The results of the particle size distribution curve as obtained from Zetasizer, Nanoseries Instrument (Nano 25, Malvern Instruments, Worcestershire, UK) are presented in Figure 7.5a, b.

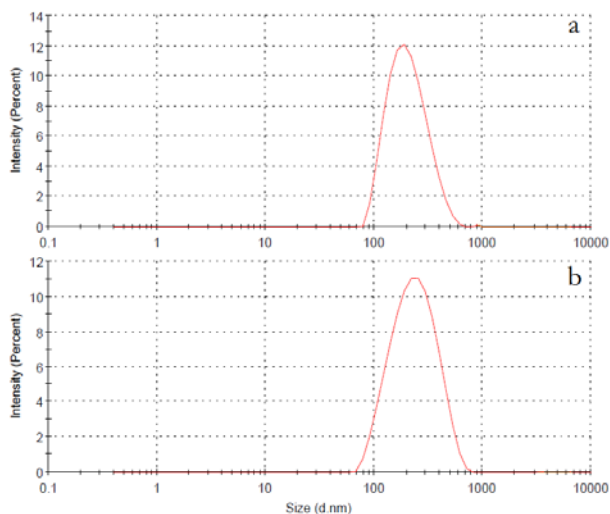


**Figure 7.5a:** Particle size distribution of PLGA-Ag85A NPs before freeze drying  
**b:** Particle size distribution of PLGA-Ag85A NPs after freeze drying

#### 7.11.2 Morphology of PLGA-Ag85A NPs

Scanning electron microscopy (SEM) and Transmission electron microscopy (TEM) was used to visualize the size, shape, and surface morphology of PLGA nanoparticles. Results of SEM and TEM of PLGA-Ag85 NPs showed spherical shape and smooth surface morphology with small (Figure 7.6a and 7.6b).

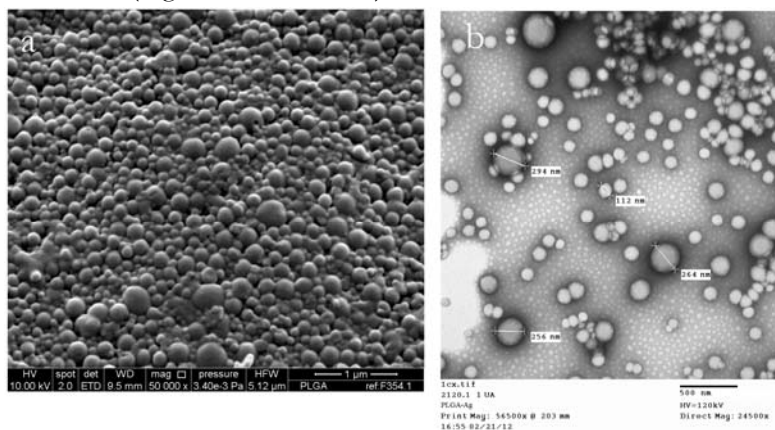


**Figure 7.6; a)** Scanning Electron micrograph of PLGA-Ag85A NPs  
**b)** Transmission Electron micrograph (TEM) of PLGA-Ag85A NPs

### 7.11.3 Solid state characterization of PLGA-Ag85A NPs

#### 7.11.3.1 Differential Scanning Calorimetry (DSC)

As Ag85A was in the liquid form, we carried out DSC studies with ovalbumin loaded formulation. Thermographs of pure ovalbumin, PLGA, PLGA-O-alb physical mixture, blank PLGA NPs and PLGA-Ag85A NP formulation were obtained and are presented in figure 7.7. Ovalbumin was characterized by broad endothermic peak at 50 °C and one more endothermic peak at 150 °C. Occurrence of both the peaks showed thermal denaturation of protein, whereas PLGA produced endothermic peak at 50°C, which is its characteristic feature of glass transition temperature ( $T_g$ ) as reported previously (Photchanachai et.al., 2002; Shi et.al., 2010). Physical mixture of PLGA and O-alb also showed a small endothermic peak at round 50°C, which may be corresponding to PLGA. Finally, when PLGA-Ag85A NPs was tested, single endothermic peak at 50 °C with reduced intensity of PLGA was observed, indicating formation of NPs with the molecular dispersion of Ag85A in the PLGA NPs. As we could not carry out the DSC studies of Ag85A in its free state and as physical mixture with PLGA due to its liquid form, as a reference free ovalbumin, its physical mixture with PLGA and blank PLGA NPs were tested (Shi, 2010). Results of the DSC studies revealed that, thermal behavior of PLGA-Ag85A NPs was similar to that of blank PLGA NPs with the characteristics small endothermic peak of reduced intensity of PLGA in both the blank and Ag85A loaded PLGA NP formulation. These results showed equivalent  $T_g$  of PLGA in all the samples tested. Similar results were reported by Shi et.al., for the TB antigen incorporated PLGA microparticles (Shi, 2010).

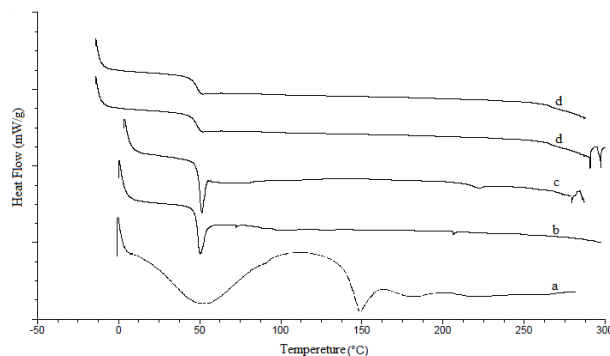


**Figure 7.7:** DSC Thermograms of – a) Pure Ovalbumin; b) Pure PLGA; c) PLGA-Ova physical mixture; d) Blank PLGA NPs ; e) PLGA-Ag85A NPs

#### 7.11.3.2 X-ray powder diffraction (XRD)

Figure 7.8 depicts the X-ray diffractograms of pure PLGA, blank PLGA NPs and Ag85A loaded PLGA NPs. Powder XRD pattern featured characteristics crystalline peaks for PLGA at around 2 theta value of 20°. It was found that parent PLGA showed sharp peak. X-Ray powder diffraction analyses of the blank PLGA NPs and Ag85A loaded PLGA NPs showed similar peak as that of pure PLGA. However, in this case intensity was found to be diminished along with the broad and diffused peak, suggesting successful formation of PLGA NPs with the amorphous or disordered-crystalline structure of the polymer matrix. In addition, similarity in the XRD spectra of PLGA blank NPs and PLGA-Ag85A NPs

indicated molecular dispersion of Ag85A in the PLGA NPs. As reported in literature, existence of broad diffuse peak in XRD observations are often consistent with nanoparticulate formulations consisting of binary components (Parlati et.al., 2009).

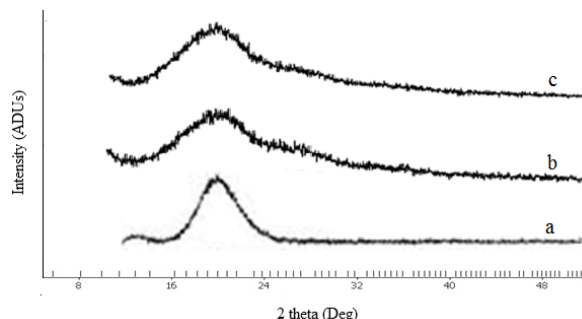


**Figure 7.8:** X-Ray Diffraction patterns of – a) Pure PLGA ; b) Blank PLGA NPs; c) PLGA-Ag85A NPs

### 7.12 Structural integrity of PLGA-Ag85A using SDS-PAGE analysis

Sodium dodecyl sulfate polyacrylamide gel electrophoresis (SDS-PAGE) of Ag85A loaded PLGA nanoparticle formulation is presented in figure 7.9. Figure presents bands of protein marker (1), native antigen (2), Blank PLGA NPs (3), PLGA-Ag85A NPs (4) and PLGA-Ag85A NPs after 2 months storage (5). The electrophoretic analysis of the entrapped Ag85A showed identical band to that of native Ag85A (as shown in Figure 7.9). No additional bands were observed when PLGA-Ag85A NPs were tested, indicating the absence of any molecular weight aggregates or fragments greater or less than the molecular weight of Ag85A (32 kDa). This result suggests that the structural integrity of Ag85A was retained even after its encapsulation in PLGA NPs. Blank PLGA NPs loaded at lane 3 was devoid of any traces of Ag85A. Lane 5 in the series represents a band for Ag85A in PLGA-Ag85A NPs after 2 months of storage period at ambient temperature of 10-15 °C. A clear band resembling to the one observed in the lane 2 and 4 is an indication of the stability and structural integrity of the Ag85A in PLGA NPs up to 2 months storage period. Hence, it can be assumed that no chemical modification, non-covalent aggregation or significant degradation of Ag85A occurred during the process of nanoparticle preparation and 2 months period of storage at 10-15 °C.

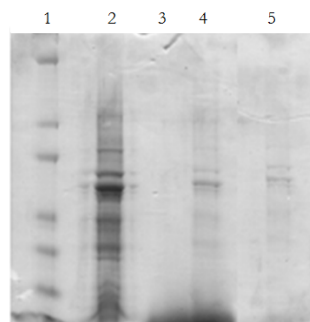


**Figure 7.9:** SDS-PAGE analysis of PLGA-Ag85A NPs, 1) Protein Marker; 2) Native Ag85A; 3) Blank PLGA-NPs; 4) PLGA-Ag85A NPs; 5) PLGA-Ag85A NPs after 2 months

**7.13 In-vitro aerodynamic performance - pulmonary deposition of NPs**

Current study was aimed to deliver Ag85A incorporated PLGA nanoparticles in the lung via nebulization therapy for better therapeutic outcome against TB. In order to aerosolize NPs, correct aerodynamic properties of particles are prerequisite so that nebulized powder can efficiently aerosolize to reach required sites of the lungs. Well known localization of MTB, their proliferation and accumulation in the macrophages within the lung (Hirota and Terada, 2012; Vadwai et.al., 2011) made the delivery of particles to lungs promising for effective therapeutic purpose.

NPs were dispersed in double distilled water and suspension was nebulized using PariBoy air-jet nebulizer with compressed air using an Inhaler Boy compressor. Table 7.17 presents the data for the deposition of PLGA-Ag85A NPs following aerosolisation. Results indicated deposition of PLGA-Ag85A NPs formulation in Stage 2 ( $21.25 \pm 5.73 \mu\text{g}$ ) of the TSI having effective cut-off diameter of  $6.8 \mu\text{m}$ , whereas high deposition of the NP formulation was observed at throat and stage 1 ( $27.78 \pm 2.09 \mu\text{g}$ ). However, no significant difference in the deposition at these two stages was noted. Nebulization efficiency of the NP formulation was found to be  $78.43 \pm 4.54\%$  of the anticipated amount of protein and  $30.01 \pm 8.09\%$  of the dose nebulized was found to be respirable fraction (Table 7.17) suggesting that the formulation can be predicted to demonstrate deposition in the lower respiratory tract. Deposition of PLGA-Ag85A NP formulation in all stages of the TSI including device, throat, stage 1 and stage 2 was falling between 75% and 125% of mass balance, which is in accordance with the criteria stated as per British Pharmacopoeia (British Pharmacopoeia, 2012).

**Table 7.17.** Pulmonary deposition of the PLGA-Ag85A NPs (P1) Measured by TSI

Batch	Inhaled Dose ( $\mu\text{g}$ )	Delivered Dose ( $\mu\text{g}$ )	FPD ( $\mu\text{g}$ )	NE %	RF (%)	FPF (%)
P1	70.8	$55.53 \pm 9.08$	$21.25 \pm 5.73$	$78.43 \pm 4.54$	$30.01 \pm 8.09$	$38.27 \pm 8.47$

( $\pm$  SD,  $n = 3$  - Mean  $\pm$  Standard Deviation) ; NE – Nebulization efficiency; RF – Respirable fraction; FPF – Fine particle fraction; FPD - Fine particle Dose.

**7.14 In-vitro release studies**

In-vitro release profile of PLGA-Ag85A NPs is shown in figure 7.9, as percentage cumulative drug release vs time. Release study was carried out in simulated lung fluid (SLF 4, pH 7.4) so as to mimic the biological environment within the lungs. Results of the release studies showed biphasic release of protein. Almost 15 % ( $13.54 \pm 4.94\%$ ) of protein was found to be released during the first 2 hrs, followed by the continuous release up to  $46.68 \pm 5.02\%$  by the end of 12 hr. Thereafter, slow and steady release of protein ( $61.46 \pm 4.74$ ) was observed up to the study period of 48 hrs. Similar pattern have been previously reported for the release of proteins such as BSA and ovalbumin (Blanco et.al., 1997). At the first phase of upto 12 hrs,  $46.68 \pm 5.02\%$  of Ag85A was released, which may have been possibly due to dissolution and passive diffusion of Ag85A located on or near the

## Chapter 7 - Preparation of PLGA-Ag85A Nanoparticles

surface of nanoparticles, whereas a second phase (beyond 12 hrs) was characterized by the slow and steady release of Ag85A, which could be attributed to the release of Ag85A from the core of PLGA nanoparticles. Hence, biphasic release pattern of the formulation can be ascribed to the localization of Ag85A onto and within nanoparticle formulation. The data obtained is in support with the reports published by Blanco et. al., (Blanco et.al., 1997).

Mathematical modeling of the release profiles using zero order, first order, Higuchi, Hixon Crowell and Korsmeyers Peppas model was undertaken to understand the kinetics of protein release from PLGA nanoparticle formulation (Costa et.al., 2001). The results of model fittings as analyzed employing different mathematical models are presented in Table 7.18. The curve fitting of release data to Korsmeyers and Peppas model showed higher correlation coefficient value ( $r^2$  value of 0.9039) (Costa et.al., 2001). This model suggested Fickian diffusion mechanism based on the  $n$  value determination ( $n$  values of 0.4695). Thus, main mechanism for the transport of Ag85A from the PLGA nanoparticles was found to be controlled by Fickian diffusion, indicating Korsmeyers and Peppas model owing to diffusion of protein from the PLGA NPs.

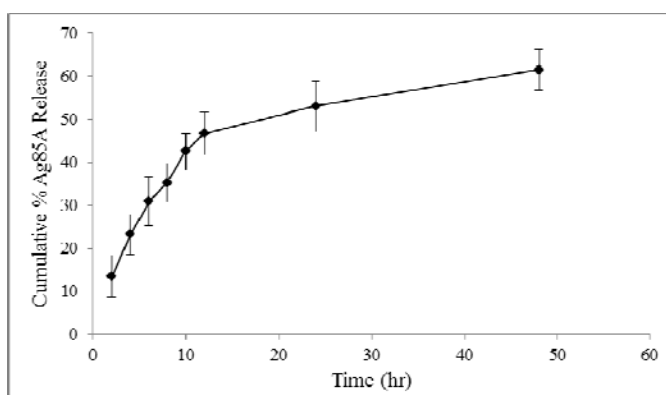


**Figure 7.10:** Cumulative percent release (CPR) of Ag85A from Ag85A loaded PLGA NPs  
( $n=3$  determinations  $\pm$ SD)

**Table 7.18. Release kinetics of PLGA-Ag85A NPs**

Model	$R^2$	Slope	Intercept
Zero order	0.7199	0.881	25.773
First order	0.5368	0.0103	1.3965
Higuchi Square root	0.8705	8.3284	10.063
Hixon- Crowell	0.601	0.0261	2.9345
Korsmeyer Peppas	<b>0.9039</b>	0.4695 ( $n$ )	1.0899

### 7.15 Stability Studies

PLGA-Ag85A NPs were subjected to storage stability study in terms of protein content (Ag85A), particle size and PDI for the period of 2 month at ambient temperature (10- 20 °C). Results of stability study indicated physical stability of the PLGA-Ag85A NPs for upto 2 months period at RT in desiccator (Table 7.19). No significant difference was noted in the

## Chapter 7 - Preparation of PLGA-Ag85A Nanoparticles

---

drug content, particle size and PDI values of PLGA-Ag85A NPs (Table 7.19). Particle size of the formulation was found to be almost similar even after 2 months storage period ( $239.07 \pm 15.62$  nm) however, increased PDI values ( $0.45 \pm 0.062$ ) were noted which could be attributed to the slight aggregation of the formulation. Results of the stability studies confirmed the stability of PLGA-Ag85A NPs at RT (10-20 °C). Considering the results of this study, 10-20 °C could be an effective storage temperature.

**Table 7.19.** Stability of PLGA-Ag85A NPs at RT (10- 20 °C)

Sr. No	Time (Months)	Drug Content (%)	Particle Size (nm)	PDI
1	Initial	100	$240.03 \pm 3.33$	$0.34 \pm 0.015$
2	2	$97.63 \pm 4.99$	$239.07 \pm 15.62$	$0.45 \pm 0.062$

n=3 determinations,  $\pm$  SD values

### References

Alex R., Bodmeier R. (1990) Encapsulation of water-soluble drugs by a modified solvent evaporation method. I. Effect of process and formulation variables on drug entrapment. *Journal of Microencapsulation*, 7, 347–355.

Atkins T.W., Peacock J. (1996) Incorporation and release of bovine serum albumin from poly-hydroxybutyrate-hydroxyvalerate microcapsules. *Journal of Microencapsulation*, 13, 709–717.

Bilati, U., Allémann, E. and Doelker, E. (2009) Poly(D,L-lactide-co-glycolide) protein-loaded nanoparticles prepared by the double emulsion method—processing and formulation issues for enhanced entrapment efficiency', *Journal of Microencapsulation*, 22 (2), 205 - 214

Blanco M.D., Alonso M.J. (1997) Development and Characterization of protein loaded poly(lactide-co-glycolide) nanospheres, *E. J. Pharm and Biopharm*, 43, 287-294.

Bolton S., Charles S. *Pharmaceutical Statistics*. New York, NY: Marcel Dekker Inc; 2004. pp. 249–255.

British Pharmacopoeia (2012) Appendix XII C. Consistency of Formulated Preparations, *British Pharmacopoeia Volume V*, British Pharmacopoeia, 2012 online.

Cohen-Sela E., Chorny M., Koroukhov N., Danenberg H.D., Golomb G. (2009) A new double emulsion solvent diffusion technique for encapsulating hydrophilic molecules in PLGA nanoparticles, *Journal of Controlled Release*, 133, 90–95

Compton O.C., Osterloh F.E. (2007) Evolution of Size and Shape in the Colloidal Crystallization of Gold Nanoparticles, *J. Am. Chem. Soc.*, 129, 7793-7798

Conway B.R., Alpar H.O. (1996) Double emulsion microencapsulation of proteins as model antigens using polylactide polymers: effect of emulsifier on the microsphere characteristics and release kinetics. *European Journal of Pharmaceutics and Biopharmaceutics*, 42, 42–48.

Desai, T.R., Hancock, R.E.W., Finlay, W.H., 2002. A facile method of delivery of liposomes by nebulization. *J. Control. Release*, 84, 69–78.

Hallworth, G.W., Westmorel, D.G., 1987. The twin impinger: a simple device for assessing the delivery of drugs from metered dose pressurized aerosol inhalers. *J. Pharm. Pharmacol.* 39, 966–972

Hirota K., and Terada H. (2012). *Endocytosis of Particle Formulations by Macrophages and Its Application to Clinical Treatment*, Molecular Regulation of Endocytosis, Dr. Brian Ceresa (Ed.), ISBN: 978-953-51-0662-3, InTech, DOI: 10.5772/45820. Available from:

## Chapter 7 - Preparation of PLGA-Ag85A Nanoparticles

---

<http://www.intechopen.com/books/molecular-regulation-of-endocytosis/endocytosis-of-particle-formulations-by-macrophages-and-its-application-to-clinical-treatment> (Date accessed May 2013).

Holzer M., Vogel V., Mäntele W., Schwartz D., Haase W., Langer K. (2009) Physico-chemical characterisation of PLGA nanoparticles after freeze-drying and storage. *European Journal of Pharmaceutics and Biopharmaceutics*, 72, 428–437

Jeffery H., Davis S.S., O'Hagan D.T. (1993) The preparation and characterization of poly(lactide-co-glycolide) microparticles. II. The entrapment of a model protein using a (water-in-oil)-in-water emulsion solvent evaporation technique. *Pharmaceutical Research*, 10, 362–368.

Kirby D. J., Rosenkrands, I., Agger E. M., Andersen P., Coombes A.G. A. and Perrie Y. (2008) PLGA microspheres for the delivery of a novel subunit TB vaccine, *Journal of Drug Targeting*, 16 (4), 282 — 293

Li H-Y., Seville P.C. (2010) Novel pMDI formulations for pulmonary delivery of proteins, *International Journal of Pharmaceutics*, 385, 73–78

Li X., Deng X., Yuan M., Xiong C., Huang Z., Zhang Y., Jia W. (1999) Investigation on process parameters involved in preparation of poly-D,LL-lactide-poly(ethylene glycol) microspheres containing *Leptospira Interrogans* antigens. *International Journal of Pharmaceutics*, 178, 245–255.

Liu J., Gong T., Fu H., Wang C., Wang X., Chena Q., Zhang Q., Hea Q., Zhang Z. (2008) Solid lipid nanoparticles for pulmonary delivery of insulin. *Int. J. Pharm.* 356, 333–344

Mainardes R.M., Evangelista R.C. (2005) PLGA nanoparticles containing praziquantel: effect of formulation variables on size distribution. *International Journal of Pharmaceutics*, 290, 137–144

Matilainen, L., Järvinen, K., Toropainen, T., Näsä, E., Auriola, S., Järvinen, T., Jarho, P., 2006. In vitro evaluation of the effect of cyclodextrin complexation on pulmonary deposition of a peptide, cyclosporin A. *Int. J. Pharm.* 318, 41-48

Meng F.T., Ma G.H., Qiu W., Su Z.G. (2003) W/ O / W double emulsion technique using ethyl acetate as organic solvent: effects of its diffusion rate on the characteristics of microparticles. *Journal of Controlled Release*, 91, 407–416

Murakami H., Kobayashi M., Takeuchi H., Kawashima Y. (1999) Preparation of poly(DL-lactide-co-glycolide) nanoparticles by modified spontaneous emulsification solvent diffusion method. *International Journal of Pharmaceutics*, 187, 143–152

Nasr M., Nawaz S., Elhissi A. (2012) Amphotericin B lipid nanoemulsion aerosols for targeting peripheral respiratory airways via nebulization. *Int. J. Pharm.* 436, 611– 616

Parlati C., Colombo P., Buttini F., Young P.M., Adi H., Ammit A.J., and Traini D. (2009) Pulmonary Spray Dried Powders of Tobramycin Containing Sodium Stearate to Improve Aerosolization Efficiency, *Pharmaceutical Research*, 26, 5, 1084-1092.

Photchanachai S., Mehta A., and Kitabatake N. (2002) Heating of an Ovalbumin Solution at Neutral pH and High Temperature, *Biosci. Biotechnol. Biochem.*, 66 (8), 1635–1640

Rafati H, Coombes AGA, Adler J, Holland J, Davis SS. (1997) Protein-loaded poly(D,L-lactide-co-glycolide) microparticles for oral administration: formulation, structural and release characteristics. *Journal of Controlled Release* 43:89–102.

Ranjan A.P., Mukerjee A., Helson L. and Vishwanatha J.K. (2012) Scale up, optimization and stability analysis of Curcumin C3 complex-loaded nanoparticles for cancer therapy. *Journal of Nanobiotechnology*, 10, 38

Sahoo S.K., Panyam J., Prabha S., Labhassetwar V. (2002) Residual polyvinyl alcohol associated with poly (D,L-lactide-coglycolide) nanoparticles affects their physical properties and cellular uptake. *Journal of Controlled Release*, 82, 105–114

Shah P.P., Mashru R.C., Rane Y.M., Thakkar A. (2008) Design and Optimization of Mefloquine Hydrochloride Microparticles for Bitter Taste Masking. *AAPS PharmSciTech.* 9 (2), 377–389.

Shi S., and Hickey A.J. (2010) PLGA Microparticles in Respirable Sizes Enhance an In Vitro T Cell Response to Recombinant Mycobacterium Tuberculosis Antigen TB10.4-Ag85B, *Pharmaceutical Research*, 27 (2), 350-360

Shi S. (2010) Rational Design, Manufacture and Evaluation of Respirable TB Subunit Vaccines. A dissertation submitted to the faculty of the University of North Carolina at Chapel Hill, Eshelman School of Pharmacy.

Vadwai V., Daver G., Udwardia Z., Sadani M., Shetty A., et al. (2011) Clonal Population of *Mycobacterium tuberculosis* Strains Reside within Multiple Lung Cavities. *PLoS ONE*, 6 (9), e24770. doi:10.1371/journal.pone.0024770.

Yang Y.Y., Chung T.S., Ng N.P. (2001) Morphology, drug distribution, and in vitro release profiles of biodegradable polymeric microspheres containing protein fabricated by double-emulsion solvent extraction/evaporation method. *Biomaterials*, 22, 231–241.

## **Chapter 7 - Preparation of PLGA-Ag85A Nanoparticles**

---

Zambaux M.F., Bonneaux F., Gref R. et al., (1998) Influence of of the drug incorporated in experimental parameters on the characteristics of poly (lactic acid) nanoparticles prepared by a double emulsion method, J. control Controlled Release, 50 (1–3), 31–40.

### 8.0 Preparation of Rifampicin Loaded HCD (HCD-Rif) Nanoparticles

#### 8.1 Materials

Rifampicin was purchased from Sigma-Aldrich (St-Louis, USA). Chitosan oligosaccharide (MW > 5kDa; degree of deacetylation (DDA) 80-90%) was supplied by Kitto Life Co. Ltd. (Kyongki-Do, Seol Korea). Octanoyl chloride, methane sulfonic acid, sodium bicarbonate, Poloxomer, Poly vinyl alcohol were purchased from Sigma-Aldrich (St-Louis, USA). Cellulose dialysis tubing (Molecular weight cut of 12-14000 Da, 5000 Da) was purchased from Medicell international Ltd., (London, UK). Dimethyl sulfoxide (DMSO, anhydrous), methanol, ethanol, chloroform, dichloromethane (DCM), acetone etc. and all other HPLC grade solvents were obtained from Sigma-Aldrich (St-Louis, USA).

#### 8.2 Equipments

1. High speed magnetic stirrer (Fisher Brand, UK)
2. Probe Sonicator (Labsonic® P, Sartorius Biotech GmbH, Germany)
3. UV-VIS Spectrophotometer (Jenway UV/Vis Spectrophotometer, UK)
4. Fourier Transform Infra-red spectrophotometer (FTIR) (Perkin Elmer, USA)
5. Differential Scanning Calorimeter DSC Q 2000, (TA Instruments, UK)
6. Zetasizer, Nanoseries Instrument (Nano 25, Malvern Instruments, UK)
7. High speed Centrifuge (Sigma 3K30, Germany & Sigma Laboratory Centrifuge, 3K30, UK)
8. Scanning Electron Microscope (FEI XL30 TMP, Philips, Netherlands)
9. X-Ray Diffractometer (Oxford Diffraction Xcalibur novaT, UK)
10. Twin Stage Impinger (Copley, UK)
11. Bath Sonicator, (Ultrawave Ltd, UK)
12. Transmission Electron Microscopy (TEM, Philips Electron Optics BV, Netherlands)
13. Lyophilizer (VirTis Co. Inc., UK)

#### 8.3 Preparation of HCD-Rif nanoparticles (HCD-Rif NPs)

HCD nanoparticles were prepared by multiple emulsion solvent evaporation technique as per previously reported method with slight modifications (Pandey et.al., 2003). Accurately weighed 50 mg of HCD was dissolved in 1.5 ml of dichloromethane, required quantity of rifampicin was dissolved in it with agitation until complete dissolution. Organic phase was emulsified immediately with aqueous phase by sonication for 15 sec at 15 Amp to form primary emulsion. The emulsion obtained was then poured into 10 ml of aqueous phase containing 0.5 % PVA and sonicated at 15 Amp for 30 sec. Resultant multiple emulsion was magnetically stirred (RO 10 power IKA WERKE, Staufen, Germany) at 25-30°C for about 4 hrs to remove organic phase. Recovery of nanoparticles formed was done by centrifugation at 21000 rpm for 30 min (Sigma Laboratory Centrifuge, 3K30, UK). Samples were washed thrice with fresh deionised water to remove any residual surfactant (PVA) and free drug. Lyophilization (VirTis Co. Inc., UK) of the nanoparticles suspension was carried out by addition of cryoprotectant, trehalose dehydrate (1 % w/v) as per the reports of Holzer et.al., (Holzer et.al., 2009). Similar protocol was followed to prepare blank HCD NPs without rifampicin.

**8.3.1 Optimization of preliminary parameters**

Preliminary optimization study was carried out to understand the influence of possible parameters affecting the formation of nanoparticles, in terms of their MPS, PDI and zeta potential. Initially, sonication time was optimized and sonication pulse required for the preparation of blank NPs was selected by preparing batches according to formula mentioned in table 8.1. Later on, parameters such as sonication time, solvent, surfactant and surfactant concentration were selected and optimized by designing the experiment as per  $2^3$  factorial design on the basis of MPS and PDI (Table 8.2 and Table 8.3). Once these formulation parameters were selected and optimized, final formula optimization was carried out utilizing  $3^2$  factorial design.

**8.3.1.1 Selection of sonication time**

Varied sonication times (15, 30 and 45 sec) were chosen to prepare different batches of nanoparticles at the stage of primary and secondary emulsion preparation. Particle size, PDI and zeta potential were determined to identify optimum sonication time required for the preparation of nanoparticles. Sonication pulse of 15 W was utilized for primary and secondary emulsion during nanoparticle preparation. Following formula as given in Table 8.1 was employed for the preparation NPs.

**Table 8.1. Composition of blank nanoparticles**

Component	Quantity
HCD	50 (mg)
Vol. of organic phase	3.5 ml
Vol. of Internal Aqueous Phase	0.5 ml
Vol. of External Aqueous Phase	10 ml
Surfactant (PVA) concentration in external aqueous phase	1 % w/v

**8.3.1.2 Selection of Solvent, surfactant and surfactant concentration**

Formulation of NPs using DESE method is usually achieved by preparing polymer solutions in volatile solvents such as dichloromethane (DCM), ethyl acetate (EtOAc) and chloroform. As compared to more hydrophobic DCM and chloroform ( $\text{CHCl}_3$ ), ethyl acetate (EtOAc) has been the choice of solvent due to its less toxic nature. However, most researchers employ DCM to manufacture NPs in the view of its favorable physical properties (low boiling point of  $40.1^\circ\text{C}$  and less water solubility - 1.60%) which helps easy evaporation of organic solvent and also solubilizes large amount of polymer (Meng et. al., 2003). Hence, we chose DCM and EtOAc for the preparation blank NPs to fit in the  $2^3$  factorial design in order to select solvent which gives optimum MPS and PDI values.

Two surfactants namely Pluronic® F 127 and polyvinyl alcohol (PVA) were selected and two concentrations (0.5 and 1 %) of each surfactant were chosen to use in the external aqueous phase and study their influence on the preparation of nanoparticle.

Preliminary optimization was done as per  $2^3$  factorial design (Table 8.2 and 8.3) by using 3 variables (solvent, surfactant and surfactant concentration) varying at two levels. Batches were prepared according to design of experiment as tabulated in table 8.3 and nanoparticles were assessed based on the mean particle size (MPS) and PDI.

**Table 8.2.** Preliminary parameters for optimization of blank nanoparticle formulation

Independent Factors	Levels used, Actual (coded)	
	Low (-1)	High (+1)
X <sub>1</sub> - Solvent	DCM	EtoAc
X <sub>2</sub> - Surfactant Conc. (%w/v)	0.5	1
X <sub>3</sub> – Surfactant	P F 127	PVP
Dependent Variables	Constraint	
Particle Size nm	Minimize	
PDI	Minimize	

Solvents : DCM – Dichloromethane; EtoAc- Ethyl Acetate;  
Surfactants: P F 127 – Pluronic F 127; PVA – Polyvinyl alcohol

**Table 8.3.** Formulation of the blank nanoparticles using  $2^3$  factorial design (Coded values)

Batch No.	Solvent	Surfactant Conc. (%w/v)	Surfactant
B1	-1	-1	-1
B2	1	-1	-1
B3	-1	1	-1
B4	1	1	-1
B5	-1	-1	1
B6	1	-1	1
B7	-1	1	1
B8	1	1	1

### 8.3.2 Optimization of MPS and EE by Factorial design

After optimizing process and formulation parameters for blank NPs, drug loaded NPs were optimized. For the preparation of rifampicin (Rif) loaded HCD NPs (HCD-Rif NPs), process parameters such as sonication time, organic solvent, surfactant, and concentration of surfactant were set as per preliminary optimization studies as described above. A  $3^2$  randomized full factorial design was utilized to optimize the concentrations of PLGA and rifampicin concentration and to study their influence on mean particle size (MPS) and entrapment efficiency (EE). A  $3^2$  randomized full factorial design involves evaluation of two factors, each at 3 levels. Accordingly 9 possible combinations of experimental trials were prepared with three replicates. The replicate experimental runs were carried out in complete randomized manner. The concentration of polymer (X<sub>1</sub>) and concentration of Rif (X<sub>2</sub>) were selected as independent variables. Two dependent variables namely, MPS (Y1) and EE (Y2)

were selected as response parameters. A statistical model incorporating interactive and polynomial terms was used to evaluate the responses. The response surface curves and contour plots were prepared to study the effects of independent variables. All the statistical operations were carried out using Design Expert software (version 8.0.7.1) (Stat-Ease Inc, Minneapolis, USA), Statistica (Stat soft, Tulsa, USA) and Microsoft Excel 2010 (I) (Gurgaon, India). Table 8.4 and Table 8.5 represent experimental design, their factor combinations, and the translation of the coded levels to the experimental units employed during the study.

**Table 8.4.** Factorial design parameters for optimization of HCD-Rif nanoparticles

Independent Factors	Levels used, Actual (coded value)		
	Low (-1)	Medium (0)	High (+1)
X <sub>1</sub> - PLGA Concentration (mg)	50	75	100
X <sub>2</sub> - Concentration of Rif (mg)	5	10	15
<b>Dependent Variables</b>	<b>Constraint</b>		
Y1 = Particle Size nm	Minimize		
Y2 = % EE	Maximize		

**Table 8.5.** Formulation of the nanoparticles utilizing 3<sup>2</sup> factorial design (Coded values)

Batch No.	C1	C2	C3	C4	C5	C6	C7	C8	C9
X <sub>1</sub>	-1	-1	-1	0	0	0	+1	+1	+1
X <sub>2</sub>	-1	0	+1	-1	0	+1	-1	0	+1

### 8.3.3 Optimization Data Analysis

The optimization of parameters in the current study was carried out by applying various Response Surface Methodology (RSM) computations using Design Expert® software (version 8.0.5.2, Stat-Ease Inc, Minneapolis, MN), Statistica (Stat soft, Tulsa, USA) and Microsoft Excel 2010. Multiple regression analysis (MLRA) approach was used to generate polynomial models (including interaction and quadratic terms) for the response variable. The general form of MLRA model can be represented as given in the equation 1.

$$Y = b_0 + b_1X_1 + b_2X_2 + b_3X_1^2 + b_4X_2^2 + b_5X_1X_2 + b_6X_1^2X_2 + b_7X_1X_2^2 \text{-----(1)}$$

The model is similar to the one described in the section 5.3.3 of this thesis.

Where  $b_0$  is the intercept representing the arithmetic average of all quantitative outcomes of 9 runs;  $b_1$  to  $b_7$  are the coefficients calculated from the observed experimental values of Y; and  $X_1$  and  $X_2$  are the coded levels of the independent variables. The terms  $X_1X_2$  represents interaction term, while  $X_i^2$  ( $i = 1$  to  $2$ ) denotes quadratic terms. The main effects ( $X_1$  and  $X_2$ ) represent the average result of changing one factor at a time from its low to high value. The interaction terms ( $X_1X_2$ ) indicate changes in the response parameters when two factors are simultaneously changed. The polynomial terms ( $X_1^2$  and  $X_2^2$ ) are included to investigate nonlinearity. The polynomial equation as mentioned above was used to conclude the results based on the values of magnitude of coefficients and the mathematical sign (positive or

negative) it carries. A positive sign signifies a synergistic effect, whereas negative sign indicates antagonistic effect (Bolton S., 2004).

Statistical validity of the polynomials was determined on the basis of ANOVA provision in the Design Expert ®software and Microsoft Excel (I) (Gurgaon, India). Significance level was considered at  $P < 0.05$ . The best fitting mathematical model was selected based on the comparisons of several statistical parameters including the coefficient of variation (CV), the multiple correlation coefficient ( $R^2$ ), adjusted multiple correlation coefficient (Adj  $R^2$ ), and the predicted residual sum of squares (PRESS) provided by the software. Among them, PRESS indicates how well the model fits the data, and for the chosen model it should be small relative to the other models under consideration (Bolton S., 2004). Also, the 3-D response surface graphs and the 2-D contour plots were generated by the Statistica® software.

### 8.3.4 Lyophilization of nanoparticles

The final optimized batch of HCD-Rif NPs was lyophilized (VirTis Co. Inc., UK) using trehalose dehydrate (1 % w/w) as cryoprotectant. The concentration of the cryoprotectant was selected based on the earlier reports (Holzer et.al., 2009). Briefly, 1 % cryoprotectant was added in each batch of HCD-Rif NPs and lyophilized for 38 hrs under vacuum. After specified time, vacuum was released, samples were withdrawn, tightly sealed and kept in desiccator until use.

## 8.4 Characterization of HCD-Rif Nanoparticles

### 8.4.1 Mean particle size (MPS) and zeta potential (ZP)

Dynamic light scattering (DLS) and laser doppler velocimetry (LDV) was employed to measure particle size and zeta potential of the particles respectively using Zetasizer, Nanoseries Instrument (Nano 25, Malvern Instruments, Worcestershire, UK). The nanoparticles were re-dispersed in deionized water, sonicated (bath sonicator) for 5 min and the resultant samples were examined for particle size and zeta potential.

### 8.4.2 Rifampicin loading and encapsulation efficiency (EE)

The entrapment of Rif in NPs was evaluated by dissolving HCD-Rif NPs in methanol and analysed using UV-VIS spectrophotometer. Known amount of Rif loaded nanoparticles were suspended in methanol, allowed to stand for around 10-15 min and water was added in a sufficient amount to precipitate HCD. Suspension obtained was centrifuged (Bio Rad Centrifuge, UK) and the concentration of Rif in the supernatant was determined using UV-VIS spectrophotometer (Jenway UV/Vis Spectrophotometer, Staffordshire, UK) at 475 nm (Benetton et.al., 1998). Analysis was performed in triplicate for each batch of drug loaded NPs. The drug loading and entrapment efficiency was calculated using following formulae and presented as mean of each of the parameter:

$$\text{Yield (\%)} = \frac{\text{Weight of NP recovered}}{\text{Weight of Drug, polymer and excipient}} \times 100 \text{-----(2)}$$

$$\text{Drug Loading (\%)} = \frac{\text{Weight of Rif in NP}}{\text{Weight of NP recovered}} \times 100 \text{-----(3)}$$

$$\text{Entrapment Efficiency (\%)} = \frac{\text{Weight of Rif in NP}}{\text{Weight of Rif fed initially}} \times 100 \text{-----(4)}$$

#### 8.4.3 Morphology

Lyophilized nanoparticles were subjected to Scanning Electron Microscopy (SEM) and Transmission Electron Microscopy (TEM) to study their shape and surface morphology. The samples were mounted onto the SEM sample holder and subjected to gold coating in a vacuum chamber and images were recorded at the required magnification at the acceleration voltage of 10 kV using FEI XL30 TMP SEM (FEI XL30 TMP, Philips, Netherlands). In case of TEM, a drop of nanoparticle suspension was stained with phototungstic acid and placed on a coated carbon grid and vacuum dried. The grid was then examined immediately under TEM (Philips Electron Optics BV, Netherlands) and the electron micrographs were obtained.

#### 8.4.4 DSC and XRD studies

Crystallinity of the drug in freeze dried HCD-Rif NPs was examined by Differential Scanning Calorimetry (DSC) and X-Ray Diffractometry (XRD). Differential Scanning Calorimeter (DSC Q 2000, TA Instruments, USA) was used to determine thermal property of the freeze-dried nanoparticles and plain Rif. Correctly weighed samples (around 3-5 mg) of the stated materials were placed in hermetically sealed aluminum pans, whereas sealed empty aluminum pan was used as a reference. Heating runs for each sample was set from 10 °C to 300 °C at 10 °C min<sup>-1</sup> in a nitrogen atmosphere to get the heating scan (thermographs). X-ray powder diffractometry was carried out using an X-ray diffractometer (Oxford Diffraction Xcalibur novaT, UK) and diffractograms obtained were analyzed to understand physical state of the powder. The samples were mounted on a sample holder and X-RD patterns were recorded in the range of 5–50° at the speed of 5° per min.

#### 8.5 In-vitro aerosolization & lung deposition using Twin Stage Impinger (TSI)

HCD-Rif nanoparticle formulations were analyzed to study their aerosolization performance using TSI as shown in figure 8.1 (Copley Scientific Ltd., Nottingham, UK) as per the specifications given in British Pharmacopoeia (British Pharmacopoeia, 2012). In brief, HCD-Rif NPs sample of HCD-Rif NPs was prepared by dispersing it in deionized water. The upper and lower stages of the impinger corresponding to upper and lower respiratory tracts were filled with 7 and 30 mL of deionized water respectively. The nebulizer was operated until “dryness” (i.e. when aerosol generation completely ceased) and maximum output was achieved by gentle tapping of the nebulizer wall during the sputtering period towards the end of nebulization. Each stage of TSI was rinsed with small known quantity of methanol, samples were collected & required volume was methanol was added for the extraction of Rif and the volume of the stages 0, 1 and 2 was made upto 20, 20 and 25 ml respectively with deionized water. The samples were then taken from each stage (lower and upper stages) and amount of Rif deposited in the different stages of impinger was analyzed using UV-VIS spectrophotometer (Jenway UV/Vis Spectrophotometer, Staffordshire, UK). Experiment

was performed thrice and the aerodynamic behavior of the nanoparticles suspension was evaluated by calculating nebulization efficiency (NE) or aerosol output (total aerosolized mass of Rif detected in the nebulizer, throat, Stage 1 and Stage 2) (Desai et al., 2002) and respirable fraction (RF) (Matilainen et al., 2006) using equation 5 and 6. In addition, percent fine particle fraction (FPF) was also calculated as the ratio of fine particle dose (FPD - i.e. mass of Rif deposited in stage 2 to recovered dose (RD) (Liu et.al., 2008; Li et.al., 2010).

$$\text{Nebulization efficiency} = \frac{\text{Aerosolized Drug Mass}}{\text{Drug Mass Loaded in nebulizer}} \times 100 \quad \text{-----(5)}$$

$$\text{Respirable Fraction (\%)} = \frac{\text{Drug Mass Deposited in Stage 2}}{\text{Drug Mass Loaded in nebulizer}} \times 100 \quad \text{-----(6)}$$



**Figure 8.1: Assembly of Twin stage Impinger**

### 8.6 In-vitro release studies

Rifampicin loaded HCD nanoparticles were tested for their ability to release Rif from the HCD NPs. In-vitro release study was carried out in dark by dialysis method using modified release technique (Marques et. al., 2011). Simulated lung fluid (SLF - pH 7.4) with 200 µg/ml of ascorbic acid (as an antioxidant to prevent oxidative degradation of rifampicin) was used as dissolution media. A known amount of Rif loaded HCD NPs were dispersed in SLF and transferred to dialysis membrane of which one end was previously sealed with dialysis tubing clamp. After complete transfer of the formulation, another end of the dialysis membrane was sealed and placed in a beaker containing 25 ml of SLF as external release media under stirring at 37°C. At selected time intervals, suitable aliquots were withdrawn from the external medium, diluted as required and analyzed by HPLC (Agilent Technologies 1200 series) at 335 nm (Tatarczak et.al., 2006). Sink condition was maintained (after withdrawal of aliquot at each time points) by replenishing the same amount of blank media. The experiment was carried out in triplicate and results of the release study were plotted as percent cumulative drug release *vs* time with the ± standard deviation values.

### 8.6.1 HPLC analysis

The amount of Rif released from HCD-Rif NPs was analyzed by HPLC system (Agilent Technologies 1200 series) equipped with a UV detector to quantify the amount of rifampicin release. The injection volume was 10  $\mu$ l. Chromatography was performed with a column (Ascentis C18, 150 x 4.6mm, 5 $\mu$ m, Supelco, Sigma-Aldrich, USA). Mobile phase composed of tetrahydrofuran (THF)/phosphate buffer (30/70 %) at a flow rate of 1.0 ml/min and a detection wavelength of 335 nm (Tatarczak et. al., 2006). The column temperature was set to 40 °C. The retention time of rifampicin was 3.5 min. Calibration curves for rifampicin (correlation coefficient was 0.9993) at concentrations varying from 5 to 80  $\mu$ g/ml was used for analysis as described in the chapter 3.

### 8.7 Stability study

Lyophilized HCD-Rif nanoparticles were stored in desiccator for 2 months at room temperature (10-15 °C) to determine their stability. After two months period of storage, required quantity of samples (2 mg) were taken and rehydrated to determine particle size & percentage of Rif in the formulation (HCD-Rif nanoparticles) in order to assess storage stability.

### 8.8 Statistical analysis

The experiments were performed in triplicate and the data collected in this study was expressed as the mean value  $\pm$  standard deviation.

## 8.9 Results and Discussion

### 8.9.1 Preparation of nanoparticles and characterization

Chitosan nanoparticles have been prepared using many methods such as ionic gelation, complex coacervation, emulsion cross-linking, and spray drying (Grenha et.al., 2012). In addition, polymeric micelles (amphiphilic, self-assembly) prepared using modified chitosan derivatives have also been explored in the drug delivery (Haung et.al., 2010; Aranaz et.al., 2010; Li et.al., 2011; Hu et.al., 2013). However, till date no reports are available for the preparation of nanoparticles directly from hydrophobic chitosan derivatives (HCD) using multiple emulsion solvent evaporation technique. Hence, the current investigation was directed to assess the feasibility of HCD in the preparation of nanoparticles (NPs) and evaluate the potential of HCD to incorporate of drug (rifampicin) into NPs, considering its effectiveness to deliver right active in the treatment of TB via pulmonary route. DESE method was successfully utilized for the preparation of NPs from HCD. The method was found to be simple and efficient in order to prepare NPs. Initially blank HCD NPs were prepared during the course of optimization. Preliminary optimization helped to select certain parameters such as sonication time, solvent, surfactant and concentration of surfactant. Once the preliminary parameters were chosen, rifampicin loaded HCD NPs were prepared and optimized employing 3<sup>2</sup> factorial design. Following sections deals with the optimization of various parameters during the course of final formula optimization.

## 8.9.2 Optimization of Parameters by preparing blank HCD NPs

### 8.9.2.1 Sonication Time (ST)

Parameters selected for the preparation of blank HCD NPs were on the line of PLGA NPs (as described in the chapter 5). At the onset, sonication time, a critical factor in the preparation of NPs by multiple emulsion solvent evaporation method was optimized by varying ST to determine optimum value, based on the results of particle size and PDI evaluation. Sonication pulse was selected to be 15 based on the preliminary particle preparation studies. Sonication time was varied from 15, 30, 45 sec. to prepare HCD NPs for both primary and secondary emulsion preparation. Sonication time producing optimum average particle size & PDI was determined and presented in Table 8.6. It was found that increase in the time of sonication at both primary and secondary emulsion preparation showed decrease in the particle size. Initially, sonication time at primary emulsion was varied from 15 - 45 sec and secondary emulsion was kept constant at 45 sec. In all the three batches reasonable particle sizes and PDI were observed and therefore first batch, where sonication time of 15 sec was applied selected. Sonication time for secondary emulsion was also optimized by varying time between 15- 45 sec, with the 15 sec sonication at primary emulsion. Particles were found to aggregate where less sonication time of 15 sec was used at secondary emulsion and hence found unsuitable for the preparation of NPs. Sonication time of 15 and 30 sec. for primary emulsion and secondary emulsion preparation respectively yielded particle size of  $139 \pm 5.11$  and PDI of  $0.223 \pm 0.132$  without any aggregation. Hence, 15 and 30 seconds time of sonication was optimized for the further preparation of NPs.

**Table 8.6. Optimization of sonication time during primary and secondary emulsion**

Optimization of sonication time for primary emulsion					
Batch	Sonication time (Sec)		MPS (nm)	PDI	Remark
	Primary emulsion	Secondary emulsion			
1ST	15	45	$132.53 \pm 25.31$	$0.251 \pm 0.028$	G
2ST	30	45	$127.92 \pm 41.99$	$0.265 \pm 0.083$	G
3ST	45	45	$122.13 \pm 64.65$	$0.293 \pm 0.075$	G
Optimization of sonication time for secondary emulsion					
1ST	15	15	$239.57 \pm 33.01$	$0.56 \pm 0.312$	AG
2ST	15	30	$139 \pm 5.11$	$0.223 \pm 0.132$	G
3ST	15	45	$129.2 \pm 7.23$	$0.272 \pm 0.084$	G

n = 3;  $\pm$  Standard Deviation; G – Good; AG – Aggregate

### 8.9.2.2 Selection of solvent, surfactant and surfactant concentration

By maintaining certain parameters constant and varying solvent, surfactant & surfactant concentration, HCD NPs were prepared by applying  $2^3$  factorial design of experiment (Table 8.1 & 7.2). Constant parameters included polymer concentration (50 mg); organic Phase (3.5 ml); internal aqueous phase (0.5 ml); external aqueous phase (10 ml) and sonication pulse (15) and sonication time (15 & 30 sec.), whereas solvent (DCM & EtoAc), Surfactant (PVP & Pluronic F 127) and surfactant concentration (0.5 & 1 %) were variable factors.

### 8.9.2.2.1 Selection of solvent

Double emulsion solvent evaporation method is usually executed by preparing emulsions of polymer solutions in volatile solvents. DCM, ethyl acetate and chloroform are widely used solvents for the preparation of NPs using DESE method. Based on the previous results in our lab, we excluded chloroform due to production of large aggregates. Therefore, we chose to optimize best solvent between DCM and EtoAc.

While comparing DCM and EtoAc, we observed that EtoAc produced smaller particles than that of DCM. However, no significant difference was noted between the particle sizes and hence both the solvents were considered suitable for the preparation of nanosized particles using HCD polymer. With the exception of DCM in combination with PF127 (Batch 1 and 3), all other combination of variables were able to produce particle sizes in the range of 100-150 nm. Thus, ability of EtoAc to yield smaller particles sizes and its better toxicological profile (than DCM and chloroform) suggested benefits of EtoAc in the preparation of NPs. However, certain drawbacks associated with the ethyl acetate including its high boiling point (77.1°C) and high water solubility (8.7%) leads to longer contact time of NPs with ethyl acetate, thereby increased degradation and secondarily, longer duration of contact of NPs with the external aqueous phase induces diffusion of drug molecule from the NPs into external aqueous phase leading to reduced entrapment efficiency (Meng et. al., 2003; Mainardes et.al., 2005). These drawbacks compels the exclusion of EtoAc for the preparation of NPs. As observed from the studies carried out using extensively used and FDA approved polymer PLGA (Bilati et.al., 2009). Bilati et.al., observed that the replacement of ethyl acetate (approximately 80%) by DCM (nearly 100 %) systematically promoted protein entrapment. Therefore, DCM was chosen over EtoAc as optimized solvent for the preparation of further batches of HCD NPs. The selection of DCM is also backed with the favorable physical properties of DCM as reported in the literature, such as low boiling point (40.1°C) and less water solubility (1.60%) required for the easy removal of organic solvent while evaporation and helps to solubilize large amount of polymer respectively (Meng et. al., 2003).

### 8.9.2.2.2 Selection of surfactant and surfactant concentration

Batches were prepared by varying surfactant and their concentration. After preparation of batches, mean particle size (MPS) and PDI were determined and tabulated in Table 8.7. Results of the optimization parameters indicated that, particle size was dependent on the surfactant and its concentration. Results showed MPS ranging from 100-700 nm. Increase in the concentration of surfactant demonstrated decreased particle size. This trend was observed in all the batches prepared (B1-B8) and results are corresponding to the reports published by Cohen-Sela et. al., (Cohen-Sela et. al., 2009). Among all the batches, batch B1 & B3 yielded higher particle size of  $708.97 \pm 94.10$  &  $631.33 \pm 206.17$  nm respectively with higher PDI values ( $0.751 \pm 0.16$  &  $0.629 \pm 0.052$ ). Batch B2 & B4 showed particle size of  $236.53 \pm 4.47$  &  $208.63 \pm 2.04$  nm with smaller PDI values, whereas all other batches exhibited particles size below 200 nm. It was ascertained that batches B1 and B3 prepared using DCM as solvent and Pluronic F127 as surfactant rendered higher MPS as compared to other

batches of NPs. In addition, these batches also showed aggregation. Therefore, batch B1 and B3 considered unsuitable for the preparation of NPs.

As stated above, MPS of the NPs been found to be a function of surfactant concentration in the external aqueous phase. Increase in the concentration of surfactant from 0.5 to 1 % w/v resulted in variable decrease in the MPS. Highest difference in the particle size of around 100 nm was noted between the batch B1 and B3 ( $708.97 \pm 94.10$  to  $631.33 \pm 206.17$  nm), when surfactant (pluronic F127) concentration was increased from 0.5 to 1 % w/v and NPs were prepared using DCM as solvent. On the other hand, when pluronic F127 was replaced with the same concentration of PVA, small MPS of  $139.3 \pm 5.112$  and  $125.47 \pm 3.53$  nm was observed from batches B5 and B7 respectively.

**Table 8.7: Results of optimization parameters (solvent, surfactant & surfactant concentration)**

Batch Code	Solvent	Surfactant Conc. (%w/v)	Surfactant	MPS (nm)	PDI	ZP (mV)	Remark
B1	DCM	0.5	PF127	$708.97 \pm 94.10$	$0.751 \pm 0.16$	$14.633 \pm 1.097$	AG
B2	EtoAc	0.5	PF127	$236.53 \pm 4.47$	$0.149 \pm 0.004$	$7.327 \pm 0.476$	G
B3	DCM	1	PF127	$631.33 \pm 206.16$	$0.629 \pm 0.052$	$16.63 \pm 0.404$	AG
B4	EtoAc	1	PF127	$208.63 \pm 2.04$	$0.054 \pm 0.031$	$9.167 \pm 1.254$	G
B5	DCM	0.5	PVA	$139.3 \pm 5.112$	$0.228 \pm 0.13$	$12.83 \pm 0.473$	G
B6	EtoAc	0.5	PVA	$134.3 \pm 1.36$	$0.159 \pm 0.092$	$13 \pm 0.3$	G
B7	DCM	1	PVA	$125.47 \pm 3.53$	$0.221 \pm 0.128$	$6.203 \pm 0.270$	G
B8	EtoAc	1	PVA	$133.2 \pm 0.99$	$0.122 \pm 0.009$	$10.83 \pm 0.603$	G

G - Good; AG - Aggregate; DCM – Dichloromethane; EtoAc – Ethyl Acetate; PF127 – Pluronic F 127; PVA – Polyvinylalcohol. n = 3;  $\pm$  Standard Deviation

Similar trend of decreasing particle size with increase in surfactant concentration was observed in all the batches prepared and in all the combinations of solvent and surfactants (DCM, EtoAc and PF 127, PVP). Previous studies also reported decrease in the particle size with increase in the surfactant concentration (Sahoo et.al., 2002; Zambaux et.al., 1998). Reduction in the particle size may be attributed to increased concentration of surfactant leading to more stable and uniform sized particles with low polydispersity index. However, higher surfactant concentration is not suggested due to its ability to hinder in-vivo degradation of NPs and carcinogenicity. Therefore, nanoparticles prepared with lower level of surfactant concentration are always preferred over higher concentration. The data obtained in this study suggested that the lower concentration of PVP and PF 127 (0.5% w/v) yielded smaller MPS from HCD NP formulations, which is in compliance with the earlier reports (Ranjan et. al., 2012). Hence, 0.5 % w/v of surfactant concentration was selected for the preparation of NPs. It is well known that, particle size is inversely proportional to the concentration of surfactant. At low surfactant concentration, surfactants evoke particle aggregation due to the reduced particle energy causing less coating of the particles by surfactant leading to low total surface area, whereas higher or critical concentration of

surfactant coats entire particle and hence system consists of small and stabilised particles (Prozorov et.al., 1999). This phenomenon can be expected due to stabilising function of surfactant and it is assumed that insufficient amount of surfactant fails to stabilise entire volume of NPs resulting in agglomerates of larger size (Mainardes & Evangelista, 2005). Accordingly, results obtained in this experiment showed that 0.5% w/v of surfactant PVP in batch B5 lead to smaller particle size ( $139.3 \pm 5.112$  nm) in comparison to the batch B1 prepared using 0.5% w/v PF 127 ( $708.97 \pm 94.10$  nm), suggesting that PF 127 may not have been able to coat all the particles leading to agglomeration in the view of less concentration of PF 127. Hence, PVP at the concentration of 0.5 % w/v which produced smaller particle size was chosen as optimized surfactant for the preparation of HCD NPs. Results of these studies are tabulated in Table 8.7 detailing factors at three levels and their responses in terms of MPS, PDI and ZP.

### 8.9.3 Optimization of formulation by Factorial design

Based on the preliminary formulation optimization studies, various process parameters required for preparation of HCD NPs were selected, which helped to avoid the complexity of experimental design. Thus, optimized parameters such as organic Phase (DCM - 3.5 ml); internal aqueous phase (0.5 ml); external aqueous phase (10 ml, 0.5% PVA); sonication pulse (15 W) and sonication time of 15 & 30 sec. for primary and secondary emulsion respectively were kept constant in factorial design studies. Influence of parameters such as concentration of HCD ( $X_1$ ) and Rifampicin ( $X_2$ ) was optimized by applying on  $3^2$  factorial design of experiment consisting of nine formulation batches with random variation of Rif and HCD at three levels. Table 8.7 enlists the combination of independent variables and observed responses in terms of mean particle size and entrapment efficiency for all the nine formulations.

#### 8.9.3.1 Effect of formulation variables on the response parameters

Nine formulations of HCD-Rif nanoparticles were prepared according to  $3^2$  factorial design and correlation between independent factors and their response parameters in terms of MPS and EE was statistically analyzed using ANOVA (Microsoft Excel Corp, India) and Statistica Stat soft Inc (Tulsa, USA) by generating various polynomial equations, response surface and contour plots. The data analyzed from the software's is discussed herein, depicting the effects of variables on the respective response parameters (Y1 and Y2).

**Table 8.8.** Response parameters for NPs prepared as per 3<sup>2</sup> factorial design.

Batch	HCD (mg)	Rif (mg)	Response (Y1) MPS (nm)	PDI	Response (Y2) EE (%)
C1	50	5	242.8±44.36	0.300±0.084	36.83±9.35
C2	50	10	214.4±26.58	0.292±0.036	28.77±0.44
<b>C3</b>	<b>50</b>	<b>15</b>	<b>253.43±19.06</b>	<b>0.323±0.059</b>	<b>64.86±7.73</b>
C4	75	5	242.37±55.54	0.536±0.272	27.87±4.46
C5	75	10	208.17±26.81	0.426±0.137	25.4±3.77
C6	75	15	276.8±58.58	0.327±0.107	58.33±7.27
C7	100	5	267.2±24.98	0.482±0.025	38.62±4.062
C8	100	10	269.2±107.55	0.447±0.035	27.21±0.94
C9	100	15	323.57±65.80	0.413±0.188	56.72±2.037

n = 3; ± Standard Deviation. Rif – Rifampicin; MPS – Mean Particle size; PDI – Polydispersity index; EE – Entrapment Efficiency;

Results of response variables obtained from design of experiment (DoE) were fitted in simple linear equation, interactive equation or quadratic model equation (Eq. 7, 8 & 9 respectively) using multiple regression analysis and F-statistic to find out statistically significant terms.

$$Y = b_0 + b_1X_1 + b_2X_2 \tag{7}$$

$$Y = b_0 + b_1X_1 + b_2X_2 + b_{12}X_1X_2 \tag{8}$$

$$Y = b_0 + b_1X_1 + b_2X_2 + b_{11}X_{11} + b_{22}X_{22} + b_{12}X_1X_2 \tag{9}$$

Multiple regressions analysis revealed significant influence of factors X<sub>1</sub>, X<sub>2</sub> on the response parameter MPS, whereas % EE was found to be significantly influenced (*p* < 0.05) by the factors X<sub>2</sub>, & X<sub>22</sub>. The multiple regression analysis suggested quadratic model as shown in equation 10 and 11 for both MPS and EE respectively. The observed and predicted values of MPS and EE for all the batches of HCD-Rif NPs are tabulated in Table 8.10 and 8.11 respectively along with their percent relative error (%RE) values as calculated using equation 12 given below.

$$Y1 = 217.71 + 24.89 X_1 + 16.91 X_2 + 19.32 X_{11} + 37.11 X_{22} + 11.44 X_1X_2 \text{ -----(10)}$$

$$Y2 = 23.81 - 1.32 X_1 + 12.76 X_2 + 4.97 X_{11} + 20.08 X_{22} - 2.48 X_1X_2 \text{ -----(11)}$$

$$\% \text{ Relative Error (RE)} = \frac{\text{Observed FS} - \text{Predicted FS}}{\text{Predicted FS}} \times 100 \text{ -----(12)}$$

**Table 8.9.** Other evaluation parameters for NPs prepared as per 3<sup>2</sup> factorial design.

Batch	ZP (mV)	Yield (%)	DL (%)
C1	18.83±8.44	60.79±1.43	2.88±0.66
C2	20.57±8.17	59.88±1.93	4.37±0.18
<b>C3</b>	<b>23.33±2.83</b>	<b>62.49±3.63</b>	<b>13.51±0.81</b>
C4	28.8±3.13	65.31±4.73	1.64±0.16
C5	29.03±13.27	64.84±4.55	2.89±0.26
C6	25±3.035	65.24±4.24	9.58±1.03
C7	35.9±2.066	69.29±2.40	1.79±0.13
C8	31.67±1.793	68.10±1.71	2.49±0.03
C9	27.3±6.49	68.55±2.46	7.52±0.02

n = 3; ± Standard Deviation. DL – Drug loading; ZP – Zeta Potential.

**Table 8.10.** Observed and Predicted values of response parameter – MPS (Y1)

Batch	Predicted Y1	Observed Y1	Residual	%RE
C1	243.78	242.8±44.36	-0.975	-0.399
C2	212.14	214.4±26.58	2.26	1.065
C3	254.72	253.43±19.06	-1.285	-0.504
C4	237.91	242.37±55.54	4.46	1.875
C5	217.71	208.17±26.81	-9.54	-4.382
C6	271.72	276.8±58.58	5.08	1.869
C7	270.69	267.2±24.98	-3.485	-1.288
C8	261.92	269.2±107.55	7.28	2.779
C9	327.37	323.57±65.80	-3.795	-1.159

**Table 8.11.** Observed and Predicted values of response parameter - EE (Y2)

Batch	Predicted Y2	Observed Y2	Residuals	%RE
C1	34.93	36.83±9.35	1.89	5.43
C2	30.09	28.77±0.44	-1.33	-4.41
C3	65.43	64.86±7.73	-0.57	-0.87
C4	31.13	27.87±4.46	-3.26	-10.46
C5	23.81	25.4±3.77	1.58	6.65
C6	56.66	58.33±7.27	1.67	2.95
C7	37.26	38.62±4.062	1.36	3.65
C8	27.46	27.21±0.94	-0.26	-0.93
C9	57.83	56.72±2.037	-1.10	-1.91

Regression output and full model responses for dependent variables viz. MPS and EE of formulation HCD-Rif NPs are displayed in Table 8.12. The MPS & EE observed after random combinations of three levels of two independent variables (X1 and X2) were

subjected to multiple regression analysis & the full model second order polynomial equation was obtained, which revealed significance ( $p < 0.05$ ) of the full model second order polynomial equation for MPS & EE. In a multiple regression analysis, if the values of “probability  $> F$ ” are less than 0.05, indicates model terms are significant. In our experiment, analysis of full model polynomial equation showed that “probability  $< F$ ” (0.012), which is less than 0.05 and hence model terms are significant (equation 10 & 11).

The F values for MPS & EE obtained by full model were found to be 25.33 & 45.33 respectively, while corresponding calculated F values ( $F_{cal}$ ) were 0.34 and 0.11 ( $p > 0.05$ ) respectively indicated significance ( $p > 0.05$ ). In addition, the goodness of fit of the model was checked by the correlation coefficient ( $R^2$ ). The correlation coefficient ( $R^2$ ) values of MPS (0.9967) and EE (0.9869) showed the total variability in the model. The value of adjusted correlation coefficient (adj  $R^2$ ) for MPS was found to be 0.9383, whereas 0.9652 for EE as obtained from the full model regression analysis. The predicted  $R^2$  values of MPS and EE were found to be in the reasonable agreement with the adj  $R^2$  values, suggesting high significance of the model ( $R^2$  value nearing to 1), which is corresponding to an excellent correlation between the independent variables. Thus, closeness of  $R^2$  values to 1 for both MPS and EE indicated accuracy of the model. Moreover, values of “probability  $> F$ ” were found to be very less than 0.05, implying that the models terms viz. concentration of HCD and Rif are highly significant ( $p$  value  $< 0.05$ ). Thus, all of the above considerations indicate that the model can effectively explain 99% variation around the mean value.

It was observed that, the MPS values were ranging from  $208.17 \pm 26.81$  to  $323.57 \pm 65.80$  nm and entrapment efficiency (EE) of Rif in HCD NPs was falling between  $25.4 \pm 3.77$  to  $64.86 \pm 7.73$  %. A considerably high entrapment of rifampicin ( $64.86 \pm 7.73$  %) in HCD NPs was achieved at low levels (-1) of X1 (50mg) and high level of X2 (15 mg) from the batch F3. Equations 10 & 11 displays the quantitative effect of formulation components (independent variables X1 and X2) on response parameters (Y1 & Y2), in the form of corresponding polynomial equations and regression coefficients for Mean particle size (MPS – Y1) and Mean % entrapment efficiency (EE - Y2).

Each coefficient in the equation (10) and (11) was evaluated and the significance was determined on the basis of the  $p$  values as tabulated in Table 8.12. Smaller the  $p$  value, the more significant is the corresponding coefficient. The data obtained from full model of MPS confirms that the main effects of the independent variables ( $X_1$ ,  $X_2$  &  $X_{22}$ ) were significant factors for prediction of MPS as their  $p$  values fall well below 0.05 ( $p < 0.05$ ), while the interaction term  $X_1X_2$  has little predictive effect as their  $p$  values were above 0.05 ( $p > 0.05$ ) and hence excluded from the model. From the results of EE,  $p$  values below 0.05 ( $p < 0.05$ ) were noted for the independent variables  $X_2$ ,  $X_{22}$  suggesting their significant effect. Remaining factors such as  $X_{22}$  and the interaction term  $X_1X_2$  had  $p$  values ( $p > 0.05$ ) and therefore they were considered less important in the given model.

The coefficients of the two independent variables in quadratic Eq. (10) were compared and the coefficient value for  $X_1$  ( $b_1 = 24.89$ ) was found to be maximum suggesting it to be the major contributing factor which affects the MPS of HCD-Rif NPs. On the other hand, quadratic Eq. (11) showed maximum coefficient values for independent variable  $X_2$  ( $b_1 = 12.76$ ) & hence it was the major factor affecting EE. In both the cases, positive values of  $X_1$  &  $X_2$  are an indication of synergistic effect of HCD & Rif concentration on MPS & EE. Significance of quadratic model terms  $X_1$  &  $X_2$  in equation 10 (MPS), whereas significance of quadratic terms  $X_2$  and  $X_{22}$  in equation 11 suggested nonlinearity in the ability of independent variables ( $X_1$  and  $X_2$ ) to influence MPS and EE respectively. The combined effect of factors  $X_1$  and  $X_2$  can be further elucidated with the help of response surface curve, contour plots as shown in fig. 2(a,b) and 3(a,b) respectively, demonstrating variation in  $Y_1$  and  $Y_2$  as mentioned above and act as a function of HCD and Rif concentration.

**Table 8.12:** Response of full model of HCD-Rif NPs

	MPS		EE	
	Coefficients	<i>p</i> -value	Coefficients	<i>p</i> -value
X1	24.89	0.0059*	-1.317	0.343
X2	16.905	0.0173*	12.76	0.002*
X11	19.32	0.0508	4.969	0.092
X22	37.105	0.0089*	20.08	0.002*
X1X2	11.435	0.0772	-2.482	0.1823
Intercept	217.71	5.69E-05 <sup>#</sup>	23.81	0.0016 <sup>#</sup>

\* Statistically significant ( $p < 0.05$ ). <sup>#</sup> Significance of F value.

The Predicted Residual Sum of Squares (PRESS) is also known as sum of squared residuals (SSR) or the sum of squared errors of prediction (SSE). PRESS value indicates how well the model fits the data, and it is recommended that, for the chosen model the value of PRESS should be relatively small as compared to the other models under consideration (Shah et.al., 2008). The polynomial model which shows lower PRESS value determines the fitness of data and hence such model is selected. In the given experiment, PRESS value was calculated for the full and reduced polynomial model for both the independent variables ( $Y_1$  &  $Y_2$ ). Results indicated the suitability of full polynomial model as compared to reduced one, owing to its smaller PRESS values for both  $Y_1$  (223.96) and  $Y_2$  (24.73), whereas reduced model showed higher PRESS values for  $Y_1$  (1493.53) and  $Y_2$  (109.17).

Figure 8.2(a, b) and 8.3 (a, b) represents contour plots and 3D response surface plot for both the response parameters MPS and EE respectively, depicting the effects of independent variables  $X_1$  and  $X_2$  on dependent variables  $Y_1$  and  $Y_2$ . No significant difference in the MPS and EE was noted, when the value of  $X_1$  was varied from low (-1) to high (+1) level and keeping  $X_2$  constant at low level (-1). In the similar set up of experiment, when the value of  $X_2$  was increased from low level (-1) to medium level (0), slight decrease in the particle size was noted which also led to corresponding decrease in the % EE. Further increase in the concentration of  $X_2$  substantially increased EE, while small extent in the increase of MPS

was observed. Comparing MPS, it was observed that small MPS in the range of  $208.17 \pm 26.81$  to  $323.57 \pm 65.80$  nm were obtained from all the batches (C1 to C9), amongst smallest value of  $208.17 \pm 26.81$  nm was obtained at medium level of  $X_1$  &  $X_2$  from batch C5. Same batch demonstrated smallest EE ( $25.4 \pm 3.77$ ). In a different combination, where values of  $X_2$  were increased from low (-1) to high (+1) level and  $X_1$  kept constant at low level (-1), results showed slight decrease ( $214.4 \pm 26.58$  nm) in value of MPS initially at medium level of  $X_1$  (0), which further increased ( $253.43 \pm 19.06$  nm) at high level (+1) of  $X_1$ . Entrapment efficiency also showed similar trend ( $28.77 \pm 0.44$  ( $X_1 - 0$ ) &  $64.86 \pm 7.73$  ( $X_1 - +1$ ) %) with increased concentration of Rif. Such non-linearity in the influence of  $X_1$  &  $X_2$  on the MPS & EE was observed in all the batches. Among all the batches tested, optimum MPS with maximum EE was obtained from the batch C3 formulated with the combination of low level of  $X_1$  (50 mg) and high (+1) level of  $X_2$  (15 mg). The results can be observed from the contour plots, 3D response surface plot as displayed in figure 8.2(a, b) & 3 (a, b). The predicted and observed values of response parameter (MPS) are shown in Table 8.10, whereas data of predicted and observed values for EE is tabulated in Table 8.11. Low percent relative error values (below 10 %) and small residuals were demonstrated by full polynomial model of MPS and EE (Table 8.10 & 8.11), confirming the reasonable agreement between predicted and experimental values and indicated suitability of the model. ANOVA full model results of MPS and EE are given in Table 8.13 and 8.14 respectively.

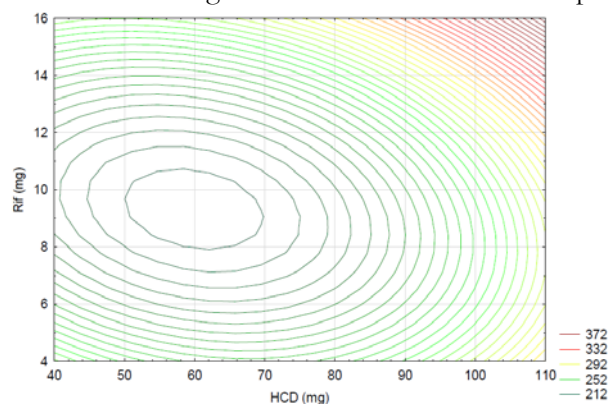


Figure 8.2(a): Contour plot showing the effect of independent factors on MPS

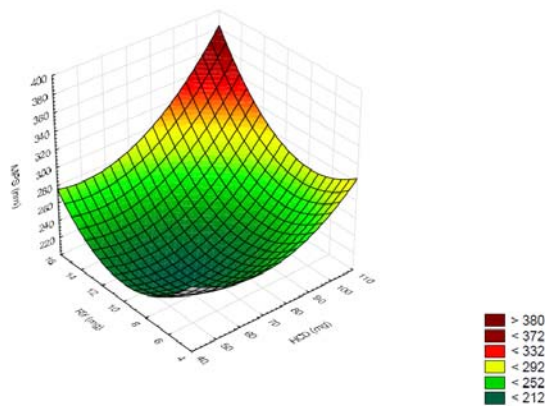


Figure 8.2(b): Response surface plot showing the effect of independent factors on MPS

**Table 8.13.** Analysis of variance (ANOVA) of MPS for full models of HCD-Rif NPs

	df	SS	MS	F	R <sup>2</sup>	Adj R <sup>2</sup>
Regression	5	9454.8705	1890.9741	25.32953765	0.9769	0.9383
Residual	3	223.9647	74.6549	--	--	--
Total	8	9678.8352	--	--	--	--

*df* degrees of freedom, *SS* sum of squares, *MS* mean of squares, *F* Fischer's ratio, *R*<sup>2</sup> regression coefficient; MPS – Mean Particle Size.

**Table 8.14.** Analysis of variance (ANOVA) of EE for full models of HCD-Rif NPs

	df	SS	MS	F	R <sup>2</sup>	Adj R <sup>2</sup>
Regression	5	1868.546735	373.7093469	45.33110211	0.9869	0.9652
Residual	3	24.73198287	8.243994289	--	--	--
Total	8	1893.278717	--	--	--	--

*df* degrees of freedom, *SS* sum of squares, *MS* mean of squares, *F* Fischer's ratio, *R*<sup>2</sup> regression coefficient ; EE – Entrapment efficiency

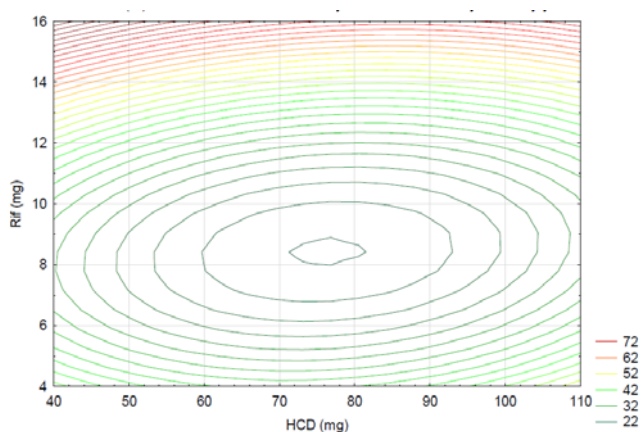


**Figure 8.3(a):** Contour plot showing the effect of independent factors on EE

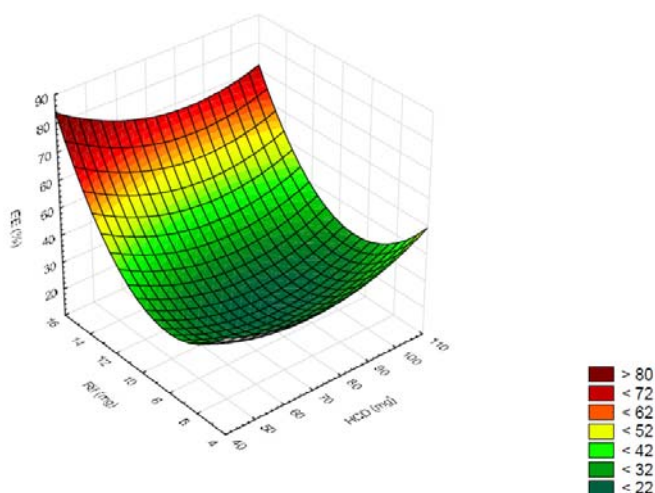


**Figure 8.3(b):** Contour plot showing the effect of independent factors on EE

**8.9.3.2 Effect of polymer concentration and theoretical drug loading on MPS, EE & ZP**

As stated in the earlier paragraph under section 7.3.9.1, a non-linear influence of theoretical drug loading (DL) on MPS was observed. At low theoretical DL (5 mg), MPS of  $242.8 \pm 44.36$  nm was obtained. Increase in the theoretical DL to double (10 mg) showed negative influence on MPS with the small MPS ( $214.4 \pm 26.58$  nm). Further increase in theoretical DL (15 mg) increased MPS to  $253.43 \pm 19.06$  nm. Similar results were obtained even when the concentration of polymer was increased from 50 to 75 and 100 mg. Such a non-linear relation between the theoretical DL and polymer concentration was also observed by Doan et. al., (Doan et.al., 2011). Although MPS from all the batches were obtained in the range of  $208.17 \pm 26.81$  to  $323.57 \pm 65.80$  nm, large MPS was observed when the concentration of polymer and drug was increased. Formulation C1-C3 consisting of lowest concentration of HCD (50 mg) and varying amount of Rif (5-15 mg) showed lowest values of PDI ( $0.292 \pm 0.036$  to  $0.323 \pm 0.059$ ), whereas increased concentration of HCD to 75 and 100 mg led to increase in the PDI values suggesting varying particle distribution ( $PDI > 0.4$ ). Slight increase in the MPS ( $276.8 \pm 58.58$  nm &  $323.57 \pm 65.80$  with PDI of  $0.427 \pm 0.107$  &  $0.413 \pm 0.188$ ) with increased amount of HCD (75 & 100 mg) may be due to increase in the viscosity of organic phase to a smaller extent, which might have caused hindrance in the efficiency of sonication. Reports also suggested possible collision and merger of nanoparticles leading to large MPS, when higher polymer concentration was used for the preparation of NPs (Li et. al., 1999; Benoit et al. 1999; Murakami et.al., 1999). Based on the results of this study, batch C3 composed of 50 mg of polymer and 15 mg of Rif exhibited optimum particle size with uniform size distribution as compared to other batches prepared with other combinations of HCD:Rif concentration.

Factorial design of experiment yielded formulation batches with the variable entrapment efficiencies of Rif in HCD. At low level of polymer concentration (50 mg), highest entrapment efficiency of  $64.86 \pm 7.73\%$  was obtained, when the theoretical DL was kept at higher level of 15 mg (batch C3). Similar pattern of results in terms of increased EE was observed when the amount of HCD was increased to 75 and 100 mg in batch C6 and C9 with the corresponding EE of  $58.33 \pm 7.27$  &  $56.72 \pm 2.037$  % respectively. Use of highest HCD concentration (100 mg) for the preparation of NPs led to slight decrease in the EE, which may be due to enhanced viscosity of the system contributing to hampered sonication and stirring. (Kirby et. al., 2008). Considerably low EE of  $36.83 \pm 9.35$  &  $28.77 \pm 0.44$  was noted at low theoretical DL of 5 and 10 mg respectively. Same trend was noted in all the batches studied. Thus, a non-linearity in the EE was observed on varying theoretical DL from 5 to 15 mg. Similar results are also reported, where decreased EE with increase in theoretical DL was observed (Bilati et.al., 2009; Alex and Bodmeier 1990; Conway and Alpar 1996; Yang et al. 2001). In addition, literature contrasting the results are also published, which revealed that increased theoretical DL is associated with increased EE and size (Doan et. al., 2011; Bilati et.al., 2009; Atkins and Peacock 1996; Jeffery et al. 1993). PDI is an important factor determining variability in the particle size in a sample of particles. Smaller PDI values close to 0 are always preferred as it suggests narrow range of size distribution

(Ranjan et al. 2012). Results of this study demonstrated higher PDI values (>0.4) of the batches prepared using higher amount of HCD (Table 8.7).

In addition, positive zeta potential conferred by the polymers is always preferred in the delivery of small and macromolecules due to advantages such as ease in surface assimilation of genetic materials such pDNA, RNA etc., drugs and even proteins, their ability to interact with cells thereby providing high transfection efficiency (Lubben et.al., 2001). Moreover, cationic polymers have also been explored for the purification of water (Harleman et.al., 1996). The current investigation was directed to modify chitosan into its hydrophobic derivative while keeping it charge intact. It was observed that all the batches from C1 to C9 showed positive ZP ranging from 18.83±8.44 to 35.9±2.066 mV. Although no correlation between charge on the particles and amount of drug was seen, increment in the polymer concentration showcased positive influence on the charge. This enhancement in the ZP can be rated as C1<C4<C7 (18.83±8.44 < 28.8±3.13 < 35.9±2.066 mV) and C2<C5<C8 & C3<C6<C9 (Table 8.7) with respect to increase in polymer concentration. Increased ZP value of the rifampicin loaded HCD NPs, as compared to their blank counterparts were observed. This increased ZP could be attributed to the particle associated rifampicin (adsorbed), which might have influenced surface charge owing to the presence of amino groups in the rifampicin molecule (Manca et. al., 2008).

**8.9.3.3 Optimization of Responses Using Desirability Function (www.itl.nist.gov)**

The difficulty of multiple and sometimes opposing responses is usually overcome by the optimization technique involving desirability function. Each response is associated with its own partial desirability function. The value of 1 for the desirability function is always preferred as it is considered optimum, while value zero completely outcast the result and is treated unacceptable. The desirability for each response can be calculated at a given response point in the experimental design. When the goal is to minimize the given response following formula can be used to calculate individual desirability.

$$d_i(Y_i) = \frac{Y_i(mps) - U_i}{T_i - U_i} \text{-----13}$$

Where  $d_i$  is individual desirability,  $Y_i$  (mps) is experimental results of response MPS.  $U_i$  and  $T_i$  stands for maximum and target MPS. Similarly, if one want to maximize the stated response, equation 14 can be availed to calculate individual desirability.

$$d_i(Y_i) = \frac{Y_i(ee) - L_i}{T_i - L_i} \text{-----14}$$

Where  $d_i$  is individual desirability,  $Y_i$  (e) is experimental results of response MPS.  $T_i$  and  $L_i$  stands for minimum and target EE respectively. Once we get this, we can calculate combined desirability (D) using equation 15, which involves multiplication of individual desirability.

$$D = \{(d_1(Y_1) \times d_2(Y_2) \times \dots \times d_n(Y_n))\}^{1/k} \text{-----15}$$

Where, k denotes total number of responses.

Optimum parameters for the formulation were generated utilizing a numerical optimization technique by the desirability approach. Response parameters such as Y1 and Y2 were optimized and the optimized formula was finalized by keeping the mean particle diameter in range of 200 to 300 nm and EE between 50 and 70%. Batch C3 (containing low (-1) level of variable X<sub>1</sub> and high level of variable X<sub>2</sub>) resulted in the optimum formula. Individual desirability for MPS and EE was calculated which found to be 1, indicating acceptability of the model for the optimization of formula. Similarly, overall desirability for the current model was also found to be 1, indicating suitability of the model for optimization purpose. Moreover, the result of the experimental and predicted values for MPS and EE confirmed the practicability and validity of the model. Relative errors for both MPS and EE were found to be below 10 % indicating that the Response Surface Methodology (RSM) optimization technique was appropriate for optimization for the preparation of NPs from novel polymer and incorporation of Rif in HCD NPs.

#### 8.9.3.4 Optimized Formulation

The rigorous optimization process yielded optimum values of the independent variable to build a final formula. Formulation was prepared according to the optimized formula as shown in Table 8.15.

**Table 8.15.** Optimized formula for HCD-Rif NPs

Parameters	Value
HCD (mg)	50 mg
Vol. of organic Phase (ml)	3.5 ml
Rifampicin concentration (mg)	15
Vol. of internal aqueous Phase (ml)	0.5
Surfactant in external aqueous phase	PVA
Concentration of surfactant in external aqueous phase (% w/v)	0.5
Vol. of external aqueous Phase (ml)	10

**Table 8.16.** The predicted and observed response variables of the optimized HCD-Rif NPs

	Y1 (nm)	Y2 (%)
<b>Predicted</b>	254.72	65.43
<b>Observed</b>	253.43±19.06	64.86±7.73
<b>% RE</b>	0.504	0.87
<b>Residuals</b>	-1.285	-0.57
<b>ZP Observed</b>	23.33±2.83	

Lyophilization of HCD-Rif NPs was done in the presence of trehalose as cryoprotective agent in the concentration 1% as reported elsewhere. Almost comparable results were achieved in the samples before (BL) and after lyophilization (AL). The presence of 1% trehalose during lyophilization did not show substantial influence on the MPS. HCD-Rif NPs showed MPS of 231.9± 20.37 nm BL, which was increased to 253.43±19.06 nm AL,

indicating the suitability of the trehalose as cyoprotectant during lyophilization in the concentration used. Results are presented in Table 8.16.

## 8.10 Particle Characterization

### 8.10.1 Particle Size

HCD-Rif NPs prepared as per the the optimized final formula were centrifuged, washed to remove any untrapped materials (Rif and PVA) and particle size, PDI & ZP was determined prior to freeze drying (FD), which exhibited mean particle size of  $231.9 \pm 20.37$  nm with the polydispersity index values of  $0.384 \pm 0.022$  as evidenced from the distribution curve presented in figure 8.4a. These particles diaplyed ZP of  $28.2 \pm 1.67$  mV. After freeze drying (with the aid of trehalose as cryoprotectant in the concentration of 1 % w/v) MPS and PDI of  $253.43 \pm 19.06$  nm and  $0.323 \pm 0.059$  respectively were noted (Table 8.16), suggesting slight increment in the MPS (Figure 8.4b), whereas almost similar ZP was observed.

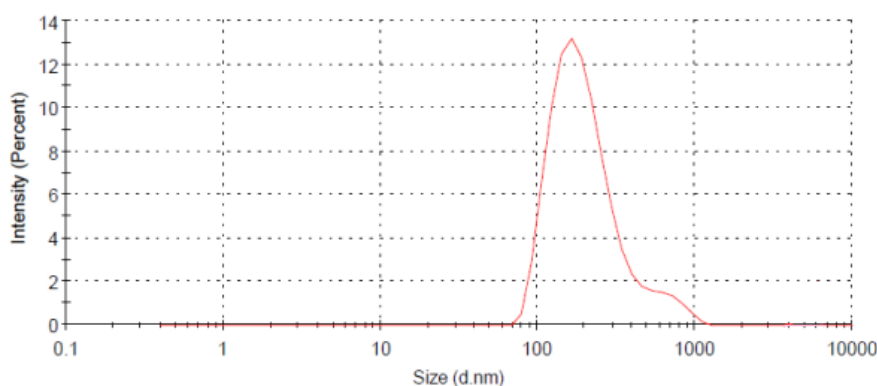


**Figure 8.4a:** Particle size distribution of HCD-Rif NPs before freeze drying

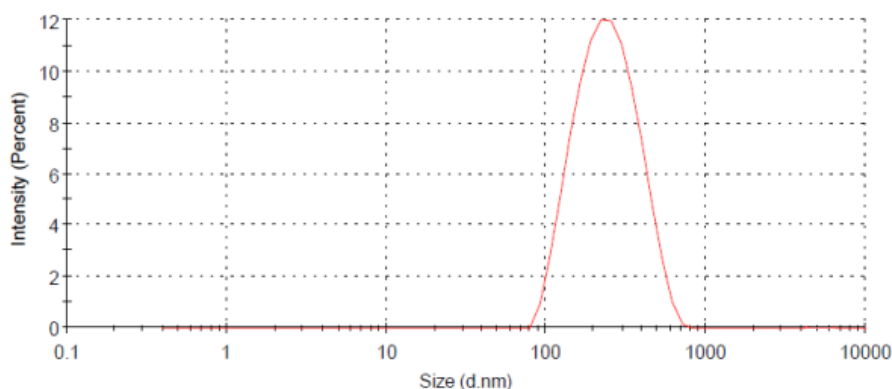


**Figure 8.4b:** Particle size distribution of HCD-Rif NPs after freeze drying

### 8.10.2 Morphology of HCD-Rif NPs after FD

Size, shape, and surface morphology of nanoparticles were visualized by scanning electron microscopy (SEM) and TEM (Figure 8.5a and b) respectively. HCD-Rif NPs showed small particle diameter, spherical shape and smooth surface morphology. Particles size as observed from the SEM and TEM images was found to be uniform.

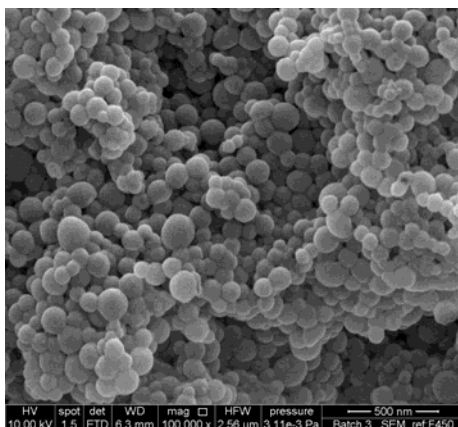


**Figure 8.5a:** Scanning Electron micrographs of HCD-Rif NPs

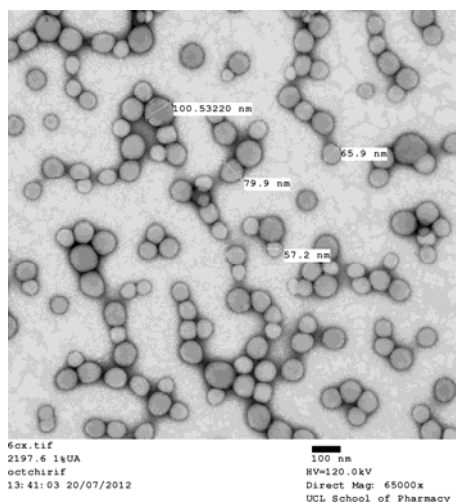


**Figure 8.5b:** Transmission Electron micrographs of HCD-Rif NPs

### 8.10.3 Solid state characterization of HCD-Rif NPs

#### 8.10.3.1 Differential Scanning Calorimeter (DSC)

Thermal analysis of rifampicin, HCD, HCD-Rif physical mixture and HCD-Rif NPs formulation was performed using DSC (DSC Q 2000, TA Instruments, USA) and the data obtained in the form of thermographs are presented in Figure 8.6. Thermograph revealed a characteristic exothermic peak at 260°C for rifampicin. As discussed in the thermal analysis section of chapter 6, no endothermic and exothermic peak between 20 to 300 °C was noticed from the DSC spectra of HCD. However, an exothermic peak can be expected beyond 300°C in the DSC spectra of chitosan, which is attributed to monomer dehydration, glycoside bond cleavage and decomposition of the acetyl and deacetylated units of chitosan. Similar results are reported by Ma et. al., and Zong et. al. (Ma et.al., 2008; Zong et al. 2000). Similar to HCD, physical mixture of HCD and rifampicin did not show any endothermic or exothermic peak for HCD, but exothermic peak corresponding to rifampicin was observed at 260°C. Owing to the absence of endothermic or exothermic peak in HCD thermographs, DSC thermographs of HCD-Rif NPs formulation was also devoid of endothermic or

exothermic peaks. In addition, absence of peak for rifampicin in the HCD-Rif NPs suggested molecular dispersion of rifampicin in HCD NPs.

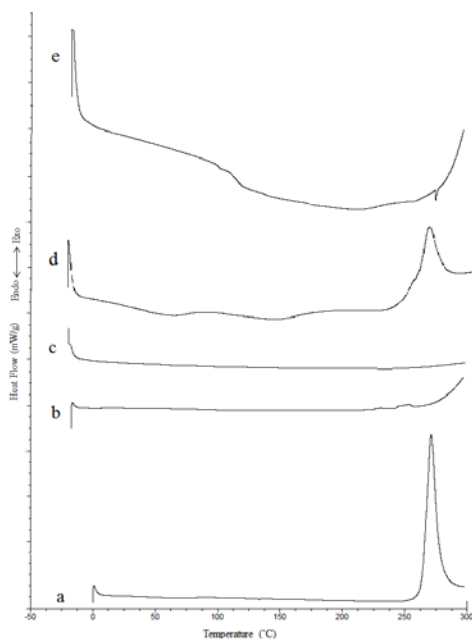


**Figure 8.6:** DSC Thermograms of – a) Rif; b) chitosan; c) HCD; d) HCD-Rif physical mixture; e) HCD-Rif NPs

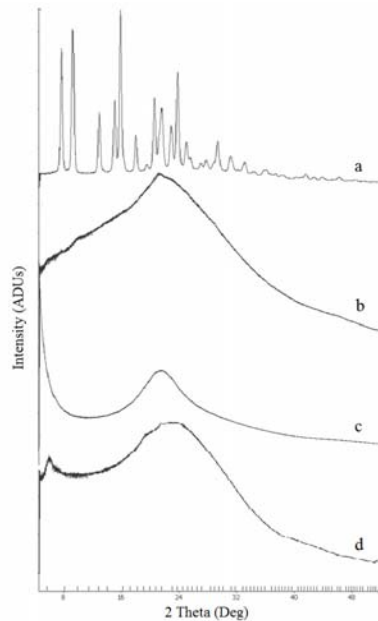


**Figure 8.7:** X-Ray Diffractograms of – a) Rif ; b) Chitosan c) HCD; d) HCD-Rif NPs.

### 8.10.3.2 X-ray powder diffraction (XRD)

X-ray diffractograms of rifampicin, chitosan, HCD & HCD-Rif NPs are displayed in figure 8.7. Characteristics crystalline peaks at  $2\theta$  values of  $13^\circ$  and  $15^\circ$  for rifampicin were observed

in the powder XRD diffractograms. XRD of Rif suggested crystalline nature of rifampicin. Parent chitosan (chitosan >5K) showed a characteristic broad peak of moderately low intensity at around 20°, whereas sharp peak at 20° and a new peak of higher intensity below 2 theta value of 8 was observed in the XRD spectra of HCD. XRD studies revealed a broad diffuse peak for rifampicin loaded NPs (HCD-Rif NPs). The absence of crystalline peak of rifampicin in the HCD-Rif NPs suggested the presence of rifampicin in amorphous form in HCD NPs and its molecular dispersion in HCD NPs. Presence of broad diffuse peak in XRD diffractograms of rifampicin loaded HCD NPs is a general characteristics for the systems composed of binary components (Parlati et. al., 2009). Results revealed from the XRD and DSC studies proved that crystallinity of rifampicin was altered by its encapsulation into HCD nanoparticle formulation.

### 8.11 In-vitro Pulmonary Deposition using Twin Stage Impinger (TSI)

Sample for TSI studies was prepared by dispersing 10 mg of HCD-Rif NPs in deionized water. HCD-Rif NPs dispersion was then nebulized using PariBoy air-jet nebulizer with compressed air using an Inhaler Boy compressor. The data obtained after nebulization of HCD-Rif NPs using TSI is presented in Table 8.17. Nebulization studies demonstrated pulmonary deposition ( $0.4488 \pm 0.057$  mg) of HCD-Rif NPs in Stage 2 of the TSI, which corresponds to  $33.15 \pm 4.24$  % of HCD-Rif NPs suggesting the effective particle size below of 6.8 μm. Maximum deposition of the formulation was observed at device+throat ( $0.5098 \pm 0.026$  mg equating to  $49.24 \pm 2.50$  %). Even after tapping of the device with finger, presence of certain amount was rifampicin in the device was noted, which is reported as combined amount of rifampicin in the device and throat, whereas stage 1 showed lowest amount of deposition with the values of about  $7.41 \pm 4.31$  μg of Rif. Various parameters to determine the aerosolization of HCD-Rif NPs were calculated. Nebulization efficiency of the HCD-Rif NPs was calculated to be  $76.47 \pm 4.33$ % of the total amount of rifampicin delivered, out of which  $30.01 \pm 8.09$  % of the dose was detected as respirable fraction (Table 8.17). Results of nebulization suggested the suitability of formulation to deliver rifampicin in the lower respiratory tract. In conformity to the British Pharmacopoeia standards (British Pharmacopoeia, 2012) deposition of HCD-Rif NPs in all stages of the TSI including device, throat, stage 1 and stage 2 was found to be in between 75% and 125% of mass balance.

**Table 8.17:** Parameter for Pulmonary Deposition of HCD-Rif NPs as Measured by TSI

Batch	Inhaled Dose (mg)	Delivered Dose (mg)	FPD (mg)	NE %	RF (%)	FPF (%)
Batch C3 (HCD-Rif NPs)	1.345	$1.035 \pm 0.128$	$0.45 \pm 0.057$	$76.47 \pm 4.33$	$33.15 \pm 4.24$	$43.35 \pm 3.23$

( $\pm$  SD,  $n = 3$  - Mean  $\pm$  Standard Deviation) ; NE - Nebulization efficiency; RF - Respirable fraction; FPF - Fine particle fraction; FPD – Fine particle dose.

## 8.12 In-vitro release studies

The cumulative percentage release of Rif from Rifampicin suspension (Rif-S) and HCD-Rif NPs were investigated in vitro over a period of 2 and 72 h respectively. Each sample was analyzed in triplicate and release curves plotted from the average values are displayed as percentages cumulative drug release *vs* time in figure 8.8. Simulated lung fluid (SLF 4, pH 7.4) was used as a release medium, which mimics the biological environment within the lungs. Results showed immediate release of almost all the amount of rifampicin ( $87.65 \pm 10.29\%$ ) from Rif-S into release medium, whereas release of rifampicin was found to be retarded from the HCD NPs. HCD-Rif NPs displayed initial rifampicin release of  $5.23 \pm 3.15\%$ , which is the onset of rifampicin release from the HCD-Rif NPs, suggesting ability of the polymer matrix to control the release of drug. HCD-Rif NPs showed sustained and steady release over the entire period of study up to 72 hr, with the biphasic drug release pattern. Initially sustained release phase was observed until 6 hr, which was followed by a steady and slow drug release. In the initial phase (up to 6 hr),  $45.97 \pm 2.99\%$  of rifampicin release was noted, which may have been possibly due to dissolution and passive diffusion of Rif located on or near the surface of nanoparticles. In addition, penetration of aqueous release medium (SLF pH 7.4) into the hydrophobic polymeric matrix leading to slow dissolution and thereby diffusion of the drug from the HCD NP matrix may have also caused sustained initial release up to 6 hr. After this, release phase was proceeded by further slowing down release of drug giving rise to almost 75 % of drug by the end of 72hr. Second phase of drug release, probably due to the diminution of rifampicin in the polymeric matrix, leading to reduced concentration gradient, causing less amount of drug to be available for release. Hence, biphasic release pattern of the formulation can be ascribed to the localization of rifampicin onto and within immediate layer and core of nanoparticle formulation. These results were found to be in agreement with the observation described by Klariæ et. al., (Klariæ et.al., 2012).

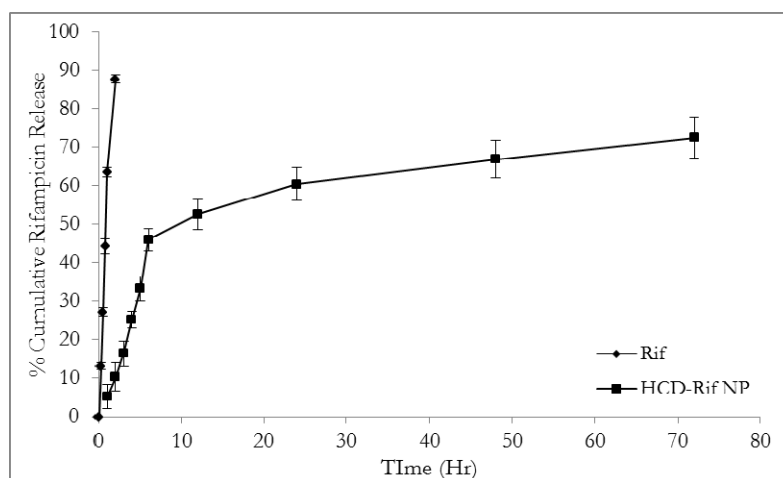


**Figure 8.8:** Percent cumulative release (PCR) of HCD-Rif nanoparticles  
*(n= 3 determinations ±SD)*

Release profiles obtained were fitted using various mathematical models such as zero order, first order, Higuchi, Hixon Crowell and Korsmeyers Peppas to understand the kinetics of

drug release from HCD nanoparticles (Costa et. al., 2001). The results of different model fittings are given in Table 8.18. Amongst various models tested, the curve fitting of release data to Korsmeyers and Peppas model represented higher value of correlation coefficient ( $r^2$  value of 0.8243) with the 'n' value (0.911, which is  $0.5 < n < 1$ ), suggesting anomalous transport (non-fickian) mechanism for the release of rifampicin. This is indicated that Korsmeyers and Peppas model satisfactorily represented the data owing to diffusion of rifampicin from the HCD NPs.

**Table 8.18: Release kinetics Rifampicin from HCD-Rif NPs**

Model	R <sup>2</sup>	Slope	Intercept
Zero order	0.6601	0.8216	24.32
First order	0.4234	0.0163	1.4353
Higuchi Square root	0.8153	4.3375	8.8426
Hixon- Crowell	0.5115	0.025	2.7661
Korsmeyer Peppas	<b>0.8243</b>	<b>0.5764 (n)</b>	0.9615

### 8.13 Stability Studies

HCD-Rif NPs were assessed for their ability to retain particle size and PDI along with the content of rifampicin over the period of 2 months storage at ambient temperature (10-15 °C) in order to check the stability of formulation. Results of stability study showed stability of HCD-Rif NPs for the period of up to 2 months storage at RT in desiccator under dark condition (Table 8.19). No significant difference was noted in the drug content, particle size and PDI values of HCD-Rif NPs (Table 8.19). Particle size of the formulation was found to be slightly increased after 2 months storage period ( $261.73 \pm 16.37$  nm) with the corresponding increment in PDI ( $0.402 \pm 0.014$ ). This slight increase in the particle size, may be due to agglomeration of the formulation. Moreover, analysis of drug content after two months storage period revealed slight decrease in the content of rifampicin in the HCD-Rif NPs. However, no significant reduction in the drug content was observed. Results of this study confirmed the stability of HCD-Rif NPs at room temperature (10-15 °C). Hence, 10-15 °C was considered to be an effective storage temperature.

**Table 8.19: Stability of HCD-Rif NPs at RT (10- 15 °C)**

Sr. No	Time (Months)	Drug Content (%)	MPS (nm)	PDI
1	Initial	100	$253.43 \pm 19.06$	$0.323 \pm 0.059$
2	2	$98.03 \pm 5.26$	$261.73 \pm 16.37$	$0.402 \pm 0.014$

n=3 determinations,  $\pm$  SD values

### References

- Alex R., Bodmeier R. (1990) Encapsulation of water-soluble drugs by a modified solvent evaporation method. I. Effect of process and formulation variables on drug entrapment. *Journal of Microencapsulation*, 7, 347–355
- Aranaz I., Harris R., and Heras A. (2010) Chitosan Amphiphilic Derivatives. *Chemistry and Applications, Current Organic Chemistry*, 14, 308-330
- Atkins T.W., Peacock J. (1996) The incorporation and release of bovine serum albumin from polyhydroxybutyratehydroxyvalerate microcapsules. *Journal of Microencapsulation*, 13, 709–717.
- Benetton S.A., Kedor-Hackmann E.R.M., Santoro M.I.R.M., Borges V.M. (1998) Visible spectrophotometric and first-derivative UV spectrophotometric determination of rifampicin and isoniazid in pharmaceutical preparations, *Talanta*, 47,3, 639–643.
- Bilati, U., Allémann, E. and Doelker, E. (2009) Poly(D,L-lactide-co-glycolide) protein-loaded nanoparticles prepared by the double emulsion method—processing and formulation issues for enhanced entrapment efficiency', *Journal of Microencapsulation*, 22 (2), 205 — 214
- Bolton S., Charles S. *Pharmaceutical Statistics*. New York, NY: Marcel Dekker Inc; 2004. pp. 249–255.
- British Pharmacopoeia (2012) Appendix XII C. Consistency of Formulated Preparations, *British Pharmacopoeia Volume V*, British Pharmacopoeia, 2012 online.
- Cohen-Sela E., Chorny M., Koroukhov N., Danenberg H.D., Golomb G. (2009) A new double emulsion solvent diffusion technique for encapsulating hydrophilic molecules in PLGA nanoparticles, *Journal of Controlled Release*, 133, 90–95
- Conway B.R., Alpar H.O. (1996) Double emulsion microencapsulation of proteins as model antigens using polylactide polymers: effect of emulsifier on the microsphere characteristics and release kinetics. *European Journal of Pharmaceutics and Biopharmaceutics*, 42, 42–48.
- Costa P., Lobo J. (2001) Modeling and comparison of dissolution profiles, *European J. of Pharm. Sci.*, 13, 123–133
- Desai, T.R., Hancock, R.E.W., Finlay, W.H., 2002. A facile method of delivery of liposomes by nebulization. *J. Control. Release*, 84, 69–78.
- Doan T.V.P., Couet W., Olivier J.C. (2011) Formulation and in vitro characterization of inhalable rifampicin-loaded PLGA microspheres for sustained lung delivery, *International Journal of Pharmaceutics*, 414, 112– 117.
- Grenha A. (2012) Chitosan nanoparticles: a survey of preparation methods. *J. Drug Target.*, 20 (4), 291-300.
- Hallworth, G.W., Westmorel, D.G., 1987. The twin impinger: a simple devise for assessing the delivery of drugs from metered dose pressurized aerosol inhalers. *J. Pharm. Pharmacol.* 39, 966–972.
- Harleman D.R.F., Murcott S.E. (1996) Method of drinking water treatment with natural cationic polymers, US 5543056 A, Publication date, Aug 6.
- Huang Y., Yu H., Guo L., Huang Q. (2010) Structure and Self-Assembly Properties of a New Chitosan-Based Amphiphile, *J.Phys.Chem. B*, 114, 7719-7726.

## Chapter 8 - Preparation of HCD-Rif Nanoparticles

---

Holzer M., Vogel V., Mäntele W., Schwartz D., Haase W., Langer K. (2009) Physico-chemical characterisation of PLGA nanoparticles after freeze-drying and storage. *European Journal of Pharmaceutics and Biopharmaceutics*, 72, 428–437

Hu L., Suna Y. and Wu Y. (2013) Advances in chitosan-based drug delivery vehicles, *Nanoscale*, 5, 3103

Jeffery H., Davis S.S., O'Hagan D.T. (1993) The preparation and characterization of poly(lactide-co-glycolide) microparticles. II. The entrapment of a model protein using a (water-in-oil)-in-water emulsion solvent evaporation technique. *Pharmaceutical Research*, 10, 362–368.

Kirby D. J., Rosenkrands, I., Agger E. M., Andersen P., Coombes A.G. A. and Perrie Y. (2008) PLGA microspheres for the delivery of a novel subunit TB vaccine, *Journal of Drug Targeting*, 16 (4), 282 — 293

Klariã D., Hafner A., Zubèiã S., Dürrigl M., and Filipoviã-Grèiã J. (2012) Spray-dried Microspheres Based on Chitosan and and Lecithin Cyclosporin A Delivery System. *Chem. Biochem. Eng. Q.* 26, 4, 355–364

Li H-Y., Seville P.C. (2010) Novel pMDI formulations for pulmonary delivery of proteins, *International Journal of Pharmaceutics*, 385, 73–78

Li Y., Zhang S., Meng X., Chen X., Ren G. (2011) The preparation and characterization of a novel amphiphilic oleoyl-carboxymethyl chitosan self-assembled nanoparticles, *Carbohydrate Polymers*, 83, 130–136

Liu J., Gong T., Fu H., Wang C., Wang X., Chena Q., Zhang Q., Hea Q., Zhang Z. (2008) Solid lipid nanoparticles for pulmonary delivery of insulin. *Int. J. Pharm.* 356, 333–344

Lubben I.M.V, Verhoef J.C., Borchard G., Junginger H.E, (2001) Chitosan and its derivatives in mucosal drug and vaccine delivery, *European Journal of Pharmaceutical Sciences*, 14, 201–207.

Ma G., Yang D., Zhou Y., Xiao M., Kennedy J.F., Nie J. (2008) Preparation and characterization of water-soluble N-alkylated chitosan. *Carbohydrate Polymers*. 74, 121–126.

Mainardes R.M., Evangelista R.C. (2005) PLGA nanoparticles containing praziquantel: effect of formulation variables on size distribution, *International Journal of Pharmaceutics*, 290, 137–144

Manca M-L., Mourtas S., Dracopoulos V., Fadda A.M., Antimisariis S.G. (2008) PLGA, chitosan or chitosan-coated PLGA microparticles for alveolar delivery? A comparative study of particle stability during nebulization, *Colloids and Surfaces B: Biointerfaces*, 62, 220–231

Matilainen, L., Järvinen, K., Toropainen, T., N'asi, E., Auriola, S., Järvinen, T., Jarho, P., 2006. In vitro evaluation of the effect of cyclodextrin complexation on pulmonary deposition of a peptide, cyclosporin A. *Int. J. Pharm.* 318, 41-48

Meng F.T., Ma G.H., Qiu W., Su Z.G. (2003) W/ O / W double emulsion technique using ethyl acetate as organic solvent: effects of its diffusion rate on the characteristics of microparticles. *Journal of Controlled Release*, 91, 407–416

Murakami H., Kobayashi M., Takeuchi H., Kawashima Y. (1999) Preparation of poly(DL-lactide-co-glycolide) nanoparticles by modified spontaneous emulsification solvent diffusion method. *International Journal of Pharmaceutics*, 187, 143–152

## Chapter 8 - Preparation of HCD-Rif Nanoparticles

---

Nasr M., Nawaz S., Elhissi A. (2012) Amphotericin B lipid nanoemulsion aerosols for targeting peripheral respiratory airways via nebulization. *Int. J. Pharm.* 436, 611– 616.

NIST/SEMATECH e-Handbook of Statistical Methods,

<http://www.itl.nist.gov/div898/handbook/>, date (accessed June 2013)

(Link to specific page –

<http://www.itl.nist.gov/div898/handbook/pri/section5/pri5322.htm>)

Pandey R., Sharma A., Zahoor A., Sharma S., Khuller G. K., and Prasad B. (2003) Poly (DL-lactide-co-glycolide) nanoparticle-based inhalable sustained drug delivery system for experimental tuberculosis. *Journal of Antimicrobial Chemotherapy*, 52, 981–986

Parlati C., Colombo P., Buttini F., Young P.M., Adi H., Ammit A.J., and Traini D. (2009) Pulmonary Spray Dried Powders of Tobramycin Containing Sodium Stearate to Improve Aerosolization Efficiency, *Pharmaceutical Research*, 26, 5, 1084-1092.

Prozorov T., Kataby G., Prozorov R., Gedanken A. (1999) Effect of surfactant concentration on the size of coated ferromagnetic nanoparticles, *Thin Solid Films*, 340, 189-193

Ranjan A.P., Mukerjee A., Helson L. and Vishwanatha J.K. (2012) Scale up, optimization and stability analysis of Curcumin C3 complex-loaded nanoparticles for cancer therapy. *Journal of Nanobiotechnology*, 10, 38

Sahoo S.K., Panyam J., Prabha S., Labhasetwar V. (2002) Residual polyvinyl alcohol associated with poly (D,L-lactide-coglycolide) nanoparticles affects their physical properties and cellular uptake. *Journal of Controlled Release*, 82, 105–114

Shah P.P., Mashru R.C., Rane Y.M., Thakkar A. (2008) Design and Optimization of Mefloquine Hydrochloride Microparticles for Bitter Taste Masking. *AAPS PharmSciTech.* 9 (2), 377–389.

Tatarczak M., Fliieger J., and Szumilo H. (2005), High-Performance Liquid-Chromatographic Determination of Rifampicin in Complex Pharmaceutical Preparation and in Serum Mycobacterium Tuberculosis-Infected Patients, *Acta Poloniae Pharmaceutica - Drug Research*, 62, 4, 251-256.

Tien C.L., Lacroix M., Ispas-Szabo P., Mateescu M. (2003) N-acylated chitosan: hydrophobic matrices for controlled drug release, *Journal of Controlled Release*, 93, 1, 1-13.

Yang Y.Y., Chung T.S., Ng N.P. (2001) Morphology, drug distribution, and in vitro release profiles of biodegradable polymeric microspheres containing protein fabricated by double-emulsion solvent extraction/evaporation method. *Biomaterials*, 22, 231–241.

Zambaux M.F., Bonneaux F., Gref R. et al., (1998) Influence of the drug incorporated in experimental parameters on the characteristics of poly (lactic acid) nanoparticles prepared by a double emulsion method, *J. control Controlled Release*, 50 (1–3), 31–40.

Zong Z., Kimura Y., Takahashi M., Yamane H. (2000) Characterization of chemical and solid state structures of acylated chitosans. *Polymer.* 41, 899–906.

### 9.0 Preparation of HCD-Ag85A Nanoparticles

#### 9.1 Materials

Ag85A was obtained as gift by TB Vaccine Testing & Research Material Contract (TBVTRMC) Colorado State University, (Colorado, USA). Chitosan oligosaccharide (MW > 5kDa; degree of deacetylation (DDA) 80-90%) was supplied by Kitto Life Co. Ltd. (Kyongki-Do, Seol Korea). Fluorescein isothiocyanate (FITC), octanoyl chlorides, methane sulfonic acid, sodium bicarbonate, Poloxomer, Poly vinyl alcohol were purchased from Sigma-Aldrich (St-Louis, USA). Cellulose dialysis tubing (Molecular weight cut of 12-14kDa, 3-5 kDa) were purchased from Medicell international Ltd., (London, UK). Dimethyl sulfoxide (anhydrous), methanol, ethanol, chloroform, dichloromethane (DCM), acetone etc. and all other HPLC grade solvents were obtained from Sigma-Aldrich (St-Louis, USA).

#### 9.2 Equipments

1. High speed magnetic stirrer (FisherBrand, UK)
2. Probe Sonicator (Labsonic® P, Sartorius Biotech GmbH, Germany)
3. UV-VIS Spectrophotometer (Jenway UV/Vis Spectrophotometer, UK)
4. Fourier Transform Infra-red spectrophotometer (FTIR) (Perkin Elmer, USA)
5. Differential Scanning Calorimeter DSC Q 2000, (TA Instruments, UK)
6. Zetasizer, Nanoseries Instrument (Nano 25, Malvern Instruments, UK)
7. High speed Centrifuge (Sigma 3K30, Sigma Laboratory Centrifuge, 3K30, UK)
8. Scanning Electron Microscope (FEI XL30 TMP, Philips, Netherlands)
9. X-Ray Diffractometer (Oxford Diffraction Xcalibur novaT, UK)
10. Twin Stage Impinger (Copley, UK)
11. Bath Sonicator, (Ultrawave Ltd, UK)
12. Transmission Electron Microscopy (TEM, Philips Electron Optics BV, Netherlands)
13. Fluorescence spectrometer (LS 55, Fluorescence spectrometer, Perkin Elmer, USA).
14. Rotary evaporator (Hei-VAP Advantage Rotary Evaporator, Heidolph, Germany)
15. Lyophilizer (VirTis Advantage, SP Scientific, USA)

#### 9.3 Preparation of nanoparticles by multiple emulsification technique

HCD-Ag85A nanoparticles were developed by using double emulsion solvent evaporation technique. Briefly, 50 mg of HCD was dissolved in 3.5 ml of DCM, specified amount of subunit protein, Ag85A in 0.5 ml of deionised water was added to the organic phase and sonicated to form w/o primary emulsion at 15 W for 25 sec in ice bath. Primary emulsion was immediately transferred to large aqueous phase of 10 ml aided with 0.5 % PVA and sonicated for 50 seconds at pulse rate of 15 W. Resultant multiple emulsion was stirred at 25-30 °C on multiple station magnetic stirrer (RO 10 power IKA WERKE, Staufen, Germany) to evaporate organic solvent. Nanoparticles were recovered by centrifugation (Sigma Laboratory Centrifuge, 3K30, UK) at 21000 rpm for 30 min and washed thrice with fresh deionized water to polish off the NPs from any residual PVA and untrapped Ag85A. Finally, NPs were dispersed in deionized water and lyophilized (VirTis Advantage, SP Scientific, USA) using trehalose dehydrate as cryoprotectant at the concentration of 1% w/v

as reported by Holzer et. al., (Holzer et. al., 2009). Similar protocol was followed to prepare blank NPs without Ag85A.

### 9.3.1 Optimization of parameters

Preliminary optimizations of various parameters influencing the formation of nanoparticles in terms of size, PDI and charge were similar to those presented elaborately in the chapter 8. These include selection of solvent, surfactant optimization and selection of surfactant concentration. However, sonication time was optimized separately for the preparation of HCD nanoparticles loaded with Ag85A, because the optimized sonication time for rifampicin loaded HCD NPs was found to be unsuitable to prepare Ag85A entrapped HCD NPs.

#### 9.3.1.1 Selection of sonication time

HCD-Ag85A NPs were formulated according to the optimized formula as mentioned in chapter 8. Batches were prepared according to the optimized formula by incorporating Ag85A (250 µg) and by varying sonication time as 25, 35 and 50 sec (for primary and secondary emulsion) and sonication time selected on the basis of optimum MPS, PDI and zeta potential value.

### 9.4 Preparation of FITC labeled HCD

FITC is an amine reactive fluorescent dye. Labeling of FITC on HCD was based on the conjugation of isothiocyanate group of FITC onto primary amine groups of the chitosan (figure 9.1). The fluorescent labeled HCD was synthesized according to the method adopted by Jia et.al., and Haung et.al., (Jia et.al., 2009 & Huang et.al., 2002). In brief, 1% (w/v) of chitosan was accurately weighed and dissolved in 10 mL mixture of anhydrous methanol and dichloromethane (DCM). Flask was sealed, nitrogen gas was bubbled into the solution under stirring for half an hour to remove oxygen. Later on, 5 ml of FITC dissolved in anhydrous methanol in the concentration of 4 mg/ml and added drop-wise to the previous solution with constant stirring. The reaction was continued in the dark for 5-6 hr at room temperature. After 6 hrs, the solvent was evaporated using rotary evaporator (Hei-VAP Advantage Rotary Evaporator, Heidolph, Schwabach, Germany). Solid material obtained was dissolved in the mixture of methanol and DCM followed by rotary evaporation (Hei-VAP Advantage Rotary Evaporator, Heidolph, Schwabach, Germany). This procedure was carried out thrice and solid FITC-HCD was then extensively dialyzed in distilled water under dark conditions, with water being replaced every 6 hr. This procedure was continued till complete removal of unreacted FITC, which was confirmed by absence of fluorescence at excitation and emission maxima of 492 and 518 nm, respectively (LS 55 Fluorescence Spectrometer, Perkin-Elmer, UK). Labeling efficiency (percent weight of FITC to weight of the FITC-HCD, %w/w) was calculated by measuring the fluorescence intensity of the FITC-HCD solution against a standard solution of FITC. For that, specified amount of FITC-HCD was dissolved in methanol, required aliquots were withdrawn and volume was made up with water to measure fluorescence intensity. The fluorometer was previously calibrated with standard solutions of 0.01 and 2 µg/ml of FITC in the same solvent. FITC-HCD was

utilized for the preparation of FITC-HCD NPs as described in section 9.3, and these NPs were availed for in-vitro pulmonary deposition in twin stage impinger.

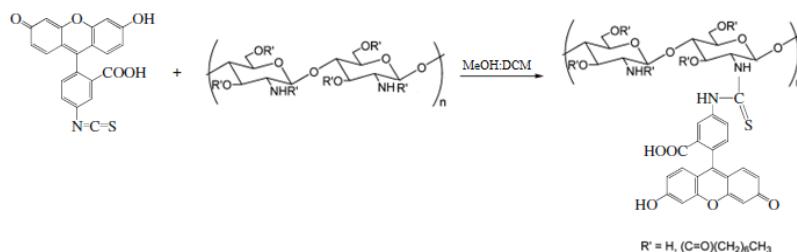


Figure 9.1: Schematic of FITC-HCD preparation

### 9.5 Protein adsorption onto HCD Nanoparticles

Blank HCD NPs were used to evaluate the adsorbing efficacy of Ag85A. Batches were prepared by incubating specified quantity of Ag85A with HCD NPs suspension. Briefly, known amount of previously prepared blank HCD NPs were suspended in 2 ml of deionized water, to which specific amount of protein (Ag85A) solution (0.25 - 1 mg) was added and incubated overnight at room temperature (15-20 °C). After incubation period, suspension was centrifuged at 13,000 rpm for 30 min, clear supernatant was collected and the amount of free Ag85A was determined using BCA protein estimation kit by UV-VIS spectrophotometer (Jenway UV/Vis Spectrophotometer, Staffordshire, UK) at 562 nm.

### 9.6 Characterization of HCD-Ag85A NPs

#### 9.6.1 Particle characterization of HCD-Ag85A NPs and FITC-HCD NPs

Dynamic light scattering (DLS) and laser doppler velocimetry (LDV) was used to measure the particle size and zeta potential of the particles respectively. For this purpose, Zetasizer, Nanoseries Instrument (Nano 25, Malvern Instruments, Worcestershire, UK) was employed. The particles were dispersed in deionized water and sonicated in Ultrawave bath sonicator (Ultrawave Ltd, Cardiff, UK) for 5 min and the resultant samples were used for the measurement of particle size, polydispersity index (PDI) and zeta potential.

#### 9.6.2 Loading efficiency and Protein loading

Protein loading was determined by indirect method. Supernatant obtained after washings of NPs was collected and used to quantify the total amount of free Ag85A using BCA protein estimation kit by UV-VIS spectrophotometer (Jenway UV/Vis Spectrophotometer, Staffordshire, UK) at 562 nm. Supernatant obtained from Blank NPs was used for correction of samples. From these results, total amount of Ag85A loaded in the HCD NPs was calculated in terms of loading capacity and loading efficiency using following equations (2 & 3). The analysis was carried out in triplicate for each batch of drug loaded NPs separately.

$$\text{Yield (\%)} = \frac{\text{Weight of NPs recovered}}{\text{weight of protein/polymer/excipients}} \times 100 \quad \text{-----(1)}$$

$$\text{Loading Capacity} = \frac{\text{Total amount of protein} - \text{Free protein}}{\text{Weight of NPs}} \text{-----}(2)$$

$$\text{Loading Efficiency (\%)} = \frac{\text{Total amount of protein} - \text{Free protein}}{\text{Total amount of protein}} \times 100 \text{-----}(3)$$

### 9.6.3 Morphological characterization

A small sample of freeze dried particles was placed on Scanning Electron Microscope (FEI XL30 TMP, Philips, Netherlands) stub. Samples were sputter coated with gold and examined to determine shape and surface morphology of NPs. In Transmission Electron Microscopy (TEM), a drop of nanoparticle suspension was placed on a coated carbon grid and vacuum dried. The grid was then examined immediately under Transmission Electron microscope (TEM, Philips Electron Optics BV, Netherlands). The electron micrographs were obtained after suitable magnifications.

### 9.6.4 DSC and XRD studies

Thermal property of the freeze-dried nanoparticles and plain protein (O-alb) was investigated with a Differential Scanning Calorimeter (DSC Q 2000, TA Instruments, USA). Accurately weighed samples (3-5 mg) were placed in hermetically closed aluminum pans and empty aluminum pan was used as a reference. Heating scans by heat runs for each sample was set from 10 °C to 300 °C at 10 °C min<sup>-1</sup> in a nitrogen atmosphere. The X-RD patterns were recorded using an X-ray diffractometer (Oxford Diffraction Xcalibur novaT, UK). The samples were mounted on a sample holder and X-RD patterns were recorded in the range of 5–50° at the speed of 5° per min.

### 9.7 Antigen Integrity by SDS-PAGE Analysis

Ag85A encapsulated in HCD NPs was analyzed using SDS PAGE to determine integrity of antigen in the NPs. Accurately weighed, 2 mg of HCD-Ag85A nanoparticles (1 - immediately after preparation & lyophilization and 2 - after two-months storage of NPs) were taken. In both the cases, NPs were dispersed in 200 µL SDS sampling buffer composed of bromophenol blue, which acted as reducing agent. Dispersed samples were kept aside for extraction for 15 min and then boiled in water bath at around 90 °C for 5 min in order to denature the protein. Resultant composition was centrifuged for 5 min at 12, 000 g prior to loading into wells of the SDS PAGE gel. Similar treatments were given to blank NPs and pure antigen and 20µL samples from each preparation were loaded into a 12% SDSPAGE gel (Biorad, Hercules, CA). Visualization of proteins was done using Coomassie Blue staining.

### 9.8 In-vitro aerosolization and lung deposition using Twin Stage Impinger (TSI)

FITC-HCD nanoparticles were analyzed using the Twin Stage Impinger (Copley Scientific Ltd., Nottingham, UK) as per the specifications given in British Pharmacopoeia (British Pharmacopoeia, 2011) to understand the pattern of aerosolisation. The upper and lower stages of the impinger were filled with 7 mL and 30 mL mixture of methanol & water (1:1 v/v) respectively and device was operated as mentioned in the previous chapter 7. Each stage

of TSI was rinsed with methanol: water, samples were collected and the volume of the stages 0, 1 and 2 was made upto 10, 20 and 35 ml respectively. The samples were taken from each stage (lower and upper stages) for analysis of FITC deposited (as FITC-HCD NPs) in the different stages of the impinger and quantified by Fluorescence spectrometer (LS 55, Fluorescence spectrometer, Perkin Elmer, Wellesley, USA). Experiment was performed thrice and the aerosolization property of the FITC-HCD nanoparticles suspension was evaluated in terms of nebulization efficiency (NE) or aerosol output (total aerosolized mass of FITC detected in the nebulizer, throat, Stage 1 and Stage 2) (Desai et al., 2002) and respirable fraction (RF) (Matilainen et al., 2006) as calculated using following formulae. In addition, percent fine particle fraction (FPF) was calculated as the ratio of fine particle dose (FPD) i.e. protein mass deposited in stage 2 to recovered dose (RD), expressed as a percentage (Liu et.al., 2008; Li et.al., 2010).

$$NE (\%) = \frac{\text{Aerosolized Protein}}{\text{Protein Mass Loaded in nebulizer}} \times 100 \text{-----(5)}$$

$$RF (\%) = \frac{\text{Mass of Protein deposited in Stage 2 of TSI}}{\text{Protein Mass Loaded in nebulizer}} \times 100 \text{-----(6)}$$

### 9.9 In-vitro release studies

Release study of HCD-Ag85A nanoparticles was executed in micro centrifuge tube using modified release medium, simulated lung fluid (SLF - pH 7.4) as suggested by Marques et.al., (Marques et. al., 2011). Specified quantity of Ag85A loaded HCD NPs was weighed, transferred to micro centrifuge tube and dispersed in SLF. Micro centrifuge tubes were kept under shaking in water bath at 37°C. At predetermined time intervals, aliquots from the release medium were withdrawn, diluted as required, centrifuged at 13000 rpm (Bio-Rad Laboratory Centrifuge) and supernatants were analyzed for Ag85A content using QuantiPro™ BCA assay kit at 562 nm (Sigma Aldrich, St. Louis, USA). After each aliquot withdrawal, same amount of blank media (kept in water bath at 37°C) was replenished in order to maintain sink condition. A calibration curve was prepared prior to the start of dissolution using a SLF (correlation coefficient was 0.9993). The experiment was done in triplicate and the results are reported as percent cumulative drug release *vs* time with ± standard deviation.

### 9.10 Stability study of HCD-Ag85A nanoparticles

Lyophilized Ag85A-loaded HCD nanoparticle was tested by storing the samples in desiccator for 2 months period at room temperature (10-15 °C). After two months, 2 mg of samples were withdrawn, rehydrated and the particle size and PDI were measured to assess any influence on stated parameters. Content of Ag85A was analyzed qualitatively using SDS PAGE and any loss of Ag85A during storage at a specified condition.

### 9.11 Statistical analysis

The experiments were performed in triplicate. The data collected in this study were expressed as the mean value ± standard deviation.

**9.12 Results and Discussion****9.12.1 Preparation and characterization of nanoparticles**

Various authors have reported preparation methods of chitosan nanoparticles, for instance ionic gelation, complex coacervation, emulsion cross-linking, and spray drying (Grenha et.al., 2012). Recent practice in the preparation of nanoparticles for application in drug and vaccine delivery include self-assembling nanoparticles, polymeric micelles prepared from amphiphilic polymers (achieved by modification of chitosan) (Haung et.al., 2010; Aranaz et.al., 2010; Li et.al., 2011; Hu et.al., 2013). However, application of hydrophobic chitosan derivative (HCD) in its native form for the preparation of nanoparticles is yet to be explored. In view of this, our investigation was focused to assess the feasibility of HCD in the preparation of nanoparticles (NPs). Results of our studies as discussed in chapter 7) indicated that HCD can be efficiently used for the preparation of NPs in the same way as that of PLGA. Additionally, HCD provides certain advantageous features of chitosan such as positive charge, mucoadhesivity etc. which are otherwise lacking in PLGA. As promising results were obtained, we evaluated the potentiality of HCD NPs to encapsulate protein (Ag85A) and also determined its protein adsorption capacity.

**9.12.1.1 Optimization of Parameters by preparing blank HCD NPs**

Formula for the preparation of HCD NPs was utilized as described in chapter 8, where full optimization study of formulation parameters was carried. This includes sonication pulse, solvent selection, surfactant and its concentration and final formula was optimized with the help of 3<sup>2</sup> full factorial design of experiment. After preparation of HCD NPs using the same formula, we found that sonication time as used for the preparation of rifampicin loaded HCD NPs was unsuitable for the preparation of NPs loaded with Ag85A as it resulted in higher particle size (567±96.45 nm). This suggested that, sonication time acts as an important factor for the preparation of NPs while using multiple emulsion technique. Therefore, sonication time was chosen as a parameter to optimize for the preparation of HCD-Ag85A NPs and optimum value was selected based on the particle size and PDI. Following parameters as determined in the previous experiments were used for the preparation of HCD NPs:

- Polymer concentration (50 mg)
- Organic phase (3.5 ml)
- Internal aqueous phase (0.5 ml)
- External aqueous phase (10 ml, 1% PVA) and
- Sonication pulse (15 W).

At the first instance, sonication time was increased and varied from 25-50 sec for primary emulsion, whereas 50 sec was set for the preparation of secondary emulsion. In all the three batches small particle sizes and PDI were observed. Therefore, a batch which required minimum time (25 sec) for the preparation of primary emulsion was selected. Similarly, sonication time for secondary emulsion was optimized by varying time from 25- 50 sec,. These batches were prepared by keeping sonication time of 25 sec at primary emulsion stage. At the lowest sonication times used, particles showed acceptable particles size of

337.18±13.17 nm, the presence of lumps indicated unsuitability of the small sonication time for the preparation of NPs. Sonication time of 25 and 35 sec. at primary emulsion and secondary emulsion respectively yielded particle size of 296.22 ±5.84 and PDI of 0.192 ±0.137. However, we chose 25 and 50 seconds time of sonication (which showed comparable results of MPS and PDI (229.60 ±7.35 nm and 0.165 ±0.044) as that of 25 and 35 sec time) for the further preparation of NPs considering that increase in the quantity of protein may cause inefficient sonication leading to aggregation. Table 9.1 presents the data of sonication time optimization.

**Table 9.1:– Optimization of sonication time during primary and secondary emulsification**

Optimization of sonication time for primary emulsion					
Sr. No.	Sonication time (Sec)		MPS (nm)	Mean PDI	Remark
	Primary emulsion	Secondary emulsion			
0	15	30	567±96.45	0.629±0.052	AG
<b>1</b>	<b>25</b>	<b>50</b>	<b>232.42±19.12</b>	<b>0.264 ±0.028</b>	<b>G</b>
2	35	50	203.25±11.66	0.203 ±0.059	G
3	50	50	160.82±14.71	0.103 ±0.083	G
Optimization of sonication time for secondary emulsion					
1	25	25	337.18±13.17	0.570 ±0.222	AG
2	25	35	296.22±5.84	0.192 ±0.137	G
<b>3</b>	<b>25</b>	<b>50</b>	<b>229.60 ±7.35</b>	<b>0.165 ±0.044</b>	<b>G</b>

n = 3; ± Standard Deviation; G – Good; AG – Aggregate

#### 9.12.1.2 Formulation optimization

Formulation of Ag85A encapsulated HCD NPs was carried out according to the optimized formula as shown below in Table 9.2. HCD nanoparticles were prepared by varying Ag85A concentration from 250-1000 µg. The batch of HCD NPs producing higher entrapment efficiency was considered as optimized batch.

**Table 9.2. Formulation of HCD-Ag NPs**

Parameters	Blank-HC-Ag 0	E-HC-Ag 1	E-HC-Ag 2	E-HC-Ag 3
Batches				
HCD (mg)	50 mg	50 mg	50 mg	50 mg
Organic Phase (ml)	3.5 ml	3.5 ml	3.5 ml	3.5 ml
Ag85A concentration (µg)	00	250	500	1000
Internal aqueous Phase (ml)	0.5	0.5	0.5	0.5
Concentration of surfactant (% w/v)	0.5	0.5	0.5	0.5
Surfactant in external aqueous phase	PVA	PVA	PVA	PVA
External aqueous Phase (EAP) (ml)	10	10	10	10
Sonication time for primary & sec emulsion (Seconds)	25 & 50	25 & 50	25 & 50	25 & 50

## Chapter 9 - Preparation of HCD-Ag85A Nanoparticles

All the batches of HCD-Ag85A NPs composing different amount of Ag85A were assessed for their mean particle size (MPS), polydispersity index (PDI) and zeta potential (ZP) values before lyophilization and their respective results are reported in table 9.3. After washing of HCD-Ag85A NPs with deionized water, dispersion of formulations in fresh deionized water were subjected to lyophilization in presence of cryoprotective agent (trehalose dehydrate) in the concentration 1 % w/v as reported elsewhere (Holzer et.al., 2009). As expected, slightly increased size of the particles was observed after lyophilization. However, no substantial difference was noted before and after lyophilization, indicating the suitability of trehalose as the cyoprotectant during lyophilization in the concentration used. Results of this study are tabulated in table 9.4. Along with the results of particle characterization, table 9.4 also tabulates loading capacity and loading efficiency of Ag85A in HCD NPs. As stated earlier, four formulations of HCD-Ag85A NPs were formulated by varying the amount of theoretical Ag85A loading from 00-1000 µg. Concentration of Ag85A in the batch E-HC-Ag 1 was found to be negative (which ruled out the utilization of this batch), though it yielded  $107.87 \pm 6.67$  and  $3.19 \pm 0.16$  of loading efficiency and loading capacity respectively. Second Batch, E-HC- Ag 2 showed highest LE of  $97.39 \pm 1.06$  % was considered to be an optimized batch for further experiments among the batches prepared using encapsulation methodology.

**Table 9.3. MPS, PDI and ZP of HCD-Ag85A NPs before freeze drying**

Batch	MPS (nm)	Mean PDI	Mean Zeta (mV)
<b>HC-Ag 0</b>	247.13±1.19	0.265±0.023	21.67±0.23
<b>HC-Ag 1</b>	246.23±2.45	0.233±0.019	23.13±0.95
<b>HC-Ag 2</b>	229.13±1.50	0.185±0.019	26.43±0.76
<b>HC-Ag 3</b>	271.23±2.40	0.299±0.012	22.5±0.5

n = 3; ± Standard Deviation; MPS – mean particle size; PDI - polydispersity index and Zp – zeta potential

**Table 9.4. MPS, PDI and ZP with LC and LE of HCD-Ag85A NPs after freeze drying**

Batch	MPS (nm)	Mean PDI	Mean Zeta (mV)	LC (w/w)	LE (%)
<b>HC-Ag 0</b>	269.1±10.15	0.317±0.019	25.07±0.32	00	00
<b>E-HC-Ag 1</b>	315.3667±3.16	0.410±0.023	28.23±1.02	3.19±0.16	107.87±6.67
<b>E-HC-Ag 2</b>	<b>241.5333±1.17</b>	<b>0.222±0.011</b>	<b>28.73±0.78</b>	<b>5.837±0.09</b>	<b>97.39±1.06</b>
<b>E-HC-Ag 3</b>	246.7±2.86	0.257±0.023	36.03±0.31	11.07±0.33	91.89±3.03

n = 3; ± Standard Deviation; LC – Loading capacity; LE – % Loading Efficiency

Secondly, owing to the cationic nature of HCD, NPs prepared using HCD were also tested for adsorption of Ag85A. Results indicated increased adsorption of Ag85A onto HCD NPs until 250 µg of Ag85A, with the loading efficiency of  $80.67 \pm 0.95\%$  in batch A-HC-Ag 0250. Lowest loading efficiency of  $66.44 \pm 2.83\%$  was observed from the batch A-HC-Ag 0100. However, after 250 µg of Ag85A, reduced loading efficiency ( $77.26 \pm 0.95$  %) was noted. Overall loading efficiency of HCD NPs could be rated as A-HC-Ag 0100 < A-HC-Ag 0200 < A-HC-Ag 0250 > A-HC-Ag 0300. Adsorption efficiency of Ag85A on HCD NPs was found to be in the range of 65-80%. The protein adsorbing efficacy of HCD NPs could be

attributed to the net positive charge on the HCD NPs. However, LE obtained after adsorption of Ag85A was less in all the cases as compared to LE of HCD NPs, where Ag85A was entrapped (Table 9.5). Hence, among the batches prepared by encapsulation and adsorption of Ag85A, batch E-HC- Ag 2, which exhibited high LE was considered as final formulation for further characterization studies.

**Table 9.5 – LC and LE of Ag85A adsorbed on blank HCD NPs (A-HC-Ag 0)**

Batch HC-Ag: Ag85A Adsorbed ( $\mu\text{g}$ )	Loading Capacity (w/w)	Loading Efficiency (%)
A- HC-Ag 0100	0.0033 $\pm$ 0.00057	66.44 $\pm$ 2.83
A- HC-Ag 0200	0.0084 $\pm$ 0.00018	70.96 $\pm$ 0.45
A- HC-Ag 0250	0.0153 $\pm$ 0.00048	80.67 $\pm$ 0.95
A- HC-Ag 0300	0.0164 $\pm$ 0.00057	77.26 $\pm$ 0.95

n = 3;  $\pm$  Standard Deviation; LC – Loading capacity; LE – % Loading Efficiency  
A- HC-Ag 0100 indicates, a blank batch of NPs (A-HC-Ag 0) was used with prefix 0 means blank NPs and suffix stands for respective amount of Ag85A used for the absorption.

### 9.12.2 Labeling efficiency of FITC to HCD

The conjugation reaction between FITC and HCD occurred due to presence of primary amino group of D-glucosamine in HCD and isothiocyanate group of FITC (Fig 8.1). The reaction yielded a fluorescent yellow colored FITC-HCD and labeling efficiency of the weight fraction of FITC per unit weight of HCD was found to be 1.78% (w/w). Dialysis of the final product (FITC-HCD) was carried out until no fluorescence was detected in the dialysis medium. Therefore, the fluorescent labeling of HCD using FITC can be considered as a stable.

## 9.13 Particle Characterization

### 9.13.1 Particle Size

HCD-Ag85A NPs exhibited mean particle size of 229.13 $\pm$ 1.50 nm with the PDI values of 0.185 $\pm$ 0.019 (figure 9.1b). After freeze drying, MPS and PDI of 241.53 $\pm$ 1.17 nm and 0.222 $\pm$ 0.011 respectively were noted (Table 9.4), suggesting slight increment in the MPS). Zeta potential value of HCD-Ag85A nanoparticles prepared in this study was found to be 26.43 $\pm$ 0.76 before freeze drying and 28.73 $\pm$ 0.78 mV after freeze drying (Figure 9.1c), suggesting no substantial variation in the ZP values. Moreover, positive ZP indicated stable HCD-Ag85A NPs (Table 9.4).

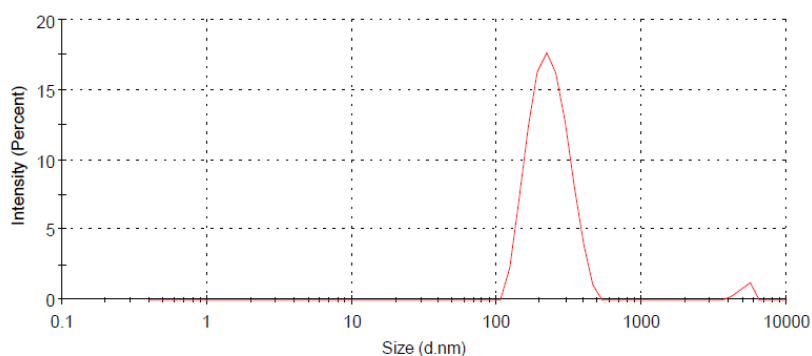


**Figure 9.1a:** Particle size distribution of HCD-Ag85A NPs before Freeze Drying

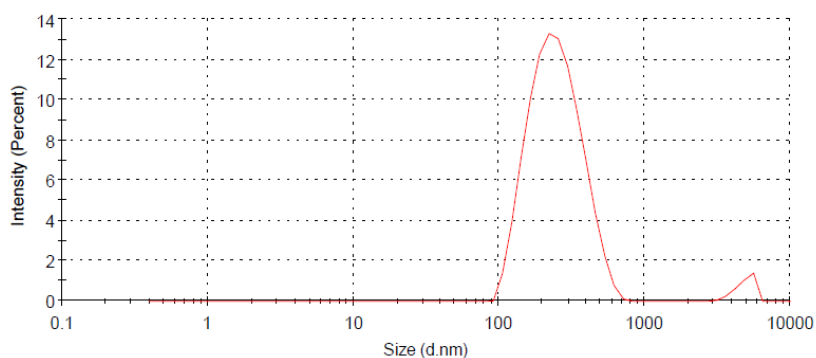


**Figure 9.1b:** Particle size distribution of HCD-Ag85A NPs after Freeze Drying

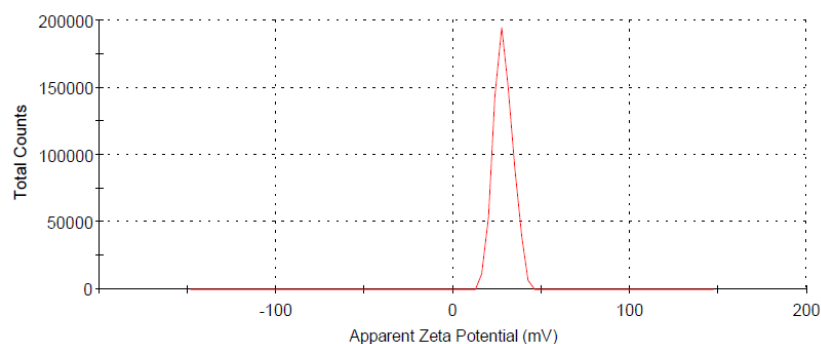


**Figure 9.1c:** Zeta potential of HCD-Ag85A NPs after Freeze Drying

FITC-HCD was utilized for the preparation of nanoparticles employing the same optimized formula as tabulated in table 9.4. Nanoparticles prepared using FITC-HCD was used for nebulization and cell line studies. Important characteristics of nanoparticles such as particle size, PDI and zeta potential were measured. FITC conjugated HCD NPs had small particle size with low PDI and positive surface potential values. The size of the FITC-HCD NPs was found to be  $177.83 \pm 8.05$  with the PDI of  $0.11 \pm 0.01$  (Figure 9.2a). This particle size was found to be substantially smaller as compared to the one obtained from batch HC-Ag 0 NPs (MPS of  $269.1 \pm 10.15$  and PDI of  $0.317 \pm 0.019$ ) and even less than that of batch HC-Ag 2 (Figure 9.1b). Results of the zeta potential indicated positive surface potential ( $10.83 \pm 2.87$ ) (Fig 2b), although less than the NPs prepared without FITC, which may be due to occupation of free amine groups by the FITC (Jia et. al., 2009).

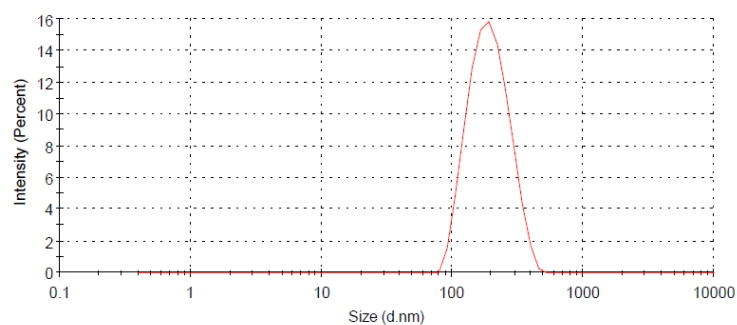


**Figure 9.2a:** Particle size distribution of FITC-HCD NPs after Freeze Drying

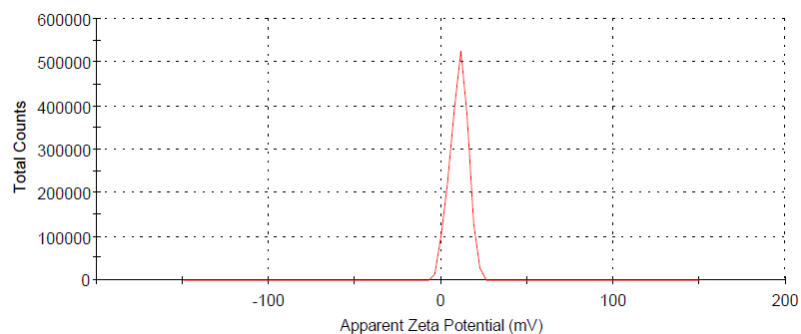


**Figure 9.2b:** Zeta potential of FITC-HCD NPs after Freeze Drying

### 9.13.2 Morphology of HCD-Rif NPs after Freeze Drying

Scanning and Transmission Electron Micrographs are depicted in Figure 9.3 a and b respectively. HCD-Ag85A NPs showed spherical shape and smooth surface morphology. Particles size was found uniform in SEM and TEM images.

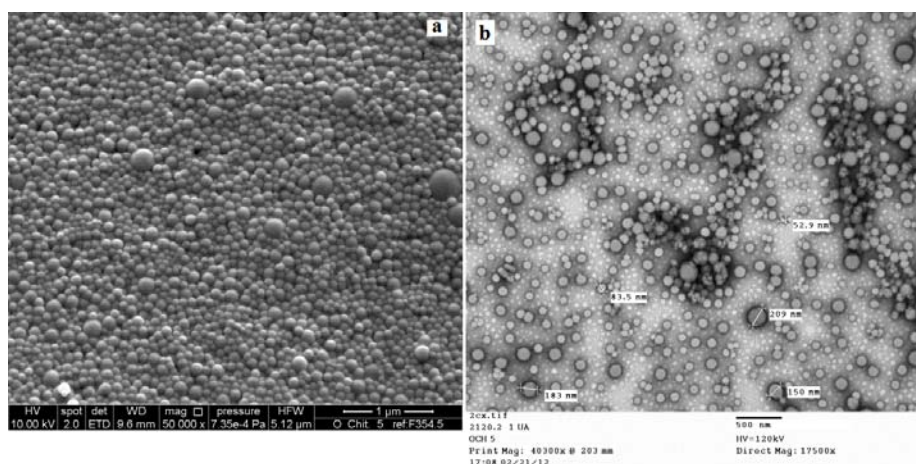


**Figure 9.3, a)** Scanning Electron micrographs of HCD-Ag85A NPs ;  
**b)** Transmission Electron micrographs of HCD-Ag85A NPs

### 9.13.3 Solid state characterization of HCD-Ag85A NPs

#### 9.13.3.1 Thermal Analysis

Figure 9.4 depicts scans obtained after thermal analysis of ovalbumin (O-alb), HCD, HCD-O-alb physical mixture, HCD-O-alb NPs and HCD-Ag85A NPs using Differential Scanning Calorimeter (DSC Q 2000, TA Instruments, USA). Thermograph of ovalbumin revealed a characteristic broad exothermic peak at 50 °C and endothermic peak at 150 °C indicating thermal denaturation of protein. Thermal analysis of HCD showed beginning of baseline exothermic deviation at around 300 °C, which suggested the onset of thermal decomposition of the crystalline regions of HCD. Similar results are reported in the literature (Zong et.al., 2000; Borges et.al., 2005; Ma et. al., 2008). DSC curve of physical mixture of HCD and ovalbumin did not show any peak corresponding to either HCD or ovalbumin, but a small curvature at 200 °C was noted, which may be due to shifting of the ovalbumin peak to higher temperature. Similar results are published by the Hitachi Hitech Science Corporation, where studies were conducted to determine the effect of sugar on thermal stability of proteins and observed that increased concentration of sugars tended to increase denaturation peak of ovalbumin (Application brief by Hitachi, 1986). Owing to the absence of endothermic or exothermic peak in HCD thermographs, DSC thermographs of HCD-O-alb NPs and HCD-Ag85A NPs also revealed absence of endothermic or exothermic peaks. However, a peak of reduced intensity was observed in both the HCD-O-alb NPs and HCD-Ag85A NPs at around 150 °C, which may be corresponding to the presence of surface associated ovalbumin and Ag85A on HCD NPs. However, reduced intensity of peaks (O-alb and Ag85A) indicated molecular dispersion and encapsulation of O-alb and Ag85A within HCD NPs.

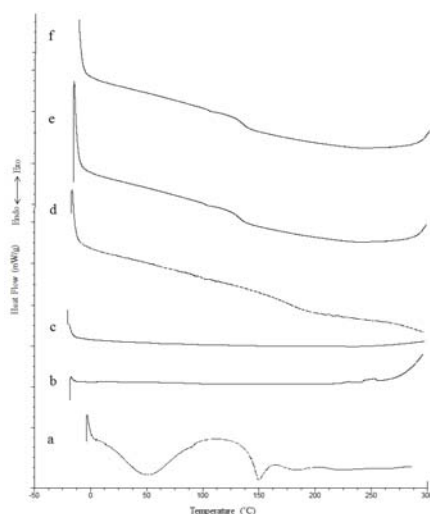


**Figure 9.4:** DSC Thermograms of – a) O-alb; b) Chitosan; c) HCD; d) HCD-O-alb physical mixture; e) HCD-O-alb NPs; f) HCD-Ag85A NPs

#### 9.13.3.2 X-ray powder diffraction

X-ray diffractograms of pure chitosan, pure HCD, blank HCD NPs and HCD-Ag85A NPs are displayed in figure 9.5. A characteristic broader peak of moderately low intensity for parent chitosan (chitosan >5K) was observed at around 20°, whereas HCD showed a sharp

peak of higher intensity at  $20^\circ$ . In addition to this, a new peak of higher intensity below  $2\theta$  value of 8 was also observed in the XRD spectra of HCD. These results are resembling to those reported by Tien et al., which suggested a more crystalline and stable structure of HCD attributed to the hydrophobic side chains as compared to the parent chitosan (Tien et.al., 2003). A broad diffuse peak was observed from the XRD spectra of blank HCD NPs and Ag85A encapsulated HCD NPs, which may be due to presence of HCD NPs and HCD-Ag85A nanoparticles in amorphous form. The reduction in the intensity of crystalline peak of HCD NPs suggested molecular dispersion and matrix formation of HCD NPs. Similar results without any extra peak implicative of Ag85A in XRD of HCD-Ag85A NPs indicated the molecular dispersion of Ag85A and hence successful formulation of Ag85A loaded NPs from HCD. This confirms the suitability of modified chitosan (HCD) for the preparation of NPs for the encapsulation of Ag85.

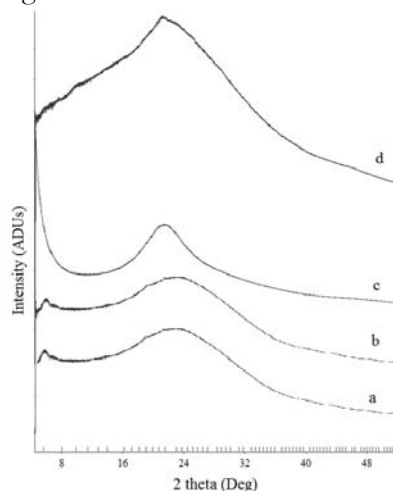


**Figure 9.5:** X-Ray Diffractograms of – a) HCD-Ag85A NPs; b) Blank HCD NPs; c) HCD; d) Chitosan

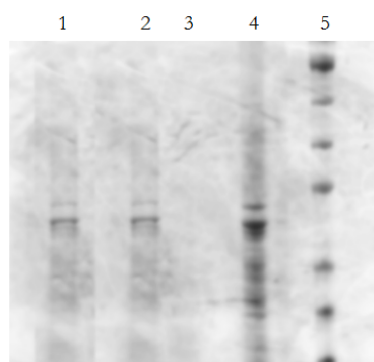


**Figure 9.6:** SDS-PAGE analysis of HCD-Ag85A NPs, 1) HCD-Ag85A NPs after 2 months of storage ; 2) HCD-Ag85A NPs; 3) Blank HCD-NPs; 4) Native Ag85A; 5) Protein Marker

### 9.14 SDS-PAGE analysis of HCD-Ag85A and its structural integrity

Ag85A encapsulated HCD NP formulations was characterized by performing Sodium dodecyl sulfate polyacrylamide gel electrophoresis (SDS-PAGE) of plane Ag85A, blank HCD NPs and Ag85A loaded HCD nanoparticle formulation and compared with the

standard protein marker, in order to identify Ag85A based on molecular weight which is carried on SDS PAGE. Results of this study are pictured in figure 9.6. Figure displays a band of protein marker (5), native antigen (4), Blank HCD NPs (3), HCD-Ag85A NPs (2) and HCD-Ag85A NPs after 2 months (1). The electrophoretic mobility of Ag85A from the HCD NPs was found to be excellent based on the quality of band observed after SDS-PAGE analysis of the entrapped Ag85A (Lane 2), whereas the lane where blank HCD NPs was run showed absence of Ag85A band. Similarly, lane 1 represents a band of Ag85A from the HCD NPs formulation, which was stored in a desiccator at room temperature of 15-20°C. Matching band in the lane 1 as compared to the one observed in lane 2 suggests the stability of Ag85A in HCD NPS at room temperature. Resembling intensity of the bands (lane 1 and 2) also indicates similar concentration of Ag85A during the course of storage (Fig 8.6). In addition, there may not be any molecular weight aggregates or fragments larger or smaller than the molecular weight of 32 kDa (Ag85A) due to absence of any kind of extra bands in the lane 1 and 2. This suggests retention of structural integrity of Ag85A after its encapsulation in HCD NPs and even after storage of HCD-Ag85A NPs for 2 months at ambient temperature of 10-15 °C. Based on the results obtained, no chemical modification, non-covalent aggregation or significant degradation of Ag85A occurred either during the process of nanoparticle formation or after 2 months storage at ambient temperature (10-15 °C).

### 9.15 In-vitro Pulmonary Deposition using Twin Stage Impinger (TSI)

Considering the benefices of pulmonary delivery in MTB, we chose to nebulize HCD-Ag85A NPs. FITC-HCD NPs were prepared and used for the nebulization study to find out the in-vitro pulmonary deposition behavior of nanoparticles using Twin Stage Impinger (TSI).

FITC-HCD NPs (2 mg) were dispersed in deionized water and nebulized using PariBoy air-jet nebulizer with compressed air using an Inhaler Boy compressor. The data obtained after nebulization of FITC-HCD-Rif NPs using TSI is tabulated in Table 9.6. Nebulization studies demonstrated moderate deposition ( $16.77 \pm 0.94 \mu\text{g}$ ) of FITC-HCD NPs in Stage 2 of the TSI, which corresponds to  $31.51 \pm 1.77 \%$  of FITC-HCD NPs suggesting that specified percentage of FITC-HCD NPs ( $31.51 \pm 1.77 \%$ ) had effective particle size below  $6.8 \mu\text{m}$ . This indicates that respirable fraction of the FITC-HCD NPs was around  $31.51 \pm 1.77 \%$  of the delivered dose. Certain amount of formulation was also noted at the device, even after tapping of the device with finger, therefore combined amount of FITC-HCD NPs in the device and throat are reported. Thus, maximum deposition of the formulation was found to be at the device and throat ( $7.08 \pm 1.83 \mu\text{g}$  at device and  $15.58 \pm 0.82 \mu\text{g}$ ) collectively which comes about  $42.57 \pm 4.99 \%$ . About  $7.08 \pm 1.83 \mu\text{g}$  of FITC-HCD NP was quantified in the device. Various parameters to determine the aerosolization of FITC-HCD NPs were calculated. Nebulization efficiency of the HCD-Rif NPs was calculated to be  $74.07 \pm 0.74 \%$  of the total amount of dose of formulation delivered, out of which  $31.51 \pm 1.77 \%$  of the dose was detected as respirable fraction (Table 9.6). Results of nebulization suggested the deposition of HCD-NPs in the lower respiratory tract. The results of the given study comply with the pharmacopoeial standards (British Pharmacopoeia, 2012).

**Table 9.6:** Parameter for Pulmonary Deposition of FITC-HCD NPs as Measured by TSI

Batch	Product Name	Inhaled Dose ( $\mu\text{g}$ )	Dose Delivered ( $\mu\text{g}$ )	FPD ( $\mu\text{g}$ )	NE %	RF (%)	FPF (%)
Batch 2	FITC-HCD 02 NPs	53.23	39.43 $\pm$ 0.39	16.77 $\pm$ 0.94	74.07 $\pm$ 0.74	31.51 $\pm$ 1.77	43.45 $\pm$ 1.02

( $\pm$  SD,  $n = 3$  - Mean  $\pm$  Standard Deviation) ; NE - Nebulization efficiency; RF - Respirable fraction; FPF - Fine particle fraction; FPD – Fine particle dose.

### 9.16 In-vitro release studies

The cumulative percentage release of Ag85A from HCD-Ag85A NPs showed biphasic release pattern (figure 9.7). Initially, burst release of Ag85A within first 2 hrs of study (28.14 $\pm$ 2.05 %) from HCD NPs was noted. As per Gan et al. the burst is more likely due to rapid release of surface associated protein. Therefore, burst release of Ag85A may be attributed to immediate dissolution of surface adsorbed Ag85A upon contact with SLF. Release study demonstrated biphasic release pattern with sustained and steady release of Ag85A over the entire period of study up to 48 hr. Initially sustained release phase was observed until 12 hr, followed by a steady and slow drug release. In the initial phase, 48.15 $\pm$ 7.52 % of the Ag85A was released from HCD-Ag85A NPs by the end of 8 hrs. This phase of release may be due to combined contribution of dissolution and passive diffusion of Ag85A from the matrix of HCD NPs. Thereafter, second phase lasted over the period entire of study with the 77.01 $\pm$ 4.44 % of Ag85A release by the end of 48 hrs. During this phase, there could have been penetration of aqueous release medium (SLF pH 7.4) into the hydrophobic polymeric matrix leading to slow dissolution and thereby diffusion of the drug from the HCD NPs. In addition, continuous declining concentration of Ag85A might have caused reduced concentration gradient, leading to less amount of Ag85A to be available for release. In sum, biphasic release of Ag85A from the HCD NPs with sustained release of Ag85A was observed. These results were found to be in agreement with the observation described by Klari  et. al., (Klari  et.al., 2012).

Release profiles obtained were fitted using various mathematical models such as zero order, first order, Higuchi, Hixon Crowell and Korsmeyers Peppas to understand the kinetics of Ag85A release from HCD nanoparticles (Costa et. al., 2001). The results of different model fittings are given in Table 9.7. Amongst various models tested, the curve fitting of release data to Higuchi square root model showed higher value for correlation coefficient ( $r^2=0.9516$ ), indicating dominant diffusion mechanism for the release of Ag85A from HCD NPs. In addition, release data showed model fitting to Korsmeyers and Peppas model ( $r^2$  value of 0.9749) (Costa et. al., 2001) and suggested anomalous transport (non-fickian) mechanism for the release of Ag85A based on the ‘n’ value of 0.3023, which is  $0.5 < n < 1$  ( $R^2$  value of 0.9749). This is indicated that both the models viz. Higuchi and Korsmeyers and Peppas model satisfactorily represented the data owing to diffusion of Ag85A from NPs.

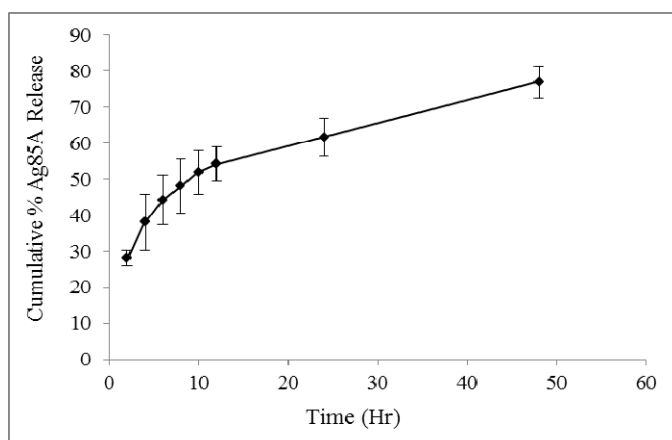


**Figure 9.7:** Cumulative % release of Ag85A from HCD-Ag 02 NPs.  
(*n* = 3 determinations  $\pm$ SD)

**Table 9.7:** Kinetics model fitting of in vitro release data of HCD-Rif NPs

Model	R <sup>2</sup>	Slope	Intercept
Zero order	0.85	0.899	32.67
First order	0.5884	0.0065	1.6438
Higuchi Square root	0.9516	8.1863	22.66
Hixon- Crowell	0.7568	0.021	3.3657
Korsemeyer Peppas	0.9749	0.3023 (n)	1.3937

### 9.17 Stability Studies

Results of the study showed no significant difference in particle size of HCD-Ag85A NPs (241.63 $\pm$ 8.35 nm) after 1 month stability, whereas increased particles size (289.43 $\pm$ 14.27 nm) was observed by the end of 2 months storage at RT (Table 9.8). Particle size was increased after 2 months storage at 10-15 °C. Increase in the particle size may be attributed to agglomeration of the NPs during the storage period. Results of the SDS-PAGE analysis showed similar band intensity of Ag85A in the HCD-Ag85A NPs immediately and after the storage of 2 months period, indicating resembling concentration of the AG85a in NPs.

**Table 9.8:** Stability of HCD-Ag85A NPs at RT (10-15 °C)

Sr. No	Time (Months)	MPS (nm)	PDI
1	Initial	241.5333 $\pm$ 1.17	0.222 $\pm$ 0.011
2	1	241.63 $\pm$ 8.35	0.253 $\pm$ 0.046
3	2	289.43 $\pm$ 14.27	0.372 $\pm$ 0.069

**n=3 determinations,  $\pm$  SD values**

### References

- Application brief, (1986) Thermal Denaturation of proteins I, effects of salt, sugars additives and pH. Hitachi Hitech Science Corporation. TA No. 31, July 1986.
- Aranaz I., Harris R., and Heras A. (2010) Chitosan Amphiphilic Derivatives. *Chemistry and Applications, Current Organic Chemistry*, 14, 308-330.
- Borges O., Borchard G., Verhoef J.C., De Sousa A., Junginger H.E. (2005) Preparation of coated nanoparticles for a new mucosal vaccine delivery system. *International Journal of Pharmaceutics*, 299, 155–166.
- British Pharmacopoeia (2012) Appendix XII C. Consistency of Formulated Preparations, *British Pharmacopoeia Volume V*, British Pharmacopoeia, 2012 online.
- Costa P., Lobo J. (2001) Modeling and comparison of dissolution profiles, *European J. of Pharm. Sci.*, 13, 123–133.
- Desai, T.R., Hancock, R.E.W., Finlay, W.H., 2002. A facile method of delivery of liposomes by nebulization. *J. Control. Release*, 84, 69–78.
- Grenha A. (2012) Chitosan nanoparticles: a survey of preparation methods. *J. Drug Target.*, 20 (4), 291-300.
- Huang Y., Yu H., Guo L., Huang Q. (2010) Structure and Self-Assembly Properties of a New Chitosan-Based Amphiphile, *J.Phys.Chem. B*, 114, 7719-7726.
- Holzer M., Vogel V., Mäntele W., Schwartz D., Haase W., Langer K. (2009) Physico-chemical characterisation of PLGA nanoparticles after freeze-drying and storage. *European Journal of Pharmaceutics and Biopharmaceutics*, 72, 428–437.  
<http://www.hitachi-hitech-science.com> (Assessed on July 2013)
- Huang, M., Ma, Z., Khor, E., & Lim, L. Y. (2002). Uptake of FITC-chitosan nanoparticles by A549 cells. *Pharmaceutical Research*, 19(10), 1488–1494.
- Jia X., Chen X., Xu Y., Han X., Xu Z. (2009) Tracing transport of chitosan nanoparticles and molecules in Caco-2 cells by fluorescent labeling. *Carbohydrate Polymers*, 78, 323–329.
- Klariæ D., Hafner A., Zubèia S., Dürriql M., and Filipovia-Grèia J. (2012) Spray-dried Microspheres Based on Chitosan and and Lecithin Cyclosporin A Delivery System. *Chem. Biochem. Eng. Q.* 26, 4, 355–364.
- Li H-Y., Seville P.C. (2010) Novel pMDI formulations for pulmonary delivery of proteins, *International Journal of Pharmaceutics*, 385, 73–78.
- Li Y., Zhang S., Meng X., Chen X., Ren G. (2011) The preparation and characterization of a novel amphiphilic oleoyl-carboxymethyl chitosan self-assembled nanoparticles, *Carbohydrate Polymers*, 83, 130–136.
- Liu J., Gongta T., Fu H., Wang C., Wang X., Chena Q., Zhang Q., Hea Q., Zhang Z. (2008) Solid lipid nanoparticles for pulmonary delivery of insulin. *Int. J. Pharm.* 356, 333–344.

## Chapter 9 - Preparation of HCD-Ag85A Nanoparticles

---

Lu D. (2007) *Aerosol Delivery of Recombinant Antigen 85B in Microparticle Vaccine Systems for Protection against Tuberculosis*, Chapel Hill, NC. PhD Dissertation.

Ma G., Yang D., Zhou Y., Xiao M., Kennedy J.F., Nie J. (2008) Preparation and characterization of water-soluble N-alkylated chitosan. *Carbohydrate Polymers*. 74, 121–126.

Marques M.R.C., Loebenberg R., and Almukainzi M. (2011) Simulated Biological Fluids with possible application in Dissolution Testing/. *Dissolution Technologies*, August, 15-28.

Matilainen, L., Järvinen, K., Toropainen, T., Näsäi, E., Auriola, S., Järvinen, T., Jarho, P., 2006. In vitro evaluation of the effect of cyclodextrin complexation on pulmonary deposition of a peptide, cyclosporin A. *Int. J. Pharm.* 318, 41-48.

Tien C.L., Lacroix M., Ispas-Szabo P., Mateescu M. (2003) N-acylated chitosan: hydrophobic matrices for controlled drug release, *Journal of Controlled Release*, 93, 1, 1-13.

Zong Z., Kimura Y., Takahashi M., Yamane H. (2000) Characterization of chemical and solid state structures of acylated Chitosans. *Polymer*. 41, 899–906.

Gan Q., Wang T. (2007) Chitosan nanoparticle as protein delivery carrier—Systematic examination of fabrication conditions for efficient loading and release *Colloids and Surfaces B: Biointerfaces* 59 (2007) 24-34.

### 10.0 Preparation of HCD-Rif Nano Spray Dried Powder for Inhalation

#### 10.1 Materials

Rifampicin was purchased from Sigma-Aldrich (St-Louis, USA). Chitosan oligosaccharide (MW > 5kDa; degree of deacetylation (DDA) 80-90%) was supplied by Kitto Life Co. Ltd. (Kyongki-Do, Seol Korea). Cellulose dialysis tubing (Molecular weight cut of 12-14000 Da, 5000 Da) were purchased from Medicell international Ltd., (London, UK). Dimethyl sulfoxide (DMSO, anhydrous), Octanoyl chloride, methane sulfonic acid, sodium stearate, sodium bicarbonate were obtained from Sigma-Aldrich (St-Louis, USA). Acetonitrile, methanol, ethanol, chloroform, dichloromethane (DCM), acetone etc. and all other HPLC grade solvents were obtained from Sigma-Aldrich (St-Louis, USA).

#### 10.2 Equipments

1. High speed magnetic stirrer (FisherBrand, Loughborough, UK)
2. Nano spray Dryer B-90 (Buchi, Oldham, UK)
3. UV-VIS Spectrophotometer (Jenway UV/Vis Spectrophotometer, Staffordshire, UK)
4. Fourier Transform Infra-red spectrophotometer (FTIR) (Perkin Elmer, MA, USA)
5. Differential Scanning Calorimeter DSC Q 2000, (TA Instruments, New Castle, UK)
6. Zetasizer, Nanoseries Instrument (Nano 25, Malvern Instruments, Worcestershire, UK)
7. Laser diffraction using HELOS particle size analyzer (Sympatech Inc., Lawrenceville, NJ, USA)
8. Scanning Electron Microscope (FEI XL30 TMP, Philips, Netherlands)
9. X-Ray Diffractometer (Oxford Diffraction Xcalibur novaT X-ray diffractometer; Oxford Diffraction Ltd., Abingdon, UK)
10. HPLC system (1200 series, Agilent Technologies, Berkshire, UK)
11. Next Generation Impactor (Copley, Nottingham, UK)

#### 10.3 Preparation of nano-spray dried powder for inhalation (NSDPI)

Preparation of powder in the form of nano sized particles was carried out by the Nano Spray dryer B-90 (Buchi, UK). To obtain drug loaded particles, 50 mg of HCD was accurately weighed and dissolved in 20 ml of methanol. To it, 25 mg of rifampicin was dissolved and batches were prepared with and without addition of sodium stearate (2 mg, 4 % w/w calculated based on the weight of HCD). Excipients and rifampicin was dissolved in methanol, stirred to produce a clear solution and subjected for nano spray drying (B-90 Nano Spray Dryer, Buchi, UK). At the same time, rifampicin alone was also spray dried by preparing a solution of rifampicin (25 mg) in specified volume of methanol. For the purpose of spray drying, mesh of 7.0  $\mu\text{m}$  was used along with 60 Hz ultrasonic frequency for the actuator. The product obtained was collected and weighed to determine the yield.

The Nano Spray Dryer B-90 was operated in a closed-mode configuration, where instrument was connected to a cooling unit, the Inert Loop B-295 in order to have safe operation of solvents. Inert gas (Nitrogen) was used at 1.5 bars to prevent explosion of gas mixture and

## Chapter 10 - Preparation of HCD-Rif particles by NSD

an electric field was generated using CO<sub>2</sub> gas at 1.5 bars for separation of the particles. The following operating conditions for the experiments were selected from the reports of Gautier et. al., and kept constant at: the drying gas flow rate – 120 l/min; Inlet temperature - 80 °C ; Outlet temperature – 61 °C ; Head temperature – 94 °C; Pressure – 39mbar ; Spray rate – 100 % ; Spray mesh - 7.0 µm (Gautier et.al., 2010). Figure 10.1a-c displays nano spray dryer used for the current study, spray pattern through nozzle and representative SEM image as per Buchi.

All the experiments were carried out in dark conditions considering light sensitivity of rifampicin.

### 10.3.1 Principle of Nano Spray Dryer B-90

Nano Spray Dryer B-90 is 4<sup>th</sup> generation of laboratory scale spray dryer. Unlike conventional spray dryers, atomization in Nano Spray Dryer B-90 occurs through piezoelectric crystal driven actuator (vibrating mesh technology), which triggers vibration of a thin, perforated, stainless steel membrane placed in a small spray cap for generation of the droplets. Spray caps are made up of different mesh size (4.0, 5.5 and 7.0 µm) in order to manipulate the average droplet size between 8 and 21 µm. It can be operated in open mode (aqueous solvent) or closed mode (organic solvent) depending upon the solvent used for sample dissolution. The liquid sample (either organic/aqueous solution or dispersion) is fed through a peristaltic pump at the desired flow rate and actuator is driven using ultrasonic frequency, which further activates the vibration of thin membrane leading to expulsion of continuous mist of precisely sized droplets per second with very narrow size distribution. At the same time, drying gas enters in laminar flow from the top of the instrument into the drying chamber and is heated up to the set inlet temperature, which helps the ultra-fine droplets to dry into solid particles. These extremely fine solid particles are then electrostatically charged (by dry N<sub>2</sub> and CO<sub>2</sub> gases) and deposited at the surface of the collecting electrode. Finally the resulting powder deposited is collected using a rubber spatula.

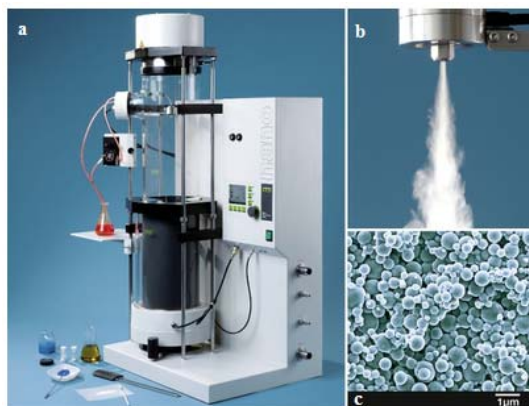


**Figure 10.1:** Buchi B-90, Nano Spray Dryer; a) Nano spray dryer; b) spray pattern produced by nozzle; c) representative SEM image

### 10.3.2 Drug loading (DL) and encapsulation efficiency (EE)

The drug entrapped in the NPs was determined using UV spectrophotometer. Known amount of drug loaded Nano spray dried powder was dissolved in methanol to dissolve the particles and small amount of water was added to precipitate the polymer. Resultant suspension was filtered through a sterile 0.22  $\mu\text{m}$  filter (Millex-MP, Millipore, Carrigtwohill, Ireland) and the concentration of rifampicin in the filtrate was determined using UV-VIS spectrophotometer (Jenway UV/Vis Spectrophotometer, Staffordshire, UK) at 475 nm (Benetton et.al., 1998). The analysis was carried out in triplicate for each batch of drug loaded NPs. The drug loading and entrapment efficiency was calculated using following formulae:

$$\text{Yield (\%)} = \frac{\text{Weight of NP recovered}}{\text{Weight of Drug, polymer and excipients}} \times 100$$

$$\text{Drug Loading (\%)} = \frac{\text{Weight of Rif in NP}}{\text{Weight of NP recovered}} \times 100$$

$$\text{Entrapment Efficiency (\%)} = \frac{\text{Weight of Rif in NP}}{\text{Weight of Rif fed initially}} \times 100$$

### 10.3.3 Particle size and zeta potential

The particle size and zeta potential of the particles was measured by dynamic light scattering (DLS) and laser doppler velocimetry (LDV) respectively using Zetasizer, Nanoseries Instrument (Nano 25, Malvern Instruments, Worcestershire, UK). The particles were redispersed in deionized water and sonicated in bath sonicator for 5 min and the particle size and zeta potential of resultant samples was determined.

### 10.3.4 Shape, surface morphology and Solid state characterization

The shape and surface morphology of the nanoparticles was evaluated by Scanning Electron Microscopy (SEM) (FEI XL30 TMP, Philips, Netherlands).

DSC measurement of rifampicin, HCD and drug loaded nano spray dried nanoparticles (Rif-NSD) was carried out to determine thermal behavior and crystallinity of the formulations using DSC instrument (DSC Q 2000, TA Instruments, USA). Similar parameters and cycle were used for DSC study of HCD nano spray dried powder as mentioned in chapter 5. NSD powders were also characterized using X-ray powder diffractometer (Oxford Diffraction Xcalibur novaT, UK)

### 10.3.5 Powder characterization using Sympatec

The volume median diameter of the nano spray dried powder was measured by laser diffraction using HELOS particle size analyzer incorporating RODOS dry powder dispersing unit (Sympatec Inc., Lawrenceville, NJ, USA) at an adopted pressure of 4 mbar. Approximately 5-10 mg of each powder sample was taken and studies were carried out in triplicate. The results were recorded using HELOS system and data obtained was expressed as the volume weighted mean particle size. The span of the volume distribution, a measure of

## Chapter 10 - Preparation of HCD-Rif particles by NSD

the width of the volume distribution relative to the median diameter ( $D_{v50}$ ), was derived from equation given below –

$$\text{Span} = \frac{D_{v90} - D_{v10}}{D_{v50}}$$

Where,  $D_{v10}$ ,  $D_{v50}$  &  $D_{v90}$  stands for the diameter sizes of a given percentage of particles smaller than the specified size. A high value for the SPAN is an indication for wider particle size distribution.

### 10.4 In-vitro aerosolization & lung deposition using Next Generation Impactor (NGI)

The deposition of particles in the lung was evaluated using NGI (Copley, UK). A vacuum pump connected to NGI was operated at a flow rate of 60 ml/min which was calibrated using flow meter (Copley, UK). Five capsules were filled with approximately 3-5 mg of nano spray dried powder. The filled capsules were then inhaled through mouth piece for 6 sec. at room temperature. The amount of rifampicin retained in the inhaler mouthpiece and deposited in each stage of the NGI was determined using HPLC (Agilent Technologies 1200 series) at a wavelength of 335 nm (Tatarczak et.al., 2006). The mass median aerodynamic diameter (MMAD) and geometric standard deviation (GSD) were calculated after plotting cumulative amount of drug deposited in each stage of the NGI *vs* their corresponding aerodynamic diameter using log probability paper as shown in equation below. Emitted dose (ED) and fine particle fraction (FPF) were calculated using following equations for ED and FPF. Each measurement was carried out in triplicate and the average values are reported.

$$\text{MMAD} = D_v 50 \%$$

$$\text{GSD} = \sqrt{\frac{84.1 \% \text{ undersize}}{15.9 \% \text{ undersize}}}$$

$$\text{ED} = \frac{\text{Amt. of Rif recovered in NGI}}{\text{Amt. of Rif initially loaded}}$$

$$\text{FPF} = \frac{\text{Amt. of Rif recovered in NGI from stage 3 to filter}}{\text{Amt. of Rif initially loaded}}$$

### 10.5 In-vitro release studies

*In-vitro* release studies of rifampicin from HCD nanoparticles was carried out in dark by dialysis method using modified release technique (Marques et. al., 2011). Simulated lung fluid (SLF) (pH 7.4) with 200  $\mu\text{g}/\text{ml}$  of ascorbic acid (as an antioxidant to prevent oxidative degradation of rifampicin) was used as dissolution media. A known amount of Rif loaded NSD powder formulation dispersed in SLF was taken in dialysis membrane (3.5 kDa molecular weight cut-off, Medicell International Ltd., Liverpool, UK). The membrane was sealed using dialysis tubing clamps and placed in a beaker containing 25 ml of SLF as external release media under stirring at 37°C. At selected time intervals, aliquots were

withdrawn from the external media, diluted as required and analyzed by HPLC (Agilent Technologies 1200 series) at 335 nm (Tatarczak et.al., 2006). After the aliquots were withdrawn, media was replenished with the same amount of blank media in order to maintain sink condition. A calibration curve was prepared prior to the start of dissolution using a SLF (correlation coefficient was 0.9993). The results were plotted as percent cumulative drug release *vs* time. The experiment was done in triplicate and reported as  $\pm$  standard deviation.

### 10.5.1 HPLC analysis

The amount of rifampicin in samples obtained after studies using next generation impacter (NGI) and in-vitro release studies were determined by HPLC (1200 series, Agilent Technologies) equipped with a UV detector. The injection volume was 10  $\mu$ l. Chromatography was performed with a column (Ascentis C18, 150 x 4.6mm, 5 $\mu$ m, Supelco, Sigma-Aldrich, USA). Mobile phase composed of tetrahydrofuran (THF)/phosphate buffer (30/70 %) at a flow rate of 1.0 ml/min and a detection wavelength of 335 nm (Tatarczak et.al., 2006). The column temperature was set to 40 °C. The retention time of rifampicin was 3.5 min. Calibration curves for rifampicin (correlation coefficient was 0.9993) at concentrations varying from 5 to 80  $\mu$ g/ml was used for analysis.

### 10.6 Stability study

The stability of formulations was studied by storing samples in glass vials at room temperature (15-20 °C) under dark conditions for up to 2 months period. Samples were withdrawn and assessed for the drug content and particle size.

### 10.7 Statistical analysis

The experiments were performed in triplicate. The data presented in this study are expressed as the mean value  $\pm$  standard deviation.

## 10.8 Results and Discussion

### 10.8.1 Preparation of HCD nano spray dried powder for inhalation (NSDPI) and characterization

The aim of the current study was to investigate the feasibility of synthesized polymer (HCD) in the preparation of nanoparticles using nano spray drying technique. Nanoparticles were successfully prepared by nanospray drying method. The method was found to be simple and efficient in order to prepare dry powder formulation. Two batches of HCD nano spray dried (NSD) powder formulations were prepared (HCD-Rif and HCD-Rif-NaSt) with or without sodium stearate (4% w/w, calculated on weight basis of HCD), as it is known that sodium stearate is tend to enhance aerosolization property of particles (Parlati et al., 2009). Similarly, rifampicin alone was also nano spray dried for comparison. The solvent selection in the process of spray drying is considered to be important step because of its control over inlet spray-drying temperature and influence on the drug loading. Methanol was selected for the solubilization of HCD and Rif as both the materials were freely soluble in methanol and hence it was chosen as the appropriate organic solvent.

Percent process yield of the nanospray dried particles was found to be in the range of 30 -55 %. Highest yield of  $55.42 \pm 1.87\%$  was obtained from batch NSD 1, which was made up of HCD and rifampicin. However, addition of sodium stearate as adjunct in the preparation of NSD decreased the yield of particles ( $44.95 \pm 1.08$ ). NSD powder prepared using rifampicin alone (batch NSD 0) showed lowest yield among formulations tested. This may be attributed to hygroscopicity of the rifampicin, which led to the adherence of the powder onto the walls of collecting chamber. Moreover, hygroscopic nature of rifampicin made it difficult to scratch off the powder from collecting chamber leading to low yield. The yields obtained after nano spray drying of HCD+Rifampicin and HCD+Rifampicin+Sodium stearate were found to be  $55.42 \pm 1.87$  and  $44.95 \pm 1.08$  % respectively. These results are in agreement with the data published by Gautier et. al. (Gautier et al., 2010), where they reported high yield with large sample size. Data for percent drug loading and entrapment efficiency are tabulated in table 10.1.

**Table 10.1 : Percent yield, Drug loading and Entrapment efficiency**

Batch	Product Name	Yield (%)	DL (%)	EE (%)	MPS ( $\mu\text{m}$ )	PDI	ZP (mV)
NSD 0	Rif NSD	$25.44 \pm 1.14$	---	$25.44 \pm 1.14$	--	--	--
NSD 1	HCD-Rif NSD	$55.42 \pm 1.87$	$26.7 \pm 2.29$	$44.31 \pm 2.39$	$4.37 \pm 0.46$	> 0.5	$8.91 \pm 1.27$
NSD 2	HCD-Rif-NaSt NSD	$44.95 \pm 1.08$	$20.22 \pm 1.94$	$27.96 \pm 2.05$	$4.58 \pm 0.22$	> 0.5	- $70.4 \pm 1.63$

*± SD of three determinations; Rif – Rifampicin; DL – Drug Loading; EE – entrapment efficiency; PS – particle size; PDI - poly dispersity index; ZP – zeta potential.*

### 10.8.2 Particle Size analysis of HCD NSDPI

Particle size analysis was carried out by dynamic light scattering (DLS) using Zetasizer, Nanoseries Instrument (Nano 25, Malvern Instruments, Worcestershire, UK). As dry powder was prepared using nano spray dryer, we expected size of particles in the nano range. However, it showed large particle size, which were in the microns range as shown in the table 10.2. Poly dispersity index (PDI) of the particles was also found to be high (> 0.5). In addition, we measured dry powder particle size by Sympatec, which gives good information about powder flowability based on the size distribution analysis. The particle size and density distribution curve of each formulation is presented in figure 10.2. Particle size analysis indicated that the NSD powder formulations had multi-modal size distribution within a size range effective for pulmonary delivery (1-5  $\mu\text{m}$ ). However, variations in size within and between the samples were observed. The particle size distribution curve of the nano spray-dried powdered formulation determined using sympatec (laser diffraction) is depicted in figure 10.2 and the particle size analysis parameters are summarized in Table 10.2. The data is expressed in terms of the particle diameter at 10, 50, and 90 % of the volume distribution ( $D_{V10}$ ,  $D_{V50}$  &  $D_{V90}$ , respectively). The span of the volume distribution, a measure of the

width of the volume distribution relative to the median diameter ( $D_{v50}$ ), was also determined. A high value for the SPAN is an indication for wider particle size distribution. Span values for both the formulations (HCD-Rif and HCD-Rif-NaSt NSD) were found to be small indicating no particle aggregation and unimodal particle size distribution. It was observed that 50<sup>th</sup> and 90<sup>th</sup> percentile undersize ( $D_{v50}$  &  $D_{v90}$ ) was found to vary in batch NSD1 and NSD2. Nevertheless, respirable particle size was obtained from both the batches NSD1 (without sodium stearate) and NSD2 (with sodium stearate).  $D_{v50}$  &  $D_{v90}$  values of NSD batch 1 were found to be  $1.73 \pm 0.02$  ( $D_{v50}$ ),  $4.61 \pm 0.1$  ( $D_{v90}$ )  $\mu\text{m}$  respectively, whereas these values were found to be increased in the formulation containing sodium stearate ( $2.91 \pm 0.04$  ( $D_{v50}$ ) &  $6.64 \pm 0.89$   $\mu\text{m}$  ( $D_{v90}$ )). It was expected that, sodium stearate should improve the aerosolization of NSD powders. However, no significant difference in the powder properties was observed in NSD1 and NSD2. But little improvement in powder properties in terms of particle aggregation and distribution was noted based on the smaller span values of batch NSD2 ( $1.93 \pm 0.27$ ) as compared to NSD1 ( $2.42 \pm 0.45$ ).

Zeta potential observed for the batch NSD 1 was on the positive side (table 10.2), indicating that NSD particles may have retained inherent nature of chitosan even after preparation of HCD and its spray dried powder formulation and could be beneficial in-vivo while interacting with the cells due to negatively charged cell surface. However, addition of sodium stearate in the HCD-Rif formulation led to transformation of zeta potential to extreme negative side with the value of  $-70.4 \pm 1.63$ . This may be attributed to the localization of negative ions on the surface of particles. It is well known that, dissociation of sodium stearate ( $\text{CH}_3(\text{CH}_2)_{16}\text{COO}^- \text{Na}^+$ ) in water leads to  $\text{RCOO}^-$  and  $\text{Na}^+$  ions. The  $\text{RCOO}^-$  ions consists of two parts, one, a long hydrocarbon chain R (non polar 'tail') which is hydrophobic, and another  $-\text{COO}^-$  (polar ionic 'head'), having hydrophilic nature. Therefore, once particles coated with sodium stearate dispersed in water,  $\text{RCOO}^-$  ions present on the surface projects  $-\text{COO}^-$  groups in water and the hydrocarbon chains R stays away from it. Based on this assumption, it can be devised that negative charge of HCD-Rif-NaSt could be due to ionization of sodium stearate leading to arrangement of negatively charged groups in water upon dispersion of particles in water. Similar results were published by Song et. al., where they reported change in the potential from positive to negative with increase in the concentration of surfactant (sodium stearate). They also noticed increase in zeta potential at higher concentration of about 4 % w/w and suggested it may be due to compression of electrical double layer by excess of sodium ions resulting into increased ionic strength of the medium (Song et.al., 1997).

### 10.8.3 Morphology of HCD NSDPI

Scanning electron microscopy (SEM) was used to visualize the size, shape, and surface morphology of nano spray dried particles. Scanning electron micrographs of pure rifampicin and nanospray dried powder formulations are shown in figure 10.3 (a, b, c, d). NSD powders showed symmetrical shape and smooth surface morphology. From the micrographs it can be noted that, the presence of adjunct (NaSt) did not affect particle geometry or morphology as no substantial difference was observed between the three formulations.

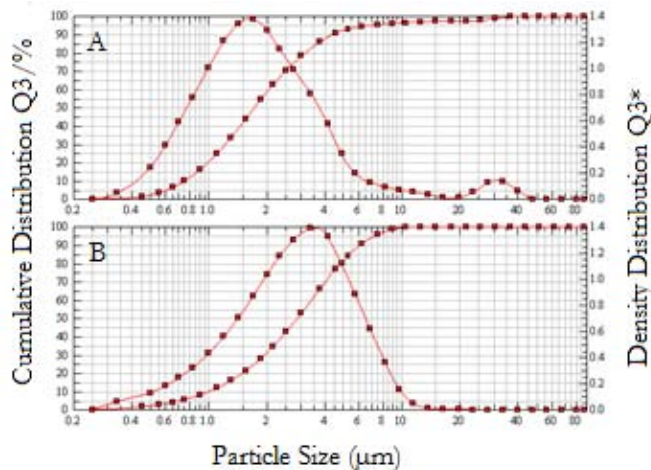


Figure 10.2: Particle size distributions of nano spray dried particles -  
 A) HCD-Rif NSD; B) HCD-Rif-NaSt NSD

Table 10. 2: Particle Size Distribution Data of Dry Powders Analyzed by Sympatec

Batch	Product Name	D <sub>10</sub> (µm)	D <sub>50</sub> (µm)	D <sub>90</sub> (µm)	Span
NSD 1	HCD-Rif NSD	0.76±0.01	1.73±0.02	4.61±0.26	2.42±0.45
NSD 2	HCD-Rif-NaSt NSD	1.01±0.04	2.91±0.04	6.64±0.89	1.93±0.27

(± SD, n = 3)

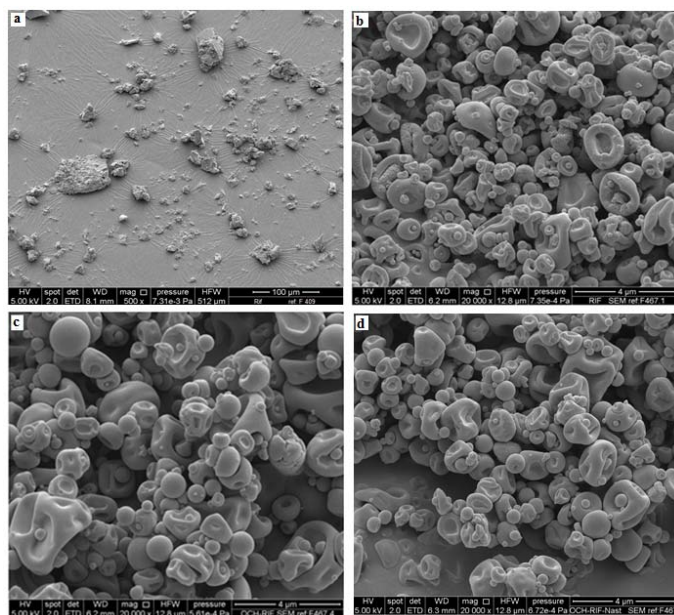


Figure 10.3: Scanning Electron micrographs of ;  
 a) Rif as supplied; NSD powder of - b) Rif ; c) HCD-Rif ; d) HCD-Rif-NaSt

### 10.8.4 FTIR analysis

The result of the FTIR indicated that rifampicin (as purchased) showed a sharp peak at  $3,485\text{ cm}^{-1}$  corresponding to OH functional groups, bands near  $2,810\text{ cm}^{-1}$  representing N-CH<sub>3</sub> band, characteristic absorption band at about  $1,724\text{ cm}^{-1}$  for acetyl C=O, sharp peaks at  $1,641$  and  $1563\text{ cm}^{-1}$  representing the furanone C=O and amide C=O group, respectively. Moreover, a band at  $1255\text{ cm}^{-1}$  (-C-O-C- ether group) was also observed in the pure rifampicin FTIR spectra. The FTIR spectra of pure rifampicin, chitosan and HCD are presented in Figure 10.4.

FTIR spectra of HCD as mentioned in the synthetic part of this thesis (chapter 5) showed the presence of characteristic bands  $\sim$  at  $1740\text{ cm}^{-1}$ , (for octanoyl groups),  $1655\text{ cm}^{-1}$ , (carbonyl stretching of amide band I - secondary amides) and  $1555\text{ cm}^{-1}$  (N-H bending vibrations of the amide band II) (Tien et.al., 2003). In addition, a sharp increase in the intensity of the bands near  $2810\text{--}2980\text{ cm}^{-1}$  evidenced the introduction of alkyl substituent at the amino sites of chitosan and introduction of a new band at  $1457\text{ cm}^{-1}$  representing angular deformation of C-H bond.

FTIR spectral analysis of nano spray dried powder formulation indicated specific functional groups of HCD and rifampicin, similar to those observed in the FTIR spectra of pure HCD and rifampicin. Upon analyzing FTIR spectra of HCD-RIF NSD, a sharp peak at  $1643$  corresponding to the furanone C=O and another peak at  $1559\text{ cm}^{-1}$  for amide C=O group present in the rifampicin were observed. In addition, a characteristic band at around  $1250\text{ cm}^{-1}$  standing for -C-O-C- ether group and aromatic C-H bending representing at  $724\text{ cm}^{-1}$  can be clearly seen in the FTIR spectra of HCD-Rif-NSD formulation, which were otherwise completely absent in the native HCD. These results confirmed that there were no interaction between the drug and HCD during preparation of NSD powder. The intensity of bands in NSD powder were found to be smaller as compared to the bands observed in pure rifampicin spectra due to incorporation of rifampicin in the polymer matrix. Similar findings are reported in the literature by Rastogi et.al., (Rastogi et al.2007). Thus, the study suggests non-existence of any chemical interaction between functional group of HCD and rifampicin that could alter the chemical structure of the drug and hence they are found to be compatible with each other.

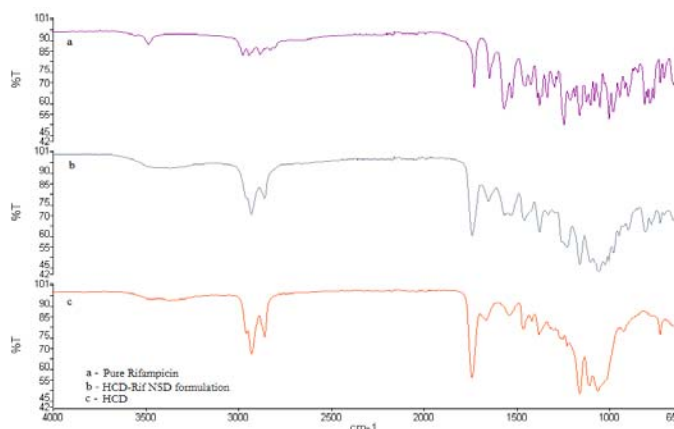


**Figure 10.4:** FTIR Spectra of - a) Rif; b) HCD; c) HCD-Rif NSD formulation

### 10.8.5 Solid state characterization of HCD-Rif nano spray dried powder

#### 10.8.5.1 Differential Scanning Calorimetry (DSC)

DSC thermograms of the pure rifampicin, chitosan, HCD, HCD-Rif physical mixture and NSD formulation are displayed in Figure 10.5. DSC thermogram of rifampicin showed a characteristic exothermic peak at 260°C. As discussed in the chapter 5, DSC studies of chitosan required two cycles of heating and cooling runs due to its moisture and thermal history. Accordingly we performed two runs, which helped to eliminate the effects of moisture absorption as observed in chitosan at round 100 °C (data not shown).

According to the reports published by Grant et.al., and Ma et.al., (Grant et.al., 1990; Ma et.al., 2008), chitosan yields an exothermic peak at around 300-320 °C due to decomposition of the acetyl and deacetylated units of chitosan. Similar trend with the shift of thermogram to higher temperature was observed by them for the acylated chitosan derivatives. In conformation with these results, this study demonstrated absence of exothermic peak in DSC thermogram of both chitosan and HCD upto 300 °C indicating enhanced thermal stability of the HCD between 20 to 300 °C., but an exothermic peak can be expected beyond 300°C for chitosan due to slight curvature in the thermograph, which could be an indication for the beginning of decomposition of chitosan from 260 °C. However, thermogram of HCD did not show such curvature may indicate that there could be shift in temperature for thermal decomposition of the crystalline regions of HCD suggesting improved thermal stability. In addition, absence of glass transition temperature in chitosan and HCD DSC thermograms was found to be in compliance with the reports published by Ma et.al., and Zong et al. (Zong et al. 2000; Ma et.al., 2008).

Physical mixture of HCD-Rif showed a clear peak at 260 °C corresponding to the thermal decomposition of rifampicin. However, no glass transition temperature (T<sub>g</sub>) was observed in physical mixture of HCD and rifampicin as observed in the thermograms of pure HCD. As we did not notice any endothermic or exothermic peak and T<sub>g</sub> in pure HCD thermographs, no endothermic or exothermic peak and T<sub>g</sub> was observed in the DSC thermographs of HCD-Rif NSD and HCD-Rif-NaSt NSD powders. Absence of peak for rifampicin in the DSC thermogram of HCD-Rif NSD and HCD-Rif-NaSt NSD powders indicated the molecular dispersion of rifampicin in the polymeric nanoparticle prepared by nano spray drying. The absence of exothermic peak for rifampicin (as observed in pure rifampicin) in HCD NSD powders confirmed the presence of rifampicin in its amorphous form HCD NSD powders. These results are also corresponding to the results obtained in FTIR studies (Figure 10.5).

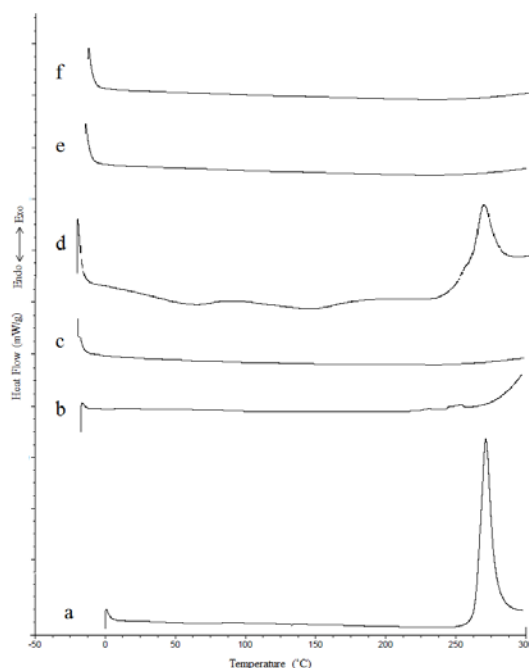


**Figure 10.5:** DSC Thermograms of – a) Rif; b) Chitosan; c) HCD; d) HCD+Rif physical mixture; e) HCD-Rif NSD formulation; f) HCD-Rif-NaSt NSD formulation

#### 10.8.5.2 X-ray powder diffraction

Figure 10.6 represents the X-ray diffractograms of pure rifampicin, sodium stearate, pure chitosan, HCD, HCD-Rif-NSD and HCD-Rif-NaSt NSD formulation. Powder X-Ray Diffractogram featured characteristics crystalline peaks for rifampicin form I at  $2\theta$  values of  $13^\circ$  and  $15^\circ$  indicating presence of rifampicin in crystalline form. Similarly, sodium stearate showed crystalline peaks at  $2\theta$  values of  $16^\circ$ ,  $20^\circ$  and  $23^\circ$ . As discussed in the chapter 5, similar results of XRD for parent chitosan and HCD was obtained. Tien et al., reported major change at  $19.4 \text{ \AA}$ , below  $2\theta$  value of 8, corresponding to more crystalline and stable organization of hydrophobic chitosan than the parent chitosan (Tien et al., 2003), which is induced by the hydrophobic side chains, thereby enhancing its stability. Results of this study also demonstrated low intensity peak for chitosan and exhibition of a new peak below  $2\theta$  value of 8 for HCD suggesting more crystalline nature of HCD than parent chitosan. X-Ray powder diffraction analyses of the nano spray dried samples as displayed in figure 10.6e also showed similar peak to that of HCD. However, the absence of crystalline peaks of rifampicin (as observed in figure 10.6a) in the HCD-Rif NSD formulation suggested the presence of rifampicin in amorphous form in the NSD formulations prepared by Nano Spray Drying method. Existence of diffuse peak in XRD observations are often consistent with spray drying of many organic materials, specifically those consisting of binary components (Corrigan et al., 2006; Parlati et al., 2009).

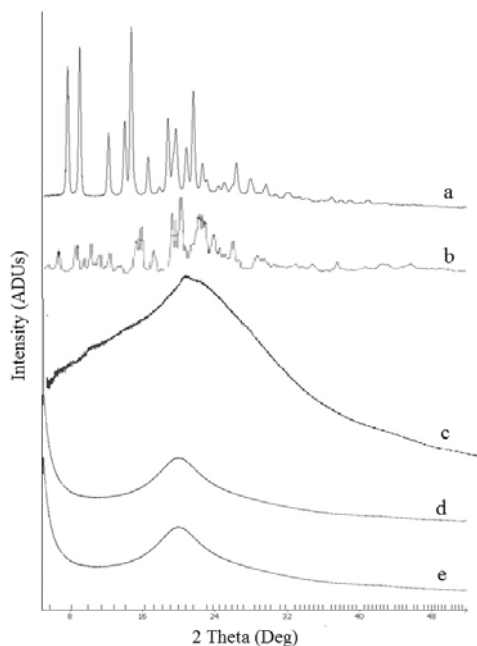


**Figure 10.6:** X-Ray Diffractograms of – a) Rif ; b) Sodium Stearate; c) Chitosan  
d) HCD; e) HCD-Rif NSD formulation

#### 10.8.6 In-vitro aerodynamic performance (Pulmonary Deposition)

The aim of current study was to maximize the concentration of rifampicin in the lung via dry powder inhalation therapy, which ultimately helps to reduce the systemic drug concentration and hence toxicity associated with it. In order to aerosolize dry powders, correct aerodynamic properties of particles are prerequisite so that dry powder can efficiently aerosolize to reach required sites of the lungs for uptake by the macrophages (a primary site of MTB localization) to combat TB. It is well known that a clonal population of *M. tuberculosis* localizes within the lung and forms multiple cavities leading to tissue necrosis and destruction of the lung (Vadwai et.al., 2011). Upon ingestion of MTB by the host, instead of its digestion by host macrophages, they proliferate and accumulate in the macrophages (Hirota and Terada, 2012). Thus, the delivery of particles having optimum size (median size 1–5  $\mu\text{m}$  required for peripheral lung deposition) containing antituberculosis agents in the form of dry powder inhalation to lungs would be effective for TB therapy.

In the view of this, aerodynamic characteristics of NSD powder formulations for inhalation was determined in simulated breathing conditions using next generation impactor (NGI). NGI is an instrument used to evaluate inhalation aerosol performance and determine its likely functioning in-vivo, upon inhalation of the product. Aerodynamic characteristics of the dry powders are evaluated based on the mass median aerodynamic diameter (MMAD) and by the in vitro fine particle fraction (FPF) representing the percentage of the emitted dose possessing aerodynamic diameter of 1-5  $\mu\text{m}$ . FPF determined by in-vitro techniques present great information for drug targeting to lungs, because inhaled infectious organism usually targets the lower respiratory tract and thus it becomes a primary site of infection that results from inhalation.

Deposition of NSD powder formulation as carried out using next generation impactor (NGI) is presented in figure 10.7, displaying the lung deposition (device & capsule, throat and NGI stages) of pure rifampicin, HCD-Rif NSD and HCD-Rif-NaSt NSD powder formulations after aerosolization. The in vitro respirability parameters are tabulated in Table 10.3. The measured fine particle fraction (FPF) for pure rifampicin, HCD-Rif and HCD-Rif-NaSt NSD powder formulation was found to be  $1.85 \pm 0.29\%$ ,  $52.92 \pm 2.92\%$  and  $54.33 \pm 3.21\%$  respectively (Table 10.3). The aerosolization and deposition of pure rifampicin without carrier system (HCD) showed poorest performance with the FPF of just  $1.85 \pm 0.29\%$  and highest MMAD of  $23.47 \pm 9.16$ , which may be attributed to the agglomeration of rifampicin due to absence of any lipophilic adjunct to enhance dispersibility. Very poor deposition properties after aerosolization of pure rifampicin was observed because more than 50% of the emitted dose was arrested well before the first stage of NGI which is corresponding to the particle size of more than  $8.06 \mu\text{m}$  (figure 10.7). Aerosolization of pure rifampicin showed highest deposition at device & capsule (DC) and throat ( $0.73 \pm 0.066$  and  $1.51 \pm 0.23$ ) suggesting cohesiveness of pure rifampicin powder.

In contrast to deposition of pure rifampicin from NGI studies, nano spray drying (NSD) of rifampicin with HCD significantly improved the powder dispersibility. HCD-Rif NSD powder formulation showed highest FPF of  $52.92 \pm 2.92\%$  with MMAD of  $3.63 \pm 0.39 \mu\text{m}$  and GSD of  $2.37 \pm 0.13$ . Subsequently, addition of another lipophilic adjunct (sodium stearate) to the HCD-Rif mixture and its NSD powder formulation (HCD-Rif-NaSt NSD) also exhibited comparable FPF ( $54.33 \pm 3.21\%$ ) to that of HCD-Rif NSD. In addition, MMAD and GSD of HCD-Rif-NaSt NSD were found to be  $3.05 \pm 0.13 \mu\text{m}$  and  $2.25 \pm 0.05$  respectively. The results of MMADs correlate well with the aerosol sizing as obtained by laser diffraction dry powder dispersion unit (described earlier). The formulation of rifampicin with HCD (with or without sodium stearate), significantly reduced the retention of NSD powder in DC and throat (Figure 10.7) and also enhanced powder flow, which may be attributed to the decrease in interfacial interaction between particles. This can be observed by comparative analysis of the NSD powder formulation (HCD-Rif and HCD-Rif-NaSt) deposition from stage-3 to the micro-orifice collection plate (respirable size ranges) as shown in figure 10.7. As per the reports, lipophilic adjunct (Sodium stearate) helps to improve the dispersibility of dry powder. However, in our study no significant increase in the FPF was noted even after addition of sodium stearate with HCD. Instead, we noted almost similar (only slightly increased) FPF from HCD-Rif-NaSt NSD than HCD-Rif NSD formulation. Similar FPF values from both the formulations may be attributed to resembling particle size and surface morphology of the HCD-Rif NSD formulations as observed from particle size analysis and scanning electron microscopy respectively. Previous studies have shown that addition of small amount of various compounds such as mannitol, PLA, PLGA, chitosan, or cyclodextrin can improve rifampicin particles dispersibility (Mizoe et.al., 2008; Doan et.al., 2009; Zarua et.al., 2009; Coowanitwong et.al., 2008). Lipopolymeric materials, chitosan coated liposomes and solid lipid nanoparticles have also been employed in rifampicin formulations (Vadakkan et.al., 2013; Pandey et.al., 2005; Zarua et.al., 2009). These studies have reported FPF value as high as 68.4% and as low as 22 %. However, no study is yet

## Chapter 10 - Preparation of HCD-Rif particles by NSD

conducted on the development of rifampicin particles using nano spray drying with the aid of chitosan and sodium stearate for pulmonary delivery. Sodium stearate was used as lipophilic adjunct to promote microparticle aerosolization and protect them from environmental humidity. In comparison to these studies, FPF value obtained in our study indicated better respirability with the FPF value of  $52.92 \pm 2.92\%$  and  $54.33 \pm 3.21\%$  for HCD-Rif and HCD-Rif-NaSt respectively. Results of the present study showed that deposition of HCD-Rif NSD and HCD-Rif-NaSt NSD powder formulations in all stages of the NGI including inhaler, mouthpiece and throat was found to be between 75% and 125%, which is in accordance with the criteria stated as per British Pharmacopoeia (British Pharmacopoeia, 2012).

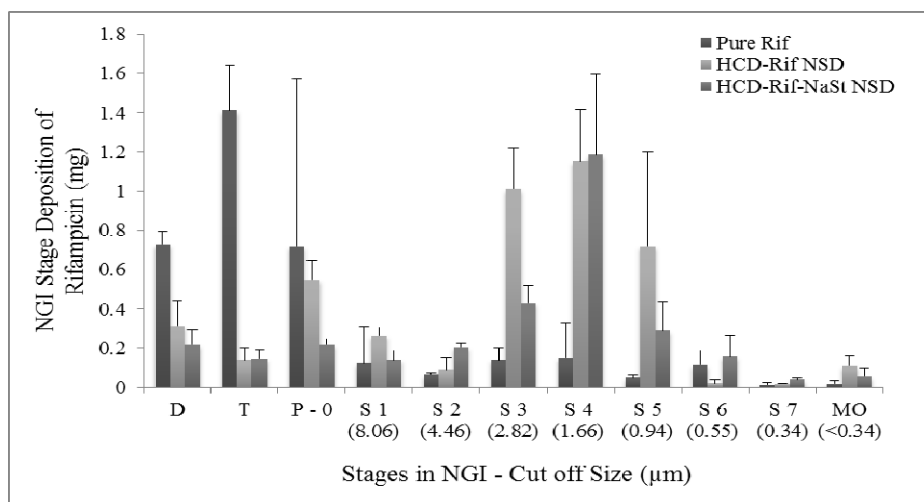


**Figure 10.7:** Next Generation Impactor stage deposition of pure rifampicin, HCD-Rif NSD, HCD-Rif-NaSt NSD. ( $n=3$ ; mean  $\pm$  standard deviation)

**Table 10.3:** Deposition Parameter of the Different Formulations Measured by NGI

Batch	Product Name	Inhaled Dose (mg)	Dose Delivered (mg)	ED %	FPF (%)	MMAD ( $\mu\text{m}$ )	GSD
NSD 1	Pure Rif	$21.4 \pm 0.15$	$3.18 \pm 0.11$	$14.84 \pm 0.53$	$1.85 \pm 0.29$	$23.47 \pm 9.16$	$5.29 \pm 1.58$
NSD 2	HCD-Rif NSD	$5.70 \pm 0.30$	$4.38 \pm 0.15$	$76.83 \pm 2.54$	$52.92 \pm 2.92$	$3.63 \pm 0.39$	$2.37 \pm 0.13$
NSD 3	HCD-Rif-NaSt NSD	$3.97 \pm 0.16$	$3.09 \pm 0.05$	$77.89 \pm 1.28$	$54.33 \pm 3.21$	$3.05 \pm 0.13$	$2.25 \pm 0.05$

( $\pm SD$ ,  $n = 3$  - Mean  $\pm$  Standard Deviation)

ED – Emitted Dose; FPF – Fine particle fraction; MMAD – Mass median aerodynamic diameter; GSD – Geometric standard deviation

### 10.8.7 In-vitro release of rifampicin

The drug release profiles of pure rifampicin, HCD-Rif NSD and HCD-Rif-NaSt NSD powder formulations are presented as percentage cumulative drug release plotted as function of time in figure 10.8. Release study was carried out in dark using simulated lung fluid (SLF

## Chapter 10 - Preparation of HCD-Rif particles by NSD

---

4, pH 7.4) so as to mimic the biological environment within the lungs. A small quantity of ascorbic acid was added to the release medium in order to avoid degradation of rifampicin. Results indicated that  $87.65 \pm 1.09$  % of rifampicin was dissolved in the SLF (pH 7.4) from pure rifampicin suspension within 2 hours, whereas HCD-Rif and HCD-Rif-NaSt NSD (figure 10.8) released  $26.668 \pm 2.173$  % and  $46.45 \pm 1.85$  % of rifampicin in 12 and 48 hr respectively. Similarly, HCD-Rif-NaSt NSD formulation took 72 hrs to release  $50.95 \pm 4.72$  % of rifampicin. The slow release of rifampicin from the NSD formulations may be attributed to the hydrophobic barrier confronted by HCD, which may have restricted access of water for the dissolution of the drug. The results obtained in this study are in agreement to the reports published by Tien et. al., where they formulated tablets utilizing non modified and acylated chitosan. They found that tablets prepared with non-modified chitosan rapidly disintegrated, whereas those formulated using acylated chitosans remained intact in aqueous medium without any erosion and sticking (Tien et. al., 2003). However, their reports pertaining to release of drug from octanoyl chitosan showed ability to control the release of drug to a limited extent (4-6 hrs to release acetaminophen). In contrast to these, our results suggested controlled release of rifampicin from HCD NSD powder formulation ( $61.72 \pm 1.81$  %) over a period of 72 hrs.

As seen from the results of HCD-Rif-NaSt NSD formulation, slow and prolonged release of rifampicin may be attributed to the inclusion of a lipophilic adjunct (sodium stearate) in the formulation. HCD was itself hydrophobic and addition of sodium stearate (another hydrophobic agent) may have slowed down the release of rifampicin by almost 10%. In a report by Parlati et.al., who prepared tobramycin particles by spray drying and studied the influence of sodium stearate (NaSt) on particle characteristics, they observed decrease in dissolution rate of powders containing sodium stearate in the range of 0% to 1% w/w due to increasing concentration of the sodium stearate on the particle surface, affecting wetting and dissolution (Parlati et. al., 2009).

Release profiles showed biphasic release pattern from both the formulations (HCD-Rif NSD and HCD-Rif-NaSt NSD). If we observe the graph presented in the inset, it can be easily identified that around 20 % of rifampicin was released by the end of 6 hrs period, the first phase of the release, which may have been possibly due to dissolution and passive diffusion of rifampicin located on or near the NSD powder surface. Six hours onwards, release was found to be slowed down, a second phase, which may have been portioned owing to rifampicin encapsulation within the core of NSD powder formulation. These results were found to be in agreement with the observation described by Klariæ et.al., (Klariæ et.al., 2012). From the results obtained, it was observed that, HCD-Rif-NaSt NSD formulation released less amount of rifampicin ( $50.95 \pm 4.72$  %) as compared to HCD-Rif NSD ( $61.72 \pm 1.81$  %), which may be attributed to additional hydrophobic layer formed by the sodium stearate on NSD particles.

It is well known that control of drug release can be obtained by hydrophobic polymers or substitution of hydrophobic moieties on the polymers. In later case, it is mostly dependent

on the degree of substitution and hence solubility. In the view of this, the HCD synthesized in our laboratory is clearly unique in terms of its solubility in comparison to those reported in the literature (Tien et. al., 2003; Jiang et. al., 2006; Jiang et.al., 2006; Li et.al., 2009; Haung et.al., 2010). As HCD was found to be insoluble in water and soluble in ranges of common organic solvents (discussed in previous section). Moreover, inherent properties of the chitosan such as positive charge will surely add up to the benefits by enhancing its interaction with the negatively charged cell surface leading to ease in transportation across the lipoidal cell membrane.

Furthermore, we analyzed the in-vitro release data to reveal the mechanism of drug release from spray dried HCD-Rif NSD and HCD-Rif-NaSt NSD powder formulation for inhalation (Costa et. al., 2001). Drug release vs time curve fitting into Higuchi model indicated that drug followed diffusion release mechanism with the  $r^2$  of 0.966 and 0.975 for HCD-Rif NSD and HCD-Rif-NaSt NSD formulation respectively. However, this model could not distinguish between fickian and non-fickian transport mechanism. Hence, existence of any deviation from fickian release mechanism was derived from Korsemeyers Peppas model. Results of the Korsemeyers Peppas model fitting indicated non-fickian drug transport from both HCD-Rif NSD ( $n=0.85$ ) and HCD-Rif-NaSt NSD ( $n=0.87$ ) formulations. Hence, the main mechanism of drug transport from the HCD NSD particles was controlled by anomalous transport (non-fickian diffusion).

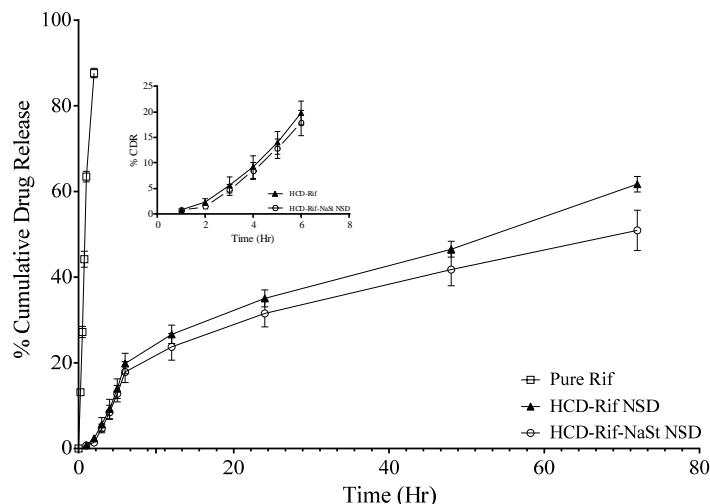


**Figure 10.8:** Percent cumulative drug release (CDR) of rifampicin, HCD-Rif NSD and HCD-Rif-NaSt NSD powder formulation. ( $n=3$  determinations  $\pm$ SD)

### 10.8.8 Stability study

HCD-Rif NSD powder formulations were assessed for stability with respect to drug content and particle size for 2 months at ambient temperature (10-20 °C) in dark. Results of stability study are tabulated in table 10.4. No significant difference was observed in drug content in the NSD powder formulations. However, particle size was of both the formulations NSD1

## Chapter 10 - Preparation of HCD-Rif particles by NSD

and NSD 2 was found to be increased ( $5.03\pm 4.93$  and  $5.8\pm 3.4$   $\mu\text{m}$ ) after 2 months. Increased particle size may be attributed to the aggregation of the particles upon storage.

**Table 10.4:** Stability of HCD-Rif NSD formulation at RT (10-20 °C)

Sr. No.	Time (Months)	Drug Content (%)		Particle Size ( $\mu\text{m}$ )	
		HCD-Rif (NSD 1)	HCD-Rif-NaSt (NSD 2)	HCD-Rif (NSD 1)	HCD-Rif-NaSt (NSD 2)
1	Initial	100	100	$4.37\pm 0.46$	$4.58\pm 0.22$
2	2	$99.25\pm 1.021$	$98.87\pm 1.251$	$5.03\pm 4.93$	$5.8\pm 3.4$

SD – standard deviation values within the formulation

### 10.8.9 Conclusions

Hydrophobic chitosan derivative was synthesized and characterized for physicochemical properties. Substitution of octanoyl groups (formation of hydrophobic chitosan derivative - HCD) on to the parent chitosan moiety was confirmed based on the results of FTIR,  $^1\text{H-NMR}$ . Thermal stability and crystallinity of the polymer was also determined. Further on, HCD was employed to check its feasibility in the preparation nano spray dried powder formulations with or without lipophilic adjunct (sodium stearate) so as to improve the aerosolization efficiency of dry powder formulation. The aerosol performance of the nano spray-dried powders formulations (HCD-Rif and HCD-Rif-NaSt) presented MMAD ( $3.63\pm 0.39$  &  $3.05\pm 0.13$ ) within the range of 1-5  $\mu\text{m}$  suggesting the utility of HCD in the formulation of DPI for pulmonary delivery. Similarly, more than 50 % aerosol performance in terms of FPF was also observed from the in-vitro lung deposition studies of HCD-Rif and HCD-Rif-NaSt NSD powder formulations. Release studies confirmed the applicability of HCD in controlling the release of drug. Almost 60 % and 50 % of drug was released from HCD-Rif NSD and HCD-Rif-NaSt NSD powder formulation respectively by the end of 72 hrs. In sum, it is envisaged that the HCD could be an effective carrier system for controlled drug and protein delivery. HCD was also found suitable for nano spray drying and this approach could provide a feasible and attractive alternative for the preparation of dry powder inhalation, which can give rise to a new terminology called nano spray dried powder inhalation (NSDPI) for encapsulation of range of antibiotics to improve therapeutic outcomes for patients suffering from draining respiratory diseases such as MTB.

## Chapter 10 - Preparation of HCD-Rif particles by NSD

---

### References

- Agrawal S., Ashokraj Y., Bharatam P.V., Pillai O., Panchagnula R. (2004) Solid-state characterization of rifampicin samples and its biopharmaceutic relevance. *Eur J. of Pharm. Sci.* 22, 2–3, 127–144.
- Benetton S.A., Kedor-Hackmann E.R.M., Santoro M.I.R.M., Borges V.M. (1998) Visible spectrophotometric and first-derivative UV spectrophotometric determination of rifampicin and isoniazid in pharmaceutical preparations, *Talanta*, 47,3, 639–643.
- British Pharmacopoeia (2012) Appendix XII C. Consistency of Formulated Preparations, British Pharmacopoeia Volume V, British Pharmacopoeia, 2012 online.
- Choudhari Y.M., Detane S.V., Mourya V.K., et.al., (2012) Low molecular weight palmitoyl chitosan: Synthesis, characterization and nanoparticle preparation, *Adv. Mat. Lett.*, 3, 6,487-492
- Chen C., Tao S., Qiu X., Ren X., Hu S. (2013) Long-alkane-chain modified N-phthaloyl chitosan membranes with controlled permeability. *Carbohydrate Polymers*, 91, 269– 276.
- Choi C.Y., Kim S.B., Pak P.K., Yoo D.I., Chung Y.S. (2007) Effect of *N*-acylation on structure and properties of chitosan fibers. *Carbohydrate Polymers*, 68, 122–127.
- Coowanitwong I., Arya V., Kulvanich P., and Hochhaus G. (2008) Slow Release Formulations of Inhaled Rifampin. *The AAPS Journal*, 10(2), 342-348.
- Corrigan D.O., Corrigan O.I., and Healy A.M. (2006) Physicochemical and in vitro deposition properties of salbutamol sulphate/ipatropium bromide and salbutamol sulphate/excipient spray dried mixtures for use in dry powder inhalers. *Int. J. Pharm.*, 322, 22–30.
- Costa P., Lobo J. (2001) Modeling and comparison of dissolution profiles, *European J. of Pharm. Sci.*, 13, 123–133
- Doan T.V.P., Olivier J.C. (2009) Preparation of rifampicin-loaded PLGA microspheres for lung delivery as aerosol by premix membrane homogenization. *International Journal of Pharmaceutics* 382, 61–66
- Gautier S., Arpagaus C., Schafroth N., Meuri M., Deschamps A., and Maquet V. (2010), Very fine chitosan microparticles with narrow & controlled size distribution using spray-drying technologies, *Drug Delivery Technology*, 10, 8, 30-37.
- Haung Y., Yu H., Guo L., Huang Q. (2010) Structure and Self-Assembly Properties of a New Chitosan-Based Amphiphile, *J.Phys.Chem. B*, 114, 7719-7726
- Hirota K., and Terada H. (2012). Endocytosis of Particle Formulations by Macrophages and Its Application to Clinical Treatment, *Molecular Regulation of Endocytosis*, Dr. Brian Ceresa (Ed.), ISBN: 978-953-51-0662-3, InTech, DOI: 10.5772/45820. Available from: <http://www.intechopen.com/books/molecular-regulation-of-endocytosis/endocytosis-of-particle-formulations-by-macrophages-and-its-application-to-clinical-treatment> (Date accessed May 2013).

Jiang G., Quan D., Liao K., Wang H. (2006) Preparation of polymeric micelles based on chitosan bearing a small amount of highly hydrophobic groups, *Carbohydrate Polymers*, 66, 4, 514–520.

Jiang G., Quan D., Liao K., Wang H. (2006) Novel polymer micelles prepared from chitosan grafted hydrophobic palmitoyl groups for drug delivery. *Mol Pharm.* 3, 2, 152-60.

Klariæ D., Hafner A., Zubèiæ S., Dürriigl M., and Filipoviæ-Grèiæ J. (2012) Spray-dried Microspheres Based on Chitosan and and LecithinCyclosporin A Delivery System. *Chem. Biochem. Eng. Q.* 26, 4, 355–364.

Li Y.Y., Chen X.G., Zhang J., Liu C.S., Xue Y.P., Sun G.Z., Zhang W.F. (2009) In Vitro Release of Rifampicin and Biocompatibility of Oleoylchitosan Nanoparticles. *Journal of Applied Polymer Science*, 111, 2269–2274.

Luangtana-anan M., Limmatvapirat S., Nunthanid J., Chalongsuk R., Yamamoto K. (2010) Polyethylene Glycol on Stability of Chitosan Microparticulate Carrier for Protein, *AAPS PharmSciTech.* 11(3), 1376–1382.

Ma G., Yang D., Zhou Y., Xiao M., Kennedy J.F., Nie J. (2008) Preparation and characterization of water-soluble N-alkylated chitosan. *Carbohydrate Polymers.* 74, 121–126.

Manca M-L., Mourtas S., Dracopoulos V., Fadda A.M., Antimisiaris S.G. (2008) PLGA, chitosan or chitosan-coated PLGA microparticlesfor alveolar delivery? A comparative study of particle stability during nebulization. *Colloids and Surfaces B: Biointerfaces*, 62, 220–231

Marques M.R.C., Loebenberg R., and Almukainzi M. (2011) Simulated Biological Fluids with possible application in Dissolution Testing. *Dissolution Technologies*, August, 15-28.

Mizoe T., Ozeki T., and Okada H. (2008) Application of a Four- fluid Nozzle Spray Drier to Prepare Inhalable Rifampicin-containing Mannitol Microparticles. *AAPS PharmSciTech*, 9, 3, 755-761.

Pandey R., Khuller G.K. (2005) Solid lipid particle-based inhalable sustained drug delivery system against experimental tuberculosis. *Tuberculosis.* 85, 227–234.

Parlati C., Colombo P., Buttini F., Young P.M., Adi H., Ammit A.J., and Traini D. (2009) Pulmonary Spray Dried Powders of Tobramycin Containing Sodium Stearate to Improve Aerosolization Efficiency, *Pharmaceutical Research*, 26, 5, 1084-1092.

Sipos P., Rajkó R., Pintye-Hódi K., Erős I., Szabó-Révész P. (2011) Formulation Optimization of Sustained-Release Ammonio Methacrylate Copolymer Microspheres. Effects of Log P and Concentration of Polar Cosolvents, and Role of the Drug/Copolymer Ratio, *Pharmaceutics*, 3, 830-847.

Song M-G., Kim J-Y., Kim J-D. (1997) the electrostatic and rheological properties of precipitated calcium carbonate with sodium stearate and calcium ions, *Applied Chemistry*, 1, 2, 389-391.

## Chapter 10 - Preparation of HCD-Rif particles by NSD

---

Tatarczak M., Flieger J., and Szumilo H. (2005), High-Performance Liquid-Chromatographic Determination of Rifampicin in Complex Pharmaceutical Preparation and in Serum Mycobacterium Tuberculosis-Infected Patients, *Acta Poloniae Pharmaceutica - Drug Research*, 62, 4, 251-256.

Tien C.L., Lacroix M., Ispas-Szabo P., Mateescu M. (2003) N-acylated chitosan: hydrophobic matrices for controlled drug release, *Journal of Controlled Release*, 93, 1, 1-13.

Vadakkan M. V., Annapoorna K., Sivakumar K. C., Mundayoor S. Vinod Kumar G.S. (2013) Dry powder cationic lipopolymeric nanomicelle inhalation for targeted delivery of antitubercular drug to alveolar macrophage. *International Journal of Nanomedicine*, 8, 2871–2885.

Vadwai V., Daver G., Udwardia Z., Sadani M., Shetty A., et al. (2011) Clonal Population of *Mycobacterium tuberculosis* Strains Reside within Multiple Lung Cavities. *PLoS ONE*, 6, 9, e24770. doi:10.1371/journal.pone.0024770.

Yang Y., Bajaj N., Xu P., Ohn K., Tsifansky M.D., Yeo Y. . (2009) Development of highly porous large PLGA microparticles for pulmonary drug delivery. *Biomaterials*, 30, 10, 1947-53.

Zarua M., Manca M-L., Faddab A.M., Antimisiaris S.G. (2009) Chitosan-coated liposomes for delivery to lungs by nebulization. *Colloids and Surfaces B: Biointerfaces*, 71, 88–95.

Zong Z., Kimura Y., Takahashi M., Yamane H. (2000) Characterization of chemical and solid state structures of acylated Chitosans. *Polymer*. 41, 899–906.

### 11.0 Preparation of modified chitosan derivative (MCD)-Rif Nano Spray Dried Powder for Inhalation

#### 11.1 Materials

Rifampicin was purchased from Sigma-Aldrich (St-Louis, USA). Chitosan oligosaccharide (MW 1kDa; degree of deacetylation (DDA) 80-90%) was supplied by Kitto Life Co. Ltd. (Kyongki-Do, Seol Korea). Cellulose dialysis tubing (Molecular weight cut of 12-14000 Da, 5000 Da) were purchased from Medicell international Ltd., (London, UK). Dimethyl sulfoxide (anhydrous), octanoyl chloride, methane sulfonic acid, L- leucine, sodium bicarbonate, acetonitrile, methanol, ethanol, chloroform, dichloromethane (DCM), acetone etc were obtained from Sigma-Aldrich (St-Louis, USA). All other HPLC grade solvents were obtained from Sigma-Aldrich (St-Louis, USA).

#### 11.2 Equipment

1. High speed magnetic stirrer (FisherBrand, Loughborough, UK)
2. Nano spray Dryer B-90 (Buchi, Oldham, UK)
3. UV-VIS Spectrophotometer (Jenway UV/Vis Spectrophotometer, Staffordshire, UK)
4. Fourier Transform Infra-red spectrophotometer (FTIR) (Perkin Elmer, MA, USA)
5. Differential Scanning Calorimeter DSC Q 2000, (TA Instruments, New Castle, UK)
6. Zetasizer, Nanoseries Instrument (Nano 25, Malvern Instruments, Worcestershire, UK)
7. Laser diffraction using HELOS particle size analyzer (Sympatech Inc., Lawrenceville, NJ, USA)
8. Scanning Electron Microscope (FEI XL30 TMP, Philips, Netherlands)
9. X-Ray Diffractometer (Oxford Diffraction Xcalibur novaT X-ray diffractometer; Oxford Diffraction Ltd., Abingdon, UK)
10. HPLC system (1200 series, Agilent Technologies, Berkshire, UK)
11. Next Generation Impactor (Copley, Nottingham, UK)

#### 11.3 Preparation of nano-spray dried powder formulation for inhalation (NSDPI)

Preparation of particles was carried out by the Nano Spray dryer B-90 (Buchi, UK). Drug loaded particles were obtained by dissolving 100 mg of MCD and 50 mg of rifampicin in 50 ml of water:methanol (70:30% w/v). Batches were prepared with and without addition of L-leucine (25 mg), maintaining the 3% of solid content in water:methanol (70:30% w/v), stirred to produce a clear solution and then subjected to nano spray drying using Nano Spray Dryer B-90. At the same time, rifampicin alone was also spray dried by preparing a solution of rifampicin (25 mg) in 25 ml of methanol. For the purpose of spray drying, mesh size of 7.0  $\mu\text{m}$  was used with 60 Hz ultrasonic frequency for the actuator. The product obtained was collected and weighed to determine the yield.

The Nano Spray Dryer B-90 was operated in open-mode configuration. The operating conditions for the experiments were selected from the reports of Gautier et. al., and kept constant at: the drying gas flow rate – 120 l/min; Inlet temperature - 120°C ; Outlet

## Chapter 11 - Preparation of MCD-Rif particles by NSD

---

temperature – 61 °C ; Head temperature – 94 °C; Pressure – 39mbar ; Spray rate – 100 % ; Spray mesh - 7.0 µm (Gautier et.al., 2010).

### ***11.3.1 Encapsulation efficiency (EE) and drug loading (DL)***

The drug entrapped in the NSD powder formulations was analyzed using UV spectrophotometer (Jenway UV/Vis Spectrophotometer, Staffordshire, UK). Known amount of drug loaded Nano spray dried powder was dissolved in methanol to dissolve the particles and volume was made with water. Resultant solution was analyzed to determine the concentration of rifampicin in the samples using UV-VIS Spectrophotometer (Benetton et.al., 1998). The analysis was carried out in triplicate for each batch of drug loaded NPs. The drug loading and entrapment efficiency was calculated using following formulae:

$$\text{Yield (\%)} = \frac{\text{Weight of NP recovered}}{\text{Weight of Drug, polymer and excipient}} \times 100$$

$$\text{Drug Loading (\%)} = \frac{\text{Weight of Rif in NP}}{\text{Weight of NP recovered}} \times 100$$

$$\text{Entrapment Efficiency (\%)} = \frac{\text{Weight of Rif in NP}}{\text{Weight of Rif fed initially}} \times 100$$

### ***11.3.2 Particle size and zeta potential***

Dynamic light scattering (DLS) and laser doppler velocimetry (LDV) were used for the measurement of particle size and zeta potential of the NSD powder particles respectively using Zetasizer, Nanoseries Instrument (Nano 25, Malvern Instruments, Worcestershire, UK). The particles were suspended in deionized water, sonicated in bath sonicator for 2 min and the resultant samples were examined to determine particle size and zeta potential.

### ***11.3.3 Shape and surface morphology and Solid state characterization***

The shape and surface morphology of the nanoparticles was evaluated by FEI XL30 TMP SEM (FEI XL30 TMP, Philips, Netherlands). DSC measurement of pure drug, pure polymer and drug loaded nano spray dried nanoparticles (Rif-NSD) was carried out to determine thermal behavior and crystallinity of the formulations using DSC instrument (DSC Q 2000, TA Instruments, USA). Similar parameters and cycles were used for DSC study as used for the HCD. Crystallinity of the formulations was also determined using X-ray powder diffraction (Oxford Diffraction Xcalibur novaT)

### ***11.3.4 Dry powder characterization using Sympatec***

The volume median diameter of the nano spray dried powder was measured by laser diffraction using HELOS particle size analyzer incorporating RODOS dry powder dispersing unit (Sympatec Inc., Lawrenceville, NJ, USA) at an adopted pressure of 4 mbar. Approximately 5-10 mg of NSD powder formulations was taken in a small cuvette and subjected to in build inhalation system of Sympatec. All measurements were performed in triplicate. The results were recorded using HELOS system and data obtained was expressed as the volume weighted mean particle size.  $Dv_{10}$ ,  $Dv_{50}$  &  $Dv_{90}$  values for the diameter sizes of

## Chapter 11 - Preparation of MCD-Rif particles by NSD

a given percentage of particles smaller than the specified size were obtained from in build software system. Span of the volume distribution, a measure of the width of the volume distribution relative to the median diameter ( $Dv_{50}$ ), was calculated from equation given below-

$$\text{Span} = \frac{Dv90 - Dv10}{Dv50}$$

A high value for the SPAN is an indication for wider particle size distribution.

### 11.4 In-vitro aerosolization and lung deposition using Next Generation Impactor (NGI)

The aerosolization properties of the NSD powder formulations were determined in-vitro using NGI (Copley, UK), which gives good information about deposition of particles in the lungs. A vacuum pump connected to NGI was operated at a flow rate of 60 ml/min which was calibrated using flow meter (Copley, UK). Five capsules each containing approximately 3-5 mg of nano spray dried powder were taken. The filled capsules were then inhaled through mouth piece for 6 sec. at room temperature. The amount of rifampicin retained in the inhaler mouthpiece and deposited in each stage of the NGI was determined using UV-VIS Spectrophotometer (Jenway UV/Vis Spectrophotometer, Staffordshire, UK) at a wavelength of 475 nm (Benetton et.al., 1998). The mass median aerodynamic diameter (MMAD) and geometric standard deviation (GSD) were calculated after plotting cumulative amount of drug deposited in each stage of the NGI *vs* their corresponding aerodynamic diameter using log probability paper using equations 1 and 2. Emitted dose (ED) and fine particle fraction (FPF) were calculated using equation 3 and 4. Each measurement was carried out in triplicate and the average values are reported.

$$\text{MMAD} = Dv\ 50\ \% \text{-----(1)}$$

$$\text{GSD} = \sqrt{\frac{04.1\ \% \text{ undersize}}{15.9\ \% \text{ undersize}}} \text{-----(2)}$$

$$\text{ED} = \frac{\text{Amt. of Rif recovered in NGI}}{\text{Amt. of Rif initially loaded}} \text{-----(3)}$$

$$\text{FPF} = \frac{\text{Amt. of Rif recovered in NGI from stage 3 to filter}}{\text{Amt. of Rif initially loaded}} \text{-----(4)}$$

### 11.5 In-vitro release studies

*In-vitro* release studies of rifampicin from MCD nanoparticles was carried out in dark by dialysis method using modified release technique (Marques et. al., 2011). The method utilized for this study was similar to the one described in chapter 9. In brief, known amount of Rif loaded NSD powder formulation was dispersed in SLF (pH 7.4) supplemented with 200 µg/ml of ascorbic acid and transferred to dialysis membrane (3.5 kDa molecular weight cut-off, Medicell International Ltd., Liverpool, UK). Dialysis membrane was sealed with the help of dialysis tubing clamps and placed in a beaker containing 25 ml of SLF as external release media under stirring at 37°C. At selected time intervals, aliquots were withdrawn from the external media, diluted as required and analyzed by HPLC (1200 series, Agilent

## Chapter 11 - Preparation of MCD-Rif particles by NSD

---

Technologies) at 335 nm (Tatarczak et.al., 2006). The results obtained were plotted as percent cumulative drug release *vs* time. The experiment was performed in triplicate and the results are reported as  $\pm$  standard deviation. Sink condition was also maintained as discussed in chapter 9.

### 11.5.1 HPLC analysis

The amount of rifampicin in samples obtained after release studies were determined by HPLC system (1200 series, Agilent Technologies) equipped with a UV detector. The injection volume was 10  $\mu$ l. Chromatography was performed with a column (Ascentis C18, 150 x 4.6mm, 5 $\mu$ m, Supelco, Sigma-Aldrich, USA). Mobile phase composed of tetrahydrofuran (THF)/phosphate buffer (30/70 %) at a flow rate of 1.0 ml/min and a detection wavelength of 335 nm (Tatarczak et.al., 2006). The column temperature was set to 40 °C. The retention time of rifampicin was 3.5 min. Calibration curves for rifampicin (correlation coefficient was 0.9993) at concentrations varying from 5 to 80  $\mu$ g/ml was used for analysis.

### 11.6 Stability study

Formulations were stored in tightly closed glass vial at room temperature (15-20 °C) for up to 2 month period in dark to check the stability. Periodically, samples were withdrawn and assayed to determine drug content. Particle size & zeta potential were also measured.

### 11.7 Statistical analysis

The experiments were performed at least in triplicate on separate occasions. The data collected in this study were expressed as the mean value  $\pm$  standard deviation.

## 11.8 Results and Discussion

### 11.8.1 Preparation of modified chitosan derivative (MCD) nano spray dried powder for inhalation (NSDPI) and characterization

The current study was undertaken to investigate the feasibility of MCD in the preparation of nanoparticles using nano spray drying technique. Nanospray drying method was found to be simple and efficient to prepare dry powder formulation and it was utilized successfully. Two batches of MCD nano spray dried (NSD) powder formulations were prepared with (MCD-Rif-Leu) or without addition of leucine (25 mg) (MCD-Rif). Similarly, rifampicin alone was also nano spray dried for comparison. The solvent selection in the process of spray drying is considered to be important step because of its control over inlet spray-drying temperature and influence on the drug loading. Due to varied solubility of MCD, Rif and leucine (MCD and leucine are soluble in water and methanol and Rif in methanol), water:methanol in the ratio of 70:30% v/v was chosen as a solvent system for development of NSD powder.

Percent yield of the nanospray dried particles was found to be in the range of 25 -85 %. Batch NSD 1 showed highest yield of 84.22 $\pm$ 2.69%, which was made up of MCD and rifampicin, whereas, addition of leucine as lipophilic adjunct was found to decrease the yield of particles (68.56 $\pm$ 2.83) (Table 11.1). Ruso et.al., also reported such kind of behavior in the

## Chapter 11 - Preparation of MCD-Rif particles by NSD

yield of gentamicin particles prepared using increasing concentration of leucine (Ruso et al., 2012). Data utilized for NSD powder formulation of rifampicin alone (batch NSD 0) is similar as discussed in the chapter 9, which showed lowest yield among all formulations. Results obtained after nano spray drying of rifampicin with MCD and MCD plus leucine denoted as batch NSD1 (84.22±2.69%) and NSD2 (68.56±2.83%) respectively showed high yield, which may be due to higher sample size of more than 100 mg. These results are in compliance with the reports published by Gautier et al., (Gautier et al., 2010), who claims for higher yields of chitosan NSD powders with sample size above 100mg. It was observed that batch NSD 1 had highest entrapment efficiency (45.25±0.76) as compared to batch NSD 2 (35.69±0.81). Percent drug loading and entrapment efficiency of both the formulations are presented in table 11.1.

**Table 11.1 : Percent yield, Drug loading (DL) and Entrapment efficiency (EE)**

Yield, Drug Loading and EE				
Batch	Product Name	Yield (%)	DL (%)	EE (%)
NSD 0	Pure Rif NSD	25.44±1.14	---	25.44±1.14
NSD 1	MCD-Rif NSD	84.22±2.69	17.91±0.28	45.25±0.76
NSD 2	MCD-Rif-L NSD	68.56±2.83	17.36±0.33	35.69±0.81
PS, PDI and ZP				
Batch	Product Name	PS (nm)	PDI	ZP (mV)
NSD 0	Pure Rif NSD	--	--	--
NSD 1	MCD-Rif NSD	222.08±2.54	0.320±0.069	27.39±8.58
NSD 2	MCD-Rif-L NSD	228.91±9.52	0.542±0.046	13.33±6.82

*± SD of three determinations; Rif – Rifampicin*

### 11.8.2 Particle Size analysis of MCD NSDPI

Particle size in the range of nanometers was expected due to preparation of particles using nano spray drying method. For this purpose, Zetasizer, Nanoseries Instrument (Nano 25, Malvern Instruments, Worcestershire, UK), which is based on the principle of dynamic light scattering (DLS) was utilized. Particle size of batch NSD 1 and NSD 2 was found to be 222.08±2.54 & 228.91±9.52 nm, with the poly dispersity index (PDI) of 0.320±0.069 and 0.542±0.046 respectively. Small particle size obtained may be due to concurrent hydrophilicity and hydrophobicity of the MCD, which may have caused micelle formation leading to smaller particle size (Haung et al., 2010). In addition to hydrodynamic particle size, dry powder particle size was also measured using sympatec, which provides good information about powder properties for pulmonary delivery based on the size distribution analysis. The particle size and density distribution of each formulation is presented in figure 11.1. Particle size analysis indicated that the NSD powder formulations had multimodal size distribution within a size range effective for pulmonary delivery (1-5 µm). Variations in size within and between the samples were observed from 1.10±0.006 to 7.24±0.12. The particle size distribution curve of the nano spray-dried powdered formulation determined using

## Chapter 11 - Preparation of MCD-Rif particles by NSD

Sympatec is shown in figure 11.1 and the particle size analysis parameters are summarized in Table 11.2. The data is expressed in terms of the particle diameter at 10, 50, and 90 % of the particle volume distribution ( $D_{V_{10}}$ ,  $D_{V_{50}}$  &  $D_{V_{90}}$ , respectively). The span of the volume distribution, a measure of the width of the volume distribution relative to the median diameter ( $D_{V_{50}}$ ), was also determined. High value for the SPAN is an indication for wider particle size distribution. However, span values for both the formulations (MCD-Rif and MCD-Rif-Leu NSD) were found to be small ( $1.94 \pm 0.04$  &  $2.00 \pm 0.17$ ) suggesting uni-modal particle size distribution. It was observed that 50<sup>th</sup> and 90<sup>th</sup> percentile undersize ( $D_{V_{50}}$  &  $D_{V_{90}}$ ) was varied in two formulations.  $D_{V_{50}}$  &  $D_{V_{90}}$  values of NSD batch 1 were found to be  $3.17 \pm 0.08$  ( $D_{V_{50}}$ ),  $7.24 \pm 0.12$  ( $D_{V_{90}}$ )  $\mu\text{m}$  respectively, whereas these values were found to be slightly decreased in the formulation containing leucine ( $2.91 \pm 0.04$  ( $D_{V_{50}}$ ) &  $6.99 \pm 0.22$   $\mu\text{m}$  ( $D_{V_{90}}$ )). Decreased particle size in MCD NSD powder formulations, may be due to presence of leucine which enhanced particle properties for aerosolization. However, no significant difference in this observation was noted. Nevertheless, NSD batches showed respirable particle size in both cases, with (NSD2) or without leucine (NSD1).

Zeta potential observed for the batch NSD 1 was on the positive side (table 11.2), MCD-Rif and MCD-Rif-L NSD powder formulation showed zeta potential of  $27.39 \pm 8.58$  and  $13.33 \pm 6.82$  respectively, indicating that NSD particles have retained inherent charge of chitosan even after preparation of MCD and its spray dried powder formulation. This also confirms the applicability of methanesulfonic acid for the preparation of o-octanoyl chitosan leaving amine groups free to bestow positive charge on MCD.

**Table 11.2 :** Particle Size Distribution Data of Dry Powders Analyzed by Sympatec

Batch	Product Name	$D_{10}$ ( $\mu\text{m}$ )	$D_{50}$ ( $\mu\text{m}$ )	$D_{90}$ ( $\mu\text{m}$ )	Span
NSD 1	MCD-Rif NSD	$1.10 \pm 0.006$	$3.17 \pm 0.08$	$7.24 \pm 0.12$	$1.94 \pm 0.04$
NSD 2	MCD-Rif-Nast NSD	$1.03 \pm 0.16$	$2.99 \pm 0.31$	$6.99 \pm 0.22$	$2.00 \pm 0.17$

( $\pm SD$ ,  $n = 3$ )

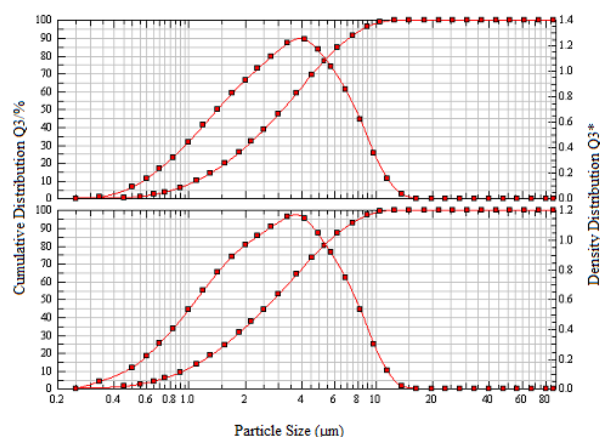


**Figure 11.1:** Particle size distributions of nano spray dried particles - MCD-Rif NSD & MCD-Rif-L NSD

### 11.8.3 Morphology of MCD NSDPI

Scanning electron microscopy (SEM) was used to visualize the size, shape, and surface morphology of nano spray dried particles. Scanning electron micrographs of nanospray dried powder formulations are shown in figure 2 (a, b & c). NSD powders showed small particle diameter and irregular surface morphology. In general, the particles displayed smooth surface but were observed to show wrinkled and collapsed morphology. Pure rifampicin particles showed irregular surface morphology, whereas MCD-Rif and MCD-Rif-L NSD showed wrinkled and collapsed structure. However, all particles were found to have smooth surface. From the micrographs it can be noted that, the presence of adjunct (Leucine) did not affect particle geometry or morphology and hence no substantial difference was observed between the two formulations (MCD-Rif and MCD-Rif-L NSD). Nevertheless, the presence of MCD and L-leucine affected the particle shape and surface morphology as compared to particle morphology of pure rifampicin. These results are in agreement with the reports published by Raula et al. As per Raula et al., surface-active properties of L-leucine molecules in aqueous solutions make them to accumulate at an air–water interface. L-leucine molecules form a coating layer on the surface of droplets, thereby preventing the penetration of water vapour through it, which leads to balloon like expansion of the surface layer. Subsequently, complete evaporation of the water causes break down of the surface layer resulting into wrinkled structure (Raula et al., 2007). Similar results were observed in our study conducted on MCD-Rif-L NSD powder formulation, which may be due to the phenomenon as described by Raula et.al. Noteworthy, similar particle surface morphology was observed from MCD-Rif NSD powder formulation, again which may be due to surface active properties of MCD (acylated chitosan derivative) and its ability to form a coating layer resembling to that of L-leucine. Wrinkled particle surface morphology has been shown to be beneficial for particles intended for inhalation due to reduced contact areas and interparticulate cohesion between corrugated particles, which ultimately leads to better powder dispersion as compared to spherical particles (Lechuga-Ballesteros et.al., 2008; Russo et.al 2012).

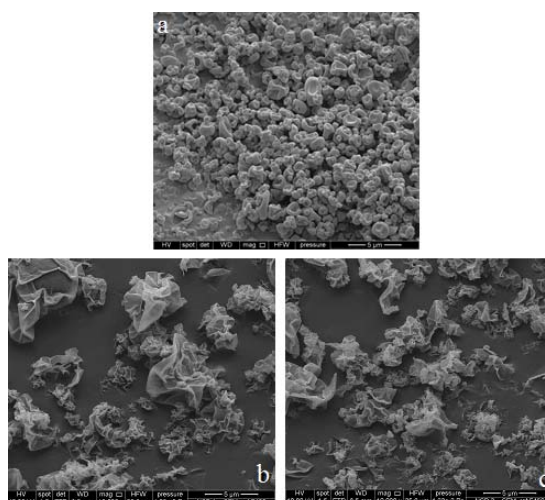


**Figure 11.2:** Scanning Electron micrographs of nano spray dried particles of ;  
a) Rifampicin; b) MCD-Rif; c) MCD-Rif-Leu

### 11.8.4 FTIR analysis

The FTIR spectra of rifampicin indicated that the rifampicin utilized in our study was in the crystalline state form I (Figure 11.3). In this regards, Agrawal et al. reported FTIR as a qualitative technique to identify the crystalline (form I and II) and amorphous forms of rifampicin (Agrawal et. al., 2004). The result of the FTIR indicated that rifampicin (as purchased) showed a sharp peak at  $3485\text{ cm}^{-1}$  corresponding to OH functional groups, bands near  $2810\text{ cm}^{-1}$  representing N-CH<sub>3</sub> band, characteristic absorption band at about  $1,724\text{ cm}^{-1}$  for acetyl C=O, sharp peaks at  $1641$  and  $1563\text{ cm}^{-1}$  representing the furanone C=O and amide C=O group, respectively. Moreover, a band at  $1255\text{ cm}^{-1}$  (-C-O-C- ether group) was also observed in the pure rifampicin FTIR spectra.

FTIR spectra of MCD as mentioned in the synthetic part of this paper showed the presence of characteristic bands  $\sim$  at  $1738.15\text{ cm}^{-1}$ , (for octanoyl groups),  $1610.50\text{ cm}^{-1}$ , (carbonyl stretching of amide band I - secondary amides) and  $1512.42\text{ cm}^{-1}$  (N-H bending vibrations of the amide band II) (Tien et.al., 2003). However, no change in the intensity of the bands near  $2810\text{--}2980\text{ cm}^{-1}$  was observed, which are corresponding to the hydroxyl and amine group of the chitosan chain. Results evidenced the introduction of a characteristic band at  $1738.15\text{ cm}^{-1}$ , which indicated substitution of ester group in the synthesized product, which was absent in the parent chitosan suggesting alkyl substituent at the hydroxyl position. This might be leaving amine position free and therefore we may consider synthesis of O-Octanoyl chitosan derivative. These results are in support with the results of Peesan et.al., (Peesan et.al., 2006).

A peak at  $1643$  corresponding to the furanone C=O and another peak at  $1559\text{ cm}^{-1}$  for amide C=O group were observed in the FTIR spectra of MCD-Rif NSD and MCD-Rif-L NSD. Moreover, a characteristic band for -C-O-C- ether group and aromatic C-H bending was also noted at around  $1250\text{ cm}^{-1}$  and  $724\text{ cm}^{-1}$  respectively. These bands were completely absent in the MCD, confirming no interaction between the drug and MCD in the formulation. However, the sizes of bands were smaller as compared to the bands observed in pure rifampicin spectra, which could be due to complete masking of the drug by the polymer and smaller amount of rifampicin adsorbed on the surface of the particles. These results are in accordance with the reports published by Rastogi et.al., (Rastogi et al.2007). Results of the study suggested compatibility of the rifampicin and MCD due to absence of any chemical interaction between functional group of MCD and rifampicin.

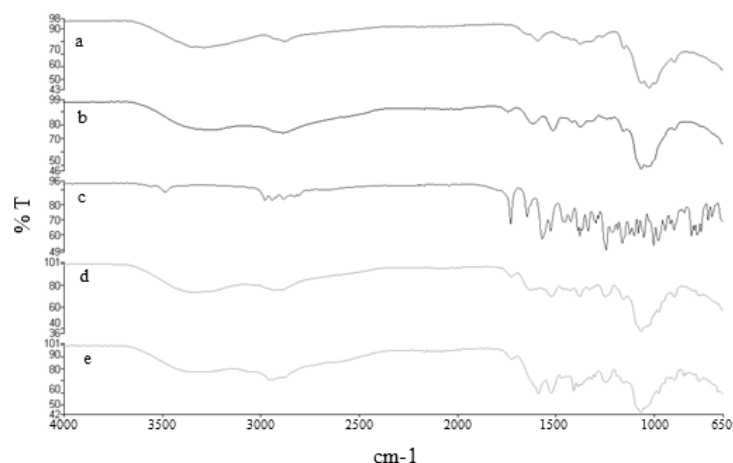


**Figure 11.3:** FTIR Spectra of - a) Chitosan; b) MCD; c) Rifampicin; d) MCD-Rif NSD & e) MCD-Rif-Leucin NSD formulation

### 11.8.5 Solid state characterization MCD-Rif Nano Spray Dried Powder

#### 11.8.5.1 Differential Scanning Calorimetry (DSC)

Differential scanning calorimetry of the rifampicin, chitosan, MCD (acylated chitosan), MCD-Rif physical mixture and NSD formulation was carried out and thermograms are displayed in figure 11.4. Results of the thermograms indicated a characteristic exothermic peak at 260°C for rifampicin showed, indicating the process of thermal decomposition and the presence of rifampicin in its polymorphic form I (figure 11.4a). This form also suggests that it is more thermally stable (Alves et.al., 2010). In the view of chitosan's moisture and thermal history, two cycles of heating and cooling runs were employed in the current experiment in order to eliminate the effects of moisture absorption. In compliance to the reports, we observed a broad endothermic peak at 100 °C corresponding to loss of residual water (data not shown, was observed in the initial run) and exothermic peak could be expected somewhere beyond 300°C, which may be due to monomer dehydration, glycoside bond cleavage and decomposition of the acetyl and deacetylated units of chitosan.

Results of the DSC studies of MCD showed absence of endothermic and exothermic peak upto 300 °C. Instead, a slight depression was seen near 300°C and hence an endothermic peak can be expected beyond 300 °C, which can be assigned to the thermal decomposition of the crystalline regions in MCD. Moreover, Choi et. al., also suggested shift in the peak to higher temperature indicating improved thermal stability. These results are in agreement with the reports published by Choi et. al., (Choi et.al., 2007). Based on these results, it can be concluded that there is improved thermal stability of MCD as compared to chitosan. In addition, no obvious glass transition ( $T_g$ ) was observed in both chitosan and MCD, which is supported by the results published by Zong et al. and Ma et.al., (Zong et al. 2000; Ma et.al., 2008). However, no discussion was provided for the absence of  $T_g$ . Similar results were observed for the physical mixture of MCD and Rif. As we did not notice any endothermic or exothermic peak in pure MCD thermographs, DSC thermographs of MCD-Rif NSD formulation also had no endothermic or exothermic peaks. In addition, no rifampicin peak

was observed in the MCD NSD formulation, indicating that the drug is not in crystalline form and is molecularly dispersed in the polymeric nanoparticle prepared by nano spray drying. These results are also corresponding to the results obtained in FTIR studies (figure 11.3).

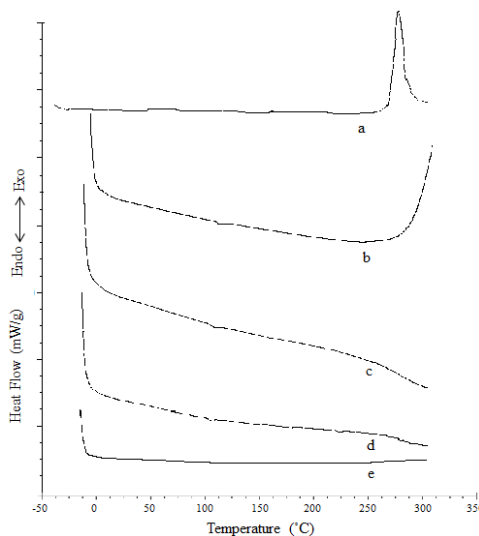


**Figure 11.4:** DSC Thermograms of – a) Rif; b) Chitosan; c) MCD; d) MCD+Rif physical mixture; e) MCD-Rif NSD formulation

### 11.8.5.2 X-ray powder diffraction

X-ray diffractograms of rifampicin, chitosan, MCD, MCD-Rif-NSD and MCD-Rif-Leu NSD formulation are presented in Figure 11.5. Results of the study showed A characteristics crystalline peaks for rifampicin form I at  $2\theta$  values of  $13^\circ$  and  $15^\circ$ , may be due to presence of rifampicin in its crystalline form. Parent chitosan showed peaks of moderately low intensity and broader than that of MCD. MCD did not show new peak below  $2\theta$  value of 8 as observed in case of HCD, but significant change in the band region below  $2\theta$  value of 8 can be seen from the XRD spectra of MCD. This change may be attributed to the more crystalline nature of MCD due to incorporation of hydrophobic side chains to that of parent chitosan. Results of this study are in agreement with the reports published by Tien et al., who reported major change at  $19.4 \text{ \AA}$  below  $2\theta$  value of 8, corresponding to more crystalline and stable organization of acylated chitosan derivative (Tien et.al., 2003). X-Ray powder diffraction analyses of the nano spray dried samples (MCD-Rif NSD and MCD-Rif-Leu NSD) are also displayed in figure 11.5. XRD spectra of both MCD-Rif NSD and MCD-Rif-Leu NSD was found to be resembling to that of plane MCD, which made it difficult to understand the crystallinity of MCD NSD formulation. However, absence of any peak of rifampicin in the MCD NSD powder formulation suggested the presence of rifampicin in solid amorphous state in both formulations prepared by nano spray drying technology. Broad diffused XRD spectra are often consistent with spray drying of organic materials consisting of binary components (Corrigan et.al., 2006; Parlati et.al., 2009). These results are in support with the results of SEM (Figure 11.2) indicating smooth surface morphology.

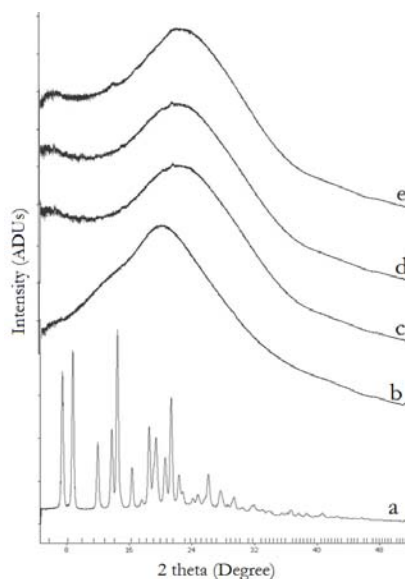


**Figure 11.5:** X-Ray Diffratograms of – a) Rif; b) Chitosan  
c) MCD; d) MCD-Rif NSD & e) MCD-Rif-Leu NSD formulation

#### 11.8.6 In-vitro aerodynamic performance (Pulmonary Deposition)

The present work was aimed to increase the concentration of rifampicin in the lung via dry powder inhalation therapy in order to reduce the systemic drug concentration and toxicity associated with it. Proper aerodynamic properties of particles are prerequisite to efficiently aerosolize the dry powder to reach the required sites of lungs, thereby increase macrophages uptake (a primary site of MTB localization) to combat TB. Well known localization of *M. tuberculosis* within the lung leading to tissue necrosis and destruction of the lung (Vadwai et.al., 2011) and its ability to proliferate and accumulate in the macrophages (Hirota and Terada, 2012) makes lung an excellent site for administration of drugs. Therefore, delivery of particles having optimum size of 1–5  $\mu\text{m}$ , incorporating antituberculosis agents in the form of dry powder inhalation to lungs becomes an effective TB therapy.

Aerosolization of NSD powder formulation was carried out using next generation impactor (NGI) and results obtained are presented in figure 11.6. Figure 11.6 presents the deposition of pure rifampicin, and rifampicin incorporated MCD NSD particles on different stages of NGI (device & capsule, throat and NGI stages). The in vitro respirability parameters obtained after NGI experiments and calculated using respective equations as given in method section are tabulated in Table 11.3. The fine particle fraction (FPF) calculated for pure rifampicin, MCD-Rif and MCD-Rif-L NSD powder formulation was found to be  $1.85 \pm 0.29\%$ ,  $74.55 \pm 4.01\%$  and  $61.48 \pm 3.88\%$  respectively (Table 11.3). The aerosolization and deposition of pure rifampicin in the different stages of NGI showed most hapless performance with the FPF of just  $1.85 \pm 0.29\%$  and highest MMAD of  $23.47 \pm 9.16$ . These results may be ascribed to the aggregation of rifampicin in absence of any lipophilic adjunct, which usually enhances powder flowability. Detailed discussion on this is presented in chapter 9. Several particle parameters haven been found to affect powder dispersibility including size distribution, morphology, surface roughness, surface hydrophobicity, surface

## Chapter 11 - Preparation of MCD-Rif particles by NSD

---

energy and density (Vehring et.al., 2008). Dispersibility of cohesive powders has been increased by mixing pure drug powder with carrier particles or lipophilic additives such as amino acids (e.g. leucine, trileucine), lecithin, chitosan, sodium stearate and magnesium stearate etc. to modulate interparticle forces (Vehring et.al., 2008). Leucine, like any other lipophilic adjunct helps to improve flowability/dispersibility of the dry powder. Several studies reported enhanced dispersion of the drug powders blended with carrier particles with the addition of L-leucine (Raula et.al., 2007; Vehring et.al., 2008; Raula et.al., 2009; Russo et.al., 2012). However, to our knowledge no studies have been undertaken to investigate the feasibility of modified chitosan as dispersing agent. Therefore, we have prepared batches incorporating dispersibility enhancers such as modified chitosan and leucine (Vehring et.al., 2008), to encapsulate rifampicin and to improve the surface properties of the particles

After preparation of MCD NSD powder formulations, significant improvement in the powder characteristics and in-vitro deposition in the lung was observed. Highest FPF of  $74.55 \pm 4.01\%$  with MMAD of  $1.53 \pm 0.17 \mu\text{m}$  and GSD of  $4.1 \pm 1.42$  was noted from MCD-Rif NSD powder formulation, whereas formulation prepared incorporating additional lipophilic adjunct exhibited (MCD-Rif-L NSD powder formulation) less FPF ( $61.48 \pm 3.88\%$ ) as compared to MCD-Rif NSD. In addition, MMAD and GSD of MCD-Rif-L NSD were found to be  $1.96 \pm 0.16 \mu\text{m}$  and  $1.8 \pm 0.09$  respectively. The results of MMADs correlate well with the aerosol sizing as obtained by laser diffraction dry powder dispersion unit (described earlier). The formulation prepared using MCD (with or without leucine) showed significant reduction in the retention of MCD NSD powder in DC and throat (Fig 6) may be due to enhanced powder flow properties attributed to the decreased interfacial interaction between particles. Comparative analysis of rifampicin deposition from NSD powder formulation (Pure rifampicin, MCD-Rif and MCD-Rif-L NSD powder) on stage-3 to the micro-orifice collection plate (respirable size ranges) is presented in figure 11.6. As mentioned earlier, various studies have reported enhancement in dispersibility of powders blended with hydrophobic adjunct L-leucine (Raula et. al., 2007; Vehring et.al., 2008; Raula et.al., 2009; Russo et.al., 2012). Similarly, we have also observed enhanced dispersability of fine drug particles by using L-leucine, which may be due to formation of surface layer by a method of droplet-drying leading to improved dispersion as reported by Raula et.al., (Raula et al., 2007; Raula et.al., 2009). In this case, they reported that L-leucine gets diffused on the surface of droplet before drying of the particles and eventually forms a coating layer on the surface of the particles. Improved flowability can be seen from the comparative deposition of rifampicin on each stage of NGI in figure 11.6. Despite this fact, we noted decreased FPF after addition of leucine with drug and MCD particles. In relation to this, Rabinovich et al. reported that the flowability and dispersibility of a powder are not only dependent on the surface material but particle shape and surface roughness (size and density of surface materials) also have similar impact (Rabinovich et al., 2000). Moreover, initial saturation of leucine is also reported as an important factor which influences dispersability of the powder. Low initial saturation of leucine in the droplet causes another component to precipitate, and hence crystallization of leucine may be inhibited (Vehring et.al., 2008; Chen et.al., 2005; Padhi et.a., 2006; Najafabadi et.al., 2004). Chen et.al., reported absence of crystalline leucine

when a small amount of leucine was added to disodium cromoglycate at low initial leucine saturation of  $S = 0.02$  (Chen et.al., 2005). The initial saturation of leucine has also been evidenced from a study on tobramycin by Padhi et.al., they found that the dispersibility of powder increases with increase in the concentration of leucine (Padhi et.al., 2006). In agreement with these results, undoubtedly L-leucine has resulted enhanced dispersability, which may be either due to optimum or high initial concentration of leucine leading to comparable dispersibility to that of the formulation devoid of leucine (MCD-Rif NSD). However, if there is high initial concentration of leucine, increase in the dry particle size is expected, which is undesirable for pulmonary administration (Vehring et.al., 2008). In relation to this, if we carefully observe figure 11.6, it can be easily identified that addition of L-leucine has significantly reduced fine particles below  $0.3 \mu\text{m}$ , whereas formulation devoid of L-leucine showed higher deposition of particles at the micro orifice (MO), which led to decrease in the FPF of MCD-Rif-L NSD powder formulation almost by 10 %. In addition, a small increase in the deposition of MCD-Rif-L NSD at DC and throat was also observed, indicating that there could be small increase in the particle size attributed to high initial concentration of leucine, which might have increased the dry particle size leading to reduced FPF.

In addition, upon comparison of two chitosan derivatives tested, we found higher FPF in case of MCD, whereas HCD (which was more hydrophobic in nature) resulted small FPF of  $52.92 \pm 2.92$ . Although both of them were good at producing dry powder for inhalation by nano spray drying technique. In connection to this, Learoyd et.al., reported dependency of FPF on molecular weight of polymeric material. Learoyd et.al., formulated terbutaline sulfate containing chitosan microspheres, with and without leucine to increase the aerosolization. They found emitted dose of greater than 90% and aerodynamic diameter between  $1-3 \mu\text{m}$  in a formulation containing leucine. One interesting finding noted by them was decrease in the FPF with increase in the molecular weight of chitosan. Accordingly, our study indicated that MCD, an acylated derivative of chitosan 1k showed higher FPF ( $74.55 \pm 4.01\%$ ), whereas another acylated derivative synthesized using chitosan  $> 5 \text{ k}$  resulted lower FPF ( $52.92 \pm 2.92$ ) as compared to the one prepared with lower molecular weight chitosan (1k). However, both the types of chitosan were able to produce nano spray dried powder for inhalation. These results are exactly matching with the reports published by Leayords et.al., (Leayords et.al.). Deposition of MCD-Rif NSD and MCD-Rif-L NSD powder formulations in all stages of the NGI including inhaler, mouthpiece and throat was ranging from 75% and 125% of mass balance, which is in accordance with the criteria stated as per British Pharmacopoeia (British Pharmacopoeia, 2012).

## Chapter 11 - Preparation of MCD-Rif particles by NSD

**Table 11.3:** Deposition Parameter of the Different Formulations Measured by NGI

Batch	Product Name	Inhaled Dose (mg)	ED (mg)	% ED	FPF (%)	MMAD* (µm)	GSD*
NSD 0	Pure Rif	21.4 ±0.15	3.18±0.11	14.84±0.53	1.85±0.29	23.47± 9.16	5.29±1.58
NSD 1	MCD-Rif NSD	3.58 ±0.30	3.17±0.18	88.42±5.01	74.55±4.01	1.53±0.17	4.1±1.42
NSD 2	MCD-Rif-L NSD	3.46±0.16	2.82±0.10	81.90±2.98	61.48±3.88	1.96±0.16	1.8±0.09

(± SD, n = 3 - Mean ± Standard Deviation; \*±SD, n=4 determinations)

ED – Emitted Dose; FPF – Fine particle fraction; MMAD – Mass median aerodynamic diameter; GSD – Geometric standard deviation

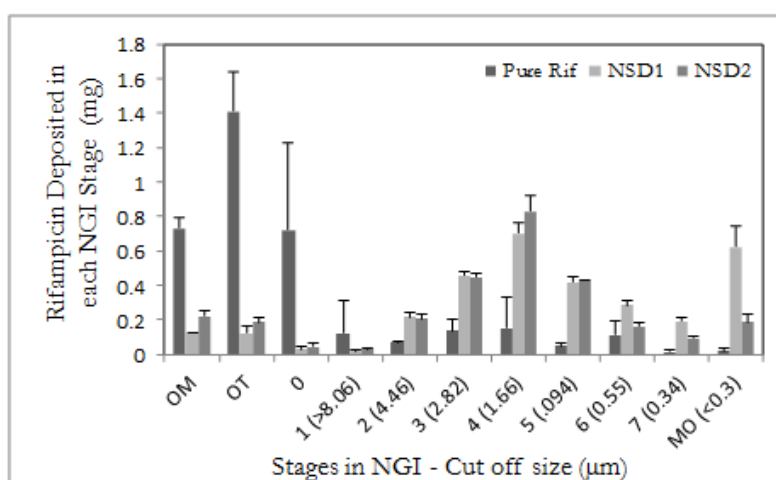


**Figure 11.6:** Next Generation Impactor stage deposition of Rifampicin, MCD-Rif NSD, MCD-Rif-Leucine NSD. (n=3; mean ± standard deviation)

### 11.8.7 In-vitro release of rifampicin

Figure 11.7 represents the drug release profiles as a function of percentage cumulative drug release vs time of rifampicin, MCD-Rif NSD and MCD-Rif-L NSD powder formulations. Results showed 87.65±1.09 % dissolution of rifampicin in the SLF (pH 7.4) within 2 hours, whereas, release of rifampicin was found to be controlled from both MCD NSD powder formulations viz. MCD-Rif and MCD-Rif-L NSD. Results demonstrated that MCD-Rif NSD powder formulation released 32.45±3.48 % and 64.53±3.48 % of rifampicin in 4 and 6 hr respectively, whereas MCD-Rif-L NSD formulation released 51.18±1.82 % of rifampicin by the end of 6 hr. Both the formulations revealed slow release of rifampicin from the NSD powder formulations, which may be due to hydrophobic barrier presented by the modified chitosan derivative (MCD). Similar results are reported by Tien et. al., in which drug release rates from tablets prepared using non modified & acylated chitosan was studied. They reported rapid disintegration of the tablets formulated with non-modified chitosan, whereas they noted controlled release of drug from tablets prepared using acylated chitosan without any erosion and sticking (Tien et.al., 2003). However, their reports indicated that octanoyl chitosan could release drug to a limited extent (4-6 hrs to release acetaminophen). On the

contrary, results of this study showed drug release over a period of 12 hrs from MCD NSD powder formulations. As shown in figure 11.7, almost 100 % ( $99.63 \% \pm 8.79 \%$ ) and 90% ( $89.71 \pm 3.71 \%$ ) of rifampicin was dissolved from MCD-Rif NSD and MCD-Rif-L NSD powder formulation respectively. Incorporation of an adjunct (leucine) in MCD-Rif NSD formulation has shown retardation in the release of rifampicin, which may be due to additional hydrophobicity conferred by the leucine leading to restricted entry of water for the dissolution of drug. Hydrophobicity of the MCD, was itself controlling the release of drug and hence addition of leucine (another hydrophobic agent) might have slowed down the release of rifampicin by encapsulating the system.

MCD-Rif NSD and MCD-Rif-Leu NSD powder formulations showed biphasic release pattern. The first phase of the release was found upto 6 hrs, where steady and almost linear release of drug was observed. Later on, rifampicin release was slowed down (second phase), which could be due to the release of rifampicin encapsulated within the core of NSD powder formulation. These results were found to be in agreement with the observation described by Klariæ et. al., (Klariæ et.al., 2012). However, release profiles did not uncover any release mechanism which rifampicin might have followed. Hence, in-vitro drug release data from MCD-Rif NSD formulations was analyzed to reveal the drug release mechanism (Costa et. al., 2001).

The results of curve fitting for MCD-Rif NSD formulations analyzed using various mathematical models (zero order, first order, Higuchi, Korsmeyers and peppas) are presented in Table 11.5. The plot of percent cumulative drug release vs. square root of time for MCD-Rif NSD formulation showed higher correlation coefficient value ( $r^2=0.973$ ), indicating that the release followed Higuchi square root model, which suggested release of rifampicin from MCD-Rif NSD formulation was mainly dominated by diffusion mechanism. On the contrary, MCD-Rif-L NSD formulation showed higher coefficient value ( $r^2=0.979$ ) with the plot of % CDR vs time corresponding to zero order model, advising drug release was independent of time and may be controlled by the dissolution mechanism. This type of behavior could be due to MCD and leucine layer formed to encapsulate rifampicin as discussed earlier in this chapter. However, both the formulations showed different release mechanism. Hence to find out the release mechanism, release curve data was analyzed by Korsmeyers and Peppas model (Kosmidis et.al., 2003), which resulted super case II transport mechanism for both MCD-Rif NSD and MCD-Rif-L NSD formulations with the n values 2.059 and 1.998 respectively. Thus, main mechanism for the drug transport from the MCD NSD particles was found to be controlled by super case II transport. This indicated that Korsmeyers and Peppas model satisfactorily represented the release data.

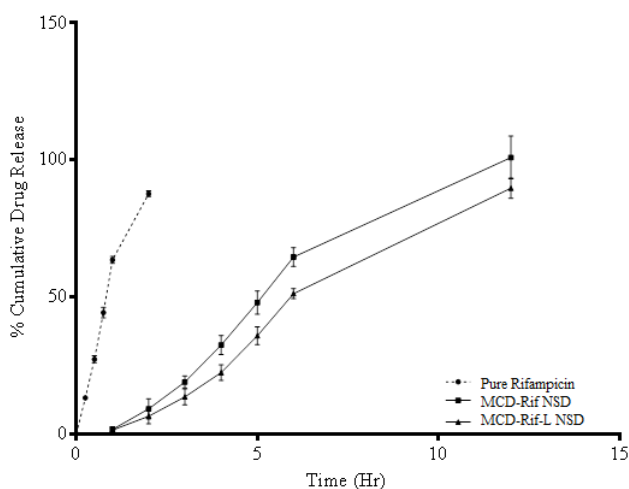


Figure 11.7: Percent cumulative drug release (% CDR) of Rifampicin, MCD-Rif NSD and MCD-Rif-L NSD powder formulation. ( $n=3$  determinations  $\pm$ SD)

Table 11.4: Kinetics model fitting of in vitro release data of MCD-Rif NSD powder formulation

Model	R <sup>2</sup>		Slope		Intercept	
	MCD-Rif	MCD-Rif-L	MCD-Rif	MCD-Rif-L	MCD-Rif	MCD-Rif-L
Zero order	0.958	<b>0.979</b>	9.385	8.41	-4.913	-8.162
First order	0.6496	0.7081	0.1361	0.1419	0.7066	0.5654
Higuchi	<b>0.973</b>	0.9597	43.22	38.05	-48.93	-46.22
Hixon-Crowell	0.9598	0.9331	81.26	71.77	-89.90	-82.51
Korsemeyer Peppas	0.9917	0.9978	2.059 (n)	1.998 (n)	0.2604	0.1632

### 11.8.8 Stability Studies

Stability study of MCD-Rif NSD powder formulations was carried out in terms of drug content and particle size for 2 month at ambient temperature (10-20 °C) in dark. Results of stability study are tabulated in table 11.5. No significant difference was noted in the drug content, particle size and PDI values of MCD NSD (MCD-Rif and MCD-Rif-L) powder formulations. The results suggested ability of MCD NSD powder formulations to remain stable at room temperature (RT). Therefore, RT could be considered as suitable storage condition for both the formulations.

**Table 11.5: Stability of MCD-Rif NSD formulation at RT (10-20 °C)**

Sr. No	Time (Months)	Drug Content (%)		Particle Size in nm (PDI)	
		MCD-Rif	MCD-Rif-L	MCD-Rif	MCD-Rif-L
1	Initial	100	100	222.08±2.54 (0.320±0.069)	228.91±9.52 (0.542±0.046)
2	2	98.54±0.094	99.01±0.61	224.44±10.36 (0.35±0.069)	227.12±9.34 (0.036±0.035)

n=3 determinations, ± SD values

### 11.8.9 Conclusions

An acyl (octanoyl) chitosan derivative i.e. MCD was synthesized and characterized for physicochemical properties. Substitution of MCD on to the parent chitosan moiety was confirmed based on the results of FTIR, <sup>1</sup>H-NMR. DSC studies confirmed thermal stability, whereas XRD spectra have showed crystallinity of MCD. Moreover, MCD was employed to check its feasibility in the preparation nano spray dried powder formulations with or without amino acid adjunct (L-Leucine) in order to improve the aerosolization efficiency of dry powder formulation. The aerosol performance of the nano spray-dried powders formulations (MCD-Rif and MCD-Rif-L) presented MMAD (1.53±0.171 & 1.96±0.167) within the range of 1-5 μm suggesting suitability of MCD in the formulation of DPI for pulmonary delivery. Similarly, aerosol performance of >50 % FPF was also observed from the in-vitro lung deposition studies of MCD-Rif and MCD-Rif-L NSD powder formulations. Release studies confirmed the applicability of MCD in controlling the release of drug. More than 80 % of drug was released from MCD-Rif NSD and MCD-Rif-L NSD powder formulation by the end of 12 hrs. In sum, it is envisaged that the MCD could be an effective carrier system for controlled drug delivery. MCD was found suitable for nano spray drying and this approach could provide a feasible and attractive alternative for the preparation of nano spray dried powder inhalation (NSDPI) for encapsulation of range of antibiotics to improve therapeutic outcomes for patients suffering from draining respiratory diseases such as MTB.

### References

- Alves R., Reis T.V., Cides da Silva L.C., Storpirtis S., Mercuri L.P., Matos J.R. (2010) Thermal behavior and decomposition kinetics of rifampicin polymorphs under isothermal and non-isothermal conditions. *Brazilian Journal of Pharmaceutical Sciences*, 46, 2, 343-351.
- Benetton S.A., Kedor-Hackmann E.R.M., Santoro M.I.R.M., Borges V.M. (1998) Visible spectrophotometric and first-derivative UV spectrophotometric determination of rifampicin and isoniazid in pharmaceutical preparations, *Talanta*, 47,3, 639–643.
- British Pharmacopoeia (2012) Appendix XII C. Consistency of Formulated Preparations, *British Pharmacopoeia Volume V*, British Pharmacopoeia, 2012 online.
- Chen N.Y., Schekunov B.Y., Tong H.H., Chow A.H., Savage C., Wu J., Chan H.K. (2005) Effect of amino acids on the dispersion of disodium cromoglycate powders. *J. Pharm. Sci.* 94, 10, 2289-2300.
- Choi C.Y., Kim S.B., Pak P.K., Yoo D.I., Chung Y.S. (2007) Effect of *N*-acylation on structure and properties of chitosan fibers. *Carbohydrate Polymers*, 68, 122–127.
- Choudhari Y.M., Detane S.V., Mourya V.K., et.al., (2012) Low molecular weight palmitoyl chitosan: Synthesis, characterization and nanoparticle preparation, *Adv. Mat. Lett.*, 3, 6,487-492
- Corrigan D.O., Corrigan O.I., and Healy A.M. (2006) Physicochemical and in vitro deposition properties of salbutamol sulphate/ipatropium bromide and salbutamol sulphate/excipient spray dried mixtures for use in dry powder inhalers. *Int. J. Pharm.*, 322, 22–30.
- Costa P., Lobo J. (2001) Modeling and comparison of dissolution profiles, *European J. of Pharm. Sci.*, 13, 123–133
- Gautier S., Arpagaus C., Schafroth N., Meuri M., Deschamps A., and Maquet V. (2010), Very fine chitosan microparticles with narrow & controlled size distribution using spray-drying technologies, *Drug Delivery Technology*, 10, 8, 30-37.
- Hirota K., and Terada H. (2012). *Endocytosis of Particle Formulations by Macrophages and Its Application to Clinical Treatment*, Molecular Regulation of Endocytosis, Dr. Brian Ceresa (Ed.), ISBN: 978-953-51-0662-3, InTech, DOI: 10.5772/45820. Available from: <http://www.intechopen.com/books/molecular-regulation-of-endocytosis/endocytosis-of-particle-formulations-by-macrophages-and-its-application-to-clinical-treatment> (Date accessed May 2013).

## Chapter 11 - Preparation of MCD-Rif particles by NSD

---

Klariæ D., Hafner A., Zubèiæ S., Dürriigl M., and Filipoviæ-Grèiæ J. (2012) Spray-dried Microspheres Based on Chitosan and and LecithinCyclosporin A Delivery System. *Chem. Biochem. Eng. Q.* 26, 4, 355–364

Kosmidis K., Rinaki E., Argyrakis P., Macheras P. (2003) Analysis of Case II drug transport with radial and axial release from cylinders. *International Journal of Pharmaceutics*, 254, 183–188.

Lechuga-Ballesteros D., Charan C., Stults C.L.M., Stevenson C.L., Miller D.P., Vehring R., Tep V., Kuo M-C. (2008) Trileucine Improves Aerosol Performance and Stability of Spray-Dried Powders for Inhalation, *J Pharm Sci*, 97,1, 287-302. (DOI 10.1002/jps.21078).

Lehrman S.R., Stevenson C., Yang B. (2003) Modulating charge density to produce improvements in the characteristics of spray-dried proteins. WO 2003035028 A1, May 1, 2003

Ma G., Yang D., Zhou Y., Xiao M., Kennedy J.F., Nie J. (2008) Preparation and characterization of water-soluble N-alkylated chitosan. *Carbohydrate Polymers*. 74, 121–126.

Marques M.R.C., Loebenberg R., and Almukainzi M. (2011) Simulated Biological Fluids with possible application in Dissolution Testing/. *Dissolution Technologies*, August, 15-28.

Najafabadi A.R., Gilani K., Barghi M., Rafiee-Tehrani M. (2004) The effect of vehicle on physical properties and aerosolisation behaviour of disodium cromoglycate microparticles spray dried alone or with L-leucine. *Int J Pharm*, 285, 1-2, 97-108

Padhi B.K., Chougule M.B., Misra A. (2006) Optimization of formulation components and characterization of large respirable powders containing high therapeutic payload. *Pharm Dev Technol.* 2006;11(4):465-75.

Parlati C., Colombo P., Buttini F., Young P.M., Adi H., Ammit A.J., and Traini D. (2009) Pulmonary Spray Dried Powders of Tobramycin Containing Sodium Stearate to Improve Aerosolization Efficiency, *Pharmaceutical Research*, 26, 5, 1084-1092.

Peesan M., Sirivat A., Supaphol P., Rujiravanit R. (2006) Dilute solution properties of hexanoyl chitosan in chloroform, dichloromethane, and tetrahydrofuran, *Carbohydrate Polymers* 64 (2006) 175–183

Rabinovich Y.I., Adler J.J., Ata A., Singh R.K., Moudgil B.M. (2000) Adhesion between Nanoscale Rough Surfaces. *J Colloid Interface Sci*, 232, 1, 10-16

## Chapter 11 - Preparation of MCD-Rif particles by NSD

---

Raula J., Kurkela J.A., Brown D.P., Kauppinen E.I. (2007) Study of the dispersion behaviour of L-leucine containing microparticles synthesized with an aerosol flow reactor method, *Powder Technology*, 177, 125–132

Raula J., Lahde A., Kauppinen E.I. (2009) Aerosolization behavior of carrier-free L-leucine coated salbutamol sulphate powders. *Int J Pharm.* 2009 Jan 5;365(1-2):18-25

Russo P., Santoro A., Prota L., Stigliani M., and Aquino R.P. (2012). Development and Investigation of Dry Powder Inhalers for Cystic Fibrosis, Recent Advances in Novel Drug Carrier Systems, PhD. Ali Demir Sezer (Ed.), ISBN: 978-953-51-0810-8, InTech, DOI: 10.5772/51408. Available from: <http://www.intechopen.com/books/recent-advances-in-novel-drug-carrier-systems/development-and-investigation-of-dry-powder-inhalers-for-cystic-fibrosis>

Tatarczak M., Flieger J., and Szumilo H. (2005), High-Performance Liquid-Chromatographic Determination of Rifampicin in Complex Pharmaceutical Preparation and in Serum Mycobacterium Tuberculosis-Infected Patients, *Acta Poloniae Pharmaceutica - Drug Research*, 62, 4, 251-256.

Tien C.L., Lacroix M., Ispas-Szabo P., Mateescu M. (2003) N-acylated chitosan: hydrophobic matrices for controlled drug release, *Journal of Controlled Release*, 93, 1, 1-13.

Vadwai V., Daver G., Udawadia Z., Sadani M., Shetty A., et al. (2011) Clonal Population of *Mycobacterium tuberculosis* Strains Reside within Multiple Lung Cavities. *PLoS ONE*, 6, 9, e24770. doi:10.1371/journal.pone.0024770.

Vehring R. (2008) Pharmaceutical Particle Engineering via Spray Drying, *Pharmaceutical Research*, 25, 5, 999-1022.

Yang Y., Bajaj N., Xu P., Ohn K., Tsifansky M.D., Yeo Y. (2009) Development of highly porous large PLGA microparticles for pulmonary drug delivery. *Biomaterials*, 30, 10, 1947-53.

Zong Z., Kimura Y., Takahashi M., Yamane H. (2000) Characterization of chemical and solid state structures of acylated Chitosans. *Polymer*. 41, 899–906.

### 12.0 In-vitro Cell line studies

#### 12.1 Materials

Hydrophobic chitosan derivative, Modified Chitosan Derivative as prepared in our laboratory. Fluorescein isothiocyanate (FITC), (3-[4,5-dimethyl-thiazole-2-yl]-2,5-diphenyl tetrazolium bromide) (MTT), L-glutamine, gentamycin sulfate, fetal bovine serum (FBS), 4'-6-diamidino-2-phenylindole (DAPI) and dimethyl sulfoxide (DMSO), RPMI-1640 medium, FBS, Antimycotic antibiotic, Ficol (Histopaque 1.077g/ml) were purchased from Sigma-Aldrich (St-Louis, USA). LD column was purchased from Miltenyi Biotec (UK), Fixable Live/Dead Violet stain, Zenon-PE fluorescent labelling kit, G1 isotype, G2a isotype ab and G2b isotype ab was procured from AbD Serotec (UK). Cytokine IL-10, IL-12, TNF- $\alpha$ , Streptavidin-PE kits and isotype goat biotin were purchased from R & D systems (Minneapolis, USA). MHC-II DR was obtained from AbD Serotec (UK), CD16 was purchased from Enzo Life Sciences (UK). All other reagents and solvents were obtained from Sigma-Aldrich (St-Louis, USA).

#### 12.2 Equipments

1. Centrifuge (Sigma 3K30, Germany & Sigma Laboratory Centrifuge, 3K30, UK)
2. Bath Sonicator (Ultrawave Ltd, Cardiff, UK)
3. Fluorescence spectrometer (LS 55, Fluorescence spectrometer, Perkin Elmer, Wellesley, USA).
4. ELISA plate reader (SpectraMAX 190, Molecular Devices, UK)
5. Flow Cytometer (MACSQuant, Miltenyi Biotec, UK)

#### 12.3 Cytotoxicity studies

Cell culture system consisting of cell lines derived from human or animals have been established and are routinely used for screening of various formulations and polymers in-vitro. The advantages of application of cell lines include easy handling, retention of organ specific properties by cell lines, unlimited source of self-replication which can be grown in infinite quantities as much as we want, high degree of homogeneity. Although contamination of the cell lines is most common drawback associated with cell culture system, replacement of cell lines from frozen stock overcomes this disadvantage.

There are several parameters for the screening of cytotoxicity or cell death, which are based on the determination of membrane integrity, cellular metabolite content, mitochondrial function and lysosomal function (Weyermann *et.al.*, 2004; Li, 2005; Ekwall *et.al.*, 1990).

**Membrane integrity** is classical endpoint for cytotoxicity, where increased amount of cytoplasmic enzymes (e.g. lactate dehydrogenase) in the culture medium is determined. Lactate dehydrogenase (LDH) is a stable cytoplasmic enzyme present in all cells, which releases into cell culture medium upon damage to the plasma membrane. Activity of LDH is determined with the help of enzymatic test. First step of enzymatic test involves reduction of NAD<sup>+</sup> to NADH/H<sup>+</sup> by the LDH catalyzed conversion of lactate to pyruvate, whereas, catalyst (diaphorase) transfers H/H<sup>+</sup> from NADH/H<sup>+</sup> to the tetrazolium salt 2-(4-

iodophenyl)-3-(4-nitrophenyl)-5-phenyltetrazolium chloride (INT), which is reduced to a red formazan in the second step. In certain cases, e.g. when basal level of cytoplasmic enzymes in hepatocytes is too high, sensitivity of method is limited.

In **cellular metabolite content**, estimation of cellular ATP is the most commonly measured metabolite and is determined based on the knowledge that dead or damaged cells contain little or no ATP. A bioluminescence assay is to be carried out in which catalysis of luciferase leads to the formation of light from ATP and luciferin and the intensity of emitted light is directly proportional to the concentration of ATP. This assay allows the use of as little as few hundred cells per assay.

Thirdly, assessment cytotoxicity by **mitochondrial function** is by using a well-known chemical called (3-[4,5-dimethyl-thiazole-2-yl]-2,5-diphenyl tetrazolium bromide) (MTT). MTT gets reduced to blue coloured crystals only in presence of metabolically active cells (viable cells). These crystals can be solubilized and quantified by using spectrophotometric assay. This assay is also called as MTT assay.

In **lysosomal functions test**, neutral red (3-amino-*m*-dimethylamino-2-methylphenazine hydrochloride) uptake assay is used to measure the cell viability as reflected by lysosomal functions based on the uptake and subsequent lysosomal accumulation of the supravital dye (neutral red). In case of cell damage or cell death, small amount of neutral red will be taken up by the cells. Assay of dye extracted from the cells has been shown to be linear with cell numbers, both by direct cell counts and by protein estimation of cell populations. Finally apoptosis, where induction of programmed cell death or apoptosis is carried out.

Depending upon the requirement of final outcome, cytotoxicity can be assessed. On one hand the ability of test compounds to inhibit the growth of cells is important in cancer therapeutics, whereas intactness of cell viability is tested in order to study the suitability of polymers for their application in drug and vaccine delivery. In this experiment, we analyzed the ability of test compounds to have minimum inhibition on growth of cells and their maximum uptake in the cells.

### 12.4 MTT assay of HCD and MCD on A549 cells

MTT cell proliferation assay for HCD and MCD was performed using MTT dye reduction assay according to the method described by Kroll (2011). The cytotoxicity profiles of HCD and MCD was evaluated over 48 hr in adenocarcinomic human alveolar basal epithelial cell line, A549. The cells (passage no. 45-49) were cultured in 96-well plates with 100  $\mu$ l RPMI-1640 medium supplemented with 10% foetal bovine serum (FBS) and 1% antimycotic solution as antibiotic (complete medium) for 24 hr in a humidified 5% CO<sub>2</sub>/95% incubator at 37°C. Then, 100  $\mu$ l of freshly prepared sample dispersions in complete medium were added to the wells to an appropriate concentration (0 - 5 mg/ml) ( $n = 3$ ), and 10% dimethyl sulfoxide (DMSO) as a positive control and incubated for a further 48 hr, followed by the addition of 40  $\mu$ g/ml MTT solution (5 mg/ml in PBS, pH 7.4) to each well. After incubating

the plates for 2 hr, the medium was carefully removed and any formazan crystals generated were solubilized with 100  $\mu$ l of DMSO and optical density (OD or absorbance) was measured using ELISA plate reader (SpectraMAX 190, Molecular Devices) at 570 nm. The MTT test was performed in triplicate and the results were expressed as percentage of cell growth with respect to the control wells (only the cells in the medium). The relative cell viability (%) was calculated using following equation:

$$\text{Cell viability (\%)} = \frac{\text{OD of test well}}{\text{OD of reference well}} \times 100$$

### 12.5 Cell viability and Cellular uptake studies in porcine monocyte

Cell cytotoxicity study was also carried out using freshly prepared porcine monocytes. Nanoparticles and polymers were diluted to specific concentration of 10 to 100  $\mu$ g/ml and freshly isolated monocytes were pulsed for 2 hours both at 4°C (surface binding control) and at 37°C. The MTT test was performed in triplicate and the results were expressed as percentage of cell growth with respect to the control wells (only the cells in the medium). The relative cell viability (%) was calculated.

Cellular uptake study of the HCD was carried out by using HCD covalently labeled with FITC, and its nanoparticles. Freshly prepared porcine monocyte cells were seeded at a density of  $5 \times 10^4$  cells per well in a 48-well plate in RPMI medium containing 10% FBS and incubated for 24 h to achieve ~60–70% confluency. Nanoparticles/polymers at the specific concentration were added to each well and freshly isolated porcine monocytes were pulsed for 2 hrs either at 4°C (surface binding control) or at 37°C. The uptake process was terminated by removing the media containing nanoparticles/polymers and washed with PBS. The percentages of FITC positive cells were determined by fluorescence activated cell sorting (FACS) analysis of the cells using a flow cytometer (MACSQuant, Miltenyi Biotec, UK).

### 12.6 Immunostimulatory study in porcine monocyte, B cells and dendritic cells

In response to the stimuli by pathogenic materials, various pro-inflammatory chemicals called cytokines are released in the body. Therefore, in order to study the ability of our formulations to stimulate release of cytokines was studied. Induction of cytokine release after activation of cells using nanoparticles was tested on freshly prepared porcine monocytes, B cells and enriched dendritic cells. The supernatants were collected and analyzed for presence of cytokine by ELISA. Different cytokines such as TNF- $\alpha$ , IL-12 and IL-10 were identified and assayed.

In addition, immunostimulatory effect of particles in terms of CD16 and MHC-II DQ expression was carried out on freshly prepared porcine monocytes. The monocytes were stained with either a CD16 antibody or an MHC-II DQ antibody with live/dead dye and analysed the cells using a flow cytometer (MACSQuant, Miltenyi Biotec, UK) to determine the expression pattern of cells after activation with the nanoparticles (HCD-NPs).

### 12.6.1 Isolation and culture of peripheral blood mononuclear cells (PBMCs)

Heparinized venous blood was obtained from pig 6162. Peripheral blood mononuclear cells (PBMCs) were isolated by Ficoll-Hypaque (Ficoll 6,42% (Sigma Aldrich, St. Louis), around 30 ml of heparin blood was layered over Ficoll-Hypaque and centrifuged for 25 mins at 2500rpm at room temperature (RT) with breaks off. The buffy coat layer was aspirated and washed with 50ml cold sterile PBS. After that, RBC's were lysed for 6 mins at RT with BD Pharmlyse and cells were washed twice with 50ml cold PBS. Cells were then resuspended in 20ml cold RPMI and counted on the flow cytometer (MACSQuant, Miltenyi Biotec).

**FACs buffer:** Mixture of PBS with 1% FBS and 0.09% sodium azide.

#### 12.6.1.1 Removal of monocytes

1. Cells were spun down and 10ul CD14 beads/ $10^7$  cells were added to it (Miltenyi Biotec)
2. Cells were incubated for 15 mins at RT and after incubation, washed with PBS containing 2% FBS.
3. The LD column (Miltenyi Biotec) was assembled and wet with 2ml Magnetic-activated cell sorting (MACs) buffer.
4. Cells were resuspended at  $1.25 \times 10^8$  per 500ul of MACs buffer so as to make 1ml per column.
5. Finally cells were applied to column(s), washed twice with 1ml MACs buffer. Thus, 3 ml of positive fraction was eluted in MACs buffer (per column). Elute was collected to get the monocyte and this CD14 negative fraction was preserved for isolation of B cells and enriched dendritic cells.

#### Isolation of Monocytes

1. Positive fraction was eluted into 3 ml MACs buffer (per column) as mentioned above.
2. After that, LS column (only one needed) was set up and wetted with 500ul MACs buffer.
3. Cells were applied to column and washed thrice with 3ml MAC buffer.
4. Resultant monocytes were eluted in 5 ml of RPMI.

#### Isolation of B cells

1. B cells were isolated from negative fraction as obtained from CD 14 cells. Washed once with 2% FBS and counted on flow cytometer ( $2.71 \times 10^8$  total).
2. Cells were spun down and aCD21 100ul/ $10^8$  cells at a dilution of 1:10 = 10ul CD21 antibody was added to it.
3. Cells were incubated for 15 mins at RT and washed once in 2% FBS.
4. Thereafter, 271ul IgG beads (10ul/ $10^7$  cells) were added to it and incubated for 15mins at 4 °C.
5. Again cells were washed once with 2% FBS, resuspended at  $10^8/500$ ul MACs buffer.

6. Finally, LS column was set up (only one needed), wetted with 500ul MACs buffer and cell were applied.
7. Cells were washed thrice with 3ml MACs buffer and elution of B cells was carried out using 5ml of RPMI.

### **Isolation of Enriched Dendritic cells (DCs)**

1. Took CD14 negative fraction as mentioned above. Cells were spun down and CD172a antibody 1ul/10<sup>7</sup> cells were added to it. Cells were washed down side of falcon with 10x 2% FBS i.e 490ul.
2. Obtained cells were incubated for 30 mins 4 °C.
3. After incubation period, cells were washed once in 2% FBS
4. After that, IgG beads at 10ul/10<sup>7</sup> cells (490ul) were added to it and incubated for 15 mins at 4 °C.
5. Cells were again washed once with 2% FBS and resuspended at 10<sup>8</sup>/500ul in PBS.
6. LS column (only one needed) was set up, wetted with 500ul MACs buffer and cells were applied to column. Washings were done three times with 3ml MACs buffer and enriched dendritic cells were eluted into 10ml RPMI.

### **12.6.2 Cytokine Assay**

Nanoparticle formulations were suspended at the concentration of 1mg/ml in water and sonicated for 5mins. Stock of nanoparticles was diluted to 100 µg/ml, 33 µg/ml and 11 µg/ml and 50 µl of nanoparticles were added to 50ul of cells per well. Plate was incubated at 37°C for 2 hours. After incubation time, cells were washed thrice with PBS containing 2% FBS and once with RPMI. Then cells were resuspended in 200 µl RPMI and incubated overnight at 37°C. RPMI alone was considered negative control, whereas positive control was Aditipoline (3.2 µl (at 1mg/ml) + 1596.8 µl RPMI) used 100ul/well (+100 µl cells) giving a final concentration of 1ug/ml. After overnight incubation of cells, they were spun down and supernatant was collected for cytokine ELISA, whereas cells were used for the expression of MHC II and CD16 cells.

Concentration of various cytokines such as TNF- $\alpha$ , IL-10, and IL-12 in cell culture supernatants was determined by enzyme-linked immunosorbent assay (ELISA) using kits Duo set from R&D Systems (Minneapolis, MN, USA) according to manufacturer's directions.

#### **12.6.2.1 ELISA Protocol (Manufacturers Protocol, R & D systems)**

##### **Preparation of Plate**

1. Capture Antibody was diluted to the working concentration in PBS without carrier protein.
1. A 96-well microplate was immediately coated with 100 µL per well of the diluted Capture Antibody, the plate was sealed and incubated overnight at RT.
2. After that, each well was aspirated and washed with Wash Buffer. The process was repeated thrice. Complete removal of liquid at each step was essential for good

performance. After the last wash, any remaining Wash Buffer was removed by aspirating or by inverting the plate and blotting it against clean paper towels.

3. Plates were then blocked by adding 300  $\mu\text{L}$  of Reagent Diluent to each well and incubated at RT for a minimum of 1 hour.
4. Thereafter, aspiration/washing as in step 2 was repeated and the plates were made ready for sample addition.

### Assay Procedure

1. 100  $\mu\text{L}$  of sample or standards in Reagent Diluent, or an appropriate diluent was added per well. The plate was covered with an adhesive strip and incubated for 2 hours at RT.
2. Aspiration/washing as mentioned in step 2 of Plate Preparation was repeated.
3. 100  $\mu\text{L}$  of the Detection Antibody was diluted in Reagent Diluent and added to each well. The plate was covered with a new adhesive strip and incubated again for 2 hours at RT.
4. Aspiration/washing as mentioned in step 2 of Plate Preparation was repeated.
5. 100  $\mu\text{L}$  of the working dilution of Streptavidin-HRP was added to each well, the plate was covered and incubated for 20 minutes at RT. Precaution was taken to avoid placing the plate in direct light.
6. Aspiration/washing as mentioned in step 2 of Plate Preparation was repeated.
7. 100  $\mu\text{L}$  of substrate solution was added to each well and the plate was incubated for 20 minutes at RT. Same precaution to avoid direct exposure to light was taken.
8. 50  $\mu\text{L}$  of Stop Solution was added to each well and thorough mixing was ensured by gentle tapping the plate.
9. Finally, the optical density of each well was determined immediately, using a microplate reader set to 450 nm.

### 12.6.3 Analysis of T cell activation (Maturation Marker Staining)

After overnight incubation of cells (porcine monocyte) as mentioned in A-12.6.2, cells obtained were used for analysis of T cell activation (maturation marker staining). Cells were stained with Fixable Live/Dead Violet stain (Invitrogen, UK) in a dilution of 1:50 in PBS. Specified amount of cells (5  $\mu\text{l}$ ) per well were added and incubated for 20 mins at RT in the dark. Cells were washed once with PBS, centrifuged for 3 mins at 2000rpm, flick off supernatant and vortexed. Then surface stains were added as mentioned below:

MHC-II DR (AbD Serotec, UK), CD16 (Enzo Life Sciences, UK) and their isotype controls were fluorescently labeled using a Zenon-PE kit (Invitrogen, UK) according to manufacturer's instructions. Briefly:

1. 2  $\mu\text{l}$  DR ab + 10  $\mu\text{l}$  G2b-PE zenon label (incubated for 5 mins) + 10  $\mu\text{l}$  Blocking buffer (incubated for 5 mins) + 308  $\mu\text{l}$  FACS buffer.
2. 20  $\mu\text{l}$  G2b isotype ab + 10  $\mu\text{l}$  G2b-PE zenon label (incubated for 5 mins) + 10  $\mu\text{l}$  Blocking buffer (incubated for 5 mins) + 290  $\mu\text{l}$  FACS buffer
3. 4.5  $\mu\text{l}$  CD16 ab + 22.5ul G1-AlexaFluor647 zenon label (5mins) + 22.5ul Blocking buffer (5mins) + 198ul FACS buffer

4. 20  $\mu$ l G1 isotype Ab (AbD Serotec) + 10ul zenon labeled ab + 5ul G1-AlexaFluor647 zenon label (5mins) + 5ul blocking buffer (5mins) + 35ul FACS buffer.
5. All samples were stored at 4 °C in the dark until flow cytometry analysis. Samples of 5  $\mu$ l per well was used for the flow cytometry.

Surface antibodies were incubated with cells for 30 mins at 4°C, washed as above. Secondary ab (Streptavidin-PE, R&D, Minneapolis, USA) was added to MHC II and CD 16/isotype wells at a dilution of 1:20 (5  $\mu$ l per well) and incubated for 10 min at RT, again washed as above. Cells were then resuspended in 200  $\mu$ l of FACS buffer and analyzed using flow cytometer (MACSQuant, Miltenyi Biotec, UK). PE voltage was kept the same for each marker and cell type.

## 12.7 Results and Discussion

### 12.7.1 Cytotoxicity studies of HCD and MCD

A very important criterion to determine the suitability of polymers in drug delivery is their cytotoxicity. It is reported that cationic agents usually confer severe cytotoxicity due to their ability to interact with cell membrane and other negatively charged cellular components or proteins (Lv et. al., 2006). Therefore, less cytotoxic materials are always preferred while choosing carrier for vaccine or drug delivery. Chitosan and its derivatives are reported to be less cytotoxic than other cationic polymers such as poly-lysine and polyethyleneimine (Dai et. al., 2011; Hoskins et. al., 2012). However, the cytotoxicity caused due to chitosan and its derivative is mainly a matter of type of chitosan derivative as well as the type of cells under study (Lv et. al., 2006; Weng et. al., 2008). This study has used chitosan derivatives and demonstrated the viability of cells treated with HCD and MCD by MTT assay. Figure 12.1a & 12.1b shows in vitro cytotoxicity of HCD and MCD in A549 cells. Data are expressed as mean  $\pm$  S.D. (n = 3) as depicted in Table 12.1. Results indicated that both the polymers (HCD and MCD) did not show significant changes in the cell viability at the tested concentrations in comparison to the negative control (taken as 100% viability) and positive control (100 % cytotoxicity; Fig. 12.1c). Therefore, MTT assay results confirmed the in vitro biocompatibility of HCD and MCD, which is important for the development of successful vaccine and drug delivery systems.

Table 12.1: In vitro cytotoxicity of controls and polymers HCD & MCD in A 549 cells

Conc. ( $\mu$ g/ml)	% Cell Viability			
	RPMI	HCD	RPMI	MCD
0	100 $\pm$ 17.51	88.8 $\pm$ 12.69	100 $\pm$ 8.24	81.05 $\pm$ 6.68
0.078125	91.6 $\pm$ 4.72	81.34 $\pm$ 3.4	108.95 $\pm$ 15.16	88.3 $\pm$ 12.29
0.15625	87.67 $\pm$ 13.79	77.86 $\pm$ 10	116.55 $\pm$ 4.34	94.47 $\pm$ 3.51
0.3125	95.93 $\pm$ 3.17	85.19 $\pm$ 2.3	106.33 $\pm$ 7.88	86.18 $\pm$ 6.38
0.625	99.57 $\pm$ 15.82	88.42 $\pm$ 11.47	109.57 $\pm$ 3.03	88.8 $\pm$ 2.45
1.25	86.59 $\pm$ 8.71	76.9 $\pm$ 5.47	90.7 $\pm$ 10.93	73.51 $\pm$ 8.86
2.5	83.38 $\pm$ 11.24	74.05 $\pm$ 8.15	86.71 $\pm$ 13.2	70.28 $\pm$ 10.7

n = 3;  $\pm$  SD; HCD – Hydrophobic chitosan derivative; MCD – Modified chitosan derivative

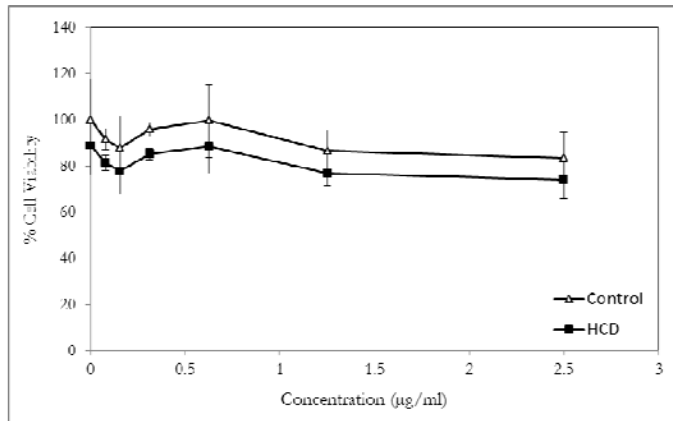


Figure 12.1a: In vitro cytotoxicity of ( $\Delta$ ) RPMI control and ( $\blacksquare$ ) HCD in A 549 cells

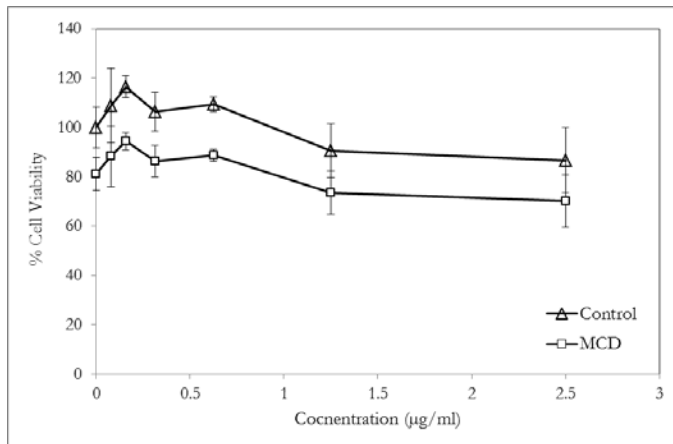


Figure 12.1b: In vitro cytotoxicity of ( $\Delta$ ) RPMI control and ( $\blacksquare$ ) MCD in A 549 cells

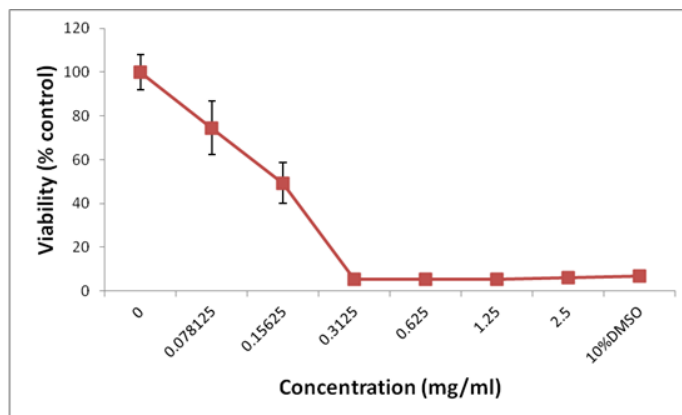


Figure 12.1c: In vitro cytotoxicity of DMSO control in A 549 cells

### 12.7.2 Cytotoxicity and cellular uptake study

Cell viability was evaluated to ensure that low levels of cytokine secretion were not caused by cell death during the period of treatment. Results of the viability are shown in figure 12.2, which indicated no deleterious effect of the particle concentration up to 100  $\mu\text{g}/\text{ml}$  on cells.

After the cytotoxicity studies, similar concentrations were used in the uptake studies. Results of the uptake studies are graphed in figure 12.3a and 3b, representing cellular uptake of Prep 1 (HCD-Ag NPs), Prep 2 (HCD NPs and Ag85A), Prep 3 (Blank HCD NPs), Prep 4 (HCD-FITC NPs) at 37 and 4  $^{\circ}\text{C}$ . Out of 4 preparations, prep 4 was FITC labeled, whereas others were having slight auto fluorescing property. It was observed that Prep 4 which is made up of HCD-FITC indicated highest cellular uptake of almost 100 % at 37  $^{\circ}\text{C}$ , suggesting the suitability of utilization of formulation at normal physiological temperature, whereas same formulations at 4  $^{\circ}\text{C}$  showed less uptake. All other formulations which were not FITC labeled showed less in-vitro cellular uptake at both 37 and 4  $^{\circ}\text{C}$ . This may be due to use of unlabeled polymers and formulations. All other preparations displayed cellular uptake below 20 %. Thus, Prep 4 showed almost 5 fold increase in the cellular uptake indicating efficient cell uptake of HCD NPs. Since HCD polymers consist of both cationic amino groups and hydrophobic octanoyl moieties, both, charge attraction and hydrophobic interactions may have played an important role in the cellular uptake process (Piest and Engbersen, 2010). Studies have shown efficient cellular uptake without adverse effect on the viability of the cells (porcine monocytes) indicating that formulations and polymers were devoid of toxicity on the cells (Figure 12.2).

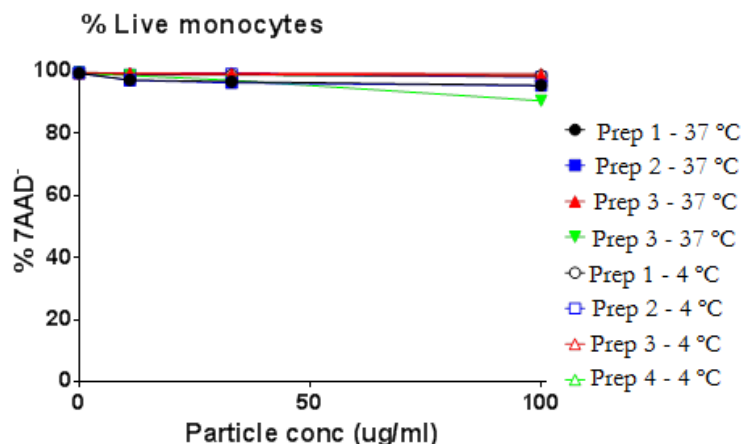


Figure 12.2: In vitro cytotoxicity of HCD polymers and HCD NPs in porcine monocytes.

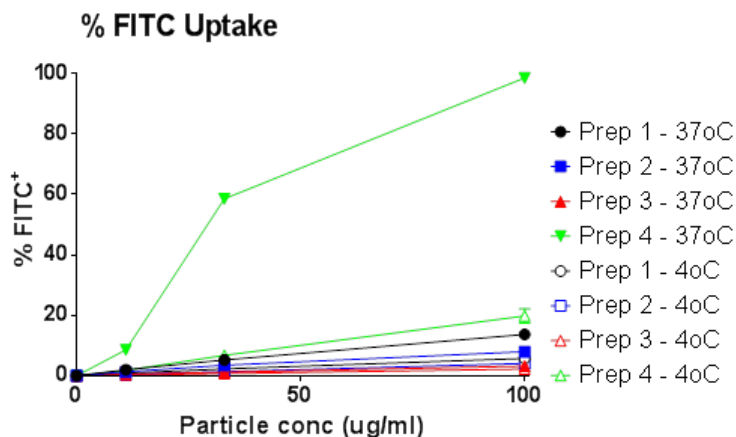


Figure 12.3a: Cell uptake of formulation and polymers at 37 and 4 °C

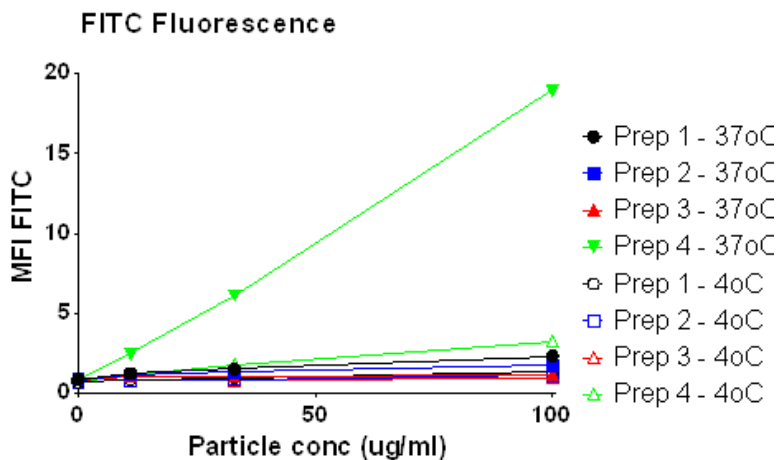


Figure 12.3b: Cell uptake of formulation and polymers at 37 and 4 °C

### 12.7.3 Immunostimulatory study

Cytokine production was performed in the porcine monocytes, B cells and enriched dendritic cells. Cytokines were assayed using specified ELISA's and concentrations were expressed as pg/mL. Cytokines namely IL- 10, IL- 12 and TNF $\alpha$  were selected for the study and the results for each of cytokine in different cell type are displayed in figure A12.4a, 4b and 4c. As shown in figures, significant induction of these cytokines (IL- 10, IL- 12 and TNF $\alpha$ ) was observed from all preparations in different cell culture except the performance of preparation 3 in porcine monocyte.

#### 12.7.3.1 Assay of IL-10

It was observed that, Prep 1 and 2 augmented secretion of IL-10 (in monocytes) with the concentration of more than 1500 pg/ml at all concentration levels of formulations, whereas Prep 4 showed increasing secretion of IL-10 with increase in its concentration of prep 4. At high concentration, more than 1500 pg/ml of L-10 was noted. Prep 3 (blank HCD NPs) exhibited less than 100 pg/ml of IL-10 at all concentration levels (Figure 12.4a). In case of B

cells, all of the preparations (prep 1 - 4) showed increased IL-10 secretion at their low concentration (Figure A12.4a), whereas increased concentration of all preparations showed reduced secretion of IL-10. Concentration of IL-10 secretion in enriched dendritic cells was found to be similar to that secreted in the B cells. Prep 1 and 2 secreted 40 - 45 pg/ml of IL-10 at their higher concentration of 100 µg/ml, whereas prep 3 and 4 showed IL-10 secretion between 27-33 pg/ml. Although secretion of IL-10 in both B cells and enriched dendritic cells was found to be much less as compared to monocytes, production of IL-10 in all the cells was noted. It is now well known that, macrophages and T lymphocytes produce IL-10 during *M. tuberculosis* infection. IL-10 was described as a cytokine synthesis inhibitory factor (CSIF) in the lieu of its ability to inhibit the T lymphocyte production of cytokines (Cavalcanti et.al., 2012). IL-10 acts by inhibiting the production of pro-inflammatory cytokines (IFN- $\gamma$ , TNF- $\alpha$  and IL-12) and the action of antigen presenting cells, blocking the activation of T lymphocytes through the inhibition of expression of MHC class II molecules (Cavalcanti et.al., 2012). Therefore, it has an immunoregulatory function. IL-10 is considered primarily as an inhibitory cytokine, which is vital for the adequate balance between inflammatory and immunopathological responses. However, the increase in IL-10 levels appears to support the mycobacterial survival in the host (Cavalcanti et. al., 2012). Certain studies have also demonstrated no increased levels of IL-10 in PBMCs from patients with active TB in response to mycobacterial antigens (McDyer et. al., 1997). Our experiment has demonstrated production of IL-10 in response to the stimuli of HCD NPs and Ag85A. Ag85A is a recombinant protein, which might have stimulated the production of IL-10, whereas HCD NPs may have acted as adjuvant to further enhance the production of IL-10.

### **12.7.3.2 Assay of IL-12**

Secondly, levels of IL-12 in all the cell types (monocytes, B cells and enriched dendritic cells) were found to be augmented with the stimulation of all the preparations. More than 200 pg/ml concentration of IL-12 was noted in all the cells (Figure 12.4b). However, secretion of IL-12 was found to be very less as compared to the secretion of IL-10, which may be due to inhibitory effect of IL-10. Similar studies are reported by Murthy et. al., where they demonstrated diminished production of four pro-inflammatory cytokines including IL-12 by the addition of exogenous IL-10 to the cultures. The inhibition of endogenous IL-10 function by added anti-IL-10 Ab seemed to reduce production only of IL-12 and IL-6 (Murthy et. al., 1997). In addition, no correlation could be derived between the concentration of different preparations and secretion of IL-12 in different cells.

### **12.7.3.3 Assay of TNF- $\alpha$**

In the third case, levels of TNF- $\alpha$  were analyzed in monocytes, B cells and enriched dendritic cells. Higher secretion of TNF- $\alpha$  (1000 pg/ml) was noted in porcine monocytes upon stimulation by all the preparations at all concentrations except prep 3 (Figure 12.4c). However, concentration of secreted TNF- $\alpha$  was found to be less in comparison to IL-10. Reduced concentration of TNF- $\alpha$  may be due to inhibitory effect of IL-10 as mentioned earlier. Secretion of TNF- $\alpha$  from B cells and enriched dendritic cells was significantly less as compared to IL-12, whereas little higher concentration of TNF- $\alpha$  was noted as compared to

IL-10 in B cells and enriched dendritic cells. The tumor necrosis factor (TNF, TNF- $\alpha$ ) is considered as a necrosis inducer in sarcomas (*in vivo*). In case of mycobacterial infection, TNF- $\alpha$  plays a vital role by acting upon wide variety of cells (such as activated macrophages, T lymphocytes, and dendritic cells), which helps controlling MTB infection. TNF- $\alpha$  is believed to act in association with IFN- $\gamma$  by stimulating the production of reactive nitrogen intermediates (RNIs), which augments the tuberculostatic function of macrophages. In addition, TNF- $\alpha$  has been also found to stimulate the migration of immune cells to the infection site leading to formation of granuloma, thereby controlling the disease progression (Cavalcanti et. al., 2012). In connection to this, there are reports in the literature, which revealed expression of TNF- $\alpha$  in MTB-infected tissues during the whole latent phase of infection, which suggested possible role of TNF- $\alpha$  in the control of the bacillus multiplication in association with other cytokines like IFN- $\gamma$  (Dlugovitzky et.al., 2000; Al-Attiyah et.al., 2012). Dlugovitzky et. al., reported increased levels of TNF- $\alpha$  in culture supernatants of peripheral blood mononucleated cells (PBMCs) from patients with pulmonary tuberculosis indicating stimulation of TNF- $\alpha$  due to presence of mycobacterial antigens in the TB patients (Dlugovitzky et.al., 2000; Al-Attiyah et.al., 2012). Moreover, reverse effect is also reported in the literature. Mohan et. al., reported that neutralization of TNF- $\alpha$  in murine models resulted in tuberculosis aggravation or reactivation (Mohan et. al., 2001). In this experiment, we observed production of TNF- $\alpha$  in all the cell types tested with all stimuli, with the higher production being obtained in porcine monocytes upon stimulation by Ag85A and HCD NPs.

In this experiment, we have assessed different preparations (Prep 1, Prep 2, Prep 3 and Prep 4) composed of HCD nanoparticles and Ag85A to stimulate monocytes, B cells and enriched dendritic cells to produce detectable levels of IL-10, IL-12 and TNF- $\alpha$ . Cytokines were quantified in overnight cultures using specific ELISAs (as described by manufacturer's instructions). It was observed that all cytokines were detectable at the lowest stimulant concentrations of 11  $\mu\text{g}/\text{ml}$ . Cytokine, IL-10 was produced at relatively high levels (1,600 pg/ml) in response to a dose as low as 11  $\mu\text{g}/\text{ml}$ , whereas lowest response was produced by prep 3 in porcine monocyte. However, in all the cases, all preparations showed induction of cytokines tested (IL- 10, IL- 12 and TNF- $\alpha$ ), suggesting immunostimulatory effect of formulations, which may be attributed to the presence of stimuli, Ag85A and hydrophobic chitosan derivative for its possible adjuvant activity. Based on the findings presented in this study, our data suggested that HCD NPs has immunological adjuvant activity on the specific cellular and humoral immune responses to Ag85A in-vitro.

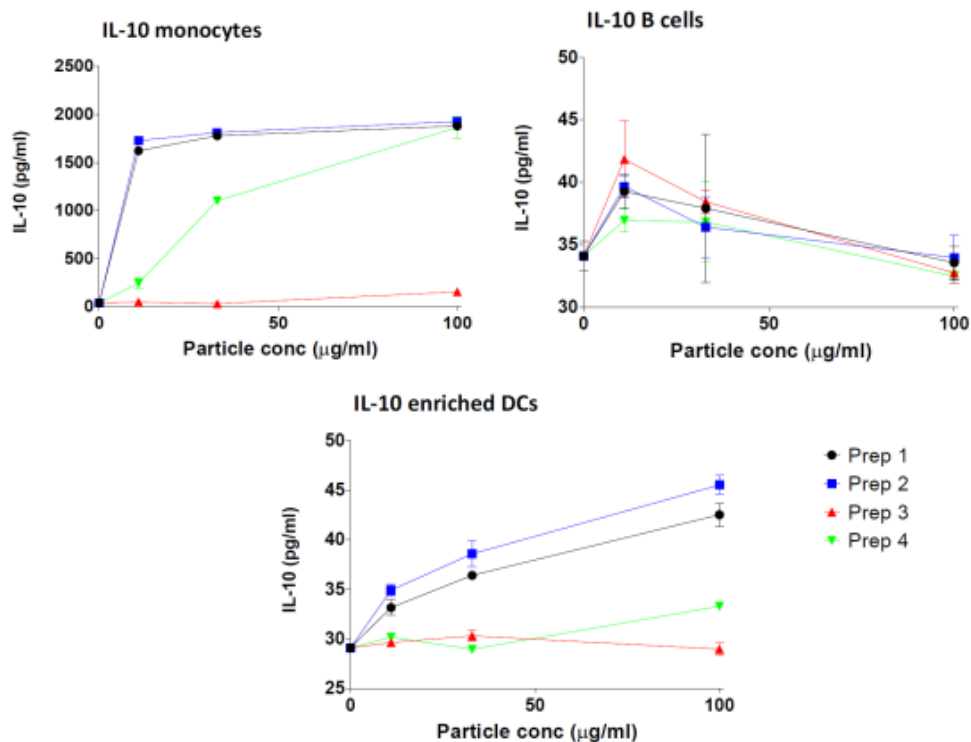


Figure 12.4a: Cytokine, IL-10 induction in monocyte, B Cells and Enriched DCs upon immunostimulation by Nanoparticles

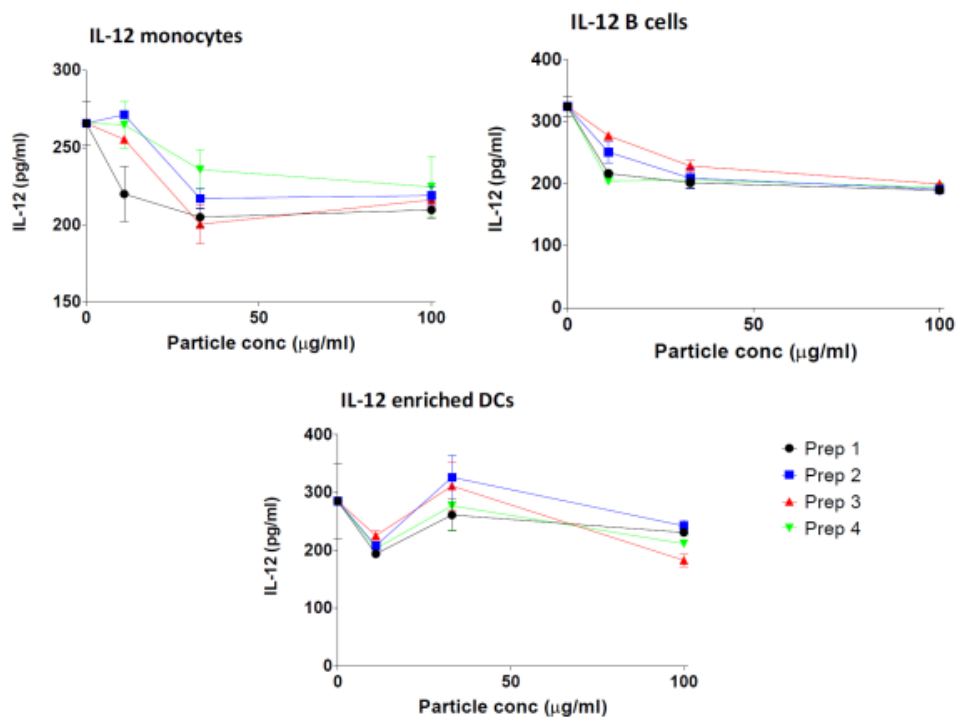


Figure 12.4b: Cytokine, IL-12 induction in monocyte, B Cells and Enriched DCs upon immunostimulation by Nanoparticles

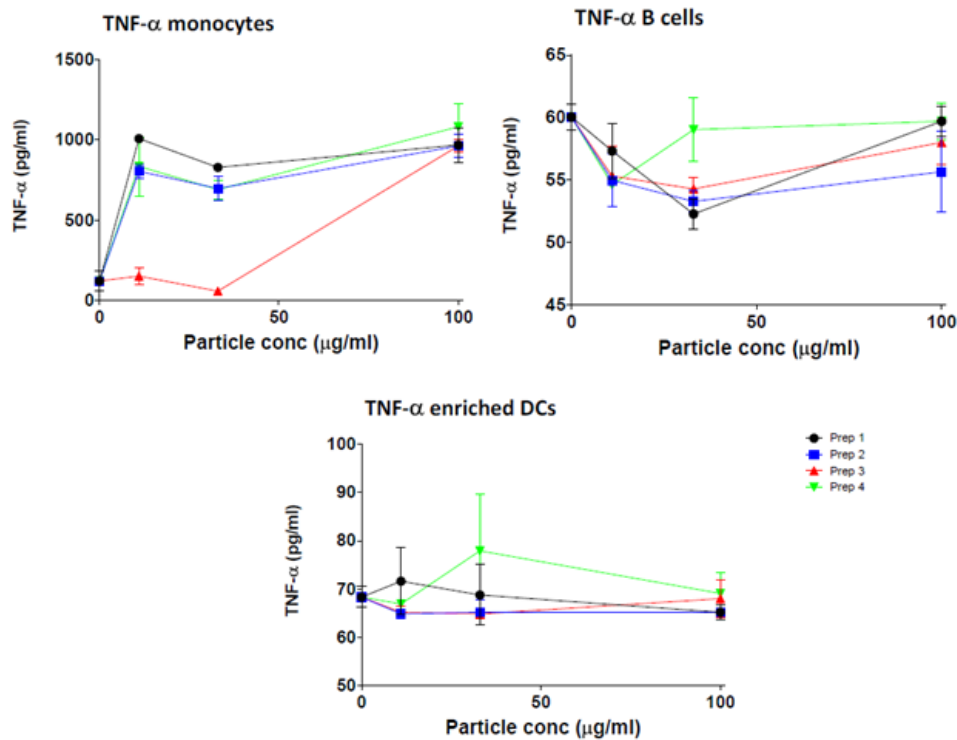


Figure 12.4c: Cytokine, TNF- $\alpha$  induction in monocyte, B Cells and Enriched DCs upon immunostimulation by Nanoparticles

#### 12.7.4 Analysis of T cell activation

Analysis of CD 16 and MHC II expression was performed and upon analyzing the results of CD 16 and MHC-II expression, it was observed that all preparations (Prep 1-4) and lipopolysaccharide (LPS) were able to induce CD16 expression. Results showed down regulation of CD16 in all the preparations except prep 3 (Figure 12.5a). As shown in figure A12.5a, prep 3 stand out with higher stimulation of co-stimulatory molecule, CD 16, whereas preparations 1, 2 & 4 showed very less stimulation. In connection to this, a study published by Balboa et al. suggests that a CD16 (+) subpopulation may represent an immune evasion strategy that ultimately favors persistence of Mycobacterium tuberculosis (Balboa et. al., 2013). In addition, Lugo-Villarino and Neyrolles also discussed about the possible role of CD16 on the function of CD16 (+) monocytes in health and disease. Thus, in accordance with these reports, results of our study indicated down regulation of CD16, indicating favorable response of formulation tested (Lugo-Villarino and Neyrolles, 2013).

On the other hand, up regulation of MHC-II expression was noted from all the preparations. Highest induction was observed from prep 4 (higher than LPS), suggesting ability of FITC-HCD NPs to stimulate MHC-II for the production of antibodies (Figure 12.5b). In addition, all other preparations also showed up regulation of MHC - II expression and, thus, stimulatory effect on the induction of antigen specific antibodies. In connection to this, Henderson *et al* reported that human monocyte derived DC efficiently phagocytosed *M.*

*tuberculosis*, suggesting a possible role of this cell in the early response to TB infection. They reported, up regulation of MHC I and MHC II (CD40, CD54, CD58, and CD80 molecules) upon infection with MTB (Henderson et.al., 1997). Considering this report, up-regulation of MHC II in our experiment may help to release antibodies and cytokines. However, it is still not clearly understood that whether the interaction between dendritic cells and *M. tuberculosis antigen* represents a defense mechanism by the invaded host, or helping the invader to evade the defense mechanism of the host.

Particulate antigen delivery systems are of interest due to their stable nature and ability to act as adjuvant. Their attraction is based on the various properties they confer such as enhancing antigen stability, easy to target particulate systems and of course their ability to control the release for a long duration of time. Particulate systems carrying antigen are known to generate immune response and stimulate cytotoxic T cell response due to antigen associated with the particles. This is due to unique ability of certain antigen processing cells (APCs) to internalize particulate matters and bacteria. Thus, particulate matters carrying antigen, first get recognized by the cells, which activates phagocytosis of antigenic materials and particles to process and present themselves and antigenic materials to other cells of immune system (Thiele et. al., 2001). Further presentation of cells to MHC I and II on APCs to stimulate cellular and humoral immunity. Considering this fact, nanoparticles of HCD incorporating Ag85A may have enhanced up regulation of MHC class II, which might further helps to enhance cellular and humoral immunity.

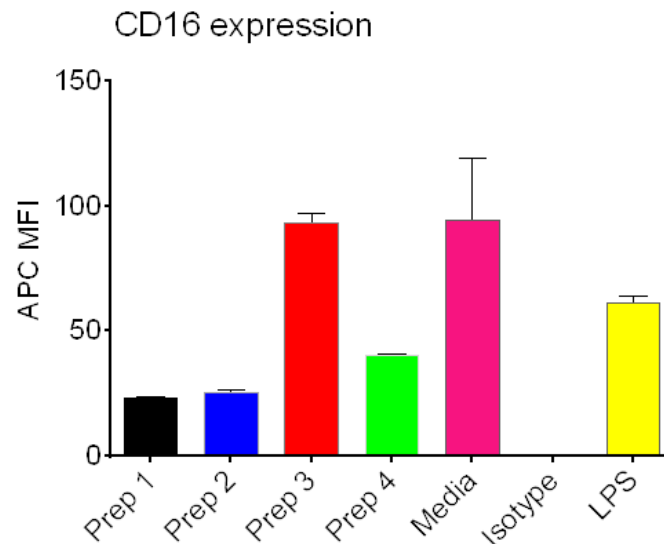


Figure 12.5a: Expression of CD 16 upon immunostimulation with formulation and polymers

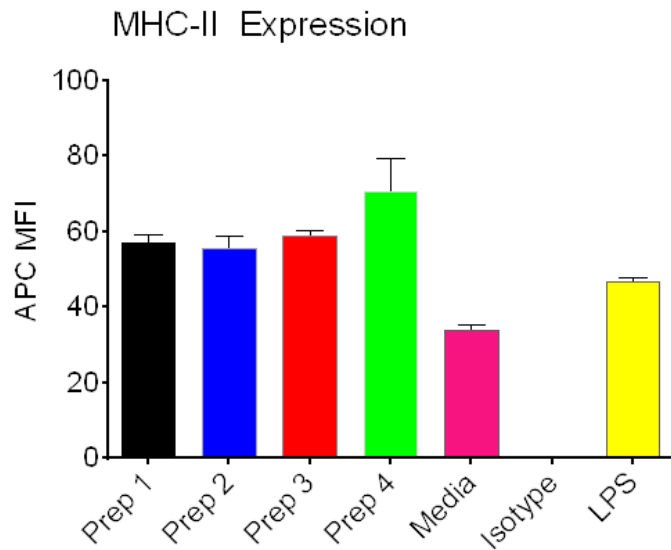


Figure 12.5b: Expression of MHC-II upon immunostimulation with formulation and polymers

### References

- Al-Attayah R., El-Shazly A., and Mustafa A. S. (2012) Comparative analysis of spontaneous and mycobacterial antigen-induced secretion of Th1, Th2 and pro-inflammatory cytokines by peripheral blood mononuclear cells of tuberculosis patients, *Scandinavian Journal of Immunology*, 75 (6) 623- 632.
- Balboa L., Romero M. M., Laborde E., Sabio Y. G. C. A., Basile J. I., Schierloh P., Yokobori N. (2013) Impaired dendritic cell differentiation of CD16-positive monocytes in tuberculosis: role of p38 MAPkinase. *Eur. J Immunol.* 43, 335–347.
- Cavalcanti Y.V.N., Brelaz M.C.A., Neves J.K.D., Ferraz J.C., and Pereira V.R.P. (2012) Role of TNF-Alpha, IFN-Gamma, and IL-10 in the Development of Pulmonary Tuberculosis. *Pulmonary Medicine*. Article ID 745483, 1-10.
- Dai J., Zou S., Pei Y., Cheng D., Ai H., Shuai X. (2011) Polyethylenimine-grafted copolymer of poly(l-lysine) and poly(ethylene glycol) for gene delivery, *Biomaterials*, 32, 6, 1694- 1705.
- Dlugovitzky D., Bay M. L., Rateni L. (2000) Influence of disease severity on nitrite and cytokine production by peripheral blood mononuclear cells (PBMC) from patients with pulmonary tuberculosis (TB), *Clinical and Experimental Immunology*, 122 (3), 343–349.
- Ekwall B., Silano V., Paganuzzi-Stammati A., Zucco F. (1990) Chapter 7 - Toxicity Tests with Mammalian Cell Cultures. Edited by P. Bourdeau et. al., *Short-term Toxicity Tests for Non genotoxic Effects*. John Wiley & Sons Ltd.
- Eyles J. E., Williamson E.D., Alpar H.O. (1999). Immunological response to nasal delivery of free and encapsulated tetanus toxoid: studies on he effect of vehicle volume. *Int. Jour. Pharmaceutics*, 189, 75-79.
- Henderson R.A., Watkins S.C., Flynn J.L. (1997) Activation of human dendritic cells following infection with Mycobacterium tuberculosis. *J Immunol.*, 159, 635-643.
- Hoskins C., Cuschieri A. and Wang L. (2012) The cytotoxicity of polycationic iron oxide nanoparticles: Common endpoint assays and alternative approaches for improved understanding of cellular response mechanism, *Journal of Nanobiotechnology*, 10, 15.
- Kroll A., Dierker C., Rommel C., Hahn D., Wohlleben W., Schulze-Isfort S., Göbbert C., Voetz M., Hardinghaus F., Schnekenburger J. (2011) Cytotoxicity screening of 23 engineered nanomaterial using a test matrix of ten cell lines and three different assays, *Particle and Fibre Toxicology*, 8, 9.
- Li A. (2005) preclinical in-vitro screening assays for drug like properties. *Drug Discovery Today. Technologies*, 2(2), 179-185.

## Chapter 12 - In-vitro Cell Line Studies

---

Lugo-Villarino G., Neyrolles O. (2013) Dressed not to kill: CD16+ monocytes impair immune defence against tuberculosis. *Eur J Immunol.* 43(2), 327-30

Lv H., Zhang S., Wang B., Cui S., Yan J. (2006) Toxicity of cationic lipids and cationic polymers in gene delivery, *Journal of Controlled Release*, 114, 100 - 109.

McDyer J. F., Hackley M. N., Walsh T. E., Cook J. L., and Seder R. A. (1997) Patients with multidrug-resistant tuberculosis with low CD4+ T cell counts have impaired Th1 responses, *Journal of Immunology*, 158 (1), 492–500

Mohan V. P., Scanga C. A., Yu K. (2001) Effects of tumor necrosis factor  $\alpha$  on host immune response in chronic persistent tuberculosis: possible role for limiting pathology. *Infection and Immunity*, 69(3),1847–1855.

Murthy P. K., Dennis V.A., Lasater B.L., and Philipp m.t. (2000) Interleukin-10 Modulates Proinflammatory Cytokines in the Human Monocytic Cell Line THP-1 Stimulated with *Borrelia burgdorferi* Lipoproteins. *Infection and Immunity*, 68 (12), 6663–6669.

Piest M., & Engbersen J. F. J. (2010) Effects of charge density and hydrophobicity of poly (amido amine)s for non-viral gene delivery. *Journal of Controlled Release*, 148, 83–90.

Thiele L., Rothen-Rutishauser B., Jilek S., Wunderli-Allenspach H., Merkle H.P., Walter E. (2001) Evaluation of particle uptake in human blood monocyte-derived cells in vitro. Does phagocytosis activity of dendritic cells measure up with macrophages? *Journal of Controlled Release*. 76, 59–71

Weng L., Romanov A., Rooney J., Chen W. (2008) Non-cytotoxic, in situ gelable hydrogels composed of N-carboxyethyl chitosan and oxidized dextran, *Biomaterials*, 29, 3905–3913.

Weyermann J. org., Lochmann D., Zimmer A. (2004) A practical note on the use of cytotoxicity assays, *International Journal of Pharmaceutics*. 288, 369–376.

### 13.0 In-vivo Immunization Studies

#### 13.1 Materials

IgG2a primary monoclonal antibody was supplied by Colorado State University (USA) under material transfer agreement. Mouse INF- $\gamma$  ELISA assay kit was purchased from Koma Biotech Inc. (Seoul, Korea). Bacillus Calmette Guerin lyophilized vaccine was purchased from Serum Institute of India (Pune, India). Goat anti mouse IgG2a-AP secondary antibodies were purchased from Santa Cruz Biotechnology, Inc. (Texas, USA). Sodium chloride, formalin was obtained from Sigma-Aldrich (St-Louis, USA). Disodium hydrogen orthophosphate, potassium dihydrogen orthophosphate, potassium chloride, sodium citrate were purchased from SD Fine Chemicals (Mumbai, India). All other solvents and reagents used were obtained from Sigma-Aldrich (St-Louis, USA).

#### 13.2 Equipments

1. Ultrasonic bath-sonicator (Asha analytical Instruments, Pvt. Ltd. Secunderabad, India)
2. Digital PH meter (Systronics, India)
3. Tissue homogenizer (RQ 127A Remi, Mumbai, India)
4. Centrifuge (R8C Remi, Mumbai, India)
5. ELISA reader (Infinite® F500, Tecan, UK)

### 13.3 In-vivo immunization studies

#### 13.3.1 Animals

Female, 6-week-old BALB/c mice were obtained and housed at the animal facility centre of J.S.S College of Pharmacy (Ooty, India). All experiments were approved and conducted in accordance with the guidelines of the Institutional Animal Ethical Committee of the J.S.S College of Pharmacy. Animals were housed for acclimatization for 1 week prior to the experiments at the animal resource facilities of the College. They had free access to food and water, with 12 h light/dark cycle.

#### 13.3.2 Immunization procedure

The immunogenicity of the formulations (HCD-Ag85A and PLGA-Ag85A) were assessed in female BALB/c mice (6–8 weeks age). Animals were housed in groups of six ( $n = 6$ ) with free access to food and water. All animals were withdrawn of food intake 3 hr prior to immunization. Protocol followed for the immunization study was approved by institutional Animals Ethical Committee of J.S.S. College of Pharmacy (Ooty, India). The studies were carried out as per the guidelines of Council for the Purpose of Control and Supervision of Experiments on Animals (CPCSEA), Ministry of Social Justice and Empowerment, Government of India. In order to produce an immune response, required quantity of (equivalent to 5  $\mu$ g of Ag85A) of both the formulations (HCD-Ag85A and PLGA-Ag85A), pure Ag85A along with adjuvant alum and blank HCD-NPs & PLGA-NPs were administered either subcutaneously (by injection) or intranasally (as small drops with the help of micropipette) by preparing suspension of each formulation under test in 50  $\mu$ l of PBS on day 1 (Eyles et.al., 1999) as shown in table 13.1. Same doses of all preparations and

formulations were administered subsequently on day 14 and 28 of the immunization experiment as booster doses. Mice were also immunized with subcutaneous (SC) injection of 0.1 ml of marketed BCG vaccine (Serum Institute of India, Pune) for comparison. Same dose of BCG vaccine was administered on 14 and 28<sup>th</sup> day as booster doses.

**Table 13.1: Group of animals under immunization study**

Group No.	Each Group of six Animals / Title of Group for SC & IN administration
	<b>Subcutaneous (SC) administration</b>
Group 1	Un-Treated mice - control
Group 2	BCG vaccinated mice
Group 3	Antigens Ag85A in PBS + Alum
Group 4	Blank HCD NPs
Group 5	Blank PLGA NPs
Group 6	Antigen Ag85A entrapped HCD NPs (HCD-Ag85A NPs)
Group 7	Antigen Ag85A entrapped PLGA NPs (PLGA-Ag85A NPs)
	<b>Intra nasal (IN) administration</b>
Group 8	Antigens Ag85A in PBS + Alum
Group 9	Blank HCD NPs
Group 10	Blank PLGA NPs
Group 11	Antigen Ag85A entrapped HCD NPs (HCD-Ag85A NPs)
Group 12	Antigen Ag85A entrapped PLGA NPs (PLGA-Ag85A NPs)

After immunization, animals were bled by superficial venupuncture on 7, 21 and 35 day of the experiment and blood was collected to determine production of antibody. On 42<sup>nd</sup> day, all animals were sacrificed by administering thiopentone (80mgkg<sup>-1</sup>, i.p.) to induce terminal euthanasia. Blood samples from all the animal groups were collected by cardiac puncture prior to humane killing by euthanasia. Afterwards, broncho alveolar fluid (BALF), spleen and inguinal lymph nodes homogenates were collected and preserved at -20 °C until analysis.

### 13.3.3 Collection of samples

#### 13.3.3.1 Blood

Blood collection was carried out on 7, 21, 35 and 42 day after immunization. After first dosing, blood samples were taken from the superficial tail vein, whereas at the end of the experiment blood samples were collected by cardiac puncture. Blood samples were then centrifuged at 5000 rpm for 10 min. and samples obtained were stored at -20 °C until analysis.

### 13.3.3.2 Bronchoalveolar lavage fluid (BALF)

The mice were sacrificed by administering thiopentone ( $80\text{mgkg}^{-1}$ , i.p.) on 42<sup>nd</sup> day. A tracheal cannula was inserted via mid cervical incision and lavaged with 2 ml of ice cold phosphate buffered saline (PBS, pH=7.4) as shown in figure 13.1. After collecting the broncho alveolar lavage fluid (BALF), the lungs of the mice were removed and stored in 10% neutral formalin for routine histology using H&E staining. BALF was stored at  $-20\text{ }^{\circ}\text{C}$  until analysis.

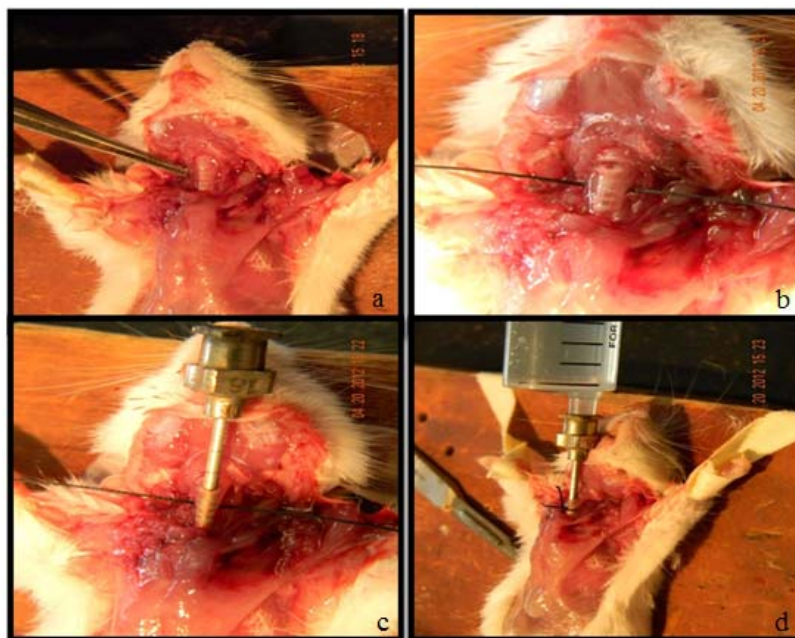


**Figure 13.1:** Process for collection of BALF. (a) picture displaying trachea; (b) a small horizontal incision made on trachea ; (c) picture showing tracheal cannulation using 18 no. needle; (d) collection of BALF by flushing lungs with 2 ml of ice cold phosphate buffered saline (PBS, pH=7.4).

### 13.3.3.3 Spleen and lymph node

After euthanasia, spleen and lymph nodes were aseptically removed and suspended in PBS (pH 7.4) for 1-2 hrs in separate micro centrifuge tubes. Spleen and lymph node tissues were then homogenized (RQ 127A Remi, Mumbai, India). The homogenates obtained were incubated in an ice-bath for 1-2 hr below  $0\text{ }^{\circ}\text{C}$  and the insoluble matters were settled down. Supernatant were then centrifuged at  $2000 \times g$  for 20 min (R8C Remi, Mumbai, India) and the clear supernatants were stored at  $-20\text{ }^{\circ}\text{C}$  until further analysis. This clear supernatants were used for estimation of cytokine (INF- $\gamma$ ) by ELISA according to manufacturer's directions. In addition, it was also utilized for the detection of Ag85A specific IgG2a antibody using ELISA.

After collection of all the samples, BALF, spleen and lymph node homogenate were tested for production of INF- $\gamma$  cytokine using ELISA assay as per manufacturer's directions. Samples (Blood, spleen and lymph node homogenate) were also titrated for the detection of

Ag85A specific IgG2a antibody using isotypes secondary antibody (IgG2a-AP) by ELISA assay.

### 13.4 Cytokine Assay

Cytokine assay was performed as per manufacturer's directions (Komma Biotech Inc., Seoul, Korea). Composition of Cytokine assay kit is mentioned in table 13.2.

**Table 13.2:** Composition of Cytokine (Mouse INF- $\gamma$ ) ELISA assay kit

Component	Description
Pre-Coated 96 well ELISA microplate	Antigen-affinity purified Rat anti-Mouse IFN- $\gamma$ pre-coated 96 well plate
Detection Antibody (Lyophilized)	Biotinylated antigen-affinity purified Rabbit anti- Mouse IFN- $\gamma$
Standard Protein (Lyophilized)	Recombinant Mouse IFN- $\gamma$
Color Development Enzyme	Streptavidin-HRP conjugate
Assay Diluent	0.1% BSA in PBS
Color development Reagent A	TMB solution
Color development Reagent B	Substrate (H <sub>2</sub> O <sub>2</sub> ) Solution
Stop Solution	2M H <sub>2</sub> SO <sub>4</sub>
PBS powder	Pouch for 1 L
Tween-20 (50%)	1 ml

#### 13.4.1 Reconstitution and Storage

- 1) **Mouse IFN-gamma Standard:** 2 ng (1 vial) of recombinant Mouse IFN-gamma was reconstituted in 40  $\mu$ l sterile water to produce a concentration of 0.05  $\mu$ g/ml.
- 2) **Detection Antibody:** 0  $\mu$ g/ml (1 vial) of biotinylated antigen-affinity purified anti-Mouse IFN-gamma was reconstituted in 250  $\mu$ l sterile water.
- 3) **Note:** Reconstituted solutions are stable at -20°C for up to 2 months. Do not repeat frozen and thawing.

**All preparations were mixed thoroughly and warmed up to RT before use.**

- 1) **Washing Solution (PBST):** PBS powder (1 pouch) was dissolved in sterile water and made upto 900 mL, then 1 ml of Tween-20 (50%) was added to this solution, mixed well and volume was made upto 1 L.
- 2) **Sample dilution:** Samples were diluted to a proper concentration in assay diluent. **(Note:** Dilute the samples, based on the expected concentration of the analyte, to fall within the concentration range of the standards).
- 3) **Detection Antibody:** Reconstituted detection antibody was diluted in assay diluent to a concentration of 0  $\mu$ g/ml (1:20 dilution).
- 4) **Color Development Enzyme:** The Streptavidin-HRP conjugate was diluted as 1:20 in assay diluent.
- 5) **Color development solution:** 1 volume of color development reagent A and 2 volume of reagent B (1:2) were mixed prior to use.

### 13.4.2 Preparation of Standard Solutions

Standards and samples were diluted in assay diluent at 1:2 serial dilutions as given in table 13.3 and analyzed using ELISA plate reader (Infinite® F500, Tecan, UK).

**Table 13.3:** Preparation of Standard Solutions

Step	Dilution Method	Standard conc. (pg/ml)
Step A	15 µl of Standard + 0.485 ml of Assay Diluent	1500
Step B	Step A 0.25 ml of Step A + 0.25 ml of Assay Diluent	750
Step C	Step B 0.25 ml of Step A + 0.25 ml of Assay Diluent	375
Step D	Step C 0.25 ml of Step A + 0.25 ml of Assay Diluent	187.5
Step E	Step D 0.25 ml of Step A + 0.25 ml of Assay Diluent	93.75
Step F	Step E 0.25 ml of Step A + 0.25 ml of Assay Diluent	46.875
Step G	Step F 0.25 ml of Step A + 0.25 ml of Assay Diluent	23.4375

### 13.4.3 ELISA Protocol

1. 200 µl of washing solution was added to each well and the wells were aspirated to remove liquid. Washing of the well plate was carried out thrice using 300 µl of washing solution per well. After the last wash, plate was inverted to remove residual solution and blotted on paper towel. (**Note:** Not to dry the wells completely and hence it is necessary to immediately go on next step).
2. After the washing step, 100 µl of standards or samples were added to each well in duplicate. The plate was covered with the sealer which was provided with the kit and incubated at room temperature for at least 2 hours.
3. Wells were again aspirated to remove liquid and the plate was washed 4 times similar to that mentioned in step 1.
4. After second washing step, 100 µl of the diluted detection antibody was added per well. The plate was covered with sealer and incubated at room temperature for 2 hours.
5. After 2 hrs, wells were aspirated and washed again for 4 times as mentioned in step 1.
6. Later, 100 µl of the diluted color development enzyme (1:20 dilute) was added to per well and the plate was covered with sealer. The plate was incubated for 30 minutes at ambient temperature (15-18 °C). After 30 min., wells were again aspirated and washed 4 times as described in step 1.
7. Thereafter, 100 µl of color development solution was added to each well and the plate was incubated for about 15 min. at ambient temperature (15-18 °C) for a proper color development. (20-25 minutes). Color reaction was stopped reaction by adding 100 µl of stop solution to each well and plate was read at 450 nm wavelength using a micro titer plate reader. (**Note:** Please be aware that the color may develop more quickly or more slowly than the recommended incubation time depending on the localized room temperature. Please visually monitor the color development to optimize the incubation time).

### 13.5 ELISA assay for detection of Ag85A specific IgG2a antibody

Sera from immunized mice were collected by superficial tail vein at regular intervals and after the last immunization, whereas blood samples before sacrificing were collected by cardiac puncture. Levels of anti-Ag85A total-immunoglobulin G (IgG2a) antibodies in individual sera, BALF, spleen and inguinal lymph node homogenates were determined by ELISA micro plate reader using native Ag85A for coating (1 µg/well) and isotype rat anti-mouse secondary antibody (IgG2a-AP) and the concentration of both the antibodies was determined by analysing at 492 nm.

In brief, serum from control and immunized mice were collected on 7<sup>th</sup>, 21<sup>st</sup>, 35<sup>th</sup> and 42<sup>nd</sup> day after the first and subsequent booster doses of each immunization scheme. To assess antigen-specific antibody levels, 96-well plates (Maxisorp Nunc-Immuno plates, Roskilde, Denmark) were treated with 0.1 mL of purified protein, Ag85A (1 µg/well) in coating solution. 100 µL solution of Ag85A in 100 mM coating buffer (carbonate buffer, pH 9.2) was transferred to 96 well plates. The plate was incubated overnight (about 14-16 hours) at 2-8°C to coat the antigen to the wells of the plate. The antigen solution was withdrawn from the wells and blocked with 200 µL of blocking buffer (1X PBS containing 0.5% BSA+ 0.02% sodium azide). The plate was left aside for about 3-4 hours at RT to allow antigen bind with surface of well. The content was discarded and washed once with 1X PBS solution (1X PBS containing + 0.02% sodium azide). 100 µL of IgG2a, primary antibody (serial dilutions in PBST) was transferred to proteins Ag85A coated wells and incubated at RT for 4 hrs. After the incubation period, wells were washed thrice with PBST (1X PBS+ 0.05% Tween 20, pH 7.4) and 100 µL of previously diluted rat anti mouse IgG2a-AP secondary antibody (alkaline phosphatase conjugated) was added to each well in a dilution of 1:2000 (100 µL/well). Plates were then kept aside for 1 hr at RT. Wells were again washed 3 times with PBST with the interval of three minutes and 100 µL of pNPP substrate (in diethanolamine buffer) was added to each well and incubated at RT for 20 min. Reaction was monitored qualitatively by visual inspection (development of yellow colour) and quantitatively with a microtiter plate reader. Reaction was stopped by adding 100 µL 0.1M EDTA and the absorbance was measured at 405 nm using ELISA plate reader (Infinite® F500, Tecan, UK).

Detection of IgG2a in the samples, blood, lymph node, spleen was performed utilizing same protocol as mentioned above. Only standard primary antibody was replaced by respective sample. Each sample was diluted to 1:200 in PBST prior to use in ELISA assay.

### 13.6 Histopathology studies of lung tissue

After thirty five days of intra nasal administration of formulations, the mice were sacrificed on 42<sup>nd</sup> day and the right lungs were removed. The lungs from each group of mice were placed in 50 mL of formalin (20 % formaldehyde solution) and histopathology studies were carried out (Lifeguard Laboratories, Bangalore). In brief, the left lungs were fixed in 10% (v/v) neutral buffered formalin. Samples were removed by section of lung lobes that had been processed with paraffin wax. The sections were stained with hematoxylin and eosin for routine evaluation with Alizarin red to detect calcified lesions.

### 13.7 Statistical analysis

The data were represented as mean  $\pm$  SD ( $n = 6$ ) and analyzed using GraphPad Prism version 4.03 for Windows (GraphPad Software, San Diego, CA). The data were compared using 1 way ANOVA. The data was tested by dunnett's post hoc test (\* $P < 0.05$ , \*\* $P < 0.01$ ,  $P < 0.001$  vs. control).

### 13.8 Results and Discussions

For the complete eradication of MTB, a vaccine should generate the complete spectrum of immunity including humoral, mucosal as well as cellular immune response. Hence, to confirm cellular immunity, the endogenous cytokine levels (IFN- $\gamma$ ) were determined after 42 days of immunization. Interferon gamma (IFN- $\gamma$ ) is secreted by Th1 cells leading to sequential events for the generation of IgG2a (Chong et.al., 2005). In order to evaluate the potential of HCD-Ag85A NPs to induce the generation of protective cytokine INF- $\gamma$  and Ag85A specific antibodies namely IgG2a, immunization studies after subcutaneous and nasal administration were performed. Figure 13.2 represents, the mean INF- $\gamma$  values expressed as concentration (pg/ml), whereas generation of IgG2a is expressed as ng/ml and presented in figure 13.3.

#### 13.8.1 Cytokine (INF- $\gamma$ ) levels in BALF, lymph node and spleen

Cytokine (IFN- $\gamma$ ) assay in BALF, lymph node and spleen was performed and results are tabulated in table 13.4. It was observed that, concentration of IFN- $\gamma$  in BLAF was found to be high in mice belonging to group 2 and 3 ( $539 \pm 159.3$  &  $605 \pm 127.5$  pg/ml), which were immunized with marketed BCG vaccine and pure Ag85a+alum by subcutaneous route as compared to the nasally administered HCD-Ag85A NPs and PLGA-Ag85A NPs formulation ( $99.88 \pm 46$  &  $118.9 \pm 64.16$  pg/ml) (group 11 and 12). When intra-nasally administered HCD-Ag85A NPs and PLGA-Ag85A NPs formulations were compared with their subcutaneous counterpart, the results highlighted better production of IFN- $\gamma$  from the later with the values of  $123.7 \pm 58.44$  and  $300.9 \pm 125$  pg/ml. With all other groups, less than 200 pg/ml of IFN- $\gamma$  generation was observed.

In case of IFN- $\gamma$  production in lymph nodes, results showed higher values from the group 2, 3, 6, 7, 11 and 12 with the corresponding IFN- $\gamma$  values of  $395.7 \pm 98.38$ ,  $546.7 \pm 131.4$ ,  $394.2 \pm 85.74$ ,  $439.2 \pm 118.8$ ,  $423.2 \pm 46.97$ ,  $525.3 \pm 101.3$  respectively. These results showed effectiveness of intra-nasally administered HCD-Ag85A NPs to produce IFN- $\gamma$  in comparison to the marketed BCG and the mixture of Ag85A with alum. However, results of the PLGA-Ag85A NPs administered by nasal route showed high IFN- $\gamma$  release as compared to the results obtained from the mixture of Ag85A with alum. HCD-Ag85A NPs administered by nasal route exhibited higher IFN- $\gamma$  response as compared to marketed BCG vaccine (SC), indicating effectiveness of the formulation for the generation of protective cytokine.

In the third case, production of IFN- $\gamma$  in the spleen was assessed. Results of this study also indicated highest production of IFN- $\gamma$  from the mixture of Ag85A with alum

## Chapter 13 - In-vivo Immunization Studies

( $516.7 \pm 132.3$  pg/ml), whereas second highest production was noted from intra-nasally administered PLGA-Ag85A NPs ( $479.1 \pm 100.2$  pg/ml) followed by HCD-Ag85A NPs, which produced  $418 \pm 46.57$  pg/ml of cytokine after nasal administration. Result obtained from the nasal administration of HCD-Ag85A NPs was found to be higher in comparison to the response obtained after subcutaneous administration of marketed BCG vaccine suggesting more efficient immunological response even though by non-parenteral route.

In all the cases, IFN- $\gamma$  production was more by the alum adsorbed Ag85A. Intra-nasally administered HCD-Ag85A NPs and PLGA-Ag85A NPs showed comparable responses for the production of IFN- $\gamma$  in all the cases as compared to the marketed BCG and alum adsorbed Ag85A, except BALF, where these formulations exhibited very less responses. The overall results of this study indicated that the nasal immunization using nanoparticles based formulation resulted into induction of Th1 (Type 1 T helper cells) cell mediated immunity. However, studies using more cytokines are recommended to identify the ability of the said formulation to induce Th2 cells for the development of humoral immunity.

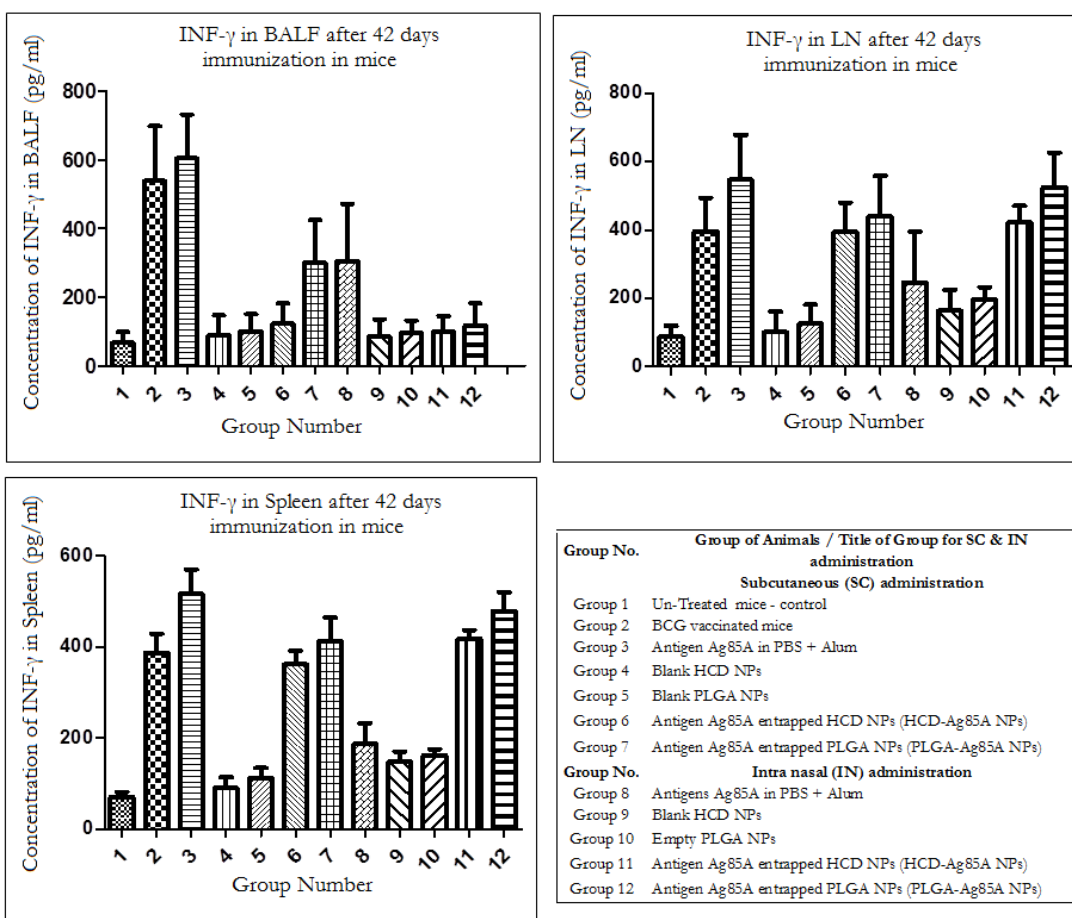


**Figure 13.2:** Cytokine (INF- $\gamma$ ) levels in BALF, lymph node and spleen after 42 days immunization in mice with different formulations.

### **13.8.2 Immunological responses by detection of IgG2a antibody**

To investigate the suitability of the Ag85A loaded HCD nanoparticles for pulmonary delivery, we compared the levels of IgG2a in serum, lymph node and spleen of mice after subcutaneous (SC) and intranasal (IN) vaccination with marketed BCG vaccine, soluble antigen co-administered with alum, HCD-Ag85A NPs and PLGA-Ag85A NPs.

#### **13.8.2.1 IgG2a in BALF**

Results of this study are tabulated in table 13.5. Anti-Ag85A antibody, IgG2a detected in BALF was found to be less as compared to that observed in all other organs (discussed below). Among all the formulations tested, high titer (IgG2a) concentration was noted from IN administered PLGA-Ag85A NPs ( $209.1 \pm 25.96$  ng/ml) as well as HCD-Ag85A NPs ( $198 \pm 5.94$  ng/ml). These formulations were able to generate almost double concentration of IgG2a as compared to intra-nasally administered alum adsorbed Ag85A ( $104 \pm 3.085$  ng/ml). Similarly, SC administered HCD-Ag85A and PLGA-Ag85A NPs also showed more immune responses than BCG vaccine and alum adsorbed Ag85A. Generation of anti-Ag85A IgG2a antibody in BALF clearly indicates the ability of these formulations (HCD-Ag85A & PLGA-Ag85A NPs) to produce mucosal immune responses. Results suggested possibility of immune adjuvant property of the HCD and PLGA NPs might have caused high mucosal and systemic concentration of protective IgG2a.

#### **13.8.2.2 IgG2a in blood**

After subcutaneous immunization of mice with different formulations, serum samples showed highest immunological response from PLGA-Ag85A NPs ( $253.9 \pm 2.669$  ng/ml), whereas alum adsorbed Ag85A demonstrated second highest response ( $245.7 \pm 2.51$  ng/ml). HCD-Ag85A NPs generated  $214.1 \pm 6.222$  ng/ml of IgG2a. Upon intra-nasal administration of different formulations, it was observed that PLGA-Ag85A NPs and HCD-Ag85A NPs exhibited comparable immunological responses with the IgG2a levels of  $307.8 \pm 1.866$  and  $265.9 \pm 2.198$  ng/ml respectively (Table 13.6). On comparing immunological responses after SC and IN route, both the nanoparticulate formulations composing Ag85A presented high IgG2a production indicating better immunogenicity as compared to marketed BCG vaccine (Figure 13.3). Moreover, the serum antibody responses elicited by IN immunization with HCD-Ag85A NPs and PLGA-Ag85A NPs were significantly higher than those achieved after conventional SC injection of marketed BCG vaccine and blank HCD and PLGA NPs after both SC and IN administration ( $P < 0.001$ ) (Fig. 13.3). Altogether, these results suggested strong immunostimulating effect of HCD-Ag85A NPs and PLGA-Ag85A NPs upon IN administration.

We also evaluated production of IgG2a at different time points after immunization with first and booster dose of formulations (Figure 13.4). Table 13.5 tabulates the data of IgG2a at different time points. We immunized animals at 0, 14 and 28<sup>th</sup> day and samples were collected at 7, 21, 35 and 42<sup>nd</sup> day. Results showed that IN administered HCD-Ag85A NPs elicited slightly delayed immunological response ( $135.9 \pm 2.198$  ng/ml) as compared to alum adsorbed Ag85A ( $205.7 \pm 2.51$  ng/ml) and PLGA-Ag85A NPs ( $237.4 \pm 1.995$  ng/ml) after IN

administration, which may be attributed to the ability of HCD NPs to control the release of Ag85A. On subsequent days, increasing concentration of IgG2a antibody was produced by the HCD-Ag85A NPs indicating enhanced immunological response of HCD-Ag85A NPs after IN administration. The levels of IgG2a were found to be high as compared to those achieved by alum adsorbed Ag85A and marketed BCG vaccine (Table 13.5; figure 13.3). On the other hand, PLGA-Ag85A NPs also showed stronger immunological response. These results suggest the property of HCD NPs to control the release of antigen as well as its application as a potential alternative adjuvant. In addition, continuous release of Ag85A suggested the ability of HCD NPs to preserve the antigens immunogenicity. Similar reports are published by Prego et.al., and Amidi et. al., where they discussed about the delayed immunological response from chitosan nanoparticles as compared to soluble antigen (Prego et. al., 2010; Amidi et. al., 2007).

### ***13.8.2.3 IgG2a in Lymph Nodes***

Amount of anti-Ag85A (IgG2a) production was also identified in lymph nodes. As expected, blank nanoparticles elicited poor immunological response in terms of specific IgG2a response after SC and IN administration, whereas immune responses achieved with Ag85A loaded HCD and PLGA NPs were higher as compared to any other formulation tested (Table 13.6 and Figure 13.3). These formulations showed significantly higher immunological response as compared to the response observed from marketed BCG vaccine and alum adsorbed Ag85A. Thus, these results indicated the application of HCD NPs and PLGA NPs as potential vaccine adjuvants.

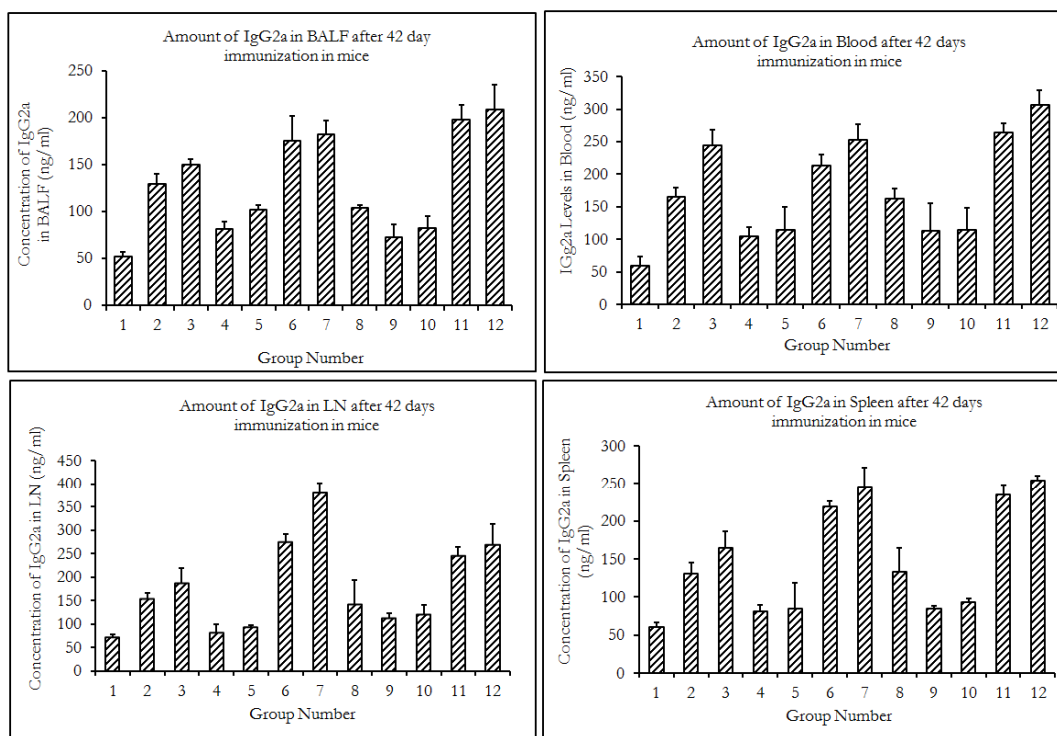
### ***13.8.2.4 IgG2a in Spleen***

Significantly high titers of antibody (IgG2a) were detected in spleen of mice immunized with SC and IN administered HCD-Ag85A NPs as well as PLGA-Ag85A NPs. IgG2a titers obtained were higher than those achieved after immunization with SC and IN administration marketed BCG vaccine and alum adsorbed Ag85A (Table 13.6, Figure 13.3). Results of the study tabulated in table 13.6 clearly illustrates almost 2 fold and 1.5 fold increase in the immune responses of IN HCD-Ag85A NPs as compared to BCD vaccine and alum adsorbed Ag85A. Similar results were found in case of PLGA-Ag85A NPs, in fact higher responses were observed. Thus, these results strongly suggest the immune adjuvant activity of HCD and PLGA NPs in conjunction with Ag85A.

To summarize, the results of in vivo immunization study conclusively indicate that HCD NPs can be considered as a new and promising adjuvant candidate for enhancing and prolonging the immune response of Ag85A after SC and IN administration. Additionally, it may provide advantages over the traditional adjuvant, alum salts. Moreover, 1) simple technique to prepare NPs helps to encapsulate antigen and other immunostimulants); 2) controlled release offered by HCD NPs due to delayed release of antigen from HCD NPs; 3) ability to protect antigen from deleterious external environment could prove to be beneficial in the vaccine delivery. The results of our studies are in accordance with the earlier reports, which demonstrated the immune adjuvant property of chitosan (Bivas-Benita et. al., 2004;

Ghendon, 2008; Illum et. al., 2001). Higher immunological responses from the HCD-Ag85 NPs may be attributed to the mucoadhesive nature of chitosan, which helps to decrease the clearance from the local site and its ability to transiently open the tight junctions of the mucosal membrane (Illum et. al., 2001).

Among all the formulations, PLGA-Ag85A NPs demonstrated best immunological responses after both SC and IN administration. Literature survey also revealed immunostimulatory properties of PLGA particles for various protein antigens (Shi et. al., 2002; Chong et. al., 2005). It is reported that, size of the particles is important for the uptake by the antigen presenting cells (APC). Small particles of size <500 nm have been shown to induce higher immunological responses as compared to large particles having size of > 2  $\mu\text{m}$  (Chong et. al., 2005; Nixon et.al., 1996). Results of this experiment showed higher IgG2a levels and INF- $\gamma$  level in BALF, blood, lymph node and spleen, which may be attributed to the enhanced uptake of the PLGA-Ag85A NPs by dendritic cells and macrophages, thereby enhancing the processing and presentation of the encapsulated Ag85A and the immune effects observed in this study. Similar explanation may be true for the HCD-Ag85A NPs, because enhancement of the immunological responses by HCD-Ag85A NPs were found to be next to PLGA-Ag85A NPs. Lastly, in vivo behaviour of these formulations suggested their potential utility as an adjuvant for the generation of mucosal as well as systemic immunity.



**Subcutaneous (SC) administration:**

Group 1 - Untreated mice, control; Group 2 - BCG vaccinated mice  
 Group 3 - Antigens Ag85A in PBS + Alum; Group 4 - Blank HCD NPs; Group 5 - Blank PLGA NPs;  
 Group 6 - Antigen Ag85A entrapped HCD NPs (HCD-Ag85A NPs);  
 Group 7 - Antigen Ag85A entrapped PLGA NPs (PLGA-Ag85A NPs).

**Intra nasal (IN) administration:**

Group 8 - Antigens Ag85A in PBS + Alum; Group 9 - Blank HCD NPs; Group 10 - Blank PLGA NPs;  
 Group 11 - Antigen Ag85A entrapped HCD NPs (HCD-Ag85A NPs);  
 Group 12 - Antigen Ag85A entrapped PLGA NPs (PLGA-Ag85A NPs)

**Figure 13.3:** Levels of IgG2a in BALF, blood, LN and spleen after 42 days immunization in mice. BALF - Bronchoalveolar fluid, LN - Lymph node.

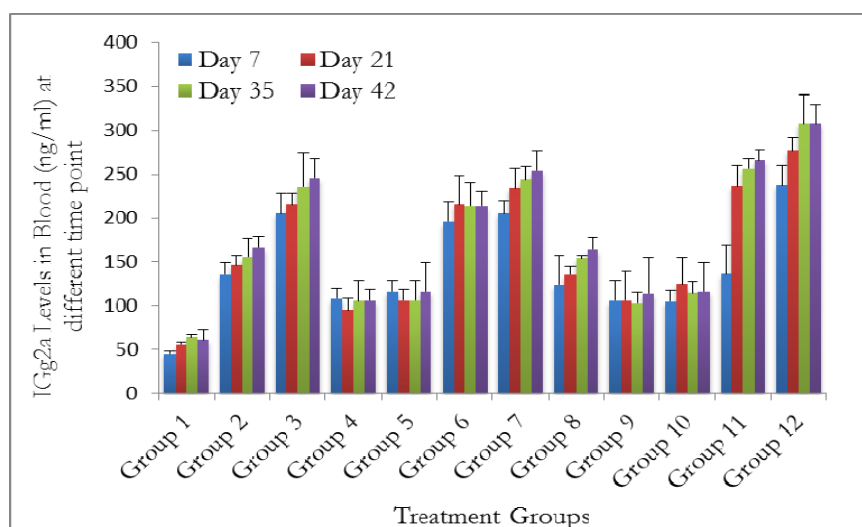


**Figure 13.4:** Levels of IgG2a in blood at different time points after immunization of mice with different formulations.

Table 13.4: Cytokine (INF- $\gamma$ ) levels in BALF, Lymph node (LN) and spleen after 42 days immunization

Group		1	2	3	4	5	6	7	8	9	10	11	12
Organ		1	2	3	4	5	6	7	8	9	10	11	12
Conc. of INF- $\gamma$ (pg/ml)	BALF	68.65 $\pm$ 31.21	539 $\pm$ 159.3***	605 $\pm$ 127.5***	90.43 $\pm$ 58.19 <sup>NS</sup>	101.5 $\pm$ 49.36 <sup>NS</sup>	123.7 $\pm$ 58.44 <sup>NS</sup>	300.9 $\pm$ 125**	306.5 $\pm$ 166**	86.32 $\pm$ 50.03 <sup>NS</sup>	96.99 $\pm$ 36.01 <sup>NS</sup>	99.88 $\pm$ 46 <sup>NS</sup>	118.9 $\pm$ 64.16 <sup>NS</sup>
	LN	88.38 $\pm$ 31.1	395.7 $\pm$ 98.38***	546.7 $\pm$ 131.4***	101.3 $\pm$ 59.56 <sup>NS</sup>	126.3 $\pm$ 54.59 <sup>NS</sup>	394.2 $\pm$ 85.74***	439.2 $\pm$ 118.8***	246.5 $\pm$ 149.3*	163.5 $\pm$ 61.74 <sup>NS</sup>	197 $\pm$ 36.01 <sup>NS</sup>	423.2 $\pm$ 46.97***	525.3 $\pm$ 101.3***
	Spleen	71.22 $\pm$ 25.93	387.4 $\pm$ 102.4***	516.7 $\pm$ 132.3***	90.59 $\pm$ 58.17 <sup>NS</sup>	112.6 $\pm$ 53.72 <sup>NS</sup>	362.2 $\pm$ 73.34***	412.7 $\pm$ 127.3***	187.2 $\pm$ 111.7 <sup>NS</sup>	147.7 $\pm$ 56.58 <sup>NS</sup>	163 $\pm$ 31.3 <sup>NS</sup>	418 $\pm$ 46.57***	479.1 $\pm$ 100.2***

n = 6, Mean  $\pm$  SD; BALF – Broncho-alveolar fluid; LN - Lymph node; S - Spleen

Table 13.5: Specific antibody (IgG2a) levels in Blood at different time point

Group		1	2	3	4	5	6	7	8	9	10	11	12
Days		1	2	3	4	5	6	7	8	9	10	11	12
Conc. of IgG2a (ng/ml)	7	45.51 $\pm$ 2.24	135.7 $\pm$ 13.61	205.7 $\pm$ 22.55	108.4 $\pm$ 11.16	116 $\pm$ 13.11	195.7 $\pm$ 22.64	205.7 $\pm$ 14.02	124 $\pm$ 33.09	105.7 $\pm$ 23.19	104.5 $\pm$ 13.62	135.9 $\pm$ 32.85	237.4 $\pm$ 21.97
	21	56.01 $\pm$ 1.83	146.2 $\pm$ 10.91	215.7 $\pm$ 12.19	95.26 $\pm$ 13.37	106 $\pm$ 13.23	215.7 $\pm$ 32.56	234.1 $\pm$ 22.49	135.7 $\pm$ 9.14	105.7 $\pm$ 32.92	124.5 $\pm$ 31.15	235.9 $\pm$ 24.35	277.4 $\pm$ 14.58
	35	64.17 $\pm$ 3.26	156.2 $\pm$ 20.84	235.7 $\pm$ 38.57	105.3 $\pm$ 23.44	116 $\pm$ 23.19	214.1 $\pm$ 26.28	243.9 $\pm$ 14.89	154 $\pm$ 3.36	103.7 $\pm$ 14.74	114.5 $\pm$ 13.51	255.9 $\pm$ 12.19	307.8 $\pm$ 32.65
	42	61.01 $\pm$ 11.87***	166.2 $\pm$ 12.58***	245.7 $\pm$ 22.51***	105.8 $\pm$ 12.68***	116 $\pm$ 33.34***	214.1 $\pm$ 16.22***	253.9 $\pm$ 22.67***	164 $\pm$ 13.85***	113.7 $\pm$ 41.15***	116 $\pm$ 32.94***	265.9 $\pm$ 12.39***	307.8 $\pm$ 21.76***

n = 6, Mean  $\pm$  SD

Table 13.6: Specific antibody (IgG2a) levels in BALF, lymph node and spleen after 42 days immunization

Group		1	2	3	4	5	6	7	8	9	10	11	12
Organ													
Conc. of IgG2a (ng/ml)	BALF	52.34± 4.43	129.5± 10.58***	150.5± 5.74***	81.76± 7.74**	102.6± 4.54***	175.6± 26.2***	182.2± 15.03***	104± 3.09***	72.82± 3.52 <sup>NS</sup>	82.82± 12.28	198± 15.94***	209.1± 25.96***
	LN	72.34± 4.82	154± 12.85***	187.4± 32.45***	81.76± 17.92 <sup>NS</sup>	92.64± 4.74 <sup>NS</sup>	275.1± 16.77***	382.2± 18.73***	142.3± 51.23***	113.8± 9.12**	121.3± 19.96***	246.4± 18.34***	269.1± 44.28***
	Spleen	62.17± 4.17	132.4± 13.43***	165.7± 20.51***	81.76± 7.92***	85.98± 33.11***	220.1± 6.12***	247.2± 24.56***	134± 30.09***	85.66± 3.19***	94.49± 3.15***	235.9± 12.19***	255.8± 3.89***

n = 6, Mean ± SD; BALF – Broncho-alveolar fluid; LN – Lymph node

#### Subcutaneous (SC) administration

Group 1 - Untreated mice - control

Group 2 - BCG vaccinated mice

Group 3 - Antigens Ag85A in PBS + Alum

Group 4 - Blank HCD NPs

Group 5 - Blank PLGA NPs

Group 6 - Antigen Ag85A entrapped HCD NPs (HCD-Ag85A NPs)

Group 7 - Antigen Ag85A entrapped PLGA NPs (PLGA-Ag85A NPs)

#### Intra nasal (IN) administration

Group 8 - Antigens Ag85A in PBS + Alum

Group 9 - Blank HCD NPs

Group 10 - Blank PLGA NPs

Group 11 - Antigen Ag85A entrapped HCD NPs (HCD-Ag85A NPs)

Group 12 - Antigen Ag85A entrapped PLGA NPs (PLGA-Ag85A NPs)

Each value presented in table 13.4, 13.5, 13.6 represent the mean + standard deviation (n=6)

Comparison of all formulations was made with control and significance level was indicated as below -

- \*P<0.05
- \*\*P<0.01
- \*\*\*P<0.001
- Ns-non significant

### 13.8.3 Histopathological studies of lungs

Results of the histopathological studies are given in figure 13.5. Group 1, which was control without administering any formulation, indicated apparent and distinct epithelium of alveoli and bronchi lining without accumulations. Cilia were found to be in the active phase and stray areas of congestion were observed (Figure 13.5a). In case of group 8 (Alum+antigen, IN), entire organ appeared moderately congested with undrained blood from major venous system. Mild to moderate degree of alveolar disruptions were observed, which may be due to direct antigen antibody reaction and uncontrolled release of inflammatory mediators (figure 13.5b). Group 9 (blank HCD NPs) and Group 10 (blank PLGA NPs) demonstrated moderate to severe damage to alveoli & lining epithelium and alveolar architecture damage to greater extent with massive congestion (figure 13.5c, d), which may be because NPs alone may have been recognised as foreign materials by the body's defence mechanism leading to activation of macrophages and release of inflammatory mediators.

In case of group 11 (HCD-Ag85A NPs) and group 12 (PLGA-Ag85A NPs), moderate degree of structural damage to the lining epithelium of bronchioles and alveolar septa along with the areas of congestion were observed. Lesser damage of the lung was noted from the group 11 and 12 as compared to group 9 and 10. This may be due to preliminary release of inflammatory mediators and enzymes by the macrophages recognizing formulations as foreign materials, followed by release of Ag85A from the HCD-Ag85A NPs and PLGA-Ag85A NPs. Release of Ag85A helps to initiate production of repairing enzymes and cytokines in order to heal the tissue (as it will be recognized by the memory T cells as MTB antigen) (Figure 13.5e, f). Thus, results of histopathological studies of lungs after 42 days of immunization with HCD-Ag85A and PLGA-Ag85A NPs indicate that they may be considered safe for prolonged lung delivery.

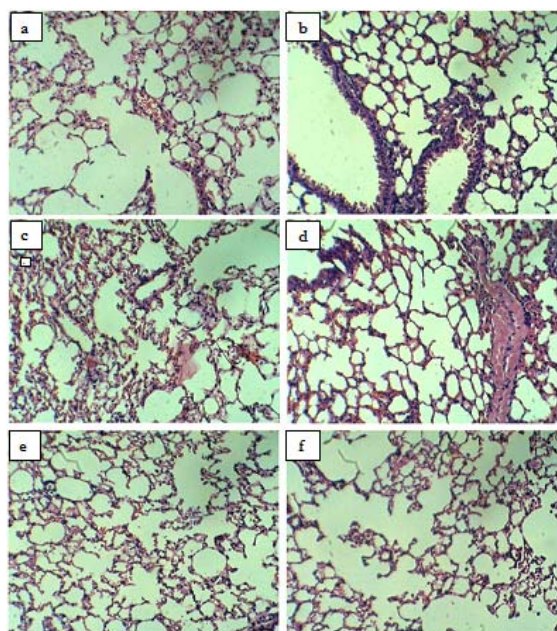


**Figure 13.5:** Histopathological changes in mice lung samples after 42 days immunization.

- a) Group 1 - Control, no treatment
- b) Group 8 - Ag85A + Alum
- c) Group 9 - Blank HCD NPs
- d) Group 10 - Blank PLGA-NPs
- e) Group 11 - HCD-Ag85A NPs
- f) Group 12 - PLGA-Ag85A NPs

### References

- Amidi M., Romeijn S.G., Verhoef J.C., Junginger H.E., Bungener L., Huckriede A., Crommelin D.J.A., Jiskoo W. (2007) N-Trimethyl chitosan (TMC) nanoparticles loaded with influenza subunit antigen for intranasal vaccination: Biological properties and immunogenicity in a mouse model. *Vaccine*, 25, 144-153.
- Bivas-Benita M., Meijgaarden K.E.V., Franken K.L.M.C, Junginger H.E., Borchard G., Ottenhoff T.M.H., Geluk A. (2004) Pulmonary delivery of chitosan-DNA nanoparticles enhances the immunogenicity of a DNA vaccine encoding HLA-A\*0201-restricted T-cell epitopes of *Mycobacterium tuberculosis*. *Vaccine* 22 (2004) 1609-1615.
- Chong C.S.W., Cao M., Wong W.W., Fischer K.P., Addison W.R., Kwon W.R., Tyrrell D.L., Samuel J. (2005) Enhancement of T helper type 1 immune responses against hepatitis B virus core antigen by PLGA nanoparticle vaccine delivery. *Journal of Controlled Release*, 102(1), 85-99.
- Eyles, J.E., Williamson, E.D., Alpar, H.O. (1999). Immunological response to nasal delivery of free and encapsulated tetanus toxoid: studies on the effect of vehicle volume. *Int. Jour. Pharmaceutics*, 189, 75-79.
- Shi L., Caulfield M.J., Chern R.T, Wilson R.A., Sanyal G., Volkin D.B. (2002) Pharmaceutical and immunological evaluation of a single-shot hepatitis B vaccine formulated with PLGA microspheres. *Journal of Pharmaceutical Sciences*, 91 (4), 1019-1035.
- Ghendon Y., Markushin S., Krivtsov G., Akopova I. (2008) Chitosan as an adjuvant for parenterally administered inactivated influenza vaccines. *Arch. Virol.* 153, 831–837.
- Illum L., Jabbal-Gill I., Hinchcliffe M., Fisher A.N., Davis S.S. (2001) Chitosan as a novel nasal delivery system for vaccines. *Advanced Drug Delivery Reviews*, 51, 81-96.
- Nixon D.F., Hioe C., Chen P.D., Bian Z., Kuebler P., Li M.L., Qiu H., Li X.M., Singh, M. Richardson A. (1996) Synthetic peptides entrapped in microparticles can elicit cytotoxic T cell activity, *Vaccine*, 14, 1523-1530.
- Prego C., Paolicelli P., Díaz B., Vicente S., Sánchez A., González-Fernández A., Alonso M.J. (2010) Chitosan-based nanoparticles for improving immunization against hepatitis B infection. *Vaccine*, 28, 2607-2614.

### 14.0 Summary and Conclusions

#### 14.1 Introduction

Tuberculosis (TB) is a major global health problem caused by *Mycobacterium tuberculosis* (MTB) and *Mycobacterium bovis*. It is a leading cause of morbidity, which infects one-third of the world's population of which 8-10 million develop active disease and 2 million die every year. (Shegokar et al., 2011) Despite the impressive results and remarkable accomplishments with the help of current BCG vaccine and drug therapy, there is a still need to further improve on vaccine and drug delivery research and development to combat deadly tuberculosis to provide complete protection, especially in developing nations (Schroder et al., 2001). This is due to ineffectiveness of BCG vaccine in pulmonary TB & adults, tedious & lengthy process required for combination antibiotics therapy leading to various systemic side effects and poor patient compliance. In addition, co-infection with HIV and mutation of MTB (due to generation of drug resistant mutants of MTB) make the disease even worse. Therefore, effective vaccination for TB with the subunit vaccines for improved immunizations and treatment of TB with less frequent dosing, reduced dose of drugs and duration of therapy are at the priority in order to save many lives.

Large numbers of protein vaccine candidates have been selected from *MTB* antigens in animal models. Among them, Ag85A is the most investigated protein and examined at preclinical and clinical level. However, a major drawback of protein vaccine is low immunogenicity especially by mucosal routes, therefore adjuvant co-administration is advised and currently research is still under progress to increase the immunogenicity of subunit protein vaccines by adjuvant effects of nanoparticulate delivery systems with due concerns to its safety. Considering this fact, research was envisaged to formulate Ag85A (proteins) entrapped nanoparticulate delivery systems for the localized delivery to lung.

World health organization (WHO) has recommended drug regimen for treatment of *MTB* infection, which is a combination of rifampicin, isoniazid, pyrazinamide and ethambutol to be taken for the six months. Amongst, rifampicin is a first-line drug used for the treatment of tuberculosis since 1970. Despite the availability of an effective therapeutic regimen for TB, high dose, patient non-compliance (due to long duration of therapy) causes emergence of multi drug resistance (MDR) and extensive drug resistance (XDR) and thus, unsuccessful treatment of tuberculosis. Moreover, less macrophage uptake of rifampicin, non-localized delivery of drugs and associated adverse effects are another concerns with the current rifampicin therapy. As rifampicin is a first line drug for the treatment of TB, many research groups have addressed these challenges. However, research is still underway to accomplish bountiful delivery system for ATDs, using alternative route of administration. Thereof, we have chosen rifampicin to address the challenges associated with the current therapy by formulating it into a newly developed polymeric system via alternative route.

The pulmonary route of drug and vaccine administration has achieved considerable attention by the scientific communities owing to the benefits presented by this route in the treatment of many deadly diseases including TB. Currently, pulmonary delivery research mainly focuses on nanotechnology based strategies for the delivery of antigens and drugs to improve the

localization of nano sized particles in the lungs, thereby generating local action with sustained release and improved therapeutic effects. Over the past decade, large number of biodegradable materials of natural and synthetic origin have been utilized in controlled drug delivery for the formulation of micro and nanoparticles. Among them, chitosan and PLGA are at the priority in drug/vaccine delivery research. PLGA is a GRAS and widely used polymer, whereas chitosan is natural polymer and its application presents many benefits in drug delivery. Considering, unusual combination of biological activities plus mechanical and physical properties including presence of primary amine groups, positive charge, mucoadhesive nature and its ability to efficiently permeate across absorptive epithelia, chitosan is more suitable polymer in sustained and targeted drug delivery. In addition, ability of chitosan particles to interact with the mannose receptors of macrophages leading to immunoadjuvant activity makes it worthwhile polymer for vaccine delivery. However, the application of chitosan is limited due to its poor solubility in water and organic solvents. Therefore, investigations are focused on the synthesis of modified chitosan derivatives to overcome its solubility issues.

### 14.2 Aims and Objectives

The present investigation was aimed at the development of nanoparticulate vaccine and drug delivery systems using PLGA and chitosan derivatives loaded with Ag85A and rifampicin for pulmonary mucosal delivery to improve the immunogenicity and therapy against TB respectively.

The main objectives of the study were:

1) To formulate and evaluate PLGA nanoparticles encapsulating Ag85A protein for pulmonary delivery in TB; 2) To synthesize and characterize chitosan derivatives; 3) to formulate and evaluate rifampicin and Ag85A entrapped chitosan derivatives nanoparticles for pulmonary delivery in the treatment of TB. These objectives were undertaken in order to, 1) improve the immunogenicity of subunit vaccine and provide its sustained localized delivery to the lungs owing to its incorporation into nanoparticulate delivery system; 2) ameliorate antitubercular activity of rifampicin and overall management of TB by increasing the macrophage uptake, improving patient compliance and reducing adverse effects due to localized pulmonary delivery of rifampicin from particulate delivery system.

It was envisaged that -

- 1) Ag85A and rifampicin loaded nanoparticles prepared using PLGA and chitosan derivatives will provide sustained release rate of Ag85A and rifampicin.
- 2) Ag85A loaded nanoparticles prepared using PLGA and chitosan derivatives may render improved immunogenicity along with adjuvant effect.
- 3) Rifampicin loaded chitosan derivatives nanoparticles may improve therapeutic efficacy of rifampicin due to local delivery of the formulation to lungs.

### 14.3 Experimental

#### 14.3.1 Vaccine preparation, extraction, expression and purification

Ag85A was used as subunit vaccine in the present study. pDNA encoding Ag85A protein was used for its expression in *E. coli* BL21 DE3 strain. After expressing Ag85A in bacterial system, it was successfully extracted using probe sonication and purified with the help of His Bind spin columns. Characterization of purified Ag85A using SDS PAGE indicated successful purification of Ag85A due to presence of clear and single band of 32 kDa protein, Ag85A. Antigenicity of protein as performed using ELISA assay was found to be 98.33 % for Ag85A 1 and 91.66 % for Ag 85 A R1 (refolded Ag85A). These results suggested successful expression and purification of vaccine, Ag85A. Purified Ag85A was further used for the formulation.

#### 14.3.2 Synthesis of chitosan derivatives - hydrophobic chitosan derivative (HCD) and modified chitosan derivative (MCD)

Hydrophobic chitosan (octanoyl chitosan) was prepared using acylation reaction with the help of methanesulfonic acid. Degree of acylation (DA) for HCD was found to be  $44.05 \pm 1.75$  %. HCD showed excellent (based on the visual inspection of samples) solubility in a range of organic solvents, whereas it was found to be insoluble in water which may be due to introduction of hydrophobic octanoyl groups to the parent chitosan. Structural analysis of HCD using FTIR studies indicated the presence of new absorption bands in the FTIR spectra of HCD at  $\sim 1740$   $\text{cm}^{-1}$  corresponding to reaction between octanoyl and amine and hydroxyl groups of the chitosan, which confirmed the substitution of octanoyl groups on chitosan.  $^1\text{H-NMR}$  analysis of HCD showed new peaks at 0.75, 1.15, 1.48 and 2.20 ppm due to alkyl proton of chitosan upon reaction with octanoyl chloride indicating conjugation of octanoyl groups to the parent chitosan leading to formation of octanoyl chitosan (HCD). Differential scanning calorimetry (DSC) and X-Ray powder diffraction (XRD) studies suggested the crystalline nature of HCD.

Similarly, synthesis of MCD was carried out using acylation reaction. Solubility studies of the MCD showed it to be soluble in water, methanol, ethanol, whereas it was found to be insoluble in various other organic solvents. Degree of acylation of acyl groups (DA) for MCD was found to be  $0.99 \pm 0.001$  %, which was very small as compared to HCD. Synthesis of MCD was confirmed by FTIR and NMR analysis due to incorporation of new absorption bands at  $\sim 1738.15$   $\text{cm}^{-1}$  as observed in the FTIR spectra of MCD, whereas new peaks at 0.84, 1.25 and 1.57 ppm attributed to the  $-\text{CH}_3$ ,  $-\text{CH}_2-$  and  $-\text{CH}_2-(\text{CO})$  groups of the octanoyl chloride chains confirming the conjugation of octanoyl onto parent chitosan.

#### 14.3.3 Formulation and characterization of Ag85A-PLGA NPs

Preparation of Ag85A loaded PLGA nanoparticles were carried out by double emulsion solvent evaporation technique. The process and formulation parameters were optimized systematically. After preliminary experiments, critical parameters were identified. The important parameters such as concentration drug and polymer were optimized by  $3^2$  factorial design. The optimized formulation consisted of 50 mg of PLGA, 3.5 ml of organic phase,

## Chapter 14 - Summary and Conclusions

---

0.25 mg Ag85A, 1% PVA and 10 ml of external medium volume. The optimized batch of nanoparticles was evaluated for particle size, zeta potential, surface morphology, protein content, protein integrity, in-vitro deposition, in vitro protein release, stability studies and in-vivo immunization studies. DSC and XRD studies indicated successful encapsulation of Ag85A in PLGA NPs.

PLGA-Ag85A NPs showed particle size of  $240.03 \pm 3.33$  nm (PDI of  $0.34 \pm 0.015$ ) and zeta potential was  $-29.4 \pm 0.35$  mV. The TEM and SEM micrographs of PLGA-Ag85A NPs confirmed the particle size in the nanometer range. Nanoparticles with spherical shape were observed in SEM images. XRD and DSC studies showed change in crystallinity of nanoparticle formulation prepared using PLGA. In XRD studies, similarity of blank and Ag85A loaded PLGA NPs confirmed the presence of PLGA NPs in amorphous form. DSC thermograms of model protein, ovalbumin (O-alb) showed a single sharp endothermic peak at 50 and 150 °C ascribed to the thermal denaturation of O-alb, whereas PLGA also showed an endothermic peak at 50°C corresponding to its Tg. Reduction in intensity or disappearance of these endothermic peaks in the PLGA-Ag85A NPs indicated amorphous nature of PLGA NPs.

Entrapment efficiency of PLGA-Ag85A formulation was found to be  $76.45 \pm 5.58$  % which indicated successful entrapment of Ag85A in the PLGA NPs. Structural integrity of Ag85A in PLGA NPs was confirmed by SDS PAGE analysis, which showed a sharp band at 32 kDa. Upon studying particle deposition in lungs using TSI, nebulization efficiency of the NP formulation was found to be  $78.43 \pm 4.54$ % of the anticipated amount of protein, whereas  $30.01 \pm 8.09$  % of the dose nebulized was found to be respirable fraction. In addition, fine particle fraction was found to be  $38.27 \pm 8.47$  %. Overall results of the deposition study suggested that the formulation can be predicted to demonstrate moderate deposition in the lower respiratory tract. Results of the release studies showed biphasic release pattern. Fast release (burst release) of protein was observed in the first phase, whereas second phase was characterized by slow release of Ag85A. Almost 15 % ( $13.54 \pm 4.94$ %) of protein was found to be released during the first 2 hrs, followed by the continuous release up to  $46.68 \pm 5.02$  % by the end of 12 hr. Thereafter, slow and steady release of protein ( $61.46 \pm 4.74$ ) was observed up to the study period of 48 hrs suggesting sustained release pattern of Ag85A from PLGA NPs. The main mechanism for the transport of Ag85A from the PLGA nanoparticles was found to be controlled by Fickian diffusion as represented by the n value and owing to diffusion of protein from the polymeric core.

### 14.3.4 Formulation and characterization of HCD-Rifampicin NPs

Application of HCD for the preparation of HCD nanoparticles using multiple solvent evaporation was carried out. Results of the study showed that HCD nanoparticles can be successfully prepared using multiple emulsion solvent evaporation technique. This technique was further utilized for the incorporation of Ag85A and rifampicin in the HCD NPs. Preliminary formulation parameters were optimized systematically and critical parameters were identified. After preliminary experiments, important parameters (concentration drug

and polymer) were optimized employing  $3^2$  factorial design of experiment. The optimized batch of nanoparticles was evaluated for particle size, zeta potential, surface morphology, physicochemical property, drug content, in vitro drug release, protein content, in-vitro deposition, in vitro protein release, stability studies. DSC and XRD studies indicated successful encapsulation of Rif in HCD NPs.

HCD-Rif NPs showed mean particle size (MPS) and PDI of  $253.43 \pm 19.06$  nm and  $0.323 \pm 0.059$  respectively, whereas zeta potential was  $28.2 \pm 1.67$  mV. The TEM and SEM micrographs of HCD-Rif NPs confirmed the presence of particles in the nanometer range, with spherical shape. XRD and DSC studies showed change in crystallinity of rifampicin as compared to pure rifampicin. XRD studies clearly showed that crystalline nature of pure rifampicin disappeared in HCD-Rif NPs, confirming amorphous state of HCD NPs. DSC thermograph revealed a characteristic exothermic peak at  $260^\circ\text{C}$  for pure rifampicin, whereas no endothermic and exothermic peak upto  $300^\circ\text{C}$  were noticed from the DSC spectra of HCD. DSC thermograph of HCD-Rif NPs formulation was also devoid of endothermic or exothermic peaks. No peak of rifampicin was observed in the HCD-Rif NPs hinting the complete molecular dispersion of rifampicin in HCD NPs and its presence in amorphous form.

Entrapment efficiency of HCD-Rif formulation was found to be  $64.86 \pm 7.73$  %, suggesting good entrapment of rifampicin in HCD NPs. In-vitro aerosolization studies using TSI determined the particle deposition in lungs, nebulization efficiency of the HCD-Rif NPs was calculated to be  $76.47 \pm 4.33$ % of the total amount of rifampicin delivered, out of which  $30.01 \pm 8.09$  % of the dose was detected as respirable fraction. Fine particle fraction was found to be  $43.35 \pm 3.23$  %. Results of nebulization study suggested the suitability of formulation to deliver rifampicin in the lower respiratory tract. In conformity to the British Pharmacopoeia standards (British Pharmacopoeia, 2012) deposition of HCD-Rif NPs in all stages of the TSI including device, throat, stage 1 and stage 2 was found to be in between 75% and 125% of mass balance. Results obtained from in-vitro release study of rifampicin suspension (Rif-S) showed immediate release of  $87.65 \pm 10.29$ % within 2 hrs into release medium, whereas biphasic release pattern was observed from the HCD-Rif NPs. In the initial phase,  $45.97 \pm 2.99$  % of rifampicin release was noted up to 6 hr, whereas sustained and steady release was observed over the entire period of study (up to 72 hr) with the rifampicin release of about 75 %. Thus, release of rifampicin was found to be retarded from the HCD NPs. Amongst various models tested, the curve fitting of release data to Korsmeyer's and Peppas model showed higher value for correlation coefficient ( $r^2$  value of 0.8243), which suggested anomalous transport (non-fickian) mechanism for the release of drug based on the 'n' value (0.911, which is  $0.5 < n < 1$ ). This indicated that Korsmeyer's and Peppas model satisfactorily represented the data owing to diffusion of rifampicin from the core of HCD nanoparticles.

### 14.3.5 Formulation and characterization of HCD-Ag85A NPs

Preparation of Ag85A loaded HCD nanoparticles were carried out by double emulsion solvent evaporation technique. The process and formulation parameters were optimized systematically. After preliminary experiments, critical parameters (particle size and entrapment efficiency) were identified by varying Ag85A concentration. In addition, adsorption efficiency of the HCD nanoparticles was also determined. The optimized batch of nanoparticles was evaluated for particle size, zeta potential, surface morphology, DSC, XRD studies, protein integrity, protein content, in-vitro deposition, in vitro protein release, stability studies and in-vivo immunization studies.

The optimized formulation of HCD-Ag85A NPs showed particle size of  $241.53 \pm 1.17$  nm (PDI of  $0.222 \pm 0.011$ ) and zeta potential was found to be  $28.73 \pm 0.78$  mV. FITC labeled HCD was synthesized and labeling efficiency was calculated. The reaction yielded a fluorescent yellow colored FITC-HCD polymer and labeling efficiency of the weight fraction of FITC per unit weight of chitosan was found to be 1.78% (w/w). FITC-HCD polymer was further utilized for the preparation of nanoparticles employing the same optimized formula and important characteristics of nanoparticles such as particle size, PDI and zeta potential were measured. The size of the FITC-HCD NPs was found to be  $177.83 \pm 8.05$  with the PDI of  $0.11 \pm 0.01$ . This particle size was found to be substantially smaller as compared to the one obtained from blank HCD-NPs (MPS of  $269.1 \pm 10.15$  and PDI of  $0.317 \pm 0.019$ ) and even less than that of optimized batch HCD-Ag85A NPs. Results of the zeta potential indicated positive surface potential ( $10.83 \pm 2.87$ ), although less than the NPs prepared without FITC, which may be due to occupation of free amine groups by the FITC.

SEM images indicated small particle diameter and spherical surface morphology of HCD-Ag85A NPs. Particles size was found to be small even and uniform in SEM and TEM images similar to that obtained from Zetasizer, Nanoseries Instrument. XRD and DSC studies showed change in crystallinity of nanoparticulate formulation prepared using HCD. In XRD studies, similarity of blank and Ag85A loaded HCD NPs confirmed the amorphous state of HCD NPs. A broad diffuse peak was observed from the XRD spectra of blank HCD NPs and Ag85A encapsulated HCD NPs, which may be due to presence of HCD NPs and HCD-Ag85A nanoparticles in amorphous form. DSC Thermograph of O-alb (which is used as a reference protein) revealed a characteristic broad exothermic peak at  $50$  °C and one more endothermic peak at  $150$  °C for ovalbumin. DSC thermographs of HCD-O-alb NPs and HCD-Ag85A formulations revealed absence of peaks related to O-alb/Ag85A confirmed the molecular dispersion and encapsulation of O-alb and Ag85A within the core of HCD nanoparticles.

Entrapment efficiency of HCD-Ag85A formulation was found to be  $97.39 \pm 1.06$  %, suggesting excellent entrapment of Ag85A in HCD NPs. The electrophoretic mobility of Ag85A from the HCD NPs was found to be excellent based on the quality of band (32 kDa) observed after SDS-PAGE analysis of the entrapped Ag85A, whereas blank HCD NPs showed absence of Ag85A band. No molecular weight aggregates or fragments larger or

smaller than the molecular weight of 32 kDa (Ag85A) due to absence of any kind of extra bands were observed suggesting retention of structural integrity of Ag85A after its encapsulation in HCD NPs. Similar band intensity was obtained even after storage of HCD-Ag85A NPs for 2 months at ambient temperature of 10-15 °C, indicating stability of Ag85A in HCD NPs. In-vitro pulmonary deposition of particles was carried out by TSI using FITC labeled HCD NPs. Nebulization efficiency of the FITC-HCD NP formulation was found to be  $74.07 \pm 0.74$  % of the anticipated amount of FITC, whereas  $31.51 \pm 1.77$ % of the dose nebulized was found to be respirable fraction. In addition, fine particle fraction was found to be  $43.45 \pm 1.02$  %. Overall results of the deposition study suggested that the formulation can be predicted to demonstrate moderate deposition in the lower respiratory tract.

Results of the release studies showed biphasic release pattern. Results showed initial burst release of Ag85A within first 2 hrs of study ( $28.14 \pm 2.05$  %) from HCD NPs. This may be due to surface desorption of protein molecules from the nanoparticles. In the initial phase, formulation took 8 hrs to release almost 50 % ( $48.15 \pm 7.52$  %) of the Ag85A from HCD-Ag85A NPs, indicating ability of HCD NP to act as barrier membrane for the release of Ag85A. Release of remaining Ag85A lasted over the entire period of study with  $77.01 \pm 4.44$  % of Ag85A release by the end of 48 hrs suggesting sustained release pattern of Ag85A from HCD NPs. Amongst various models tested, the curve fitting of release data to Higuchi square root model showed higher value for correlation coefficient ( $r^2=0.9516$ ), indicating dominant diffusion mechanism for the release of Ag85A from HCD NPs. However, release data fitting to Korsmeyer's and Peppas model showed exact transport mechanism with the  $r^2$  value of 0.9749. It suggested anomalous transport (non-fickian) mechanism for the release of Ag85A based on the 'n' value of 0.3023 ( $0.5 < n < 1$ ), which indicated that Korsmeyer's and Peppas model satisfactorily represented the data owing to diffusion of Ag85A from the core of HCD NPs.

### 14.3.6 Formulation and characterization of HCD-Rif nano spray dried powder for inhalation (HCD-Rif NSDPI)

Preparation of dry powder for inhalation in the form of nano sized particles was carried out by the Nano Spray dryer B-90 (Buchi, UK). The Nano Spray Dryer B-90 was operated in a closed-mode configuration. To obtain drug loaded particles, HCD was accurately weighed and dissolved in methanol. To it, rifampicin was dissolved and batches were prepared with and without addition of sodium stearate. Excipients and rifampicin was dissolved in methanol, stirred to produce clear solution and subjected for nano spray drying (B-90 Nano Spray Dryer, Buchi, UK). Two formulations viz. HCD-Rif NSDPI (NSD1) and other containing sodium stearate (HCD-Rif-NaSt NSDPI - NSD2) were prepared and characterized for physicochemical property. Formulations were evaluated for particle size, PDI and zeta potential, drug content, surface morphology, in-vitro lung deposition, in-vitro release rate and stability studies. DSC & XRD studies indicated successful encapsulation of rifampicin in HCD NSDPI.

## Chapter 14 - Summary and Conclusions

---

Particle size for both the formulations was found to be  $4.37 \pm 0.46$  and  $4.58 \pm 0.22$   $\mu\text{m}$  with the PDI values of more than 0.5. Zeta potential of NSD1 was noted to be  $8.91 \pm 1.27$ , whereas  $-70.4 \pm 1.63$  was observed for the formulation containing sodium stearate (NSD2), which could be attributed to the dissociation of sodium stearate leading to high negative charge. The particle size distribution curve of the nano spray-dried powder formulation determined using Sympatec was expressed in terms of the particle diameter at 10, 50, and 90 % of the volume distribution ( $D_{v_{10}}$ ,  $D_{v_{50}}$  &  $D_{v_{90}}$ , respectively). Span values for both the formulations (HCD-Rif and HCD-Rif-NaSt NSD) were found to be small indicating no particle aggregation and unimodal particle size distribution. It was observed that 50<sup>th</sup> and 90<sup>th</sup> percentile undersize ( $D_{v_{50}}$  &  $D_{v_{90}}$ ) was found to vary in batch NSD1 and NSD2. Nevertheless, respirable particle size was obtained from both the batches NSD1 (without sodium stearate) and NSD2 (with sodium stearate).  $D_{v_{50}}$  &  $D_{v_{90}}$  values of NSD batch 1 were found to be  $1.73 \pm 0.02$  ( $D_{v_{50}}$ ),  $4.61 \pm 0.1$  ( $D_{v_{90}}$ )  $\mu\text{m}$  respectively, whereas these values were found to be increased in the formulation containing sodium stearate ( $2.91 \pm 0.04$  for  $D_{v_{50}}$  &  $6.64 \pm 0.89$   $\mu\text{m}$  for  $D_{v_{90}}$ ). It was expected that, sodium stearate should improve the aerosolization of NSD powders. However, no significant difference in the powder properties was observed in NSD1 and NSD2. But little improvement in powder properties in terms of particle aggregation and distribution was noted based on the smaller span values of batch NSD2 ( $1.93 \pm 0.27$ ) as compared to NSD1 ( $2.42 \pm 0.45$ ). Both NSD powders showed acceptable particle diameter for respiration with the symmetrical shape for all the samples tested. In general, the particles displayed smooth surfaces, which may be attributed to application of nano spray drying for the preparation of particles.

Structural analysis of HCD-Rif NSD using FTIR showed a sharp peak at 1643 corresponding to the furanone C=O of rifampicin and another peak at  $1559 \text{ cm}^{-1}$  for amide C=O group were observed indicating entrapment of rifampicin in the both the NSD powders. FTIR spectral analysis of nano spray dried powder formulation indicated specific functional groups of HCD and rifampicin, similar to those observed in the FTIR spectra of pure HCD and rifampicin suggesting non-existence of any chemical interaction between functional group of HCD and rifampicin that could alter the chemical structure of the drug and hence they are found to be compatible with each other. DSC thermogram of rifampicin showed a characteristic exothermic peak at  $260^\circ\text{C}$ , whereas no exothermic or endothermic peak were noted for HCD. Absence of the peak for rifampicin in the DSC thermogram of HCD-Rif NSD and HCD-Rif-NaSt NSD powders indicated the molecular dispersion of rifampicin in the polymeric nanoparticle prepared by nano spray drying. This also confirmed the presence of rifampicin in its amorphous form in HCD NSD powders. Similarly, the absence of crystalline peaks of rifampicin in X-Ray powder diffractometry of HCD-Rif NSD formulation suggested the presence of rifampicin in solid amorphous form in the NSD formulations prepared by Nano Spray Drying method.

In-vitro aerosolization study was carried out using next generation impactor. The measured fine particle fraction (FPF) for pure rifampicin, HCD-Rif and HCD-Rif-NaSt NSD powder formulation was found to be  $52.92 \pm 2.92\%$  and  $54.33 \pm 3.21\%$  respectively. The aerosolization

and deposition of pure rifampicin (without carrier system - HCD) showed poorest performance with the FPF of just  $1.85 \pm 0.29\%$  and highest MMAD of  $23.47 \pm 9.16$ , which may be attributed to the agglomeration of rifampicin due to absence of any lipophilic adjunct to enhance dispersibility and more than 50% of the emitted dose was arrested well before the first stage of NGI which is corresponding to the particle size of more than  $8.06 \mu\text{m}$ . Nano spray drying (NSD) of rifampicin using HCD significantly improved the powder characteristics. HCD-Rif NSD powder formulation showed highest FPF of  $52.92 \pm 2.92\%$  with MMAD of  $3.63 \pm 0.39 \mu\text{m}$  and GSD of  $2.37 \pm 0.13$ . Subsequently, addition of another lipophilic adjunct (sodium stearate) to the HCD-Rif mixture and its NSD powder formulation (HCD-Rif-NaSt NSD) also exhibited comparable FPF ( $54.33 \pm 3.21\%$ ) to that of HCD-Rif NSD. In addition, MMAD and GSD of HCD-Rif-NaSt NSD were found to be  $3.05 \pm 0.13 \mu\text{m}$  and  $2.25 \pm 0.05$  respectively. In sum, results of NGI studies suggested that the addition of HCD helped to improve powder characteristics of pure rifampicin for lung delivery using dry powder inhaler. Deposition of HCD-Rif NSD and HCD-Rif-NaSt NSD powder formulations in all stages of the NGI including inhaler, mouthpiece and throat was falling between 75% and 125% of mass balance, which is in accordance with the criteria stated as per British Pharmacopoeia.

Results of in-vitro release studies showed  $87.65 \pm 1.09\%$  release of rifampicin in the SLF (pH 7.4) within 2 hours, whereas, HCD-Rif and HCD-Rif-NaSt NSD formulation were able to control the release of rifampicin. HCD-Rif NSD powder formulation released  $26.668 \pm 2.173$  and  $46.45 \pm 1.85\%$  of rifampicin in 12 and 48 hr respectively,  $61.72 \pm 1.81\%$  of rifampicin was released after 72 hrs, whereas HCD-Rif-NaSt NSD formulation released  $50.95 \pm 4.72\%$  of rifampicin after 72 hrs. The slow release of rifampicin from both the NSD powders may be attributed to the extensive hydrophobic barrier confronted by HCD, which may have restricted access of water for the dissolution of the drug. Release profiles showed biphasic release pattern from both the formulations (HCD-Rif NSD and HCD-Rif-NaSt NSD), which may be attributed to the varying localization of rifampicin on and within NSD formulation. Around 20 % of rifampicin was released by the end of 6 hrs period, the first phase of the release. Thereafter, release was found to be slowed down, a second phase, which may have been portioned owing to rifampicin encapsulation within the core of NSD powder formulation. Results of the model fitting indicated non-fickian drug transport for both HCD-Rif NSD ( $n=0.85$ ) and HCD-Rif-NaSt NSD ( $n=0.87$ ) formulations. The results of the stability study at room temperature indicated that storage of NSD formulations at RT did not influence drug content, particle size and zeta potential and hence RT could be considered as suitable storage condition for both the formulations.

### 14.3.7 Formulation and characterization of MCD-Rif nano spray dried powder for inhalation (MCD-Rif NSDPI)

Preparation of dry powder for inhalation in the form of nano sized particles was carried out by the Nano Spray dryer B-90 (Buchi, UK). The Nano Spray Dryer B-90 was operated in open-mode configuration. Drug loaded particles were obtained by dissolving MCD and rifampicin in water:methanol (70:30% w/v). Batches were prepared with and without

## Chapter 14 - Summary and Conclusions

---

addition of L- leucine in water:methanol (70:30% w/v). The content was stirred to produce a clear solution and then subjected to nano spray drying using Nano Spray Dryer B-90. At the same time, rifampicin alone was also spray dried by preparing a solution of rifampicin in methanol. Two formulations viz. MCD-Rif NSDPI (NSD1) and other with leucine (MCD-Rif-Leu NSDPI – NSD2) were prepared and characterized for physicochemical property. NSDPI obtained were evaluated for particle size, PDI and zeta potential, drug content, physicochemical properties, surface morphology, in-vitro lung deposition, in-vitro release rate and stability studies.

Particle size for both the formulations was found to be  $222.08 \pm 2.54$  and  $228.91 \pm 9.52$  nm with the corresponding PDI values of  $0.320 \pm 0.069$  and  $0.542 \pm 0.046$  respectively. Zeta potential of NSD1 was noted to be  $19.10 \pm 1.05$ , whereas  $22.23 \pm 2.22$  was observed for the formulation containing leucine (NSD2). Entrapment efficiency for both NSD1 and NSD 2 was found to be  $45.25 \pm 0.76$  and  $35.69 \pm 0.81$  % respectively. The particle size distribution curve of the nano spray-dried powder formulation determined using Sympatec was expressed in terms of the particle diameter at 10, 50, and 90 % of the volume distribution ( $D_{v_{10}}$ ,  $D_{v_{50}}$  &  $D_{v_{90}}$ , respectively). Span values for both the formulations (MCD-Rif and MCD-Rif-Leu NSD) were found to be small ( $1.94 \pm 0.04$  &  $2.00 \pm 0.17$ ) indicating no particle aggregation and unimodal particle size distribution. It was observed that 50<sup>th</sup> and 90<sup>th</sup> percentile undersize ( $D_{v_{50}}$  &  $D_{v_{90}}$ ) was varied in two formulations.  $D_{v_{50}}$  &  $D_{v_{90}}$  values of NSD batch 1 were found to be  $3.17 \pm 0.08$  ( $D_{v_{50}}$ ),  $7.24 \pm 0.12$  ( $D_{v_{90}}$ )  $\mu\text{m}$  respectively, whereas these values were found to be slightly decreased in the formulation containing leucine ( $2.91 \pm 0.04$  ( $D_{v_{50}}$ ) &  $6.99 \pm 0.22$   $\mu\text{m}$  ( $D_{v_{90}}$ )). Decreased particle size of MCD NSD 2 powder formulations, may be due to presence of leucine which enhanced particle properties for aerosolization. NSD batches showed respirable particle size in both cases, with (NSD2) or without leucine (NSD1). In general, the particles (NSD1 and NSD2) displayed irregular to wrinkled and collapsed shape with smooth surface morphology.

Structural analysis of MCD-RIF NSD using FTIR showed a peak at 1643 corresponding to the furanone C=O and another peak at  $1559 \text{ cm}^{-1}$  for amide C=O group were observed in the FTIR spectra of MCD-Rif NSD and MCD-Rif-Leu NSD. Moreover, a characteristic band for –C–O–C– ether group and aromatic C-H bending was also noted at around  $1250 \text{ cm}^{-1}$  and  $724 \text{ cm}^{-1}$  respectively, indicating entrapment of rifampicin in the both the NSD powders. These bands were completely absent in the MCD, confirming no interaction between the drug and MCD in the formulation. DSC thermogram of rifampicin showed a characteristic exothermic peak at  $260^\circ\text{C}$ . As we did not notice any endothermic or exothermic peak in pure MCD thermographs, DSC thermographs of MCD-Rif NSD formulation also had no endothermic or exothermic peaks. In addition, no rifampicin peak was observed in the MCD NSD formulation, indicating that the drug was in molecularly dispersed in the polymeric nanoparticle prepared by nano spray drying. XRD spectra of both MCD-Rif NSD and MCD-Rif-Leu NSD showed absence of any peak of rifampicin in the MCD NSD powder formulation suggested the presence of rifampicin in solid amorphous state in both formulations prepared by nano spray drying technology.

In-vitro aerosolization study of MCD-Rif NSD powder was carried out using next generation impactor. The measured fine particle fraction (FPF) for pure rifampicin, MCD-Rif and MCD-Rif-Leu NSD powder formulation was found to be  $74.55 \pm 4.01$  % and  $61.48 \pm 3.88$  % respectively. The aerosolization and deposition of pure rifampicin without carrier system (MCD) showed poorest performance, whereas nano spray drying (NSD) of rifampicin using MCD significantly improved the powder characteristics. After preparation of MCD NSD powder formulations, significant improvement in the powder characteristics and in-vitro deposition in the lung was observed. Highest FPF of  $74.55 \pm 4.01$ % with MMAD of  $1.53 \pm 0.17$   $\mu\text{m}$  and GSD of  $4.1 \pm 1.42$  was noted from MCD-Rif NSD powder formulation, whereas formulation prepared incorporating additional lipophilic adjunct (MCD-Rif-L NSD powder formulation) exhibited less FPF ( $61.48 \pm 3.88$ %) as compared to MCD-Rif NSD. In addition, MMAD and GSD of MCD-Rif-L NSD were found to be  $1.96 \pm 0.16$   $\mu\text{m}$  and  $1.8 \pm 0.09$  respectively. These results suggested the applicability of MCD-Rif NSDPI for incorporation of rifampicin for lung delivery. Deposition of MCD-Rif NSD and MCD-Rif-L NSD powder formulations in all stages of the NGI including inhaler, mouthpiece and throat was ranging from 75% and 125% of mass balance, which is in accordance with the criteria stated as per British Pharmacopoeia.

Results of in-vitro release studies indicated  $87.65 \pm 1.09$  % release of rifampicin in the SLF (pH 7.4) within 2 hours, whereas, MCD-Rif and MCD-Rif-Leu NSD formulation were able to control the release of rifampicin. Results demonstrated that MCD-Rif NSD powder formulation released  $32.45 \pm 3.48$   $64.53 \pm 3.48$  % of rifampicin in 4 and 6 hr respectively, whereas, MCD-Rif-Leu NSD formulation released  $51.18 \pm 1.82$  % of rifampicin by the end of 6 hr. Both the formulations revealed slow release of rifampicin from the NSD powder formulations, which may be due to hydrophobic barrier presented by the modified chitosan derivative (MCD). MCD-Rif NSD and MCD-Rif-Leu NSD powder formulations showed biphasic release pattern, which could be attributed to the localized rifampicin within NSD formulation. The first phase of the release was found upto 6 hrs, where steady and almost linear release of drug was observed. Later on, rifampicin release was slowed down (second phase), which could be due to the release of rifampicin encapsulated within the core of NSD powder formulation. The main mechanism for the drug transport from the MCD NSD particles was found to be controlled by super case II transport, which is a combination of diffusion and polymer chain relaxation. The results of the stability study at room temperature indicated that storage of NSD formulations at RT did not influence drug content, particle size and zeta potential and hence RT could be considered as suitable storage condition for both the formulations.

### 14.3.8 In-vitro cell line studies

Synthesized polymers (HCD and MCD) were tested for cytotoxicity using MTT assay. The cytotoxicity profiles of HCD and MCD was evaluated over 48 hr in adenocarcinomic human alveolar basal epithelial cell line, A549. Results indicated that both the polymers (HCD and MCD) showed cell viability at the tested concentrations (0- 2.5  $\mu\text{g}/\text{ml}$ ) in comparison to the negative control (taken as 100% viability) and positive control (100 % cytotoxicity). MTT

## Chapter 14 - Summary and Conclusions

---

assay results confirmed the *in vitro* biocompatibility of HCD and MCD, which is important for their application in successful vaccine and drug delivery systems.

A cytotoxicity study was performed on porcine monocytes to ensure that the concentrations used in the experiments are not deleterious to cells. Results of this study also indicated non-toxic nature of the Prep 1 (HCD-Ag NPs), Prep 2 (HCD NPs + Ag85A), Prep 3 (HCD Blank NPs), Prep 4 (HCD-FITC NPs) at the temperatures of 37 and 4 °C suggesting suitability of the polymer and formulations for drug and vaccine delivery. Cellular uptake was determined using freshly prepared porcine monocytes. It was observed that Prep 4 (FITC-HCD NP) indicated highest cellular uptake of almost 100 % at 37 °C, whereas same formulations at 4 °C showed less uptake suggesting the suitability of utilization of formulation at normal physiological temperature. All other formulations which were not FITC labeled but had auto fluorescing property showed less cellular uptake at both 37 and 4 °C. All other preparations displayed % cellular uptake below 20 %. Thus, prep 4 showed almost 5 fold increases in the cellular uptake indicating suitability of its administration for improved therapeutic efficacy in the treatment of TB. Hence, efficient uptake of FITC-HCD NPs indicated suitability of HCD NPs for drug and vaccine delivery and thus, more uptake will help to either neutralize MTB present in the macrophages or vaccine preparation will help to induce immunostimulatory effect.

Immunostimulatory effect of the formulations was studied in two steps; first by analyzing cytokine production and second by analyzing T cell activation. Cytokine production was performed in the porcine monocytes, B cells and enriched dendritic cells and assayed using specified ELISA's and cytokine concentrations were expressed as pg/mL. Cytokines namely IL- 10, IL- 12 and TNF $\alpha$  were selected for the study and the results for each of cytokine in different cell type. Experiments conducted with Prep 1, Prep 2, Prep 3 and Prep 4 were able to stimulate monocytes, B cells and enriched dendritic cells to produce detectable levels of IL-10, IL-12 and TNF- $\alpha$ . It was observed that all cytokines were detectable at the lowest stimulant concentrations of 11  $\mu$ g/ml. Cytokine, IL-10 was produced at relatively high levels (1,600 pg/ml) in response to a dose as low as 11  $\mu$ g/ml of prep 1 and 2 in porcine monocyte, whereas prep 3 showed lowest stimulation of IL-10 production. In case of IL-10, 10-1600 pg/ml of IL-10 was secreted from monocytes, whereas 30-45 pg/ml of IL-10 was secreted from both B cells and DCs. Around 200 – 300 pg/ml of IL-12 was found to be released from all the cells. Lastly, TNF- $\alpha$  showed increased production from monocytes (20-1000 pg/ml), whereas approximately 50 – 60 and 60 – 80 pg/ml of TNF- $\alpha$  was found to be secreted from B cells and DCs respectively. Based on these results it can be concluded that higher levels of IL-10 was released from monocytes, whereas all other preparations were also able to stimulate the production of cytokine in all cells. Secondly, immunostimulatory effect of nanoparticles was determined by analyzing CD 16 and MHC II expression. Upon analyzing the results of CD 16 and MHC-II expression, it was observed that all preparations (Prep 1-4) and lipopolysaccharide (LPS) were able to induce CD16 expression. Results showed down regulation of CD16 in all the preparations except prep 3, whereas preparations 1, 2 & 4 showed very less stimulation. On the other hand, up regulation of MHC-II

expression was noted from all the preparations. All preparations showed up-regulation of MHC II, with highest stimulation was observed from prep 4, suggesting ability of HCD NPs and its Ag85A counterpart to stimulate MHC-II for the production of antibodies.

### 14.3.9 In-vivo immunization studies

*In vivo* studies were performed on Balb/c mice as per the guidelines of Institutional Animal Ethics Committee. In-vivo studies were carried out at two levels – 1) cytokine assay and 2) in-vivo immunization studies. Cytokine ELISA assay performed on bronchoalveolar fluid (BALF) and spleen and lymph nodes confirmed release of cytokine, INF- $\alpha$ . Cytokine (IFN- $\gamma$ ) assay in BALF, lymph node and spleen was performed and it was observed that, concentration of IFN- $\gamma$  in BLAF was found to be high in mice belonging to group 2 and 3 ( $539 \pm 159.3$  &  $605 \pm 127.5$  pg/ml), which were immunized with marketed BCG vaccine and pure Ag85a+alum by subcutaneous route as compared to the nasally administered HCD-Ag85A NPs and PLGA-Ag85A NPs formulation ( $99.88 \pm 46$  &  $118.9 \pm 64.16$  pg/ml) (group 11 and 12). When intra-nasally administered HCD-Ag85A NPs and PLGA-Ag85A NPs formulations were compared with their subcutaneous counterpart, the results highlighted better production of IFN- $\gamma$  from the later with the values of  $123.7 \pm 58.44$  and  $300.9 \pm 125$  pg/ml. With all other groups, less than 200 pg/ml of IFN- $\gamma$  generation was observed. In all the cases, IFN- $\gamma$  production was dominated by the alum adsorbed Ag85A. Similarly, intra-nasally administered HCD-Ag85A NPs and PLGA-Ag85A NPs showed comparable responses for the production of IFN- $\gamma$  in all the cases (lymph nodes and spleen) as compared to the marketed BCG and alum adsorbed Ag85A, except BALF, where these formulations exhibited very less responses. The overall results of this study indicated that the nasal immunization using nanoparticles based formulation resulted in the induction of Th1 (cell mediated) immunity. However, studies using more cytokines are recommended to identify the ability of the said formulation to induce Th2 cells for the development of humoral immunity.

Suitability of the Ag85A loaded HCD nanoparticles for intranasal vaccination was investigated by comparing the serum, lymph node and spleen responses of mice after subcutaneous (SC) and intranasal (IN) vaccination with marketed BCG vaccine, soluble antigen co-administered with alum, HCD-Ag85A NPs and PLGA-Ag85A NPs.

The serum antibody responses elicited by IN immunization with HCD-Ag85A NPs and PLGA-Ag85A NPs were significantly higher than those achieved after conventional SC injection of marketed BCG vaccine and blank HCD and PLGA NPs after both SC and IN administration ( $P < 0.001$ ). Altogether, these results suggested strong immunostimulating effect of HCD-Ag85A NPs and PLGA-Ag85A NPs upon IN administration. In addition, results showed that HCD-Ag85A NPs elicited slightly delayed immunological response ( $135.9 \pm 2.198$ ) as compared to the alum adsorbed Ag85A ( $205.7 \pm 2.51$ ) indicating ability of HCD NPs to control the release of Ag85A. On subsequent days, concentration of IgG2a antibody attained in mice showed increasing immunological response for HCD-Ag85A NPs, which even exceeded the levels, achieved by alum adsorbed Ag85A and marketed BCG

vaccine. Similarly, PLGA-Ag85A NPs also showed better levels of IgG2a as compared to marketed BCG vaccine and blank HCD and PLGA NPs after both SC and IN administration. Secondly, we have estimated the amount of anti-Ag85A (IgG2a) production in lymph nodes and spleen and the immune response achieved with Ag85A loaded HCD and PLGA NPs following SC and IN administration was found to be higher as compared to any other formulation tested.

In sum, based on the results of *in vivo* immunization study, we may conclude that HCD-Ag85A NPs could be considered as a new and promising adjuvant candidate for enhancing and prolonging the immune response of Ag85A after SC and IN administration. PLGA-Ag85A NPs demonstrated best immunological responses among all formulations after both SC and IN administration, of which immunostimulatory properties for various protein antigens are already reported. However, interesting feature of our experiment is achievement of higher immunological responses from HCD-Ag85A NPs and PLGA-Ag85A NPs as compared to marketed BCG vaccine (which is known to be standard) and alum adsorbed Ag85A (which is traditional and only approved adjuvant to date).

### 14.4 Conclusions

In the present investigations, two chitosan derivatives, hydrophobic chitosan derivative (HCD) and modified chitosan derivative (MCD) were synthesized to overcome the current limitations of chitosan. Thereafter, nanoparticulate delivery systems were prepared by double emulsion solvent evaporation using PLGA and hydrophobic chitosan derivative (HCD) for pulmonary delivery of Ag85A and rifampicin to improve immunostimulatory effect of Ag85A and therapeutic efficacy of rifampicin. In addition, nano spray drying technique was utilized for the preparation of rifampicin incorporated HCD and MCD particles as dry powder inhalation. Results of physicochemical characterization showed successful entrapment of Ag85A and rifampicin in HCD, whereas *in-vitro* lung deposition and release studies revealed more than 30-40 % deposition of nanoparticles in lungs and sustained with biphasic release pattern respectively. Results of the physicochemical properties indicated formation of rifampicin incorporated MCD nano spray dried particles, whereas *in-vitro* lung deposition studies showed more deposition of MCD-rif NSD particles as compared to HCD-Rif particles. Results of *in-vitro* cytotoxicity study by MTT assay showed no-toxicity of HCD and MCD, indicating their suitability for application in delivery of vaccines and drugs. Uptake studies in porcine monocytes revealed 100 % uptake of FITC-HCD NPs suggesting ability of NPs incorporated either Ag85A or rifampicin will be efficiently taken up by the macrophages, where MTB thrives, thus, improved disease control can be achieved. Immunostimulatory studies in terms of cytokine assay and T cell activation was carried out in porcine monocyte, B cells and enriched dendritic cells. Results showed production of IL-10, IL-12 and TNF- $\alpha$  in porcine monocyte, B cells and enriched dendritic cells in response to the stimuli conferred by HCD NPs and Ag85A. HCD NPs and Ag85A were also able to stimulate CD 16 and MHC-II cells, which may leads to stimulation of Th1 and Th2 cells to releases cytokines. Activation of Th1 cells help releasing INF- $\alpha$ , TNF, whereas Th2 releases IL-2, IL-4, IL- 10, IL- 12 etc. Thus, activation of Th1 and Th2 in our studies, indicated

induction of cell mediated and humoral immunity conferred by HCD-Ag85A NPs. In vivo studies confirmed generation of cytokine, INF- $\alpha$  in bronchoalveolar fluid (BALF), spleen and inguinal lymph nodes, whereas Ag85A specific IgG2a antibody was detected in serum, lymph node and spleen indicating systemic immunological response.

In sum, based on the results of in vivo immunization study, HCD-Ag85A NPs may be considered as a new and promising adjuvant candidate for enhancing and prolonging the immune response of Ag85A after SC and IN administration. PLGA-Ag85A NPs demonstrated best immunological responses among all formulations after both SC and IN administration, whose immunostimulatory properties for various protein antigens are already reported. However, interesting feature of our experiment was achievement of higher immunological responses from HCD-Ag85A NPs and PLGA-Ag85A NPs as compared to marketed BCG vaccine, which is known to be standard and alum adsorbed Ag85A, which is traditional and only approved adjuvant to date. Moreover, the new hydrophobic chitosan derivative synthesized by us, which exhibited interesting in vitro and in vivo features hold promise as a better alternative for vaccine delivery of subunit antigens over conventional or routine adjuvants such as alum.

However, further investigations in animals for protection efficacy and human beings under clinical conditions are necessary before they can be commercially exploited.